ASTROPHYSICS AND SPACE SCIENCE PROCEEDINGS

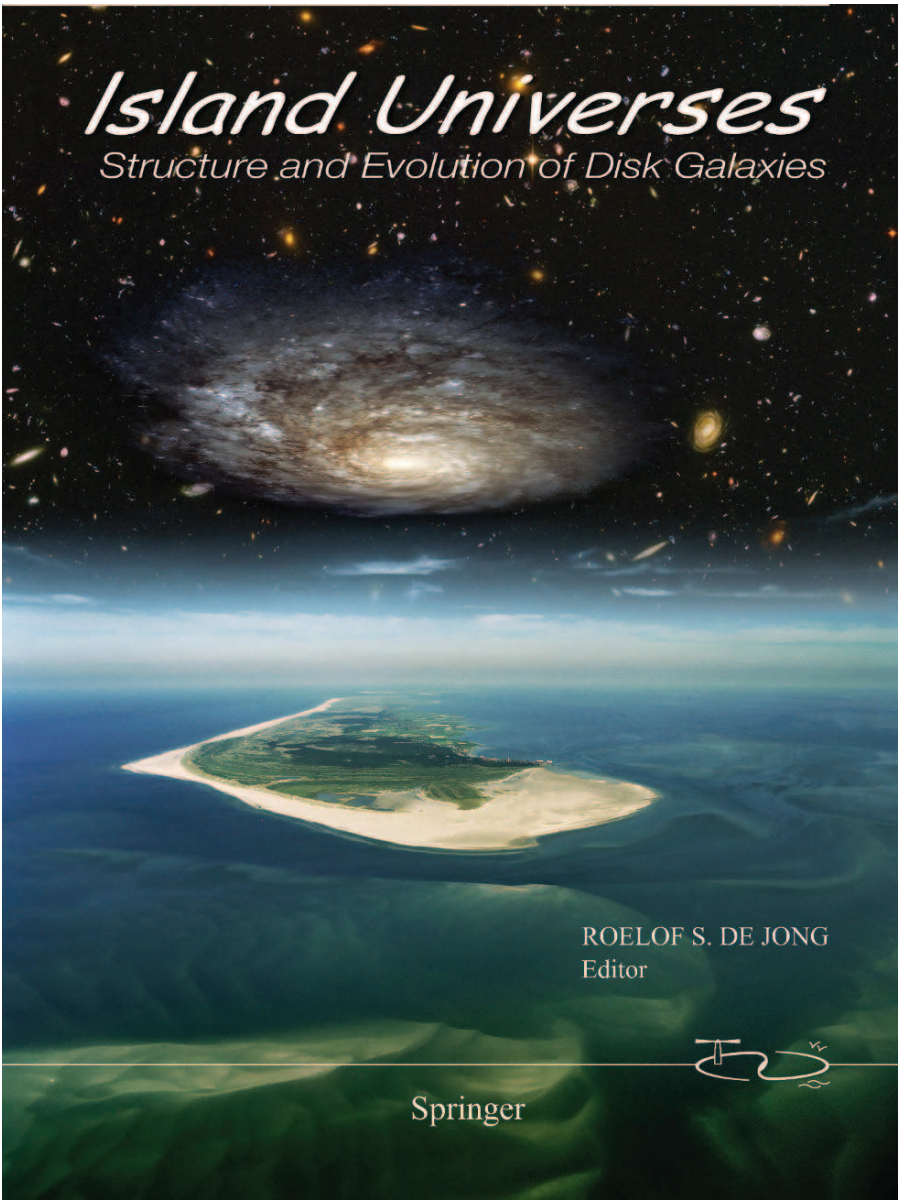

ISLAND UNIVERSES

ISLAND UNIVERSES

STRUCTURE AND EVOLUTION OF DISK GALAXIES

by

R. S. DE JONG
Space Telescope Science Institute, Baltimore, MD, U.S.A.

Springer

A C.I.P. Catalogue record for this book is available from the Library of Congress.

ISBN-10 1-4020-5572-2 (HB)
ISBN-13 978-1-4020-5572-0 (HB)
ISBN-10 1-4020-5573-0 (e-book)
ISBN-13 978-1-4020-5573-7 (e-book)

Published by Springer,
P.O. Box 17, 3300 AA Dordrecht, The Netherlands.

www.springer.com

Printed on acid-free paper

All Rights Reserved
© 2007 Springer
No part of this work may be reproduced, stored in a retrieval system, or transmitted
in any form or by any means, electronic, mechanical, photocopying, microfilming, recording
or otherwise, without written permission from the Publisher, with the exception
of any material supplied specifically for the purpose of being entered
and executed on a computer system, for exclusive use by the purchaser of the work.

Contents

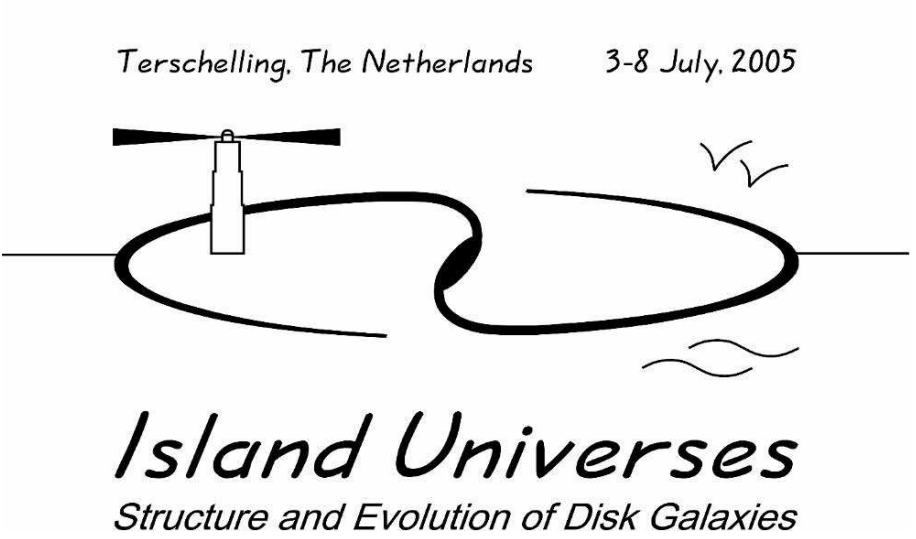

Foreword

Piet van der Kruit

Kapteyn Astronomical Institute, University of Groningen, The Netherlands
vdkruit@astro.rug.nl

In the first place I would like to say that I am extremely grateful that this conference took place. It was a very stimulating and exciting meeting. The speakers and contributors to the discussion were all very inspiring and the Scientific Organising Committee put together a most interesting program. It was also helpful that the meeting was held in the same place where we were staying and had our meals, the Schylge Hotel on the beautiful Frisian island of Terschelling. I am very pleased that so many young astronomers took part and made use of the many opportunities at meals and in the evenings to talk to older astronomers. For me personally it was great to see many colleagues that have worked in the same field as I and whom I often have known and respected for many years.

I first of all would like to thank those former students of mine that took the initiative to hold this symposium and subsequently did most of the hard work of organising it: Erwin de Blok (although really and truly a student of Thijs van der Hulst), Richard de Grijs, Roelof de Jong, Johan Knapen and Eline Tolstoy (whose real supervisor was Abi Saha). In particular I am very grateful to Roelof de Jong, who chaired the Scientific Organising Committee, designed the poster and the logo and edited these proceedings. And also to Eline Tolstoy, who chaired the Local Organising Committee. I know it took both of them valuable time that they would have devoted to research, but what they did here was certainly also an important contribution to astronomy.

I thank all members of the SOC for all their input; with a few exceptions they are colleagues that I had collaborations with over the years. I have been very impressed by the way in which the LOC organized the meeting, took care of all arrangements and gave the participants all support they required. Greta, Peter, Isabel, Hans, Eline, Thijs, Hennie and Jackie: it was wonderful. And I thank all participants for this stimulating week. I would like to thank three more persons in particular. I thank Mike Disney for the very nice portret reproduced in this book and his afterdinner speech at the conference barbecue, which was followed by a very moving applause for me by all attending. And I thank Ken Freeman for giving the opening review (as I had the honor to do at his conference on Dunk Island) and Tim de Zeeuw for doing me the honor of giving the conference summary.

Tim de Zeeuw and Ken Freeman mentioned in their contributions the "van der Kruit guilder". I would like to take this opportunity to tell the background of this, since most of the credit for it should go to Leonard Searle.

We were writing paper III and IV in our series in September 1981 during a visit that Leonard made to Groningen. I said to him that I felt he should be first author on paper IV. He immediately refused, arguing that I had initiated the project, produced most of the ideas and had done most the work. My reply was that it had been very much a collaboration and that therefere I felt it would be very appropriate. Leonard thought about it overnight (he woke up early because he still suffered from jetlag) but stayed firmly with his opinion, even to the extent that he felt we should make a joke about it. He therefore had made up the text of a possible footnote to the title of paper IV and he showed it to me. I gave in, to a large extent because I so much liked the footnote. It was included precisely as Leonard suggested and for completeness I cite it: *"The order of the authors' names in this series of papers has been decided in each case by tossing a coin. The coin used for this purpose is fully described in a forthcoming monograph "The van der Kruitguilder" to be published in the Series "Curiosités Numismatiques", Monte Carlo."*

In those days we had no Internet or preprint servers and preprints were distributed on paper. Also there was no ADS and most institutes had especially printed postcards to fill out and sent to authors requesting reprints after publication. After the preprints of papers III and IV went out, I started getting such postcards requesting preprints of the monograph in the footnote. So after a few of these I made up the page that Tim has included in his contribution to this book and sent that in return. However, it was Leonard who first suggested the footnote and composed it.

For the record I note that the coin has been "used" also by Rosie Wyse (after asking me for permission) for a paper she wrote with Gerry Gilmore (Wyse & Gilmore, 1986, A.J. 91, 855). On the first page a footnote appears: *"The order of the authors' names was decided by tossing a coin. This coin, the van der Kruit guilder (van der Kruit and Searle 1986), was kindly made available to the first author by P.C. van der Kruit."* The year was now 1986. Indeed the list of references at the end of the Wise & Gilmore paper contains "van der Kruit, P.C. and Searle, L. (1986), In *Curiosités Numismatiques* (to be published)".

PIET VAN DER KRUIT

Piet van der Kruit as drawn by Mike Disney.

Former and current students of Prof. Piet van der Kruit. Fltr: Benne Holwerda, Richard de Grijs, Erwin de Blok, Piet van der Kruit, Roelof de Jong, Jonathan Heiner, Eline Tolstoy, Johan Knapen.

Preface

The *Island Universe: Structure and Evolution of Disk Galaxies* conference was held on the island of Terschelling from 3–8 July, 2005. It was attended by 125 registered participants coming from 23 different countries. A total of 54 oral papers were delivered including a conference summary. Furthermore, more than 50 posters were presented, which were summarized in two short presentations.

The idea for the meeting originated when Prof. Piet van der Kruit met with some former students and indicated that he was interested in organizing a conference. When Piet subsequently was appointed on a new honorary chair — the Jacobus C. Kapteyn Professorship in Astronomy — a reason to organize the meeting had been found. We would organize the meeting to celebrate Piet's achievements in astronomy and thank him for his generous contributions to astro-politics and administration.

The topic of the conference had to be a tribute to Piet's life long science interest: the properties of disk galaxies. The goal of the meeting was to take inventory of our current knowledge of the structure and content of disk galaxies, to present models of formation and evolution leading to disk galaxies, and to bring together observers and theorists to investigate paths for future research.

The band of former students was expanded to a full SOC (see xix), an LOC was formed at the Kapteyn Astronomical Institute, and the organization of the meeting started in earnest. While Piet had indicated that he would like the meeting to take place on Svalbard/Spitsbergen, it was quickly determined that this was not practical for logistical and financial reasons. We were lucky to find as a very good alternative conference center and hotel "Schylge" on the island of Terschelling, which allowed us to board all participants at the same place where the oral and poster presentations were delivered, without even to have to share the hotel with any other guests. This remote location, away from the daily bustle, significantly contributed to the success of the meeting.

The meeting was organized along eight broad topics. Each topic was introduced by a review speaker, followed by invited and contributed presentations. The same structure as used during the meeting is used in these proceedings, with the contributions ordered within each topic as they were presented during the meeting, followed by the poster contributions that fit best in that session. I hope these proceedings will portrait the atmosphere of an fruitful and enjoyable meeting, and carry the invitation for the next (at Spitsbergen?).

Acknowledgements

The "Island Universes" conference and these proceedings would not have been possible without the support of a large number of people and institutions.

First and foremost I want to thank Piet van der Kruit, without whose continued support for me and his other (former) students (see p. xvi) this conference and these proceedings never would have been.

I want to thank the Science Organizing Committee for helping me to make a very interesting and stimulating science program, that fostered lots of good discussions. I am very much indebted to the Local Organizing Committee for their tireless efforts before the meeting and their excellent support during the meeting, making everything run so smoothly.

The conference received financial support from the annual grant of the Faculty of Mathematics and Natural Sciences awarded to Prof. van der Kruit for his J.C. Kapteyn Professorship, the Kapteyn Astronomical Institute, the Koninklijke Nederlandse Akademie van Wetenschappen (KNAW), the Leids Kerkhoven-Bosscha Fonds (LKBF), Netherlands Research School for Astronomy (NOVA), and the Netherlands Organisation for Scientific Research (NWO).

ROELOF S. DE JONG

Science Organizing Committee:

Chairperson:	Roelof de Jong
Other members:	Ron Allen, Julianne Dalcanton, Erwin de Blok, Richard de Grijs, Ken Freeman, Johan Knapen, Rob Kennicutt, Jerry Sellwood, Eline Tolstoy, Jacqueline van Gorkom, Thijs van der Hulst, Piet van der Kruit.

Local Organizing Committee:

Chairperson:	Eline Tolstoy
Other members:	Greta de Vries, Peter Kamphuis, Isabel Pérez Martín, Hans Terlouw, Thijs van der Hulst, Piet van der Kruit, Hennie Zondervan, Jackie Zwegers

Image credits:

Page ii images:	Terschelling: © Aerophoto-Schiphol b.v. Hubble Ultra Deep Field & NGC 4414: © STScI/NASA
Illustration and logo design:	© Roelof de Jong
Other photographs:	© Stéphane Courteau, except © Piet van der Kruit p. 374, 536, 578 © Fabio Governato p. 346 © Benne Holwerda p. 570, 582 bottom

List of Participants

Roberto Abraham	Dept. of Astronomy & Astrophysics, University of Toronto
Emma Allard	Univsersity of Hertfordshire
Paul Allen	Mount Stromlo Observatory
João Alves	ESO
David Andersen	NRC Herzberg Institute of Astrophysics
E. Athanassoula	Observatoire de Marseille
Steven Bamford	University of Nottingham
Jesus Falcon Barroso	Leiden Observatory
Peter Barthel	Kapteyn Astronomical Institute
Giuseppina Battaglia	Kapteyn Astronomical Institute
Amanda Bauer	University of Texas at Austin
Eric Bell	Max-Planck-Institut für Astronomie
Matthew Bershady	University of Wisconsin
Giuseppe Bertin	Dipartimento di Fisica, Università di Milano
Yury Bialetski	ESO
James Binney	Oxford University
Torsten Böker	European Space Agency
Ian Bonnell	University of St Andrews
Albert Bosma	Observatoire de Marseille
Robert Braun	ASTRON
Chris Brook	Université Laval
Alyson Brooks	University of Washington
James Bullock	UC Irvine
Martin Bureau	University of Oxford
David Burstein	Arizona State University
Scott Chapman	Caltech
Chin-Wei Chen	Graduate Institute of Astronomy, National Central University
Daniel Christlein	Yale University & Universidad de Chile
Lodovico Coccato	Kapteyn Astronomical Institute
Enrico Maria Corsini	Dipartimento di Astronomia, Università di Padova
Stéphane Courteau	Queen's University
Hugh Crowl	Yale University
Barbara Cunow	Department of Mathematical Sciences, University of South Africa
Julianne Dalcanton	University of Washington
Ivana Damjanov	Astronomical Observatory of Belgrade
Erwin de Blok	RSAA, Mount Stromlo
Richard de Grijs	University of Sheffield

Roelof de Jong	Space Telescope Science Institute
Tim de Zeeuw	Leiden Observatory
Ralf-Juergen Dettmar	Astronomical Institute, Ruhr-University Bochum
Mike Disney	Cardiff University
Clare Dobbs	School of Physics & Astronomy, University of St Andrews
Michael Andrew Dopita	RSAA, Australian National University
Bruce Elmegreen	IBM T.J. Watson Research Center
Debra Elmegreen	Vassar College
Michael Fall	Space Telescope Science Institute
Kambiz Fathi	Rochester Institute of Technology
Annette Ferguson	Institute for Astronomy, University of Edinburgh
Filippo Fraternali	Theoretical Physics, University of Oxford
Ken Freeman	RSAA, Mount Stromlo
Peter Frinchaboy	University of Virginia
Jose Funes	Vatican Observatory
Katia Ganda	Kapteyn Astronomical Institute
Fabio Governato	INAF - University of Washington
Preben Grosbol	European Southern Observatory
Puragra (Raja) Guhathakurta	UCO/Lick Observatory, Univ. of California Santa Cruz
Asao Habe	Graduate School of Science, Hokkaido University
George Heald	University of New Mexico
Jonathan Heiner	Space Telescope Science Institute
Philippe Héraudeau	Kapteyn Astronomical Institute
Benne Willem Holwerda	Kapteyn Astronomical Institute
Chanda Jog	Indian Institute of Science
Rachel Johnson	Oxford University
Bernard Jones	Kapteyn Astronomical Institute
Nadejda Kaltcheva	University of Wisconsin – Oshkosh
Peter Kamphuis	Kapteyn Astronomical Institute
Susan Kassin	UCO/Lick Observatory, Univ. of California, Santa Cruz
Robert Kennicutt	Steward Observatory
Lisa Kewley	Institute for Astronomy, Univ. of Hawaii
Johan Knapen	University of Hertfordshire
Karen Knierman	Steward Observatory, University of Arizona
David Koo	UCO/Lick Obs., Univ. of California, Santa Cruz
Nario Kuno	Nobeyama Radio Observatory
Lerothodi Leeuw	University of Chicago
Yang-Shyang Li	Kapteyn Astronomical Institute
Ute Lisenfeld	Universidad de Granada, Spain
Jochen Liske	ESO
Donald Lynden-Bell	Institute of Astronomy, Cambridge
Lauren MacArthur	University of British Columbia
George Mamatsashvili	Center for Plasma Astrophysics, Abastumani Astroph. Obs.
Hidenori Matsui	Graduate School of Science, Hokkaido University
Lynn Matthews	Harvard-Smithsonian Center for Astrophysics
Sharon Meidt	University of New Mexico
Bhasker Moorthy	New Mexico State University
Marcelo Daniel Mora	ESO

Eric Murphy	Yale University
Preethi Nair	University of Toronto
Colin Norman	The Johns Hopkins University
Tetyana Nykytyuk	Main Astron. Obs. of National Academy of Sciences of Ukraine
Sachiko Onodera	Institute of Astronomy, University of Tokyo
Panos Patsis	Research Center for Astronomy, Academy of Athens
Isabel Pérez Martin	Kapteyn Astronomical Institute
Max Pettini	Institute of Astronomy, Cambridge
Daniel Pisano	Naval Research Laboratory
Michael Pohlen	Kapteyn Astronomical Instituut
Laura Portinari	Tuorla Observatory, Turku University
Michael Regan	Space Telescope Science Institute
Dominik Rosenbaum	Astronomisches Institut Ruhr Universtität Bochum
Joern Rossa	Space Telescope Science Institute
Renzo Sancisi	Osservatorio Astronomico di Bologna & Kapteyn Astron. Institute
Jerry Sellwood	Rutgers University
Joe Silk	Astrophysics, University of Oxford
Leonie Snijders	Leiden Observatory
Jesper Sommer-Larsen	Niels Bohr Institute
Mario Soto	Sterrewacht Leiden
Jaroslaw Stasielak	Institute of Physics, Jagellonian University
Annapurni Subramaniam	Indian Institute of Astrophysics
Claire Thomas	Liverpool John Moores University
Eline Tolstoy	Kapteyn Astronomical Institute
Clemens Trachternach	Astronomisches Institut Ruhr Universtität Bochum
Ignacio Trujillo	Max-Planck-Institute für Astronomie
Tjeerd van Albada	Kapteyn Astronomical Institute
J.M. van der Hulst	Kapteyn Astronomical Institute
Piet van der Kruit	Kapteyn Astronomical Institute
Jacqueline van Gorkom	Columbia University
Lottie van Starkenburg	Leiden Observatory
Kim Venn	University of Victoria
Marc Verheijen	Kapteyn Astronomical Institute
Nicole Vogt	New Mexico State University
Kyle Westfall	University of Wisconsin
Tony Wong	CSIRO ATNF and University of New South Wales
Revaz Yves	Geneva Observatory
Dennis Zaritsky	University of Arizona
Saleem Zaroubi	Kapteyn Astronomical Institute
Hennie Zondervan	Kapteyn Astronomical Institute
Martin Zwaan	ESO
Jackie Zwegers	Kapteyn Astronomical Institute

I

PROPERTIES OF STELLAR DISKS

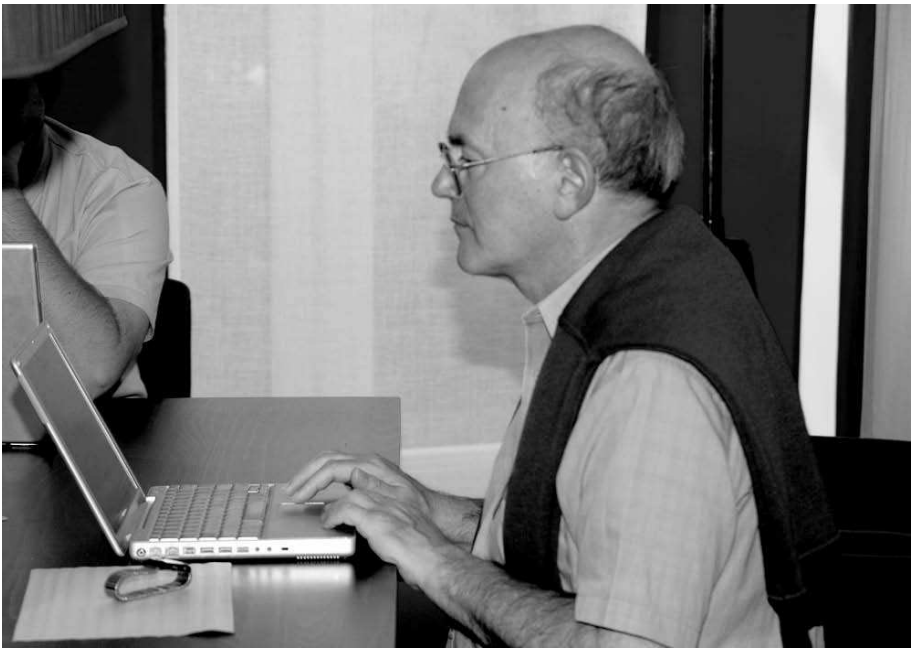

Ken Freeman at work.

STELLAR DISKS

K.C. Freeman

Research School of Astronomy & Astrophysics, The Australian National University
kcf@mso.anu.edu.au

Abstract I review the properties of galactic stellar disks. The review includes the famous van der Kruit & Searle papers of the early 1980s, recent work on the structure of the outer regions of galactic disks including the problem of the radial truncation of disks, and galactic thick disks.

Keywords: galaxies: spiral - galaxies: structure - galaxies: halo - galaxies: abundances

1. Introduction

The disk is the defining stellar component of disk galaxies. It is the end product of the dissipation of most of the baryons, and contains almost all of the baryonic angular momentum. Understanding its formation is probably the most important goal of galaxy formation theory.

Out of the chaotic hierarchical disk formation process come galactic disks with a high level of regularity in their structure and scaling laws. We need to understand the reasons for this regularity. In a series of four papers, following on from van der Kruit (1979), van der Kruit & Searle (1981a,b; 1982a,b) used surface photometry of a sample of edge-on spirals to establish most of the basic properties of disk galaxies, and laid the foundations of today's studies of galactic disks.

2. The van der Kruit & Searle Papers

Van der Kruit & Searle (vdKS) established:

- the underlying structure of galactic disks. The luminosity density distribution $L(R, z)$ is roughly exponential in radius R and height z, following a distribution of the form

$$L(R, z) = L_\circ \exp(-R/h_R)\mathrm{sech}^2(\mathrm{z}/\mathrm{z}_\circ)$$

or

$$L(R, z) = L_\circ \exp(-R/h_R) \exp(-z/h_z)$$

R. S. de Jong, Island Universes, 3–16.
© 2007 *Springer.*

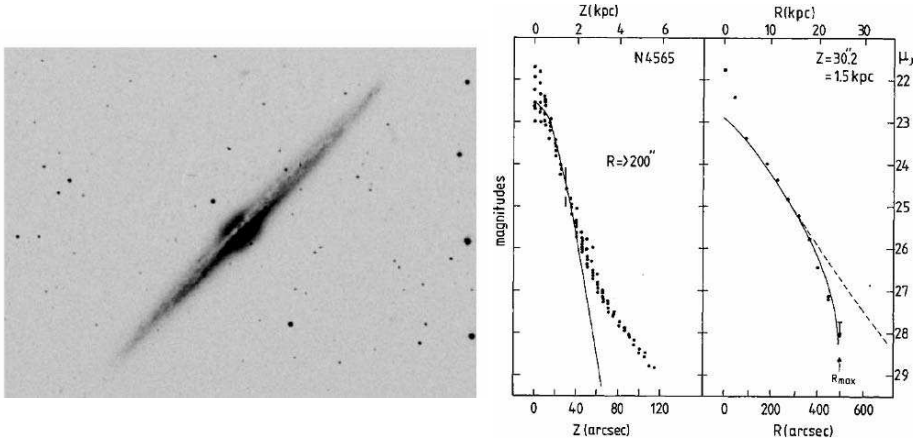

Figure 1. The galaxy NGC 4565 (left panel) and its surface brightness profiles in z and R, from van der Kruit & Searle (1981a). The $z-$profile shows the dominance of the thick disk above a height $z = 50$ arcsec. The $R-$profile shows the onset of radial truncation at a radius $R = 300$ arcsec.

with the vertical scaleheight h_z or $z_\circ$ approximately independent of radius.

- that this form of the luminosity distribution $L(R, z)$ holds out to $R = 3$ to 5 radial scale lengths, after which it is often truncated.

- the prevalence of thick disks which envelop the $L(R, z)$ light distribution of the thin disks.

Figure 1 shows one of the edge-on galaxies (NGC 4565) investigated by vdKS. This system has a small bulge and a prominent thick disk. The disk properties which vdKS established are clearly visible in their surface photometry for this galaxy.

From Jeans' equations, and assuming constant M/L ratio throughout the disk, the approximately double exponential structure with its constant scaleheight implies that the stellar velocity dispersion components in the disk should change with radius as $\sigma \sim \exp(-R/2h_R)$. This exponential decline in velocity dispersion is observed in the Milky Way and other spirals. Figure 2 shows the radial change in velocity dispersion observed by van der Kruit & Freeman (1986) for the disk of the spiral NGC 5247, and by Lewis & Freeman (1989) for the disk of the Milky Way.

Simulations of disk formation show a complex interplay of gravitational and hydro-dynamical effects. The details are not well understood, and the reason for the exponential form of the radial light distribution is not yet clear. Extreme options include

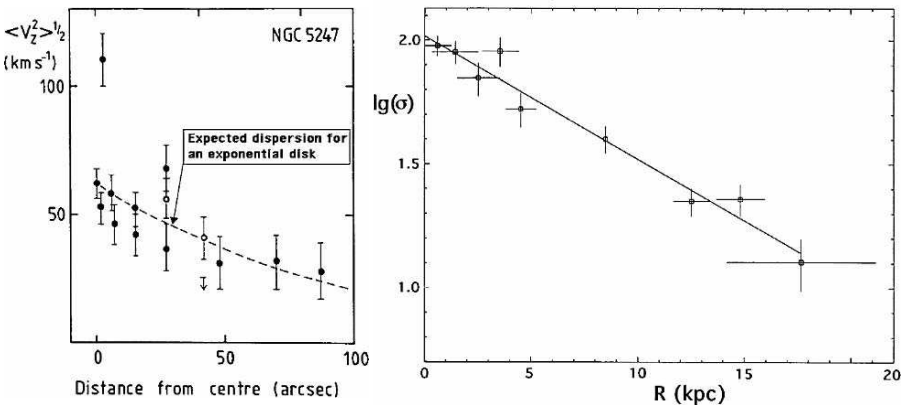

Figure 2. *Left:* The radial decrease of the z-component of the velocity dispersion in the spiral NGC 5247 (from van der Kruit & Freeman 1986). *Right:* The radial decrease of the R-component of the velocity dispersion for the thin disk of the Milky Way (from Lewis & Freeman 1989). The disk of the Milky Way is approximately exponential in R and z, with scaleheight of about 300 pc and scalelength of about 3.5 kpc. The velocity dispersion decreases from about 100 km/s near the center (similar to the velocity dispersion of the bulge) to about 15 km/s at a radius of 18 kpc.

- the collapse of a torqued gas cloud with the appropriate internal angular momentum distribution $M(j)$ within a dark halo, conserving its $M(j)$ to give an exponential gas disk in place before star formation began (e.g., Fall & Efstathiou 1980).

- the gas in the disk is radially redistributed by viscous torques: this process tends to an exponential disk if the star formation timescale $\sim$ viscous timescale (e.g., Lin & Pringle 1987).

The vertical structure of disks (Fig. 3) is directly associated with their star formation history and dynamical history. Spiral arm heating, scattering by giant molecular clouds, accretion and warping can all contribute to heating the disk vertically and generating a a vertical scale height h_z for the old thin disk that is usually about 200 to 300 pc.

3. The Outer Regions of Disks

First we discuss the radial truncation of galactic disks. The truncation is more easily seen in in edge-on galaxies than in face-on galaxies. Figure 4 shows two images of the edge-on spiral NGC 4565, printed with different stretches. In the deep stretch, one can see that the disk appears thicker in z, but its radial extent has hardly changed. Figure 5 shows the correlation between the truncation radius $R_{\rm max}$ and the radial scalelength for a sample of edge-on disks.

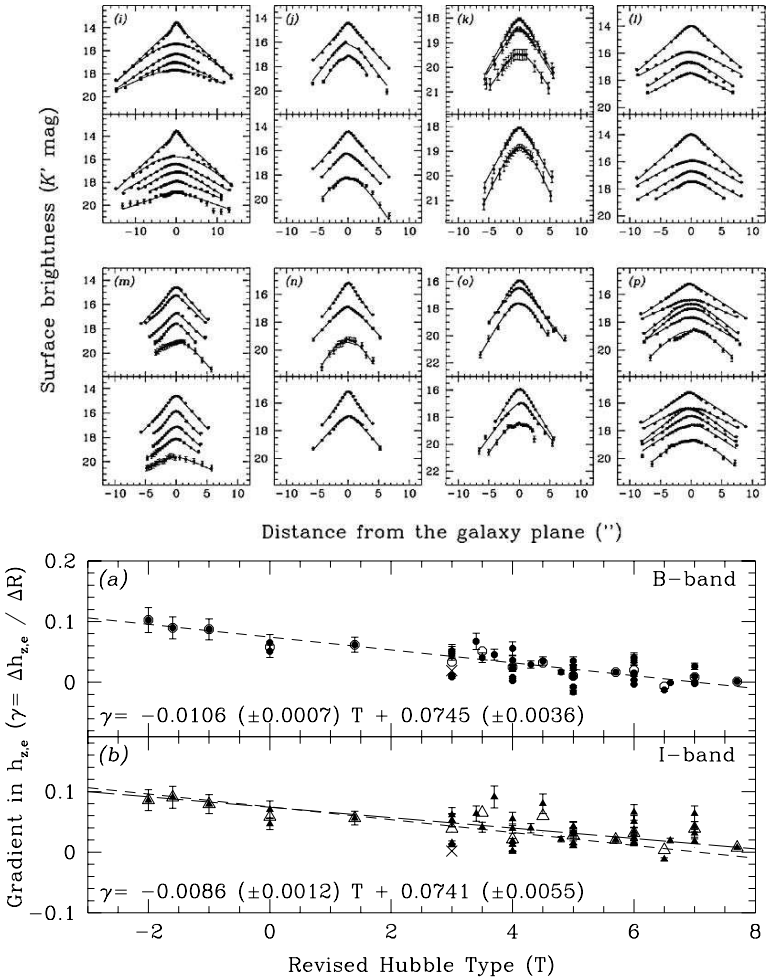

Figure 3. *Top:* Vertical brightness profiles in a sample of edge-on disk galaxies. Each panel shows the approximately exponential surface brightness distribution for one galaxy, at a range of radial distances from their centers (de Grijs et al. 1997). *Bottom:* The radial variation of the scaleheight as a function of Hubble type, for a sample of edge-on galaxies from de Grijs & Peletier (1997). The earlier-type galaxies show a gradient in the scaleheight, with h_z increasing with radius. For the spirals later than T = 5 (Sc), the gradient in scaleheight is small.

The surface brightness profile of the Local Group spiral M33 has recently been measured to very faint levels (about 31 mag arcsec^{-2}) by Ferguson et al. (2006), using surface photometry and star counts. This galaxy shows a classical exponential disk extending to a truncation radius of about 5 radial scale lengths, beyond which the surface brightness profile breaks to a steeper exponential with a much shorter scale length. This double exponential radial structure is a common form of radial truncation. Ferguson et al. were able to

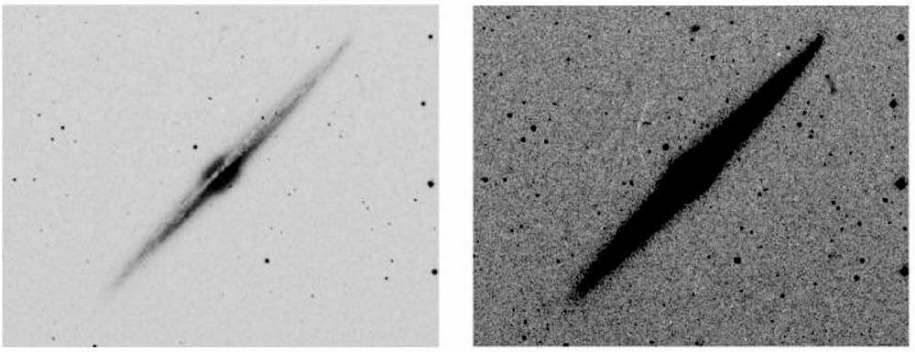

Figure 4. The edge-on spiral NGC 4565. The image (from the DSS) is shown at two different stretches to illustrate the radial truncation of the thin disk.

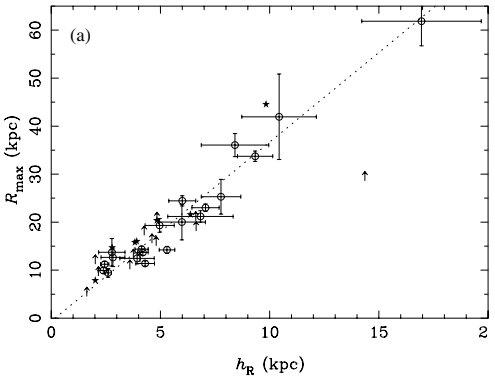

Figure 5. For a sample of 34 edge-on disk galaxies, Kregel et al. (2002) find $R_{\rm max}/h_R = 3.6 \pm 0.6$.

trace the stellar disk of M33 out to a radius of about 1 degree; the HI distribution extends even further (Corbelli et al. 1989).

What is the origin of the radial truncation of galactic disks? Here are a few of the many possibilities which have been discussed.

- the truncation radius is associated with the maximum angular momentum of the disk baryons in the proto-galaxy. This now seems unlikely because many disks have HI extending well beyond the truncation radius.

- star formation is believed to be regulated by disk instability (Kennicutt 1989), and the truncation radius is where the gas density goes below the critical value for star formation. This seems a likely explanation.

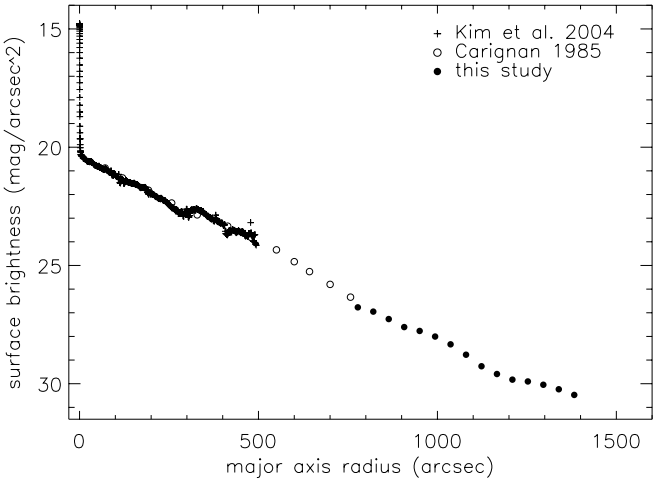

Figure 6. The surface brightness profile of NGC 300 shows no truncation out to a radius of about 10 scale lengths (Bland-Hawthorn et al. 2005).

- disks continue to grow by accretion up to the present time, and the truncation radius is the radius to which the disk has grown today. This seems unlikely: although the outer disks of spirals do appear to be younger than the inner disks, they are still typically many Gyr old (e.g., Bell & de Jong 2000). In some galaxies, like M83 and the Milky Way, star formation continues in the outer disk but there is an underlying old component. The color-magnitude diagram of the stars in the outer disk of M33 (Ferguson et al, in preparation) shows an intermediate/old, fairly metal-poor ([Fe/H] ~ -1.2) stellar population dominating the outer disk of M33.

Although radial truncation of disks is common, it is not ubiquitous. Bland-Hawthorn et al. (2005) have measured the structure of the late-type Sculptor group spiral NGC 300, which is rather similar to M33 but about 3 times more distant. Combining surface photometry from other sources with deep star counts from images with the Gemini GMOS, complete to magnitude $r' = 27$, the disk of NGC 300 appears to be exponential for at least 10 scale lengths without truncation (see Figure 6). As for M33, the HI distribution extends beyond the maximum radius reached by the star counts.

Pohlen & Trujillo (2006) propose three classes of structure in the outer regions of disks. Type I is like NGC 300, showing a single untruncated exponential disk out to the limit of the photometry. Type II is like M33, with an inner exponential disk breaking to a steeper exponential disk in the outer regions. In the type III systems, there are again two exponential components, but the outer component has a *longer* scalelength than the inner component.

The structure and truncation of outer disks is not understood yet: it remains an interesting problem.

Recent HI observations by Koribalski et al. (unpublished) of the nearby giant spiral M83 shows a complex filamentary structure in its outer disk, extending to a radius of about 100 kpc. Some of these filaments coincide with the faint outer optical structures observed earlier by Malin & Hadley (1997); others do not. Some of the outer HI filaments are sites of star formation observed with GALEX (Thilker et al. 2005). The HI structure has the appearance of tidal filaments, possibly HI extracted from the inner disk of M83 by tidal interaction with a nearby dwarf galaxy. The presence of star formation in these filaments may be demonstrating a way of building an outer stellar disk through tidal interactions of the inner disk. The very extended star formation in the outer disk of M83 is particularly interesting in the context of new results on the outer disk of M31 and the Milky Way.

4. The Outer Regions of M31 and the Galaxy

HST photometry of stars in the outermost regions of M31 give an estimate of the stellar metallicity distribution (e.g., Worthey et al. 2005). Figure 7 shows how the abundance gradient in M31 continues out to a radius of about 15 kpc, but thereafter the mean stellar metallicity remains constant with radius at about $[Z/H] = -0.5$ out to a distance of 50 kpc. Irwin et al. (2005) show that the surface brightness distribution along the minor axis shows the usual $r^{\frac{1}{4}}$ distribution out to about 15 kpc, but thereafter is approximately exponential to a radius of about 50 kpc, indicating the presence of an extended outer exponential disk. Guhathakurta et al. (this conference) argue that the halo of M31 extends even further, out to a radius of about 150 kpc.

New kinematical data confirms that the disk of M31 extends beyond 50 kpc (10 scalelengths). The outer disk is rotating almost as rapidly as the inner disk (Ibata et al. 2005), with a small rotational lag and a velocity dispersion of about 30 km s^{-1}. Stars in fields out to 80 kpc, away from the M31 stellar stream, have typical lags of 54 km s^{-1} and dispersions of 37 km s^{-1}. Ibata et al. argue that the outer disk formed from accretion of many small subgalactic structures. Its disk-like stellar kinematics indicate that the accreted matter probably came into M31 in mainly gaseous form, rather in already formed stars. The color-magnitude diagrams in the outer disk of M31 suggests that the stars of the outer disk are fairly old (several Gyr), as in M33 and the Galaxy. The red giant branch colors indicates a (47 Tuc)-like stellar population in outer disk, similar over wide range in radius, and consistent with the observed constant chemical abundance in the outer disk.

The abundance distribution in the outer disk of the Milky Way appears remarkably similar to that of M31. Yong et al. (2005) and Carney et al. (2005)

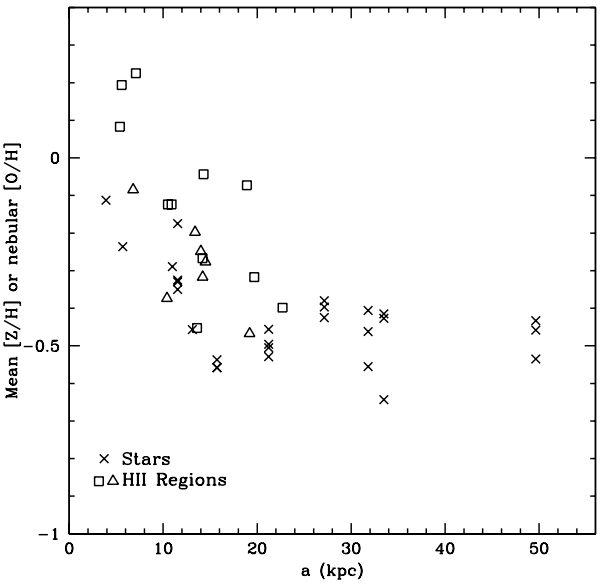

Figure 7. The metallicity gradient in the disk of M31 (Worthey et al. (2005). The gradient bottoms out at a radius of about 15 kpc and an abundance of [Z/H]~ -0.5.

measured the chemical properties of open clusters and stars in the outer disk. The radial abundance gradient for the open clusters (ages 1 to 5 Gyr) in the galactic disk bottoms out, at a radial R_G = 10 to 12 kpc (R_G = 15 kpc in M31), and at an abundance of [Fe/H] = -0.5 (as in M31). The outer disk is α-enhanced, with [α/Fe] = + 0.2, and is also Eu-enhanced, indicating a fairly rapid history of star formation and chemical evolution in the outer disk. Yong et al. argue that the outer disk stars formed from reservoir of gas that had a different star formation history from the solar neighborhood (for which the star formation rate has been roughly constant over the last 10 Gyr: e.g. Rocha-Pinto et al. 2000). Star formation in the outer disk may have been triggered by a merger event.

Carney et al. (2005) also measured abundances in Cepheids of the outer disk, which are significantly younger than their 1-5 Gyr-old open clusters. The Cepheids show a weaker abundance gradient than the clusters, and they are also less alpha-enhanced: see Figure 8. The abundance gradient in the galactic disk has flattened with time, as the associated duration of chemical evolution has lengthened, from the open clusters to the Cepheids, with abundances tending towards the solar values.

To summarize this section on outer disks:

- tidal effects as in M83 may contributed to building up the very extended disks of some spirals. Gas tidal stripped from the inner galaxy builds up

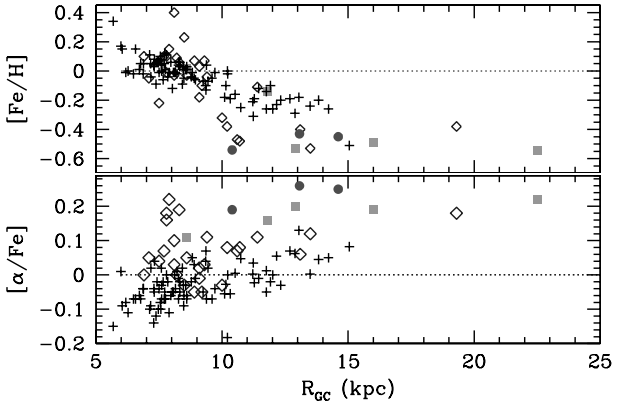

Figure 8. The radial abundance gradient in the outer disk of the Milky Way (from Carney et al. 2005). The + symbols show Cepheids, and the other symbols are open clusters in the Galaxy. The Cepheids are younger than the open clusters. The abundance gradient in the disk has flattened with time, tending towards solar values.

the outer disk. In M83, a low level of star formation is observed in the outer gas.

- the disks of some spirals, like M31 and NGC 300, extend out beyond 10 radial scale lengths.
- the outer disks of M31, M33 and the Milky Way include a stellar population that is at least several Gyr old.
- the radial abundance profiles in the outer disks of M31 and the Galaxy are approximately constant at [Fe/H] ~ -0.5 beyond a radius of about 15 kpc. The older stars of the outer galactic disk show α-enhancement, indicating a relatively short duration of chemical evolution.

5. Thick Disks

Most spirals have a second disk component, the thick disk, enveloping the thin disk. Figure 9 shows the thick disk of the edge-on S0 galaxy NGC 4762. This galaxy has an unusually prominent thick disk that is readily visible in images. Our Galaxy has a thick disk with a mass about 10% of the mass of the thin disk. It is old (> 12 Gyr) and significantly more metal poor than the thin disk: its mean [Fe/H] ~ -0.7 and it is α-enhanced, as seen in Figure 10. It is rapidly rotating, lagging the rotation of the thin disk by only about 50 km s^{-1}: see Freeman & Bland-Hawthorn (2002) for references.

Figure 11 shows a 2MASS image of the edge-on spiral NGC 5907. Only the thin disk is visible, but surface photometry shows a prominent thick disk appearing at a surface brightness of ~ 25 R mag arcsec $^{-2}$.

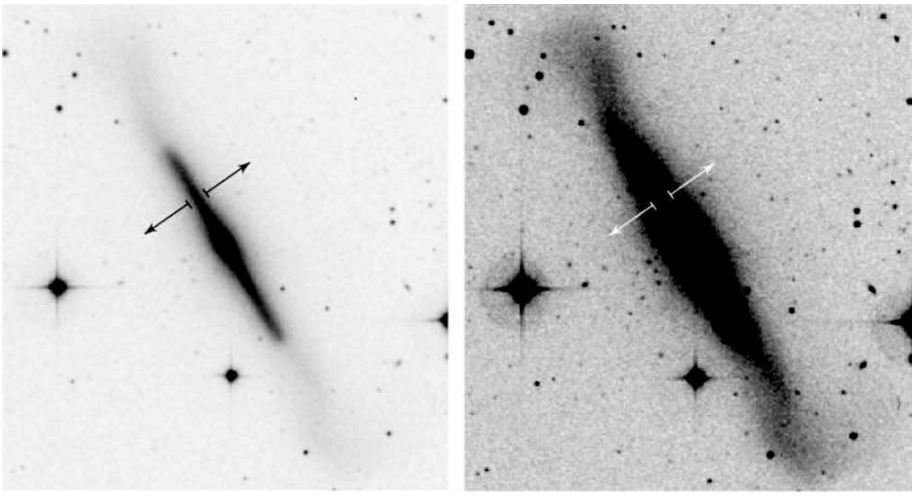

Figure 9. The edge-on S0 galaxy NGC 4762. The blunt ends of the arrow show the approximate extent of the thin disk. The thick disk can be seen in the deeper stretch extending vertically well beyond the thin disk.

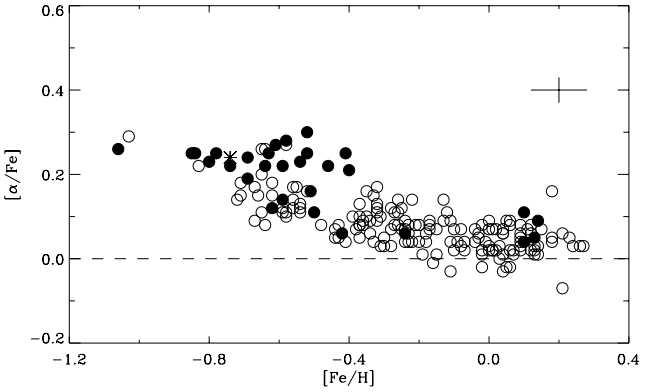

Figure 10. [α/Fe] vs. [Fe/H] for stars of the galactic thin (open circles) and thick (filled circles) disks (selected kinematically), showing the $\alpha-$ enhancement of most of the thick disk stars. Higher [α/Fe] is associated with more rapid star formation. From Nissen (2004).

Dalcanton & Bernstein (2002) made BRK surface photometry of 47 late-type edge-on disk galaxies. They find that all are embedded in a flattened low surface brightness red envelope or thick disk. From their colors, they estimate that the typical ages of these red envelopes are > 6 Gyr and that they are not very metal poor, so they appear similar to the thick disk of the Milky Way. They argue that the formation of a thick disk is a nearly universal feature of formation of disk galaxies.

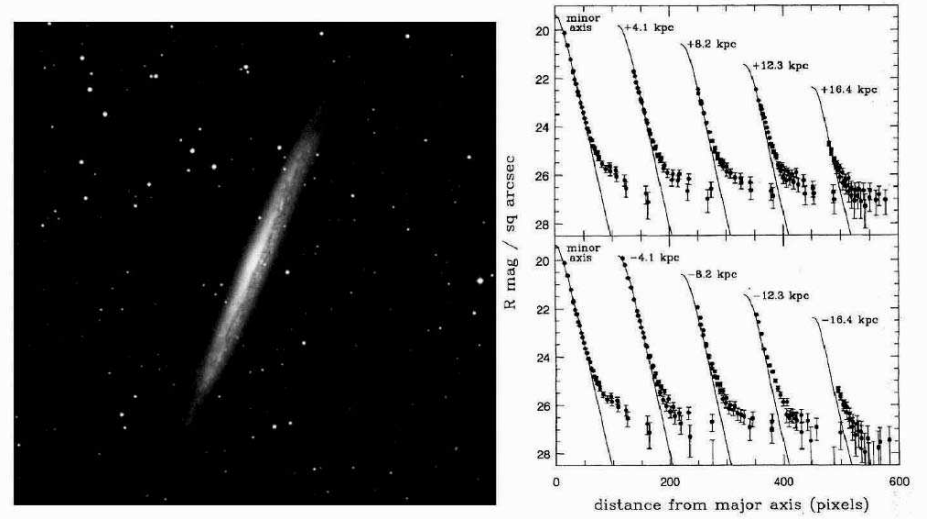

Figure 11. *Left:* Image of the edge-on galaxy NGC 5907. *Right:* Vertical surface brightness profiles at different radii: the curve shows the surface brightness distribution of the thin disk. The thick disk appears in all of the vertical cuts at a surface brightness of about 25 R mag arcsec^{-2} (from Morrison et al. 1994).

To summarize the current view of thick disks: thick disks are almost ubiquitous and appear to form early ($>$ 6 Gyr ago, 12 Gyr ago in the Galaxy) and rapidly, through the heating of the early thin disk in an epoch of merging (e.g., Quinn & Goodman 1986) or from early accretion of satellites, probably in mainly gaseous form (e.g., Brook et al. 2004). Thick disks appear to be dynamically and chemically distinct from the thin disks of their parent galaxies.

Yoachim & Dalcanton (2005) have made an interesting first measurement of the rotation of the thick disks in two edge-on spirals. This is a difficult observation, because it is necessary to separate the contributions of the thin and thick disks to the spectra of the faint regions away from the equatorial plane, using the surface photometry of the individual galaxies. For one of their galaxies (FGC 227), their data indicate that the thick disk may be counter-rotating relative to the thin disk. If this turns out to be correct, then it would exclude heating of an early thin disk as the origin for the thick disk in this galaxy.

At least one edge-on disk galaxy, NGC 4244 (Fry et al. 1999) appears to be a pure thin disk. Surface brightness cuts perpendicular to its disk show only a single exponential component, with no indication of a thick disk component down to a surface brightness level of about $\mu(R) = 28$ mag acrsec^{-2} (see Fig. 12).

The existence of such a pure disk galaxy is interesting because, at least for some late-type disks

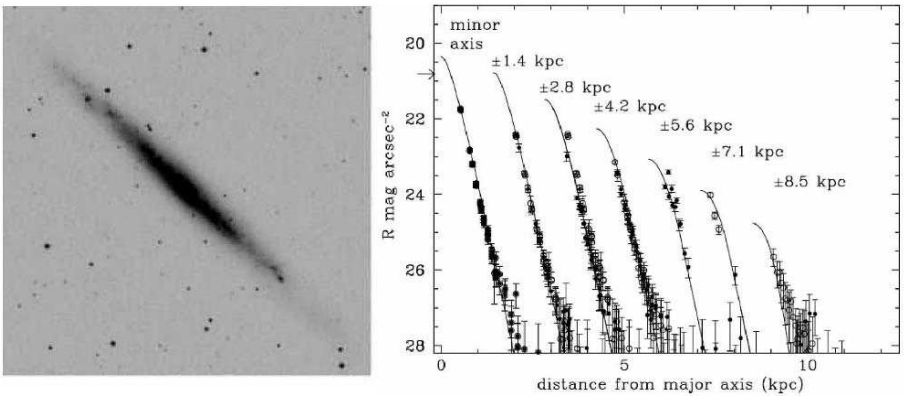

Figure 12. *Left:* Image of the edge-on galaxy NGC 4244. *Right:* Vertical surface brightness profiles at different radii: the curve shows the surface brightness distribution of the thin disk. From Fry et al. (1999).

- the star formation did not start before the gas had settled to the disk plane
- since the onset of star formation in the disk, the the disk has suffered no significant dynamical disturbance from internal or external sources

We note that pure disk galaxies like NGC 4244 are not readily produced in ΛCDM simulations, because there is too much merger activity.

How did pure disk galaxies avoid any significant star formation until the baryons had settled to thin disk? We might expect that the aggregation process with its interacting lumps of dark matter and baryons should lead to star formation as it does in present-day interacting systems. The baryons need to be maintained in a state such that they can settle quiescently to the disk, for example via winds or baryon blowout driven by early star formation and supernovae (e.g., Sommer-Larsen et al. 1999).

6. Summary

- disks typically have the exponential structure in R and z: some are truncated radially at a few scalelengths
- the radial exponential structure and radial truncation of galactic disks are still not well understood
- thick disks are very common but not 100% ubiquitous
- the existence of pure (thin) disk galaxies means that at least some disks form in a very quiescent manner, with no star formation until the disk had settled, and with an undisturbed history thereafter.

7. Conclusion

Best wishes to Piet van der Kruit on his appointment to the Jacobus Kapteyn chair. I express my appreciation for the illumination which he and his students have brought to the subject of disk galaxies, and my gratitude for a long and continuing collaboration.

References

Bland-Hawthorn, J., Vlajic, M., Freeman, K.C., Draine, B.T. 2005. ApJ, 629, 239
Bell, E.F. de Jong, R.S. 2000. MNRAS, 312, 497
Brook, C.B. et al. 2004. ApJ, 612, 894
Carney, B.W. et al. 2005. AJ, 130, 1111
Corbelli, E., Schneider, S.E., Salpeter, E.E. 1989. AJ, 97, 390
Dalcanton, J.J., Bernstein, R.A., 2002. AJ, 124, 1328
de Grijs, R., Peletier, R.F., van der Kruit, P.C. 1997. A&A, 327, 966
de Grijs, R., Peletier, R.F. 1997. A&A, 320, L21
Fall, S.M., Efstathious, G.P. 1980. MNRAS, 193, 189
Freeman, K.C., Bland-Hawthorn, J. 2002. ARAA, 40, 487
Fry, A. et al. 1999, AJ, 118, 1209
Ferguson, A., Irwin, I., Chapman, S., Ibata, R., Lewis, G. & Tanvir, N. 2006, these proceedings, p. 239
Ibata, R. et al. 2005. ApJ, 634, 287
Irwin, M. et al. 2005. ApJ, 628, L105
Kennicutt, R. 1989. ApJ, 344, 685
Kregel, M., van der Kruit, P.C., de Grijs, R. 2002. MNRAS, 334, 646
Lewis, J.R., Freeman, K.C. 1989. AJ, 97, 139
Lin, D.N.C., Pringle, J.E. 1987. ApJ, 320, L87
Morrison, H.L., Boroson, T.A., Harding, P. 1994. AJ, 108, 1191
Malin, D.F., Hadley, B. 1997. Proc. Astr. Soc. Austr., 14, 52
Nissen, P. 2004. in “Origin & Evolution of the Elements", ed. A. McWilliam & M. Rauch (Cambridge: CUP), p 154 (astroph/0310326)
Pohlen, M., Trujillo, I. 2006, these proceedings, p. 253
Quinn, P.J., Goodman, J. 1986. ApJ, 309, 472
Rocha-Pinto, H. et al. 2000. A&A, 358, 869
Sommer-Larsen, J. et al. 1999. ApJ, 519, 501
Thilker, D.A. et al. 2005. ApJ, 619, L79
van der Kruit, P.C. 1979. A&AS, 38, 15
van der Kruit, P.C., Searle, L. 1981a. A&A, 95, 105
van der Kruit, P.C., Searle, L. 1981b. A&A, 95, 116
van der Kruit, P.C., Searle, L. 1982a. A&A, 110, 61
van der Kruit, P.C., Searle, L. 1982b. A&A, 110, 79
van der Kruit, P.C., Freeman, K.C. 1986. ApJ, 303, 556
Worthey, G. et al. 2005. ApJ, 631, 820
Yoachim, P., Dalcanton, J.J. 2005. ApJ, 624, 701
Yong, D. et al. 2005. AJ, 130, 597

Martin Bureau, Raja Guhathakurta, and Jacqueline van Gorkom.

Julianne Dalcanton, Rob Kennicutt, Dennis Zaritsky, and James Bullock.

DISENTANGLING STAR FORMATION, ENVIRONMENT, AND MORPHOLOGY IN GALAXY EVOLUTION

Daniel Christlein[1] and Ann Zabludoff[2]

[1] *Universidad de Chile & Yale University, USA*

[2] *University of Arizona, Tucson, USA*

Abstract Statistical studies of galaxies have matured beyond the calculation of luminosity functions, and by simultaneously analyzing a large number of parameters, such as star formation rates, morphology, and environment, new insights into the mechanisms that drive the evolution of galaxies can be gained.

We present a study of the photometric and spectroscopic properties of galaxies in six nearby, rich clusters. The primary issues that we address are: 1) variations of the luminosity function between the field, groups, and clusters, and what this implies for environmental influences, 2) Luminosity Functions for bulges and disks, how they vary with morphology, and what this implies for the mechanisms by which early-type galaxies are formed in dense environments, and 3) whether residual correlations between star formation and environment exist after taking into account the fundamental differences in morphology, stellar mass, and stellar age that already exist between galaxy populations in different environments, and what this implies for the mechanisms that influence star formation.

Keywords: galaxies: evolution - galaxies: structure - galaxies: fundamental parameters - galaxies: clusters

1. Introduction

Fundamental properties of galaxies, such as star formation and morphology, are known to vary with environment (e.g., Dressler 1980; Lewis et al. 2002; Gómez et al. 2003). However, our understanding of the mechanisms that shape these correlations is much less secure. Does the luminosity function (LF) vary across environments (Christlein & Zabludoff 2003; de Propris et al. 2003)? What mechanisms generate the morphology-density relation? What mechanisms generate the star formation-environment relation? Such questions cannot be answered by looking at the variation of any single galaxy property with environment. But modern galaxy surveys are gathering a large number

R. S. de Jong, Island Universes, 17–22.
© 2007 *Springer.*

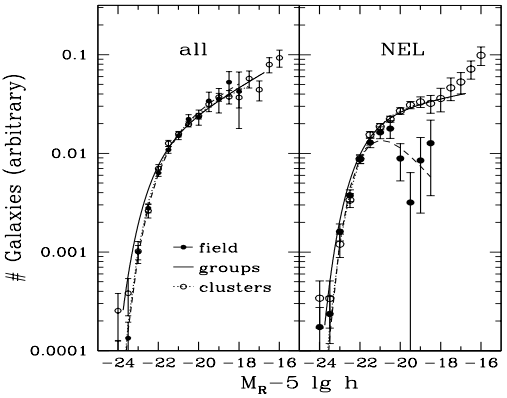

Figure 1. Luminosity functions for all (left) and non-emission line (quiescent) galaxies (right) in the field (solid points), groups (solid line), and clusters (open circles). The overall luminosity function shows very little variation with environment, but the faint end slope of the NEL LF steepens significantly between the field and group samples. The LFs in groups and clusters are consistent again.

of parameters for each object, including magnitudes, redshifts, morphologies, star formation indices, etc. Approaching such multi-dimensional datasets with powerful tools and well-defined physical questions will provide new insight into the problems above.

This work is an analysis of a photometric (R-band) and spectroscopic survey of galaxies in six nearby clusters which combines information on environment, star formation, morphology, luminosity, and other variables. It aims to provide constraints on some of the environmental mechanisms that affect the evolution of galaxies in dense environments and demonstrate techniques to approach such a multi-dimensional dataset.

2. Luminosity and Environment

Variations of the luminosity functions contain signatures of possible environmental variations in galaxy formation efficiency as well as subsequent environmental effects on a galaxy's star formation history and current star formation rate. They are thus a fundamental test for models of galaxy formation and evolution. However, the methods used to calculate luminosity functions in the densest, cluster environments — statistical background subtraction — can be biased (Valotto, Moore, & Lambas 2001), creating a long-standing uncertainty about the environmental dependence of the LF. A careful study of the LF in clusters and comparison to other environments requires a sample with spectroscopic membership confirmation, such as ours.

Figure 1 shows our luminosity functions for the complete field and cluster samples, as well as for non-emission line (NEL; predominantly quiescent) galaxies. NEL galaxies are defined to be galaxies with an equivalent width

of the [OII]3727 doublet of less than 5Å. A luminosity function for groups (Zabludoff & Mulchaey 2001) is also overplotted. There are no significant differences between field and cluster LFs under a χ^2 test or a comparison of the best-fit Schechter parameters. The only discrepancy is that the number of extremely bright ($M_R < -22.5$) galaxies in clusters cannot be reproduced by randomly sampling the field LF. We do not find a significant difference in the LF of emission line (EL) galaxies either (but caution that the statistics are worse than for the overall sample). Their LF is steep both in the field and in clusters. However, we find a significant difference for the NEL galaxies, in the sense of a steepening of the faint end slope, as we go from the field to clusters. A possible explanation for all these observations is that the predominant environmental effect is to curtail star formation rates in dense environments, so that the faint end of the NEL LF is filled up with galaxies originally drawn from the steep EL LF, while preserving the shape of the overall LF.

In what kind of environment does this turnover from shallow to steep faint end slopes of the NEL LF occur? As Fig. 1 shows, the faint end slope is only shallow in the field environment. In the intermediate, group environment, it is already as steep as in clusters. Hence, if this environmental variation of the LF is a diagnostic of environmental effects on the star formation properties of galaxies, the effects in question are already important in intermediate, group-like environments.

3. Morphology and Luminosity

One of the best-known correlation between environment and galaxy properties is the morphology-density relation (Dressler 1980), which states that the relative abundance of early-type galaxies, particularly S0s, is larger in dense environments than in the field. Models suggest that this may be the result of environmental mechanisms that either diminish the disk luminosity (such as ram-pressure stripping (Gunn &Gott 1972), or strangulation (Larson, Tinsley & Caldwell 1980, Balogh, Navarro, & Morris 2002; Bekki, Couch, & Shioya 2002)) or that enhance the bulge (such as tidal interactions and mergers; Barnes 1999; Bekki 1998; Mihos & Hernquist 1994). Distinguishing between these models requires a comparison of bulge and disk LFs along the morphological sequence.

We calculate bulge fractions (B/T) for our galaxy sample using the GIM2D code (Simard et al. 2002), use them to determine bulge and disk LFs, and fit Schechter functions (Schechter 1976) to them. We then examine their variation with morphology (i.e., with the bulge fraction itself). In doing so, we are asking whether early-type galaxies are early-type galaxies because their bulges are brighter, or because their disks are fainter. Because plotting bulge and disk LFs as a function of B/T will automatically introduce correlations, we use a

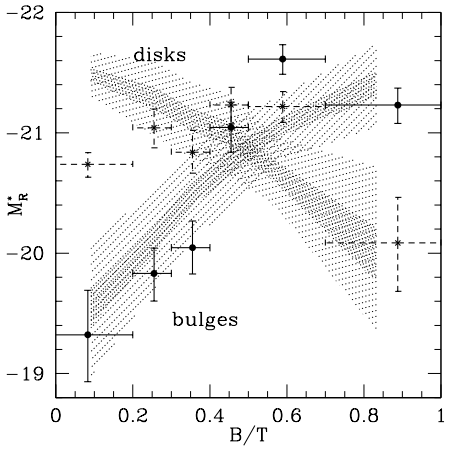

Figure 2. Variation of the characteristic bright end magnitude, M^*, of the LFs for bulges and disks with B/T. Shaded areas show prediction from a Monte Carlo model, assuming no correlation between B/T and luminosity. The observed variation is inconsistent with either that null hypothesis or with disk fading models. It is consistent with models that populate the early-type region of the morphological sequence by bulge-enhancing processes.

Monte Carlo algorithm to determine how the bright end magnitude, M^*, would vary if all galaxies, regardless of morphology, were drawn from the same LF.

Figure 2 shows the dependence of M^* on B/T for disks and bulges. Shaded regions show how M^* varies in our Monte Carlo simulation. The figure shows that bulge luminosities increase more steeply than the Monte Carlo prediction. Disk luminosities remain almost constant along the morphological sequence, while the simulation predicts a fading. These results clearly rule out the null hypothesis of the Monte Carlo simulation, and are in even stronger disagreement with disk fading models, which would predict earlier-type galaxies to have fainter disks. However, they match perfectly a model in which early-type galaxies with $B/T > 0.3$ are made by increasing the bulge luminosity of galaxies drawn from a universal LF and assumed to have $B/T = 0.3$ (characteristic of early-type spirals). This applies not only over the full range of B/T, but even over relatively small ranges; i.e., it is not possible to make intermediate-type, S0-like, galaxies from later-type galaxies by disk fading. This shows that bulge-enhancing transformations must at least have played a role in creating the bright population of early-type galaxies in our cluster sample. We caution that, since we use the characteristic bright end magnitude, M^*, as our statistic, this test is by design insensitive to transformations affecting fainter galaxies.

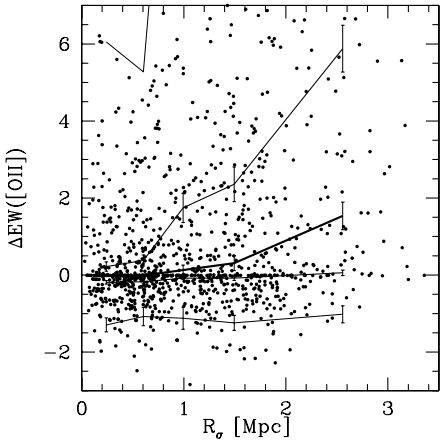

Figure 3. Residual correlation between [OII] equivalent width and environment. Even after removing the effects of population gradients in stellar age, stellar mass, and morphology, a residual effect of environment on star formation remains.

4. Star Formation and Environment

It has long been known and more recently established quantitatively (Lewis et al. 2002; Gómez et al. 2003) that galaxies have lower star formation rates in dense environments. However, the galaxy populations in dense environments are different from those in sparse environments in many regards: they are older, possibly more massive, and of earlier morphologies. All these properties, by themselves, go with lower star formation rates. Is the star formation gradient thus nothing more than a reflection of the presence of old, evolved galaxies in clusters? Or is it indicative of ongoing environmental processes lowering star formation rates in dense environments? In other words, does a galaxy with the same stellar age, same mass, and same morphology still have lower star formation rates in dense environments than in sparse ones?

To answer this, it is necessary to account for the three known gradients of galaxy properties with environment — stellar mass, stellar age, and morphology — and examine whether residual star formation gradients remain. Mathematically, we do so with the aid of partial rank correlation coefficients (Kendall & Stuart 1977). We quantify star formation with the equivalent width of the [OII]3727 doublet, morphology with B/T, stellar age with the D4000 index. We use 2MASS photometry, in combination with D4000, to calculate stellar masses. We parametrize environment with the radial projected distance from the cluster center. In our sample, this is tightly correlated with local projected galaxy number density, so that this choice of environmental variable does not imply a premise regarding the environmental mechanism.

Figure 3 shows the residual $[OII]$ E.W. for each galaxy after subtracting an expectation value derived from linear partial regression, as a function of radius. Lines indicate various percentiles of the distribution at any given radius. A weak, but significant residual correlation remains. At $r = 0.221$, the partial correlation coefficient is significantly different from zero at the 8 σ level. Therefore, differences between the galaxy populations in different environments with regard to stellar age, stellar mass, and morphology are not strong enough to explain the star formation gradient. We conclude that ongoing effects of environment are responsible for the lowered star formation rates in dense environments. This also confirms findings (Kauffmann et al. 2004) that star formation varies more strongly with environment than any other variable.

5. Conclusion

The overall R-band luminosity function varies little between environments, but the LF of quiescent galaxies is much steeper in clusters than in the field. This is consistent with a picture in which environment principally affects star formation rather than individual R-band luminosities. We have also demonstrated that the turnover in the LF occurs between the general field and groups, indicating that the responsible transformation mechanisms work in intermediate-density environments. We have isolated one possible mechanism by demonstrating that cluster galaxies with intermediate bulge fractions (typical of S0s) can only be made from late-type galaxies if bulge-enhancing processes, such as tidal interactions and mergers, are involved. Such interactions are most efficient in intermediate-density environments, such as groups. Furthermore, we have found that the environmental variation of star formation rates cannot be explained by the known gradients in morphology, stellar mass, and stellar age — the signatures that could have been left by environmental variations of galaxy formation processes themselves. Instead, our results point to ongoing environmental effects on star formation, among which the bulge-enhancing processes found above may only be one mechanism.

References

Christlein, D., Zabludoff, A., 2003 ApJ 591, 764
de Propris, R., et al., 2003 MNRAS 342, 725
Dressler, A., 1980 ApJ 236, 351
Kauffmann, G., et al., 2004 MNRAS 353, 713
Kendall, M. G., Stuart, A., *The Advanced Theory of Statistics*, Griffin 1977
Lewis, I., et al., 2002 MNRAS 334, 673
Gómez, P. L., et al., 2003 ApJ 584, 210
Simard, L., et al., 2002 ApJS 142, 1
Valotto, C. A., Moore, B., Lambas, D. G., 2001 ApJ 546, 157
Zabludoff, A., Mulchaey, J. S., 2000 ApJ 539, 136

MEASURING STRUCTURAL PROPERTIES OF GALAXIES IN THE LOCAL UNIVERSE

Paul D. Allen[1*], Simon P. Driver[1], Jochen Liske[2] and Alister W. Graham[1]

[1]*Australian National University, Mount Stromlo Observatory, Australia.*

[2]*European Southern Observatory, Germany.*

* paul@mso.anu.edu.au

Abstract The Millennium Galaxy Catalogue provides a representative and complete sample of nearby galaxies for structural analysis. GIM2D is used to model the light profiles for over 10000 resolved galaxies, using three different schemes: $R^{1/4}$+Exponential, $R^{1/n}$+Exponential, and $R^{1/n}$. The resulting catalogues are shown to be robust for those galaxies with component half-light radii greater than the seeing.

Keywords: astronomical data bases: catalogues - galaxies: general - galaxies: fundamental parameters - galaxies: structure - galaxies: statistics.

1. Introduction

It has long been known that, although galaxies cover an expanse of quite different morphologies, they have two basic features in common, notably spheroids (or bulges) and disks. These are often observed to have different average colours, metallicities, and kinematics, justifying their treatment as distinct entities. Even at $z \sim 1$, bulges and disks are clearly in place and appear to be the dominant structural feature in the majority of galaxies (Simard et al. 1999; Ravindranath et al. 2004; Barden et al. 2005; Koo et al. 2005; Trujillo et al. 2005). Most models of galaxy formation and evolution involve separate formation scenarios for bulges and disks (e.g., Cole et al. 2000; Kormendy & Kennicutt 2004). It is possible, within the ΛCDM paradigm, to make specific predictions relating the mass and angular momentum of dark matter haloes with the observed distributions in galaxy luminosity and size as a function of redshift (e.g., Mo, Mao, & White 1998, Bouwens & Silk 2004).

Bulge-disk decomposition is therefore a popular and useful method for quantifying the morphologies of galaxies by fitting model surface brightness profiles to data. A bulge-disk model is also convenient because the surface brightness profiles of bulges can be modelled by an $R^{1/4}$ law (de Vaucouleurs

R. S. de Jong, Island Universes, 23–28.
© 2007 *Springer.*

1948), and exponential profile (Andredakis and Sanders 1994; de Jong 1996), or more optimally using a Sérsic profile (Sersic 1968; Graham & Driver 2005), and disks are observed to follow exponential laws (de Vaucouleurs 1959; Freeman 1970). Finally, software is now available which makes it a fairly straightforward task to perform bulge-disk decomposition on many thousands of galaxies (Simard et al. 2002; Peng et al. 2002; Trujillo and Aguerri 2004; de Souza et al. 2004).

Here, we discuss the use of one such publically available bulge-disk decomposition code, GIM2D (Simard et al. 2002), to provide a quantitative measure of the surface brightness profiles of 10095 galaxies in the Millennium Galaxy Catalogue (MGC). This provides a catalogue of structural measurements for a representative and complete sample of galaxies in the ($z \sim 0$) local Universe.

2. The Millennium Galaxy Catalogue

The Millennium Galaxy Catalogue[1] (MGC) is a deep ($\mu_{lim} = 26\, B$-mag arcsec^{-2}), wide area ($\sim$37.5 deg^2) imaging and redshift survey covering a 0.5 deg wide strip along the equatorial sky from 10h to 14h50$'$. The imaging was carried out using the INT Wide Field Camera (WFC). The survey region overlaps both the 2dFGRS (Colless et al. 2001), and SDSS-DR1 (Abazajian et al. 2003), providing both $u'g'r'i'z'$ photometry, and redshifts for 47.0% of the 10095 resolved galaxies with $B < 20$ mag. The remaining $B < 20$ galaxies without known redshifts were observed as targets in the spectroscopic part of the survey, MGCz. This mostly involved observations using the 2dF instrument on the AAT providing redshifts for a further 47.2% of galaxies in the sample. However, in order to avoid significant redshift incompleteness for objects with low surface brightness (see Driver et al. 2005), both 4-m (ESO/NTT and TNG) and 8-m (Gemini) observations were carried out to obtain spectra for the lowest surface brightness galaxies in the sample.

Comparison between 2dFGRS, SDSS and the MGC shows that the MGC is deeper, more complete, more precise, and of higher spatial resolution than either the 2dFGRS or SDSS-DR1 data sets (Cross et al. 2004; Driver et al. 2005). The increased depth and resolution is demonstrated in Figure 1. Full details of the MGC, including observations, data reduction, image detection and classification, are given in Liske et al. (2003). The MGC redshift survey is discussed in detail in Driver et al. (2005).

With a photometric precision of 0.03 mag, astrometric accuracy of 0.08 arcsec (Liske et al. 2006), and 96% redshift completeness to $B_{\rm MGC} = 20$ mag (increasing to 99.8% for $B_{\rm MGC} < 19.2$ mag), the MGC represents an extremely high quality and high completeness census of the nearby galaxy population.

[1]The MGC is publically available at http://www.eso.org/ $\sim$jliske/mgc

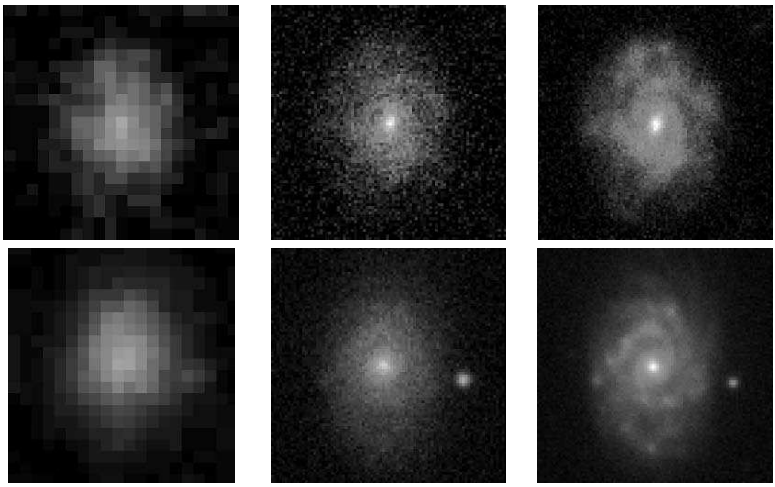

Figure 1. A comparison between Digitized Sky Survey (left, b_J-band), SDSS-DR1 (centre, g-band), and the MGC (right), for MGC18325 (upper panels), and MGC04795 (lower panels).

It is therefore the ideal data set to use for a detailed analysis of the structural composition of galaxies in the local Universe, and to provide a low redshift anchor for higher redshift studies.

3. Fitting Profiles with GIM2D

In Allen et al. (2005) the 2-D light profiles for all 10095 MGC galaxy images were modelled using the GIM2D package (Simard et al. 2002). GIM2D allows galaxies to be modelled using a single component model, or a two component model with separate profiles for the bulge and disk components. For the MGC, three schemes were used. (1) Sérsic – single component. (2) De Vaucouleurs Bulge + Exponential Disk. (3) Sérsic Bulge + Exponential Disk.

It is important to disentangle the intrinsic morphologies of galaxies from distortions that arise from the combined optical system of telescope, instrument, and atmosphere. Therefore the point spread function (PSF) was also modelled for each galaxy using stars that lie in the same frame as the galaxy. GIM2D then finds the best-fitting PSF-convolved model for each galaxy using the pixels designated as part of the object by the SEXtractor segmentation image mask (Simard et al. 2002). This resulted in three structural catalogues containing measurements of total flux, bulge to disk flux ratio (B/T), and the $x - y$ position of the central surface brightness. For bulges, effective radii (R_e), Sérsic index (n), ellipticity (ϵ), and position angle (ϕ_b) are all measured. For disks, the catalogues contain measurements of scale-length (h), inclination (i), and disk position angle (ϕ_d). Figure 2 shows example output and residual images for the galaxy MGC27301 along with the raw image, mask, and

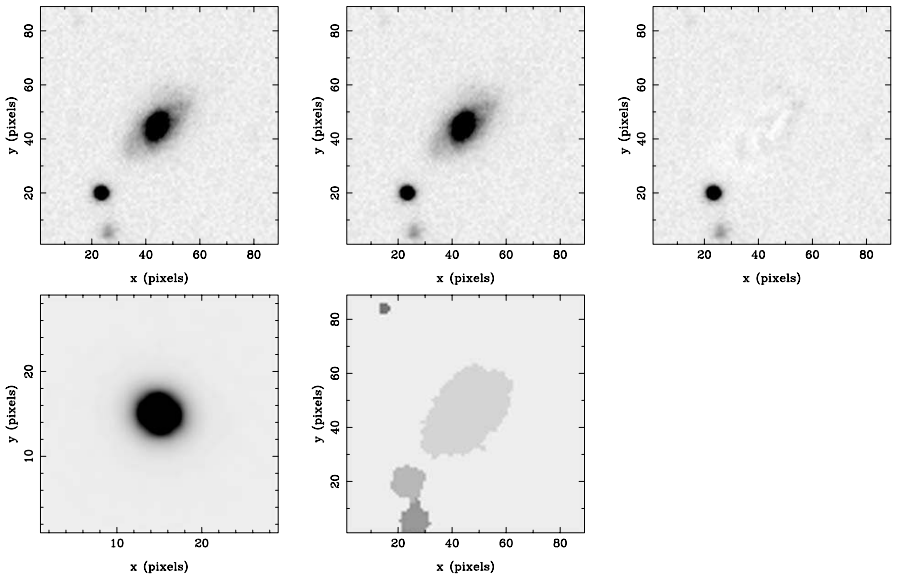

Figure 2. GIM2D input and output for the galaxy MGC27301. The output model shown is for the Sérsic+Exponential fit. The top row shows images of the galaxy (left), the GIM2D model image (centre), and the residual image showing the difference. The bottom row shows the input PSF (left), and the segmentation image or mask (centre).

PSF. Figure 3 shows a plot of the best-fitting model for this galaxy using the Sérsic+Exponential fit.

Quality Control

As an initial test of the accuracy of the GIM2D output, simple global observables such as magnitudes, half-light radii, and $x - y$ centroid positions can be compared to the values measured by other means in Liske et al. (2003). For example, differences between GIM2D output and previous measurements can be indicative of bad segmentation images. If a galaxy has been over-deblended, then the GIM2D magnitude will be an under-estimate. When two nearby galaxies are treated as one, the centroids will be grossly different, and the GIM2D magnitudes over-estimated. It was found that 222 segmentation images needed to be corrected. It is also important to ensure that the fits are interpreted correctly, as the two components can be inverted or used to fit neither a bulge nor a disk (see Allen et al. 2005).

Due to overlaps between pointings of the WFC, 702 objects had duplicate observations. In many cases the observations were carried out on a different night or even as part of different observing runs several months apart. They therefore provide an excellent test of the repeatability of GIM2D fits for a

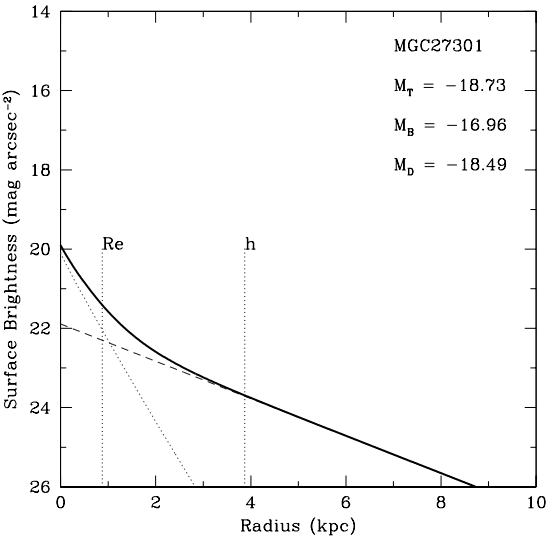

Figure 3. The best fitting profile for MGC27301 (see Figure 2) using the Sérsic+Exponential model. The blue dashed straight line represents the exponential (disk) component, and the red dotted curve corresponds to the Sérsic(bulge) component. The total profile is shown by the solid bold curve. R_e and h are also shown.

diverse and representative sample of galaxies under different conditions. The comparison reveals that if the half light radius of a component is sufficiently large ($R_e > 0.8\Gamma$ or $1.678h > 0.8\Gamma$ where Γ is the seeing FWHM), then for the Sérsic+Exponential model the standard deviations between repeat measurements are: $R_e \sim 13.2\%$, $\log(n) \sim 13.6\%$, and $h \sim 6\%$. For the component magnitudes: $M_{bulge} \sim 0.24$ mags, and $M_{disk} \sim 0.14$ mags.

4. Summary

The Millennium Galaxy Catalogue is a deep, wide survey of the local galaxy population. Its completeness, depth and resolution make it ideal for the provision of a representative sample of galaxy structural measurements at $z \sim 0$. GIM2D has been used to obtain the best-fitting Sérsic models, Sérsic+Exponential decompositions, and de Vaucouleurs+Exponential decompositions to the 100095 galaxies with $B < 20$ in the MGC. Structural catalogues are made publically available in Allen et al. (2005). With careful quality control, repeatable measurements are obtainable for galaxies that are larger than the seeing FWHM. The measured parameters can then be used to measure luminosity functions and bivariate brightness distributions (see Liske et al. 2006).

References

Abazajian, K., et al. 2003, AJ, 126, 2081

Allen, P. D., Driver, S. P., Liske, J., Graham, A., Cameron, E., Cross, N. J. G., and de Propris, R. 2005, MNRAS, submitted.

Andredakis, Y. C. and Sanders, R. H. 1994, MNRAS, 267, 283

Barden, M., et al. 2005, astro-ph/0502416.

Bouwens, R. and Silk, J. 2002, ApJ, 568, 522

Cole, S., Lacey, C. G., Baugh, C. M., and Frenk, C. S. 2000, MNRAS, 319, 168

Colless, M., et al 2001, MNRAS, 328, 1039

Cross, N. J. G., Driver, S. P., Liske, J., Lemon, D. J., Peacock, J. A., Cole, S., Norberg, P., and Sutherland, W. J. 2004, MNRAS, 349, 576

de Jong, R. S. 1996, A&AS, 118, 557

de Souza, R. E., Gadotti, D. A., and dos Anjos, S. 2004, ApJS, 153, 411

de Vaucouleurs, G. 1948, Annales d'Astrophysique, 11, 247.

de Vaucouleurs, G. 1959, Handbuch der Physik, 53, 275.

Driver, S. P., Liske, J., Cross, N. J. G., De Propris, R., and Allen, P. D. 2005, MNRAS, 360, 81

Freeman, K. C. 1970, ApJ, 160, 811.

Graham, A. W. and Driver, S. P. 2005, PASA, 22, 118.

Koo, D. C., et al 2005, ApJS, 157, 175

Kormendy, J. and Kennicutt, R. C. 2004, ARAA, 42, 603

Liske, J., Lemon, D. J., Driver, S. P., Cross, N. J. G., and Couch, W. J. 2003, MNRAS, 344, 307

Liske, J., Driver, S. P., and Allen, P. 2006, these proceedings, p. 530

Mo, H. J., Mao, S., and White, S. D. M. 1998, MNRAS, 295, 319

Peng, C. Y., Ho, L. C., Impey, C. D., and Rix, H. 2002, AJ, 124, 266

Ravindranath, S., et al 2004, ApJL, 604, L9

Sersic, J. L. 1968, Atlas de galaxias australes. Cordoba, Argentina, Observatorio Astronomico, 1968.

Simard, L., et al 1999, ApJ, 519, 563

Simard, L., et al 2002, ApJS, 142, 1

Trujillo, I. and Aguerri, J. A. L. 2004, MNRAS, 355, 82

Trujillo, I., et al 2005, astro-ph/0504225.

EXTRAGALACTIC THICK DISKS

Implications for Early Galaxy Evolution

Julianne J. Dalcanton, (with Anil C. Seth and Peter Yoachim)

University of Washington, Seattle, USA
jd@astro.washington.edu

Abstract I briefly review the growing evidence that thick stellar disks surround most edge-on disk galaxies. Recent studies show that these extragalactic thick disks have old ages, low metallicities, long scale lengths, and moderately flattened axial ratios, much like the thick disk of the Milky Way. However, the properties of thick disks change systematically with the mass of the galaxy. The thick disks of low mass galaxies are more prominent and somewhat more metal-poor than those surrounding massive disk galaxies. Given the strong evidence that thick disks are fossils from an early epoch of merging, these trends place tight constraints on the early assembly of disk galaxies.

Keywords: galaxies: structure - galaxies: stellar content - galaxies: kinematics and dynamics - galaxies: evolution

Introduction

Although thick disks are best known as a component of the Milky Way, they were actually first identified as extended faint envelopes surrounding other galaxies (Burstein, 1979; Tsikoudi, 1979). The subsequent discovery of a comparable stellar component in the Milky Way (Gilmore & Reid, 1983) drew attention away from the ambiguous interpretation of faint features in external galaxies, and instead refocused it on the wealth of data available from photometric and spectroscopic observations of individual stars within the Galaxy. These studies quickly showed that the Milky Way's thick disk is a fossil relic from an early epoch in the Galaxy's formation (see reviews by Freeman & Bland-Hawthorn 2002; Norris, 1999; Majewski, 1993; Gilmore et al., 1989). Its stars are old and metal-poor ($\langle$[Fe/H]$\rangle$ $\sim$-0.7), and show an enrichment pattern that is distinct from thin disk stars with similar iron abundances (see the recent review by Feltzing et al. 2004). These data suggest that the Milky Way thick disk is not a simple extension of the thin disk, but instead captures a unique episode early in the formation of the Galaxy.

R. S. de Jong, Island Universes, 29–40.
© 2007 *Springer.*

Given the evidence above, how does the thick disk fit into the existing paradigm of disk galaxy formation? The ages of stars in the thick disk suggest that they were formed more than 8 Gyr ago (Liu & Chaboyer 2000), when the merging rate was likely to be high. It is therefore reasonable to assume that the formation of the thick disk is somehow coupled to the mergers and interactions expected to dominated in hierarchical structure formation. Within this scenario, thick disk stars could have acquired their current large scale heights and vertical velocity dispersions in three ways. In the first and widely held view, the thick disks stars were initially formed within a thin gas disk, but were then vertically heated by one or more interactions with a satellite galaxy (e.g. Quinn et al., 1993). In the second, the thick disk stars were formed *in situ* at large scale heights during a burst of star formation, as clumps of gas coalesced to form the thin disk (e.g. Kroupa 2002; Brook et al. 2004). In the third, the thick disk stars formed outside of the galaxy in the pre-galactic fragments, which then deposited the stars in the disk (Statler, 1988; Abadi et al. 2003).

Unfortunately, it is difficult to discriminate among these very different scenarios using data from the Milky Way alone. It is therefore time to return to the broader range of galaxies that can be probed with studies of extragalactic thick disks. In the intervening years between the initial detections of Burstein (1979) and Tsikoudi (1979), there has been a steadily growing body of detections of thick disks in other galaxies (e.g., Neeser et al. 2002; Wu et al. 2002; Matthews 2000; Abe et al., 1999; Fry et al., 1999; Morrison et al., 1997; Naeslund & Joersaeter, 1997; de Grijs & van der Kruit, 1996; van Dokkum et al., 1994; Bahcall & Kylafis, 1985; Jensen & Thuan, 1982; van der Kruit & Searl, 1981; see also the compilation in Table 2 of Yoachim & Dalcanton 2005b and the review by Morrison, 1999). Recently, the pace of discovery has accelerated with the large early-type sample studied by Pohlen et al. (2004) and the late-type sample studied by Dalcanton & Bernstein (2002). In this review I first summarize the structures, stellar populations, and kinematics of the thick disk population, and argue that extragalactic thick disks are indeed reasonable analogs of the well-studied thick disk in the Milky Way. I then discuss how the growing body of data places strong constraints on the origins of thick disks, and on disk galaxy formation in general.

1. The Properties of Extragalactic Thick Disks

Until recently, most evidence for thick disks in other galaxies came from deep broad-band imaging. Starting with the seminal work of Burstein (1979) and continuing through the systematic work of Heather Morrison's group and others (see review in Morrison, 1999), analyses of vertical surface brightness profiles (i.e. parallel to the minor axis) of edge-on galaxies have typically shown breaks at large scale heights, indicative of a second, thicker disk

component that dominates at large heights and faint surface brightnesses. More recent studies have taken advantage of advances in computing power to fit the full two-dimensional light distribution to models of two superimposed disk components (e.g., Yoachim & Dalcanton 2005b; Pohlen et al. 2004). In Figure 1 I show the residuals from one- and two-disk fits to a large sample of edge-on late-type disk galaxies from the Dalcanton & Bernstein (2000) sample, as analyzed in Yoachim & Dalcanton (2005b). Fits to only a single disk leave large amounts of light at high latitudes, providing convincing evidence that there is an additional, thicker stellar component. Fits that include a second disk component do a far better job of fitting the light distribution, at all latitudes.

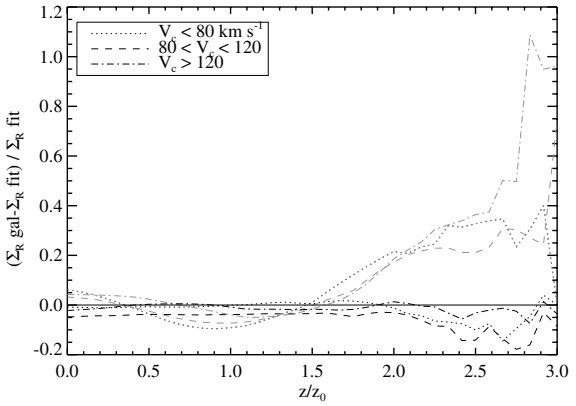

Figure 1. Residuals from single-disk (light lines) and two-disk fits (dark lines) to edge-on galaxies in different mass ranges (Yoachim & Dalcanton 2005b). All of the single-disk fits show large positive residuals at large scale-heights, for galaxies in every mass range. In contrast, including a second thick disk component reduces the residuals to $< 10\%$ at all scale heights.

The Structure of Thick Disks

Generically, all of the disk galaxies studied to date have some degree of excess light at high latitudes. While the extra-planar light seems to be well fit by an additional thick disk component, there is no guarantee that this second component is strictly analogous to the well-studied thick disk of the Milky Way. Within the Galaxy, one can identify thick disk stars by their distinct kinematic and chemical properties, whereas two-dimensional decompositions of galaxies typically have non-unique solutions that depend on the weighting, the bandpass, and the assumed underlying model.

In spite of these uncertainties, there is growing evidence that the population of extragalactic thick disks revealed by two-dimensional disk fitting are

reasonable (though probably not exact) analogs of the Milky Way's thick disk. Structurally, the secondary disk components are quite similar, and are well matched to the scale heights, scale lengths, and axial ratios (∼3-4:1) of the Milky Way thick disk, when restricted to galaxies of comparable mass (Yoachim & Dalcanton 2005b).

While it is not too surprising that extragalactic thick disks are indeed thick, other unexpected structural results have been revealed by the rapid increase in the number of well-studied systems. In particular, the thick disk component is almost always more radially extended than the embedded thin disk. Figure 2 shows the scale length ratio of the thick to thin disks from a wide variety of studies in the literature. In almost all cases, the thick disk has a longer scale length.

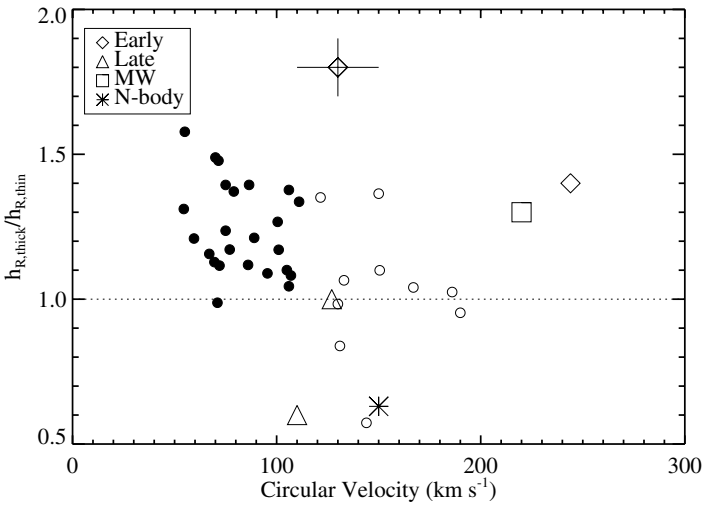

Figure 2. The ratio of thick disk to thin disk exponential scale length, as a function of galaxy rotation speed for the late-type galaxies from the Dalcanton Bernstein (2000) sample (closed and open circles) and other individual studies (triangles; Wu et al. 2002; Neeser et al. 2002; Abe et al., 1999), the Milky Way (square; Larsen & Humphreys 2003), the Pohlen et al. 2004 sample of S0's, and numerical simulations of Brook et al. 2004. In almost all cases, the thick disks have longer scale lengths than their embedded thin disks.

The Stellar Populations of Thick Disks

In addition to their structural similarities, HST imaging is now revealing similarities between the stellar populations of the Milky Way and the extragalactic thick disks. Studies of resolved extraplanar stars (Seth et al. 2005a; Seth et al. 2005b; Mould 2005) are finding that the stellar populations are

systematically older at large scale heights. Figure 3 shows that stars above the plane are dominated by old ($\sim 5-13\,\mathrm{Gyr}$) red giant branch stars, as discussed in more detail in Seth et al. (2005b). The colors of these extraplanar red giants indicate that they are exclusively metal poor, with a median metallicity of [Fe/H]$\sim$-1 in the low mass ($V_c \sim 75\,\mathrm{km\,s^{-1}}$) galaxies studied. The old red giant population seems to be well mixed vertically, and shows no evidence for the strong vertical metallicity gradients that would be expected if steady vertical heating had been solely responsible for driving each new generation of stars to larger scale heights (Seth et al. 2005b; Mould 2005). A single vertical heating event, however, could be compatible with the lack of metallicity gradient, since the resulting thickened disk would be well-mixed.

Unfortunately, extraplanar stellar populations have been studied in fewer than ten galaxies to date, and usually in a single field. The number of future studies will be limited by the relatively small numbers of galaxies that are both edge-on and close enough to resolve into stars.

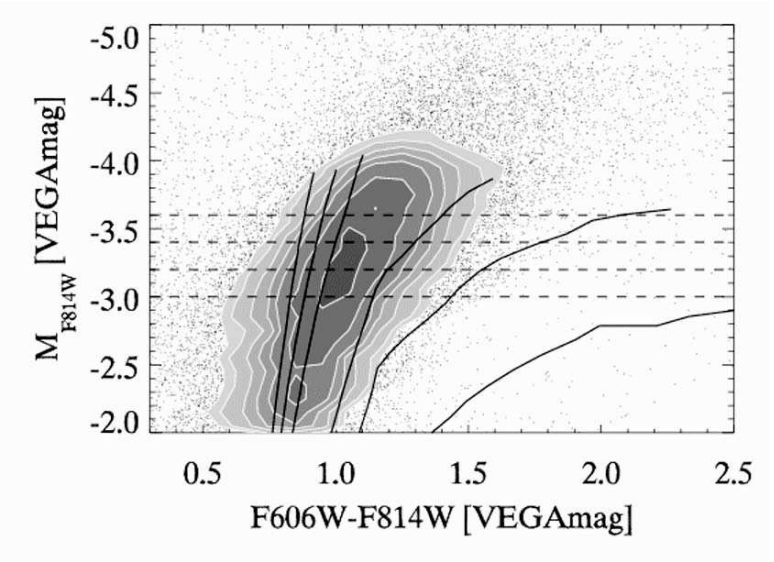

Figure 3. The color-magnitude diagram of stars more than 4 disk scale heights above the midplane, for all six galaxies in the Seth et al. (2005b) sample. The stars are clearly dominated by old red-giant stars, with no significant main sequence or AGB population. Solid lines show 10 Gyr old Padova isochrones for the RGB with [Fe/H] (from left to right) of -2.3, -1.7, -1.3, -0.7, -0.4, and 0.0. The peak of the stellar distributions fall between [Fe/H] of -1.3 and -0.7. For reference, the peak metallicities of the Milky Way's thick disk and stellar halo are [Fe/H]$\sim$-0.7 and [Fe/H]$\sim$-2.2, respectively.

The Kinematics of Thick Disks

The number of kinematic studies of extragalactic thick disks is even more sparse than the stellar population studies. Outside the Milky Way, there have only been two other published measurements of thick disk kinematics (Yoachim & Dalcanton 2005a). All three cases reveal thick disks that rotate more slowly than the embedded thin disk. However, even within such a small sample, the thick disk kinematics seem to be relatively complex. Within the Milky Way, there is evidence at large scale heights of significant kinematically distinct populations that rotate even more slowly than typical thick disk stars closer to the midplane (Gilmore et al. 2002). Among the two extragalactic thick disks studied, one shows clear evidence of *counter*-rotation. While larger samples are clearly needed before one can probe systematic variations, the current data already point to a significant degree of scatter in the relative kinematics of thin and thick disks.

2. How Do Thick Disks Form?

The data summarized above points to the following generic facts about thick disks that must be fit into the basic paradigm of disk galaxy formation:

- Thick disks are found in essentially all edge-on disks, at all Hubble types. They are therefore a generic by-product of disk galaxy formation.
- Although they are ubiquitous, there is substantial scatter in the structural properties of thick disks (see, for example, the scatter in Figure 2).
- The thick disk typically has a longer exponential scale length than the embedded thin disk.
- The stars in thick disks are dominated by old (>5 Gyr), relatively metal-poor (-1.5<[Fe/H]<-0.7) red giants, and are somewhat more metal-poor in lower-mass galaxies.
- The kinematics of thick disk stars vary widely, and show both co- and counter-rotation. However, in all cases the thick disk rotates more slowly than the thick disk.

Current models of disk formation assume that the bulk of a galaxy disk forms from accreted gas with high angular momentum. Analytic calculations assume that this gas is accreted steadily through spherical infall (e.g., Fall & Efstathiou, 1980; Dalcanton et al., 1997; van den Bosch, 1998), but recent numerical simulations have shown that even the gas accreted through clumpy hierarchical merging can maintain sufficient angular momentum to produce realistic massive disks (e.g., Governato et al. 2004). The accreted gas dissipates

and collapses into a rapidly rotating disk that then converts into stars, forming a thin disk.

Within this scenario, the natural sites of thick disk star formation are: [1] in the thin gas disk, which is later disrupted and vertically heated by satellite accretion; [2] in the merging gas clumps, as they coalesce into the thin disk (Brook et al. 2004); or [3] in the pre-galactic fragments, before the disk is formed (e.g. Abadi et al. 2003; Yoachim & Dalcanton 2005b). All three of these possibilities would naturally lead to the formation of the thick disk in a merging hierarchy. Moreover, because all three are tied to high merging rates (which peak early and decline sharply after a redshift of $\sim 1-2$), each of these scenarios naturally produces an early epoch of rapid thick disk formation, making them compatible with the old ages and high α-element abundances currently seen in thick disk stars.

Of these three scenarios, I believe that the third possibility – direct accretion of stars – is likely to dominate the production of the thick disk, although there is certainly room for the other two mechanisms to occur as well (and indeed, it would be surprising if they didn't to some degree). Although it is far more limited than the structural information currently in hand, the kinematic data strongly disfavors the vertical heating scenario. Vertical heating does little to change the angular momentum of a disk (Velazquez & White, 1999), thus making it difficult to explain why the thick disk rotates significantly more slowly than the thin disk, having no more than $\sim$50% of the rotational speed of the thin disk in all three cases studied. Likewise, it would be difficult to produce the very different scale lengths of the two disk components without their having very different angular momenta.

Long thick disk scale lengths are likewise difficult to produce in the second model, where thick disk stars form *in situ* as gas merges to form the final disk. In this case, the same accreted gas would form both the thin disk and the thick disk stars, making it likely that both would have similar radial distributions. Producing a thin disk with a shorter scale length would require that the gas left over after the thick disk stars formed had systematically lower angular momentum. This requirement seems a bit unlikely and is in conflict with the limited available kinematic data.

In contrast, the slower rotation speeds and longer scale lengths of thick disk stars drop out naturally if the stars were formed in pre-galactic fragments before being accreted onto the disk. Gas and stars behave differently during accretion, leading to a natural segregation in the properties of the thin and thick disk. The accreted gas (which forms the thin disk) can cool and dissipate, and thus will tend to contract further into the halo than the stars. As it contracts, the gas will speed up due to angular momentum conservation, producing a compact disk that rotates more rapidly than the accreted stars. In contrast, the orbits of the accreted stars cannot lose energy (except through dynamical friction),

and will tend to remain in a thicker, more radially extended distribution than the gas disk. This scenario thus naturally reproduces the larger scale height and scale length of the thick disk. Moreover, because not all of the merging satellites have the same gas-richness, some satellites may contribute the bulk of the stars to the thick disk while others contribute the bulk of the gas to the thin disk. Some kinematic and structural decoupling between the two components would therefore be expected, because different precursors may dominate production of the thick and the thin disks, and could thus easily produce the scatter seen in the observations.

If the majority of thick disk stars were indeed directly accreted, then the thick disk can constrain the typical gas-richness of the pre-galactic fragments from which the galaxy assembled. In this picture, any stars in the merging subunits were deposited in the thick disk, while any gas cooled and settled into the thin disk. The relative baryonic mass fractions of the thin and thick disks therefore constrain the ratio of stars to gas in the early galaxy. In Yoachim & Dalcanton 2005b we have inferred the luminosities of the thick and thin disks from the two-dimensional decompositions, and then adopted color-dependent stellar mass-to-light ratios to derive the stellar mass of each disk component. The resulting "baryon budget" is reproduced in Figure 4, as a function of galaxy mass for the late-type Dalcanton & Bernstein (2000) sample, after assuming that any gas is confined to the thin disk.

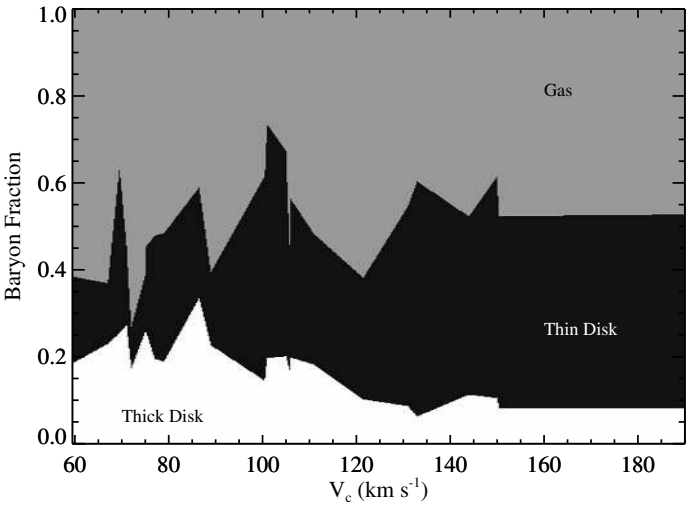

Figure 4. The baryonic mass fraction of the the thick disk stars (bottom), thin disk stars (middle), and cool gas (top) for the galaxies analyzed by Yoachim & Dalcanton (2005b), sorted by galaxy rotation speed.

Figure 4 shows a number of striking features. First, the baryonic mass fraction trapped in the thick disk is relatively small, implying that the initial galaxy disk was almost entirely gaseous ($\sim$75-90%, or more if some thick disk stars formed during the final coalescence of the disk). Second, the stellar mass of the thick disk is *larger* than the stellar mass of the thin disk in low mass galaxies. Thus, although low mass galaxies appear to be blue and young, the majority of their stars are actually quite old, as would be expected in hierarchical merging scenarios. Finally, the thick disk is increasingly important in low mass galaxies. The baryonic mass fraction locked in the thick disk increases systematically from $\sim$ 10% in high mass galaxies to up to $\sim$ 25% in low mass galaxies, implying that the precursors of low mass galaxies were more gas poor than the precursors of their high mass counterparts.

If thick disk stars are directly accreted, then the increasing importance of thick disk stars in low mass galaxies can be easily explained by supernova-driven winds in the pre-galactic fragments. The precursors of low mass galaxies are themselves likely to be lower mass than the typical sub-units which merge together to form more massive galaxies, and thus, they are more susceptible to gas loss through supernova driven winds. These winds would reduce the gas mass of the initial galaxy, and thus reduce the fraction of baryons that wind up in the thin disk. The winds would also reduce the typical metallicity of thick disk stars, and could thus nicely produce the trend toward lower thick disk metallicities in low mass galaxies (Seth et al. 2005b).

3. Prospects for the Future

Decades of painstaking work have gone into observing and characterizing the population of extragalactic thick disks. Thanks to this effort, we now have a broad understanding of the basic properties of thick disks, allowing us to finally place them within the context of galaxy formation. However, while the broad outlines of thick disk formation are in place, there are many details to be worked out. Over the next decade, I believe there are several areas where thick disk research will be critical:

- **Exploring the link between observations of thick disks at low redshift and of young galaxies at high redshift ($z > 1.5$).** There are already hints that many of the stars in clumpy, disturbed galaxies at high redshift will evolve into the thick disk population by the present day (Elmegreen & Elmegreen 2005). This likely connection makes on-going work on low-redshift thick disks crucial for understanding and interpreting high-redshift observations.

- **Linking thick disk observations to numerical studies of galaxy formation.** Simulations are just now beginning to have the resolution to tackle thick disk formation (see work by Chris Brook and Alyson Brooks

in this volume). However, because the properties of thick disks depend on star formation and gas loss in dense low mass pre-galactic fragments, simulations of thick disk formation will be highly sensitive to the adopted star formation and feedback recipes, as well as to the numerical resolution. Thus, I believe we are only in the early days of numerical exploration of thick disk formation. Perhaps the greatest long-term role for extragalactic thick disks will be as a key calibration for tuning the baryonic physics in these simulations.

- **Incorporating the thick disk component into semi-analytic models of galaxy formation.** Given that the thick disk dominates the stellar mass in low-mass disks, a recipe for including thick disks in semi-analytic models is sorely needed.

- **Exploring the connection between thick disks and bulges.** To date, large studies of thick disks have focused on either bulgeless (Dalcanton & Bernstein 2002; Yoachim & Dalcanton 2005b) or bulge-dominated (Pohlen et al. 2004) galaxies. However, there is currently no study using uniform data and analysis techniques to bridge across this wide range of galaxy types. There are hints that thick disks may be systematically "thicker" in early type galaxies (Yoachim & Dalcanton 2005b), but without uniform data, the robustness and interpretation of such conclusions is questionable. Theoretically, there is much work to be done as well. Mergers are thought to be critical to the formation of both thick disks and massive bulges, but we currently have no well-developed theory that can reliably calculate how the merging material is distributed between the bulge and the thick and thin disks.

- **Observationally and theoretically untangling thick disks and stellar halos.** As difficult as it has been to characterize extragalactic thick disks, the upcoming work to isolate stellar halos will be even harder. In the Milky Way, the thick disk makes up roughly 10% of the stars at the solar circle, while the stellar halo contributes only a tenth of a percent (Chen et al. 2001). Even with detailed studies of resolved stars (e.g., Ferguson et al. 2002), it is difficult to decide whether a given structure is an analog of the Milky Way's thick disk or its halo, if indeed they are truly distinct structures. Already, there have been extraplanar stars attributed to the thick disk that are probably distributed in a much more spherical distribution (e.g., Tikhonov et al. 2005) and which may be better assigned to an analog of the stellar halo. Simultaneously, theoretical models of stellar halo formation (Bullock & Johnston 2005) produce distributions of stars that can be relatively flattened in their inner, higher surface brightness regions. Given the only modest flattening ($\sim$3:1) of

extragalactic thick disks, it is possible that these are the same structures, in spite of the different nomenclature. As more simulations are translated to the observational plane, the correct interpretation of broad-band colors and resolved stellar populations in edge-on disks will clarify.

References

Abadi, M. G., Navarro, J. F., Steinmetz, M., & Eke, V. R. 2003, Ap.J., 597, 21
Abe, F., et al. 1999, A.J., 118, 261
Bahcall, J. N., & Kylafis, N. D. 1985, Ap.J., 288, 252
Brook, C. B., Kawata, D., Gibson, B. K., & Freeman, K. C. 2004, Ap.J., 612, 894
Bullock, J. S., & Johnston, K. V. 2005, astro-ph/0506467
Burstein, D. 1979, Ap.J., 234, 829
Carney, B. W., Latham, D. W., & Laird, J. B. 1989, A.J., 97, 423
Chen, B., et al. 2001, Ap.J., 553, 184
Dalcanton, J. J., Spergel, D. N., & Summers, F. J. 1997, Ap.J., 482, 659
Dalcanton, J. J., & Bernstein, R. A. 2000, A.J., 120, 203
Dalcanton, J. J., & Bernstein, R. A. 2002, A.J., 124, 1328
de Grijs, R., & van der Kruit, P. C. 1996, A.&Ap.Supp., 117, 19
Elmegreen, B. G., & Elmegreen, D. M. 2005, Ap.J., 627, 632
Fall, S. M., & Efstathiou, G. 1980, M.N.R.A.S., 193, 189
Feltzing, S., Bensby, T., Gesse, S., & Lundström, I. 2004, in Origin and Evolution of the Elements
Ferguson, A. M. N., Irwin, M. J., Ibata, R. A., Lewis, G. F., & Tanvir, N. R. 2002, A.J., 124, 1452
Freeman, K., & Bland-Hawthorn, J. 2002, Ann.Rev.Astr.&Ap., 40, 487
Fry, A. M., Morrison, H. L., Harding, P., & Boroson, T. A. 1999, A.J., 118, 1209
Gilmore, G., & Reid, N. 1983, M.N.R.A.S.202, 1025
Gilmore, G., Wyse, R. F. G., & Kuijken, K. 1989, Ann.Rev.Astr.&Ap., 27, 555
Gilmore, G., Wyse, R. F. G., & Norris, J. E. 2002, Ap.J.Lett., 574, L39
Governato, F., et al. 2004, Ap.J., 607, 688
Jensen, E. B., & Thuan, T. X. 1982, Ap.J.Supp, 50, 421
Kroupa, P. 2002, M.N.R.A.S., 330, 707
Larsen, J. A., & Humphreys, R. M. 2003, A.J., 125, 1958
Liu, W. M., & Chaboyer, B. 2000, Ap.J., 544, 818
Majewski, S. R. 1993, Ann.Rev.Astr.&Ap., 31, 575
Matthews, L. D. 2000, A.J., 120, 1764
Morrison, H. L., Miller, E. D., Harding, P., Stinebring, D. R., & Boroson, T. A. 1997, A.J., 113, 2061
Morrison, H. L. 1999, ASP Conf. Ser. 165: The Third Stromlo Symposium: The Galactic Halo, 165, 174
Mould, J. 2005, A.J., 129, 698
Naeslund, M., & Joersaeter, S. 1997, A.&Ap., 325, 915
Neeser, M. J., Sackett, P. D., De Marchi, G., & Paresce, F. 2002, A.&Ap., 383, 472
Norris, J. E. 1999, Ap.&Sp.Sc., 265, 213
Pohlen, M., Balcells, M., Lütticke, R., & Dettmar, R.-J. 2004, A.&Ap., 422, 465

Quinn, P. J., Hernquist, L., & Fullagar, D. P. 1993, Ap.J., 403, 74
Seth, A. C., Dalcanton, J. J., & de Jong, R. S. 2005a, A.J., 129, 1331
Seth, A. C., Dalcanton, J. J., & de Jong, R. S. 2005b, AJ, 130, 1574
Statler, T. S. 1988, Ap.J., 331, 71
Tikhonov, N. A., Galazutdinova, O. A., & Drozdovsky, I. O. 2005, A.&Ap., 431, 127
Tsikoudi, V. 1979, Ap.J., 234, 842
van den Bosch, F. C. 1998, Ap.J., 507, 601
van der Kruit, P. C., & Searle, L. 1981, A.&Ap., 95, 105
van Dokkum, P. G., Peletier, R. F., de Grijs, R., & Balcells, M. 1994, A.&Ap., 286, 415
Velazquez, H., & White, S. D. M. 1999, M.N.R.A.S., 304, 254
Wainscoat, R. J., Freeman, K. C., & Hyland, A. R. 1989, Ap.J., 337, 163
Wu, H. et al. 2002, A.J., 123, 1364
Yoachim, P., & Dalcanton, J. J. 2005a, Ap.J., 624, 701
Yoachim, P., & Dalcanton, J. J. 2005b, Ap.J., in press.

Jackie Zwegers and Hennie Zondervan of the LOC.

THE OPACITY OF SPIRAL GALAXY DISKS

Benne W. Holwerda[1,2*], R.A. González[3], Ronald J. Allen[2] and P.C. van der Kruit[1]

[1] *Kapteyn Astronomical Institute, University of Groningen, The Netherlands*

[2] *Space Telescope Science Institute, Baltimore, USA*

[3] *Centro de Radiastronomía y Astrofísica, Michoacán, Mexico*

* holwerda@stsci.edu

Abstract The opacity of foreground spiral disks can be probed from the number of distant galaxies seen through them. To calibrate this number for effects other than the dust extinction, Gonzalez et al. (1998) developed the "Synthetic Field Method". A synthetic field is an extincted Hubble Deep Field added to the science field. The relation between the dimming and the number of retrieved synthetic galaxies calibrates the number found in the science field. Here we present results from counts in 32 HST/WFPC2 fields. The relation between opacity and radius, arm and disk, surface brightness and HI are presented. The opacity is found to be caused by a clumpy distribution of clouds in the disk. The brighter parts of the disk –the center and arms– are also the more opaque ones. The dust distribution in spiral disks is found to be more extended than the stellar disk. A comparison between HI column densities and opacity shows little relation between the two.

Keywords: ISM: dust, extinction - galaxies: spiral - ISM: structure

1. Introduction

The measure and extent of the dust absorption by spiral disks has been the subject of study and even controversy for some time. New models of the disk's energy household (e.g., Dopita 2006) and a wealth of observational data (e.g., Regan 2006; Kennicutt 2006) promise a better understanding of the role of dust in the disks. Still, there are several questions regarding the distribution of dust clouds in the spiral disk which should be addressed: to which radius does dust extend and is dust spatially correlated to the stellar distribution or the atomic hydrogen gas? One possible technique to answer these questions is to use the number of distant galaxies seen through a foreground disk as an indicator of disk opacity.

R. S. de Jong, Island Universes, 41–46.
© 2007 *Springer.*

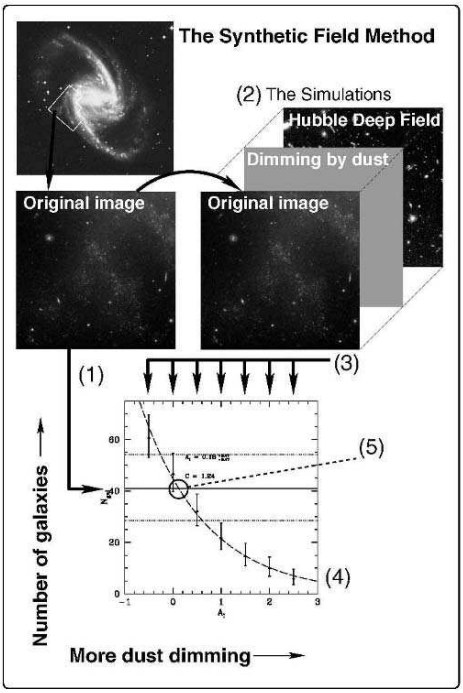

Figure 1. A schematic of the "Synthetic Field Method". First a WFPC2 field is retrieved from the HST archive and redrizzled. The steps are:
1. The number of distant galaxies in the original science field are counted.
2. The "synthetic fields" are made by combining a dimmed Hubble Deep Field with the science field.
3. The numbers of synthetic galaxies are counted in the synthetic fields.
4. $A = -2.5\log(N/N_0)$ is fitted to the number of synthetic galaxies (N) as a function of the applied dimming.
5. From the intersection between the number galaxies in the science field and the fit, the average dimming in the image is found.

2. What is the "Synthetic Field Method"?

For a useful measurement, one needs to calibrate the number of distant galaxies seen through a foreground for effects other than the extinction by dust. The calibration is done with the "Synthetic Field Method" (Fig. 1). The distant galaxies in the science field are counted (step 1). An average background field is added to the science field to create a "synthetic field". The average background field is artificially dimmed in progressive "synthetic fields" (step 2). The numbers of retrieved synthetic galaxies for each value of the dimming is found (step 3). The relation $A{=}-2.5\log(N/N_0)$ is fitted to the relation between the numbers of galaxies (N) and the dimming (A) of the synthetic fields (step 4). The free parameters are the slope (C) and the number of galaxies without any dimming (N_0). The intersection between the fit and the number of actual distant galaxies found in the science field gives the average opacity of the science field (step 5)[1]. This comparison between counts can be done for individual fields but also for multiple fields, combined based on disk characteristics: radius, arm or disk region, surface brightness or HI column density.[2]

[1] A comprehensive description of the "Synthetic Field Method" and the uncertainties involved is presented in Holwerda et al. (2005a,d) and Holwerda (2005).
[2] The numbers of distant galaxies in a single HST/WFPC2 field are only sufficient for a relatively uncertain opacity measurement. To counter this more solid angle from several HST observations need to be combined.

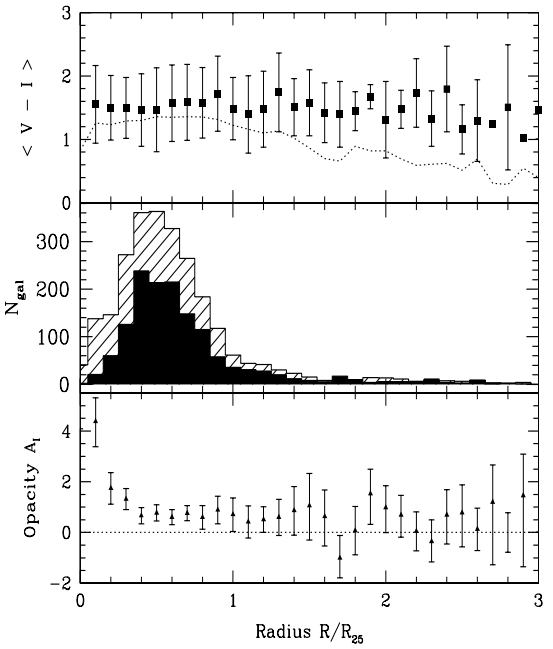

Figure 2. The stacked radial opacity profile for all 32 galaxies in the sample. The counts of galaxies were ordered according to deprojected radial distance from the foreground galaxy's center, expressed in R_{25}. Top: the average color of distant galaxies in the science fields. Middle: the number of distant galaxies in the science field (filled) and the synthetic fields without any dimming (shaded). Bottom: the disk opacity as a function of radius derived from the numbers of distant galaxies. Since most of the WFPC2 fields were pointed at the disk of these galaxies, the opacity measurements are the most accurate there (from Holwerda et al. 2005b).

3. The Opacity Profile of Spiral Disksx

Figure 2 shows the stacked radial opacity profile of our entire sample of 32 HST/WFPC2 fields. From Fig. 2, we can conclude that the average radial opacity profile of spiral galaxies remains relatively flat for most of the disk and only tapers off somewhere beyond the R_{25}. This was already suspected from sub-mm observations (e.g., Nelson et al. 1998 and Zaritsky & Christlein 2006). This profile has not been corrected for inclination effects, as this depends greatly on the assumed dust geometry.

The average color of the galaxies in the science fields does not change however (Fig. 2, top panel). If the diminishing effect of the dust in the ISM would have been due to a uniform screen, the average color would have changed with the total amount of attenuation according to an Extinction Law. However, if the dust in the disk is relatively patchy, the attenuation is derived from the number of absent galaxies while the color is from those that have been detected relatively unhindered by dust in the disk. The average disk opacity in Fig. 2 can therefore be interpreted as a cloud covering factor.

Separate profiles for the arm and disk sections of the foreground galaxy can also be made (Fig. 3). These opacity profiles show a strong radial relation in the arms and a much flatter profile in the rest of the disk. When these profiles are compared to the opacity values from occulted galaxy pairs (White et al. 2000;

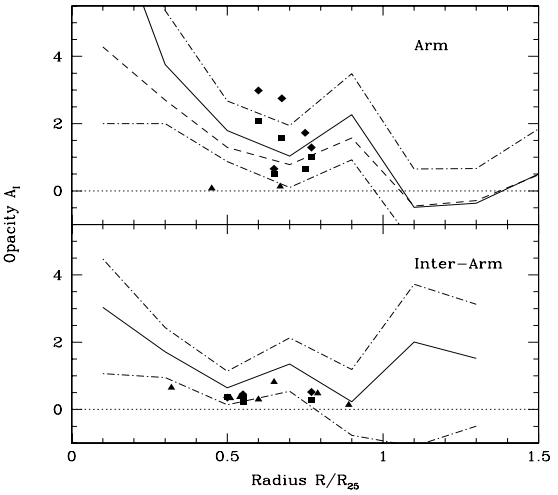

Figure 3. The stacked radial opacity profiles for the arm and inter-arm regions of the disks. The filled squares and triangles are the measurements by White et al. (2000) and Domingue et al. (2000), respectively. The dashed/dotted lines are the uncertainties in the SFM measurements. higher values for spiral arm opacity have been found in earlier photometric studies (e.g., Elmegreen 1980).

Domingue et al. 2000), there is a remarkably good agreement between these completely different methods. White et al. (2000) also found a gray behaviour but Keel & White (2001) found that the Galactic Extinction law re-emerged for measurements below a linear scale in the disk smaller than 100 pc.

4. Dust, Gas and Stars

The strong radial relation for the spiral arms hints at a direct relation between the amount of dust in the disk and the surface brightness of the disk. A similar relation between overall disk opacity and brightness was found by Tully et al. (1998) and Masters et al. (2003). However the much flatter distribution of the opacity in the rest of the disk does suggest that the dust may be more distributed like the atomic hydrogen.

To find the relation between opacity and surface brightness, each distant galaxy, from both synthetic and science fields, are flagged with the surface brightness in 2MASS images. The numbers of galaxies as a function of near-infrared surface brightness are shown in Fig. 4 for all of the disk and the arm and non-arm regions separate. As could be expected from Fig. 3, there is a strong relation between surface brightness and opacity in the arm regions but none in the non-arm part of the disk.

The relation between atomic hydrogen and dust might reveal more on the hidden constituents of the ISM. Due to limitations of the SFM measurements and lack of HI maps, Fig. 5 shows the ratio of the HI column density from radial profiles from the literature and the opacity measured from counts of galaxies in the same radial bin. No direct relation is evident, mainly because opacity profiles rise towards the center of galaxies and HI profiles stay flat or decrease. It is possible that dust correlates with the total gas content in the disk, both the molecular and the atomic.

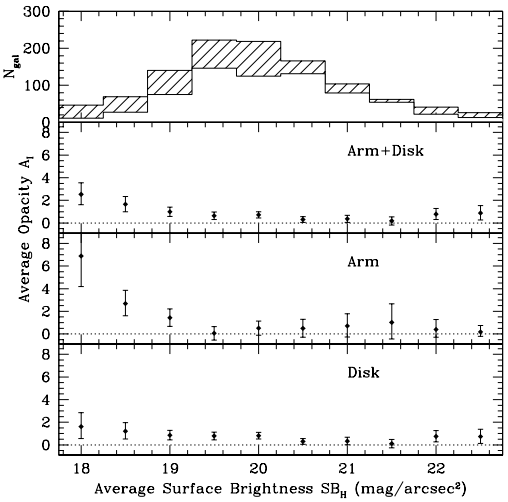

Figure 4. The disk opacity as a function of surface brightness. The distant galaxies - real and synthetic- are sorted by surface brightness in the entire sample. Top: the histograms of distant galaxies (shaded for the synthetic fields and the line for the science field). Top middle: the derived opacity as a function of surface brightness. Bottom two plots: the surface-brightness and opacity plots for the arm (top) and disk (bottom) parts of the spiral galaxy. (from Holwerda et al. 2005d)

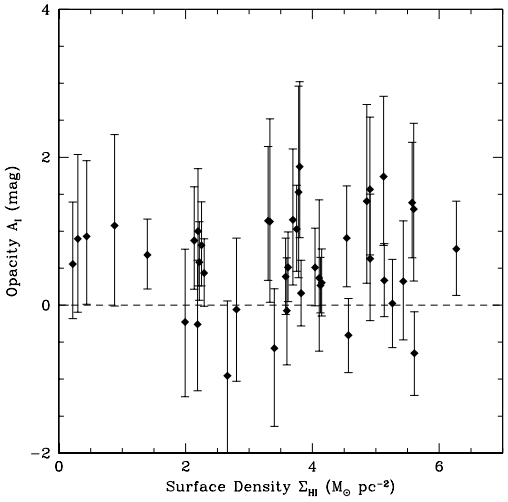

Figure 5. The ratio of HI column density and opacity in radial annuli of 0.25 R_{25}. Opacity measurements in individual galaxies remain uncertain due to cosmic variance in the number of distant galaxies behind each foreground galaxy. An improvement would include compare galaxy number directly as a function of HI column density (e.g., Cuillandre et al. 2001), much like Fig. 4. (from Holwerda et al. 2005c)

5. Final Remarks

The counts of distant galaxies have proven themselves to be a good indicator of disk opacity, provided they are calibrated with the SFM. Improved statistics from many HST fields have lent insight into the distribution of dust in the disk and into the relation with the stellar content and atomic gas. The radial opacity profile extends to well beyond the optical disk and appears caused by patchy dust. The dust clouds correlate with stellar light in the arms but there is additional constant disk component which is more dominant at higher radii.

The radial profile implies that there are dust clouds outside the optical disk. This seems in agreement with the SINGS extinction maps (Regan et al. 2006) and PAH emission maps from the SINGS project (Kennicutt 2006) but an exact comparison remains to be made. However, we know that starformation and HII regions can be found at hitherto unprecedented radii. The presence of dust is therefore not unreasonable. The question remains how much there is.

One implication of the relation between opacity and surface brightness in the arms is that a light-profile derived from the non-arm regions can be a maximum disk or a scaling of that but that a profile that includes the arm regions will be less concentrated than the actual distribution of mass. This may be another contributor to a slightly different normalization of the Bell & de Jong (2001) color-M/L relation (de Jong & Bell 2006).

The profiles of opacity and HI column density are not correlated. Since the opacity keeps rising in the center, it is very possible that the overall disk opacity relates in some way to the total gas content or just the molecular component.

A similar radial profile and HI-to-dust ratio for spiral disks have also been found in sub-mm observations of disks. This implies that a substantial fraction of the dust responsible for the disk opacity is cold.

Future application of the counts of distant galaxies include probing the edge of the dust disk, constraining the average cloud size, and a comparison with sub-mm observations to constrain dust emissivity.

References

Bell, E. F. and de Jong, R. S. 2001, ApJ, 550, 212
Cuillandre, J., Lequeux, J., Allen, R. J., Mellier, Y., and Bertin, E. 2001, ApJ, 554, 190
de Jong, R. S., Bell E. F. 2006, these proceedings, p. 107
Domingue, D. L., Keel, W. C., and White, R. E. 2000, ApJ, 545, 171
Dopita, M. 2006, these proceedings, p. 328
Elmegreen, D. M. (980, ApJS, 43:37
Holwerda, B. W. 2005, PhD thesis, University of Groningen, The Netherlands
Holwerda, B. W., Gonzalez, R. A., Allen, R. J., and van der Kruit, P. C. 2005a, AJ, 129, 1381
Holwerda, B. W., Gonzalez, R. A., Allen, R. J., and van der Kruit, P. C. 2005b, AJ, 129, 1396
Holwerda, B. W., Gonzalez, R. A., Allen, R. J., and van der Kruit, P. C. 2005c, A&A submitted
Holwerda, B. W., Gonzalez, R. A., Allen, R. J., and van der Kruit, P. C. 2005d, A&A accepted
Holwerda, B. W., Gonzalez, R. A., Allen, R. J., and van der Kruit, P. C. 2005e, A&A submitted.
Keel, W. C. and White, R. E. 2001, AJ, 121:1442
Kennicutt, R. C. 2006, these proceedings, p. 397
Masters, K. L., Giovanelli, R., and Haynes, M. P. 2003, AJ, 126, 158
Nelson, A. E., Zaritsky, D., and Cutri, R. M. (1998). AJ, 115, 2273
Regan, M. W. et al. 2006, these proceedings,p. 341
Tully, R. B. et al. 1998, AJ, 115, 2264
White, R. E., Keel, W. C., and Conselice, C. J. 2000, ApJ, 542, 761
Zaritsky, D., Christlein, D. 2006, these proceedings, p. 265

STELLAR POPULATIONS IN BULGES OF SPIRAL GALAXIES

Bhasker K. Moorthy and Jon A. Holtzman
Department of Astronomy, New Mexico State University, Las Cruces, USA

Abstract To better understand bulge formation, we have used long-slit spectroscopy and imaging to obtain luminosity-weighted (SSP) ages and abundances, line of sight velocity distributions, and bulge-to-disk decomposition for 38 spiral galaxies. We specifically included several blue bulges to see if these show evidence for secular evolution. Here we describe the stellar populations and how they relate to the kinematics and dynamics. We find that red bulges are similar to luminous ellipticals in their central line strengths, with large SSP ages and super-solar metallicities and α/Fe ratios. Blue bulges are similar to low-luminosity ellipticals in their central line strengths. They have solar α/Fe ratios and either small age or small metallicity. The colors, metallicities, and α/Fe ratios of bulges are correlated with the central velocity dispersion and maximum disk rotational velocity. Most bulges have metallicity gradients, but the metallicities of the bulge and disk are correlated. These observations suggest that the star-formation histories of ellipticals, bulges, and disks are sensitive primarily to the depth of the galactic potential well, but the scatter in the scaling relations leaves room for multiple formation mechanisms.

Keywords: galaxies: bulges - galaxies: stellar content - galaxies: abundances - galaxies: kinematics and dynamics

1. Introduction

The stellar content of bulges can provide insight into the physical mechanisms responsible for the formation and evolution of galaxies and the nature of the Hubble sequence. Some studies have found that the light profiles, colors, and kinematics of bulges are similar to those of ellipticals while others have found them to be more similar to those of disks (e.g., Carollo et al. 1997; de Jong 1996; MacArthur et al. 2004; Kormendy & Illingworth 1982). While bulges follow the fundamental plane relation of ellipticals (Falcón-Barroso et al. 2002), their scale lengths are correlated with those of their disks (Courteau et al. 1996; MacArthur et al. 2003). There are indications that the massive bulges of early-typed spirals are more similar to ellipticals, while late-typed bulges are more disk-like. As a consequence of these observations, it has been

R. S. de Jong, Island Universes, 47–52.
© 2007 *Springer.*

proposed that bulges were formed through similar mechanisms as ellipticals, such as mergers (e.g., Cole et al. 1994), or through the secular evolution of disks (see Kormendy & Kennicutt 2004 for a review).

We have conducted a multidimensional study of the bulges of 38 nearby spiral and lenticular galaxies, examining their stellar populations, structural properties, kinematics, and dynamics. We specifically included several blue bulges to see if these show evidence for secular evolution. Here we present results on the stellar populations and how they relate to the central velocity dispersion and the maximum disk rotational velocity.

Long-slit spectra covering the wavelength range 4000-7000 Å at 6–9 Å resolution were obtaining using the Double Imaging Spectrograph (DIS) on the ARC 3.5m telescope at Apache Point Observatory. The slit was placed along the major axis for nearly all the galaxies and also along the minor axis for several of the highly-inclined galaxies. Images in *BVR* were obtained using the SPIcam imager on the same telescope. We measured the strengths of the 25 Lick indices (Worthey 1994; Worthey & Ottaviani 1997) as well as several emission lines. The line strengths have been fully transformed to the Lick system and corrected for stellar motions and emission. We obtained luminosity-weighted ages and metallicities using Simple Stellar Population (SSP) models by Thomas, Maraston, & Bender (2003; hereafter TMB). Kinematics were measured using the pPXF package (Cappellari & Emsellem 2004). Bulge-to-disk decomposition was performed using the images to determine the relative contributions of bulge and disk light and to obtain structural parameters. A detailed description of the sample selection, observations, and analysis will be presented in an upcoming paper (Moorthy & Holtzman, in preparation).

2. Results

Figure 1 shows central values of the age-sensitive index Hβ and the metallicity-sensitive index [MgFe]' for bulges and ellipticals. Our central indices were measured on spectral extractions binned to match previous measurements by Trager et al. (1998) and Proctor & Sansom (2002) as closely as possible (3.3, 4.2, and 3.8 arcsec for DIS I, II, and III respectively).

Bulges can be divided into three groups depending on which region of Fig. 1 they populate: the old metal-rich region (OMRR), the young metal-rich region (YMRR), or the metal-poor region (MPR). Membership in a region is closely related to bulge color. Red bulges and Trager et al.'s ellipticals almost always populate the OMRR. One exception is IC 267 (the red filled square with [MgFe]'=1.65). This bulge has strong Balmer emission which suggests that its red color is due to dust from recent star formation as opposed to an old stellar population. The otherwise good separation between blue and red bulges in Fig. 1 indicates that $B-K$ color is sensitive to the central stellar populations

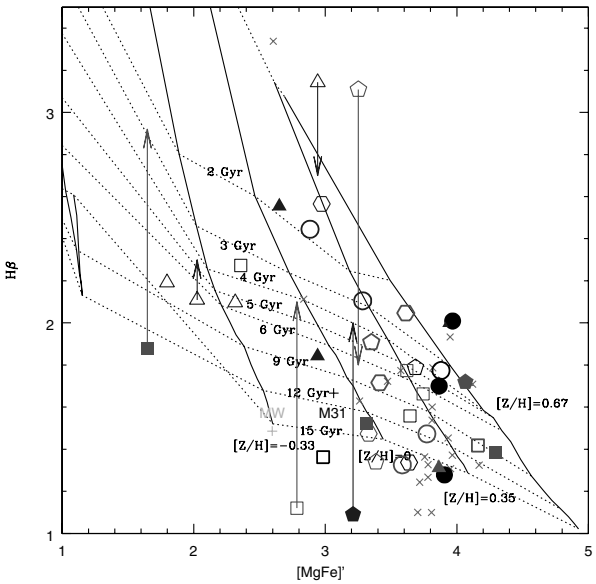

Figure 1. Hβ versus [MgFe]' in the central regions of our bulges. Magenta crosses are galaxies from Trager et al. (1998) that were classified as elliptical and had Hβ uncertainty less than 0.2 and velocity dispersion uncertainty less than or equal to 10 km s^{-1}. The Milky Way (Puzia et al. 2002) and M31 (Puzia et al. 2005) are shown as '+' symbols. For our bulges, thin open symbols represent elliptical or unbarred galaxies, thick open symbols represent boxy/peanut-shaped bulges, and filled symbols represent barred galaxies. Circles are S0's; hexagons are S0a's or Sas; pentagons are Sab's; squares are Sb's; and triangles are Sc's. Bulges are shown in blue or red based on whether they have $B-K$ color less than or greater than 4 as determined by Peletier & Balcells (1996) and de Jong (1996). Bulge color was measured at half the effective radius or 5 arcsec, whichever is larger. Bulges for which we do not have color information are in black. Where spectra exist along both minor and major axes, the average of the two values was used. For galaxies with large emission corrections, arrows show where each bulge would lie if an average of the other Balmer indices were used instead of Hβ to compute the SSP age. TMB's models are superimposed on the plot.

without being affected much by dust. However, the $B-K$ color is degenerate in age and metallicity; some bulges are blue because they are metal-poor while others are blue because they are young. Prugniel et al. (2001) identified three similar classes of bulges based on their central line strengths.

Bulges of late-typed spirals are more heterogeneous in their central line strengths than those of early-types. All the early-typed (S0-Sab) bulges have large central metallicities. The blue early-types are in the YMRR while the red early-types are in the OMRR. The MPR is populated exclusively by late-types, but late-types are also found in the other two regions.

Figure 2 shows how the central line strengths relate to central velocity dispersion and maximum disk rotational velocity. [MgFe]' is correlated with σ_0

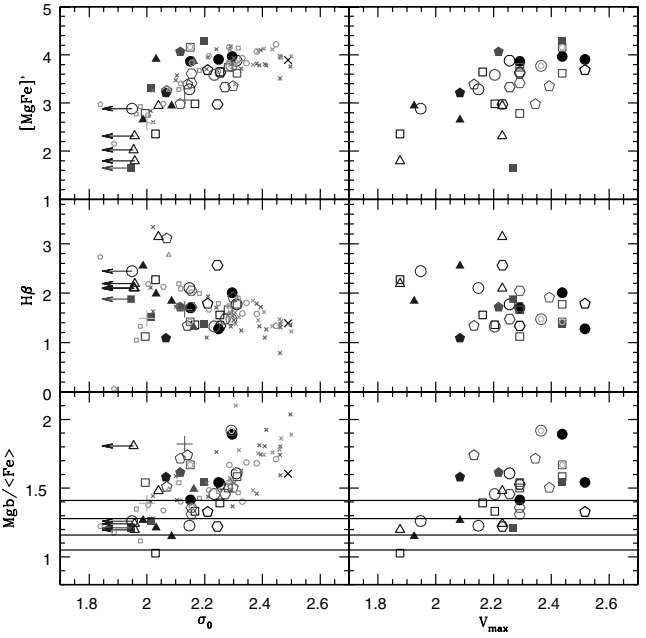

Figure 2. Central line strengths versus central velocity dispersion and maximum disk rotational velocity. Green symbols are bulges and ellipticals from Proctor & Sansom (2002). Other symbols are as in Fig. 1. Arrows represent upper limits for galaxies whose velocity dispersions are close to or below our resolution limit. In the bottom two figures, the region between the two inner horizontal lines corresponds to models with solar α/Fe for metallicities -1.35 $\leq$ [Z/H] $\leq$ 0.35 and ages from 8 to 15 Gyr (from Fig. 4 of TMB). The region within the outer lines represents models with the same metallicities and ages from 3 to 15 Gyr.

and V_{max} while Hβ is weakly anti-correlated with them. Bulges with sub-solar SSP metallicity and small SSP age ($\leq$ 2 Gyr) have small σ_0 (Log $\sigma_0 <$ 2) but not necessarily small V_{max}. Bulges with larger σ_0 are metal-rich and on average older, but at a given σ_0 the scatter in SSP age is large.

There is no systematic difference between different types of bulges or between bulges and ellipticals in the [MgFe]'-σ_0 and Hβ-σ_0 relations. Instead, there is one continuous and overlapping sequence dominated by blue bulges at small-σ_0, red bulges at intermediate-σ_0, and ellipticals at large-σ_0. In both bulges and ellipticals, [MgFe]' is correlated with σ_0 at the low-σ_0 end. As σ_0 increases beyond Log σ_0>2.2, [MgFe]' remains constant. The apparent dichotomy seen in Fig. 1, namely that late-typed blue bulges are metal-poor, while red bulges and ellipticals are metal-rich, is naturally explained by the wide range of σ_0 and V_{max} values spanned by the different types of objects. The blue late-typed bulges which populate the MPR reside in considerably shallower potential wells than the red bulges and ellipticals which populate the OMRR. It is important to note here that the predominant view that ellipticals

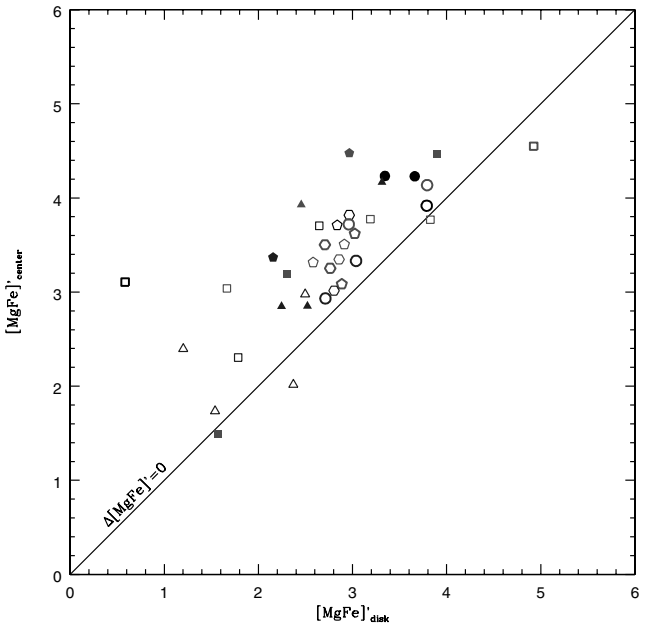

Figure 3. The [MgFe]' value at the center of the galaxy versus the value at one disk scale length. The latter was computed from a least squares fit to the [MgFe]' profile in the disk-dominated region. Symbols are as in Fig. 1.

are metal-rich (Trager et al. 2002; Denicoló et al. 2005; Thomas et al. 2005) applies only to high-σ_0 ellipticals. The only study we could find in the literature that included a large number of ellipticals with $\sigma_0 < 100$ km s^{-1} found that these objects spanned a similar range of SSP ages and metallicities as our blue bulges (Caldwell et al. 2003).

The Mgb/$\langle$Fe$\rangle$ index, which is directly related to α/Fe, is correlated with σ_0 and even more so with V$_{max}$. The most straight-forward interpretation of this is that the duration of star-formation is shorter in deeper potential wells. The tighter correlation with V$_{max}$ indicates that the star-formation timescales are more sensitive to the halo potential than the bulge potential. The Mgb/$\langle$Fe$\rangle$-σ_0 relation does not apply to blue bulges. With a couple of exceptions, blue bulges are consistent with having solar α/Fe. These have small V$_{max}$, but they do not all have small σ_0. Consequently, blue bulges have smaller Mgb/$\langle$Fe$\rangle$ ratios than red bulges or ellipticals at a given value of σ_0.

Most galaxies have a negative gradient in [MgFe]' within the bulge-dominated region and a distinct shallower gradient in the disk-dominated region. However, the [MgFe]' value at one disk scale length, which is almost always outside the bulge-dominated region, is correlated with the central value (Fig. 3). This suggests that the star-formation history of the bulge and disk are coupled.

3. Conclusion

We have studied central line strengths and line strength gradients in the bulges and inner disks of 38 nearby galaxies. The metallicities of bulges are correlated with that of their disks and similar to those of ellipticals of the same σ_0. The α/Fe values in bulges are correlated with σ_0 and even more tightly with V_{max}, suggesting that the star-formation timescales are modulated by the depths of the bulge and halo potential wells. The continuity among disks, different types of bulges, and ellipticals suggests that the star-formation histories of all of these are similarly modulated by the depth of the galactic potential well. However, the large scatter in the scaling relations leaves room for multiple formation mechanisms.

Acknowledgements It is a pleasure to thank Anatoly Klypin for innumerable helpful discussions and the organizing committee for a most beneficial and enjoyable conference.

References

Caldwell, N., Rose, J. A., & Concannon, K. D. 2003, AJ, 125, 2891
Cappellari, M., & Emsellem, E. 2004, PASP, 116, 138
Carollo, C. M., Stiavelli, M., de Zeeuw, P. T., & Mack, J. 1997, AJ 114, 2366
Cole, S., Aragón-Salamanca, A., Frenk, C. S., Navarro, J. F., & Zepf, S. E. 1994, MNRAS, 271, 781
Courteau, S., de Jong, R. S., & Broeils, A. H. 1996, ApJ, 457, L73
de Jong, R. S. 1996, A&A, 313, 377
Denicoló, G. Terlevich, R., Terlevich, E., Forbes, D. A., Terlevich, A. & Carrasco, L. 2005, MNRAS, 356, 1440
Falcón-Barroso, J., Peletier, R. F, & Balcells, M. 2002, MNRAS, 335, 741
Kormendy, J., & Kennicutt, R. C. 2004, ARA&A, 42, 603
Kormendy, J., & Illingworth, G. 1982, ApJ, 256, 460
MacArthur, L. A., Courteau, S., Bell, E. F., Holtzman, J. A. 2004, ApJS 152, 175
MacArthur, L. A., Courteau, S., & Holtzman, J. A. 2003, ApJ, 582, 689
Peletier, R. F, & Balcells, M. 1997, New Astronomy, 1, 349
Peletier, R. F, & Balcells, M. 1996, AJ, 111, 2238
Proctor, R. N., & Sansom, A. E. 2002, MNRAS, 333,517
Prugniel, P., Maubon, G. & Simien, F. 2001, A&A, 366, 68
Puzia, T. H., Perrett, K. M., & Bridges, T. J. 2005, A&A, 434, 909
Puzia, T. H., Saglia, R. P., Kissler-Patig, M., Maraston, C., Greggio, L.,
Renzini, A., & Ortolani, S. 2002, A&A, 395, 45
Thomas, D., Maraston, C., Bender, R., & de Oliveira, C. M. 2005, ApJ, 621, 673
Thomas, D., Maraston, C., & Bender, R. (TMB) 2003, MNRAS, 339, 897
Trager, S. C., Faber, S. M., Worthey, G., & González, J. J. 2000b, AJ, 120, 165
Trager, S. C., Worthey, G., Faber, S. M., Burstein, D., & González, J. J. 1998, ApJS, 116, 1
Worthey, G. 1994, ApJS, 95, 107
Worthey, G., & Ottaviani, D. L. 1997, ApJS, 111, 377

THE THIN AND THICK DISKS OF THE GALAXY: DIFFERENCES IN EVOLUTION

Tetyana V. Nykytyuk[1] and Tamara V. Mishenina[2]

[1]*Main Astronomical Observatory, Kyiv, Ukraine*
[2]*Department of Astronomy, Odessa State University, Ukraine*

Abstract The chemical evolution of the Galactic disk was investigated in framework of the opened two-zone model with gas inflow. We suppose that the Galactic disk is divided in two zones — the thin and thick disks, which separate chemically and spatially and have different evolution timescales. The Galactic evolution of magnesium was investigated for the thin and thick disks. The obtained results show that the star formation history of the thin disk is more smooth and quiet than the star formation history of the thick disk of our Galaxy. Gas infall plays an important role in creating relative abundance differences between the thin and thick disk — the inflow rate is more intense for the thick disk.

Keywords: Galaxy: evolution; Galaxy: abundances; Galaxy: structure

1. Introduction

Recent studies of kinematics and ages of disk stars of our Galaxy show the presence of two distinct populations in the Galactic disk: the thick and the thin disk. The observations show that the disk subsystems: **1)** have different scale heights (Gilmore & Raid 1983) and velocity dispersions (Soubiran et al. 2003), **2)** were formed in different epochs (Fuhrmann 1998; Bensby et al. 2003), and **3)** have different chemical characteristics: mean metallicity of the thick disk population, <[Fe/H]>, covers the range between -0.5 and -0.7 dex, while the mean value of the thin disk star metallicity is -0.17 to -0.25 dex (Soubiran et al. 2003; Wyse & Gilmore 1995); the thin and thick disk α-element abundance trends are clearly separated at [Fe/H] < 0 (Fuhrmann 1998; Bensby et al. 2003; Gratton et al. 2000); the abundance trends for Mn, Ba and Eu are also different (Nissen et al. 2000; Mashonkina & Gehren 2000, 2001).

The abundance ratios depend on the stellar nucleosynthesis, stellar lifetimes, the initial mass function and the star formation history. This allows us to use the variations of [α/Fe] ratio as an indicator of the star formation history. Since the [α/Fe] tracks of the thick and thin disks have some distinctions, we

R. S. de Jong, Island Universes, 53–56.
© 2007 *Springer.*

suppose that star formation histories of the disk components must be different. Therefore, our aim is to find those parameters of the star formation history that reproduce the observed abundance trends of the thin and thick disks of the Galaxy.

2. The Model

The Galactic disk is divided into two zones — the thin and thick disks; the mass of gas, heavy elements, stars and stellar remnants are computed as a function of time for each component. The stellar nucleosynthesis and main equations of a galactic chemical evolution are described in detail by Nykytyuk (2003, 2004). We have used the stellar yields of Portinari et al. (1998), which give underestimated Mg values. We had to lower the predicted Mg yield from the stars with 9–15 $M_{\odot}$ by a factor of 1.5 so that the model results be in good agreement with the observations.

The star formation rate $\psi(t)$ in thick and thin disks is described by exponential function (Pilyugin & Edmunds 1996):

$$\psi(t) \sim \begin{cases} t \cdot e^{-t/T_{top}}, & \mathrm{t} \leq T_{top} \\ e^{-t/T_{sfr}}, & \mathrm{t} \geq T_{top} \end{cases}$$

where T_{top} and T_{sfr} are free parameters of a star formation rate.

It is supposed that an infall of unenriched intergalactic gas takes place on the disk during the galaxy's life. The infall rate is described by a function

$$A(t) = a_0 e^{-t/T_{inf}},$$

where T_{inf} and a_0 are free model parameters (Pilyugin & Edmunds 1996).

The star formation histories of disk components were chosen such that a majority of thick disk stars were formed 10–13 Gyr ago, while thin disk stars would have ages less then 10 Gyr. It is assumed that the age of the disk of our Galaxy equals 13 Gyr (Cowan et al. 1991).

3. The Results

Figure 1 shows the model prediction for thin disk. The model predictions demonstrated in Fig. 1 were obtained with the following parameters: T_{top} = 1 Gyr, T_{sfr} = 8 Gyr and T_{inf} = 5 Gyr.

The thin disk model with the above-mentioned parameter values reproduces the $[\mathrm{Mg/Fe}]$ –$[\mathrm{Fe/H}]$ ratio quite well. The thin disk model prediction for element abundances as a function of time are lower on average when compared with the Mishenina et al. (2004) observations.

The obtained values of the parameters of the thin disk evolution are in a good agreement with parameters of the best fit model of Pilyugin & Edmunds

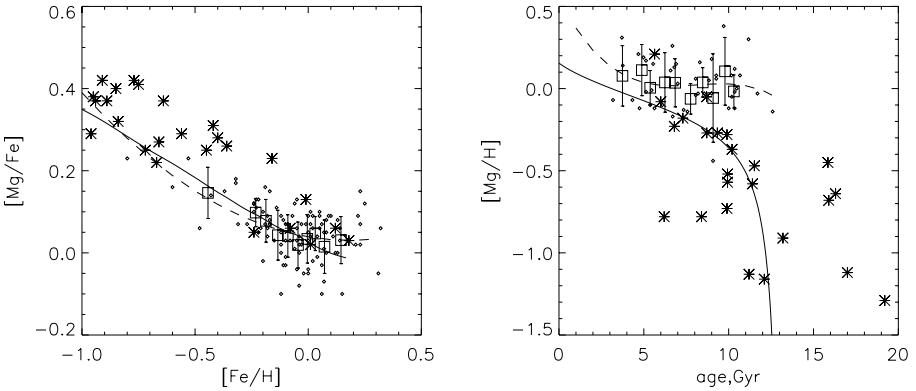

Figure 1. [Mg/Fe] vs [Fe/H] and [Mg/H] vs age diagrams for the thin disk of our Galaxy. The Galactic thin disk stars are marked by the small diamonds, the thick disk stars by the asterisks . The squares are mean observed thin disk data in 10 bins with equal numbers of stars. Dashed line is curve drawn by the least-squares method in the observed data of the thin disk. The prediction for the thin disk is indicated by solid line. Observed data are taken from Mishenina et al. (2004) and Bensby et al. (2003) (thick disk stars only).

(1996), having investigated the "age–[Fe/H]" and "age–[O/H]" ratios and the solar neighbourhood metallicity distribution function.

The model predictions for the thick disk are presented in the Fig. 2. The following parameters of thick disk evolution were found: T_{top} = 1 Gyr, T_{sfr}= 5 Gyr and T_{inf} = 7 Gyr. As Fig. 2 shows, the solid line of the prediction of thick disk model is in agreement with the dashed line obtained by least-squares fitting to the Mg relative abundance observations of thick disk stars.

Unfortunately, the number of stars belonging kinematically to the thin disk exceeds distinctly the number of stars belonging to the thick disk; there are not enough objects for which one can surely determine the ages. Therefore, the trend in the "age–[Mg/H] " diagram for the thick disk stars is less obvious than it is for the thin disk stars.

Under above mentioned model parameters we find that the star formation history of the thick disk was rather quick, as the majority of the thick disk stars in our model was formed during 2–3 Gyr and was almost stopped after 10 Gyr ago. On the contrary, the thin disk stars only begun to form 9–10 Gyr ago, and the star formation in the thin disk has gone smoothly, gradually going down to zero at our time.

The accretion of intergalactic gas has played a noticeable role in the evolution of the disk subsystems of our Galaxy. The model line of the relative abundances of the thin disk stars will change a location and approach the thick disk star region, if the mass of gas infalling on the disk at the each accretion

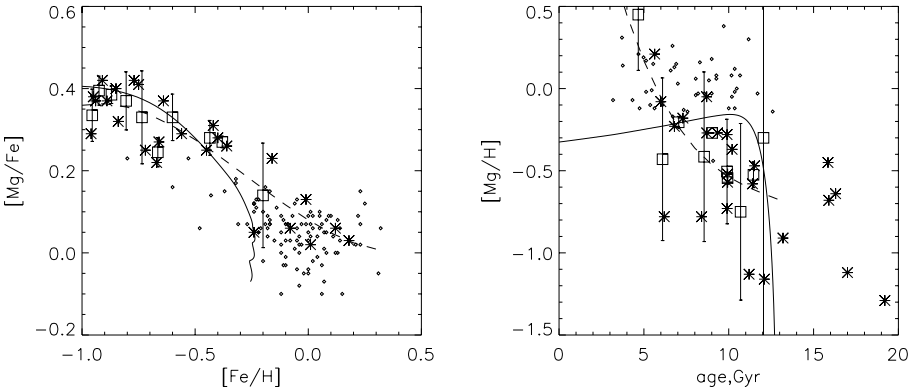

Figure 2. [Mg/Fe] vs [Fe/H] and [Mg/H] vs age diagrams for the thick disk of our Galaxy. Symbols are the same as in Fig. 1.

episode increases. In other words, the more massive accretion in a unit of time is a more characteristic feature for thick disk evolution than for thin disk.

Acknowledgements TN would like to thank Dr. H. Zondervan and the Conference Committee for the kind hospitality and partial financial support. The authors also wish to thank Drs. C. Travaglio, C. Soubiran and L.S. Pilyugin for fruitful discussion and valuable remarks.

References

Bensby, T. et al. 2003, A&A, 410, 527
Cowan, J.J. et al. 1991, ARA&A, 29, 447
Fuhrmann, K. 1998,A&A, 338, 161
Gilmore, G., Raid,N. 1983, MNRAS, 202, 1025
Gratton, R. et al. 2000, A&A, 358, 671
Mashonkina, L., Gehren, T. 2000, A&A, 364, 249
Mashonkina, L., Gehren, T. 2001, A&A, 376, 232
Mishenina, T.V. et al. 2004, A&A, 418, 551
Nissen P.E. et al. 2000, A&A, 353, 722
Nykytyuk T. 2003, KFNT, 19, 259
Nykytyuk T. 2004, KFNT, 20, 489
Pilyugin, L.S., Edmunds, M.G., 1996, A&A, 313, 783
Portinari, L. et al. 1998, A&A, 334, 505
Soubiran C. et al. 2003, A&A, 398, 141
Wyse, R.F.G., Gilmore, G. 1995, AJ, 110, 2771

THE MILKY WAY AND THE TULLY–FISHER RELATION

L. Portinari, J. Holmberg and C. Flynn

Tuorla Observatory, University of Turku, Finland

Abstract We present an updated estimate of the surface density and surface brightness in B, V, I of the local Galactic disc, based on a model for the "Solar cylinder" calibrated to reproduce Hipparcos and Tycho star counts. We discuss the mass-to-light ratio of the local stellar disc and infer the global luminosity of the Milky Way, which indicates it is underluminous with respect to the Tully–Fisher relation.

Keywords: Galaxy: fundamental parameters - Galaxy: disk - Galaxy: stellar content

1. Introduction

In the past two decades there has been a steady effort to determine the surface mass density of the local Galactic disc, excluding eventually any significant evidence for disc dark matter (e.g. Holmberg & Flynn 2000, 2004). As to luminosity, the infrared structure of the Milky Way seems well understood (Gerhard 2002), but studies in the optical typically date back to the '80s (de Vaucouleurs & Pence 1978; Ishida & Mikami 1982; Bahcall & Soneira 1980; van der Kruit 1986). Yet the surface luminosity and colours of the "Solar cylinder" are of great interest to compare to extragalactic studies, and to constrain chemo–photometric models of the Milky Way, which often serve as a calibration point for the systematic modelling of disc galaxies (Boisser & Prantzos 1999). Estimating the local multi–band surface brightness requires accurate knowledge of the vertical structure of the disc; in this respect, Galactic models have much improved after Hipparcos. Time is ripe for an update.

2. The Galactic Model and the Solar Cylinder

We derive the surface brightness of the local Galactic disc from the stellar census of the Hipparcos and Tycho catalogues, combined to a model for the vertical structure of the disc. The model consists of a thin disc, a thick disc and a stellar halo (irrelevant in this study). The vertical structure is modelled

R. S. de Jong, Island Universes, 57–60.
© 2007 *Springer.*

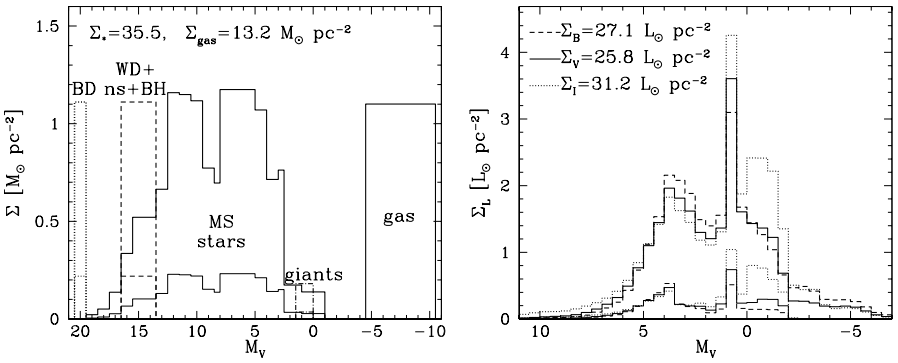

Figure 1. Mass model by Holmberg & Flynn (2004) and corresponding surface luminosity histograms in B, V, I. *Thick lines*: total mass/luminosity; *thin lines*: thick disc contribution.

as a series of components (e.g. Bahcall & Soneira 1980; van der Kruit 1988) with a different scaleheight for each component: main sequence stars of different M_V, red giants or supergiants. The V-band luminosity function and the colour distributions (B–V, V–I) vs. M_V are calibrated to reproduce the Hipparcos/Tycho star counts. The mass model is constrained from the kinematics and the vertical distribution of AF stars (within 200 pc) and of K giants (both local and out to $\sim$1 kpc toward the South Galactic Pole); for details see Holmberg et al. (1997) and Holmberg & Flynn (2000, 2004).

Figure 1 shows (a slightly updated version of) the mass model of Holmberg & Flynn (2004), and the corresponding B, V, I luminosity contribution of stars of different magnitude; the resulting global surface mass/luminosity densities are also indicated. The luminosity peak around $M_V \sim 0.5$ is due to clump giants; giant stars contribute 26 (40, 56) % of the B (V, I) surface luminosity.

Figure 2 lists the surface brightness and colours we derive for the local thin, thick and total disc, and the stellar mass-to-light ratio (M_*/L) of the Solar cylinder. We also compare our results to the theoretical colour–M_*/L relations predicted by the population synthesis models of Portinari et al. (2004) for different Initial Mass Functions (IMFs). Our Solar cylinder values are in excellent agreement with the predictions for the Kroupa and Chabrier IMFs, which have been derived for the Solar Neighbourhood — a successful consistency check.

3. From the Solar Cylinder to the Milky Way

From the surface luminosity (or density) at the Solar radius one can infer the total luminosity (or mass) of the Galactic disc by assuming an exponential profile, and the result is quite robust to the assumed scalelength R_d (e.g. Sommer–Larsen & Dolgov 2001). The Solar cylinder probes an inter-arm region so we must allow for the spiral arm contrast to derive the actual azimuthally averaged surface brightness at the Solar radius. We will henceforth focus on the I-band

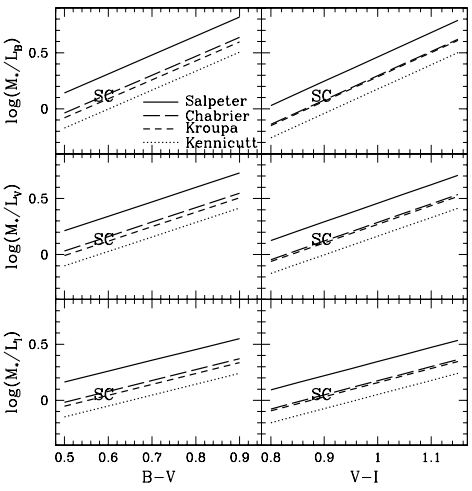

	thin disc	*thick disc*	*total*
μ_B	23.7	25.7	23.5
μ_V	23.1	24.8	22.9
μ_I	22.3	23.7	22.0
$(B–V)$	0.53	0.90	0.59
$(V–I)$	0.84	1.13	0.89

$\frac{M_*}{L_B}$	$\frac{M_*}{L_V}$	$\frac{M_*}{L_I}$
1.3	1.4	1.1

Figure 2. Model results for the surface brightness and colours of the Solar cylinder, and corresponding location with respect to the colour–M$_*$/L relations predicted for different IMFs.

as this is most typical for Tully–Fisher (TF) studies and spiral arms are not expected to induce major effects. In K-band the spiral arm enhancement is only about 10% (Drimmel & Spergel 2001; Gerhard 2002) and in the I-band the effect should be comparable (Rix & Zaritsky 1995). Figure 3a shows the total I-band luminosity and stellar mass of the Galactic disc inferred from the local surface brightness and density, including a 10% correction for spiral arms. We must further add the bulge contribution to get the total luminosity; the bulge K-band luminosity is $\sim 10^{10}$ L$_\odot$ (Kent et al. 1991; Gerhard 2002); we assume the same value in I-band, which is probably an overestimate as the bulge is mostly composed of red old populations. The total I-band luminosity of the Milky Way is thus $\sim 4 \times 10^{10}$ L$_\odot$, corresponding to $M_I \sim -22.4$. With a circular speed of $\sim 220\pm20$ km/s, the Milky Way turns out to be underluminous with respect to the TF relation defined by external spirals (Fig. 3b).

4. Conclusions

We have presented an updated estimate of the B, V, I surface brightness and colours of the "Solar cylinder" and reconstructed from the local disc brightness the total luminosity of the Milky Way, which appears to be underluminous with respect to the TF relation; although the discrepancy is not dramatic when considering the scatter in the TF relation and the uncertainty in the Milky Way values (20% assumed for the luminosity in Fig. 3). The offset might be partly due to a colour effect, if the Milky Way is a redder and earlier type spiral than the Sbc-Sc galaxies defining the TF relation (Portinari et al. 2004); however, the disc locally is quite blue ($B–V \sim 0.6$) which does not argue for significant

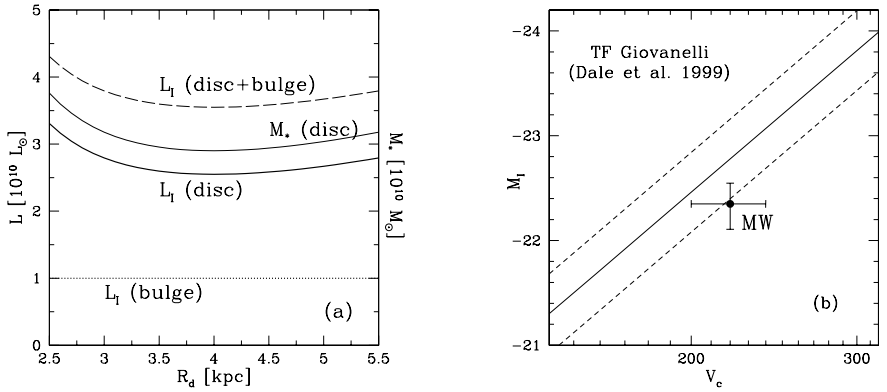

Figure 3. *(a)* Total I-band luminosity of the Milky Way inferred as a function of the assumed disc scalelength R_d. *(b)* Location of the Milky Way with respect to the I-band TF relation.

colour and M_*/L offsets between the Milky Way and Sbc–Sc spirals. All in all, the offset might indicate a problem with the luminosity zero–point of the TF relation, and/or with the M_*/L of disc galaxies. A similar conclusion is suggested also by semi–analytic models of galaxy formation (Dutton et al. 2004). The issue certainly deserves further investigation.

We are presently refining our I-band luminosity estimate with the aid of DENIS and other star counts, and defining better our errorbars; we are also extending our surface brightness determination to other photometric bands, especially in the infrared utilizing DENIS and 2MASS.

References

Bahcall J.N., Soneira R.M., 1980, ApJS 44, 73

Boissier S., Prantzos N., 1999, MNRAS 307, 857

Dale D.A., Giovanelli R., Haynes M.P., Campusano L.E., Hardy E., 1999, AJ 118, 1489

de Vaucouleurs G., Pence W.D., 1978, AJ 83, 1163

Drimmel R., Spergel D.N., 2001, ApJ 556, 181

Dutton A., van den Bosch F.C., Courteau S., Dekel A., 2004, in Baryons in Dark Matter Halos, R-J. Dettmar, U. Klein and P. Salucci (eds.), SISSA, Proceedings of Science, p. 50.1

Gerhard O.E., 2002, Space Science Reviews 100, 129

Ishida K., Mikami T., 1982, PASJ 34, 89

Holmberg J., Flynn C., 2000, MNRAS 313, 209

Holmberg J., Flynn C., 2004, MNRAS 352, 440

Holmberg J., Flynn C., Lindegren L., 1997, Hipparcos, ESA SP-402, p. 721

Kent S.M., Dame T.M., Fazio G., 1991, ApJ 378, 131

Portinari L., Sommer–Larsen J., Tantalo R., 2004, MNRAS 347, 691

Rix H.-W., Zaritsky D., 1995, ApJ 447, 82

Sommer–Larsen J., Dolgov A., 2001, ApJ 551, 608

van der Kruit P.C., 1986, A&A 157, 230

van der Kruit P.C., 1988, A&A 192, 117

THE CONTRIBUTION OF LSB GALAXIES TO THE LOCAL GALAXY NUMBER DENSITY

Clemens Trachternach*, Dominik J. Bomans, Lutz Haberzettl and Ralf-Juergen Dettmar

Astronomisches Institut Ruhr-Universitaet Bochum, Germany

* trachter@astro.rub.de

Abstract We present the results from a blind optical survey targeted on the Arecibo HI Strip Survey (AHISS). Object detection and profile fitting of the galaxies were done with automated algorithms. Our final catalogue is diameter-limited and contains 306 galaxies with diameters larger than $18''$; 148 of these galaxies were previously uncatalogued. Thereupon, we estimated the galaxy number density per square degree and compared it with other optical surveys and with the AHISS itself. Our number density is several times higher than the one from the AHISS. We discuss the selection effects for HI and optical surveys and point out the influence of different search algorithms and size estimation methods at the number density. The contribution of LSB galaxies to the local galaxy number density is about 30 % and thus not negligible.

Keywords:

1. Introduction

The importance of low surface brightness (LSB) galaxies has been established over the last ten years (e.g., Impey & Bothun 1997, Minchin et al. 2004). However, the detection of LSBs and their interpretation was influenced at all times by selection biases (e.g., Disney 1976) and the understanding of these biases. To avoid the problems resulting from the night sky brightness, HI surveys were considered as a possible alternative. Nevertheless, HI surveys are also biased due to selection effects. The question, which kind of survey is affected stronger by selection effects, if one wants to search for LSB galaxies, arises. With our work, we want to give some answers to this question. Furthermore, we want to test the influence of different object detection and data analysis methods on the galaxy number density.

R. S. de Jong, Island Universes, 61–64.
© 2007 *Springer.*

2. Data Reduction and Sample Selection

Our survey covers an effective area of 14.3 $\deg^2$ at a fixed declination of $14°12'$. This area was initially observed as a part of the blind AHISS. The data consists of two long strips in the *B*-band and was obtained at the 1.23m telescope at Calar Alto equipped with WWFPP and an exposure time of 900 s. The reduction of our data was done using an automated reduction pipeline which was specifically developed for mosaic CCD wide field imaging data (Erben et al. 2005).

Object detection. Our objects were detected using *SExtractor* (Bertin & Arnouts 1996). The use of an automated search algorithm yields several advantages (e.g., speed, uniformity in the object detection and reproducibility). Furthermore, it is possible to estimate the detection efficiency by using artificial galaxies as done in our forthcoming paper (Trachternach et al., in prep.). The star-galaxy separation was done by the use of the *SExtractor* CLASS_STAR parameter (CLASS_STAR ≤ 0.1). Thereby, 13.400 galaxy candidates remain.

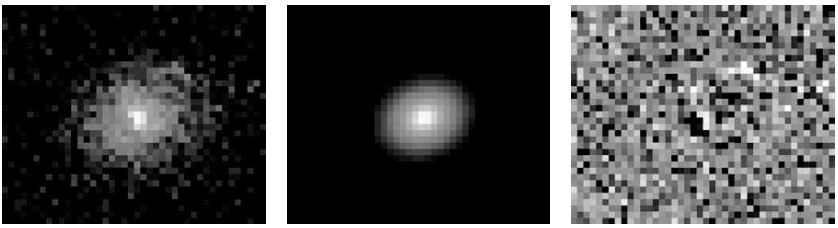

Figure 1. Thumbnail triplet of one of our galaxies. Original galaxy (left), model fit (middle) and residual image (right).

Galaxy Profile Fitting. Each of the 13.400 galaxies were fitted by an exponential profile using the galaxy fitting program Galfit (Peng et al. 2002). Galfit calculates several parameter for each galaxy and generates a triplet of thumbnails – one of the original object, a model fit and a residual image (see Figure 1). After the profile fitting, we calculated the central surface brightness. Furthermore, we have computed the sizes of our objects using the analytical function of the exponential profile in combination with the limiting surface brightness derived from *SExtractor*.

Restriction to the local universe. To remove the contribution of high redshifted galaxies, we applied a diameter criterion. A comparison with 26.000 objects from the 2dfGRS (Colless et al. 2001) showed that using a diameter limit of $18''$ restricts our sample approximately to $z \leq 0.1$. Cross-checks with

our objects which have published redshifts lead us to the same conclusion. After rejecting all galaxies with $d \leq 18''$ and manually sorting out misfitted objects and observational artifacts, 306 galaxies remain in our final catalogue.

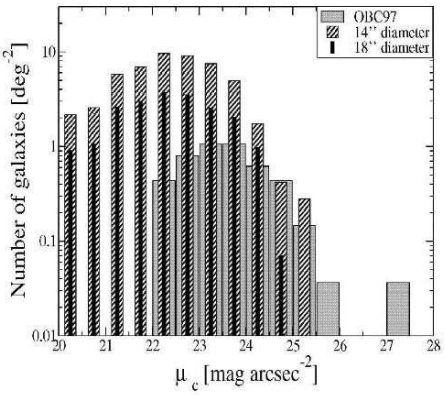

Figure 2. Number densities of our samples and the one from OBC97.

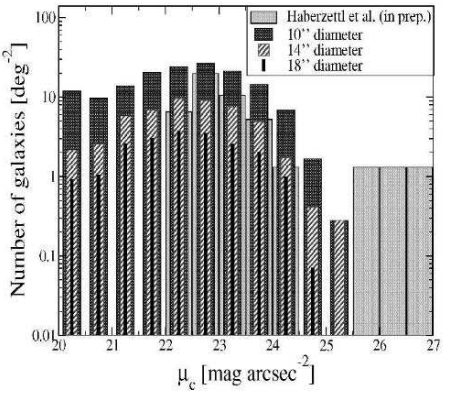

Figure 3. Number densities of our samples and the one from Haberzettl et al.

3. Results

Comparisons to other optical surveys. Figure 2 shows the comparison of our survey to the optical CCD survey from O'Neil et al. (1997, OBC97 from now on). OBC97 made their object detection and size estimation via the eye. Their limiting surface brightness is approximately $\mu_{\rm lim} \approx 27$ mag arcsec^{-2}, which is roughly two magnitudes fainter than the mean of ours ($\mu_{\rm lim} \approx 25.2$ mag arcsec^{-2}). Although our diameter limit is larger than theirs ($18''$ vs. $13\farcs5$), we found much more objects than they did. If we compare samples with the same diameter criterion, the difference is up to a factor of 5.

Another comparison is shown in Figure 3, where we compared the number density of several samples of our survey with the sample from Haberzettl et al. (2005, in prep.). Size estimation was again done visually, whereas object detection was done using *SExtractor*. Their survey is much deeper than ours ($\mu_{lim} \approx 29$ mag arcsec^{-2}) and they used a considerably smaller limiting diameter compared to us ($\mathrm{d} \geq 10\farcs75$). Although they are able to follow a galaxy to much fainter isophotes than we were able to do, the number density of their sample is comparable to our $\mathrm{d} \geq 14''$ sample. Putting these two comparisons together, we conclude that the eye is not as reliable for the detection of faint objects as an automated search algorithm. Moreover, the eye underestimates the galaxies' sizes meaning that the eye is not capable of following a galaxy as deep in the noise as we were able to do by using our analytical approach.

Comparison to the AHISS. The number density of our survey is 21.4 galaxies deg^{-2}, the one from the AHISS is 0.92 galaxies deg^{-2} (or 3 galaxies deg^{-2} if restricting the area to the one the main beam covered). All detected objects from the AHISS were found in our survey by our automated search algorithms. By comparing the number densities, one can see that our number density is 23.2 times as high as the one from the AHISS. (7.1 times by a comparison restricted to the main beam area). These differences are the result of the stronger selection effects for HI surveys in respect to optical surveys. The small search volume and the flux limit of the AHISS account for the major part of the differences between the number densities. If one extends the search volume by using better correlators, the problem of beam-filling and flux limitation becomes worse. Another selection effect is likely caused by the ionization of the neutral gas for column densities below $10^{19.5}\,\mathrm{cm}^{-2}$ due to extragalactic UV radiation (e.g., Sprayberry et al. 1998). Moreover, the column density decreases to a lower central surface brightness (e.g., Minchin et al. 2003). Thus, one needs extremely sensitive HI surveys to detect these low column densities of HI. Hence, optical surveys are – at least at the moment – more efficient in detecting LSB objects than HI surveys.

4. Conclusions

We conclude that HI surveys are – currently – less suitable than optical surveys for the detection of LSB galaxies in blind surveys due to stronger selection criteria. We show furthermore, that automated search algorithms rise the number density significantly and that a size estimation by the eye leads to underestimated sizes of the galaxies and therefore, if using a diameter limit, to a lower number density.

About 30 % of the galaxies from our survey are LSBs. Therefore, their contribution to the local galaxy number density and to the baryonic matter is not negligible.

References

Bertin, E. & Arnouts, S. 1996, A&AS 117, 393
Colless, M. et al. 2001, MNRAS 328, 1039
Disney, M. J. 1976, Nature 263, 573
Erben, T. et al. 2005, AN 326, 432
Haberzettl, L. et al. 2005, in prep.
Impey, C. D. & Bothun, G. D. 1997, ARA&A 35, 267
Minchin, R. F. et al. 2003, MNRAS 346, 787
Minchin, R. F. et al. 2004, MNRAS 355, 1303
O'Neil, K. et al. 1997, AJ 114, 2448
Peng , C. Y. et al. 2002, AJ 124, 266
Sprayberry, D. et al. 1998, ASP Conf. Ser. 136, 121
Zwaan, M. A. et al. 1997, ApJ 490, 173

II

KINEMATICS AND DYNAMICS OF DISK GALAXIES

DYNAMICS OF DISKS

James Binney

Rudolf Peierls Centre for Theoretical Physics, University of Oxford,UK
binney@thphys.ox.ac.uk

Abstract I review (i) the impact of spiral structure on the kinematics and chemistry of the solar neighbourhood and (ii) recent developments in the theory of warps. It has been suggested at age $\sim 3\,\mathrm{Gyr}$ the random velocity of a star saturates, but I show that this conjecture is excluded by Hipparcos data. Spiral structure dominates the heating of disks, but spirals don't just heat disks, they churn them. In the solar neighbourhood churning is required to explain the distribution of stars in age and metallicity. It seems likely that most of the chemically heterogeneous star streams of the solar neighbourhood owe their existence more to churning than to heating. A strong case can now be made that warps reflect misalignment between the symmetry axes of the outer dark halo and the inner disk. The inner halo is tightly coupled to the disk, so when modelling a warp it is essential to have a fully dynamical halo. Warps should now provide valuable probes of structure of dark halos in the region around visible galaxies.

Keywords: galaxies: kinematics and dynamics - stellar dynamics

1. Introduction

Galaxy disks are complex dynamical systems that are far from well understood. Within the last decade there have been important developments in our understanding of the impact that spiral structure has on the chemical and dynamical evolution of disks. Meanwhile the evidence has hardened that warps are symptoms of the misalignment of the outer and inner parts of galactic halos.

2. Disk Heating

We tend to think of waves as travelling perturbations that leave the medium that carries them unchanged after they have passed by. Actually some wave energy is always absorbed by the medium and heats it. Thus it has long been clear that spiral waves in disks must increase the random velocities of stars. An alternative heating mechanism, scattering of stars by giant gas clouds, was proposed by Spitzer & Schwarzschild (1953) and the relative importance of these two heating mechanisms was estimated by Jenkins & Binney (1990) from the

R. S. de Jong, Island Universes, 67–76.
© 2007 *Springer.*

axis ratio of the velocity ellipsoids near the Sun: σ_ϕ/σ_R is increased by cloud-scattering and reduced by wave heating. They concluded that wave heating strongly dominates.

Waves heat only resonant stars, and in a cool disk with a steady spiral pattern these stars are localised to narrow annuli around the Lindblad resonances. In the solar neighbourhood the random velocities of main-sequence stars are independent of colour for $B-V > 0.6$, but steadily increase with $B-V$ for $B-V < 0.6$ (Dehnen & Binney 1998 and Figure 1). The break in the $\sigma, B-V$ relation is called Parenago's discontinuity and occurs at the colour of stars that have main-sequence lifetimes comparable to the Hubble time. Parenago's discontinuity presumably arises because to the red of the discontinuity one sees all stars that have ever been formed, while as one moves blueward of it the oldest stars one sees get younger and younger, and young stars have not had time to pick up such large random velocities as old red stars.

Binney, Dehnen & Bertelli (2000; hereafter BDB) modelled the $\sigma, B-V$ relation and the number of main-sequence stars of each colour in a complete sample of nearly 12 000 stars with accurate Hipparcos parallaxes by assuming that the measured velocity dispersion of stars of age τ is

$$\sigma = v_{10}[(\tau+\tau_1)/(10\,\mathrm{Gyr}+\tau_1)]^\beta, \tag{1}$$

and that over the lifetime $\tau_{\max}$ of the disk the rate of formation of stars of mass M has been proportional to

$$M^{-\alpha}\exp(-\gamma t). \tag{2}$$

They were able to obtain good fits to the data for $\alpha \simeq 2.35$ (Salpeter value), $\beta \simeq 0.33$, $\gamma \simeq 0$, $\tau_1 \lesssim 0.03\,\mathrm{Gyr}$ and $\tau_{\max} \simeq 11\,\mathrm{Gyr}$. Thus BDB required the solar neighbourhood to be remarkably old, and to have formed at a very constant rate.

Edvardsson et al. (1993) obtained high-resolution spectroscopy and Strömgren photometry for a kinematically unbiased (but chemically biased) sample of 189 F and G dwarfs, and from these data Quillen & Garnett (2001) plotted velocity dispersion against age. Freeman & Bland-Hawthorn (2002) argued that these data show that the velocity dispersion rises with age only for $\tau \lesssim 3\,\mathrm{Gyr}$, and then flattens off until an age $\sim 9.5\,\mathrm{Gyr}$ is reached, where σ_R jumps by a factor $\gtrsim 1.5$. Such an evolution of σ with time would be consistent with a small value of the index β in equation (1), leading to rapid saturation of the wave-induced random velocities, combined with a merging event $9.5\,\mathrm{Gyr}$ ago, that abruptly increased the velocity dispersion of the disk that had formed by that time.

It is interesting to ask whether this interpretation of the Edvardsson et al. data is consistent with the much larger sample of Hipparcos stars discussed

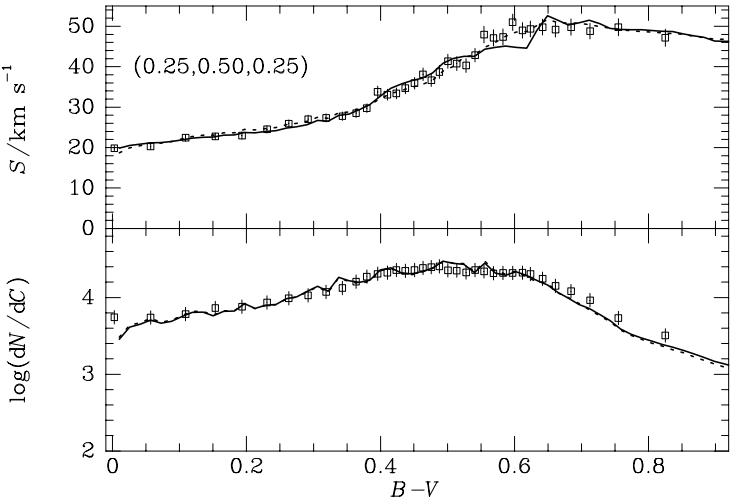

Figure 1. Top panel: velocity dispersion versus colour for a kinematically unbiased sample of main-sequence stars with accurate Hipparcos parallaxes (points) and two model curves. The dashed curve shows the steady-acceleration model whose parameters occur at the top of Table 2 of BDB. The full curve is for a model inspired by Freeman & Bland-Hawthorn (2002) and described in the text. Lower panel: number of stars at each colour in the data and in the model predictions.

by BDB. Figure 1 shows the Hipparcos data as points, and the predictions of two models as curves. The dashed curve shows a model from BDB: for this model the parameters in equations (1) and (2) are $\alpha = 2.26$, $\beta = 0.328$, $\gamma = -0.006$, $v_{10} = 58.1\,\mathrm{km\,s^{-1}}$, and $\tau_1 = 0.03\,\mathrm{Gyr}$, while the age of the disk is $\tau_{\max} = 11.2\,\mathrm{Gyr}$. The full curves in Figure 1 are for a model in which the velocity dispersion varies with age τ as

$$\sigma = \begin{cases} v_3[(\tau+\tau_1)/(3\,\mathrm{Gyr}+\tau_1)]^\beta & \text{for } \tau < 3\,\mathrm{Gyr}, \\ v_3 & \text{for } 3\,\mathrm{Gyr} \le \tau < 9.5\,\mathrm{Gyr}, \\ 1.5v_3 & \text{otherwise} \end{cases} \qquad (3)$$

as suggested from the Edvardsson sample. The parameters of this model are $\alpha = 2.29$, $\beta = 1.05$, $\gamma = 0.051$, $\tau_1 = 1.99\,\mathrm{Gyr}$, $v_3 = 45.0\,\mathrm{km\,s^{-1}}$, and $\tau_{\max} = 12\,\mathrm{Gyr}$. The parameter-optimization routine that successfully fitted to the data the dashed model based on equation (1) is clearly less successful when working from equation (3): the model falls unacceptably below the data between $B-V = 0.55$ and 0.64 as a consequence of the assumption that acceleration saturates after 3 Gyr. From this result I conclude that acceleration does not saturate at 3 Gyr, and that the contention of Freeman & Bland-Hawthorn (2002) that it does arises from an over-interpretation of the rather sparse and unrepresentative Edvardsson et al. sample. This conclusion is consistent with

the age–velocity dispersion relations derived by Gomez et al. (1998) from a different sample of Hipparcos stars – see their Figure 2.

3. Churning by Spirals

A crucial finding of Edvardsson et al. (1993) was that stars are scattered widely in the age-metallicity plane. In the conventional picture of galactic chemical evolution, the ISM at any galactocentric radius has a well defined metallicity that increases steadily with time. Consequently, all stars formed at the same time at the same radius should have the same metallicity Z. The Evdardsson et al. data imply either that there is a wide spread in the metallicity of the ISM at a given radius, or that the stars that are currently in the solar neighbourhood were formed at a wide variety of different radii.

Since stars have non-zero epicycle radii, it is clear that stars *do* move in radius, but it is straightforward to show that such movement is insufficient to account for the Edvardsson et al. data. Consider, for example, stars of age $5\,\mathrm{Gyr}$, which have $\log(Z/Z_0)$ in the range $(-0.4, 0.15)$. The radial velocity dispersion of these stars is $\sim 30\,\mathrm{km\,s^{-1}}$, so we have $v_R(\mathrm{max}) \sim 30\sqrt{2}\,\mathrm{km\,s^{-1}}$, which implies an epicycle amplitude $X \simeq 30\sqrt{2}\,\mathrm{km\,s^{-1}}/\kappa \simeq 1.2\,\mathrm{kpc}$, where $\kappa \simeq 36\,\mathrm{km\,s^{-1}}$ is the epicycle frequency. Equation (14) of Sellwood & Binney (2002) gives the change in the metallicity of the present-day ISM as $\delta\log(Z) = -0.96\delta R/R$, so stars born now at $R_0 \pm 1.2\,\mathrm{kpc}$ will be spread in metallicity by $\delta\log(Z) \simeq \pm 0.14$. If the metallicity of the ISM is everywhere increasing, as is probably the case, the range in metallicity will be somewhat narrower, whereas the measured range is nearly a factor of 2 larger.

Sellwood & Binney (2002) showed that a single transient spiral feature can shift the guiding centre of a star near corotation by $2 - 3\,\mathrm{kpc}$. The guiding-centre shifts of stars are correlated in the sense that all stars with one orbital phase relative to the spiral pattern move outwards, and an equal number with different phases move inward, with the result that the distribution of mass within the disk is unchanged. Since the gravitational potential energy of the disk is unaffected by the shifts, they do not have a tendency to heat the disk. However, the shifts do "churn" the disk in the sense that they mix the disk chemically. Churning explains the absence of a well defined metallicity-age relation: the old, metal-rich stars in the Edvardsson et al. sample were born at small radii where the metallicity quickly rose to near-solar values, and have had their guiding centres increased to near R_0. Conversely, a small number of young stars with $\log(Z/Z_0) \lesssim -0.4$ arise because some stars born at $R > R_0$ have migrated inwards.

Star streams

Hipparcos data enable one to determine the density of stars in velocity space near the Sun. Jeans' theorem implies that the isodensity surfaces should approximately coincide with the ellipsoids $U^2+\gamma^2V^2+\epsilon W^2 = \text{constant}$, where $\gamma = 2\Omega/\kappa$, with Ω the circular frequency. This expectation was confounded by Dehnen (1998), who showed that the projection of the velocity-space density onto the (U, V) plane is far from smooth and ellipsoidal. In fact, a substantial faction of the stars seem to be associated with streams that are centred on velocities that differ markedly from the local standard of rest.

It has been known for a very long time that some stars form streams. The standard explanation of this phenomenon is that each stream is a dispersing association or cluster, that has been tidally disrupted. If this hypothesis were valid, the members of any given stream should have very similar ages and metallicities. Famaey et al. (2005), who had not only proper motions and parallaxes but also spectroscopy, were able to locate individual stars in velocity space, rather than simply deriving the density of stars in a statistical manner, as Dehnen (1998) had done from Hipparcos data alone. They found that some of Dehnen's star streams contain stars with many different ages and metallicities, so they are not disrupting star clusters. Rather they must be groups of previously unrelated stars that have acquired similar peculiar velocities because they happen to have similar orbital phases with respect to a non-axisymmetric feature in the Galaxy's gravitational potential.

Dehnen (2000) made a strong case that the most extended of these streams, the Hercules stream, is comprised of stars that are resonantly trapped by the Galactic bar. Quillen & Minchev (2005) have suggest that the Pleiades/Hyades and Coma Berenices streams are generated by a two-armed spiral perturbation with a pattern speed such that the Sun lies near the 4:1 inner Lindblad resonance. Desimone, Wu & Tremaine (2004) investigated the impact on the local velocity space of a sequence of spirals that were transient rather than long-lived and therefore had less well-defined pattern speeds. When studied with the resolution of current data, the structures generated by these perturbations look moderately like the observed features, but to some extent share with the work of Quillen & Minchev (2005) the fault of producing features that are too narrow in U and too broad in V. An interesting and inadequately explored possibility is that in these heterogeneous star streams we are seeing in action the shift mechanism discussed by Sellwood & Binney (2002).

4. Warps

Despite four decades of work, there is still no consensus on the origin of warps. Warps become pronounced beyond the radius at which even a maximum disk model predicts that dark matter makes a large contribution to the

rotation curve, so it has been clear for a long time that the dynamics of warps involves, and is a probe of, the dark halo (Binney 1978). For over a decade the field was dominated by the idea of Toomre (1983) and Dekel & Shlosman (1983) that warps are "normal modes" of disks in which a fixed pattern steadily precesses in the external gravitational field of an aspherical halo (Sparke & Casertano 1988). Within the last decade it has been realized that the vertical response of the halo to the cusped gravitational field of the disk cannot be ignored. Nelson & Tremaine (1995) estimated the energy that would be gained by halo particles in the time-varying potential of the disk, and showed that it would very quickly exceed the energy of the warp, which is small. From this calculation they argued that the warp would be quickly damped. Binney, Jian & Dutta (1998) followed the dynamics of a disk of massive rings embedded in an N-body halo and showed that before the warp can damp, it distorts the halo sufficiently to change radically the torques acting on each ring, which in a normal mode are nicely adjusted to cause all rings to precess at the same rate. Consequently, a disk that is configured to be a normal mode of a rigid halo is almost immediately not a normal mode of the actual halo, and its warp winds up in a few dynamical times. The net result of this winding up is to convert the warp's energy into heat within the disk rather than within the halo, as Nelson & Tremaine had conjectured.

The failure of the normal-mode model prompted Jiang & Binney (2000; hereafter JB) to re-examine the possibility that warps are steadily forced by infall. They again simulated the disk as a series of rings embedded in an N-body halo, but now they started with the disk flat and aligned with the equatorial plane of the halo. Then they added particles to the halo on near-circular but inclined orbits. They found that the resulting enhancement in the density of the halo in the inclined torus within which mass was injected caused the disk to become warped in a fairly realistic way.

In his Rutgers thesis Juntai Shen has recently significantly improved on the models of JB in several respects. First his disks are made of stars rather than rings, which makes them more rigid since radial oscillations of stars directly couple adjacent annuli. Second his disks extend to $8R_d$, where R_d is the exponential disks' scale length, rather than to $4R_d$ as in JB. Third his simulations contain ~ 12 times as many particles as those of JB.

Rather than injecting particles with off-axis angular momentum as JB did, Shen simply adds in the potential of a slowly growing inclined ring of mean radius $15R_d$; the final mass of the torus is 2.5 times the mass of the disk. He argues that this torus would evolve dynamically on such a long timescale that its own dynamics can be ignored.

As Figure 2 shows, the torus distorts the initially flat stellar disk into a warp that is strikingly reminiscent of warps observed in HI. Moreover, Shen finds that these warps conform to Briggs (1990) rules of HI warps, namely: (i) the

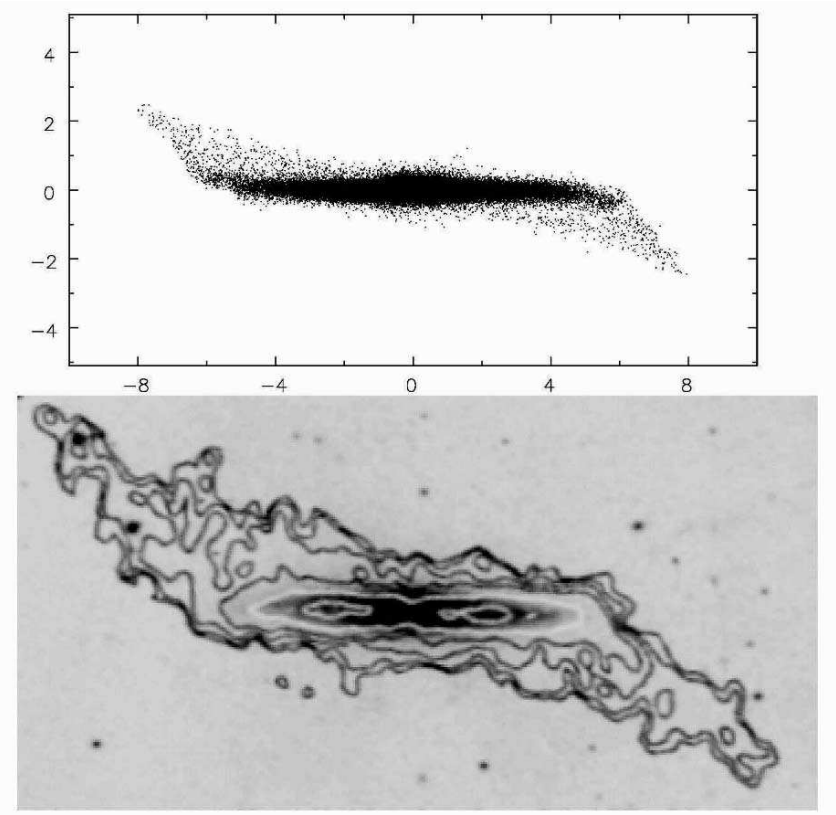

Figure 2. (top) The warp excited in a simulated stellar disk by Shen (2005) and (bottom) the HI warp of NGC 4013 observed by Bottema (1996).

disk is planar at $R \lesssim R_{25} \simeq 3R_d$ and becomes warped between R_{25} and the Holmberg radius ($R_{26.5} \simeq 4.4R_d$); (ii) the line of nodes is fairly straight inside $R_{26.5}$; (iii) outside $R_{26.5}$ the line of nodes is a loosely-wound leading spiral.

Shen confirms the result of Binney, Jiang & Dutta (1998) that at each radius the halo aligns with the local disk. The quadrupole field of the torus forces slow retrograde precession of the flat inner disk. Outer annuli of the disk are more strongly torqued by the torus, and in the absence of disk self-gravity precess faster than the inner disk, causing the line of nodes to be a trailing spiral. When the disk is realistically massive, torques on outer annuli from the inner disk slow the precession of the outer annuli so much that the line of nodes becomes a leading spiral.

The tori that drive the warp in the simulations of JB and Shen (2005) are artificial devices inspired by the idea that material that is being accreted with off-axis angular momentum would form such a torus. Polar-ring galaxies, the Magellanic stream and the ring of tidal debris from the Sagittarius dwarf galaxy

constitute hard evidence that material with off-axis angular momentum is accreted, but the mass of such material is uncertain because it depends on how much dark matter is being accreted alongside the detected baryonic matter. In fact probably the way forward is to use warps to probe the shape of the halo outside the disk, and to relate this to the visible manifestations of accretion.

5. Conclusions

Understanding disks is fundamental to understanding the structure and formation of galaxies: through most, perhaps all, of cosmic history they have been the main sites of star formation, and they are also sensitive dynamical probes of the gravitational potentials and thus mass distributions of their host galaxies. We are fortunate to live at a strategic location in a typical disk, and the last few years have been notable for a rapidly spreading appreciation of the window this gives us on the galaxy-formation process (e.g., Freeman &Bland-Hawthorn 2002).

Spiral structure is fundamental to galactic disks but we are only just beginning to understand the profound affects it has on the kinematics and chemistry of the solar neighbourhood. The tendency of spiral structure to heat disks is well known but is confined to Lindblad resonances. At corotation spiral structure has a major impact on the chemistry of the disk, but leaves the kinematic unchanged. Observations of the solar neighbourhood show that this second process, "churning", is an important one, and it seems likely that it is responsible for the existence of heterogeneous star streams.

It may be that after forty years of fumbling we finally have a grip on the origin of warps. If so, there is tremendous potential for using this widespread phenomenon to probe the dark halo and mass accretion outside disks in a way that will complement the use of spiral structure and bar dynamics to probe the dark halo within the visible parts of galaxies. The picture of the centres of dark halos that emerges from these studies conflicts with the predictions of standard CDM cosmology in interesting ways. Will these predictions fare better when tested in the circumgalactic environment? The next few years promise to be interesting.

References

Binney, J., 1978, MNRAS, 183, 779

Binney, J., Jiang, I.-G. & Dutta, S., 19998, MNRAS, 297, 1237

Binney, J., Dehnen, W. & Bertelli, G., 2000, MNRAS, 318, 658 (BDB)

Bottema, R., 1996, A&A, 306, 345

Briggs, F.H., 1990, ApJ, 352, 15

Dekel A. & Shlosman I., 1983, in IAU Symposium 100, 'Internal Kinematics and Dynamics of Galaxies', ed. E. Athanassoula, Dordrecht, Reidel, p. 187

Dehnen, W., 1998, AJ, 115, 238

Dehnen, W., 2000, AJ, 119, 800
Dehnen, W. & Binney, J., 1998, MNRAS, 298, 387
De Simone, R., Wu, X. & Tremaine, S., 2004, MNRAS, 350, 627
Edvardsson, B., Andersen, B., Gustafsson, B., Lambert, D.L., Nissen, P.E., Tomkin, J., 1993, A&A, 275, 101
Famaey, B., Jorissen, A., Luri, X., Mayor, M., Udry, S., Dejonghe, H. & Turon, C., 2005, A&A, 430, 165
Freeman, K.C. & Bland-Hawthorn, J., 2002, ARA&A, 40, 487
Gomez, A., Grenier, S., Udry, S., Haywood, M., Meillon, L., Sabas, V., Sellier, A., Morrin, D., 1998, in "Hipparcos–Venice '97", 621, ESA
Jenkins, A. & Binney, J., 1990, MNRAS, 245, 305
Jiang, I.-G. & Binney, J., 2000, MNRAS, 314, 468 (JB)
Nelson R.W., Tremaine S., 1995, MNRAS, 275, 897
Quillen & Garnett 2001
Quillen, A.C. & Minchev, I., 2005, AJ, 130, 576
Sellwood, J.A. & Binney, J., 2002, MNRAS, 336, 785
Shen, J., 2005, Rutgers University PhD Thesis.
Sparke, L.S. & Casertano, S., 1988, MNRAS, 234, 873
Spitzer, L. & Schwarzschild, M., 1953, ApJ, 118, 106
Toomre, A., 1983, in IAU Symp. 100, 'Internal Kinematics and Dynamics of Galaxies', ed. E. Athanassoula, Reidel, Dordrecht, p. 177

Renzo Sancisi, Giuseppe Bertin, and Tjeerd van Albada.

Ignacio Trujillo, Matthew Bershady, and Michael Pohlen.

CIRCULAR VELOCITY AND CENTRAL VELOCITY DISPERSION IN LOW SURFACE BRIGHTNESS GALAXIES

E.M. Corsini[1*], A. Pizzella[1], E. Dalla Bontà[1], F. Bertola[1], L. Cocato[2] and M. Sarzi[3]

[1] *Dipartimento di Astronomia, Università di Padova, Italy*

[2] *Kapteyn Astronomical Institute, University of Groningen, The Netherlands*

[3] *Physics Department, University of Oxford, UK*

* corsini@pd.astro.it

Abstract We analyzed a sample of high and low surface brightness (HSB and LSB) disc galaxies and elliptical galaxies to investigate the correlation between the circular velocity (V_c) and the central velocity dispersion (σ_c). We better defined the previous V_c–σ_c correlation for HSB and elliptical galaxies, especially at the lower end of the σ_c values.

Elliptical galaxies with V_c based on dynamical models or directly derived from the HI rotation curves follow the same relation as the HSB galaxies in the V_c–σ_c plane. On the contrary, the LSB galaxies follow a different relation, since most of them show either higher V_c (or lower σ_c) with respect to the HSB galaxies. This argues against the relevance of baryon collapse in the radial density profile of the dark matter haloes of LSB galaxies. Moreover, if the V_c–σ_c relation is equivalent to one between the mass of the dark matter halo and that of the supermassive black hole, these results suggest that the LSB galaxies host a supermassive black hole with a smaller mass compared to HSB galaxies of equal dark matter halo. On the other hand, if the fundamental correlation of SMBH mass is with the halo V_c, then LSBs should have larger black hole masses for given bulge σ_c.

Keywords: galaxies: elliptical and lenticular, cD – galaxies: fundamental parameters – galaxies: kinematics and dynamics – galaxies: spirals

1. Introduction

A possible relation between the central velocity dispersion of the spheroidal component (σ_c) and the galaxy circular velocity (V_c) measured in the flat region of the rotation curve (RC) was suggested by Whitmore et al. (1979). By measuring stellar velocity dispersions and HI line widths for a sample of 19

R. S. de Jong, Island Universes, 77–82.
© 2007 *Springer.*

spiral galaxies they found a a significant decrease in V_c/σ_c with increasing bulge-to-disk ratio. Since σ_c and V_c probe the potential of the spheroid and dark matter (DM) halo, a mean value $V_c/\sigma_c \simeq 1.7$ implies these components are dynamically separate with the bulge substantially cooler than halo.

Gerhard et al. (2001) derived the V_c–σ_c relation for the sample of giant elliptical galaxies studied by Kronawitter et al. (2000). This was explained as an indication of near dynamical homology of these objects which were selected to be nearly round and almost non-rotating elliptical galaxies. These galaxies form a unique dynamical family which scales with luminosity and effective radius. As a consequence the maximum V_c of the galaxy is correlated to its σ_c. Whether the same is true for more flattened and fainter ellipticals is still to be investigated. On the contrary, both shape and amplitude of the RC of a spiral galaxy depend on the galaxy luminosity and morphological type (e.g., Burstein & Rubin 1985). As a consequence for spiral galaxies the V_c–σ_c relation is not expected a priori.

Nevertheless, Ferrarese (2002) and Baes (2003) found that elliptical and spiral galaxies define a common V_c–σ_c relation. In particular, they find that for a given σ_c the value of V_c is independent of the morphological type. But σ_c and V_c are related to the mass of the supermassive black hole (hereafter SMBH, see Ferrarese & Ford 2005 for a review) and DM halo (e.g., Seljak 2002), respectively. Therefore Ferrarese (2002) argued that the V_c–σ_c relation is suggestive of a correlation between the mass of SMBH and DM halo.

Previous works concentrated on high surface brightness (HSB) galaxies. It is interesting to investigate whether the V_c–σ_c relation holds also for less dense objects characterized by a less steep potential well. This is the case of low surface brightness (LSB) galaxies, which are disc galaxies with a central face-on surface brightness $\mu_B \geq 22.6$ mag arcsec^{-2} (e.g., Impey et al. 1996). In Pizzella et al. (2005) we studied the behavior of LSB galaxies in the V_c–σ_c relation. Here we present our results.

2. Sample Selection

In the past years we started a scientific program aimed at deriving the detailed kinematics of ionized gas and stars in HSB and LSB galaxies in order to study their mass distribution and structural properties (e.g., Pignatelli et al. 2001).

We measured the velocity curves and velocity dispersion profiles along the major axis for both the ionized-gas and stellar components for a preliminary sample of 50 HSB galaxies [10 S0–S0/a's in Corsini et al. (2003); 7 Sa's in Bertola et al. (1996) and Corsini et al. (1999); 16 S0–Sc's in Vega Beltran et al. (2001); 17 Sb–Scd's in Pizzella et al. (2004a)] and 11 LSB galaxies (Pizzella et al. 2004b). The HSB sample consists of disc galaxies with Hubble

type ranging from S0 to Scd, an inclination $i \geq 30^\circ$ and a distance $D < 80$ Mpc. The LSB sample consists of disc galaxies with Hubble type ranging from Sa to Irr, an intermediate inclination ($30^\circ \leq i \leq 70^\circ$), and a distance $D < 65$ Mpc. In order to complete our sample of disc galaxies we included the 38 Sa-Scd galaxies previously studied by Ferrarese (2002) and the 12 Sb-Sc galaxies by Baes et al. (2003).

Finally, we considered a sample of 24 elliptical galaxies with a flat RC and for which both V_c and σ_c are available from the literature. They include 19 objects studied by Kronawitter et al. (2000) who derived V_c by dynamical modeling and 5 objects studied by Bertola et al. (1993) for which V_c is directly derived from the flat portion of their HI RCs. The addition of these galaxies will allow to test against model-dependent biases in the V_c– σ_c relation.

3. Measuring V_c and σ_c

For all the disc galaxies we obtained the ionized-gas RC. We rejected galaxies with asymmetric RCs or RCs which were not characterized by an outer flat portion. The flatness of each RC has been checked by fitting it with a linear law $V(R) = AR + B$ for $R \geq 0.35\ R_{25}$. The radial range has been chosen in order to avoid the bulge-dominated region. The RCs with $|A| \geq 2\ \mathrm{km\ s^{-1}\ kpc^{-1}}$ within 3σ have been considered not to be flat. We derived V_c by averaging the outermost values of the flat portion of the RC. We derived σ_c from the stellar kinematics by extrapolating the velocity dispersion radial profile to the centre. This has been done by fitting the innermost data points with an empirical function (either an exponential, or a Gaussian or a constant). We did not apply any aperture correction to σ_c as discussed by Pizzella et al. (2004a).

For the elliptical galaxies we obtained V_c either from the dynamical models by Gerhard et al. (2001) or from the flat portion of the HI RC. For these galaxies we relaxed the flatness criterion in favor of their large radial extension which is about 10 times larger than that of optical RCs. Aperture measurements of the stellar velocity dispersion corrected to $r_e/8$ were adopted to estimate σ_c.

4. The V_c– σ_c Relation for HSB and Elliptical Galaxies

In summary, we have 40 disc galaxies [15 from our preliminary sample, 16 from Ferrarese (2002), and 9 from Baes et al. (2003) with flat RCs extending to $\sim\ 0.8\ R_{25}$] and 24 elliptical galaxies [19 from Kronawitter et al. (2000) with flat RCs extending to about $\sim\ 0.5\ R_{25}$, 5 from Bertola et al. (1993) with flat HI RCs extending to $\sim\ 3\ R_{25}$].

A power law has been usually adopted to describe the correlation between V_c and σ_c for galaxies with $\sigma_c > 80\ \mathrm{km\ s^{-1}}$. We find

$$\log V_c = (0.74 \pm 0.07)\ \log \sigma_c + (0.80 \pm 0.15) \qquad (1)$$

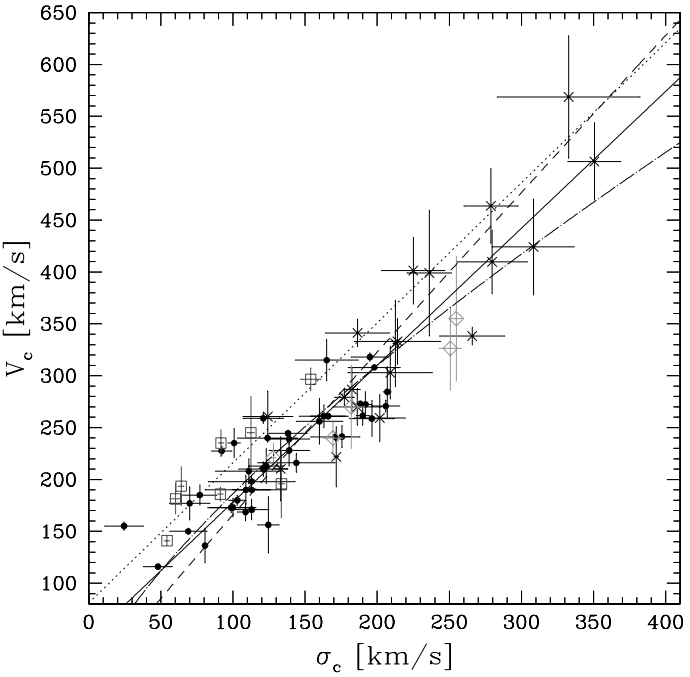

Figure 1. The correlation between V_c and σ_c. The data points corresponding to HSB galaxies (*filled circles*), LSB galaxies (*squares*), and elliptical galaxies with V_c obtained from HI data (*diamonds*) or dynamical models (*crosses*) are shown. The *dash-dotted* and *continuous line* represent the power-law (Eq. 1) and linear fit (Eq. 2) to HSB and elliptical galaxies. The *dotted line* represents the linear-law fit (Eq. 3) to LSB galaxies. For a comparison, the *dashed line* corresponds to the power-law fit to spiral galaxies with $\sigma_c > 80$ km s^{-1} by Baes et al. (2003).

with V_c and σ_c expressed in $\mathrm{km\ s^{-1}}$. The resulting power law is plotted in Fig. 1 (dash-dotted line). However, according to a χ^2 analysis the data are also consistent with a linear law out to velocity dispersions as low as $\sigma_c \approx 50$ $\mathrm{km\ s^{-1}}$

$$V_c = (1.32 \pm 0.09)\,\sigma_c + (46 \pm 14). \tag{2}$$

The resulting straight line is plotted in Fig. 1 (continuous line).

The data points corresponding to the 5 elliptical galaxies with V_c based on HI data follow the same relation as the remaining disc and elliptical galaxies. They are mostly located on the upper end of the V_c–σ_c relation derived for disc galaxies, in agreement with the findings of Bertola et al. (1993). They studied these elliptical galaxies and showed that their DM content and distribution are similar to those of spiral galaxies.

5. The V_c–σ_c Relation for LSB Galaxies

The LSB and HSB galaxies do not follow the same V_c–σ_c relation. In fact, most of the LSB galaxies are characterized by a higher V_c for a given σ_c (or a lower σ_c for a given V_c) with respect to HSB galaxies. By applying to the LSB data points the same regression analysis which has been adopted for the HSB and elliptical galaxies of the final sample, we find

$$V_c = (1.35 \pm 0.19)\,\sigma_c + (81 \pm 23) \tag{3}$$

with V_c and σ_c expressed in $\mathrm{km\ s^{-1}}$. The straight line corresponding to this fit, which is different from the one obtained for HSB and elliptical galaxies and happens to be parallel to it, is plotted in Fig. 1 (dotted line). To address the significance of this result, which is based only on 8 data points, we compared the distribution of the normalized scatter of the LSB galaxies to that of the HSB and elliptical galaxies. They are different at a high confidence level ($> 99\%$) by a Kolmogorov-Smirnov test. The fact that these objects fall in a different region of the V_c–σ_c plane confirms that LSB and HSB galaxies constitute two different classes of galaxies.

6. Conclusions

Both demographics of SMBHs and study of DM distribution in galactic nuclei benefit from the V_c–σ_c relation. The recent finding that the mass of SMBHs correlates with different properties of the host spheroid supports the idea that formation and accretion of SMBHs are closely linked to the formation and evolution of their host galaxy. A task to be pursued is to obtain a firm description of all these relationships spanning a wide range of SMBH masses and address if they hold for all Hubble types. In fact, the current demography of SMBHs suffers of important biases, related to the limited sampling over the different basic properties of their host galaxies. The finding that the V_c–σ_c relation holds for small values of σ_c points to the idea that SMBHs with masses $\mathrm{M_\bullet} < 10^6\ \mathrm{M_\odot}$ may also exist and follow the $\mathrm{M_\bullet}$-σ relation.

Moreover, it has been suggested that the V_c–σ_c relation is equivalent to one between the masses of SMBH and DM halo (Ferrarese 2002; Baes 2003) because σ_c and V_c are related to the masses of the central SMBH and DM halo, respectively. Yet, this claim is to be considered with caution, as the demography of SMBHs is still limited, in particular as far as spiral galaxies are concerned. Furthermore, the calculation of the virial mass of the DM halo from the measured V_c depends on the assumptions made for the DM density profile and the resulting rotation curve (e.g., see the prescriptions by Seljack et al. 2002). A better estimate of the virial velocity of the DM halo V_{vir} can be obtained by constraining the baryonic-to-dark matter fraction with detailed dynamical modeling of the sample galaxies. The resulting V_{vir}–σ_c relation

is expected to have a smaller scatter than the V_c–σ_c relation. If the $M_\bullet$-σ relation is to hold, the deviation of LSB galaxies *with bulge* from the V_c–σ_c of HSB and elliptical galaxies suggests that for a given DM halo mass the LSB galaxies would host a SMBH with a smaller mass compared to HSB galaxies. On the other hand, if the fundamental correlation of SMBH mass is with the halo V_c, then LSBs should have larger black-hole masses for given bulge σ_c. This should be accounted for in the theoretical and numerical investigations of the processes leading to the formation of LSB galaxies.

The collapse of baryonic matter can induce a further concentration in the DM distribution, and a deepening of the overall gravitational well in the central regions. If this is the case, the finding that at a given DM mass (as traced by V_c) the central σ_c of LSB galaxies is smaller than in their HSB counterparts, would argue against the relevance of baryon collapse in the radial density profile of DM in LSB galaxies.

References

Baes, M., Buyle, P., Hau, G. K. T., & Dejonghe, H. 2003, MNRAS, 341, L44
Bertola, F., Cinzano, P., Corsini, E. M., et al. 1996, ApJ, 458, L67
Bertola, F., Pizzella, A., Persic, M., & Salucci, P. 1993, ApJ, 416, L45
Burstein, D., & Rubin, V. C. 1985, ApJ, 297, 423
Corsini, E. M., Pizzella, A., Sarzi, M., et al. 1999, A&A, 342, 671
Corsini, E. M., Pizzella, A., Coccato, L., & Bertola, F. 2003, A&A, 408, 873
Ferrarese, L. 2002, ApJ, 578, 90
Ferrarese, L., & Ford, H. 2005, Space Science Rev., 116, 523
Gerhard, O., Kronawitter, A., Saglia, R. P., & Bender, R. 2001, AJ, 121, 1936
Kronawitter, A., Saglia, R. P., Gerhard, O., & Bender, R. 2000, A&AS, 144, 53
Impey, C. D., Sprayberry, D., Irwin, M. J., & Bothun, G. D. 1996, ApJS, 105, 209
Pignatelli, E., Corsini, E. M, Vega Beltran, J. C., et al. 2001, MNRAS, 323, 188
Pizzella, A., Corsini, E. M., Vega Beltran, J. C., & Bertola, F. 2004a, A&A, 424, 447
Pizzella, A., Corsini, E. M., Bertola, F., et al. 2004b, IAU Symp., 222, 337
Pizzella, A., Corsini, E. M., Dalla Bonta', et al. 2005, ApJ, 631, 785
Seljak, U. 2002, MNRAS, 334, 797
Vega Beltran, J. C., Pizzella, A., Corsini, E. M., et al. 2001, A&A, 374, 394
Whitmore, B. C., Schechter, P. L., & Kirshner, R. P. 1979, ApJ, 234, 68

COUNTERROTATING CORE IN THE LMC: ACCRETION AND/OR MERGER?

Annapurni Subramaniam* and Tushar P. Prabhu**

Indian Institute of Astrophysics, Bangalore, India

* purni@iiap.res.in, ** tpp@iiap.res.in

Abstract The stellar radial velocity in the central region of the Large Magellanic Cloud (LMC) is used to estimate the radial velocity curve along various position angles (PA) including the line of nodes (LON). The central part of the radial velocity profile along the LON shows a V-shaped profile instead of a straight line profile. This is a clear indication of counterrotation. To explain the observed velocity profile, we propose the existence of two disks in the inner LMC, with one counterrotating. This two disk model is found to match the HI velocities as well. The presence of a counter-rotating core could be due to internal (secondary bar) / external (gas accretion) origin.

Keywords: Magellanic Clouds - galaxies: interactions - galaxies: kinematics and dynamics

1. Introduction

The Large Magellanic Cloud (LMC) has been the subject of a large number of surveys over the years in a wide variety of wavebands (see Westerlund 1990). The radial velocity curve of the LMC was estimated up to 8 kpc by van der Marel et al. (2002) using carbon stars. The linear inner part of the rotation curve has one peculiarity, which is the presence of negative velocity near the center. This result was not given any importance in the paper due to statistically insignificant number of stars near the center. Two kinematic components in CH stars were found by Hartwick & Cowley (1988) and a lower velocity component in carbon stars was found by Graff et al. (2000). The HI velocity studies also revealed two kinematic components, the L and the D components (Rohlfs 1984; Luks & Rohlfs 1992). Double peaked HI velocities, indicating HI clouds with two velocities in the same line of sight have been found in some locations in the LMC, suggestive of HI gas being located in two layers in the LMC. The galacto-centric radial velocity curve as shown in figure 8 of Rohlfs et al. (1984) shows that the central linear part of the velocity profile has a reversal of the slope near the center. All the above point to the possibility

R. S. de Jong, Island Universes, 83–88.
© 2007 *Springer.*

of a kinematically distinct component in the inner LMC. Zhao et al. (2003) estimated and studied the radial velocity of 1347 stars in an attempt to detect the presence of a kinematically different component in the inner LMC, and assigned a probability of less than 1% for its presence. We re-analyze the above data and search for evidence of a second kinematic component in the inner LMC.

2. Rotation Curve and the V-shaped Profile

The radial velocity of 1347 stars presented by Zhao et al. (2003) is used to obtain the stellar radial velocity curves. The bar region of the LMC is more or less covered by this data. The main advantage of this data is that it is homogeneous such that the same set up is used to estimate all the velocities, thereby reducing the systematic errors. On the other hand, the observed stars do not belong to any particular evolutionary category, thus represents a heterogeneous population. We also used the stellar velocities of red super giants (Olsen & Massey 2003), carbon stars (Lunkel et al. 1997) and red giants (Cole et al. 2005). The center of the LMC is taken to be $\alpha = 05^h19^m38^s.0$; $\delta = -69^o27'5".2$ (J2000) of de Vaucouleurs & Freeman (1973), which is the optical center. The α and δ are converted to the linear X, Y co-ordinates using this center.

Stars located along PA = 130^o and located up to 0.4^o away from the PA in the perpendicular direction, on both sides are selected and their average velocity was estimated. The plot is shown in figure 1, bottom left panel. The error bars as shown in the figure indicate the dispersion in the velocity among the stars in each bin. The striking feature of the plot is the 'V' shaped velocity profile in the central region, where we expect a straight line profile corresponding to the primary bar. The radial distance along any PA is taken positive for the northern part and negative for the southern part of the LMC (Feitzinger 1980). The rotation curve as estimated from carbon stars by van der Marel et al. (2002) (their table 2) is shown as solid line. It can be seen that their suggestion of counterrotation near the center is confirmed here.

3. Two Disk Model and the Fit to the Observed Radial Velocity Profiles

We tried to model the disk of the LMC such that a counterrotating contribution is added to the main disk of the LMC. The main disk of the LMC which contains the bar and majority of the mass is responsible for most of the radial velocity curve. The LON of the counterrotating region is also found to be 130^o. Thus the inner kinematic change is produced by invoking counterrotation, with respect to the main large scale disk, whose parameters were estimated by van der Marel et al. (2002). On the other hand, the region just outside the

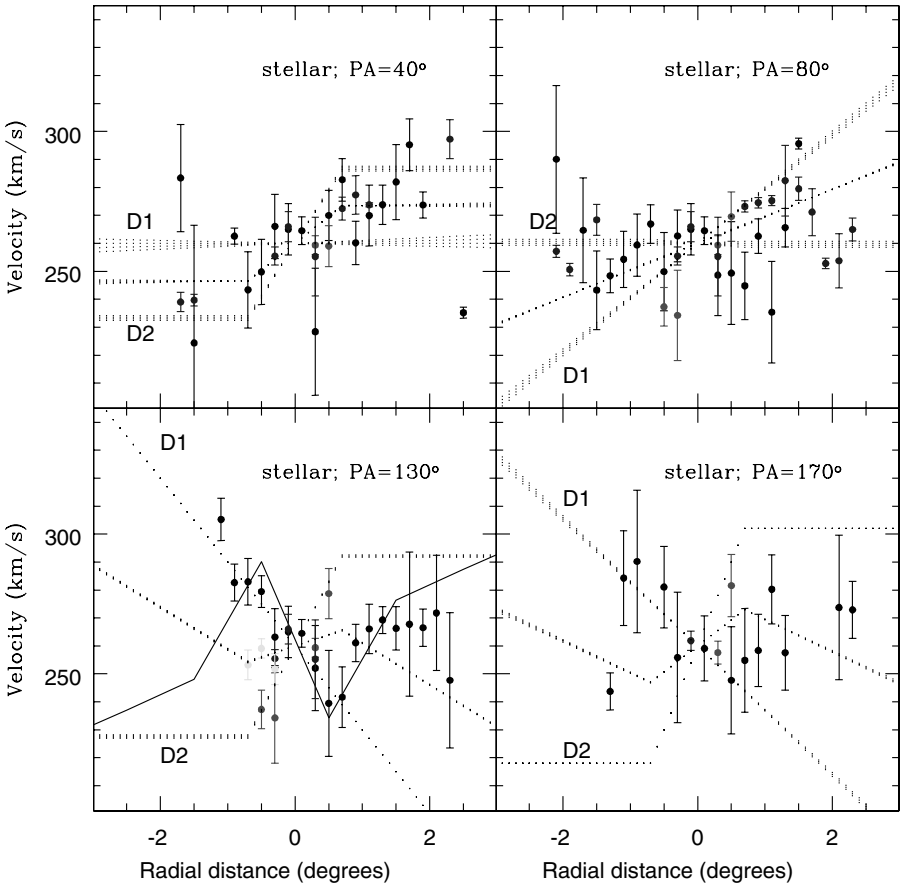

Figure 1. The radial velocity profiles of stars along various PAs. Black points indicate stellar velocities of Zhao et al. (2003), red points indicate carbon star velocities from Kunkel et al. (1997), blue points indicate velocities of red super giants from Olsen & Massey (2003) and yellow points indicate velocities of red giants from Cole et al. (2005). The bold line in the bottom left panel is the rotation curve estimated by van der Marel et al. (2002). D1 and D2 denote the disk1 and disk2 respectively. The dotted line between D1 and D2 denote the average of the two. This figure also appears in Subramaniam & Prabhu (2005).

counterrotating core was found to have a LON $\neq 130^o$. The position of the LON of this region can be estimated from the fact the there is a positive slope observed at a PA of 40^o. This indicates that the value of LON is larger than 130^o. A value of 160^o – 170^o for the PA was able to reproduce the observed slope along 40^o. It is found that the LON of HI gas is 170^o and it extends only up to 2.5 – 3.0^o. The inclination of the HI distribution was found to be similar to that of the stellar disk. Thus it is quite possible that the intermediate region between the counterrotating core and the outer LMC, is dominated by a disk, which is more of HI gas and having the above mentioned properties. The stellar data shows a lot of scatter for 170^o, probably due to the fact that the stars are quite disturbed in this region.

We generated two disks. One with the LON=130^o that follows the kinematics of the stellar disk (D1) and with an inclination of $i = 35^o$ about the LON. The other disk, that is dominated by HI gas, has the LON=170^o (D2). The detailed model can be found in Subramaniam & Prabhu (2005). In this model, there are some locations in the line of sight, where the two disks are physically and kinematically separated. Points in the line of sight which are located in two disks and separated by more than 360 pc are assumed to be physically separated. The scale-height of the HI disk was estimated to be about 180 pc (Padoan et al. 2001), thus the assumed value for separation is just enough to physically separate the disks. Locations which are in the same line of sight, but located in two disks and have more than 20 kms^{-1} difference in velocity are assumed to be kinematically separated. Figure 2 shows the predicted locations in the LMC. One of the observed features in the LMC is the presence of HI clouds in layers. The location of the double peaked clouds of Rohlfs et al. (1984) are over plotted as red points. One can see that the majority of the double peaked clouds are located within the predicted region. HI in the north-western side is matched very well. Some part of the south-east lobe of HI is found to be extended outside, and this lobe is known to extend to larger distance from the LMC, due to tidal effects Staveley-Smith et al. (2003). Thus a larger extent of the HI gas in this lobe may be expected. The more or less agreeable match between the predicted and observed locations of the double velocities indicates that the assumed two disk model is very close to the true nature of the LMC. Stars located in two disks can increase the star-star microlensing in the line of sight, thereby increasing the probability of self-lensing within the inner LMC. The locations of the observed micro-lensing events towards the LMC are shown in figure 2 as big open circles on the predicted physically and kinematically separated locations on the LMC. Many of the events can be found to fall within the predicted region. This suggests that the two disks in the inner LMC fit most of the criteria required for self-lensing within the LMC.

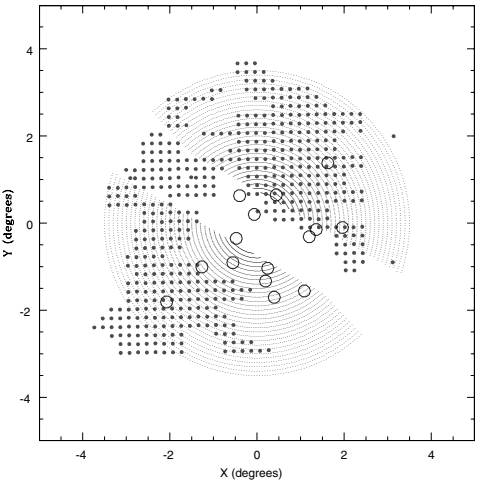

Figure 2. Locations in the LMC where the two disks are separated by more than 360 pc and have velocity differing by more than 20 kms^{-1} are shown as black points. Over plotted are the locations of HI gas (red filled circles) where two components were detected by Rohlfs et al. (1984) and the locations of the micro-lensing events identified towards the LMC (blue open circles). This figure also appears in Subramaniam & Prabhu (2005).

4. Discussion

The main result of the present study is in the identification of a counter-rotating core in the LMC. The inner LMC within a radius of 3^o is modeled as having the presence of two disks, with one counterrotating. This model is valid inside the 3^o radius. The region outside is not studied here and probably follows the parameters as estimated by van der Marel et al. (2002).

Kinematically peculiar cores are generally understood as being fossil fingerprints of merging history of host galaxies (see Mehlert et al. (1998)). The identified counterrotation may also be associated with the secondary bar of the LMC (Subramaniam (2004)). The proposed formation scheme is the accretion of a retrograde satellite. Counterrotating secondary bars could also be formed due to the instabilities in the primary bar (Friedli & Martinet (1993)). This scenario does not require any merger. Thus, the true nature and the reason for the formation of the counterrotating core in the LMC is to be understood from a wide variety of possibilities which are of external/internal origin.

In the LMC, the population I stars are found to show the kinematics of HI gas indicating that they belong to the disk2. It is possible that the young stars in the LMC are formed from the gas which has been accreted recently. Bruns et al. (2004) presented a complete HI survey of the Magellanic system. The LMC and the SMC were found to be associated with large gaseous features - the

Magellanic Bridge, the interface region, and the Magellanic stream. This gas connects the two not only in position, but also in velocity. The gas in the Magellanic Bridge has low velocities in the LMC-standard-of-rest frame making an accretion of some of this gas by the LMC very likely. Thus it is very likely that the inner gas-rich disk of the LMC could be formed from this infalling gas, which could provide new fuel to star formation.

References

Bruns et al., 2005, A&A, 432, 45
Cole, A.A., Tolstoy, E., Gallaghar, III, J.S. & Smecker-Hane, T., 2005, AJ, 129, 1465
de Vaucouleurs, G., & Freeman, K.C. 1973, Vistas Astron., 14, 163
Feitzinger, J.V., 1980, Space Sci. Rev., 27, 35
Friedli, D., & Martinet, L., 1993, A&A, 277, 27
Graff, D.S., Gould, A., Suntzeff, N.B.,& Schommer, R.A. 2000, ApJ, 540, 211
Hartwick, F.D.A., & Cowley, A.P., 1988, ApJ, 334, 135
Kunkel, W.E., Demers, S., Irwin, M.J. & Albert, L., 1997, ApJ, 488, 129
Luks, Th., & Rohlfs, K. 1992, A&A, 263, 41
Mehlert,D., Saglia, R.P., Bender, R., & Wegner, G., 1998, A&A, 332, 33
Olsen, K.A.G., & Massey, P. 2003, AJ, 126, 2867
Padoan, P., Kim, S., Goodman, A. & Staveley-Smith, L., 2001, ApJ, 555, L33
Rohlfs, K., Kreitschmann, J., Siegman, B.C., & Feitzinger, J.V. 1984, A&A, 137, 343
Staveley-Smith, L., Kim, S., Calabretta, M.R., Haynes, R.F. & Kesteven, M.J., 2003, MNRAS, 339, 87
Subramaniam, A., 2004, ApJ, 604, L41
Subramaniam, A & Prabhu, T.P., 2005, ApJ, 625, L47
van der Marel, R.P., Alves, D.R., Hardy, E., & Suntzeff, N.B., 2002, AJ, 124, 2639
Westerlund, B.E., 1990, Astronomy & Astrophysics Review, 2, 29
Zhao, H.S., Ibata, R.A., Lewis, G.F., & Irwin, M.J. 2003, MNRAS, 339, 701

HALO MASS PROFILES OF LOW SURFACE BRIGHTNESS GALAXIES

W.J.G. de Blok

RSAA, Mount Stromlo Observatory, Australia
edeblok@mso.anu.edu.au

Abstract A recent study has claimed that the rotation curves of Low Surface Brightness (LSB) galaxies are largely consistent with ΛCDM simulations, contradicting a large body of observational work that appears to show that the CDM-characteristic steep mass-density cusps are absent in real galaxies. I describe an improved analysis method that shows that only a small minority of LSB rotation curves is possibly consistent with ΛCDM simulations. The large majority prefer semi-constant kpc-sized mass-density cores.

Keywords: galaxies: kinematics and dynamics - galaxies: fundamental parameters - dark matter

1. Introduction

In recent years the inner structure of dark matter haloes has been the topic of some discussion. Low Surface Brightness (LSB) galaxies are dominated by dark matter (de Blok & McGaugh 1997), and observations suggest that these galaxies have a roughly constant dark-matter density core, with a typical size of order a few kpc. On the other hand, numerical simulations based on the (Λ)Cold Dark Matter (CDM) paradigm suggest a very steep inner mass density distribution, a so-called "cusp" (e.g., Navarro, Frenk & White 1996; Navarro, Frenk & White 1997).

In a recent paper Hayashi et al. (2004; hereafter H04) claim that the inner slope is difficult to constrain, both observationally as well as theoretically and point out that rotation curve constraints are strongest where numerical simulations are least reliable. They present a method to fit circular velocity curves derived from their high-resolution cosmological simulations as well as LSB galaxy rotation curves from Mcgaugh et al. (2001), de Blok & Bosma (2002) and Swaters et al (2003), and conclude that the observed curves *are* consistent with the CDM paradigm; a conclusion that contradicts a large body of

R. S. de Jong, Island Universes, 89–94.
© 2007 *Springer.*

observational work. To quantify the observed and simulated rotation curves they use a three-parameter fitting formula (see, e.g., Courteau 1997):

$$V(r) = \frac{V_0}{\left(1 + \left(\frac{r_t}{r}\right)^{\gamma}\right)^{1/\gamma}}. \quad (1)$$

Here V_0 is the asymptotic velocity of the flat part of the rotation curve, r_t is a scale radius (the transition radius between the rising and flat part of the rotation curve) and the parameter γ describes the abruptness of the turn-over between the rising and flat parts of the rotation curve.

Figure 9 in H04 compares the distributions of γ for observations and simulations. The LSB rotation curves show a broad distribution in γ with two peaks around $\gamma \sim 1$ and $\gamma \sim 5$. The γ distribution of the simulated CDM haloes is markedly different. It is narrow and centered around $\gamma \sim 0.6$ with a dispersion of ~ 0.4. At first sight the two distributions seem quite incompatible, and one might conclude that the LSB rotation curves are not consistent with the CDM simulations. H04 argue, however, that for most ($\sim$ 70 per cent) of the LSB galaxy rotation curves the reduced χ^2 distribution is quite broad and shallow, so that by constraining the fit to $\gamma < 1$, a fit can be found that is consistent with the simulations, at the cost of only a small increase in $\chi^2_{\rm red}$. They conclude that "this sample of LSB rotation curves is not manifestly inconsistent with the predictions of ΛCDM cosmological models" and thus contradict most observational work on LSB rotation curves which argues the opposite.

2. Slopes

To investigate the reasons behind this surprising conclusion, we investigate the logarithmic slope $\alpha(r)$ of the mass-density distribution corresponding to the rotation curve given in Eq. (1). This slope is given by

$$\alpha(r) \equiv \frac{d\log\rho}{d\log r} = -\frac{2+\gamma}{1+\left(\frac{r_t}{r}\right)^{\gamma}} + \frac{\gamma}{1+3\left(\frac{r_t}{r}\right)^{\gamma}}. \quad (2)$$

The slope thus *depends on both* γ *and* r_t. We can now compare the slopes $\alpha(r)$ of both observations and simulations. To make the comparison as fair as possible we will compare them at identical radii, and choose a radius that is well-resolved by both. In H04 the smallest reliably resolved radius, defined by the so-called convergence radius (Power et al. 2003), is $r_{\rm conv} = 0.3h^{-1}$ kpc. For $h = 0.7$ we find $r_{\rm conv} \sim 0.4$ kpc and this is the radius we choose. The slope at $r_{\rm conv}$ in the simulations varies between $\alpha \sim -1$ and ~ -1.3.

Figure 1 shows iso-slope contours in the (γ, r_t) plane, evaluated at $r = 0.4$ kpc. It is immediately obvious that α is not a unique function of γ, but depends equally strongly on r_t. Only a very small part of parameter space results in

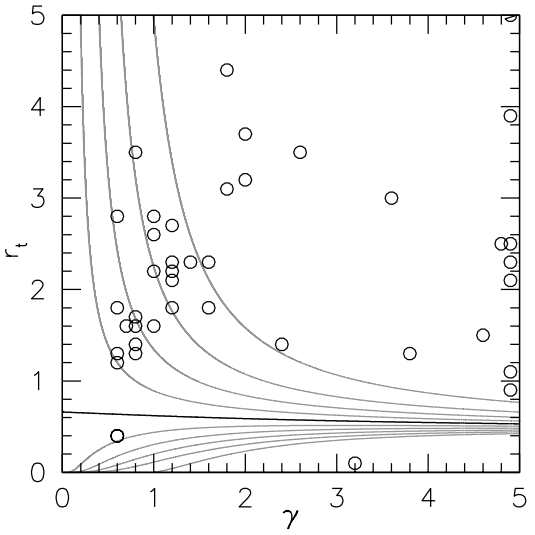

Figure 1. Distribution of slopes α in the (γ, r_t) plane evaluated at a radius of 0.4 kpc. Iso-slope contours run from $\alpha = -0.2$ (top contour) to $\alpha = -2.0$ (bottom contour) in steps of $\Delta\alpha = -0.2$. The black, almost horizontal contour indicates a slope $\alpha = -1$. Over-plotted are the best-fit (γ, r_t)-combinations for the LSB galaxies investigated in H04.

steep, CDM-compatible slopes and constraining $\gamma < 1$ still allows values up to $\alpha \sim -0.2$.

Over-plotted in Fig. 1 are the best-fit γ and r_t values of the LSB rotation curves as determined by H04. The very large majority of the galaxies have slopes inconsistent with the values $\alpha < -1$ derived in the H04 simulations. Note again that the slopes in simulations and observations are compared at *identical radii*, and that the γ and r_t values were derived using the *entirety of the rotation curves*. The constraints introduced by H04 are thus insufficient conditions for agreement with CDM, as constraining to $\gamma < 1$ does not automatically imply a mass-density slope consistent with CDM. (In their analysis H04 implicitly assumed that the slope depends on γ alone). For a more extended description of the analysis presented here see de Blok (2005).

3. Additional Constraints

Unless one is prepared to allow for shallow slopes in CDM at these radii (making it inconsistent with its own simulations) an extra constraint on the slope is needed to ensure agreement with CDM. In practice this means that (γ, r_t) parameter space needs to be searched for the minimum χ^2 value that still results in a steep slope. At 0.4 kpc the H04 simulations show slopes $-1.3 < \alpha < -1$, and strictly speaking one ought to restrict the search of

(γ, r_t) space to slopes $\alpha < -1$. However, to take into account uncertainties in data and simulations, and give the CDM models as much leeway as possible, a more liberal range of $\alpha < -0.8$ will be used. This is the steepest slope we can expect at this radius from an ultra-compact ISO halo with $R_C \sim 0.5$ kpc, and thus cleanly separates the ISO and CDM domains.

H04 determine for each LSB rotation curve the reduced χ^2 for the best-fitting (γ, r_t) model, as well as the minimum $\chi^2_{\rm red}$ value using their extra CDM constraints. They argue that for most of the galaxies the CDM constraints only cause a small increase in the *reduced* χ^2, and that therefore the CDM-constrained models are not much worse than the best-fit models. However, in order to cause the same change in *reduced* χ^2 the change in *absolute* χ^2 must be much larger for a rotation curve with a large number of data points than for a rotation curve with a small number of data points. In other words, a small change in $\chi^2_{\rm red}$ can be very significant for a curve with a large number of data points, while it can be insignificant for a curve with only a small number of data points.

The observed sample contains a large number of rotation curves, with a wide range in the number of data points, varying from ~ 10 to over 350. The relevant parameter is thus *not* the reduced χ^2, but the *change in absolute* χ^2. The confidence level of any parameter combination is given by the corresponding change in χ^2 with respect to the minimum value. For a model with three free parameters (γ, r_t, V_0) as used here, the $(1, 2, 3)\sigma$ confidence intervals for any fit are given by $\Delta\chi^2 = (3.5, 8.0, 13.9)$, respectively.

Using these criteria, a rotation curve can be defined to be consistent with CDM if the best-fit values of γ and r_t lie within 2σ of the closest (γ, r_t) combination with a $\alpha < -0.8$ slope. In order for the fit to give any meaningful constraints, one should furthermore require that the area enclosed by the 2σ confidence level is a small fraction R of the total area of parameter space investigated. If this is not the case, then any conclusions regarding agreement or disagreement with CDM are only very weak at best. Here we investigate a parameter space (γ, r_t) ranging from $(\gamma : 0 \rightarrow 5;\ r_t : 0 \rightarrow 5$ kpc) and choose a ratio $R = 0.25$. Small values of R indicate that the 2σ area is only a small fraction of total parameter space, and therefore yield significant solutions. Large values of R indicate that the fit does not constrain models in a significant way.

Of the 36 galaxies from H04 that we investigate here, 20 have well-constrained solutions $R < 0.25$. The rest are only loosely constrained and therefore cannot make strong statements regarding (dis-)agreement with CDM. Of the 20 well-constrained galaxies, 3 are consistent with CDM using our definition, and 17 are inconsistent.

This is investigated further in Fig. 2. Here R is plotted against the number of data points in each rotation curve. A distinction is made between rotation

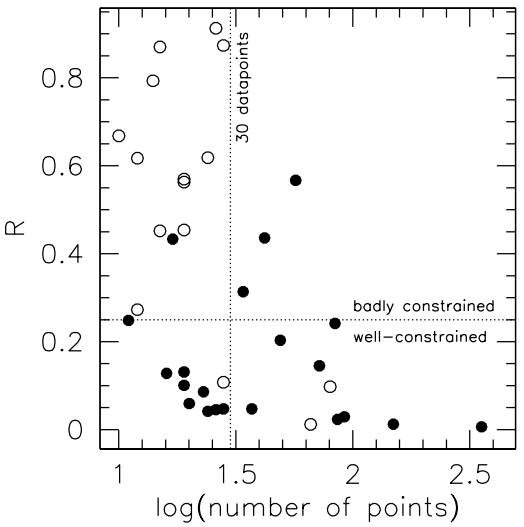

Figure 2. The ratio R of the area enclosed by the 2σ contour and the total parameter search area (see text for fuller description) plotted against the number of data-points in the rotation curve. Open circles have a best-fit (γ, r_t) within 2σ of a point with a steep slope $\alpha < -0.8$. Filled circles are more than 2σ away from such a point.

curves that are consistent with CDM and those that are inconsistent with CDM using the constraints introduced here. Firstly, of the 15 galaxies that are consistent with CDM (regardless of their value of R), 13 have less than 30 data points. Furthermore, of these 13 galaxies, only 1 has $R \leq 0.25$ (i.e. is well-constrained). Looking at the 21 galaxies that are inconsistent with CDM (independent of R), only 10 have less than 30 data points. Of these 10 galaxies, all except one have $R \leq 0.25$. Rotation curves with more than 30 data points tend to be better constrained on average, as well as have a tendency to be inconsistent with CDM. It is also interesting to note that even amongst galaxies with only a limited number of data points, the most constrained solutions (small R) tend to be those inconsistent with CDM. The majority of solutions (~ 85 per cent) that are consistent with CDM have only a small number of data points *and* are ill-constrained. These ill-constrained solutions therefore do not decide between any model one way or the other, and statements that these galaxies are consistent with CDM are thus not very strong. Of the well-constrained solutions the large majority is inconsistent with CDM. Furthermore, of the 13 galaxies with more than 30 data points only 2 are consistent with CDM. These two galaxies (NGC 3274 and NGC 4455) also happen to have the smallest optical scale-lengths and highest surface brightnesses from all galaxies with available photometry in the Mcgaugh et al. (2001), de Blok & Bosma (2002)

and Swaters et al. (2003) samples. These galaxies are therefore unlikely to be dominated by dark matter in their inner parts and it is very likely that the steep slopes in these two galaxies simply reflect the stellar mass distribution.

Amongst the rotation curves with less than 30 points there is only one galaxy with $R < 0.25$ that seems consistent with CDM. This is UGC 731, a bona-fide LSB dwarf, and is the best and only candidate in the entire observed sample for a CDM-consistent, dark-matter-dominated galaxy with a well-constrained solution. In summary, a comparison of the circular velocity profiles of CDM haloes with rotation curves of LSB galaxies indicates that the shapes and inferred central densities of most LSB galaxies are mostly *inconsistent* with those of simulated haloes within the limitations imposed by observational error.

References

Courteau, S. 1997, AJ, 114, 2402

de Blok, W. J.G., 2005, ApJ, 634, 227

de Blok, W. J. G., Bosma, A. 2002, A&A, 385, 816

de Blok, W. J. G., McGaugh, S. S. 1997, MNRAS, 290, 533

Hayashi, E., Navarro, J. F., Power, C., Jenkins, A., Frenk, C. S., White, S. D. M., Springel, V., Stadel, J., Quinn, T. R. 2004, MNRAS, 355, 794

McGaugh, S. S., Rubin, V. C., & de Blok, W. J. G. 2001, AJ, 122, 2381

Navarro, J. F., Frenk, C. S., White, S. D. M. 1996, ApJ, 462, 563

Navarro, J. F., Frenk, C. S., White, S. D. M. 1997, ApJ, 490, 493

Power, C., Navarro, J. F., Jenkins, A., Frenk, C. S., White, S. D. M., Springel, V., Stadel, J., & Quinn, T. 2003, MNRAS, 338, 14

Swaters, R. A., Madore, B. F., van den Bosch, F. C., & Balcells, M. 2003, ApJ, 583, 732

THE DISK MASS PROJECT

Breaking the disk-halo degeneracy

Marc A.W. Verheijen[1*], Matthew A. Bershady[2], Rob A. Swaters[3], David R. Andersen[4] and Kyle B. Westfall[2]

[1]*Kapteyn Astronomical Institute, University of Groningen, The Netherlands*
[2]*University of Wisconsin – Madison, USA*
[3]*University of Maryland, College Park, USA*
[4]*NRC Herzberg Institute of Astrophysics, Canada*
* verheyen@astro.rug.nl

Abstract Little is known about the content and distribution of dark matter in spiral galaxies. To break the degeneracy in galaxy rotation curve decompositions, which allows a wide range of dark matter halo density profiles, an independent measure of the mass surface density of stellar disks is needed. Here, we present our ongoing Disk Mass project, using two custom-built Integral Field Units, to measure the vertical velocity dispersion of stars in ∼40 spiral galaxies. This will provide a kinematic measurement of the stellar disk mass required to break the degeneracy, enabling us to determine the dark matter properties in spiral galaxies with unprecedented accuracy. Here we present preliminary results for three galaxies with different central disk surface brightness levels.

Keywords: galaxies: spiral — galaxies: fundamental parameters — galaxies: kinematics and dynamics — instrumentation: spectrographs

1. Motivation

A major roadblock in testing galaxy formation models is the disk-halo degeneracy: density profiles of dark matter halos as inferred from rotation curve decompositions depend critically on the adopted M/L of the disk component. An often used refuge to circumvent this degeneracy is the adoption of the maximum-disk hypothesis (van Albada & Sancisi 1986). However, this hypothesis remains unproven. Bell & De Jong (2001) showed that stellar population synthesis models yield plausible *relative* measurements of stellar M/L in old disks, but uncertainties in the IMF prevent an *absolute* measurement of stellar M/L from photometry. Another tool to determine the M/L, and specifically

R. S. de Jong, Island Universes, 95–100.
© 2007 *Springer.*

whether disks are maximal, is the Tully-Fisher relation, e.g. by looking for offsets between barred vs. un-barred galaxies, but this too is only a relative measurement. Evidently, none of these methods are suited to break the degeneracy, and without an independent measurement of the M/L of the stellar disk, it is not possible to determine the structural properties of dark matter halos from rotation curve decompositions.

A direct and absolute measurement of the M/L can be derived from the vertical component σ_z of the stellar velocity dispersion. For a locally isothermal disk, $\sigma_z = \sqrt{\pi G(M/L)\mu z_o}$, with μ the surface brightness, and z_0 the disk scale height. The latter is statistically well-determined from studies of edge-on galaxies (de Grijs & van der Kruit 1996; Kregel et al. 2002). Thus, σ_z provides a direct, kinematic estimate of the M/L of a galaxy disk and can break the disk-halo degeneracy.

This approach has been attempted before with long-slit spectroscopy on significantly inclined galaxies. For example, Bottema (1997) concluded for a sample of 12 galaxies that, on average, the stellar disk contributes at maximum some 63% to the amplitude of the rotation curve. These observations, however, barely reached 1.5 disk scale-lengths, required broad radial binning, and because of the high inclinations, the measured velocity dispersions required large and uncertain corrections for the tangential (σ_ϕ) and radial (σ_r) components of an assumed velocity dispersion ellipsoid.

2. The Disk Mass Project

Measuring σ_z in kinematically cold stellar disks requires spectroscopy at moderately high resolution (R$\approx 10^4$) of extended light at relatively low surface brightness levels ($\mu_B \approx 24$ mag/arcsec^2). Clearly, measurements of σ_z have been severely hampered by the limited signal-to-noise of the observations to date, as well as the small samples of galaxies studied so far.

With the advent of Integral Field Unit (IFU) spectroscopy, the observational situation can be dramatically improved, and significant progress in determining the mass surface densities of stellar disks can now be made. The main advantage of IFU spectroscopy over traditional long-slit studies lies in the fact that IFUs are capable to collect light from a much larger solid angle and that many IFU spectra can be combined to increase the signal-to-noise.

Capitalizing on this aspect of IFU spectroscopy, we have initiated our long-term Disk Mass project. The main goal is to measure σ_z as a function of radius out to 2.5 disk scale lengths in $\sim$40 undisturbed, nearly face-on spiral galaxies with a wide range of global properties like total luminosity, surface brightness, colour, and morphology. To achieve this, we have constructed two special-purpose wide-field fiber-based IFUs, and adopted a two-phased observational strategy extending over a 3-4 year period.

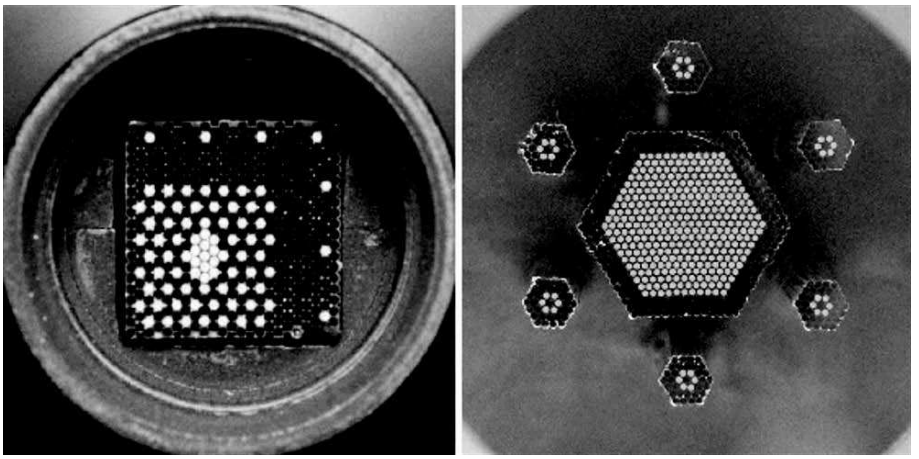

Figure 1. Two custom-built fiber-based wide-field IFUs. Active fibers are back-illuminated. Dark fibers terminate shortly behind the focal plane and serve as buffer for stress relief and to edge-protect the active fibers while polishing the fiber head.**Left:** focal plane layout of the fibers in the SparsePak IFU: the grid is filled with 3 pointings. **Right:** focal plane layout of the fibers in the P-Pak IFU. Sky fibers are located in 6 mini-IFUs surrounding the main fiber head.

Phase A aims at collecting Hα velocity fields for a parent sample of nearly phase-on spiral galaxies. From the UGC, we selected disk galaxies at $|b| \geq 25^\circ$ to minimize Galactic extinction, with diameters between $1'$ and $1.5'$ to match them to the large field-of-view of our IFUs, and with optical axis ratios of b/a$>$0.85 to ensure a nearly face-on orientation. This yielded a total sample of 470 galaxies from which we removed the strongly barred and interacting galaxies, and randomly picked galaxies to observe.

Subsequently, the regularity of the gas kinematics is evaluated from the Hα velocity fields. The main purpose is to identify kinematically disturbed disks which are likely to violate the assumption of local isothermal equilibrium, which is required when relating σ_z and disk scale height to the mass surface density of the disk. Furthermore, Andersen & Bershady (2003) have demonstrated that accurate inclinations and rotation curves can be derived for nearly face-on disks, provided a regular and symmetric Hα velocity field of high signal-to-noise. The parent sample will be expanded until 40 galaxies with regular gas kinematics have been identified.

Phase B of our project aims at measuring σ_z in the stellar disks of the subsample of 40 galaxies with regular gas kinematics. Velocity dispersions are determined from the broadening of the absorption lines in the blue part of the spectrum around 515 nm, containing absorption lines of the MgIb triplet and many Fe lines. For a selected number of galaxies, σ_z is also measured from the broadened CaII triplet absorption lines around 860 nm.

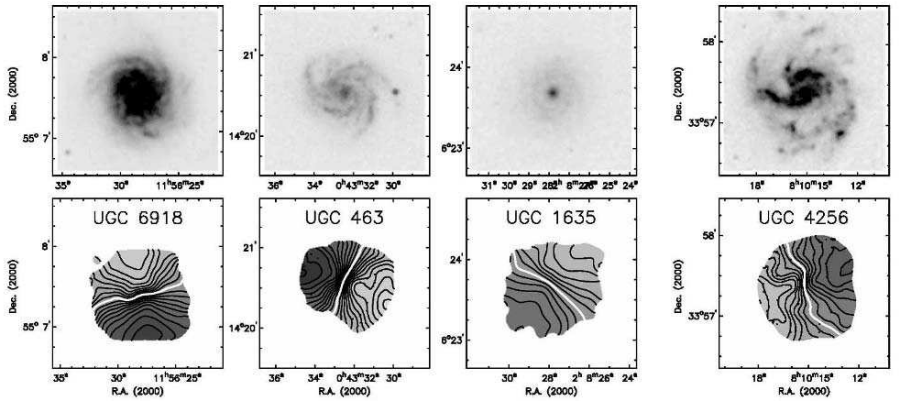

Figure 2. Examples of galaxies in the parent sample. **Upper row:** optical images at the same grayscale levels. **Bottom row:** Hα velocity fields obtained with SparsePak. The three galaxies on the left, with different central disk surface brightness levels, are suitable for follow-up observations of their stellar kinematics which are presented in Figure 3. UGC 4256 is an example of a galaxy which is too irregular, as is the case for most galaxies in our parent sample.

Apart from these spectroscopic observations with our IFUs, all galaxies in the parent sample will be imaged in the U,B,V,R,I and J,H,K passbands. All galaxies in the subsample will be imaged in neutral hydrogen to determine the contribution from the cold gas to the total surface mass density of the disks.

3. Two Custom-built Integral Field Units

As mentioned above, measuring σ_z requires spectroscopy at moderately high spectral resolution of diffuse low surface brightness light. To achieve this, we have built two special-purpose wide-field IFUs consisting of large aperture fibers which carry light from a focal plane to the pseudo-slit of a pre-existing spectrograph. The diameter of the fibers is maximized while providing a spectral resolution of no less than R$\approx$8000. The maximum number of fibers is then determined by the length of the spectrograph slit, while the layout in the focal plane is designed to span more than an arcminute on the sky. Obviously, the penalty paid for large aperture fibers is a limited angular resolution, but this is of secondary importance for our Disk Mass project.

SparsePak, built at the University of Wisconsin in Madison, contains 75 science and 7 sky fibers, each 4.7 arcsec in diameter (Fig. 1). The 25m long fibers pipe light from a $71'' \times 72''$ field-of-view (fov) at the F/6 imaging port of the 3.6m WIYN telescope at Kitt Peak to its Bench Spectrograph. SparsePak is described in detail by Bershady et al. (2004, 2005).

P-Pak, built at the AIP in Potsdam, contains 331 science and 36 sky fibers, each 2.7 arcsec in diameter (Fig. 1). The 3m long fibers carry light from a

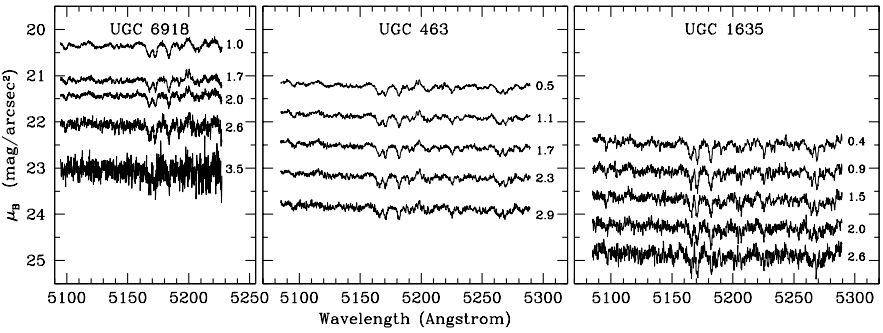

Figure 3. Azimuthally averaged absorption line spectra at 5 radial bins for 3 galaxies with different central surface brightness. Each spectrum is plotted at the corresponding surface brightness level. At the right of each spectrum, the number of disk scale lengths for the radial bin is indicated. UGC 6918 was observed for $3\times45^{\rm min}$ with SparsePak at R=11,750. UGC 463 and UGC 1635 were observed for $5\times60^{\rm min}$ with P-Pak at R=7,800. The number of averaged spectra at each radius is 6, 8, 12, 18, and 18 for SparsePak, and 18, 42, 66, 90, and 114 for P-Pak.

$64''\times74''$ hexagonal fov at the focal plane behind a F/3.5 focal reducer lens on the 3.5m Calar Alto telescope, to the collimator lens of the Cassegrain mounted PMAS spectrograph (Verheijen et al. 2004; Kelz et al. 2005). Fifteen additional fibers allow for an accurate simultaneous wavelength calibration.

4. Current Status

Phase A is effectively complete. From analyzing the gas kinematics (Fig. 2), it became clear that only about 1 in 3 galaxies have sufficiently regular gas kinematics to successfully fit a tilted-ring model to the Hα velocity field, allowing us to measure the shape and amplitude of the inner rotation curves from which to total mass (dark plus luminous) of the inner galaxy follows. Hence, a parent sample of 130 galaxies has been constructed from which a subsample of 40 regular galaxies can be selected.

We have started Phase B in the fall of 2004 and observed the stellar kinematics in the MgIb region with P-Pak for 11 galaxies. With SparsePak we have observed the MgIb kinematics for 8 and CaII kinematics of 7 galaxies. With both IFUs we have built up an extensive library of spectroscopic template stars covering a range of spectral types, metallicities and log(g).

5. First Results

Figure 3 shows, for 3 galaxies with different disk central surface brightness levels, the azimuthally averaged stellar absorption line spectra in the MgIb region of the spectra for five radial bins. Using the stellar template spectra,

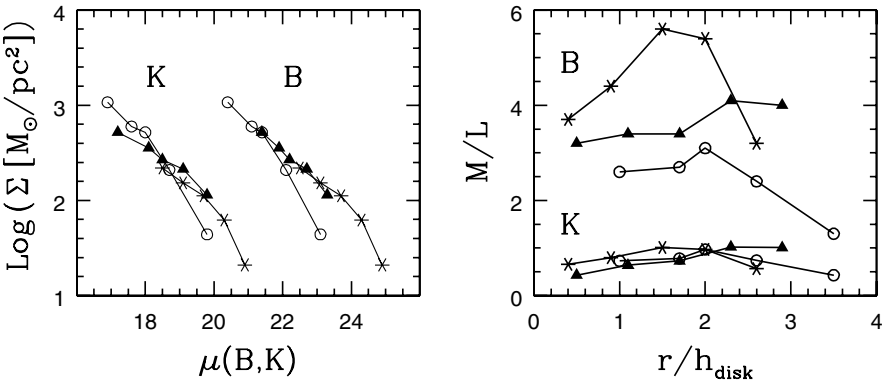

Figure 4. **Left:** Mass surface density as function of local B- and K-band surface brightness. **Right:** Mass-to-light ratios in the B- and K-band as a function of radius. Circles: UGC 6918, triangles: UGC 463, asterisks: UGC 1635. Lacking K-band photometry for UGC 1635 forced us to adopt a B−K colour constant with radius.

we have measured σ_z as a function of radius, assuming a Gaussian broadening function. Figure 4 shows the derived mass surface densities and mass-to-light ratios. Although we are dealing with three entirely different galaxies, the K-band M/L is quite similar for these galaxies while the B-band M/L seems to increase systematically with lower central disk surface brightness.

Acknowledgements This work benefits from NSF grant AST–0307417. P-Pak was developed within the ULTROS project, which is funded by the German ministry of education & research (BMBF) through Verbundforschungs grant 05–AE2BAA/4.

References

Andersen, D.R. and Bershady, M.A. 2003, ApJ, 599, 79

Bell, E.F. and de Jong, R.S. 2001, ApJ, 550, 212

Bershady, M.A., Andersen, D.R., Harker, J., Ramsey, L.W. and Verheijen, M.A.W. 2004, PASP, 116, 565

Bershady, M.A., Andersen, D.R., Verheijen, M.A.W., Westfall, K.B., Crawford, S.M. and Swaters, R.A. 2005, ApJS, 156, 311

Bottema, R. 1997, A&A, 328, 517

de Grijs, R. and van der Kruit, P.C. 1996, A&AS, 117, 19

Kelz, A., Verheijen, M.A.W., Roth, M.M., Bauer, S.M., Becker, T., Paschke, J., Popow, E., Sanchez, S.F. and Laux, U. 2005, PASP, in press

Kregel, M., van der Kruit, P.C., and de Grijs, R. 2002, MNRAS, 334, 646

van Albada, T.S. and Sancisi, R. 1886, Phil. Trans. Royal Society of London, 320, 446

Verheijen, M.A.W., Bershady, M.A., Andersen, D.R., Swaters, R.A., Westfall, K.B., Kelz, A. and Roth, M.M. 2004, AN, 325, 151

A DARK GALAXY IN THE VIRGO CLUSTER IMAGED AT 21-CM

R. F. Minchin[1,2*], M. J. Disney[2], J. I. Davies[2], A. R. Marble[3], C. D. Impey[3], P. J. Boyce[2], D. A. Garcia[2], M. Grossi[2], C. A. Jordan[4], R. H. Lang[2], S. Roberts[2], S. Sabatini[5] and W. van Driel[6]

[1]*Arecibo Observatory, Puerto Rico*

[2]*School of Physics and Astronomy, Cardiff University, UK*

[3]*Steward Observatory, University of Arizona, Tucson, USA*

[4]*Jodrell Bank Observatory, University of Manchester, UK*

[5]*Osservatorio Astronomico di Roma, Italy*

[6]*Observatoire de Paris, France*

* rminchin@naic.edu

Abstract Dark Matter supposedly dominates the extragalactic Universe (Peebles 1993; Peacock 1998; Moore et al. 1999; D'Onghi & Lake 2004), yet no dark structure of galactic proportions has ever been convincingly identified. Earlier (Minchin et al. 2005) we suggested that VIRGOHI 21, a 21-cm source we found in the Virgo Cluster at Jodrell Bank using single-dish observations (Davies et al. 2004), was probably such a dark galaxy because of its broad line-width ($\sim$200 km s^{-1}) unaccompanied by any visible gravitational source to account for it. We have now imaged VIRGOHI 21 in the neutral-hydrogen line, and have found what appears to be a dark, edge-on, spinning disc with the mass and diameter of a typical spiral galaxy. Moreover the disc has unquestionably interacted with NGC 4254, a luminous spiral with an odd one-armed morphology, but lacking the massive interactor normally linked with such a feature. Published numerical models (Vollmer et al. 2005) of NGC 4254 call for a close interaction $\sim 10^8$ years ago with a perturber of $\sim 10^{11}$ solar masses. This we take as further, independent evidence for the massive nature of VIRGOHI 21.

Keywords: galaxies: intergalactic medium - dark matter - galaxies: peculiar

1. Observations

The data were taken in March 2005 at the Westerbork Synthesis Radio Telescope (WSRT) in two full 12-hour syntheses. The velocity range between 980 and 2890 km s^{-1} was covered in 230 channels with a resolution of 10 km s^{-1}. The beam was 99×30 arc sec in size (extended North-South) and the noise was

R. S. de Jong, Island Universes, 101–106.
© 2007 *Springer.*

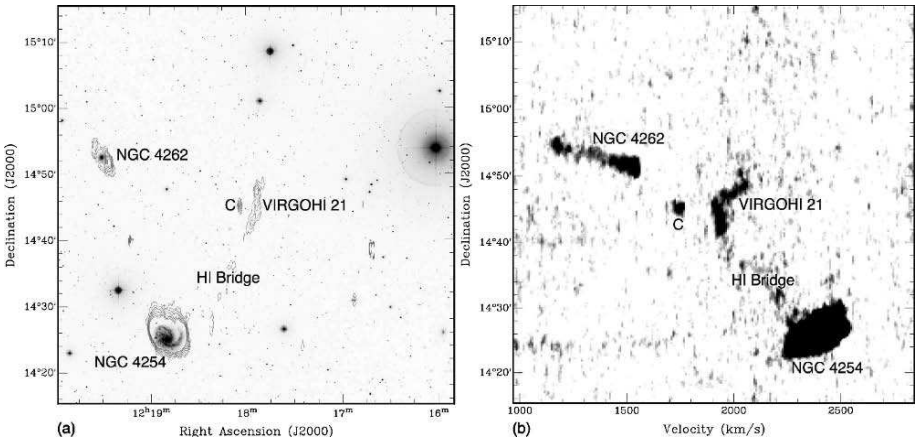

Figure 1. (a) HI contour map of the 21-cm observations, superimposed on a 1 square degree negative Digitized Sky Survey image. Contours are from 2.5×10^{19} to 2×10^{20} cm^{-2} at intervals of 2.5×10^{19} cm^{-2}.(b) Shows the declination-velocity projection of the data cube. More detail can be seen in the on-line animation of the cube.

0.3 mJy beam^{-1} channel^{-1}, giving a 5σ column-density to sources 25 km s^{-1} wide of 2×10^{19} Hydrogen atoms cm^{-2}.

Figure 1a shows a neutral Hydrogen (HI) contour map of the field superimposed on a negative optical image. VIRGOHI 21 is the elongated structure in the centre with a previously unseen bridge stretching towards the spiral galaxy NGC 4254 (bottom left). Figure 1b shows the velocity-declination projection of the full 3 dimensional data cube, an animation of which contains far more information (see http://www.astro.cf.ac.uk/groups/galaxies/slow_rot.gif).

The $\sim$25 arc minute filamentary bridge stretches from the low-velocity, western edge of NGC 4254, falling in radial velocity from 2250 km s^{-1} at declination $+14^\circ 20'$ to 1900 km s^{-1} at $+14^\circ 41'$ where it is suddenly arrested. Then at $+14^\circ 46'$ it is abruptly wrenched upwards again towards 2100 km s^{-1} at $14^\circ 49'$. Figure 2 is a blow-up of the source region superimposed on a deep CCD image, illustrating that there is no optical counterpart. Object 'A', which falls within the HI contours of the detection, has an optical redshift of $z = 0.25$.

2. Discussion

Combining the new data with the old, we argue:
(a) If attributed to gravitation, changes in velocity of galactic size over galactic scales, as seen here, require masses of galactic proportions. On dimensional grounds the velocity wrench ΔV ($\sim$200 km s^{-1}) seen at VIRGOHI 21 over a conservative length-scale Δx ($\sim$14 kpc $\simeq 5 \times 10^{22}$ cm $\simeq$ 3 arc minutes at the Virgo Cluster distance of 16 Mpc; Minchin et al. 2005) implies a mass $M \geq$

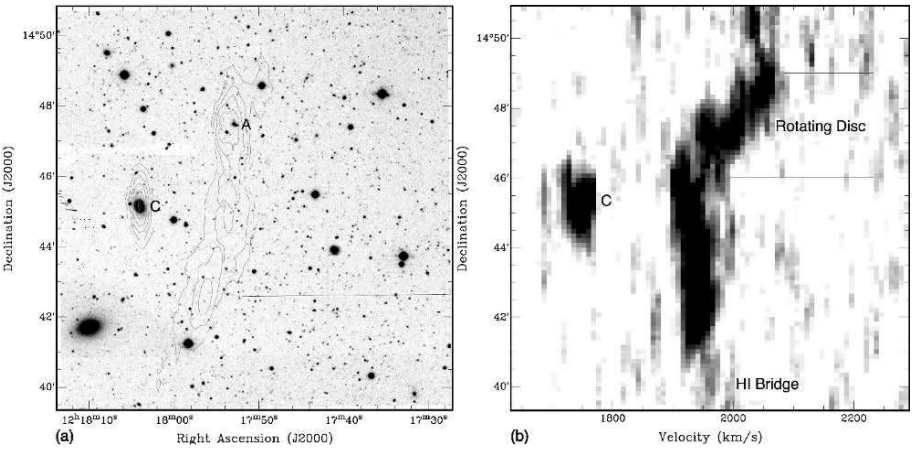

Figure 2. As Fig. 1, but expanded and superimposed on a negative of our deep CCD B-band image (Minchin et al. 2005) with a surface-brightness limit of 27.5 B mag. arcsec^{-2}.

$(\Delta V)^2 \Delta x/G \simeq 10^{10-11}$ solar masses. More specifically the gravitational (free-fall) timescale $(\Delta x)^{3/2}/(GM)^{1/2}$ needs to be $\leq \Delta x/V$, the time it takes for gas travelling at V (relative to M) to change velocity by ΔV. And where $\Delta V \sim V$, as it appears to be here (see Fig. 2b), $M \geq (\Delta V)^2 \Delta x/G$ again.

(b) The bridge between NGC 4254 and VIRGOHI 21 reveals that they have interacted. According to published numerical simulations (Vollmer et al. 2005) the morphological peculiarities of NGC 4254 can be explained by an interaction with a mass of $\sim 10^{11} M_\odot$, 3×10^8 years ago. As the projected length of the bridge is 120 kpc this would imply it has been drawn out at a projected speed of 390 km s^{-1}, which is comparable to the radial velocity difference between NGC 4254 and VIRGOHI 21 of 400 km s^{-1}.

(c) NGC 4262, the spiral to the North-East, is not involved. There is no bridge to it and the radial velocity difference between NGC 4254 and NGC 4262 is too large (900 km s^{-1}) to generate one.

(d) If object C, the HI galaxy just to the east (left) of VIRGOHI 21 (Fig. 2) were involved its mass, by (a), must be $\sim 10^{11} M_\odot$. However, its measured HI velocity distribution and size suggest a probable mass $\leq 10^9 M_\odot$, while it has a luminosity of only $10^8 L_\odot$ and an M_{HI} of $4 \times 10^6 M_\odot$. It is two orders of magnitude too undermassive and underluminous to explain the dynamics of VIRGOHI 21, while there is no sign of its interacting.

(e) The structure of VIRGOHI 21 (Fig. 2a) is centred at R.A. $12^h 17^m 52^s$ and elongated in the North-South plane between $+14°41'$ and $+14°49'$. Its remarkable velocity change (from 1900 to 2100 km s^{-1}) is, however, confined to the tilted structure (Fig. 2b) between $+14°46'$ and $+14°49'$, which closely resembles the characteristic shape of an edge-on disc (Kregel et al. 2004). If indeed

Table 1. PROPERTIES OF THE DARK DISC

Diameter $2R$, [from $+14°46'$ to $49'$]	14 kpc (4×10^{22} cm)
Circular Velocity V_c, $[(1900-2100)/2]$	100 km s^{-1}
Spin Period P, $[2\pi R/V_c]$	4×10^8 years
Total Mass M_T, $[RV_c^2/G]$	$2 \times 10^{10} M_\odot$ (solar masses)
Face-on Mass-density $[M_T/\pi R^2]$	2×10^{-2} g cm^{-2}
Hydrogen Mass M_{HI}, [flux $F_{HI} = 0.7$ Jy km s^{-1}]	$4 \times 10^7 M_\odot$
Face-on gas density N_{HI}, $[M_{HI}/\pi m_{HI} R^2]$	3×10^{19} HI atoms cm^{-2}
Total Mass to Blue Light Ratio in solar units [assuming a disc $0.5' \times 3'$]	$> 750 M_\odot/L_\odot$

what we are witnessing here is a dark, gravitationally bound, edge-on rotating disc then its properties are as presented in Table 1, with a minimum mass of $2 \times 10^{10} M_\odot$. Judging from visible disc galaxies, whose masses continue to rise beyond their HI edges (Salucci & Persic 1997), the full size and mass of such a disc could easily reach $\sim 10^{11} M_\odot$. The very low surface-brightness limits (dimmer than 27.5 Blue mag arcsec^{-2}; Minchin et al. 2005) imply that the disc has $M_{tot}/L_B > 750 M_\odot/L_\odot$, where normal galaxies have < 50.

The integrated spectrum, minus the bridge, is consistent with earlier single-dish observations, implying that the interferometer misses little HI. The surprising ease with which it has been mapped is due to two pieces of luck: it is edge on, thus increasing the apparent surface density, and most of its gas is spread over fairly low velocity widths within each synthesised beam.

The incontrovertible evidence of an interaction with NGC 4254 provides independent support for the massive nature of VIRGOHI 21. NGC 4254 is a luminous one-armed spiral galaxy, sufficiently peculiar to have attracted several studies (Iye et al 1982; Phookun et al. 1993; Vollmer et al. 2005). Single-armed spirals are invariably the result of interactions with close-by massive companions (Iye et al 1982); the lack of any visible companion thus triggered much interest. Recent numerical models by Vollmer et al. indicate that NGC 4254 "had a close and rapid encounter with a $10^{11} M_\odot$ galaxy $\sim$250 Myr ago. The tidal interaction caused the spiral structure...". Phookun et al., in a VLA study of the galaxy, find a trail of gas leading away from it (their Figure 5) in both the right direction and with exactly the right velocity-gradient required to intersect VIRGOHI 21. Thus the case for VIRGOHI 21 being the aforesaid $\sim 10^{11} M_\odot$ mass which caused the peculiarities in NGC 4254 seems strong.

Models for VIRGOHI 21 now have a number of crucial observations to explain: the broad velocity-width in a galactic volume (implying large mass); its elongated geometry; its steep velocity profile; the bridge to NGC 4254, and to no other galaxy; the damage to NGC 4254; and the lack of light.

The first hypothesis to consider is that we are detecting tidal debris left by the past interaction of NGC 4254 and another galaxy. This is rather easy to

dismiss here where the lines are so broad, and there are no such interactors visible nearby. Imagine two galaxies with radial velocities, V_1 and V_2 at either end of an approximately linear tidal bridge of physical length d pitched at an angle θ to the plane of the sky. A telescope pointed towards it has a transverse beam diameter of b at the bridge. The only significant gas motions within the bridge will be streaming velocities along its length. From end to end of the bridge the radial velocity difference is $|V_2 - V_1|$ while within the telescope beam the measured velocity width, ΔV, will be $(b/d \sin\theta) \times |V_2 - V_1|$. But, as is well known, bridges of any size arise only when the *total* velocity difference between the interacting galaxies – $|V_2 - V_1|/\cos\theta$ here – is of the same order as the circular velocity V_c in the donor (Toomre & Toomre 1972). It follows immediately that $\Delta V/V_c \simeq (b/d)\tan\theta$. Thus broad line widths $\Delta V \simeq V_c$, as here, can only be seen within a beam if *both* interactors *appear* to lie within, or very close to the beam ($d\cos\theta \leq b$). There are no such putative interactors anywhere close to VIRGOHI 21 (see figures), let alone within a beam diameter. VIRGOHI 21 cannot be such tidal debris.

Of other models that have been suggested, or that we have been able to devise, neither Ram Pressure Stripping (Oosterloo & van Gorkom 2005) nor a Group gravitational field (Bekki et al. 2005a), nor long-range interactions deliberately aimed at simulating this object (Bekki et al. 2005b) can explain the abrupt changes of velocity. A ballistic encounter of the bridge with other gas clouds would require a number of separate but neighbouring clouds travelling at improbably different velocities to account for the different kinks in VIRGOHI 21. If radiation pressure were responsible, where is the necessary powerful source? We are left with the massive dark disc model (Minchin et al. 2005) which explains all the above.

The biggest theoretical puzzle for the Dark Galaxy model of VIRGOHI 21 is its observed shortage of baryons. Visible disc galaxies typically have, in the form of stars and gas, $\sim$10 per cent of their dynamical mass in baryons, a figure consistent with cosmological models which predict $\sim$7 times as much Dark Matter as baryonic in the Universe at large (Salucci & Persic 1997). Had VIRGOHI 21 10 per cent of its mass in baryons it would contain $\sim 2 \times 10^9$ solar masses which would, if it were once in the form of HI spread evenly across the existing dynamical disc, yield a column density $\sim 10^{21}$ atoms cm^{-2} – sufficiently above the "star-formation threshold" of $\sim 10^{20}$ cm^{-2} (Martin & Kennicutt 2001), or above the Toomre criterion for gravitational instability in a rotating disc (Toomre 1964), to form stars (Verde et al. 2002). Since it apparently contains no stars it must have *and must always have had*, ten times less baryons – a phenomenon often apparent in dwarf galaxies (Mateo 1998). Only $2 \times 10^8 M_\odot$ of HI is currently detectable – and even that could have been stolen from NGC 4254 during their interaction. Ram pressure stripping of a 10^{21} cm^{-2} disc by the present intra-cluster medium in Virgo (assuming a

dynamic pressure $\sim 10^{-11}$ to 10^{-12} cgs units) is just possible numerically, but, given that clusters form late, it would be a relatively recent phenomenon – so this would only work if VIRGOHI 21 is younger than the cluster as a whole. While the interaction with NGC 4254 could certainly have removed gas, that doesn't explain the lack of star-formation prior to that relatively recent encounter. Thus 90 per cent of the baryons one might have expected to find in VIRGOHI 21 appear to be missing. Whatever the reason, the lack of baryons in such massive objects can only decrease their detectability.

Theoretical difficulties with the baryon deficiency aside, the new observations make it even harder to escape the inference that VIRGOHI 21 contains a massive dark disc.

Acknowledgements We thank the NFRA for use of the WSRT and PPARC for financial support. We would like to thank the following for useful comments: Virginia Kilborn, Erwin de Blok, Martin Zwaan and Greg Bothun. Arecibo Observatory is part of NAIC, which is operated by Cornell University under a cooperative agreement with the NSF.

References

Bekki, K., Koribalski, B. S., Ryder, S. D., & Couch, W. J., 2005, MNRAS, 357, L21
Bekki, K., Koribalski, B. S. & Kilborn, V. A., 2005b, MNRAS, 363, L21
Briggs, D. S., 1995, BAAS, 27, 1444
Davies, J. et al., 2004, MNRAS, 349, 922
D'Onghia, E & Lake, G., 2004, ApJ, 612, 628
Iye, M., Okamura, S., Watanabe, M., 1982, ApJ, 256, 103
Kregel, M., van der Kruit, P. & de Blok, W., 2004, MNRAS, 352, 787
Martin, C. & Kennicutt, R., Jr., 2001, ApJ, 555, 301
Mateo, M. L., 1998, ARA&A, 36, 435
Minchin, R. et al. 2005, ApJ, 622, L21
Moore, B. et al. 1999, ApJ, 524, L19
Oosterloo, T. & van Gorkom, J. A, 2005, A&A, 437, L19
Peacock, J. 1998, *Cosmological Physics*, Cambridge University Press, Cambridge.
Peebles, P. 1993, *Principles of Physical Cosmology*, Princeton University Press, Princeton.
Phookun, B., Vogel, S. N. & Mundy, L. G., 1993, ApJ, 418, 113
Salucci, P. & Persic, M., 1997, in *Dark and Visible Matter in Galaxies* (eds. M. Persic & P. Salucci), ASP Conf. Ser. 117, p. 1, Astron. Soc. Pacific, San Francisco.
Toomre, A. & Toomre, J., 1972, ApJ, 178, 623
Toomre, A., 1964, ApJ, 139, 1217
Verde, L., Oh, S. & Jimenez, R., 2002, MNRAS, 336, 541
Vollmer, B., Huchtmeier, W. & van Driel, W., 2005, A&A, 439, 921

COMPARING DYNAMICAL AND STELLAR POPULATION MASS-TO-LIGHT RATIO ESTIMATES

Roelof S. de Jong[1*] and Eric F. Bell[2**]

[1] *Space Telescope Science Institute, Baltimore, USA*

[2] *Max-Planck-Institut für Astronomie, Heidelberg, Germany*

* dejong@stsci.edu, ** bell@mpia.de

Abstract We investigate the mass-to-light ratios of stellar populations as predicted by stellar population synthesis codes and compare those to dynamical/gravitational measurements. In Bell & de Jong (2001) we showed that population synthesis models predict a tight relation between the color and mass-to-light ratio of a stellar population. The normalization of this relation depends critically on the shape of the stellar IMF at the low-mass end. These faint stars contribute significantly to the mass, but insignificantly to the luminosity and color of a stellar system. In Bell & de Jong (2001) we used rotation curves to normalize the relation, but rotation curves provide only an upper limit to the stellar masses in a system. Here we compare stellar and dynamical masses for a range of stellar systems in order to constrain the mass normalization of stellar population models. We find that the normalization of Bell & de Jong (2001) should be lowered by about 0.05-0.1 dex in *M/L*. This is consistent with a Kroupa (2001), Chabrier (2003), or a Kennicutt (1983) IMF, but does not leave much room for other unseen components.

Keywords: stars: mass function - galaxies: stellar content - galaxies: fundamental parameters - galaxies: kinematics and dynamics - dark matter

1. Introduction

In Bell & de Jong (2001) we showed that stellar population models predict a strong correlation between an optical color of a stellar population and its mass-to-light (*M/L*) ratio (see also e.g., Bell et al. 2003; Portinari et al. 2004). We showed that the *slope* of this relation is rather insensitive to the exact details of the star formation history and chemical enrichment of the stellar population (except for recent star bursts) and to dust reddening, owing to the well-known age/metallicity/dust degeneracy. Furthermore, the color–*M/L* slope is also rather insensitive to the IMF used. Yet, the *normalization* of the color–*M/L* relation is highly IMF dependent, shifting up and down depending on

R. S. de Jong, Island Universes, 107–116.
© 2007 *Springer.*

how many stars are present at the low-mass end of the stellar IMF (these stars contribute significantly to the mass of a population, but insignificantly to its luminosity and color).

In Bell & de Jong (2001) we used maximum disk rotation curves to constrain the normalization of the color–*M/L* relation. The predicted stellar population masses derived from the color–*M/L* relation should never over-predict the observed dynamical masses derived from rotation curves. However, while rotating gas in a disk galaxy is a very simple dynamical system and hence a clean constraint, rotation curves of disk galaxies have the disadvantage that they only provide an upper limit to *M/L* ratios once we accept that dark matter may be present in disk galaxies. There is no guarantee that there is no unseen matter contributing to the dynamical mass within the radius where the maximum disk is constrained, be it baryonic (e.g., cold molecular gas) or non-baryonic. Hence, rotation curves only provide an upper limit to the normalization of the color–*M/L* relation. Here we compare dynamical masses and masses predicted by stellar population modeling of a variety of stellar systems in order to constrain the normalization of the color–*M/L* relation[1].

2. Comparing Dynamical and Population *M/L* Estimates

In order to compare dynamical and stellar population masses we have to make a number of assumptions:

- The IMFs of the stellar populations in the different objects are the same, notwithstanding the large range in object scale sizes and masses involved.
- The stellar population models used are accurate in a relative sense (not necessary in absolute calibration).
- The stellar systems in question have not selectively lost (or accreted) stars in a particular mass range.
- Where necessary we use the HST Key Project distance scale.

We will now go through a number of dynamical/gravitational versus stellar population mass comparisons, and express the range of allowed population *M/L* ratios in terms of the IMF normalization used in Bell & de Jong (2001), i.e. a Salpeter x=1.35 IMF between 0.1 and 125 $M_{\odot}$ reduced in mass by a factor 0.7[2].

[1] In principle, any of these systems could have a dark component co-spatial with the stellar light (in some cases this is rather unlikely), and hence all comparisons are strictly speaking upper limits to the relation.

[2] We do not explicitly include a mass contribution for objects with masses less than 0.1 $M_{\odot}$; as argued later, the contribution from brown dwarf or planetary regime objects to the stellar *M/L* is expected to be 0.04 dex or less.

Globular Clusters At first sight globular clusters seem ideal targets to compare dynamical and stellar population masses: their stellar populations, dust corrections and dynamics are simple, and they are unlikely to contain large amounts of dark matter near their centers. However, mass segregation has resulted in centers of clusters being dominated by massive stars, the outer parts by lower mass stars. The outer stars are subsequently more likely to be stripped by interaction with the galaxy, making it even harder to get a good sampling of the original full IMF. Detailed dynamical modeling of Galactic globular clusters shows clear evidence of these effects, with *M/L* changing with radius (e.g., Gebhardt & Fischer 1995).

When we compute the dynamical core *M/L* ratios of Galactic globular clusters following McLaughlin (2000) and compare those to single burst *PEGASE* (Fioc & Rocca-Volmerange 1997) models using the colors and metallicities of Harris (1996), we find that the dynamical *M/L* values are much lower (by about 0.23 dex) than predicted by the single burst models of a 10–12 Gyr old population. Alternatively, we can follow a more simplified approach by using virial masses (Pryor & Meylan 1993), which are more representative of the total globular cluster. We find that the 12 Gyr stellar population masses are lower by 0.10 dex than the virial masses when using our Bell & de Jong (2001) IMF normalization, albeit with a large scatter of 0.20 dex rms (comparable to the uncertainties in the dynamical *M/L* values).

In recent years it has also become possible to measure virial masses of globular clusters in other nearby galaxies. This has the advantage that it is easier to get integrated properties the globular clusters and many objects at the same distance, but as disadvantage the limited accuracy that can be reached, even with 8 m class telescopes. The results of extra-galactic globular clusters are still inconclusive, with dynamical masses of Cen A as measured by Martini & Ho (2004) being more massive than our stellar population model predictions by 0.08 dex, but the dynamical masses of M33 (Larsen et al. 2002) being 0.27 dex lower than predicted.

Elliptical galaxies Recently, Cappellari et al. (2006) have performed a detailed analysis of dynamical and stellar populations masses of a sample of early-type galaxies. Their integral field spectrograph SAURON data allows them to derive accurate dynamical masses using Schwarzschild modeling and stellar population masses using line-strength indices modeling. Using a Kroupa (2001) IMF and Vazdekis et al. (1999) stellar population synthesis models, they find that old, fast rotating elliptical galaxies have dynamical and stellar population masses that are very similar. Younger, fast rotating elliptical galaxies have smaller stellar population masses than dynamical masses, but they can be made to agree by assuming that the young ages are the result of a superposition of a dominant, old massive population and a small, young population. However, slowly rotating, old massive elliptical galaxies seem to have higher dynamical

than stellar population *M/L* ratios, a discrepancy that cannot be solved by a super-position of young and old populations, because the population already is old according to the line indices.

Cappellari et al. (2006) argue that under the assumption that the IMF is the same for all galaxies this must mean that these massive, slowly rotating galaxies have a significant dark matter within their effective radius where the dynamical measure was made. However, once we accept that some elliptical galaxies must have a dynamically significant amount of dark matter in their central region, we cannot exclude that all elliptical galaxies have dark matter contributing to their central dynamics. Therefore, the comparison of stellar population and dynamical masses in elliptical galaxies becomes an upper limit to the normalization of the "IMF mass", identical to the maximum disk rotation curve constraint. In terms of this mass normalization, this argues for a ~ 0.05 dex lower normalization that used by Bell & de Jong (2001), given that the Vazdekis models include masses down to 0.01 $M_{\odot}$.

Maximum disk rotation curves: As described above, we used maximum disk rotation curve limits to normalize the color–*M/L* relation in Bell & de Jong (2001). In Kassin, de Jong & Weiner (2006) we have repeated this analysis, but we expanded the Verheijen (1997) Ursa Major cluster sample with 34 luminous galaxies and improved the treatment of shifting the mass models to another distance. We compared the maximum disk values to the updated color–*M/L* relations of Bell et al. (2003) and find that the Bell & de Jong (2001) normalization is fully consistent with this expanded data set. The normalization may at best be 0.05 dex higher to account for the scatter in the color–*M/L* relation.

Minimum disk rotation curves: While most galaxy rotation curves are fairly smooth, some show enough structure to allow determination of a lower limit to a stellar *M/L* to explain these structures under the assumption that the dark matter component is smooth (e.g., Noordermeer et al. 2004). Such analysis is complicated by the unknown intrinsic distribution of dark matter, the effect of adiabatic contraction, and rotation curve uncertainties (including non-circular motions). Using NGC 157 (Kassin et al. 2006) we find a lower limit of -0.3 dex with respect to the Bell & de Jong (2001) normalization to explain the strongly declining rotation curve of this galaxy. However, the large asymmetries and hence large errorbars on the rotation curve of this galaxy limits the usefulness of this galaxy. More suitable systems (mainly early-type spiral galaxies with falling rotation curves) are studied by Noordermeer (2006).

Disk velocity dispersions: The mass and scale height distribution determine the vertical velocity dispersion of a self-gravitating disk. Thus, to determine a disk mass from a measured vertical velocity dispersion in a face-on system we have to make assumptions about the (unobservable) vertical stellar distribution,while for edge-on systems, where we can measure the vertical stellar

distribution, we have to relate the observed radial and tangential velocity dispersion to the (unobservable) vertical velocity dispersion (Bottema 1997). Recently, Kregel et al. (2005) used velocity dispersions of a sample of 15 edge-on galaxies to determine a dynamical mass Tully-Fisher relation and compared it to the stellar population mass Tully-Fisher relation of Bell & de Jong (2001). They find an offset of about -0.24 dex, assuming a vertical-to-radial velocity dispersion ratio (σ_z/σ_R) of 0.6. However, the determined *M/L* ratio scales quadratically with the poorly known σ_z/σ_R ratio. To the best of our knowledge, only 3 measurements of σ_z/σ_R have been made to date, ranging between 0.5 and 0.9 (Gerssen, Kuijken, & Merrifield 2000). Without substantially better understanding of the behavior of σ_z/σ_R as a function of galaxy properties, it is unclear that one can place competitive constraints on stellar *M/L* ratios using this method.

Bar streaming motions: A galactic bar moving through the interstellar medium creates streaming motions and often a shock, the size of which depends somewhat on the pattern speed of the bar, but mostly on the mass of the bar. Weiner et al. (2001; 2004) obtained $H\alpha$ velocity fields of NGC 4123 and NGC 3095 and modeled these with fluid-dynamical models. Their models only permit a limited range in stellar *M/L*, such that the galaxies are close to maximum disk. In Fig. 1 we compare the local bar colors and the derived *M/L* values of these two galaxies to the stellar population models of a range in metallicity and with exponentially decaying star formation rates. We show the models normalized at the Bell & de Jong (2001) value on the left, reduced by 0.1 dex in *M/L* on the right. The models cover a limited area in these

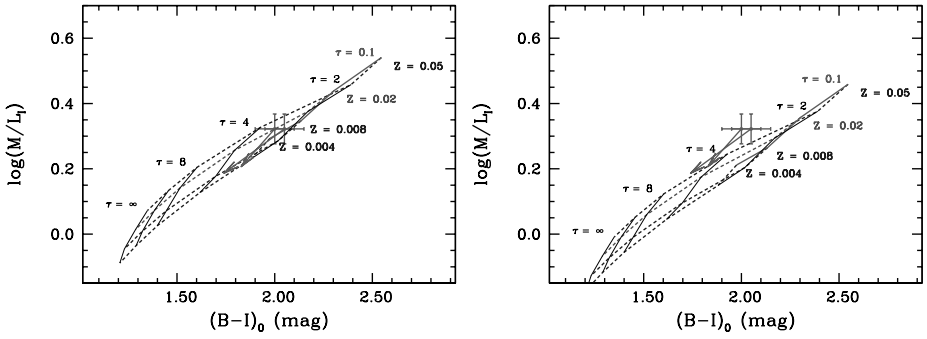

Figure 1. Comparing the Weiner et al. (2001; 2004) bar dynamics *M/L* constraints to Pégase stellar population models (Fioc & Rocca-Volmerange 1997). We plot 12 Gyr old exponential decaying star formation rate models with different decay rates τ connected by solid lines, different metallicities by dotted lines, as indicated. The two data points for NGC 4123 and NGC 3095 are indicated with formal errorbars. The arrows on the data points indicate the reddening for these galaxies according to Tully et al. (1998). On the left we show the Bell & de Jong (2001) normalization, at the right a 0.1 dex lower normalization.

diagrams, showing the age-metallicity degeneracy that makes the color–*M/L* relation work in the first place.

We expect the central region to suffer from extinction, and we have plotted indicative dereddening vectors on the measured data points. These vectors were derived from Tully et al. (1998) global galaxy reddening values, and the extinction in the central region may be somewhat higher. The left panel, where the Bell & de Jong normalization is used, shows that the raw and reddening-corrected stellar *M/L* ratios are consistent with the model normalization. The right-hand panel, with the model stellar *M/L* values decreased by 0.1 dex compared to Bell & de Jong (2001), is just consistent with the reddening-corrected data. The bar streaming motions modeling therefore provides some of the strongest constraints on our color–*M/L* normalization, allowing only a range of $\sim$0.2 dex.

Pérez et al. (2004) confirm the analysis of Weiner et al. (2001) to the extent that, for the two out of their sample of five galaxies for which they could derive *M/L* constraints, the barred galaxies had to be close to maximum disk (at least 80% stellar mass contribution in bar region).

Spiral arm streaming motions: In a similar fashion, streaming motions can be used to estimate the mass in a spiral density wave. Clearly this is a more challenging exercise, as arm-induced shocks and streaming motions are much weaker than those induced by bars. Kranz et al. (2003) studied five high surface brightness galaxies with long-slit spectra and optical/near-IR surface photometry. They can only weakly constrain stellar *M/L* (their Table 3), and find *i)* most of their sample have maximum disk *M/L* values consistent with the Bell & de Jong calibration, and *ii)* most high $v_{\rm rot}$ disks are consistent with close to maximum disk, whereas the lower rotation velocity disks could be substantially sub-maximal (with less than $\sim$60% of the disk mass coming from stars within 2.2 disk scalelengths).

Strong galaxy lensing: Strong gravitational lensing provides an estimate of the gravitational mass within the lens area with rather straightforward modeling. To compare the gravitational mass of the lens with its stellar population mass we have to correct the observed colors using k-corrections or better yet, redshift the model spectra to the lens redshift and calculate a new color–*M/L* grid in the observed bands. Furthermore, we have to realize that galaxies are younger at higher redshift and the color–*M/L* relation will shift. For simplicity we can model this with exponentially declining star formation rate models (which becomes an increasingly poorer approximation at higher redshift, because starbursts will become relatively more important). Such exponentially declining models — started 12 Gyr ago — have color–*M/L* relations in *rest-frame colors* that are decreased by 0.15 dex at redshift 1 compared to the z=0 relation.

To minimize these corrections a lensing galaxy at low redshift should be used in the gravitational to stellar mass comparison. Furthermore, the lensed images should be of small angular separation, surrounding only the central region of the lens galaxy, which is most likely to be dominated by stellar mass. We should keep in mind that any masses derived from lensing, like maximum rotation curves, only provides an upper limit to the stellar population mass estimates, as significant dark matter may be present in the centers of some galaxies as also suggested by the Cappellari et al. (2006) elliptical galaxies result.

Indications from the first studies to satisfy these criteria are encouraging. Smith et al. (2005) present an example of a low redshift (z=0.0345), tight lens, finding a $M/L_I{\sim}1.8$, $M/L_B{\sim}4.7$. Using the reported F475W and F814W observed magnitudes, galactic foreground corrections, and k-corrections assuming a non-evolving ancient galaxy template (solar metallicity and $\sim$12 Gyr old), we find excellent agreement with the predicted stellar *M/L* values, as usual accounting for gas recycling from ageing stellar populations ($M/L_{I,\mathrm{pred}}{\sim}1.8$, $M/L_{B,\mathrm{pred}}{\sim}4.5$). Koopmans et al. (2006) analyze an extensive sample of 15 lenses with z=0.06–0.33. In this case, the dynamically-derived *total M/L* scale is compared with the lensing results, finding consistency (i.e., they have roughly cross-checked the dynamical mass scale — e.g., Cappellari et al.'s scale — with the lensing scale). A more careful, explicit test of the color-derived stellar mass scale with the lensing mass scale is clearly warranted.

3. Conclusions

In Fig. 2 we give an overview of all constraints derived in the previous section on stellar population *M/L* values relative to an IMF normalization of Bell & de Jong (2001). The strongest constraints are currently provided by the Weiner et al. (2001, 2004) constraints from bar streaming motions. However, this constraint is derived from only two galaxies, and is therefore very susceptible to for instance errors in the distances to the galaxies. We have indicated in Fig. 2 the effect of 15% distance errors, which accounts for 0.075 dex offset in the *M/L* IMF normalization. Another source of uncertainty lies in the stellar population modeling. The Padova isochrone tracks (Girardi et al. 2002) are used in many of the popular models (e.g., Charlot & Bruzual 2003; Fioc & Rocca-Volmerange 1997; Vazdekis 1999) and these models all give very similar results in terms of the color–*M/L* relation. However, a class of models based on the fuel consumption theorem that treats the late stages of stellar evolution differently are giving somewhat different results, especially in the infrared where AGB and RGB stars dominate (e.g., Maraston 2005). These models have indeed a slightly steeper slope in the color–*M/L* relation, especially in the near-infrared, but surprisingly the normalizations of the different

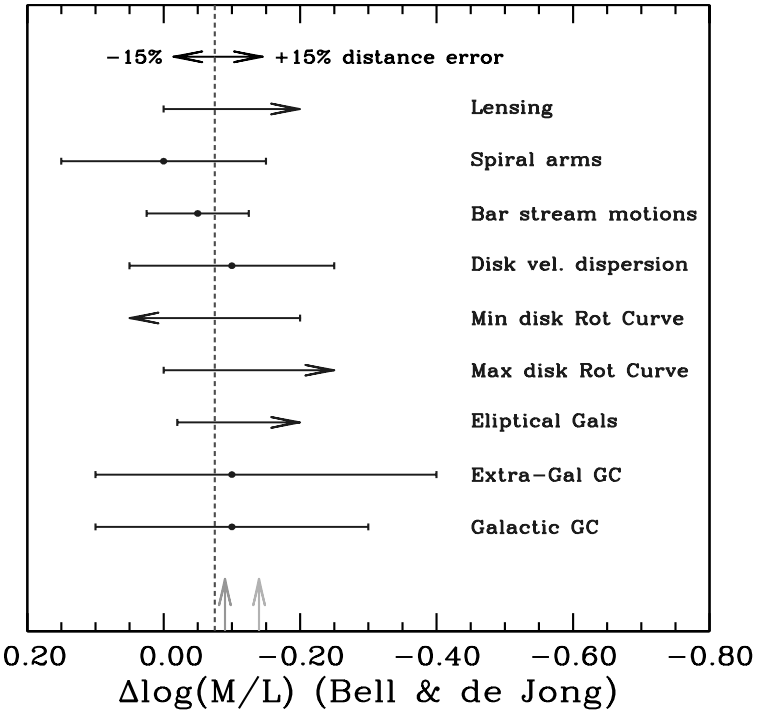

Figure 2. Overview of offsets between dynamical and stellar population mass estimates relative to the normalization of Bell & de Jong. Ranges are indicated by horizontal errorbars, upper and lower limits are indicated with horizontal arrows. The vertical dotted line indicates the our best estimate for the offset given all constraints. The uncertainty in this offset caused by 15% distance errors are indicated at the top. The vertical arrows indicate offsets expected for a Kroupa (2001) IMF (left, green) and a Kennicutt (1983) IMF (right, cyan).

sets of models are very consistent in the intermediate color range where most of the normalization constraints are derived. Combining all constraints, we argue that the most likely normalization is about 0.05–0.1 dex lower than the Bell & de Jong (2001) normalization, i.e. a Salpeter x=1.35 IMF between 0.1 and 125 $M_{\odot}$ reduced in mass by a factor 0.6 (-0.22 dex).

This normalization is consistent with for instance the Kroupa (2001) or Chabrier (2003) IMFs (offset by about -0.25 dex with respect to Salpeter IMF) and a Kennicutt (1983) IMF (-0.3 dex). It leaves however not much margin for other unseen but known mass components in the dynamical comparisons. Stellar and substellar objects below our 0.1 $M_{\odot}$ mass limit could contribute up to 10% (0.04 dex) of the IMF mass. A significant molecular gas component in the inner part of spiral galaxies could push down the rotation curve constraint. However, it is satisfying to see that the current Galactic IMF estimates give stellar mass estimates in a wide range of objects that are fully consistent with their dynamical masses.

References

Bell, E. F., & de Jong, R. S. 2001, ApJ, 550, 212
Bell, E. F., McIntosh, D. H., Katz, N., & Weinberg, M. D. 2003, ApJS, 149, 289
Bottema, R. 1997, A&A, 328, 517
Bruzual, G., & Charlot, S. 2003, MNRAS, 344, 1000
Cappellari, M., et al. 2006, MNRAS, 366, 1126
Chabrier, G. 2003, ApJ, 586, L133
Fioc, M., & Rocca-Volmerange, B. 1997, A&A, 326, 950
Gebhardt, K., & Fischer, P. 1995, AJ, 109, 209
Gerssen, J., Kuijken, K., & Merrifield, M. R. 2000, MNRAS, 317, 545
Girardi, L., Bertelli, G., Bressan, A., Chiosi, C., Groenewegen, M. A. T., Marigo, P., Salasnich, B., & Weiss, A. 2002, A&A, 391, 195
Harris, W.E. 1996, AJ, 112
Kassin, S. A., de Jong, R. S., & Weiner, B. J. 2006, ApJ, 643, 804
Kennicutt, R. C., Jr. 1983, ApJ, 272, 54
Koopmans, L.V.E., Treu, T., Bolton, A.S., Burles, S., Moustakas, L.A., 2006, submitted to ApJ (astro-ph/0601628)
Kranz, T., Slyz, A., & Rix, H.-W. 2003, ApJ, 586, 143
Kregel, M., van der Kruit, P. C., & Freeman, K. C. 2005, MNRAS, 358, 503
Kroupa, P. 2001, MNRAS, 322, 231
Larsen, S. S., Brodie, J. P., Sarajedini, A., & Huchra, J. P. 2002, AJ, 124, 2615
Maraston, C. 2005, MNRAS, 362, 799
Martini, P., & Ho, L. C. 2004, ApJ 610, 233
McLaughlin 2000, ApJ, 539, 618
Noordermeer, E. 2006, Ph.D. Thesis, University of Groningen
Noordermeer, E., van der Hulst, T., Sancisi, R., & Swaters, R. 2004, IAU Symposium, 220, 287
Pérez, I., Fux, R., & Freeman, K. 2004, A&A, 424, 799
Portinari, L., Sommer-Larsen, J., & Tantalo, R. 2004, MNRAS, 347, 691
Pryor, C., & Meylan, G. 1993, in ASP Conf. Ser. 50, Structure and Dynamics of Globular Clusters, ed. S. Djorgovski & G. Meylan (San Francisco: ASP), 357
Salpeter, E. E. 1955, ApJ, 121, 161
Smith, R. J., Blakeslee, J. P., Lucey, J. R., & Tonry, J. 2005, ApJL, 625, L103
Tully, R. B., Pierce, M. J., Huang, J.-S., Saunders, W., Verheijen, M. A. W., & Witchalls, P. L. 1998, AJ, 115, 2264
Vazdekis A., 1999, ApJ, 513, 224
Verheijen, M. A. W. 1997, Ph.D. Thesis, University of groningen
Weiner, B. J. 2004, IAU Symposium, 220, 265
Weiner, B. J., Sellwood, J. A., & Williams, T. B. 2001, ApJ, 546, 931

Roelof de Jong.

FEEDING THE NUCLEAR STARBURST IN NGC 6946

T. Böker[1], E. Schinnerer[2], E. Emsellem[3] and U. Lisenfeld[4]

[1]*European Space Agency, Noordwijk, The Netherlands*

[2]*Max-Planck-Institut für Astronomie, Heidelberg, Germany*

[3]*Centre de Recherche Astronomique de Lyon, France*

[4]*Dept. Física Teórica y del Cosmos, Universidad de Granada, Spain*

Abstract We present the highest angular resolution (0.6 arcsec) and most sensitive CO(2-1) and (1-0) observations ever made of the nuclear region of the nearby late type (Scd) spiral galaxy NGC 6946. The data - obtained with the Plateau de Bure interferometer - resolve for the first time the gas morphology inside the central 300 pc of NGC 6946. The CO maps reveal an S-shaped spiral running through a small-scale gas disk centered on the galaxy nucleus. The disk has a radius of ≈ 20 pc and shows signs for radial streaming motion towards the nucleus. Our findings suggest that significant amounts of molecular gas are currently being funneled into the very nucleus of NGC 6946, which is undergoing a period of intense star formation. Our observations provide a detailed test for models of nuclear gas spirals inside the inner Lindblad resonance as a possible funneling mechanism towards galactic nuclei, and will be used to constrain the efficiency of nuclear star formation in NGC 6946.

Keywords: galaxies: nuclei - galaxies: starburst - galaxies: kinematics and dynamics - sub-millimeter

1. Introduction

A large fraction of nearby spiral galaxies experience intense star formation within a few hundred pc from their nuclei. Many detailed studies exist of the stellar populations produced in these starbursts and the physical conditions in the ionized gas surrounding them. These studies mostly use imaging and/or spectroscopy at visible and NIR wavelengths, which yield sub-arcsecond resolution and thus allow to study star formation processes on scales of individual giant molecular clouds (a few tens of pc).

However, relatively little is known about the mechanisms that lead to the high gas densities within the central $\approx$ 100 pc that are required to tri gger such intense star formation. While much progress has been made in

R. S. de Jong, Island Universes, 117–120.
© 2007 *Springer.*

hydro-dynamical modeling of the gas flow in barred gravitational potentials (e.g., Wada & Koda 2001), there are few observational tests of these models on the scales relevant for nuclear starbursts.

The reason mostly lies in the fact that maps of the molecular gas can rarely match the spatial resolution obtained at optical/NIR wavelengths. For example, the most comprehensive interferometric CO survey of nearby galaxies, the BIMA SONG (Regan et al. 2001, Helfer et al. 2003), has a spatial resolution of $6''$, or $300\,\mathrm{pc}$ at a distance of $10\,\mathrm{Mpc}$. Until the commissioning of the Atacama Large Millimeter Array, only a few nearby galaxies offer the chance to obtain a more detailed picture of the molecular gas dynamics within and around the nuclear starbursts.

NGC 6946 provides such an opportunity. It is one of the nearest (d=$5.9\mathrm{Mpc}$, Karachentsev et al. 2000) large spiral galaxies outside the local group, and currently experiences intense star formation in its central $5''$ ($150\,\mathrm{pc}$, Engelbracht et al. 1996). It harbors a small stellar bar (major axis diameter of $\approx 220\,\mathrm{pc}$) which is most clearly visible in the K-band image of Elmegreen et al. (1998). High-resolution HST maps of the nuclear dust and emission line morphology (Martini et al. 2003, Böker et al. 1999) show a complex pattern of star formation and dense material which is difficult to interpret without kinematical information.

On larger scales, NGC 6946 has an unusual four-armed spiral structure which is traceable inwards down to scales of a few arcsec, both in the stellar light and the CO line emission (Regan & Vogel 1995). Such a morphology is rare in barred spirals, and cannot easily be explained by hydro-dynamical models of gas flows in a barred potential. The effect of the small nuclear bar on the gas dynamics in the inner kpc remained unclear from previous CO observations due to their limited spatial resolution. Here, we present new interferometric CO maps that reach $0.6''$ ($15\,\mathrm{pc}$) resolution and reveal in detail the gas flow patterns within and around the galaxy nucleus.

2. Data

The $^{12}\mathrm{CO}(1-0)$ and $^{12}\mathrm{CO}(2-1)$ lines were observed in February 2002 using the IRAM PdB interferometer with 6 antennas in its A and B configurations providing 30 baselines from 32 to 400 m. The resulting resolution is $0.58'' \times 0.48''$ (PA $-165°$) at $1.3\,\mathrm{mm}$ and $1.25'' \times 1.01''$ (PA 22°) at $2.6\,\mathrm{mm}$ using uniform weighting. The calibration and mapping were done with the GAG software packages CLIC and GRAPHIC. The bandpass was calibrated on the quasar 2037+511. For phase and amplitude calibration, 2037+511 was observed every 20 minutes. The flux calibration was also checked on this source, we achieve an accuracy of better than 15% at both wavelengths. Maps were CLEANed with 10000 iterations. The spectral resolution of the $^{12}\mathrm{CO}(1-0)$

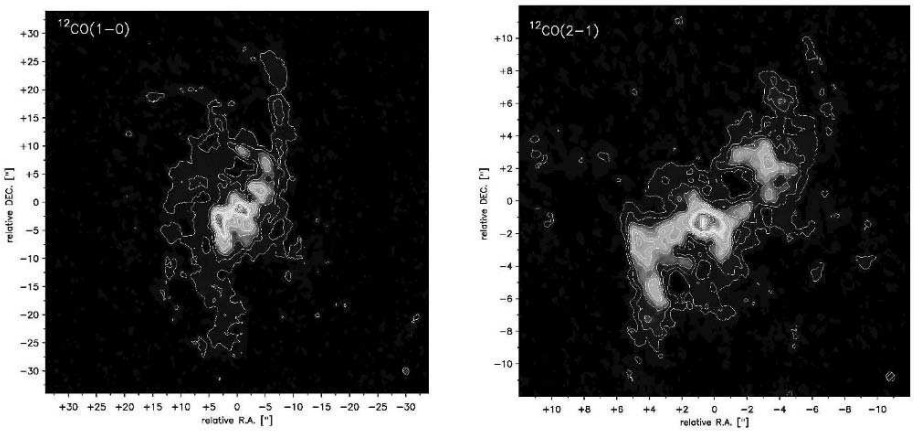

Figure 1. Intensity maps of the $^{12}\mathrm{CO}(1-0)$ (left) and $^{12}\mathrm{CO}(2-1)$ (right) emission lines. The beam sizes are indicated in the lower right, the resolution is $1.2''$ and $0.6''$ in the (1-0) and (2-1) maps, respectively. Note the S-shaped spiral structure in the $^{12}\mathrm{CO}(2-1)$ map which extends all the way into the central $2''$. The channel maps (not shown) indicate that the gas concentration inside the central $2''$ (50 pc) is in a disk configuration.

and $^{12}\mathrm{CO}(2-1)$ line data is 6 and $3\,\mathrm{km\,s^{-1}}$, respectively. The resulting intensity maps of the $^{12}\mathrm{CO}(1-0)$ and $^{12}\mathrm{CO}(2-1)$ lines are presented in Figure 1.

Our analysis of the gas kinematics is still ongoing, but the preliminary velocity map (Figure 2) shows clear deviations from the butterfly pattern expected for gas disk in circular rotation. These deviations - which are evident even within the central few pc - are indicative of radial motions towards the nucleus. This implies that molecular gas is accumulating within the central few pc, plausibly enabling star formation at very small distances from the galaxy nucleus.

3. Summary

Our observations unambiguously confirm that the molecular gas in the central kpc of NGC 6946 is distributed in a spiral pattern, rather than in a molecular bar. The arms of the outer gas spiral extend to within $\approx 5''$ (140 pc) from the nucleus, where they form an S-shape structure that runs through the nuclear starburst. We detect streaming motions along this inner S-shape structure which are consistent with gas falling towards the nuclear starburst. This indicates that the raw material for nuclear star formation is constantly being replenished. The gas dynamics can plausibly be explained by the effect of the small-scale stellar bar evident in NIR images, although detailed dynamical modeling of the observations is still in progress. The high gas densities in the nucleus are sufficient to produce intense star formation, as evident in the strong

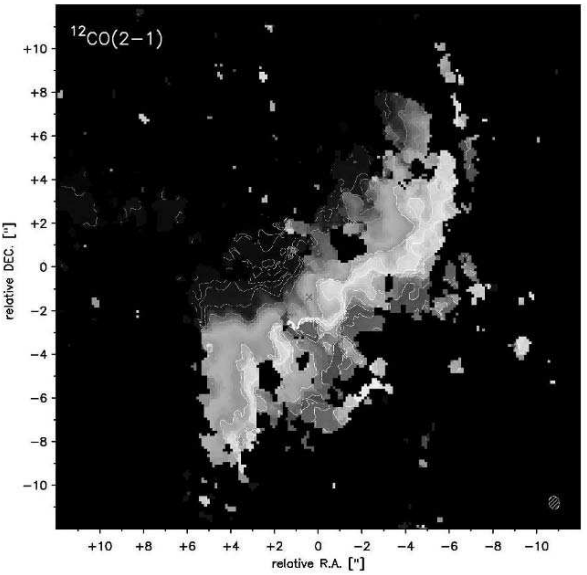

Figure 2. Velocity map of the $^{12}\mathrm{CO}(2-1)$ emission line. The pattern shows deviations from pure circular rotation, suggestive of radial motions towards the nucleus.

nuclear $\mathrm{H}\alpha$ and $\mathrm{Pa}\alpha$ emission seen in optical and NIR images (e.g., Böker et al. 1999).

References

Böker, T., et al. 1999, ApJS, 124, 95
Elmegreen, D. M., Chromey, F. R., & Santos, M. 1998, AJ, 116, 1221
Engelbracht, C. W., et al. 1996, ApJ, 467, 227
Helfer, T. T., et al. 2001, ApJS, 145, 259
Karachentsev, I. D., Sharina, M. E., & Huchtmeier, W. K. 2000, A&A, 362, 544
Martini, P. et al. 2003, ApJ, 589, 774
Regan, M. W. & Vogel, S. N. 1995, ApJL, 452, L21
Regan, M. W., et al. 2001, ApJ, 561, 218
Wada, K. & Koda, J. 2001, PASJ, 53, 1163

INTEGRAL FIELD SPECTROSCOPY OF NGC 2855 AND NGC 7049

L. Coccato[1], E. M. Corsini[2], A. Pizzella[2] and F. Bertola[2]

[1] *Kapteyn Astronomical Institute, University of Groningen, The Netherlands*
[2] *Dipartimento di Astronomia, Padova, Italy*

Abstract We present the ionized gas bidimensional velocity field of two spiral galaxies (NGC 2855 and NGC 7049) which show an S-distortion of the isovelocities. We performed models of the velocity field in order to investigate the possible presence of an inner polar disk which generate such a kinematic behaviour, or the presence of a strong internal warp of the gaseous disk. The decomposition of the surface brightness map of NGC 7049 seems to indicate the presence of an orthogonal decoupled component, while the case of NGC 2855 seems to be better explained in terms of a strong central warp of the gaseous disk.

Keywords: galaxies: kinematics and dynamics - galaxies: spirals - galaxies: structure - galaxies: individual: (NGC 2855, NGC 7049)

1. Introduction

A statistical study reveals that velocity gradients for the gaseous component along the minor axis in galaxies are quite common (Coccato et al. 2004) even if they are unexpected if the gas is moving onto circular orbits. This is a signature that the motions are not circular or the gas is not settled in a plane. Among the variety minor axis velocity gradient shapes, the particular case in which a central velocity plateau along the major axis is combined with a rotation confined only in the innermost regions of the minor axis is suggestive of the presence of an Inner Polar Disk (IPD, i.e. a dynamically and spatially coherent polar gaseous and/or stellar structures rotating in a orthogonal plane with respect the main galaxy disk). In Figure 1 we plot an example of this particular case. Because of the non-complete coverage of the velocity field, long-slit spectroscopy is not enough to fully characterise the IPDs. Integral field spectroscopy is therefore the ideal tool for these purposes. In particular, we selected two Sa galaxies, NGC 2855 and NGC 7049, whose long slit kinematics are suggestive of the presence of a IPD (Corsini et al. 2003). The correct characterisation of the velocity field is fundamental to derive the

R. S. de Jong, Island Universes, 121–124.
© 2007 *Springer.*

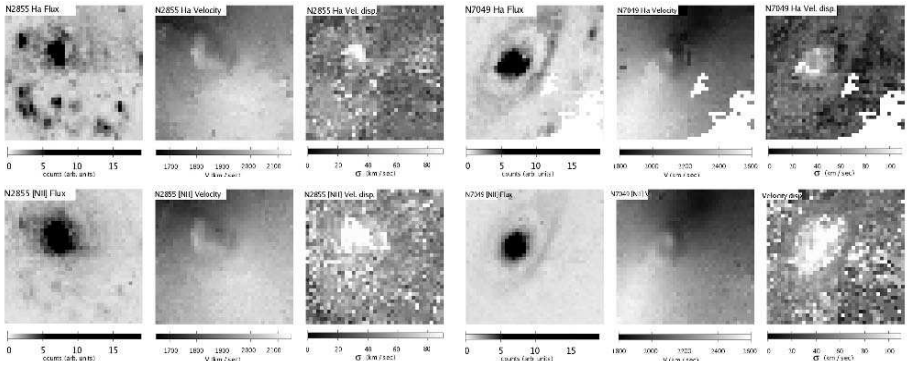

Figure 1. Observed emission line intensity map, radial velocity field and velocity dispersion field for the Hα and [N II] emission lines for the two target galaxies.

correct mass density profile, which can be underestimated if we simply assume circular motions.

2. Galaxy Sample

Spectroscopic observations were carried out at the Very Large Telescope (Paranal, Chile) using the Integral Field Unit (IFU) of the VIsible Multi Object Spectograph (VIMOS) mounted on the UT3 telescope. Data were obtained during the Period 73 (proposal I.D.: 073.B-0545) on 26 – 27 February 2004 (for NGC 2855) and 13 - 15 May 2004 (for NGC 7049). We used the red high resolution grism (HR-red) which ensured a wavelength coverage from 6300 to 8700 Å with a instrumental resolution of FWHM = 68 km/s measured at Hα. The observed field of view is $27'' \times 27''$, the spatial resolution is 0"67/fibre. The measured emission map, velocity field and velocity dispersion field for the Hα and [N II](6583) emission lines are shown in Figure 1.

3. Data Analysis

The bidimensional velocity fields reveal the presence of non circular motions in the central regions (see Figure 2). They can be due to: i) a central warping of the gaseous disk, ii) an orthogonally decoupled component (IPD), or iii) outflows.

We can exclude the case of non-circular but coplanar motions due to the triaxial potential of the bulge (de Zeeuw & Franx 1989) because this scenario is not able to reproduce the observed central plateau along the major axis (Corsini et al. 2003).

The observed kinematics of both galaxies are modelled with a tilt ring model and a two orthogonal component model, in order to understand the intrinsic geometry of the gaseous disk and derive the correct velocity. We show the

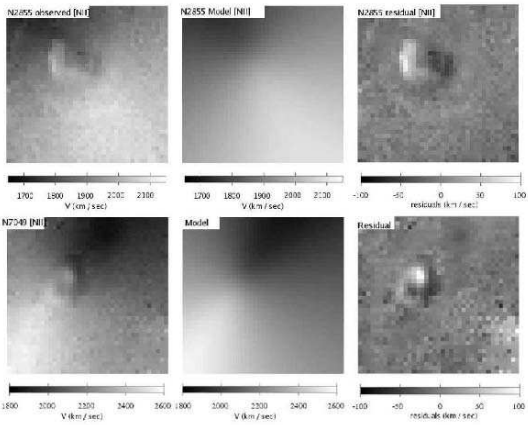

Figure 2. The observed velocity fields (left panels) were fitted with a circular model (central panels), assuming the gas is settled in a thin disk. Residuals from the model (right panels) are remarkable.

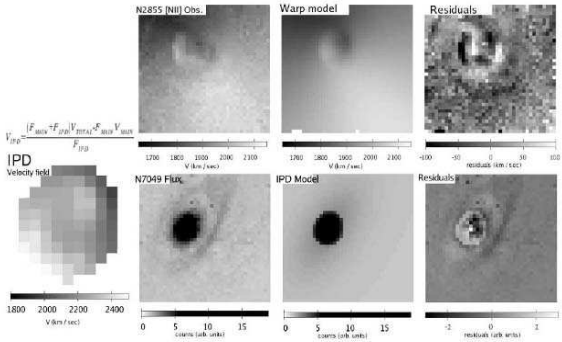

Figure 3. Upper panels: results for the tilted ring model for NGC 2855. Lower panels: results for the two component model for NGC 7049.

results in Figure 3. In the case of the tilted ring model, an arctan function is chosen to characterise the variation of the circular velocity along the radius, while both variations in the position angle and inclination of the rings are considered. In the case of two orthogonal component, the emission line map is considered as the sum of two exponential disk, the main disk and the IPD (this choice fits the emission line surface brightness profile well). The intrinsic velocity field of the IPD is derived from the total velocity field, assuming that the velocity field of the main disk is in circular motions (and derived from the model of Figure 2):

$$V_{Total} = \frac{F_{Main}V_{Main} + F_{IPD}V_{IPD}}{F_{IPD} + F_{MAIN}} \quad (1)$$

4. Conclusions

The bidimensional velocity fields showed an S-shaped distortion on the isovelocities. These deviations from the circular motions reach almost 100 $\mathrm{km\ s^{-1}}$ in the central regions.

We build a two orthogonal component model, which simulate the presence of two orthogonal gaseous disk with circular motions and exponential surface brightness profile. This model does not fit with NGC 2855 data, while for NGC 7049 it fits only for the emission line surface brightness. This mean that: i) there is no IPD in NGC 7049, or ii) there is an IPD in NGC 7049 (as suggested by the emission line map), but its motions are not circular as assumed in the model. In that case we derive its velocity field as a "weighted" subtraction from the main disk velocity field (see Equation 1).

An alternative scenario to the IPD is offered by an internal warp of the galaxy disk (for which the IPD represents an extreme configuration): the gaseous disk is formed by tilted and concentric rings, which are almost orthogonal in the central region. This scenario fits quite well the situation for NGC 2855, reproducing the S-shaped distortion of the velocity field, but not the situation of NGC 7049.

There is no evidence of a bar in NGC 2855, and the stars show regular kinematics and corotate with the gas component (Corsini et al. 2002). This indicates that the orbits in which the gas is moving are not stable (van Albada et al. 1982). In addition we have evidences that the galaxy is acquiring external material (Malin & Hadley 1997) in a direction close to the apparent minor axis. By this argument we conclude that the inner warped structure of the gaseous disk of NGC 2855 is due to an ongoing external acquisition process and it is not in equilibrium. This means that after the acquisition process is over, the gaseous disk of NGC 2855 must settle into the main galaxy equilibrium plane and, if the triaxial potential of the bulge is strong enough to allow an equilibrium plane orthogonal to the main disk (de Zeeuw & Franx 1989), the central part of the warped disk will form an IPD. In this scenario, NGC 2855 may represent a galaxy with a forming IPD.

References

Coccato, L., Corsini, E. M., Pizzella, A., et al. 2004, A&A, 416, 507
Corsini, E. M., Pizzella, A., & Bertola, F. 2002, A&A, 382, 488
Corsini, E. M., Pizzella, A., Coccato, L., & Bertola, F. 2003, A&A, 408, 873
de Zeeuw, T., & Franx, M. 1989, ApJ, 343, 617
Malin, & D., Hadley, B. 1997, PASA, 14, 52
Van Albada, G. D., Kotany, C. G., & Schwarzschil.d, M. 1982, MNRAS. 198, 303

TWO-DIMENSIONAL KINEMATICS OF A BAR AND CENTRAL DISK IN NGC 5448

Kambiz Fathi[1,2], Glenn van de Ven[3], Reynier Peletier[2], Eric Emsellem[4], Jesús Falcón–Barroso[3], Michele Cappellari[3] and Tim de Zeeuw[3]

[1]*Rochester Institute of Technology, USA*

[2]*Kapteyn Astronomical Institute, Groningen, The Netherlands*

[3]*Sterrewacht Leiden, The Netherlands*

[4]*Centre de Recherche Astronomique de Lyon, France*

Abstract We analyse SAURON kinematic maps of the inner kpc of the early-type (Sa) barred spiral galaxy NGC 5448. The observed morphology and kinematics of the emission-line gas is patchy and perturbed, indicating clear departures from circular motion. The kinematics of the stars is more regular, and displays a small inner disk-like system embedded in a large-scale rotating structure. We focus on the [O III] gas, and use a harmonic decomposition formalism to analyse the gas velocity field. The higher-order harmonic terms and the main kinematic features of the observed data are consistent with an analytically constructed simple bar model, which is derived using linear theory. Our study illustrates how the harmonic decomposition formalism can be used as a powerful tool to quantify non-circular motions in observed gas velocity fields.

Keywords: galaxies: kinematics and dynamics - galaxies: structure

1. Introduction

Line-of-sight velocity distributions are efficient probes of the dynamical structure of galaxies, and can be used to derive the mass distribution, intrinsic shape and the motions of stars and gas. Non-axisymmetric components such as bars, or external triggers, can lead to significant galaxy evolution via, e.g., redistribution of the angular momentum, triggering of star formation, or building of a central mass concentration (e.g., Shloshman et al. 1989; Knapen et al. 2000). Much can be learned about these processes by simultaneously studying both the stellar and gas dynamics of nearby galaxies by means of integral-field spectroscopy. Here we summarize such a study for the spiral galaxy NGC 5448, which was observed with SAURON as part of a representative

R. S. de Jong, Island Universes, 125–128.
© 2007 *Springer.*

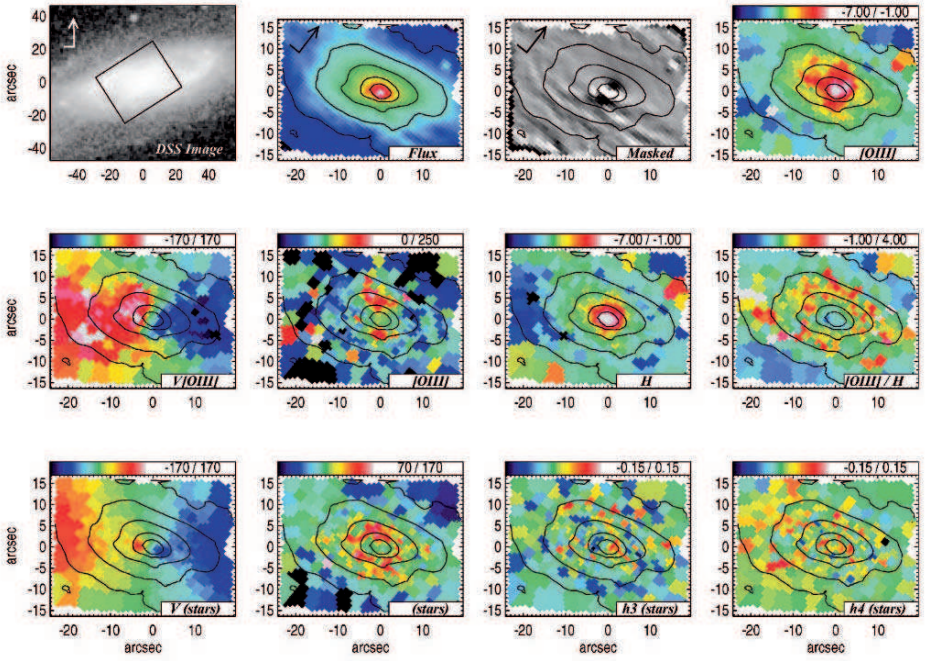

Figure 1. Top Left: Digitised Sky Survey image with SAURON footprint and north-east orientation arrow. All other panels show the SAURON data with the same orientation and overplotted contours in magnitude steps of 0.25. Two-dimensional Voronoi binning has been applied to all our maps, as described in Falcón–Barroso et al. (2005). The titles are indicated at the bottom right corner of each panel with plotting ranges according to the top color bar. All velocities and velocity dispersions are given in km s^{-1}.

survey of 72 nearby early-type galaxies (de Zeeuw et al. 2002; Falcón–Barroso et al. 2005). A more comprehensive report can be found in Fathi et al. (2005).

2. Data

We observed NGC 5448 with SAURON on April 14th 2004. Detailed specifications for the instrument, reduction procedure, and the data preparation procedure can be found in Bacon et al. (2001); Emsellem et al. (2004); Sarzi et al. (2005). The SAURON flux map in Fig. 1 displays a smooth stellar distribution and the presence of prominent dust lanes to the south of the nucleus. The stellar kinematics shows a global disk-like rotation with a smaller inner stellar disk within the central 7″ radius. Along the strong dust lanes, the gas shows a patchy distribution, with an asymmetric elongation of [O III] gas towards the east as well as the galactic poles. The gas velocity map clearly shows a prominent 'S'-shaped zero-velocity curve with sharp edges indicating very strong non-circular gas motions.

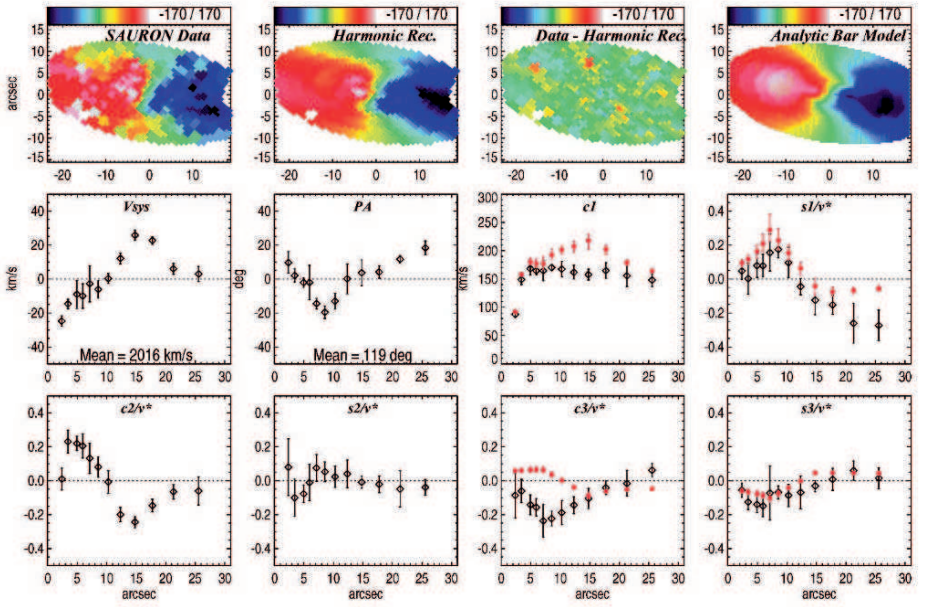

Figure 2. Top row, from left to right: observed SAURON gas velocity field of NGC 5448; the harmonic reconstruction of the SAURON gas velocity field; residual field; and the analytic bar model, which reproduces best the main kinematic features of the observed gas velocity field (in km s^{-1}). Middle and bottom row: the tilted-ring and harmonic parameters as a function of outer radius of each ring, and $v^* = c_1 \sin i$. The over-plotted red filled circles are the analytically calculated first and third harmonic terms for the bar model, with the 3σ (99.7%) confidence level error bars. The orientation of the maps is the same as in Fig. 1.

3. Analysis and Results

In order to study the gas velocity field, we apply the tilted-ring decomposition combined with the harmonic expansion formalism from Schoenmakers et al. (1997). This formalism allows us to extract the gaseous kinematic information such as the rotation curve, kinematic position angle variation, and higher harmonic terms. Wong et al. (2004) derived the higher-order harmonics for an axisymmetric potential with an $m = 2$ bar perturbation. This bar model depends on a set of parameters describing the potential, as well as the viewing angle. We construct libraries of models with different input parameters, and find that we can describe our observed velocity field with the bar model shown in Fig. 2. Thus, the radial motions of the gas are associated with that of the large-scale bar (see Fathi et al. 2005 for a detailed discussion).

NGC 5448 exhibits clear signatures of the presence of other components than a single bar, which affect the observed velocity field. Inspecting the photometry and the central parts of the gaseous and stellar velocity field, we find signatures of a central stellar disk embedded in the larger disk (see Fig. 3). We approximate the stellar velocity field with an exponential thin disk to

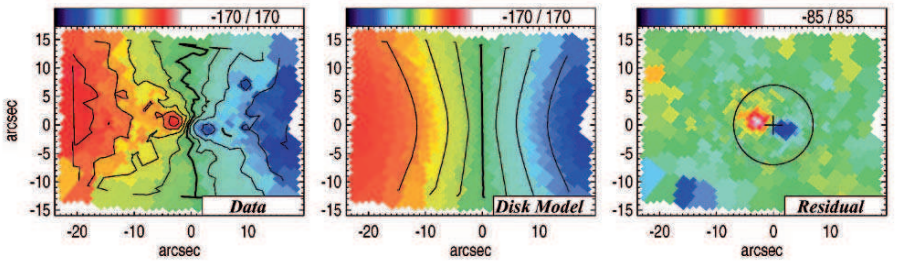

Figure 3. A thin isothermal disk model for the stellar velocity field of NGC 5448. The circle marks the 7″ region within which we find a disk-like structure. All maps are given in km s^{-1}.

emphasize the kinematic signatures of the central disk. Figure 3 illustrates our simple inclined disk model, after subtraction of which we find that the inner stellar disk-like component rotates faster than the outer disk. Fitting also an exponential disk to the region interior to the 7″ radius, we find that the central disk-like structure is misaligned with respect to the outer disk by $\sim 13°$. The stellar kinematic maps show that the central disk rotates faster than the main disk, and our observed gas distribution and kinematics indicate that this central disk also hosts gas which rotates faster than its stellar counterpart. It is known that bars are efficient in transferring mass towards the inner regions of their host galaxies. The centrally concentrated matter may be able to form a secondary bar or a central disk. Our analysis shows that the non-circular gas kinematics in NGC 5448 could be driven by the large-scale bar. The central disk could then have been formed as a result of the gas accumulation at the centre.

Acknowledgements It is a pleasure to acknowledge the entire SAURON team for their efforts in carrying out the observations and data preparation and for many fruitful discussions. KF thanks the conference organizers for all their efforts.

References

Bacon, R. et al. 2001, MNRAS, 326, 23
de Zeeuw, P. T. et al. 2002, MNRAS, 329, 513
Emsellem, E. et al. 2004, MNRAS, 352, 721
Falcón–Barroso, J. et al. 2005, MNRAS, submitted
Fathi, K. et al. 2005, MNRAS, submitted
Knapen, J. H. et al. 2000, ApJ, 528, 219
Sarzi, M. et al. 2005, MNRAS, submitted
Schoenmakers, R. H. M., Franx, M., de Zeeuw, P. T. 1997, MNRAS, 292, 349
Shlosman, I., Frank, J., Begelman, M. 1989, Nature, 338, 45
Wong, T., Blitz, L., Bosma, A. 2004, ApJ, 605, 183

DETERMINATION OF THE GALACTIC ROTATION USING OPEN STAR CLUSTERS

Preliminary Results

Peter M. Frinchaboy* and Steven R. Majewski**

Department of Astronomy, University of Virginia, USA

* pmf8b@virginia.edu, ** srm4n@virginia.edu

Abstract The dark matter distribution of the Milky Way remains among the major unsolved problems about our home galaxy. The masses of other spiral galaxies can be determined from their rotation curves through long-slit spectroscopy. But for the Milky Way obtaining the complete rotation curve is a more complex problem. By measuring the 3-dimensional motions of tracer objects the rotation curve and Galactic mass distribution can be derived, even outside the solar circle where H I tangent point analysis is not possible. We present the first findings from a project to measure the motions of open clusters, both inside and outside the solar circle. From a nearly uniform sample of spectroscopic data for large numbers of stars in over 50 open clusters in the third and fourth Galactic quadrants, we derive the speed of Galactic rotation at the solar circle as $\Theta_0 = 214^{+6}_{-9}$ km s^{-1}. Future work will include clusters in the other Galactic quadrants and analysis of the local rotation curve.

Keywords: Galaxy: open clusters and associations - Galaxy: fundamental parameters - Galaxy: structure - Galaxy: kynematics and dynamics

Considering the importance of galactic potentials in shaping the chemodynamical evolution of their stellar populations, it is unfortunate that the surface mass distribution of the Milky Way is still poorly constrained, even while our knowledge of Galactic stellar abundance distributions grows ever more detailed. One reason for this shortcoming is the difficulty of determining the Galactic rotation curve in the outer disk. The inner Galactic rotation curve has been derived from tangent point analysis of H I radial velocities (RVs; e.g., Malhotra 1995). However, outside the solar circle one must also obtain proper motions *and* reliable distances for some suitable stellar tracer population to properly derive the rotation curve. To this end, we have collected a near uniform sample of spectroscopic data from stars in over 100 open clusters at medium–high resolution ($R \sim 15,000$) using the HYDRA multi-fiber

R. S. de Jong, Island Universes, 129–132.
© 2007 *Springer.*

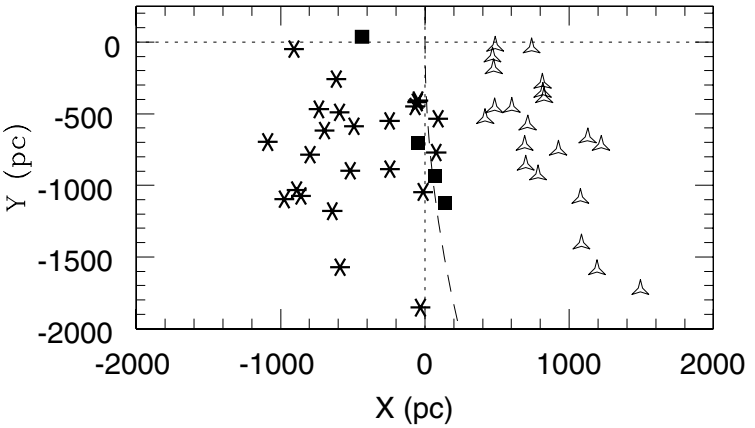

Figure 1. Visualization of the Milky Way in the X, Y coordinate system of the Galaxy with the Sun at (0,0). The 56 clusters used here (primarily in the third and fourth Galactic quadrants) are shown by their V_{lsr}: stars ($V_{lsr} > 5$ km s^{-1}), squares ($-5 < V_{lsr} < 5$ km s^{-1}), and triangles ($V_{lsr} < -5$ km s^{-1}). The transition between negative and positive V_{lsr} clusters lies near the solar circle (dashed line) as expected for well-behaved circular Galactic rotation.

spectrographs on the CTIO 4-meter and WIYN 3.5-meter telescopes. We specifically target stars for which proper motions have previously been measured (e.g., Dias et al. 2001), and place additional fibers on other stars in the field to expand the membership census in anticipation of future astrometric surveys (e.g., GAIA). The average motion of all verified members will yield a reliable, accurate systemic proper motion and RV for each cluster to trace the rotation curve. However, in this proceedings we focus specifically on an analysis of the speed of Galactic rotation at the solar circle (Θ_0) based solely on cluster RVs and positions.

Data for the sub-sample of 56 clusters presented here were all obtained using the Blanco 4-meter telescope at CTIO. The spectra were reduced using standard techniques. RVs were determined using the IRAF fxcor package as described in Frinchaboy et al., 2005. Cluster star members were isolated both from our RVs and the proper motion membership criteria of Dias et al. (2001, 2002a). We adopt a $\pm$5–10 km s^{-1} RV range to discriminate cluster members, which is several times larger than the typical individual stellar RV errors (1–2 km s^{-1}) and the expected velocity dispersions of these systems. With proper motions and RVs for each star we can, in principle, derive full space velocities, but we already have significant sensitivity to the speed of the local standard of rest through the cluster RVs and positions, for a conservative first analysis. An average of 8–9 stellar members per cluster yields a mean error in systemic velocity for all clusters used here of 3.9 km s^{-1}. The analysis was completed using distances from the Dias et al., 2002b catalog combined with our

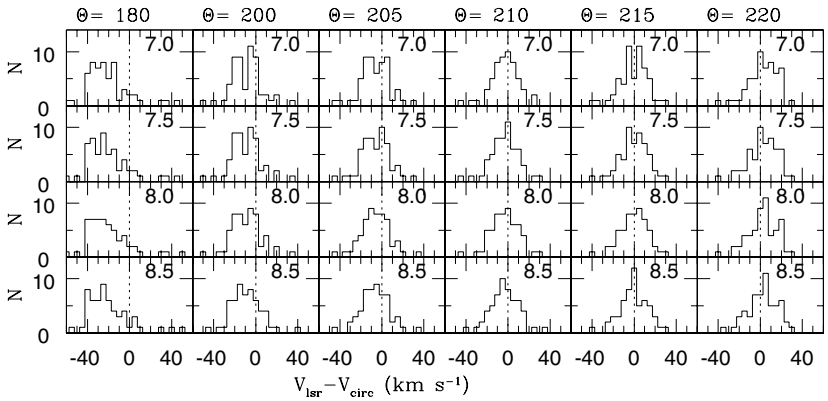

Figure 2. Histograms of the difference of $V_{lsr} - V_{circ}$ for the 56 open clusters for a range of adopted R_0 and Θ_0. The dotted line denotes a difference of zero which corresponds to a flat rotation curve at the given Θ_0

heliocentric RVs converted to V_{lsr} (see Figure 1) using the solar peculiar motion (U, V, W) velocities (10, 5.2, 7.2) km s^{-1} given in Binney & Merrifield, 199).

Under the assumption that open clusters closely trace the circular speed of the Milky Way at their Galactic radius, we can predict their expected observed V_{lsr} under an assumed rotation curve and solar Galactocentric distance (R_0). For simplicity, we assume a flat rotation curve over the relevant Galactic radii. Comparison of our measured V_{lsr}'s to derived V_{circ}'s (i.e., the V_{lsr} a cluster would have in the same position for a flat rotation curve of speed Θ_0) over a range of R_0 (7.0–8.5 kpc) and Θ_0 (180–220 km s^{-1}) reveals a systematic trend with assumed Θ_0 but little apparent sensitivity to R_0 (see Figure 2). Over this range of R_0 the mean (V_{lsr}-V_{circ}) difference was consistently closest to zero when Θ_0 ranged between only 210–215 km s^{-1}. With finer analysis of the $\Theta_0 = 210$–215 km s^{-1} region (see Figure 3), we find that (V_{lsr}-V_{circ}) $= 0.0 \pm 0.2$ km s^{-1} for $\Theta_0 = 214^{+6}_{-9}$ km s^{-1}. The quoted errors are the 3σ deviation given by the error on the mean. This Θ_0 result is in the middle of the wide range of other recent findings that range from $\Theta_0 = 184$ km s^{-1} (Olling & Merrifield, 1998) to $\Theta_0 = 255$ km s^{-1} (Uemura et al. 2000), two limiting values strongly ruled out by our open cluster velocities if the Milky Way has a well-behaved, simple, circular velocity field. Future work on this project will nearly double the number of clusters available (to approximately 100) and expand coverage to the first and second Galactic quadrants. Additionally, the proper motion data will be incorporated to investigate not only the mean Galactic rotation *curve* but whether second order variations in the local velocity field of the disk can be discerned.

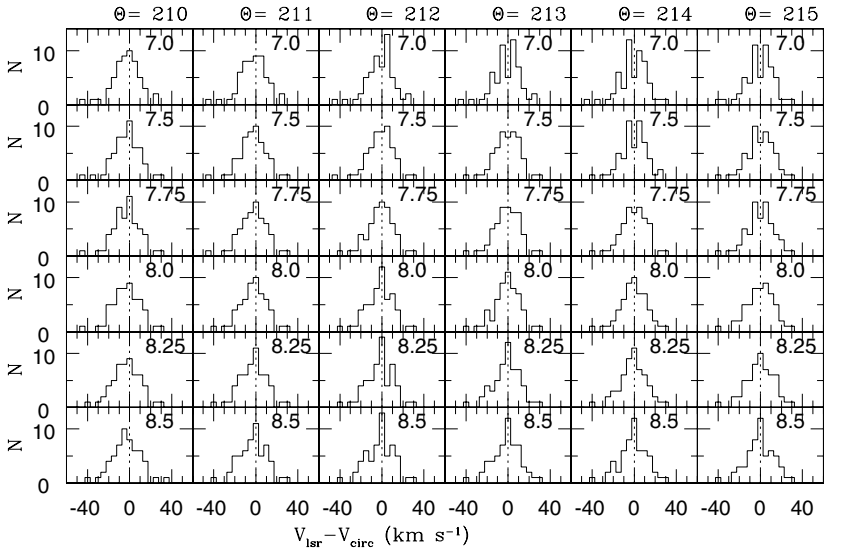

Figure 3. Same as Figure 2 with a finer grid of assumed Θ_0. We find that $\Theta_0 = 214$ km s^{-1} provides the best match to the Local Standard of Rest velocity for our preliminary cluster sample.

Acknowledgements We would like to thank the NOAO TAC for granting this project long-term status and NOAO for travel support of this thesis. We acknowledge funding by NSF grant AST-0307851, NASA/JPL contract 1228235, the David and Lucile Packard Foundation, and the F.H. Levinson Fund of the Peninsula Community Foundation. PMF also acknowledges support from the Virginia Space Grant Consortium, an AAS International Travel Grant, and the conference organizers.

References

Binney, J. & Merrifield, M., 1998, Galactic Astronomy (Princeton University Press), p. 627

Dias, W. S., Lepine, J. R. D. & Alessi, B. S. , 2001, A&A, 376, 441

Dias, W. S., Lepine, J. R. D. & Alessi, B. S. , 2002, A&A, 388, 168

Dias, W. S., Alessi, B. S. , Moitinho, Lepine, J. R. D. & Alessi, B. S. , 2002, A&A, 389, 871

Frinchaboy, P. M., Munoz, R. R., Phelps, R. L., Majewski, S. R., & Kunkel, W. E. 2005, AJ, *submitted*

Malhotra, S., 1995, ApJ, 448, 138

Olling, R. P. & Merrifield, M. R., 1998, MNRAS, 297, 943

Uemura, M., Ohashi, H., Hayakawa, T., Ishida, E., Kato, T., & Hirata, R., 2000, PASJ, 52, 143

TWO-DIMENSIONAL SPECTROSCOPY OF LATE-TYPE SPIRALS

Katia Ganda* and Reynier Peletier

Kapteyn Astronomical Institute, Unversity of Groningen, The Netherlands

* katia@astro.rug.nl

Abstract We are currently engaged in a study aimed at clarifying the nature of late-type spiral galaxies. Using the IFU SAURON we have obtained the two-dimensional stellar and gaseous kinematics for a sample of 18 galaxies spanning a range in Hubble type between Sb and Sd. Here we illustrate the applied methods and present the kinematical maps and preliminary analysis for one of our galaxies.

Keywords: galaxies: kinematics and dynamics - galaxies: individual (NGC 2964)

Introduction

The complexity and low surface brightness of spiral galaxies towards the end of the Hubble sequence is the cause of the fact that we know relatively little about them, especially about their optical properties. Recently, HST imaging showed that they can host a variety of structures: bulges, nuclear star clusters, stellar disks, small bars, double bars. We do not know really how those features were made and how they fit into an evolutionary picture. Stellar populations and kinematics, as direct tracers of the star formation and mass assembly history of the systems, would help clarify the picture. In this paper we present the first results from a study aimed at understanding the structure and star formation history of their inner parts. We focus on the two-dimensional kinematics and stellar populations using emission and absorption lines at optical wavelengths for a sample of nearby late-type spiral galaxies.

1. Sample Selection

Our sample of galaxies consists of optically selected galaxies ($B_T < 12.5$, taking RC3 values) with HST imaging available from WFPC2 and/or NICMOS. Their morphological type ranges between Sb and Sd, according to the RC3 classification. Galaxies in close interaction and Seyferts have been discarded. The resulting sample contains 18 nearby spiral galaxies.

R. S. de Jong, Island Universes, 133–136.
© 2007 *Springer.*

2. Observations and Data Reduction

We observed our sample galaxies in January 2004 using SAURON, which is a visitor instrument at the WHT in La Palma, Spain, and is a panoramic integral-field spectrograph using a lenslet array. It has a field of view of $41'' \times 33''$, with a spatial sampling of $0.''94$ and it covers the spectral window 4800-5300Å. Therefore, it allows us to measure the Hβ emission line, the [OIII] and [NI] doublets and the absorption features Hβ, Mg$_b$, FeI (Bacon et al. 2001). For each galaxy, we took 2 to 6 exposures of 1800 s. Extraction, reduction and calibration of the data were carried out using the dedicated package XSauron (de Zeeuw et al. 2002) and some IRAF tasks.

3. Kinematical Maps

On the fully reduced spectra we performed a two-dimensional binning in order to reach a minimum signal-to-noise ratio (Cappellari & Copin, 2003). The requested signal-to-noise is 60 and 5 for stars and gas respectively. We measured then the stellar kinematics using a pixel fitting method which fits to the spectra linear combinations of single age, single metallicity models convolved with a Gauss-Hermite expansion; a low-order polynomial is also included in the fit to account for small differences in the flux calibration between the galaxy and the template spectra (Cappellari & Emsellem, 2004). While fitting, the spectral regions that are potentially affected by nebular emission are masked out. This allows us to derive the mean velocity V, velocity dispersion σ and the higher order Gauss-Hermite moments h_3 and h_4. The gas kinematics was instead computed by fitting to the full spectrum (without masking) both the emission lines amplitude and the optimal combination of the stellar templates (Sarzi et al. 2005, Falcón-Barroso et al. 2005).

The stellar kinematics turns out to be often characterized by a central drop in σ, indicating a kinematically cold region; this could either be due to a central disk of newly forming stars or to the fact that the bulge is so faint. We detect a considerable amount of ionized gas in our objects, and the gas kinematical maps display often a very complicated appearance. The gas rotates faster than the stars and around the same axis, although it is in some cases misaligned with respect to the photometric minor axis. The zero-velocity lines are often wiggling, bending or S-shaped. We do not generally detect major differences between gas distribution and kinematics in Hβ and [OIII], except in one case (NGC4102, which is classified as a LINER). Overall, the sample galaxies display low [OIII]/Hβ ratios over most of the SAURON field, suggesting star formation, as expected in spiral galaxies. Here we will present an "example" galaxy, namely NGC2964.

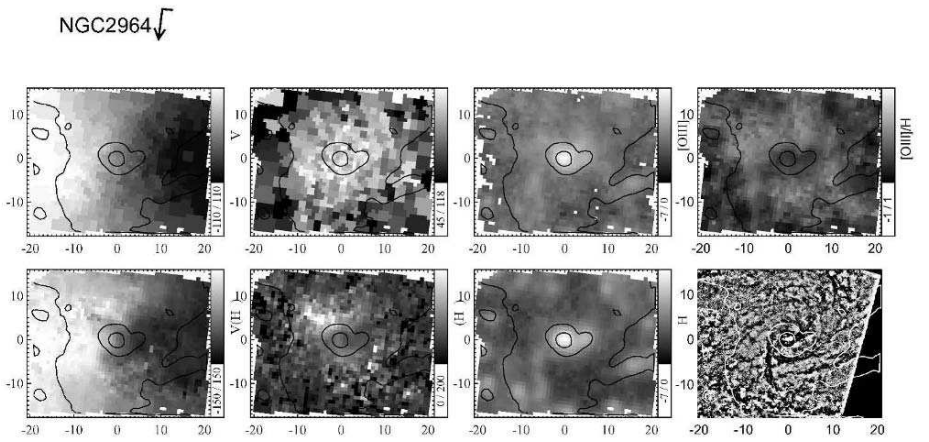

Figure 1. Stellar and gaseous kinematics for NGC2964. First row: stellar velocity and velocity dispersion; [OIII] flux, [OIII]/Hβ line ratio; second row: Hβ velocity, velocity dispersion and flux; HST unsharp-masked image. The orientation of the maps is given by the arrow and its dash, which point respectively to North and East.

4. Kinemetry Analysis

We analysed our gas velocity maps using a method called kinemetry (Krajnovíc et al., 2005, Wong et al. 2004) which performs an harmonic expansion of the map along ellipses, in a similar way to the standard approach in use in photometry:

$$V(\theta) = a_0 + a_1 \sin(\theta) + b_1 \cos(\theta) + a_3 \sin(3\theta) + b_3 \cos(3\theta) + ... \qquad (1)$$

In case of circular motions, only a_0 and b_1 are different from zero. Thus, the analysis of the behaviour of the higher order terms can teach us about the perturbations in the potential that give rise to non-circular motions. We applied the method to our Hβ velocity maps and started interpreting the output, following the approach of Wong et al. (2004). Here we present the results for NGC2964.

5. NGC2964

Our data reveal a variety of features in this galaxy (see Figure 1). The stars rotate quite regularly along the major axis, although a twist in the zero-velocity line can be seen very close to the edge of the field, on both sides. The stellar velocity dispersion increases quite smoothly moving toward the centre. The ionized gas shows a clumpy distribution, which could suggest a spiral arm structure, and complex kinematics in both lines, with a very irregular

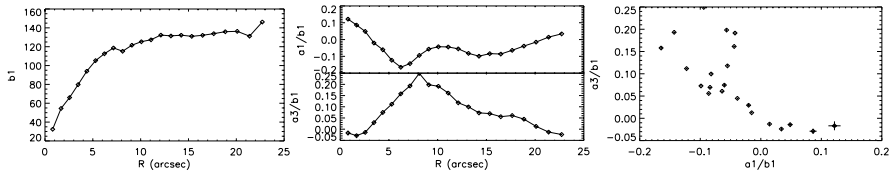

Figure 2. NGC2964: radial variations of kinemetric coefficients b_1, a_1 and a_3; diagnostic diagram a_3/b_1 vs a_1/b_1.

zero-velocity line and with the velocity dispersion peaking in a region slightly away from the very centre. The [OIII]/Hβ line ratio map assumes low values over most of the field, and is enhanced in a ring-like structure surrounding an elongated nuclear region where the ratio becomes low again. This could be a star forming region.

Kinemetry reveals the presence of non circular motions, with a minimum in a_1 and a maximum in a_3 at a radius corresponding to the location of the gas-σ peak noticed in the velocity dispersion map (see Figure 2). According to our analysis, this can be due to the presence of a bar perturbation, which is also detectable in the photometry, and/or to the spiral pattern, recognizable photometrically as well.

References

Bacon R., Copin Y., Monnet G., Miller B.W., Allington-Smith J.R., Bureau M., Carollo C.M., Davies R.L. et al., 2001, MNRAS, 326, 23

Cappellari M., Copin Y. 2003, MNRAS, 342, 345

Cappellari M., Emsellem E. 2004, PASP, 116, 138

Falcón-Barroso J. et al., 2005, in preparation

Krajnovíc D., 2005, submitted

Sarzi M., et al., 2005, submitted

Wong T., Blitz L., Bosma A., 2004,APJ, 605, 183

de Zeeuw P.T., Bureau M., Emsellem E., Bacon R., Carollo C.M., Copin Y., Davies R.L., Kuntschner H. et al., MNRAS, 329, 513

VERTICAL DISTRIBUTION OF STARS AND GAS IN A GALACTIC DISK

Chanda J. Jog

Indian Institute of Science, Bangalore, India
cjjog@physics.iisc.ernet.in

Abstract We study the vertical density distribution of stars and gas (HI and H_2) in a galactic disk which is embedded in a dark mater halo. The new feature of this work is the inclusion of gas, and the gravitational coupling between stars and gas, which has led to a more realistic treatment of a multi-component galactic disk. The gas gravity is shown to be crucially important despite the low gas mass fraction. This approach physically explains the observed scaleheight distribution of all the three disk components, including the long-standing puzzle (Oort 1962) of a constant HI scaleheight observed in the inner Galaxy. The above model is applied to two external galaxies, NGC 891 and NGC 4565, and the stellar disk is shown to be not strictly flat as was long believed, but rather it shows a moderate flaring of a factor of ~ 2 within the optical radius.

Keywords: galaxies: kinematics and dynamics - galaxies: ISM - galaxies: structure - Galaxy: structure

1. Introduction

The visible mass in a galactic disk is distributed in a thin disk, hence the planar and the vertical dynamics can be treated separately. The vertical distribution is not studied well unlike the planar mass distribution, though it is important to understand it since it acts as a tracer of the galactic potential and the disk evolution. The vertical distribution in a one-component, isothermal, self-gravitating disk was studied in a classic paper by Spitzer (1942). However, the physical origin of the thickness of stars and gas in a galactic disk and in particular their radial variation is not yet fully understood – we address this problem here.

In the past, gas gravity was often ignored even when studying the vertical distribution of gas, and the gas response to the stellar potential alone was considered. We show that stars and gas need to be treated jointly to get their correct vertical distribution. Due to its low velocity dispersion, gas forms a

R. S. de Jong, Island Universes, 137–140.
© 2007 *Springer.*

thin layer and hence affects the dynamics and the vertical distribution of stars as well, despite the low gas mass fraction.

2. Formulation of Three-Component Model

The vertical scaleheight of HI gas in the inner Galaxy is remarkably constant, which has been a long-standing puzzle (Oort 1962, Dickey & Lockman 1990). The vertical scaleheight is a measure of equilibrium between the gravitational force and the pressure. Hence the HI gas responding to the gravitational potential of an exponential stellar disk alone should show flaring, in contrast to the observed constant scaleheight.

We propose that an increase in the gravitational force due to the inclusion of gas can decrease the gas scaleheight, and study this idea quantitatively (Narayan & Jog 2002b). We formulate a general treatment, where the stars, the HI gas and the H_2 gas are treated as three gravitationally coupled disk components, embedded in a dark matter halo. Thus each disk component experiences the same joint potential due to the three disk components and the dark matter halo, but each has a different response due to its different random velocity dispersion.

The equation of hydrostatic equilibrium along z or the vertical direction for each component and the joint Poisson equation are solved together. Thus each component obeys:

$$\frac{d^2\rho_i}{dz^2} = \frac{\rho_i}{<(v_z)_i{}^2>}[-4\pi G(\rho_s + \rho_{HI} + \rho_{H_2}) + \frac{d(K_z)_{DM}}{dz}] + \frac{1}{\rho_i}(\frac{d\rho_i}{dz})^2$$

where i=1,2,3 denote the three disk components, and ρ_i and $<(v_z)_i{}^2>^{1/2}$ denote the mass density and the velocity dispersion respectively.

The above three coupled, second-order differential equations are solved numerically and iteratively, using $d\rho_i/dz = 0$ at the midplane and the observed mass surface density (Σ_i) as the two boundary conditions in each case. This results in a sech^2-like density profile for the mass density in each case, and we use its HWHM to define the vertical scaleheight.

Resulting Vertical Scaleheight vs. Radius

On using the joint potential, the HI scaleheight decreases as expected, and is in a better agreement with observations (Fig. 1), especially at large radii where the effect of gas gravity is higher because of the higher gas fraction. For H_2 gas, the joint potential gives a good agreement at all radii. In the stellar case, the joint potential gives a nearly flat curve that slowly rises with radius with a slope of 24 pc kpc^{-1} for 5-10 kpc, this agrees well with the near-IR observations (Kent et al. 1991).

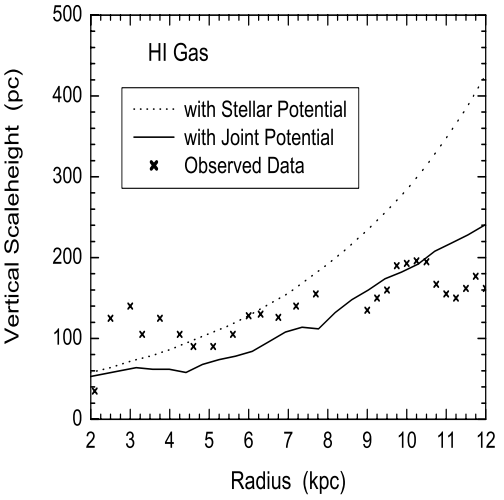

Figure 1. Galactic HI scale height as function of radius. The joint potential gives a better fit to the HI data, and explains the constant HI scaleheight observed in the inner Galaxy. The agreement is even better for a slight linear increase in the HI velocity dispersion at small radii.

3. Radially Increasing Stellar Scaleheight

We next applied this general model to two external, prototypical edge-on spiral galaxies: NGC 891 and NGC 4565, for which gas density values are known from observations - see Narayan & Jog (2002a) for details.

From the pioneering study of the vertical luminosity distribution of edge-on spiral galaxies, van der Kruit & Searle (1981a,b) concluded that the stellar vertical scaleheight in a galactic disk is constant with radius, and this is explained if the ratio $R_{vel}/R_d = 2$, where R_{vel} and R_d are the scalelengths with which the stellar velocity dispersion and disk luminosity fall off exponentially. This has been a paradigm in galactic structure for 25 years. However, there is no clear physical explanation for this. We argue that such a strict relation is unrealistic in general given the different sources of stellar heating now known to operate in a disk, such as heating via scattering off clouds or spiral arms within the galactic disk, and via heating due to tidal encounters with other galaxies.

Hence, our model is applied to NGC 891 and NGC 4565, treating the above ratio as a free parameter. The resulting stellar scaleheight is not strictly constant but instead shows flaring by a factor of ~ 2 within the optical radius (Fig. 2). This result agrees with observations (de Grijs & Peletier 1997). This is an important result for galactic structure.

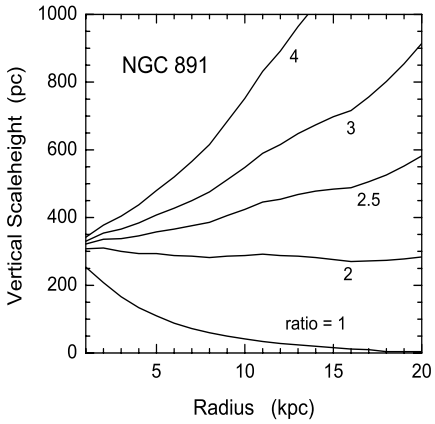

Figure 2. Resulting stellar vertical scaleheight vs. radius for different radial velocity dispersion scalelength to stellar disk scalelength ratios. In general, the stellar scaleheight shows moderate flaring when the ratio $R_{vel}/R_d > 2$.

4. Conclusions

The multi-component approach developed here cohesively explains the observed vertical scaleheights of all the three disk components, namely the stars, the HI and the H_2 gas in the inner Galaxy.

The above model is applied to two external galaxies, NGC 891 and NGC 4565, and the resulting stellar scaleheight is shown to be not constant with radius, instead it shows flaring. Such a moderate increase in stellar scaleheight is likely to be common in other galaxies as well.

References

Dickey, J.M., & Lockman, F.J. 1990, ARA&A, 28, 215
de Grijs, R., & Peletier, R.F. 1997, A & A, 320, L21
Kent, S.M., Dame, T.M., & Fazio, G. 1991, ApJ, 378, 131
Narayan, C.A., & Jog, C.J. 2002a, A & A, 390, L35
Narayan, C.A., & Jog, C.J. 2002b, A & A, 394, 89
Oort, J.H. 1962, in The Distribution and Motion of Interstellar Matter in Galaxies, IAU symp. 15, ed. L. Woltjer (New York: Benjamin), 3
Spitzer, L. 1942, ApJ, 95, 329
van der Kruit, P.C., & Searle, L. 1981a, A & A, 95, 105
van der Kruit, P.C., & Searle, L. 1981b, A & A, 95, 116

TWO DIMENSIONAL VELOCITY FIELDS OF LOW SURFACE BRIGHTNESS GALAXIES

Rachel Kuzio de Naray[1*], Stacy S. McGaugh[1**], W.J.G. de Blok[2***] and Albert Bosma[3****]

[1]*Astronomy Department, University of Maryland, USA*

[2]*Research School of Astronomy and Astrophysics, Australian National University*

[3]*Observatoire de Marseille, France*

* kuzio, ** ssm@astro.umd.edu, *** edeblok@mso.anu.edu.au, **** bosma@oamp.fr

Abstract We have obtained high resolution two-dimensional velocity fields from integral field spectroscopy along with derived rotation curves for nine low surface brightness galaxies. This is a positive step forward in terms of both data quality and number of objects studied. We fit NFW and pseudo-isothermal halo models to the observations. We find that the pseudo-isothermal halo better represents the data in most cases than the NFW halo, as the resulting concentrations for the latter are lower than would be expected from ΛCDM. Cusps can clearly be detected by this method when they are present and the data are of high quality. Yet only one of our six best cases is consistent with a cusp.

Keywords: galaxies: kinematics and dynamics - galaxies: halos - dark matter

1. Introduction

Though it is widely agreed that low surface brightness (LSB) galaxies are dark matter dominated at all radii (de Blok & McGaugh 1997) and, hence, are ideal test subjects for studying the dark matter distribution, a consensus has not yet been reached on the interpretation of their rotation curves. Are the dark matter halos of LSB galaxies "cuspy" NFW halos, as expected from cosmological numerical simulations (e.g., Navarro, Frenk & White 1997; Moore et al. 1999; Klypin et al. 2001), or are they closer to "cored" pseudo-isothermal halos? NFW halos can be fit to the observations, but the cosmological parameters implied by the fits are inconsistent with the standard ΛCDM picture (McGaugh, Barker & de Blok 2003). Pseudo-isothermal halos provide much better fits, and in the case of a power-law fit to the density, $\rho \sim r^{\alpha}$, the optimum value of α seems to be -0.2 $\pm$ 0.2 (de Blok, Bosma & McGaugh 2003). However, such models have no cosmological dependence or theoretical basis.

R. S. de Jong, Island Universes, 141–144.
© 2007 *Springer.*

In hopes of salvaging the NFW halo, a number of systematic effects have been suggested to affect the data (Swaters et al. 2003a,b).

In an effort to address these concerns, the quality of observations has been greatly improved. The first suggested effect which could "hide" a NFW-halo was beam smearing in two-dimensional 21-cm HI velocity fields. Subsequent long-slit Hα observations increased the resolution by an order of magnitude. When cusps did not appear along with the resolution increase, effects such as slit misplacement and non-circular motions came to the forefront. We address these issues with new data that is both high resolution and two-dimensional.

2. Observations

We observed twelve LSB galaxies using the DensePak Integrated Field Unit on the WIYN telescope at Kitt Peak. DensePak is comprised of 3" diameter fibers arranged in a 43" x 28" rectangle. The distances to the galaxies are such that a 3" fiber provides sub-kpc resolution. The fiber bundle orientation on the sky and number of pointings were tailored to each galaxy so that the critical central regions were covered by the fibers. Two 1800 sec exposures were taken at each pointing.

Velocities of the Hα, [NII]λ6584, [SII]λ6717 and [SII]λ6731 emission lines were measured for each fiber. The average of the measured velocities in each fiber was taken as the fiber velocity. Velocity fields were constructed by combining individual DensePak pointings and comparing an Hα flux image made from the DensePak data to an actual Hα image. Velocity fields were then transformed to rotation curves using the NEMO program ROTCUR. For three of the galaxies no useful data covering a large fraction of the galaxy has been obtained.

3. Data

As an example of the data quality, we show in Figure 1 for the galaxy UGC 5750 the location of the DensePak fibers on an image of the galaxy, the observed velocity field, the DensePak rotation curve along with previous long-slit and HI rotation curves, and the fits of some models in the log V - log r plane. As can be seen, the new data agree very well with the previous long slit data obtained by McGaugh, Rubin & de Blok (2001) and de Blok & Bosma (2002).

4. Rotation Curve Fits

We fit the combined rotation curves with pseudo-isothermal and NFW$_{free}$ halos for the minimum disk case. We also fit an NFW$_{constrained}$ halo which was required to match the velocities at the outer radii of each galaxy, in effect, constraining the concentrations to agree with cosmology. We highlight the

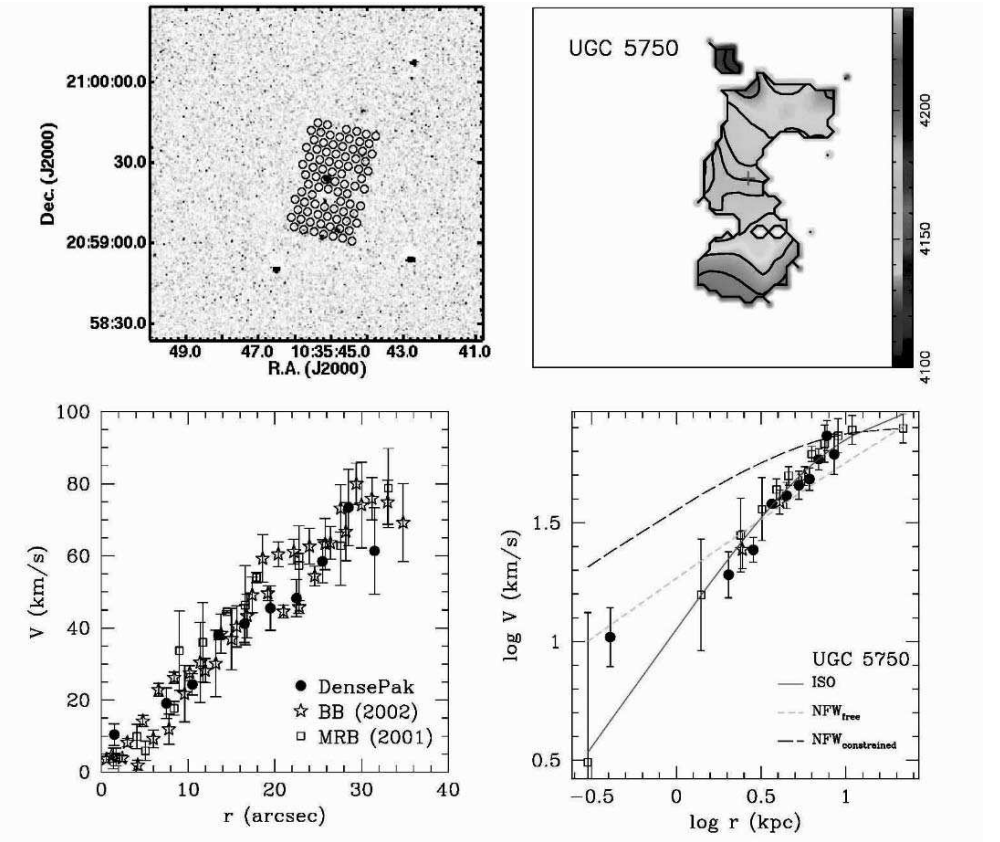

Figure 1. Top left: coverage of the DensePak data for UGC 5750, overlaid on a Hα image. Top right: observed velocity field of UGC 5750 derived from the DensePak data. Bottom left: comparison of the new rotation data for UGC 5750 with previous work by McGaugh, Rubin & de Blok (2001) and de Blok & Bosma (2002). Bottom right: Model rotation curve fits for the new data, assuming minimum disk (M/L=0). The solid (red) curve represents the best fitting pseudo-isothermal halo, the short-dashed (green) curve the best fitting free NFW halo, and the long-dashed (black) curve the best fitting constrained NFW halo.

results for UGC 5750 in Figure 1d. UGC 5750 is clearly well-fit by an pseudo-isothermal halo. We stress that the fit should extend to the whole rotation curve, and that the inner most points on their own do not constitute a good fit to a NFW halo. In our sample so far, only NGC 4395 is fit by a NFW halo. The concentrations for the other galaxies do not agree with values expected for ΛCDM.

5. Conclusions and Further Work

We have obtained velocity fields and rotation curves for a sample of LSB galaxies observed with DensePak. That we did observe one halo consistent with the expected cusp shows that cusps can be detected when they are present and the data are of high quality.

Future work will include mass-modeling, reconstruction of slit placement, and a detailed assessment of the non-circular motions possibly indicated by the twisting of the kinematic axes.

Acknowledgements This research was supported by NSF grant AST 0206078.

References

de Blok, W.J.G., & Bosma, A. 2002, A.&A., 385, 816
de Blok, W.J.G., Bosma, A., & McGaugh, S.S. 2003, MNRAS, 340, 567
de Blok, W.J.G., McGaugh, S.S., & Rubin, V.C. 2001, AJ, 122, 2396
de Blok, W.J.G., McGaugh, S.S., Bosma, A., & Rubin, V.C. 2001, ApJ, 552, L23
de Blok, W.J.G., & McGaugh, S.S. 1997, MNRAS, 290, 533
Klypin, A.A., Kravtsov, A.V., Bullock, J.S., & Primack, J.R. 2001, ApJ, 554, 903
McGaugh, S.S., Barker, M.K. & de Blok, W.J.G. 2003, ApJ, 584, 566
McGaugh, S.S., Rubin, V.C., & de Blok, W.J.G. 2001, AJ, 122, 2381
Moore, B., Quinn, T., Governato, F., Stadel, J., & Lake, G. 1999, MNRAS, 310, 1147
Navarro, J.F., Frenk, C.S., & White, S.D.M. 1997, ApJ, 490, 493
Swaters, R.A., Madore, B.F., van den Bosch, F.C., & Balcells, M. 2003, ApJ, 583, 732
Swaters, R.A., Verheijen, M.A.W., Bershady, M.A., & Andersen, D.R. 2003, ApJ, 587, L13

PATTERN SPEEDS OF SPIRAL GALAXIES USING THE TREMAINE-WEINBERG METHOD

S. E. Meidt and R. J. Rand

University of New Mexico

Keywords: galaxies: kinematics and dynamics - galaxies: spiral

Introduction

Long-lasting spiral structure in galaxies is established when density waves form a pattern that rotates at a constant angular frequency Ω_p, the pattern speed. This quantity, critical to understanding spiral structure, galaxy evolution, and the connection, if any, between bars and spirals in galaxies, is not directly measurable. Most determinations of pattern speeds have relied on identifying morphological features at certain radii as resonances, but this depends significantly on knowledge of the behavior of stars and gas at these resonances. The Tremaine-Weinberg (TW) method allows for the determination of pattern speeds based on kinematic observations in a way completely independent of resonance identification, or theories of spiral structure, relying on the identification of a tracer that obeys the continuity equation as it orbits through the pattern.

This work expands on previous studies of the TW method applied to galaxies with molecular- or HI-dominated ISMs. In galaxies where the ISM is found to be dominated by one phase, it is assumed that this component satisfies the continuity requirement; for galaxies with H_2 dominated ISMs, for instance, the TW method has successfully been applied using ^{12}CO(1-0) emission as a tracer for the molecular gas surface density (Rand & Wallin 2004).

1. The Tremaine-Weinberg Method

If the component obeys continuity as it orbits in the spiral/bar potential, Tremaine & Weinberg (1984) show that

$$\Omega_p \sin i = \frac{\int_{-\infty}^{\infty} \Sigma(X,Y) V_{\parallel} dX}{\int_{-\infty}^{\infty} \Sigma(X,Y) X dX}, \qquad (1)$$

R. S. de Jong, Island Universes, 145–148.
© 2007 *Springer.*

where (X, Y) are the sky coordinates $\parallel$ and $\perp$ to the major axis; $\Sigma(X, Y)$ is the surface density of the component; $V_{\parallel}$ is the line-of-sight velocity; and i is the inclination angle of the galaxy.

If the intensity of the component's emission traces the surface density, then, at a given Y (cf. Merrifield & Kuijken 1995),

$$\Omega_p = \frac{1}{\sin i} \frac{\int_{-\infty}^{\infty} I(X) V_{\parallel} dX}{\int_{-\infty}^{\infty} I(X) X dX} \frac{\int_{-\infty}^{\infty} I(X) dX}{\int_{-\infty}^{\infty} I(X) dX}, \tag{2}$$

and Ω_p, modulo $\sin i$, can be determined from total intensity and velocity field maps by measuring intensity-weighted averages of observed position <x> and velocity <v> along lines of constant Y (parallel to the major axis). The slope in a plot of <v> vs. <x> for such "apertures" is the pattern speed.

2. Data and Analysis

Presently, to determine the spiral density wave pattern speed, we use high-resolution CO data cubes from the BIMA Survey of Nearby Galaxies (SONG). The BIMA SONG observations include single-dish data, thereby sampling all spatial frequencies to support the continuity requirement. Pattern speed determinations for three of the galaxies in this work are presented based on CO emission data cubes alone; we cite the results of Wong & Blitz (2002), wherein radial profiles of NGC 5055, 5033, and 5457 (M101) indicate that these galaxies are molecule-dominated within the region of CO detection.

In this work, a constant conversion factor X=2$\times 10^{20}$ mol cm^{-2}(K km s^{-1})$^{-1}$ between CO intensity and H_2 column density is assumed. As demonstrated in Zimmer, Rand & McGraw (2004), the choice of conversion factor has little effect on the TW calculation. The choice, however, clearly influences assertions of molecular dominance, particularly with regard to an important suspected variation of X with metallicity, which is supported by empirical evidence for an inverse correlation (e.g., Boselli, Lequeux, & Gavazzi 2003). For the galaxies studied here, NGC 5457, 5055 and 5033, metallicity estimates are subsolar (as compiled by Pilyugin, et al. 2004), indicating that, if anything, the conversion factor underestimates the amount of H_2 present.

Inclination and position angles (PA's) used in the TW calculation are determined by fitting tilted rings to the velocity field as performed by the GIPSY task ROTCUR. As found in Debattista (2003) and Rand & Wallin (2004), the scatter in the slope of the <v> vs. <x> plot worsens for PA's further from the nominal value. Error bars reported for the pattern speed of each galaxy account for PA uncertainty and the scatter in the <v> vs. <x> plot for nominal PA.

	Morphological Type	D (Mpc)	i (^{o})	PA (^{o})	V_{sys} (km/s)	Ω_p (km/s/kpc)
NGC 5457	SAB(rs)cd	7.4	21	42 +4/-2	257	48 +7/-6
NGC 5055	SA(rs)bc	7.2	57	99 $\pm$1	506	67 $\pm$6
NGC 5033	SA(s)c	11.8	68	352 $\pm$2	880	93 +18/-39

Table 1. Properties of sample galaxies.

3. Results

Given that NGC 5457, 5055 and 5033 appear to be dominated by molecular gas in their inner disks, we can be reasonably confident that the continuity requirement of the TW method is satisfied. Table 1 lists the properties and results of the TW calculation for each of the galaxies in our sample. Figures 1a and b display an example of the line-of-sight apertures used in the TW calculation for NGC 5457 and the corresponding <v> vs. <x> plot, respectively.

4. Conclusions and Future Work

The Tremaine-Weinberg method has long been applied with much success to bars in galaxies. The relatively recent applications of the method to spiral patterns, too, are compelling: pattern speeds for M51 and M83, for example (Rand & Wallin 2004), were found to be in good agreement with those determined from resonances. Generally, however, it is unclear how reliable spi-

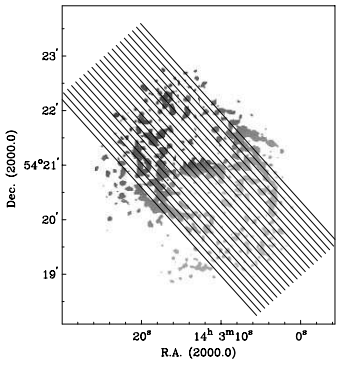

Figure 1a. First moment map of the BIMA CO data for NGC 5457 with apertures used in the TW calculation spaced at the resolution of the map shown overlayed as solid lines, with the westernmost being aperture 1.

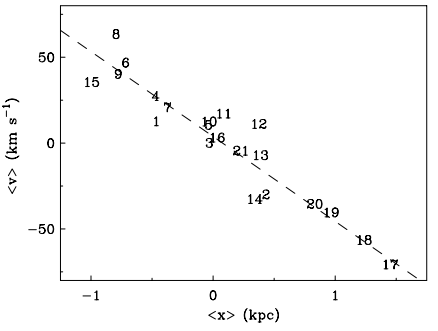

Figure 1b. Plot of <v> vs. <x> for the 21 apertures shown in Fig.1a. The dashed line is the best-fit straight line to all apertures. The corresponding value of Ω_p is 48 +7/-6 km s^{-1} kpc^{-1}.

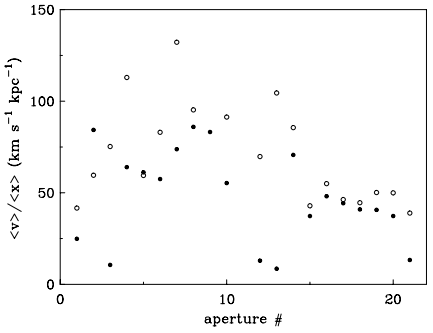

Figure 2. Plot of <v>/<x> vs. aperture number for NGC 5457 with filled and open circles representing values from the TW calculation using the original and axisymmetric velocity fields, respectively.

ral pattern speed determinations with the TW method are, considering that the converging and diverging flows responsible for the pattern are typically weaker in a spiral (e.g. Roberts & Stewart 1987) than in a bar; the method, based on the continuity equation, relies on the detection of such non-axisymmetric, or "streaming", motions that trace spiral arm surface density enhancements in order to calculate a pattern speed. It is easy to show, in the case of purely axisymmetric azimuthal motion, that the method returns a weighted average of the angular rotation frequency. This makes sense: in such a case, only a material pattern can be sustained.

To understand whether streaming motions are significantly contributing to the TW analysis, we have repeated the procedure using axisymmetric velocity fields built from the output of ROTCUR. We generally find little difference relative to the result for the original velocity field (shown here for the case of NGC 5457 in a plot of <v>/<x> vs. aperture number in Figure 2). While this may indicate a limitation of the method, it may alternatively indicate that spiral patterns are in fact close to material patterns. With M. Merrifield, we are pursuing the latter possibility, while with P. Rautiainen we are studying applications of the TW method on simulated spirals with varying pattern speeds and spiral strengths in order to assess the reliability of the method on spiral patterns.

References

Boselli, A., Lequeux, J., & Gavazzi, G. 2002, A&A, 384, 33
Debattista, V. P. 2003, MNRAS, 342, 1194
Merrifield, M. R., & Kuijken, K. 1995, MNRAS, 274, 933
Pilyugin, L. S., Vilchez, J. M., & Contini, T. 2004, A&A, 425, 849
Rand, R. J. & Wallin, J. F. 2004, ApJ, 614, 142
Roberts, W. & Stewart, G. 1987, ApJ, 314, 10
Tremaine, S. & Weinberg, M. D. 1984, ApJ, 282, L5
Wong, T. & Blitz, L. 2002, ApJ, 569, 157
Zimmer, P., Rand, R. J. & McGraw, J. T. 2004, ApJ, 607, 285

A NEW SCENARIO FOR THE ORIGIN OF GALACTIC WARPS

Yves Revaz* and Daniel Pfenniger**

Geneva Observatory, Switzerland

* yves.revaz@obs.unige.ch, ** daniel.pfenniger@obs.unige.ch

Abstract Galactic warps represent an old unresolved problem since the discovery of the HI warp of the Milky Way at the end of the fifties. In this paper, we propose a new scenario explaining a large fraction of the observed optical warps. Based on N-body simulations, we show that realistic galactic disks, where the dark matter is essentially distributed in a disk, are subject to bending instabilities. S, U-shaped, as well as asymmetric warps are spontaneously generated and in some cases are long-lived. While this scenario presents the advantage of explaining the three observed types of warps, it also brings new constraints on the dark matter distribution in spiral galaxies. Finally, it gives us a unified picture of galaxies, where galactic asymmetries like bars, spirals, and warps result from gravitational instabilities.

Keywords: galaxies: kinematics and dynamics - galaxies: structure - dark matter

1. Why Do Disk Galaxies have Often Spirals and Warps?

Here we propose that the fundamental reason why spiral galaxies present frequently warps is identical to the one why spirals have frequently spiral arms and bars: the dissipational component, gas-dust, brings these systems toward a critical state with respect to gravitational instabilities, producing spiral arms and bars in the radial direction, and warps in the vertical direction. As long as gas dissipates the dynamical reheating induced by the instabilities compensates the cooling due to radiative losses in the gas. The critical state is maintained and disk galaxies remain very responsive to perturbations.

In such conditions any perturbations, be it gas infall or interactions, trigger large and long-lived responses of the disks in the form of grand design spirals or large warps. Thus while external perturbations help galaxies to produce spirals and warps the fundamental cause why the disk response is large and slow lies in the marginally stable state of such systems reached by the secular energy losses.

R. S. de Jong, Island Universes, 149–152.
© 2007 *Springer.*

Consistent with this scenario is that gas poor disk galaxies, such as S0's possess typically only small, tightly wound spiral arms, and warps are rare. When too little gas is left it is unable to regenerate gravitational instabilities.

The interesting by-product of such a scenario is that the matter content of galaxy disks is then constraint. Several observational results, like spiral structures in HI disks (Masset & Bureau 2003), dark matter and HI correlation (Bosma 1978; Hoekstra et al. 2001; Pfenniger & Revaz 2005), star formation in low gas density regions (Cuillandre et al. 2001), and more recently, diffuse gamma-rays in the Galaxy (Grenier et al. 2001), suggest that dark baryons are in galactic disks associated to HI and classical molecular clouds. A substantial amount of matter in the disks would therefore explain many aspects of disks galaxies, and in passing warps.

Bending instabilities are Jeans-like gravitational instabilities that occur in flat systems and cause them to warp. Toomre (1966) and Araki (1985) have shown that an infinite slab of finite thickness may be unstable when the ratio of the vertical velocity dispersion σ_z to the velocity dispersion in the plane σ_u is less than 0.293 (This value is called the Araki limit). In this work we use N-body simulations to quantify the effects produced by bending instabilities in self-gravitating disks of different thicknesses, and to quantify the amount of matter that bending instabilities require in the disk in order to be unstable, and the amount of matter that is left in the halo up to the disk radius.

2. The Heavy Disk Model

We have studied the spontaneous formation of warp resulting from bending instabilities in 9 different galactic models. All mass model are composed of a bulge, an exponential stellar disk ($H_R = 2.5$, $H_z = 0.25\,\mathrm{kpc}$) and a heavy disk made of HI gas and dark matter proportional to it. With a respective mass fraction for the 3 components of 0.068, 0.206, and 0.726, the rotation curve is approximately flat up to $R = 35\,\mathrm{kpc}$. The 9 models differ only by the thickness h_{z0} and flaring R_f of the dark matter component.

The initial vertical velocity dispersion σ_z is found by satisfying the equilibrium solution of the stellar hydrodynamic equation in cylindrical coordinates, separately for each components. To set the azimuthal and radial dispersions, we have used the epicycle approximation and the ratio between the radial and vertical epicyclic frequency κ and ν. See Revaz & Pfenniger (2004) for more details on the models.

All models (from 01 to 09) are displayed on Fig. 1, where the ratio σ_z/σ_R (stability index) is plotted as a function of the vertical dispersion. This latter value gives an idea of the disk thickness. Thin disks are found at lower left end, while thick disks are found at the upper right end. The dotted line corresponds

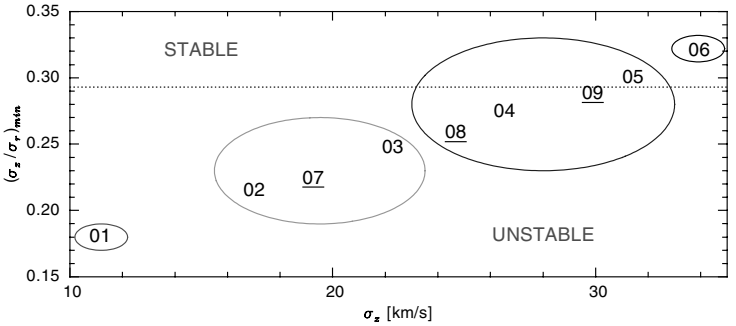

Figure 1. Ratio σ_z/σ_R as a function of the vertical dispersion σ_z at $R = 15\,\mathrm{kpc}$. The values are taken at the radius where σ_z/σ_R is minimum. The dotted line corresponds to Araki's limit.

to Araki's stability criterion $\sigma_z/\sigma_R = 0.293$. We thus expect that thinner disk will be less stable.

3. Stability as a Function of the Disk Thickness

As expected from Fig. 2., the evolution of the models depends strongly on the thickness of the heavy disk. According to their evolution, the models can be divided in four groups:

1) Model 01 has a ratio σ_z/σ_R of 0.18. It is very unstable. The bending instability occurs quickly and generates a transient asymmetric warp that extends up to $z = 4\,\mathrm{kpc}$ at $R = 35\mathrm{kpc}$ (see Fig. 2a). After the perturbation the disk is thickened and the galaxy is stabilized.

2) Models 02, 07 and 03 have still a ratio σ_z/σ_R well below the Araki limit. The bending instability occurs during the first 2 Gyr. An axisymmetric bowl mode $m = 0$ (U-shaped warp) grows during about $1\,\mathrm{Gyr}$ (Fig. 2b), before that σ_z increases and stabilizes the disk.

3) The four models 08, 04, 09 and 05 develop S-shaped warped modes ($m = 1$). Except model 05, which has a ratio $\sigma_z/\sigma_R = 0.3$ just above Araki's limit, all are unstable with respect to a bending. In the case of model 08, the warp is long-lived and lasts more than $5.5\,\mathrm{Gyr}$, corresponding to about 5 rotation times at $R = 30\,\mathrm{kpc}$ (Fig. 2c,d).

4) Model 06 has a ratio σ_z/σ_R well above 0.3. The model is stable.

These simulations show that the bending instability in heavy disk model may be at the origin of the 3 observed type of warp : S-shaped, U-shaped and asymmetric. The high frequency of observed S-shaped warps (Reshetnikov 1998) is naturally explained because S-shaped warps develop near the Araki limit (marginally unstable regime) and then are long lived.

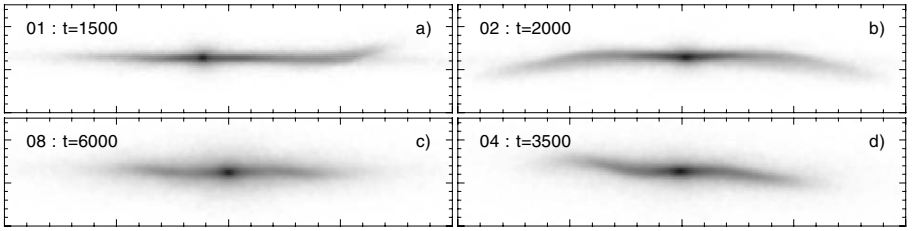

Figure 2. Edge-on projections of the models 01, 02, 08 and 04.

4. Dark Matter Constraint

The previous results have been obtained in the absence of a dark halo. We have checked up to which point the disk self-gravity leads to bending instabilities when the disk is embedded in a conventional hot halo.

For a realistic model, where a fraction $(1 - f)$ of the dark matter has been transfered into a halo, the vertical instabilities are damped if more than half of the dark mater is in the halo ($f < 0.5$). On the contrary, the disk may be unstable.

When taking into account the dissipational behavior of the gas, as this is the case in the plane for spirals, the disk is expected to reach a marginally unstable regime at the Araki limit corresponding to $f = 0.5$ in our model. We can then deduce, that half of the dark matter is situated in the disk and the other half in the halo. The flattening of our model is then in agreement with the flattening of the Milky Way, recently determined by Johnston et al. (2005), based on the study of the Sagittarius orbit.

References

Araki, S., 1985, Ph.D. Thesis, Massachusetts Inst. Technology
Bosma, A. 1978, PhD thesis, Univ. Groningen
Cuillandre, J-C., Lequeux, J., Allen, R.J., Mellier, Y., Bertin, E. 2001, ApJ, 554, 190
Grenier, I.A., Casandjian, J-M, Terrier, R. 2005, Science, 307, 1292
Hoekstra, H., van Albada, T.S., Sancisi, R. 2001, MNRAS, 323, 453
Johnston, K.V., Law, D.R., Majewski, S.R. 2005, ApJ, 619, 800
Masset, F.D., Bureau, M. 2003, ApJ, 586, 152
Pfenniger, D., Revaz, Y. 2005, A&A, 431, 511
Reshetnikov, V., Combes, F. 1998, A&A, 337, 9
Revaz, Y., Pfenniger, D. 2004, A&A, 425, 67
Toomre, A. 1966, Geophys. Fluid Dyn., 46, 111

THE 3-DIMENSIONAL DYNAMICS OF THE GALACTIC BULGE

M. Soto, K.H. Kuijken and J. Lub

Leiden Observatory, The Netherlands

Abstract We report the preliminary results of our research that includes stellar radial velocities and proper motion measurements in several windows of the Galactic Bulge, using HST images and VIMOS integral field spectroscopy. A new procedure to obtain spectra of stars in very crowded fields and to combine the information of both instruments has been developed. Using these results we have found a significant vertex deviation in two fields.

Keywords: Galaxy: bulge - Galaxy: kinematics and dynamics - stellar dynamics

1. Introduction

The center of our galaxy provide us with the closest example of bulge kinematics we can get. In spite of much work we still lack a unique detailed model to explain the kinematics within the bulge. This lack includes information about the bar.

Understanding the bulge kinematics requires knowledge of the gravitational potential that drives the stellar orbits. A suitable data set with 3-dimensional information (like two projected spatial coordinates, two proper motion coordinates, combined with radial velocities) could solve this problem (Kuijken 2004). Mechanisms to drive the galactic evolution can be inferred once we have understood the kinematics and its relation to stellar populations.

The complications to get these results are mainly related with the high extinction by foreground dust near the galactic plane. This high extinction limits the optical work to only a few windows where the extinction is relatively low and uniform. Furthermore, we must consider the fact that even in these fields with low extinction the contamination by disc stars is important (as high as 50% in some cases according to exponential models). In this sense, the use of photometric data to separate disc and bulge populations is not enough. Only combining data from new spectroscopy instrumentation with HST photometry we will be able to infer more precise conclusions about our galactic bulge.

R. S. de Jong, Island Universes, 153–156.
© 2007 *Springer.*

2. Proper Motion and Radial Velocities

Proper motion images were obtained by HST WFPC2 at two epochs. While several fields are still in progress, the three nearest fields of the galactic minor

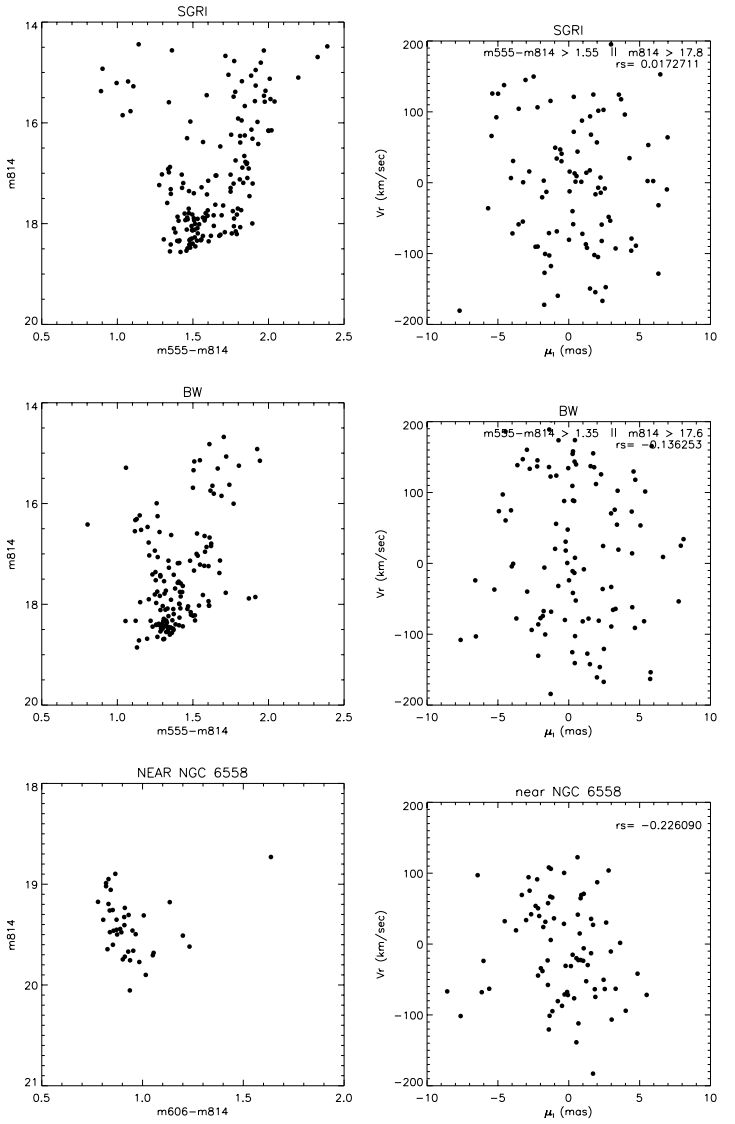

Figure 1. *Left*, Color Magnitude diagram with radial velocities for the three fields completed. *Right*, longitude proper motion μ_l and radial velocity information for the same three fields. Note the cuts in the SGR-I and Baade's Window using the respective CMD and the correlation coefficient rs. In the two bottom plots a significant vertex deviation has been found.

axis have been already completed; these are Sgr-I (l, b)=$(1.26, 2.65)$, Baade's Window (l, b)=$(1.13, -3.76)$, and *near* NGC 6558 (l, b)=$(0.28, -6.17)$.

The proper motion procedure is similar to used by Anderson & King (2000) and consists of a combination of PSF reconstruction from bright stars in the HST images, and PSF core fitting on these same crowded images (Kuijken & Rich 2002). Information from exposures at different positions was used to refine the centroids, with residual systematics on the measurements believed to be better than 1.5 mas.

Radial velocity spectra have been taken in the VLT's integral field spectrograph VIMOS/IFU in high resolution for the same three fields.

Every VIMOS/IFU image has 1600 spectra (each fiber/pixel is a spectrum), but this huge quantity of spectra does not mean a huge quantity of stars. The procedure to extract the stellar spectrum requires the organization of the reduced data in cubes and the use of the HST images for the same IFU fields. Using a suitable IFU PSF we can estimate the contribution of each HST list star in each IFU field pixel and define a matrix according to the real flux found in the IFU image. The solutions of this system correspond to the fluxes for every star in the IFU image. Repeating the same process in the spectra IFU cube for every slice (one slice per angstrom) we are able to rebuild the spectrum of each star. Performing a cross correlation with a template star we finally obtain the radial velocity in each spectrum.

3. Discusion

A clear signature of a barred bulge and therefore a non-axisymmetric potential should show a vertex deviation (angle between the long axis of the velocity ellipsoid and the line of sight).

Figure 1 combines our first results of radial velocities and proper motion measurements in the three central fields. We observe encouraging preliminary results where the signature of a vertex deviation can be inferred. We have proven the technical capacity to work in very crowded fields and get radial velocities.

This project is on-going: new data in other fields away from the galaxy minor-axis will be added. The new fields will provide us information to develop a well constrained model of the Galactic center.

References

Anderson, J. & King, I.R 2000, PASP 112, 1360
Kuijken, K. & Rich, R.M. 2002, AJ 124, 2054
Kuijken, K. 2004, ASPC 317, 310

Amanda Bauer.

ASYMMETRIC DRIFT AND THE STELLAR VELOCITY ELLIPSOID

Kyle B. Westfall[1], Matthew A. Bershady[1], Marc A. W. Verheijen[2], David R. Andersen[3] and Rob A. Swaters[4]

[1] *University of Wisconsin – Madison, USA*
[2] *Kapteyn Astronomical Institute, University of Groningen, the Netherlands*
[3] *NRC Herzberg Institute of Astrophysics, Canada*
[4] *University of Maryland, College Park, USA*

Abstract We present the decomposition of the stellar velocity ellipsoid using stellar velocity dispersions within a 40° wedge about the major-axis ($\sigma_{\rm maj}$), the epicycle approximation, and the asymmetric drift equation. Thus, we employ no fitted forms for $\sigma_{\rm maj}$ and escape interpolation errors resulting from comparisons of the major and minor axes. We apply the theoretical construction of the method to integral field data taken for NGC 3949 and NGC 3982. We derive the vertical-to-radial velocity dispersion ratio (σ_z/σ_R) and find (1) our decomposition method is accurate and reasonable, (2) NGC 3982 appears to be rather typical of an Sb type galaxy with $\sigma_z/\sigma_R = 0.73^{+0.13}_{-0.11}$ despite its high surface brightness and small size, and (3) NGC 3949 has a hot disk with $\sigma_z/\sigma_R = 1.18^{+0.36}_{-0.28}$.

Keywords: galaxies: kinematics and dynamics - galaxies: individual (NGC 3949, NGC 3982)

1. Motivation and Methodology

The shape of the stellar velocity ellipsoid, defined by σ_R, σ_ϕ, and σ_z, provides key insights into the dynamical state of a galactic disk: σ_z:σ_R provides a measure of disk heating and σ_ϕ:σ_R yields a check on the validity of the epicycle approximation (EA). Additionally, σ_R is a key component in measuring the stability criterion and in correcting rotation curves for asymmetric drift (AD), while σ_z is required for measuring the disk mass-to-light ratio. The latter is where the DiskMass survey focuses (Verheijen et al. 2004, 2005); however, in anything but face-on systems, σ_z must be extracted via decomposition of the line-of-sight (LOS) velocity dispersion. Below, we present such a decomposition for two galaxies in the DiskMass sample: NGC 3949 and NGC 3982.

Previous long-slit studies (e.g., Shapiro et al. 2003 and references therein) acquired observations along the major and minor axes and performed the

R. S. de Jong, Island Universes, 157–160.
© 2007 *Springer.*

decomposition via the EA and AD equations; using both dynamical equations overspecifies the problem such that AD is often used as a consistency check. Here, use of the SparsePak (Bershady et al. 2004, 2005) integral field unit (IFU) automatically provides multiple position angles, thereby increasing observing efficiency and ensuring signal extraction along the desired kinematic axes. Long-slit studies have also used functional forms to reduce the sensitivity of the above decomposition method to noise. Here, only measures of the LOS velocity dispersions within a 40° wedge about the major axis are used to perform the decomposition by incorporating both the EA and AD equations under some simplifying assumptions. Velocities and radii within the wedge are projected onto the major axis according to derived disk inclinations, i, and assuming near circular motion. In the end, our method requires neither fitted forms nor error-prone interpolation between the major and minor axes. Future work will compare this decomposition method with the multi-axis long-slit method and investigate effects due to use of points off the kinematic axes.

Following derivations in Binney & Tremaine (1987) and assuming (1) EA holds, (2) the velocity ellipsoid shape and orientation is independent of z ($\partial(\overline{v_R v_z})/\partial z = 0$), (3) both the space density, ν, and σ_R have an exponential fall off radially with scale lengths of h_R and $2h_R$, respectively, and (4) the circular velocity is well-represented by the gaseous velocity, v_g, the equation for the AD of the stars becomes $v_g^2 - \overline{v_*}^2 = \frac{1}{2}\sigma_R^2\left(\frac{\partial \ln \overline{v_*}}{\partial \ln R} + 4\frac{R}{h_R} - 1\right)$, where $\overline{v_*}$ is the mean stellar rotation velocity; hence, σ_R is the only unknown. The third assumption requires mass to follow light, $\Sigma \propto \sigma_z^2$, and constant velocity ellipsoid axis ratios with radius; Σ is the surface density. The major-axis dispersion is geometrically given by $\sigma_{maj}^2 = \sigma_\phi^2 \sin^2 i + (\eta\sigma_R)^2 \cos^2 i$, where $\eta = \sigma_z/\sigma_R$ is constant with radius. Finally, EA, $\sigma_\phi^2/\sigma_R^2 = \frac{1}{2}\left(\frac{\partial \ln \overline{v_*}}{\partial \ln R} + 1\right)$, completes a full set of equations for decomposition of the velocity ellipsoid.

2. Analysis

Data for testing of the above formalism was obtained during SparsePak commissioning (Bershady et al. 2005, see Table 1). Both NGC 3949 and NGC 3982 were observed for 3×2700s at one IFU position with $\lambda_c = 513.1$ nm and $\lambda/\Delta\lambda = 11700$ or 26 km s^{-1}. The velocity distribution function (VDF) of both gas and stars is parameterized by a Gaussian function. In each fiber with sufficient signal-to-noise, the gaseous VDF is extracted using fits to the [OIII] emission line; the stellar VDF is extracted using a modified cross-correlation method (Tonry & Davis 1979; Statler 1995) with HR 7615 (K0III) as the template (Westfall et al. 2005). The pointing of the IFU on the galaxy is determined *post factum* to better than 1" by minimizing the χ^2 difference between the fiber continuum flux and the surface brightness profile. Subsequent

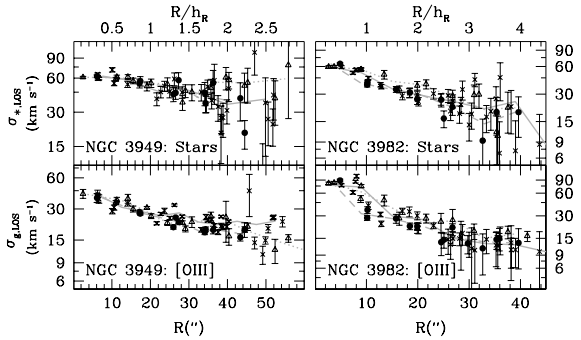

Figure 1. Measurements of the LOS dispersions in NGC 3949 (*left*) and NGC 3982 (*right*) for stars (*top*) and gas (*bottom*) as a function of galactic radius; the top axis is in units of scale length (h_R is 20 and 10 arcsec in NGC 3949 and NGC 3982, respectively). Major axis, minor axis, and in between fibers are shown as points, triangles, and crosses, respectively; "axis fibers" lie in a 40° wedge around the axis. The binned mean values are shown for the major axis, minor axis, and otherwise as dashed, dotted, and solid lines, respectively.

galactic coordinates have been deprojected according to the kinematic inclination and position angle.

Figure 1 shows LOS dispersions for both the gas, $\sigma_{g,LOS}$, and stars, $\sigma_{*,LOS}$; data points are given across the full field of the IFU with points along the major and minor axes and in between having different symbols (see caption). From this Figure note (1) there is no significant difference in σ_{LOS} along the major and minor axes for NGC 3949 and (2) the large gas dispersion within $R \leq 10$" for NGC 3982 is a result of poor single Gaussian fits to the multiple dynamical components of its LINER nucleus.

Figure 2 gives the folded gaseous and stellar rotation curves and compares the measured $\sigma_{\rm maj}$ from Figure 1 with that calculated using the formalism from §1. The value of η used in Figure 2 provides the minimum difference between the two sets of data (as measured by χ^2_ν; see Figure 3a). We find $\eta = 1.18^{+0.36}_{-0.28}$ and $\eta = 0.73^{+0.13}_{-0.11}$ for NGC 3949 and NGC 3982, respectively; errors are given by 68% confidence limits. A comparison of these values to the summary in Shapiro et al. (2003) is shown in Figure 3b. The disk of NGC 3982 is similar to other Sb types studied; however, NGC 3949 seems to have an inordinately hot disk. The latter, while peculiar, is also supported by the indifference between its major and minor axis σ_{LOS} from Figure 1 and the same indifference seen in the CaII data presented by Bershady et al. (2002). Our streamlined velocity-ellipsoid decomposition method appears accurate, as seen by comparison with (1) galaxies of a similar type for NGC 3982, and (2) data in a different spectral region for NGC 3949.

Acknowledgement This work was supported by an AAS International Travel Grant, the Wisconsin Space Grant Consortium, and NSF Grant AST-0307417.

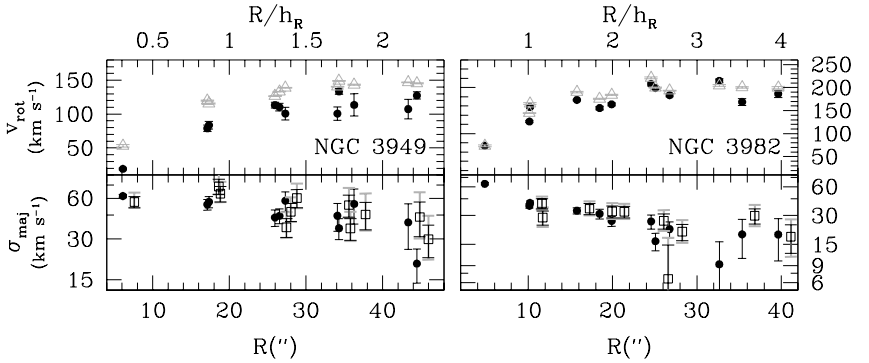

Figure 2. Comparison of measured and calculated σ_{maj} in NGC 3949 (*left*) and NGC 3982 (*right*). Top panels show the deprojected rotational velocity for both the gas (*grey triangles*) and stars (*black points*) along the major axis. Bottom panels compare the measured σ_{maj} (*points*) to those from our formalism using η as derived from Figure 3a (*squares*; offset in R for comparison). Errors on σ_{maj} are also calculated when using the 68% confidence limits for η (*grey*).

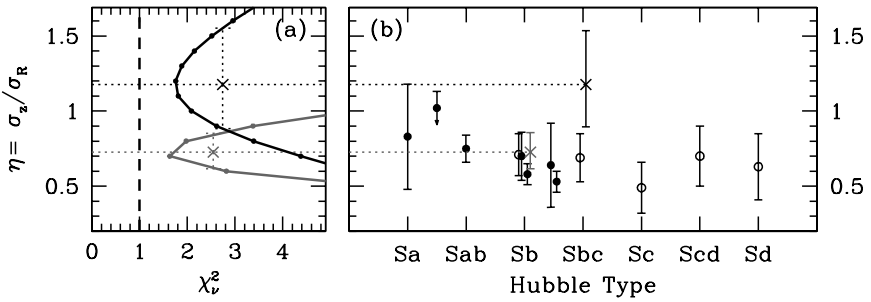

Figure 3. Derivation of the ratio $\eta = \sigma_z/\sigma_R$. In (a), the χ^2_ν statistic is used to find the best correspondence between the model and measured data sets for NGC 3949 (*black line*) and NGC 3982 (*grey line*). The 68% (1σ) confidence limits on η are determined by an increase of χ^2_ν by 1 (*dotted lines*). The disk heating of NGC 3949 (*black cross*) and NGC 3982 (*grey cross*) are placed on Figure 5 from Shapiro et al. (2003) in (b).

References

Bershady, M., Verheijen, M., Andersen, D. 2002, in Disks of Galaxies: Kinematics, Dynamics and Perturbations, eds. E. Athanassoula & A. Bosma, ASP Conference Series, 275, 43

Bershady, M. A. et al. 2004, PASP, 116, 565

Bershady, M. A. et al. 2005, ApJS, 156, 311

Binney, J. & Tremaine, S. 1987, *Galactic Dynamics* (Princeton University Press: Princeton, NJ)

Shapiro, K. L., Gerssen, J., & van der Marel, R. P. 2003, AJ, 126, 2707

Staler, T. 1995, AJ, 109, 1371

Tonry, J. & Davis, M. 1979, AJ, 84, 1511

Verheijen, M. A. W. et al. 2004, AN, 325, 151

Verheijen, M. et al. 2005, these proceedings

Westfall, K. B. et al. 2005, in prep.

III

BARS, SPIRAL STRUCTURE, AND SECULAR EVOLUTION IN DISK GALAXIES

BARS, SPIRAL STRUCTURE, AND SECULAR EVOLUTION IN DISK GALAXIES

Bruce G. Elmegreen

IBM Research Division, T.J. Watson Research Center, USA
bge@watson.ibm.com

Abstract Simulations and observations of galactic bars suggest they do not commonly evolve into bulges, although it is possible that the earliest bars formed bulges long ago, when galaxies were smaller, denser, and had more gas. The most highly evolved of today's bars may become lenses over a Hubble time. Most galaxies in the early Universe are extremely clumpy, with $\sim 10^8 - 10^9$ $M_\odot$ blue clumps that resemble in color and magnitude the isolated field objects nearby. The presence of blue and irregular bars at high redshift suggests that some bars formed primarily in the gas phase accompanied by giant starbursts, rather than in pure stellar disks like most models. Secular and non-secular processes that cause galaxies to evolve are summarized.

Keywords: galaxies: structure - galaxies: spiral - galaxies: evolution

Introduction

Secular evolution of galaxies includes too many processes to review thoroughly here. Instead, a selection of processes with contemporary interests will be discussed. They include bar evolution in the present-day Universe and at intermediate to high z, and disk formation at high z, where extremely clumpy structure seems to be common. A brief summary of secular evolution effects over a Hubble time is in Section 4. A recent review of secular evolution leading to central mass concentrations and pseudobulges was in Kormendy & Kennicutt (2004).

1. Bar Evolution

Bar Dissolution to Form a Bulge

The disk and halo of a galaxy exert negative torques on a bar and cause the bar to get stronger, longer, and slow down over time (Weinberg 1985; Debattista & Sellwood 1998, 2000; Athanassoula, Lambert, & Dehnen 2005;

R. S. de Jong, Island Universes, 163–174.
© 2007 *Springer.*

Athanassoula 2005). Bars also change their shape as more orbital families get populated. They can thicken and develop a peanut-shaped profile perpendicular to the disk as a result of a resonance between the corotating pattern period and the vertical oscillation period (Combes & Sanders 1981). They can become more squared off at the ends, or boxy, as a result of increasing populations of 4:1 orbits. Orbit families are described in Sellwood & Wilkinson (1993) and Athanassoula (2005). Gas accretion to the center and subsequent star formation can lead to a dense nucleus, which either forms an ILR or shifts the existing ILR to a larger radius. Tightly wound starburst spirals or rings may appear near these inner resonances and secondary bars can form inside (e.g., Englmaier & Shlosman 2004).

Perhaps the most startling development of the 1990's was that the growth of the ILR radius with time depopulates bar-supporting orbits (x1 orbits), which are the elongated orbits parallel to the bar out to nearly the corotation radius. This depopulation can dissolve a bar completely, forming a bulge-like concentration in the center (Hasan & Norman 1990; Friedli & Benz 1993; Hasan, Pfenniger, & Norman 1993). Norman, Sellwood, & Hasan (1996) ran 2D models of bar dissolution with 50,000 star particles, no gas and no active halo. They found that by the time 3-5% of the total disk mass shrank to the galaxy core, the bar was completely dissolved. They also confirmed this result with a 3D model using 200,000 star particles and no active halo.

Shen & Sellwood (2004) also ran 3D star models with no active halo and found in addition that bar weakening occurs in 2 phases, an initially fast stage where the bar-supporting orbits are scattered, and then a slow stage where the whole potential changes. More importantly, they pointed out that the central mass needed to destroy a bar is much larger, by a factor of 10 or more, than the nuclear black hole mass, concluding that bar destruction is in fact unlikely in real galaxies. They showed further that a dispersed central mass, as might result from gas inflow and star formation, required an even higher fraction (e.g., $> 10\%$ of the disk mass) than a point-like distribution, making the possibility that gas accretion can eventually destroy a bar (i.e., because of its central mass) seem even more remote.

Athanassoula, Lambert, & Dehnen (2005) studied bars with active halos and found that if the halo was massive, the bars survived even with a central mass of 10% of the disk mass. Bars in low-mass active halos were still destroyed, like before. The difference is that an active halo continuously removes angular momentum from the bar, strengthening it by populating x1 orbits. Then the deleterious effect of the central mass is reduced. Halos also promote spiral arm formation by the removal of disk angular momentum (Fuchs 2004).

While bars are strengthened by a loss of angular momentum to a disk or halo, thereby resisting dissolution at the ILR from a central concentration, bars also weaken by the absorption of angular momentum from gas, and thereby

become more prone to dissolution (Bournaud & Combes 2002). Gas within the bar radius shocks at the bar-leading dust lanes. The asymmetric pressures in these shocks cause the gas to lose orbital angular momentum, eventually migrating to the center. The shock is asymmetric only if there is energy dissipation; otherwise the backward impulse the gas feels when entering the shock is compensated by a forward impulse it feels when leaving the shock. From the point of view of the stars, there is a gravitational attraction to the dust lane, which is shifted forward of the orbital apocenter. Because stars in bar orbits spend a longer time at apocenter than at pericenter (on the minor axis), the time-integrated gravitational force from the gas produces a net positive torque on the stars. The resulting angular momentum gain causes the elongated stellar orbits to open up into circular orbits, which have higher angular momentum for the same energy (the same major axis length). Circularization of orbits makes the bar ultimately dissolve. Recent simulations of this effect are in Bournaud, Combes, & Semelin (2005).

Dissolution of a bar by gas torques requires a large amount of gas in the bar region, as essentially all of the angular momentum that was removed from the stars to make the bar in the first place has to be returned from the gas. If the total mass fraction of gas in the bar region is small, then the circularization of bar orbits may be minimal. Block et al. (2002) propose that continued accretion of gas onto the galaxy disk can cause a second or third event of bar dissolution if a new bar forms in the mean time. In this way, bars can dissolve but still have an approximately constant fraction over a large portion of the Hubble time, as observed by Sheth et al. (2003), Elmegreen, Elmegreen, & Hirst (2004), Jogee et al. (2004), and Zheng et al. (2005).

Bars Dissolution to Form a Lens

What is the observational evidence for bar dissolution and what happens to old bars? The evidence for bar circularization in more centrally concentrated galaxies (Das et al. 2003) does not actually indicate that bars dissolve. Dissolution may take a very long time and the observed circularization could be only the first step.

There is good evidence for some bar dissolution, however, with the resulting structure a lens (Sandage 1961; Freeman 1975; Kormendy 1977), or perhaps a pseudo-bulge (Kormendy & Kennicutt 2004). A lens is not a spheroid or part of the outer exponential disk. It is a stellar distribution in the inner region with a rather shallow brightness profile and a sharp cutoff at mid-disk radius. Outside the lens, the main disk exponential continues. Kormendy (1979) suggested that lenses are dissolved bars. That is, S0 galaxies with lenses formerly had bars. Of the 121 low-inclination, bright SB0-SBd type galaxies in Kormendy (1979), 54% of early bar types, SB0-SBa, have a lens, 0% of late bar types SBab-SBc

have a lens, and 16% of the sample have both a bar and a lens. The lens looks like it is coming from the bar in these latter cases because the lens size is the same as the bar size. The lenses in early-type non-barred galaxies are also the same size as the inner rings in barred (non-lens) galaxies for the same absolute magnitude galaxy; these rings are another measure of bar size. Lens colors are generally the same as bar colors too. Some bars even "look" like they are dissolving into a lens because the bar spreads out into a circular shape at the ends (e.g., NGC 5101). The axial ratio distribution of lenses weakly suggests they are thick (triaxial).

The presence of lenses in about half of the early-type barred galaxies (as mentioned above) but in only a small fraction of early-type non-barred galaxies suggests further that bars dissolve very slowly into lenses. The most advanced stages of dissolution are in the early-type bars, which are denser and more advanced in total evolution than late-type bars.

There are very few simulations of bar dissolution into a lens. A pure star simulation by Debattista & Sellwood (2000) shows something like a stellar ring forming at the end of the bar. Stars develop complex orbits over time, migrating between inside and outside the bar as the lens builds up.

2. Bar Dissolution into Bulges at Very Early Times

We have found that barred galaxies in the early Universe are slightly smaller than barred galaxies today, by a factor of ~ 2 in the exponential scale length (Elmegreen, Elmegreen, & Hirst 2004). Such a measurement avoids problems with cosmological surface brightness dimming. The same small sizes are observed for spiral galaxies in general, based on a sample of 269 spirals in the Hubble Ultra Deep Field (Elmegreen et al. 2005a). The presence of spirals in these high-z disk galaxies suggests that the disks are relatively massive compared to the halos at that time, unlike the inner disks of today's galaxies. This suggests, in turn, that galaxies build up from the inside out, as proposed many years ago (e.g., Larson 1976). With such a process, the dynamical time for evolution in a disk, which is proportional to the inverse square root of total density, will be shorter in the early Universe than it is today. That is, the active parts of galaxy disks are gradually evolving toward lower and lower densities and longer evolutionary timescales (a process related to "downsizing" – e.g. Tanaka et al. 2005).

The implication of increasing dynamical time in an aging Universe is that bar formation and secular dissolution should have been much faster at high redshift, in approximate proportion to the bar size. Also, the higher gas abundance in young galaxies would have led to a more rapid dissolution then too, by the Bournaud & Combes (2002) process. Thus some of the very early stages of bulge formation inside a disk (as opposed to disk accretion around a

pre-existing bulge) could have involved evolution from a bar. There is no direct evidence for this yet, however.

Observing The Youngest Bars

Observations of the youngest bars are difficult for several reasons. Figure 1 plots various observables as a function of redshift, using the WMAP cosmology (Spergel et al. 2003) and equations in Carroll, Press, & Turner (1992). Beyond $z \sim 1$, galaxies are only a few Gyr old (top left) and a normal size bar has rotated around only a few times. Thus the bar will be dynamically young and likely to appear different, perhaps more irregular or round. Also, the bar age is likely to be younger than the gas consumption time, which is typically ~ 10 orbit times (e.g., Kennicutt 1998), so the bars will still be gas-rich, like

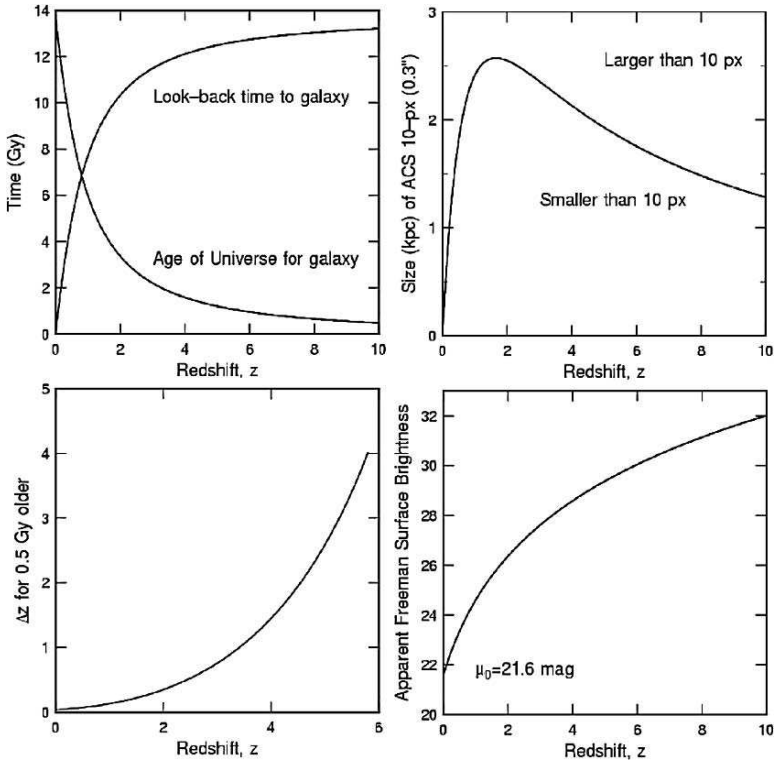

Figure 1. Four quantities from the standard ΛCDM cosmology are plotted versus redshift, z: the Universe age and look back time (top left), the physical size of a region subtending 10 pixels of the HST ACS camera (top right), the redshift range, Δz, spanning 0.5 Gyr (lower left), and the apparent surface brightness of a region having an intrinsic surface brightness equal to the standard Freeman value (lower right).

some late-type bars today. This makes them irregular also because of dust obscuration and star formation.

Second (Fig. 1 upper right), between $z \sim 0.6$ and 4.6, objects smaller than 2 kpc in physical size, such as a bar thickness, will be smaller than 10 pixels on the HST ACS camera. This makes it difficult to resolve internal structure. Bars were not easily seen in the Hubble Deep Fields North and South (e.g., Abraham et al. 1999) because of the factor of 2 lower angular resolution of the WFPC2 camera. Only the largest bars could be seen in the HDF images (Sheth et al. 2003).

Third (lower left), beyond $z \sim 3$ the redshift range corresponding to the duration of bar formation exceeds $\Delta z = 1$, which means that the bar formation process gets stretched out over a wide range of z. This is good in the sense that different stages in bar formation may be seen distinctly, but it is bad in the sense that bars beyond $z \sim 3$ will be incompletely formed and perhaps unrecognizable.

Fourth (lower right), beyond $z \sim 4$ disks with the "standard" rest-B band surface brightness of today's Freeman-disk, 21.6 mag arcsec^{-2}, are almost too faint to see. The $2-\sigma$ noise limiting surface brightness of the Hubble Ultra Deep Field is $\sim$ 26 mag arcsec^{-2} at I band, which is the deepest passband (Elmegreen et al. 2005a). At $z = 4$, a Freeman disk will have a central surface brightness of ~ 28 mag arcsec^{-2}, which requires averaging over areas at least as large as ~ 40 square pixels to observe at the $2-\sigma$ limit. Thus only large bright regions can be seen. Fortunately the intrinsic surface brightnesses of disks are higher at high redshift because of enhanced star formation, unless the extinction is also high. Whether this star formation is enough to reveal bars at this early epoch is unknown. Surface brightness limitations have already diminished the number of spiral galaxies that can be seen in the UDF (Elmegreen et al. 2005a).

The relatively late formation of disk galaxies compared to spheroids aids somewhat in the study of bar formation because it means that bars in disks form late too, when they can be more easily observed. Nevertheless, there are still considerable problems recognizing and observing young bars. The apparent loss of bars beyond $z \sim 1$ could be partly from these selection effects affects.

The Morphology of Bars out to $z \sim 1$

Most bars look different at $z = 1$ than they do today. High-z bars are typically blue and often clumpy, like giant star-forming regions (Elmegreen, Elmegreen, & Hirst 2004). Sometimes they are off-center. Perhaps this irregularity is not surprising since young disks should still be gas-rich. However, the observation implies something new about bar formation: that it could occur

in gas-rich or pure-gas disks with gas dissipation playing an important role. The bar formation models and simulations existing today are all in pure stellar or dominantly stellar systems, where orbital motions and resonances are important. In a gas rich disk, bar formation is more like a dissipative instability. Recent simulations of bar formation in a pure-gas disk are in Kaufmann et al. (2004).

3. Clumpy Structure in High-z Galaxies

Most galaxies in the Hubble Deep fields and in the Ultra Deep Field are very clumpy. Even elliptical galaxies are clumpy in their cores (Elmegreen, Elmegreen, & Ferguson 2005). A compendium of clumpy structures is shown in Figure 2.

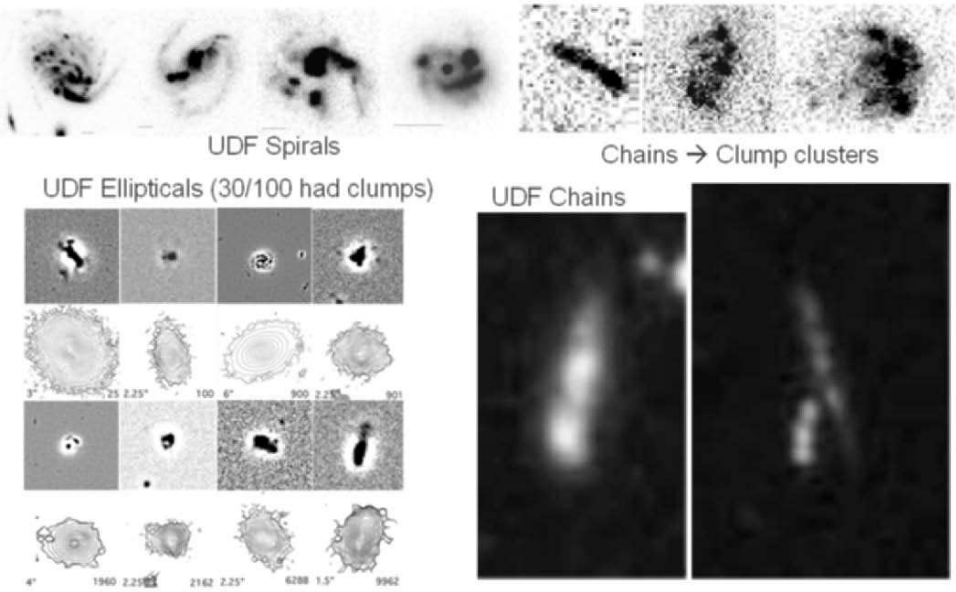

Figure 2. Mosaic of galaxy types from the HST UDF showing extremely clumpy structure. In the lower left, elliptical galaxies are shown with contours to illustrate the overall extents and with unsharp masks at the same scale to highlight the clumps.

The clumps in galaxies in the UDF contain up to 10^9 $M_\odot$ and are typically bluer than the rest of the disk or elliptical galaxy. Thus they are probably young and still forming stars. They are distinct from spiral galaxy bulges, which are redder and always centrally placed.

An examination of the colors and magnitudes of clumps in 10 highly clumpy galaxies, called "clump clusters," suggests their ages are several $\times 10^8$ years

(Elmegreen & Elmegreen 2005). This is ~ 10 times longer than the dynamical times of the clumps, meaning they are gravitationally bound like star clusters, but it is not so young that they may be interpreted as currently star-bursting. Moreover, the clumps have internal densities that are only a factor of $\sim 3-10$ above the local tidal densities in their disks, which means they should disperse relatively soon because of tidal forces. This is probably the process of disk formation; i.e., through the dissolution of giant clumps (see also Elmegreen et al. 2005b).

The origin of the clumps is unknown at the present time. They could be formed in the disks of spirals and clump cluster galaxies or in the gaseous components of elliptical galaxies as a result of gravitational instabilities (Noguchi 1999; Immeli et al. 2004a,b). They could also come in as dwarf-like galaxies from the surrounding field. Similar but isolated clumps are actually seen in these fields (Elmegreen & Elmegreen 2005; Elmegreen et al. 2005a).

4. Summary of Evolutionary Effects over a Hubble Time

Evolutionary effects may be divided into two types, non-secular, which result from one-time events, and secular, which result from a progressive slow change. Non-secular events include interactions, major mergers, and gas stripping during motion through a galaxy cluster.

Strong interactions form bars (Noguchi 1988; Gerin, Combes, & Athanassoula 1990; Sundin & Sundelius 1991; Berentzen et al. 2004). Even binary companions promote bar formation and may shift the galaxy to an earlier Hubble type because of torqued inflow (Elmegreen, Elmegreen, & Bellin 1990). Bars are also more common in perturbed galaxies (Varela et al. 2004). Major mergers form ellipticals (Toomre & Toomre 1972; Barnes & Hernquist 1992; Schweizer 1998), and in the process, they form at least the youngest halo globular clusters (Ashman & Zepf 1992), and may produce counter-rotating cores (Kannappan & Fabricant 2001).

Minor mergers are non-secular events although they may occur more or less continuously. They thicken spiral disks (Walker et al. 1996; Schwarzkopf & Dettmar 2000ab; Bertschik & Burkert 2002; Gilmore, Wyse, & Norris 2002) and may also lead to counter-rotating cores. Interactions may form dwarf galaxies in tidal tails (Zwicky 1959; Barnes & Hernquist 1992; Elmegreen, Kaufman, & Thomasson 1993; Duc, Bournaud, & Masset 2004).

Cluster ram pressure strips gas (Gunn & Gott 1972; Warmels 1988; Hoffman et al. 1988; Cayatte 1990; Crowl et al. 2005) and may promote the formation of S0 types (Larson, Tinsley, & Caldwell 1980).

Strong interactions also form ring galaxies (Theys & Spiegel 1976; Lynds & Toomre 1976), polar ring galaxies (e.g., Cox & Sparke 2004), disk warps, tidal tails, and so on (Toomre & Toomre 1972).

Secular interactions include accretion in the form of residual hierarchical build-up from outside the galaxy, continuous accretion of dwarfs (e.g., Lewis et al. 2004), galaxy harassment (e.g., Moore et al. 1996), accretion of gas (e.g., Bournaud et al. 2005), globular cluster accretion from dwarfs (e.g., Bellazzini, Ibata, & Ferraro 2004), halo streams (e.g., Ferguson et al. 2005), and so on.

Secular changes are also driven by internal processes, such as bar and spiral torques, which lead to inner disk accretion and outer disk spreading (see review in Pfenniger 2000). Gas accretion at resonances makes star-forming rings (see review in Buta & Combes 1996). Scattering and vertical resonances thicken disks. Bars dissolve into lenses and (maybe) bulges, as discussed above. And of course, gas converts into stars, while gas viscosity redistributes the disk gas.

Secular changes among galaxies with different average densities cause early Hubble types to age more quickly than late Hubble types. Most evolutionary processes are faster at higher density. As time goes by, the transition between early and late types moves, converting little-evolved galaxies, which still have a lot of gas and star formation, to highly evolved galaxies, which are inactive and fading. As galaxies progress from late to early types, they become more centrally concentrated, have less gas, less star formation, hotter disks, redder populations, and more metals. Galaxy mass and size increase over time by hierarchical buildup at $z > 1$, and they probably still increase over time today for late-type spirals as a result of continued accretion and coalescence. Still, the average mass and size of a galaxy that is actively forming stars tends to decrease with time ("downsizing"). This is because the most massive galaxies tend also to be the densest, and they completed their star formation first. Also with time, galaxies become more and more isolated, which means that flocculent spiral types and perhaps low surface brightness disks appear relatively late.

Acknowledgements Support from the National Science Foundation grant AST-0205097 is gratefully acknowledged.

References

Abraham, R. G., Merrifield, M. R., Ellis, R. S., Tanvir, N. R., & Brinchmann, J. 1999, MNRAS, 308, 569

Ashman, K.M., & Zepf, S.E. 1992, ApJ, 384, 50

Athanassoula, E. 2005, Celestial Mech. and Dynamical Astron. 91, 9

Athanassoula, E., Lambert, J. C., & Dehnen, W. 2005, MNRAS, 363, 496

Bellazzini, M., Ibata, R., & Ferraro, F.R. 2004, in Satellites and Tidal Streams, ed. F. Prada, D. Martinez Delgado, & T.J. Mahoney, ASP Conf. Ser. Vol. 327, 220

Barnes, J.E., & Hernquist, L. 1992, ARA&A, 30, 705

Barnes, J.E., & Hernquist, L. 1992, Nature, 360, 715

Berentzen, I., Athanassoula, E., Heller, C. H., & Fricke, K. J. 2004, MNRAS, 347, 220

Bertschik, M., & Burkert, A. 2002, Ap&SS, 281, 405

Block, D. L., Bournaud, F., Combes, F., Puerari, I., & Buta, R. 2002, A&A, 394, L35
Bournaud, F., & Combes, F. 2002, A&A, 392, 83
Bournaud, F., Combes, F., Jog, C.J., & Puerari, I. 2005, A&A, 435, 507
Bournaud, F., Combes, F., & Semelin, B. 2005, MNRAS, in press
Buta, R., & Combes, F. 1996, Fund. Cos. Phys., 17, 95
Carroll, S.M., Press, W.H., & Turner, E.L. 1992, ARA&A, 30, 499
Cayatte, V., van Gorkom, J. H., Balkowski, C., & Kotanyi, C. 1990, AJ, 100, 604
Combes, F., & Sanders, R.H. 1981, A&A, 96, 164
Cox, A.L. & Sparke, L.S. 2004, AJ, 128, 2013
Crowl, H.H., Kenney, J.D.P., van Gorkom, J.H., & Vollmer, B. 2005, AJ, 130, 65
Das, M., Teuben, P.J., Vogel, S.N., Regan, M.W., Sheth, K., Harris, A.I., & Jefferys, W.H. 2003, ApJ, 582, 190
Debattista, V. P., & Sellwood, J.A. 1998, ApJ, 493, L5
Debattista, V. P., & Sellwood, J.A. 2000, ApJ, 543, 704
Duc, P.-A., Bournaud, F., & Masset, F. 2004, A&A, 427, 803
Elmegreen, D.M., Elmegreen, B.G., & Bellin, A. 1990, ApJ, 364, 415
Elmegreen, B.G., Kaufman, M. & Thomasson, M. 1993, ApJ, 412, 90
Elmegreen, B.G., Elmegreen, D.M., & Hirst, A.C. 2004, ApJ, 604, L21
Elmegreen, D.M., Elmegreen, B.G., & Ferguson, T.E. 2005, ApJ, 623, L71
Elmegreen, B.G., & Elmegreen, D.M., 2005, ApJ, 627, 632
Elmegreen, D.M., Elmegreen, B.G., Rubin, D.S., & Schaffer, M.A. 2005a, ApJ, 631, 85
Elmegreen, B.G., Elmegreen, D.M., Vollbach, D.R., Foster, E.R., & Ferguson, T.E. 2005b, ApJ, in press
Englmaier, P., & Shlosman, I. 2004, ApJ, 617, L115
Ferguson, A.M.N., Johnson, R.A., Faria, D.C., Irwin, M.J., & Ibata, R.A., Johnston, K.V., Lewis, G.F., & Tanvir, N.R. 2005, ApJ, 622, L109
Freeman, K. 1975, in IAU Symposium No. 69, Dynamics of Stellar Systems, ed. A. Havli (Dordrecht: Reidel), p. 367
Friedli, D., & Benz, W. 1993, A&A, 268, 65
Fuchs, B. 2004, A&A, 419, 941
Gerin, M., Combes, F., & Athanassoula, E. 1990, A&A, 230, 37
Gilmore, G., Wyse, R.F.G., & Norris, J.E. 2002, ApJ, 574, L39
Gunn, J.E., & Gott, J.R., III, 1972, ApJ, 176, 1
Hasan, H. & Norman, C. 1990, ApJ, 361, 69
Hasan, H., Pfenniger, D., & Norman, C. 1993, ApJ, 409, 91
Hoffman, G.L., Helou, G., Salpeter, E.E. 1988, ApJ, 324, 75
Immeli, A., Samland, M., Gerhard, O., & Westera, P. 2004a, A&A, 413, 547
Immeli, A., Samland, M., Westera, P., & Gerhard, O. 2004b, ApJ, 611, 20
Jogee, S. et al. 2004, ApJL, 615, 105
Kannappan, S.J., & Fabricant, D.G. 2001, AJ, 121, 140
Kaufmann, T., Mayer, L., Moore, B., Stadel, J., & Wadsley, J. 2004, astro-ph/0412348
Kennicutt, R.C., Jr. 1998, ApJ, 498, 541
Kormendy, J. 1977, ApJ, 214, 359
Kormendy, J. 1979, ApJ, 227, 714
Kormendy, J. & Kennicutt, R.C. 2004, ARA&A, 42, 603
Larson, R.B. 1976, MNRAS, 176, 31

Larson, R.B., Tinsley, B.M., & Caldwell, C.N., 1980, ApJ, 237, 692
Lewis, G.F., Ibata, R.A., Chapman, S.C., Ferguson, A.M.N., McConnachie, A.W., Irwin, M.J., & Tanvir, N. 2004, PASA, 21, 203
Lynds, R., & Toomre, A. 1976, ApJ, 209, 382
Moore, B., Lake, G., Quinn, T., & Stadel, J. 1996, MNRAS, 304, 465
Noguchi, M. 1988, A&A, 203, 259
Noguchi, M. 1999, ApJ, 514, 77
Norman, C.A., Sellwood, J.A., & Hasan, H. 1996, ApJ, 462, 114
Pfenniger, D. 2000, in Dynamics of Galaxies: from the Early Universe to the Present, eds. F. Combes, G.A. Mamon, and V. Charmandaris. ASP Conf. Ser. Vol. 197, 413
Sandage, A. 1961, The Hubble Atlas of Galaxies, Washington: Carnegie Institution of Washington
Schwarzkopf, U., & Dettmar, R.-J. 2000a, A&A, 361, 451
Schwarzkopf, U., & Dettmar, R.-J. 2000b, A&AS, 144, 85
Schweizer, F. 1998, in Galaxies: Interactions and Induced Star Formation, Saas-Fee Advanced Course 26, Swiss Society for Astrophysics and Astronomy, XIV, eds. R. C. Kennicutt, Jr., F. Schweizer, J. E. Barnes, D. Friedli, L. Martinet, & D. Pfenniger, p. 105
Sellwood, J.A. & Wilkinson, A. 1993, Rep. Prog. Phys., 56, 173
Shen, J., & Sellwood, J.A. 2004, ApJ, 604, 614
Sheth, K., Regan, M.W., Scoville, N.Z., & Strubbe, L.E. 2003, ApJ, 592, 13
Spergel, D.N., et al. 2003, ApJS, 148, 175
Sundin, M., & Sundelius, B. 1991, A&A, 245, L5
Tanaka, M., et al. 2005, MNRAS, 362, 268
Theys, J.C., & Spiegel, E.A. 1976., ApJ, 208, 650
Toomre, A., & Toomre, J. 1972, ApJ, 178, 623
Varela, J., Moles, M., Márquez, I., Galletta, G., Masegosa, J., & Bettoni, D. 2004, A&A, 420, 873
Walker, I.R., Mihos, J.C., Hernquist, L. 1996, ApJ, 460, 121
Warmels, R.H. 1988, A&AS, 72, 427
Weinberg, M.D. 1985, MNRAS, 213, 451
Zheng, X. Z., Hammer, F., Flores, H., Assémat, F., & Rawat, A. 2005, A&A, 435, 507
Zwicky, F. 1959, Handbuch der Physik, 53, 373

Martin Bureau.

BARRED GALAXIES AND GALAXY EVOLUTION

Johan H. Knapen

Centre for Astrophysics Research, University of Hertfordshire, U.K.
j.knapen@star.herts.ac.uk

Abstract We know from near-infrared imaging that bars are present in more than three quarters of local disk galaxies. Several studies have recently led to the conclusion that the fraction, as well as the properties, of bars in galaxies have not changed much from a redshift of about unity to the present day. In this paper, I will briefly review the results on which this conclusion is based, and will discuss some of the implications of bars for the evolution of galaxies. Specifically, I will discuss the role of bars in fuelling gas from the disk to the nuclear regions, where starburst activity may ensue, and the relations of bars with the specific but important class of low-luminosity starbursts known as nuclear rings.

Keywords: galaxies: spiral - galaxies: structure - galaxies: evolution - galaxies: starburst

1. Introduction: Bars, Inflow, and Galaxy Evolution

From theoretical and numerical studies performed over the past decades it is by now well known that bars will lead to a concentration of gas toward the central regions of spiral galaxies. This is caused by the asymmetry of the gravitational potential, torquing and shocking the gas, which thus loses angular momentum and moves further in (e.g., Shlosman, Frank & Begelman 1989; Knapen et al. 1995). The resulting gas accumulation in the central regions of barred galaxies is rather difficult to confirm, but several pieces of observational evidence have been published in recent years (reviewed in more detail by Knapen 2004). Most directly relevant are observations of molecular gas, which indicate that the ratio of central to disk gas is statistically higher in barred than in non-barred galaxies (e.g., Sakamoto et al. 1999; Jogee, Scoville, & Kenney 2005).

There is also observational evidence that starburst galaxies are preferentially barred (see Roussel et al. 2001 and references therein), although these results are subject to important caveats and exclusions. For instance, Huang et al. (1996) point out that their result of more bars among starburst hosts is only valid for strong bars (SB class in the RC3 catalogue) and for early-type

R. S. de Jong, Island Universes, 175–180.
© 2007 *Springer.*

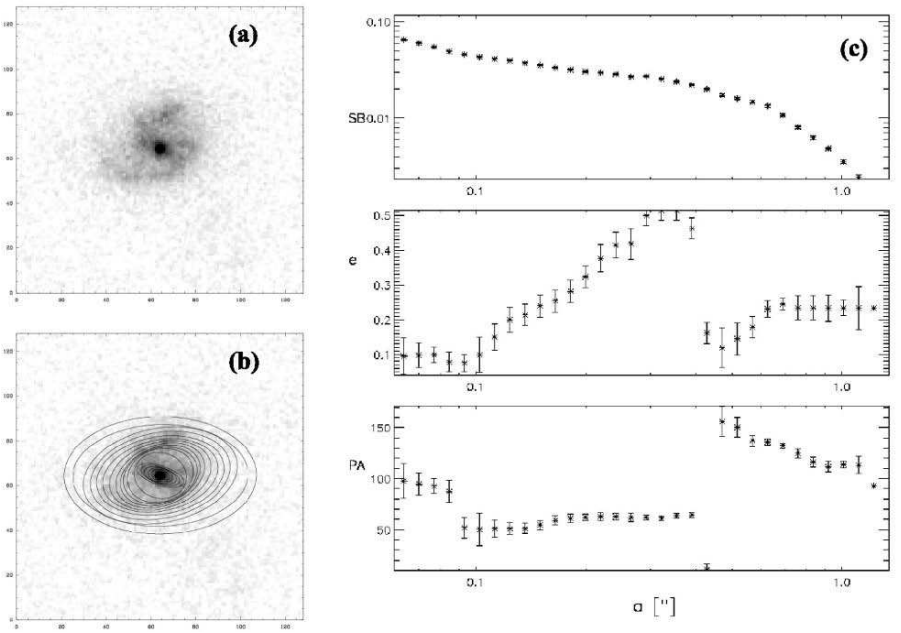

Figure 1. Illustration of how a bar at a redshift out to unity can be found in *HST* ACS data. (a): GEMS image of a galaxy at $z \sim 0.5$, showing a prominent bar and spiral arm structure. (b): the same image, but overlaid are ellipses fitted to the surface brightness distribution. The parameters of the fitted ellipses are shown graphically in (c), in the form of radial profiles of their surface brightness (top), ellipticity (middle), and position angle (bottom). The classic signature of the bar is clear in a radial range of 0.1 - 0.35 arcsec as a gradual rise and sharp fall of ellipticity with increasing radius, while the position angle is constant. Reproduced with permission from Jogee et al. (2004).

galaxies (see also Roussel et al. 2001). Perhaps more importantly, all results referred to above take the bar classifications from optical catalogues such as the RC3, whereas it is now well known that bars can be found and studied more reliably from near-IR imaging. Near-IR imaging yields higher bar fractions than optical imaging (e.g., Knapen, Shlosman & Peletier 2000; Eskridge et al. 2000), but it is unclear whether and how the use of near-IR imaging data would affect the results on the statistical relations between bars and starbursts.

But in any case, it is clear from theory, modelling and increasingly from observations that bars do concentrate matter in the central regions of their hosts. This redistribution of matter and mass has important effects on a galaxy's evolution, not only because a significant fraction of the gas which ends up in the central region will eventually be used to form stars that will add to the bulge, thus helping the process of secular evolution, but also because of the effects

of the bar on the disk and halo, as discussed elsewhere in these proceedings. The dynamics of bars and their influence on the circumnuclear regions has recently been reviewed by Kormendy & Kennicutt (2004), and previously by, e.g., Shlosman (2001).

In the rest of this short paper, we will review recent work showing that the bar fraction, as well as the properties of the bars, have been constant since a redshift of at least unity, and discuss the specific, but rather common, class of star-forming nuclear rings, which form important links between the bars and the star formation in the central regions.

2. Bars at Redshifts of Zero to Unity

Because bars form rather easily in a modelled galaxy, and remain relatively stable once formed, one would have expected that bar properties would not have varied dramatically for the past few billion years. The claim by Abraham et al. (1999), based on imaging data of the original Hubble Deep Field, of a "significant decline" in the bar fraction beyond a redshift of 0.5 was thus greeted with surprise. A number of more recent investigations, however, show convincingly that the fraction of barred galaxies in fact remains unchanged up to a redshift of $z \sim 1$, at least (Sheth et al. 2003; Elmegreen, Elmegreen & Hirst 2004; Jogee et al. 2004; Zheng et al. 2005 – see Fig. 1). Moreover, the distribution of bar properties (sizes and axial ratios) only allows for a mild evolution of galactic disks, and practically rules out a major merger-dominated evolution over the last 8 Gyr (Jogee et al. 2004).

3. Nuclear Rings

From a recent statistical study based on Hα imaging of a sample of Northern spirals[1], we now know that nuclear rings occur in around one fifth of all disk galaxies (Knapen 2005). Asymmetries in the gravitational potential, set up for instance by a bar, can lead to the occurrence of resonances in a gaseous disk. Galactic rings can form in their vicinity, and massive star formation can occur in the rings because gas concentrates near resonances (see Allard, Peletier & Knapen 2005, and these proceedings, p. 207), can become unstable, and collapse. Nuclear rings are associated with Inner Lindblad Resonances (ILRs), usually occur in barred galaxies, and have typical radii of $0.5 - 1$ kpc. Nuclear rings form significant numbers of stars which can help shape a pseudo-bulge, and so drive secular evolution (Kormendy & Kennicutt 2004).

[1]These data are part of a larger data set, consisting of images in the $B, R, I, K_{\rm s}$ broad bands, as well as in Hα, of 57 spiral galaxies. The data are described in Knapen et al. (2003, 2004a), and the images are available through the Centre de Données Stellaires.

Nuclear rings have long been known to occur preferentially in barred galaxies, and in early-type disk galaxies. Knapen (2005) quantified this, and found that the distribution of the morphological types of the nuclear ring host galaxies peaks at type Sbc, while no rings were found in types later than Scd, and very few in earlier types. In later types, the bulge may not be massive enough to ensure the presence of ILRs, whereas in earlier types, there may not be enough gas present.

Of the 12 nuclear rings in Knapen's (2005) survey, 10 occur in galaxies classified as either SAB or SB in the RC3, but two are classified as non-barred. Upon closer inspection, though, it turns out that both these galaxies, NGC 1068 and NGC 4736, do have bars, albeit rather small, and only visible in near-IR imaging (e.g., Scoville et al. 1988; Shaw et al. 1993; Knapen 2005). The nuclear ring and the bar in NGC 4736 can be seen in Fig. 2, which shows Hα and $K_{\rm s}$-band images of the central region of the galaxy. In the context of this conference, it is interesting to point out that Piet van der Kruit has studied the inner part of this galaxy with Hα imaging and optical spectroscopy which he obtained in the spring of 1973 with the 60- and 200-inch telescopes at Palomar (van der Kruit 1974, 1976).

The literature shows that almost all nuclear rings are associated with bars in their host galaxies. There are, however, a number of galaxies which have prominent nuclear rings, but which show no sign of a bar, even in the near-IR. The small disk galaxy NGC 278, for example, has enhanced massive star formation occurring in a well-defined radial range, of around 1 kpc in radius, yet no sign of a bar from optical and near-IR, ground-based or *Hubble Space Telescope* imaging (interestingly enough, the galaxy has been classified as SAB in the RC3). Imaging in 21cm HI, however, shows that the outer regions are severely distorted both in gas morphology and kinematics. This indicates that NGC 278 may have undergone a recent minor merger event. This encounter with an even smaller galaxy, now dispersed into the outer disk of NGC 278, would have caused an asymmetry of the gravitational potential, which in turn could have caused gas inflow, the formation of resonances, and ultimately the formation of the star-forming nuclear ring (Knapen et al. 2004b).

Several other galaxies in this class, non-barred but with a prominent star-forming nuclear ring, are known, although it must be stressed that these systems form a small minority, with by far most nuclear rings hosted by barred galaxies. Examples include NGC 5953 (e.g., Knapen et al. 2006), NGC 7217 (e.g., Combes et al. 2004), or NGC 7742 (e.g., Falcon-Barroso et al. 2006). The various explanations invoked to explain the nuclear rings include the presence of interactions, oval distortions, or kinematically distinct components in the central regions. In all cases, these do indicate asymmetries in the gravitational potential.

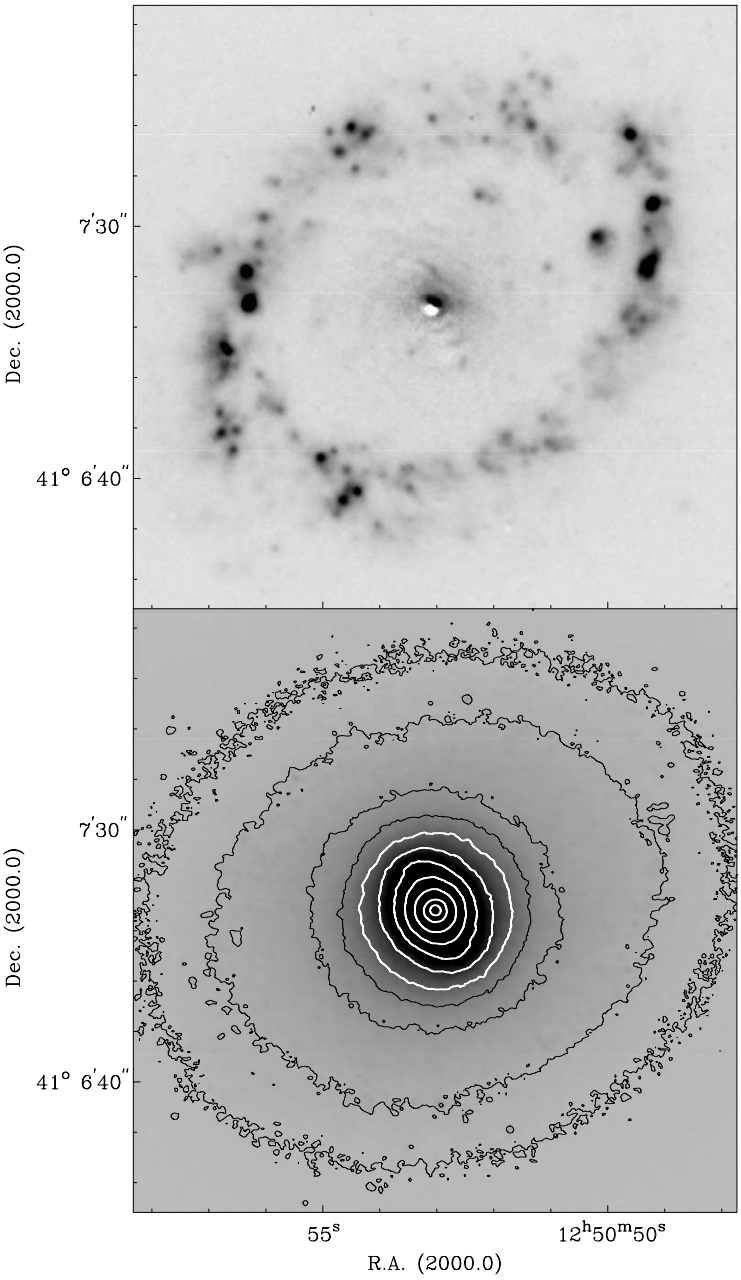

Figure 2. Images of the central region of NGC 4736, in continuum-subtracted Hα (top) and the near-IR $K_{\rm s}$-band (bottom). The area shown is 2 arcmin on the side, which corresponds to 2.4 kpc. $K_{\rm s}$-band contours are at surface brightness levels of 18 and 17, and then of 16 to 12 mag arcsec^{-2} in steps of 0.5 mag arcsec^{-2}. Based upon data from Knapen et al. (2003, 2004a).

Acknowledgements I wish to thank my collaborators on the various papers referred to above, especially Emma Allard, Shardha Jogee and Isaac Shlosman. I also acknowledge the receipt of a Leverhulme Research Fellowship.

References

Abraham, R. G., Merrifield, M. R., Ellis, R. S., Tanvir, N. R., & Brinchmann, J. 1999, MNRAS, 308, 569

Allard, E. L., Peletier, R. F., & Knapen, J. H. 2005, ApJ, 633, L25

Combes, F., et al. 2004, A&A, 414, 857

Elmegreen, B. G., Elmegreen, D. M., & Hirst, A. C. 2004, ApJ, 612, 191

Eskridge, P. B., et al. 2000, AJ, 119, 536

Falcon-Barroso, F. et al. 2006, these proceedings, p. 201

Huang, J. H., Gu, Q. S., Su, H. J., Hawarden, T. G., Liao, X. H., & Wu, G. X. 1996, A&A, 313, 13

Jogee, S., et al. 2004, ApJ, 615, L105

Jogee, S., Scoville, N., & Kenney, J. D. P. 2005, ApJ, 630, 837

Knapen, J. H. 2004, Astr. & Sp. Sc. Library, 319, 189

Knapen, J. H. 2005, A&A, 429, 141

Knapen, J. H., Beckman, J. E., Heller, C. H., Shlosman, I., & de Jong, R. S. 1995, ApJ, 454, 623

Knapen, J. H., de Jong, R. S., Stedman, S., & Bramich, D. M. 2003, MNRAS, 344, 527 (Erratum MNRAS 346, 333)

Knapen, J. H., Mazzuca, L. M., Böker, T., Shlosman, I., Colina, L., Combes, F., Axon, D. J. 2006, A&A, in press (astro-ph/0511558)

Knapen, J. H., Shlosman, I., & Peletier, R. F. 2000, ApJ, 529, 93

Knapen, J. H., Stedman, S., Bramich, D. M., Folkes, S. L., & Bradley, T. R. 2004a, A&A, 426, 1135

Knapen, J. H., Whyte, L. F., de Blok, W. J. G., & van der Hulst, J. M. 2004b, A&A, 423, 481

Kormendy, J., & Kennicutt, R. C. 2004, ARA&A, 42, 603

Roussel, H., et al. 2001, A&A, 372, 406

Sakamoto, K., Okumura, S. K., Ishizuki, S., & Scoville, N. Z. 1999, ApJ, 525, 691

Scoville, N. Z., Matthews, K., Carico, D. P., & Sanders, D. B. 1988, ApJ, 327, L61

Shaw, M. A., Combes, F., Axon, D. J., & Wright, G. S. 1993, A&A, 273, 31

Sheth, K., Regan, M. W., Scoville, N. Z., & Strubbe, L. E. 2003, ApJ, 592, L13

Shlosman, I., Frank, J., & Begelman, M. C. 1989, Nature, 338, 45

Shlosman, I. 2001, ASP Conf. Ser. 249, 55

van der Kruit, P. C. 1974, ApJ, 188, 3

van der Kruit, P. C. 1976, A&A, 52, 85

Zheng, X. Z., Hammer, F., Flores, H., Assémat, F., & Rawat, A. 2005, A&A, 435, 507

THREE-DIMENSIONAL BAR STRUCTURE AND DISC/BULGE SECULAR EVOLUTION

M. Bureau[1], G. Aronica[2,3] and E. Athanassoula[3]

[1]*Sub-Department of Astrophysics, University of Oxford, UK*

[2]*Astronomisches Institut, Ruhr-Universität Bochum, Germany*

[3]*Observatoire de Marseille, France*

Abstract *K*n-band imaging of a sample of 30 edge-on spiral galaxies with a boxy or peanut-shaped (B/PS) bulge is discussed. Galaxies with a B/PS bulge tend to have a more complex morphology than galaxies with other bulge types, unsharp-masked images revealing structures that trace the major orbit families of three-dimensional bars. Their surface brightness profiles are also more complex, typically containing 3 or more clearly separated regions, including a shallow or flat intermediate region (Freeman Type II profiles), suggestive of bar-driven transfer of angular momentum and radial redistribution of material. The data also suggest abrupt variations of the discs' scaleheights, as expected from the vertical resonances and instabilities present in barred discs but contrary to conventional wisdom. Counter to the standard 'bulge + disc' model, we thus propose that galaxies with a B/PS bulge are composed of a thin concentrated disc (a disc-like bulge) contained within a partially thick bar (the B/PS bulge), itself contained within a thin outer disc. The inner disc most likely formed through bar-driven processes while the thick bar arises from buckling instabilities. Both are strongly coupled dynamically and are formed mostly of the same (disc) material.

Keywords: galaxies: structure - galaxies: bulges - galaxies: kinematics and dynamics - galaxies: evolution

1. Introduction

Bulges are traditionally viewed as low-luminosity elliptical galaxies, suggesting a rapid formation dominated either by mergers/accretion (e.g. Searle & Zinn 1978) or possibly by dissipative gravitational collapse (e.g. Eggen et al. 1962). Those ideas have come under increasing criticism, however, and competing models where bulges grow secularly (i.e. over a long timescale and in relative isolation) are now widely discussed, many of them bar-driven (e.g. Pfenniger & Norman 1990; Friedli & Benz 1995).

R. S. de Jong, Island Universes, 181–186.
© 2007 *Springer.*

We focus here on the identification of most boxy and peanut-shaped (B/PS) bulges in edge-on spiral galaxies with part of the bars of barred spirals. N-body simulations clearly show that, whenever a disc forms a bar, a B/PS bar/bulge develops soon after (e.g. Combes & Sanders 1981; Combes et al. 1990). True peanuts are seen with the bar nearly side-on while boxier/rounder shapes are seen when the bar is closer to end-on. This view is supported by the incidence of B/PS bulges in edge-on spirals (e.g. Lütticke et al. 2000a) and by the ionized-gas and stellar kinematics of discs harbouring a B/PS bulge (e.g. Kuijken & Merrifield 1995; Bureau & Freeman 1999; Chung & Bureau 2004).

Following recent work by Lütticke et al. (2000b), we present here additional evidence for the above scenario based on *K*n-band imaging of a sample of well-studied nearby edge-on spiral galaxies with a B/PS bulge. The observations and results are described more deeply in Bureau et al. (2006) and Athanassoula et al. (2006).

2. Images

The 30 edge-on spiral galaxies of Bureau & Freeman (1999) and Chung & Bureau (2004), 24 of which have a B/PS bulge (the rest constituting a control sample), were observed at *K*n-band using CASPIR on the 2.3m telescope at Siding Spring Observatory. Both a standard image and numerous unsharp-masked images (enhancing local extrema) were produced for every galaxy. Examples are shown in Figure 1 for a B/PS bulge and a nearly bulgeless galaxy. Compared to other bands, *K*n is least hampered by dust and best traces the dominant Population II stars, sharpening the B/PS and associated features.

The unsharp-masked images highlight pervasive complex morphological structures, such as centered X features, off-centered X features, secondary maxima along the major-axis, elongated minor-axis extrema, spiral arms, etc (see Fig. 1). Most importantly, except for the minor-axis extrema, those structures are much more prevalent in galaxies with a B/PS bulge. For examples, 88% of galaxies with a B/PS bulge have either a centered or off-center X feature, while only 33% of the control galaxies do, with identical fractions for secondary major-axis maxima. The contrast between the main and control samples would in fact be even greater if the latter was not contaminated by weak B/PS bulges. Although the accretion of external material can give rise to centered X-shaped features (e.g. Hernquist & Quinn 1988), it is unlikely that long-lasting off-centered X could be produced, and those are the majority of the features observed in our sample. The orbital structure of 3D bars offers a more attractive, simple and unifying and explanation.

The most important orbit families in 3D bar models are those of the x_1 tree, elongated parallel to the bar and located within corotation. This includes the x_1 family itself (restricted to the equatorial plane) and other families

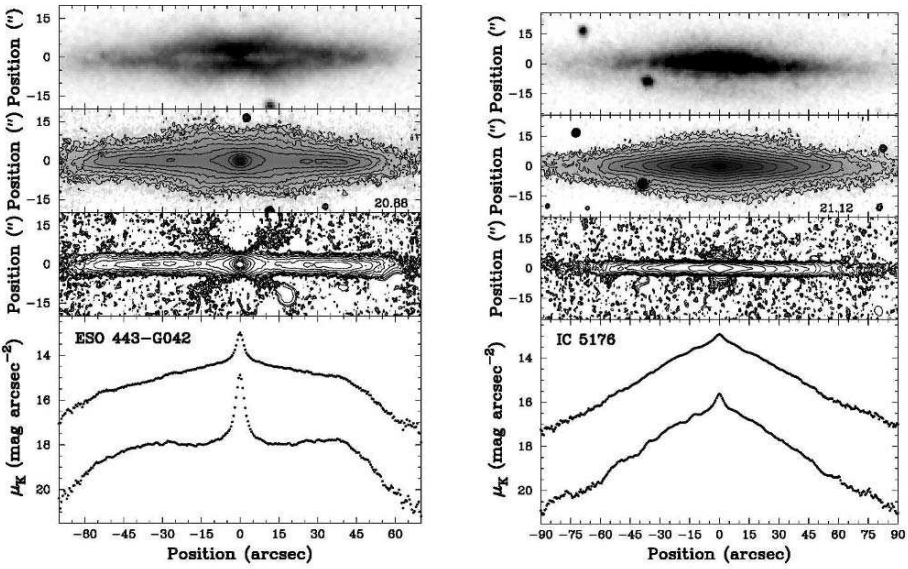

Figure 1. Images and surface brightness profiles of the galaxies ESO443-G042 (left), with a B/PS bulge, and IC5176 (right), with a nearly pure disc. From top to bottom, each panel shows first a DSS image of the galaxy, second our *K*n-band image, third an unsharp-masked *K*n-band image, and last the major-axis (fainter) and vertically-summed (brighter) surface brightness profiles, all spatially registered.

bifurcating from it at vertical resonances. The morphological features observed can be reproduced by superposing orbits of the appropriate shapes, as done by Patsis et al. (2002). This is particularly true of the (off-)centered X features which, depending on the model (mass distribution and pattern speed) and viewing angle, can *both* arise from orbit families extending vertically out of the equatorial plane. The same orbits can give rise to a number of maxima along the major-axis, similar to the secondary maxima observed. Those generally occur at larger radii than the X features and near (but within) the ends of the bar. An analogous explanation is that the secondary maxima are the edge-on projections of the inner rings present in a large fraction of barred spiral galaxies (e.g. Buta 1995) and predicted to form under the influence of bars in gas-rich and gas-poor discs (e.g. Schwartz 1981; Athanassoula & Misiriotis 2002). Unsharp-masking of barred N-body simulations also provides a perfect match to the variety of features observed, strengthening the link between them and edge-on bars (Athanassoula 2005).

3. Surface Brightness Profiles

We also extracted from our images standard major-axis surface brightness profiles and profiles summed in the vertical direction (as if the galaxies were infinitely thin). From axisymmetric face-on galaxies, we would generally expect the profiles to show only two distinct regions: a first steep region at small radii, associated with the bulge, and a second exponential region at larger radii, associated with the disc. Such profiles are however rare in our data, especially along the major-axis.

In particular, the profiles of galaxies with a B/PS bulge are again more complex than those of the control sample, in that they typically contain more distinct regions separated by clear radial breaks. For example, 96% of the galaxies with a B/PS bulge have a major-axis profile with an additional region at intermediate radii, where the profile is very shallow, even flat or slightly rising (Freeman Type II profile; see Fig. 1). The fraction for the control sample is only 50%, and the contrast between the two samples would again be sharper if they had been better selected.

Those shallow intermediate regions are particularly important as they suggest a third photometric/morphological component at moderate radii, inconsistent with a classic axisymmetric bulge + disc model. Both the central peak and the flat intermediate region are however consistent with a *single* bar viewed edge-on, with no need for a classic bulge. Indeed, Bureau & Athanassoula (2005) followed the evolution of the major-axis profile in barred N-body simulations viewed edge-on, and they convincingly showed that bar formation and evolution is associated with the buildup and continued growth of a dense central region, which would normally be identified with a bulge, and with the formation and gradual flattening of an intermediate region, in addition to the outer exponential disc. The intermediate region extends to the end of the bar, well beyond the central peak and the thickest part of the bar, as observed.

As expected from the elongated boxy/peanut shape of the bar in simulations, the observed ratio of the length of the thickest part of the bulge (or the central peak) to that of the flat intermediate region is also generally larger in peanut-shaped bulges than in boxy ones. There is however much variety, and likely many causes for it. Even so, the scatter in the ratio may well be dominated by the range of bar strengths in the sample, rather than by the range of viewing angles, as also suggested by the data of Lütticke et al. (2000b). The small ratios observed in strong peanut-shaped bulges (see Fig. 1) can then be explained only if the central peak and the thick part of the bulge are shorter in stronger bars. This is natural in barred models if the central peak is a disc-like bulge limited by the outer inner Lindblad resonance (e.g. Athanassoula 1992).

4. Bar-Driven Evolution

Athanassoula (2003) showed that much of the bar-driven evolution in discs is due to a transfer of angular momentum from the inner (barred) disc to the outer disc and halo, leading to a *radial* redistribution of matter. The majority of vertically-summed surface brightness profiles, best suited to isolate those effects, indeed show 3 or more clearly separated regions, while only one of the control galaxy does. Collapse or accretion/merger scenarios can not straightforwardly create those radial breaks or explain their spatial correlation with the ionized-gas and stellar kinematics. But if bar-driven scenarios are right, the break at the end of the intermediate region should mark the bar's end. Comparison shows that it indeed occurs where the rotation curve flattens, normally associated with the end of the bar. The break also coincides with the inner ring, when visible. As inner rings occur near the inner 4:1 and corotation resonances (e.g. Schwartz 1981), our galaxies are consistent with harbouring fast bars, as do most galaxies (e.g. Gerssen et al. 2003).

To probe the *vertical* redistribution of material predicted by bar buckling scenarios, we must compare the major-axis and vertically-summed profiles. If the stellar scaleheight was constant with radius, the two profiles would have the same functional form but different zero-points (i.e. be offset but parallel). This is clearly not the case for most galaxies, however, and the profiles of most galaxies with a B/PS bulge differ significantly (e.g. Fig. 1). Although we have amalgamated the bulge and disc by considering a single scaleheight, the functional difference between the two profiles is greatest in the flat intermediate regions, which are clearly disc material dominated. Our profiles thus clearly show that the radial scaleheight variations are real and that they occur in the discs, in direct contradiction to the common wisdom that disc scaleheights are constant (e.g. van der Kruit & Searle 1981). Athanassoula et al. (2005) show that the variations are as expected from barred N-body models.

Galaxy bulges are usually defined as either 1) the steep central component of the surface brightness profile or 2) the thick galactic component. Those definitions are normally used interchangeably, but many results show this to be grossly oversimplified (e.g. Kormendy & Kennicutt 2004). Our data clearly show that the central peak is often contained *within* the thick central component, while the shallow intermediate region always extends *beyond* the thick component (e.g. Fig. 1). Those facts are unaccounted for in classic bulge formation scenarios, but they are a natural consequence of the bar viewing angle and the fact that only part of the bar is actually thick in bar-buckling models (see Athanassoula 2005 for more on this last point).

Comparison of the major-axis and vertically-summed profiles also reveals that the central peak is more pronounced along the major-axis, so that most of the high z material belongs to the shallow intermediate region rather than the

central peak. The latter thus seems to be a thin concentrated disc, while the former appears to be thick. This is again counter to the classic bulge + disc model, but fits with the nomenclature proposed by Athanassoula (2005). The bar leads to the formation of a concentrated disc (a disc-like bulge), presumably through (bar-driven) gaseous inflow and star formation, but this disc is thin, largely decoupled from the bar, and addresses only the first bulge definition. The bar itself is thick over most but not all its length (a B/PS bulge), with a shallow profile, and addresses the second bulge definition. Like the classic models, our model comprises a number of distinct building blocks, but those are very different and tightly intertwined dynamically, emerging from the rapid radial variation of the scaleheight of the disc material, due to the weak but relentless action of bar-related resonances.

References

Athanassoula E., 1992, MNRAS, 259, 345
Athanassoula E., 2003, MNRAS, 341, 1179
Athanassoula E., 2005, MNRAS, 358, 1477
Athanassoula E., Aronica G., Bureau M., 2006, MNRAS, submitted
Athanassoula E., Misiriotis A., 2002, MNRAS, 330, 35
Bureau M., et al., 2006, MNRAS, submitted
Bureau M., Athanassoula E., 2005, ApJ, 626, 159
Bureau M., Freeman K. C., 1999, AJ, 118, 2158
Buta R., 1995, ApJS, 96, 39
Chung A., Bureau M., 2004, AJ, 127, 3192
Combes F., Debbasch F., Friedli D., Pfenniger D., 1990, A&A, 233, 82
Combes F., Sanders R. H., 1981, A&A, 96, 164
Eggen O., Lynden-Bell D., Sandage A., 1962, ApJ, 136, 748
Friedli D., Benz W., 1995, A&A, 301, 649
Gerssen J., Kuijken K., Merrifield M. R., 2003, MNRAS, 345, 261
Hernquist L., Quinn P. J., 1988, ApJ, 331, 682
Kormendy J., Kennicutt R. C. Jr., 2004, ARA&A, 42, 603
Kuijken K., Merrifield M. R., 1995, ApJ, 443, L13
Lütticke R., Dettmar R.-J., Pohlen M., 2000a, A&AS, 145, 405
Lütticke R., Dettmar R.-J., Pohlen M., 2000b, A&A, 362, 435
Patsis P. A., Skokos Ch., Athanassoula E., 2002, MNRAS, 337, 578
Pfenniger D., Norman C., 1990, ApJ, 363, 391
Schwarz M. P., 1981, ApJ, 247, 77
Searle L., Zinn R., 1978, ApJ, 225, 357
van der Kruit P. C., Searle L., 1981, A&A, 95, 105

ANOMALOUSLY WEAK DYNAMICAL FRICTION IN HALOS

J. A. Sellwood[1*] and Victor P. Debattista[2**]

[1]*Department of Physics & Astronomy, Rutgers University, Piscataway, USA*

[2]*Astronomy Department, University of Washington, Seattle, USA*

*sellwood@physics.rutgers.edu, ** debattis@astro.washington.edu

Abstract A bar rotating in a pressure-supported halo generally loses angular momentum and slows down due to dynamical friction. Valenzuela & Klypin report a counter-example of a bar that rotates in a dense halo with little friction for several Gyr, and argue that their result invalidates the claim by Debattista & Sellwood that fast bars in real galaxies require a low halo density. We show that it is possible for friction to cease for a while should the pattern speed of the bar fluctuate upward. The reduced friction is due to an anomalous gradient in the phase-space density of particles at the principal resonance created by the earlier evolution. The result obtained by Valenzuela & Klypin is probably an artifact of their adaptive mesh refinement method, but anyway could not persist in a real galaxy. The conclusion by Debattista & Sellwood still stands.

Keywords: galaxies: kinematics and dynamics - galaxies: halos - dark matter

1. Introduction

It is now well established that a bar rotating in a halo loses angular momentum through dynamical friction. This topic has received a lot of attention recently for two important reasons: (1) it offers a constraint on the density of the DM halo (Debattista & Sellwood 1998, 2000), and (2) it may flatten the density cusp (Weinberg & Katz 2002).

Both these claims have been challenged. Realistic bars in cuspy halos produce a mild density decrease at most (Holley-Bockelmann et al. 2003) or even a slight increase (Sellwood 2003), but we leave this issue aside here and concentrate instead on the density constraint. Holley-Bockelmann & Weinberg (2005) announce a preliminary report of simulations with weak friction in halos having uniform density cores, but we focus here on the older counter-example claimed by Valenzuela & Klypin (2003; hereafter VK03) of a bar that experiences little friction in a cusped dense halo.

R. S. de Jong, Island Universes, 187–194.
© 2007 *Springer.*

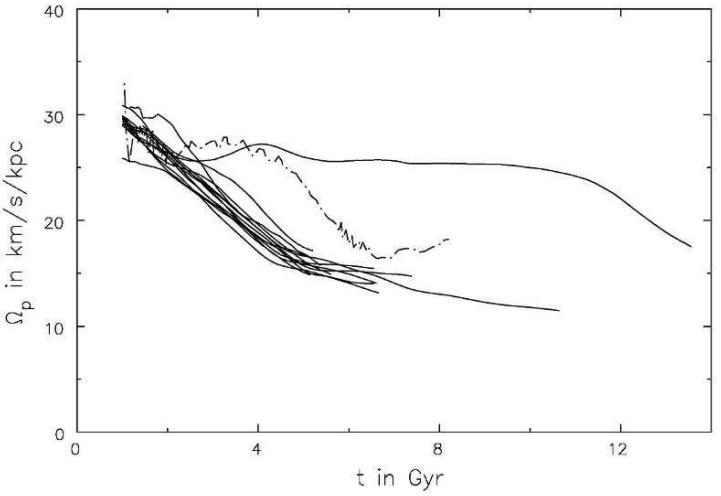

Figure 1. The time evolution of the bar pattern speed in a number of resimulations of model A_1 of VK03. The evolution reported by VK03 is reproduced as the dot-dashed line; all other lines are from simulations from the same initial particle load, but run with our code using many different sets of numerical parameters.

VK03 kindly made available the initial positions and velocities of all the particles of their model A_1, in which the bar did not slow for 2-3 Gyrs after it had formed and settled. We have used our code (Sellwood 2003) to rerun this simulation many times, and the pattern speed evolution in many of these runs is shown in Figure 1. It is striking that in most cases, the bar slowed earlier than VK03 found, but in one anomalous case, the bar stayed fast for about 10 Gyr! The anomalous result is not a consequence of some inadequate numerical parameter, since many of the other cases are from models with parameters that bracket those of the anomalous case – i.e. longer and shorter time steps, coarser and finer grids, etc.

Note that apart from the crucial delay in the onset of friction in the case by VK03 and the one anomalous case we find, the evolution is generally very similar. In particular, whenever the bar slows, it slows at a similar rate. The following sections account for the discrepancies between the results shown in Fig. 1.

2. Frictional Torque

In a classic paper, Tremaine & Weinberg (1984) laid out the mathematical apparatus for friction in a spherical system. Following the precepts of Lynden-Bell & Kalnajs (1972), they derived a formula for the torque experienced by a rotating perturbation potential, Φ_p. They work in action-angle variables (see

Binney & Tremaine 1987, §3.5). In a spherical potential, there are two non-zero actions: the total angular momentum per unit mass $L \equiv J_\phi$ and the radial action J_r, each associated with two separate frequencies, Ω and κ, which are generalizations to orbits of arbitrary eccentricity of the usual frequencies of Lindblad epicycles familiar from disk dynamics. In the limit that a constant amplitude perturbation rotates steadily at Ω_p, they showed that the net LBK torque is

$$\tau_{\rm LBK} \propto \sum_{m,k,n} \left(m\frac{\partial f}{\partial L} + k\frac{\partial f}{\partial J_r} \right) |\Phi_{mnk}|^2 \delta(n\Omega + k\kappa - m\Omega_p), \qquad (1)$$

where f is the usual distribution function and Φ_{mnk} is a Fourier coefficient of the perturbing potential. The Dirac delta function implies that the net torque is the sum of the separate contributions from resonances, where $n\Omega + k\kappa = m\Omega_p$. Because the bar pattern speed decreases, as a result of the frictional torque, this expression needs to be generalized to a time-dependent forcing (see Weinberg 2004), but the revised expression for the torque still contains the same derivatives of the distribution function.

Lynden-Bell (1979) offered a clear insight into how an orbit is affected when close to a resonance. The unperturbed orbit, which is a rosette in an inertial reference frame, closes in any frame that rotates at the rate

$$\Omega' = \Omega + k\kappa/m, \qquad (2)$$

for any pair k, m. [See e.g. Kalnajs (1977) for illustrations of several of the most important shapes.] When the pattern speed of the bar is close to Ω' for some pair k, m, the orbit can be regarded as a closed figure that precesses at the slow rate

$$\Omega_s \equiv (\Omega' - \Omega_p) \ll \Omega_p. \qquad (3)$$

Under these circumstances, the "fast action" is adiabatically invariant, while the "slow action" can suffer a large change. Things are particularly straightforward at corotation, where the fast action is the radial action, while the slow action that can suffer a large change is simply the angular momentum.

3. Restricted Simulations

Fully self-consistent simulations are complicated by evolution of the total potential, changes to the bar mass profile, etc. It is therefore easier first to try to understand "restricted" simulations in which a rigid bar rotates in halo of non-interacting test particles (Lin & Tremaine 1983; Sellwood 2004). The particles move in a rigid halo potential that is perturbed by that of the rotating bar, and the bar is accelerated in response to the vector-sum of the non-axisymmetric forces felt by the particles. Figure 2 shows an example of the pattern speed

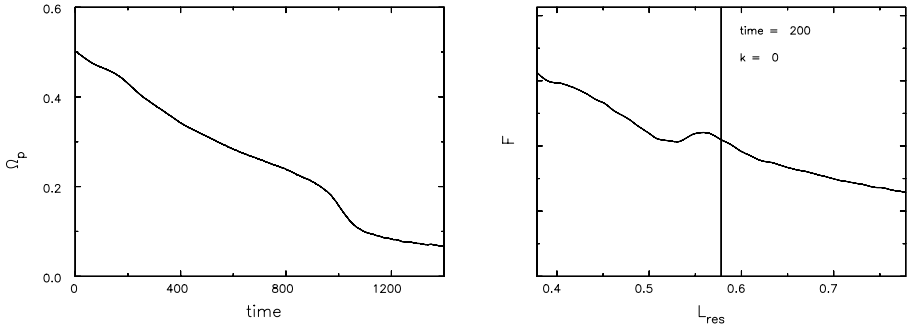

Figure 2. Left: The time evolution of the bar pattern speed in the restricted simulation discussed in §3. This simulation employs 10M particles. Right: The mean density of particles as a function of $L_{\rm res}$ at $t = 200$ in the same simulation.

evolution of a homogeneous ellipsoid with principal axes $1 : 0.5 : 0.1$ in a Hernquist (1990) halo. The bar mass is 1% of the halo mass, M_h, has a semi-major axis equal to the halo break radius r_h, and rotates initially so that it just fills its corotation circle. We use units such that $G = M_h = r_h = 1$.

At intervals during the simulation, we compute $\Omega' = \Omega + k\kappa/m$ for every particle, and calculate F, the average density of particles as a function Ω'. It is somewhat easier to understand a plot of F as a function of the angular momentum, $L_{\rm res}$, of a circular orbit that has the given $\Omega'(k, m)$.

The right-hand panel of Figure 2 shows the form of F near to corotation ($m = 2,\ k = 0$) at $t = 200$, which is typical. Near to the resonance (marked by the vertical line), particles cross corotation in both directions on horse-shoe orbits (Binney & Tremaine 1987, §7.5). The generally negative slope of F implies an excess of lower L particles that gain angular momentum and move out across the resonance, and this imbalance is responsible for friction. If the pattern speed were to stay constant, the imbalance would tend to flatten the slope of F, and the distribution of particles about the resonance would approach kinetic equilibrium in which there would be more nearly equal numbers of particles crossing in both directions. But as Ω_p declines, the resonance keeps moving to larger $L_{\rm res}$, and equilibrium is never established; instead, the density of particles about the dominant resonance(s) responsible for friction takes on the characteristic humped form shown in Fig. 2.

Friction arises principally at corotation over most of the evolution. The outer Lindblad resonance contributes in the early stages, but dominates only if the bar is unreasonably fast. The inner Lindblad resonance becomes important only when the bar is already quite slow; e.g. it is responsible for the more rapid braking around $t = 1000$ in Fig. 2.

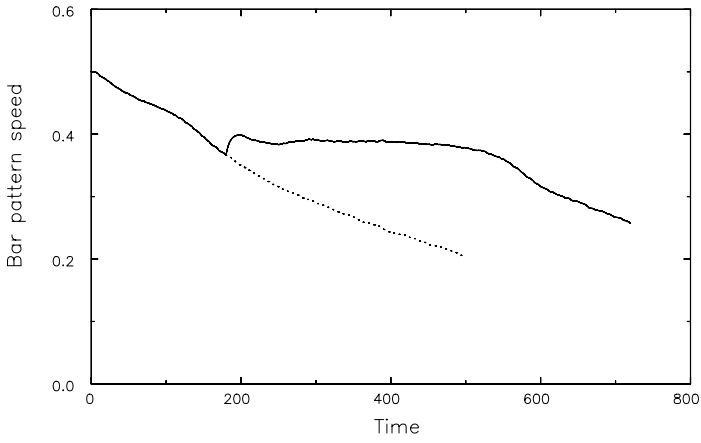

Figure 3. The solid curve shows evolution of the bar pattern speed in a restricted experiment in which the bar was reaccelerated (by external interference) between times 180 and 200, but was otherwise allowed to evolve freely. (This experiment used 1M particles.) The dotted curve shows what happens without interference.

4. Anomalous Situation

Now suppose that Ω_p rises for some reason, after having declined for some time, as illustrated in Figure 3. The shoulder in F created by the previous friction survives, but the resonance at the now higher Ω_p lies on the other side of the shoulder, as shown in Figure 4. Thus the local gradient in F has changed sign, leading to an adverse gradient for friction, and the torque from the dominant resonance disappears. Under these circumstances, a balance between gainers and losers is soon established, and the bar can rotate in a dense halo with little friction, which we describe as a "metastable state".

In fact, Ω_p declines slowly because of weak friction at other resonances, and normal friction resumes when the slope of F at the main resonance changes, as shown in the last frame of Fig. 4.

5. Self-consistent Simulations

If we now re-examine Fig. 1, we see that the period of weak friction is preceded by a small rise in the bar pattern speed in both the simulation of VK03 (dot-dashed line) and in the anomalous case we found. It is likely therefore that friction stopped for a while in both cases because the local density gradient across the principal resonance became flat, as just described.

Analysis of our simulation that displayed this behavior suggests that Ω_p rose because of an interaction between the bar and a spiral in the disk, which caused the bar to gain angular momentum. Such an event is rare; spirals generally

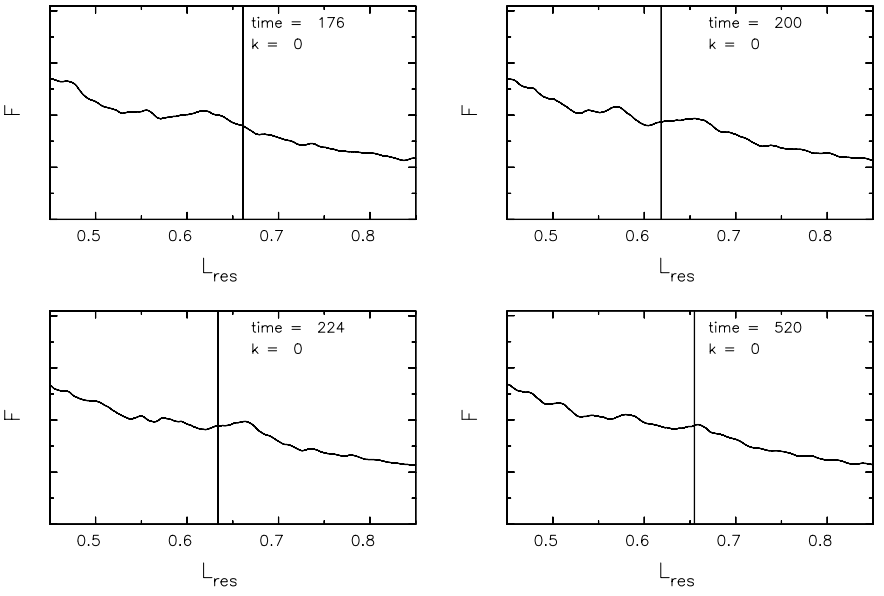

Figure 4. The mean density of particles as a function of $L_{\rm res}$ at several different times in the simulation shown in Fig. 3.

remove angular momentum from the bar at most relative phases. It is possible that VK03 were unlucky to have such an event in their case, but they report similar behavior in their model B making a chance event unlikely.

One significant difference between our code and the code used by VK03 (Kravtsov, Klypin & Khokhlov 1997) is that their resolution is adaptive, which causes gravity to strengthen at short range when the grid is refined. The increase in the local density as the bar amplitude rises causes the code to refine the grid, strengthening gravity and thereby causing the bar to contract slightly and to spin-up. We have found that a reduction of softening length in our code at this epoch also leads to a metastable state. It is likely, therefore, that their anomalous result is an artifact of their adaptive code.

6. The Metastable State is Fragile

Whatever the origin of the bar speed-up in simulations, it remains possible that the metastable state could occur in real galaxies. If friction in a dense halo can be avoided for this reason, then the observed pattern speeds will provide no constraint on the halo density.

However, further experiments in which we perturbed our model in the metastable state very slightly, revealed that the state is highly fragile. For example, a satellite of merely 1% of the galaxy mass flying by at 30 kpc is sufficient to jolt

the system out of the metastable state. We therefore conclude that anomalously weak friction is unlikely to persist for long in nature.

7. Conclusions

Tremaine & Weinberg (1984) showed that angular momentum is transferred from a rotating bar to the halo through resonant interactions. We find that friction is dominated by a single resonance at most times, and that corotation is most important for a bar with realistic pattern speed – i.e. when the bar extends almost to corotation.

Friction arises because the phase space density is a decreasing function of angular momentum in normal circumstances, causing an excess of particles that gain angular momentum over those that lose. While this process would tend to flatten the density gradient if the pattern speed remained steady, the decreasing angular speed of the bar prevents this steady state from being reached. Instead we find that the density of particles in phase space develops a shoulder, with the resonance holding station on the high-angular momentum side of the shoulder as the feature moves to larger $L_{\rm res}$.

However, if the bar is spun up slightly for some reason after a period of normal friction, the rise in the pattern speed may move the resonance to the other side of the pre-constructed shoulder. The change in the local gradient of particle density at the dominant resonance causes friction to become very weak for a while, allowing the bar to rotate almost steadily. Mild friction persists because of contributions from other, sub-dominant resonances, and normal friction resumes once the pattern speed has declined sufficiently for the gradient at the main resonance to become favorable for friction once more.

A state in which strong friction is suspended for this reason is "metastable", both because it relies on a local minimum in the phase space density, and because the state is fragile. A very mild jolt to the system is sufficient to cause normal friction to resume.

The absence of friction in the simulation $\rm A_1$ reported by Valenzuela & Klypin (2003) is probably an artifact of their code. Their adaptive grid causes gravity to strengthen as the bar density builds up, making the pattern speed of the bar rise for a purely numerical reason. Thus their claimed counter-example to the argument of Debattista & Sellwood (1998, 2000) is a numerical artifact of their method. *Pace* Holley-Bockelmann & Weinberg (2005), our constraint on halo density still stands: A *strong* bar in a *dense* halo will quickly become unacceptably slow through dynamical friction.

Acknowledgements We thank Anatoly Klypin for providing the initial positions and velocities of the particles in his model, and for many discussions. This work was supported by NASA (NAG 5-10110) and NSF (AST-0098282).

References

Binney, J. & Tremaine, S. 1987, *Galactic Dynamics* (Princeton: Princeton University Press)
Debattista, V. P. & Sellwood, J. A. 1998, Ap. J. Lett., 493, L5
Debattista, V. P. & Sellwood, J. A. 2000, Ap. J., 543, 704
Hernquist, L. 1990, Ap. J., 356, 359
Holley-Bockelmann, K., Weinberg, M. D. & Katz, N. 2003, astro-ph/0306374
Holley-Bockelmann, K. & Weinberg, M. D. 2005, DDA abstract 36.0512
Kalnajs, A. J. 1977, Ap. J., 212, 637
Kravtsov, A. V., Klypin, A. & Khokhlov, A. M. 1997, Ap. J. Suppl., 111, 73
Lin, D. N. C. & Tremaine, S. 1983, Ap. J., 264, 364
Lynden-Bell, D. 1979, MNRAS, 187, 101
Lynden-Bell, D. & Kalnajs, A. J. 1972, MNRAS, 157, 1
Sellwood, J. A. 2003, Ap. J., 587, 638
Sellwood, J. A. 2004, astro-ph/0407533
Tremaine, S. & Weinberg, M. D. 1984, MNRAS, 209, 729
Valenzuela, O. & Klypin, A. 2003, MNRAS, 345, 406
Weinberg, M. D. 2004, astro-ph/0404169
Weinberg, M. D. & Katz, N. 2002, Ap. J., 580, 627

Lia Athanassoula and Thijs van der Hulst.

HALO PROPERTIES AND SECULAR EVOLUTION IN BARRED GALAXIES

E. Athanassoula

Observatoire de Marseille Provence, France
lia@oamp.fr

Abstract The halo plays a crucial role in the evolution of barred galaxies. Its near-resonant material absorbs angular momentum emitted from some of the disc particles and helps the bar become stronger. As a result, a bar (oval) forms in the inner parts of the halo of strongly barred disc galaxies. It is thinner in the inner parts (but still considerably fatter than the disc bar) and tends to spherical at larger radii. Its length increases with time, while always staying shorter than the disc bar. It is roughly aligned with the disc bar, which it trails only slightly, and it turns with roughly the same pattern speed. The bi-symmetric component of the halo density continues well outside the halo bar, where it clearly trails behind the disc bar. The length and strength of the disc and halo bars correlate; the former being always much stronger than the latter. If the halo is composed of weakly interacting massive particles, then the formation of the halo bar, by redistributing the matter in the halo and changing its shape, could influence the expected annihilation signal. This is indeed found to be the case if the halo has a core, but not if it has a steep cusp. The formation and evolution of the bar strongly affect the halo orbits. A fraction of them becomes near-resonant, similar to the disc near-resonant orbits at the same resonance, while another fraction becomes chaotic. Finally, a massive and responsive halo makes it harder for a central mass concentration to destroy the disc bar.

Keywords: galaxies: kinematics and dynamics - galaxies: structure - galaxies: spiral - dark matter

1. The Role of the Halo in the Evolution of Barred Galaxies

As shown by N-body simulations, barred galaxies undergo considerable secular evolution (e.g., Hernquist & Weinberg 1992; Debattista & Sellwood 2000; Athanassoula & Misiriotis 2002 [AM02]; Athanassoula 2002 [A02]; Athanassoula 2003 [A03]; O'Neil & Dubinski 2003; Valenzuela & Klypin 2003; Martinez-Valpuesta & Shlosman 2004; Athanassoula 2005a; Martinez-Valpuesta, Shlosman & Heller 2005). The halo plays a major role in this, since

R. S. de Jong, Island Universes, 195–200.
© 2007 *Springer.*

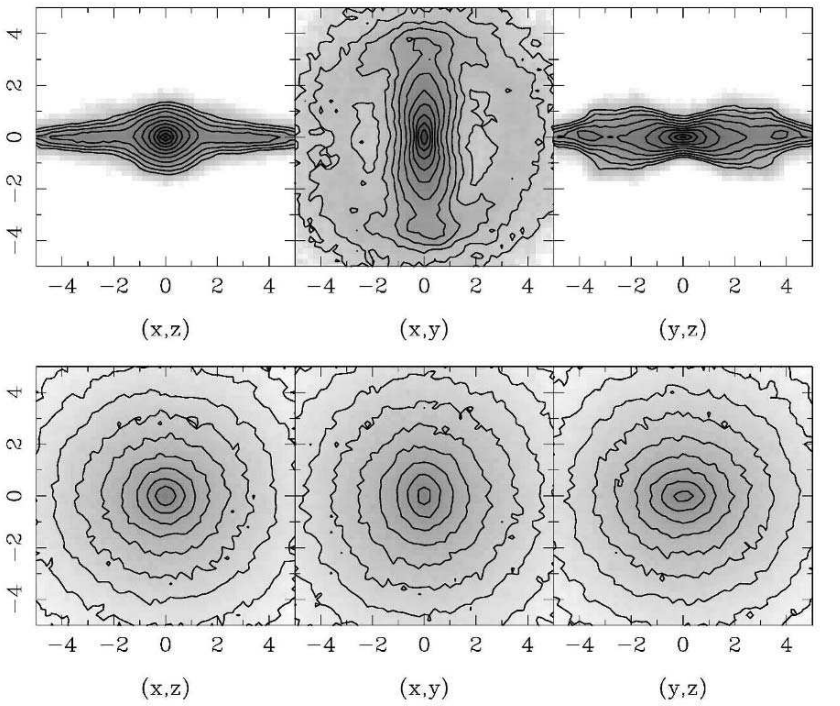

Figure 1. Three orthogonal views of the disc (upper panels) and halo component (lower panels). The central panels are face-on views, while the others are edge-on; side-on for the right panels and end-on for the left ones. Note that the halo does not stay axisymmetric, but forms an oval in its inner parts, which I call the halo bar.

it participates in the angular momentum exchange within the galaxy. In an isolated disc galaxy with little or no gas, angular momentum is emitted mainly by near-resonant material in the inner disc (bar region) and absorbed by near-resonant material in the outer disc and in the halo (A02; A03). Since the bar is a negative angular momentum feature (Kalnajs 1971; Lynden-Bell & Kalnajs 1972), by loosing angular momentum it will grow stronger (A02).

Both for the disc and for the halo, there is more angular momentum gained (or lost) at a given resonance if the density is higher there and if the near-resonant material is colder. So, for equal amounts of mass, the outer disc will absorb more angular momentum than the halo, because it is colder. There is, however, considerably less mass in the outer disc than in the halo, so the role of the halo can be very important, or even predominant (A03). Thus, bars immersed in massive responsive haloes can grow stronger than bars immersed in weaker haloes (AM02; A03) and very much stronger than bars immersed in rigid haloes (A02), since the latter can not, by their formation, absorb any angular momentum.

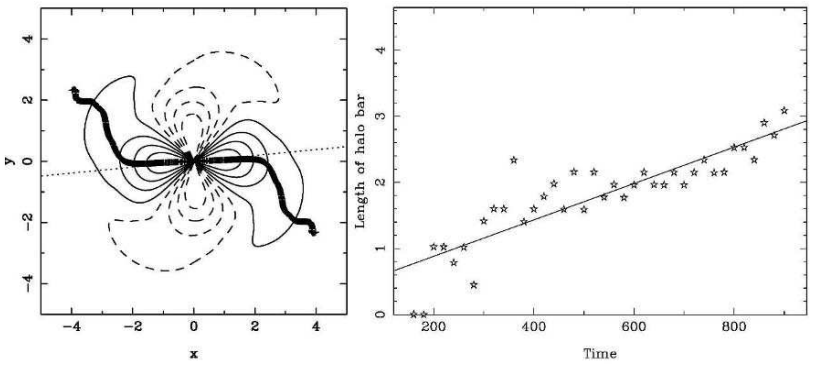

Figure 2. **Left panel** : Isocontours of the l=2 m=2 component of the halo mass distribution on the galaxy equatorial plane. Positive isocontours are given with solid lines and negative ones with dashed lines. The thin dotted line gives the position angle of the disc bar and the thick line shows the phase of the halo bar. The latter is only plotted in regions where the amplitude of the l=2 m=2 component is at least equal to 4% of its maximum amplitude. **Right panel** : Length of the halo bar as a function of time. The solid line is a least squares fit, to guide the eye.

Since the halo plays such a crucial role in the evolution, it is reasonable to expect that its properties will evolve with time, as do the bar properties. This is indeed the case. Here, I will particularly discuss the formation of an oval in the inner parts of the halo.

2. The Halo Bar

Figure 1, from a simulation similar to those described in AM02 or A03, shows three orthogonal views of the disc (upper panels) and the halo (lower panels) from a simulation at a time well after the bar has formed, i.e. while it is secularly evolving. The disc is strongly barred, and seen side-on (i.e. edge-on, with the line of sight along the bar minor axis) it shows a strong peanut. The evolution of the halo, although less spectacular, is still quite clear. The inner parts have lost their initial spherical symmetry and show a clear prolate deformation, whose principal axes are roughly aligned with those of the disc bar. Such a deformation is seen in all the simulations with a strong bar that I analysed and has also been discussed in Athanassoula (2005b [A05b]) and in Colin, Valenzuela & Klypin (2005). The axial ratio in the inner parts is roughly 0.7 and increases with radius.

Analysing the halo mass distribution in spherical harmonics, it is possible to get more information on the halo bar. The left panel of Figure 2 shows isocontours of the l=2 m=2 component, i.e. of the component that best characterises the halo bar. In the inner parts, the phase of this component seems roughly the same as the phase of the disc bar (dotted line in the figure). In fact, it trails it

very slightly, of the order of a couple of degrees so that it is not easy to discern it on the plot. I found similar phase differences at other times and in other simulations I analysed. This phase difference increases substantially at larger radii, so that the outer parts of the l=2 m=2 component look spiral-like. As can be seen in the right panel of Figure 2, the length of the halo bar increases substantially with time.

3. Halo Geometry and the WIMP Annihilation Signal

Athanassoula, Ling and Nezri (2005) studied the impact of halo shape and geometry on the expected WIMP (weakly interacting massive particle) annihilation signal from the galactic center. They find that the asphericity has a strong impact on the annihilation signal when the halo density profile has a core near the center, such as advocated by observations (Bosma 2004 and references therein), but becomes less significant for cuspy profiles, such as advocated by simulations (e.g., Navarro, Frenk & White 1997; Moore et al. 1999; Diemand et al. 2005), and negligible in the presence of a central spike.

4. Orbital Structure in Haloes

As already mentioned in section 1, the halo contains a fair fraction of near-resonant orbits. These are mainly trapped around Lagrangian periodic orbits (see Fig 12 of A05b), or around x_1-tree[1] periodic orbits (Fig 11 of A05b).

Halo particles which are near-resonant at a given time are not randomly chosen from the initial halo distribution function. Particles at near-inner Lindblad resonance had initially preferentially smaller cylindrical and spherical radii. They also had preferentially smaller values of L_z, the z component of the angular momentum. Particles at near-corotation had preferentially initially intermediate cylindrical and spherical radii (i.e. they were not located initially in the innermost or in the outermost regions). They had initially preferentially smaller values of $|u_z|$, the z velocity component, and larger values of L_z than average. To summarise, we can say that the halo particles that will become near-resonant had initially properties similar to those of the disc particles.

An important property for the evolution of the halo, and in general of the galaxy, is the fraction of chaotic orbits in its population. The most straightforward way of measuring this in simulations is to calculate the complexity of each orbit, as introduced by Kandrup, Eckstein & Bradley (1997). As shown by these authors, the complexity correlates well with the short term Lyapounov

[1]The x_1 orbits are periodic orbits elongated along the bar and closing after one rotation and two radial oscillations (Contopoulos & Grosbl 1989). The x_1-tree is the 3D extension of the x_1 family (Skokos, Patsis & Athanassoula 2002) and comprises, except for the x_1 family, other 2D and 3D families bifurcating from x_1.

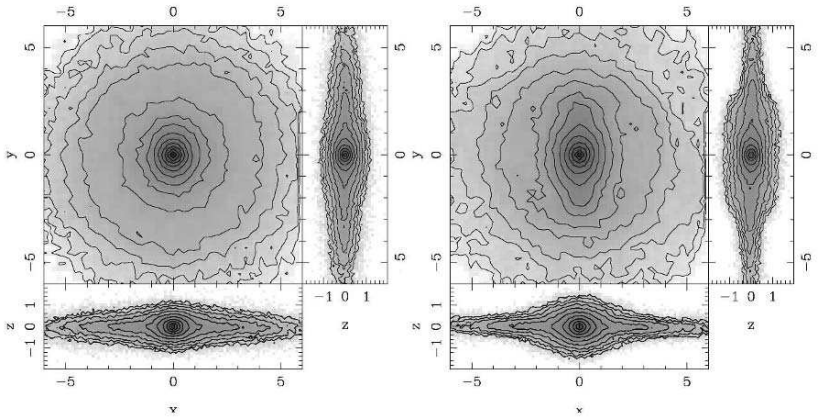

Figure 3. Density distribution in the disc of a barred galaxy after the introduction of a CMC **Left panel** : MD-type model. **Right panel** : MH-type model.

exponents, often used to measure chaos. Of course, the exact value of the fraction of chaotic orbits depends on where one sets the dividing line between a regular and a chaotic orbit. A05b calculated this fraction for different such threshold values and showed that it increases with the strength of the disc bar and that in a strongly barred galaxy as much as a quarter of the halo orbits can be chaotic.

5. Black Holes and Central Mass Concentrations in Barred Galaxies with Live Haloes

As shown both by periodic orbit calculations (Hasan & Norman 1990; Hasan, Pfenniger & Norman 1993) and by N-body simulations (Shen & Sellwood 2004 and references therein) a central mass concentration (CMC) affects the stability of x_1 orbits, making them unstable and incapable of sustaining the bar. Thus, provided the CMC is sufficiently massive and/or sufficiently centrally concentrated, it can destroy the bar, or at least considerably lower its amplitude. These simulations, however, use a rigid halo and thus are not fully-self-consistent.

Seen the important role that the response of the halo can play on the evolution of barred galaxies, Athanassoula, Lambert & Dehnen (2005) revisited this problem, now using a live halo, and I will here summarise some of their results. They find that the effect of the CMC depends drastically on the model. This is also illustrated in Figure 3, which compares the effect of a given CMC on two different barred galaxy models. The difference is quite important. In the model on the left (MD-type, according to the definition of AM02) the CMC totally destroyed the bar. But in the model on the right (MH-type) the same

CMC only decreased the bar strength, albeit substantially. In fact, the lowering of the bar strength is mainly due to a decrease of the bar length and to more axisymmetric innermost parts. The latter can be easily understood since this is the vicinity of the CMC. The CMC also causes an increase of the bar pattern speed in all cases.

The difference between these two models could be due to the role of the halo in the two cases. Indeed, in MH-type models the inner resonances in the halo are more populated, so that the halo can absorb more angular momentum, compared to MD-type haloes (A03). This extra angular momentum is taken from the bar and will, as discussed in section 1, tend to increase its strength. It will thus work against the CMC, whose effect will thus be lessened. This is indeed what the simulations of Athanassoula et al. (2005) show.

References

Athanassoula, E., 2002, ApJ, 569, L83 (A02).

Athanassoula, E., 2003, MNRAS, 341, 1179 (A03).

Athanassoula, E., 2005a, MNRAS, 358, 1477.

Athanassoula, E., 2005b, in "Nonlinear Dynamics in Astronomy and Physics (In memory of Henry E. Kandrup)", eds. S. T. Gottesman, J.-R. Buchler and M. E. Mahon, Annals of the New York Academy of Sciences, 1045, 168 (A05b).

Athanassoula, E., Lambert, J. C., Dehnen, W., 2005, MNRAS, in press and astro-ph/0507566.

Athanassoula, E., Ling, F.-S., Nezri, E., 2005, Phys. Rev. D., in press and astro-ph/0504631.

Athanassoula, E., Misiriotis, A., 2002, MNRAS, 330, 35 (AM02).

Bosma, A., 2004, in "Dark Matter in Galaxies", eds. S. D. Ryder, D. J. Pisano, M. A. Walker and K. C. Freeman, IAU symposium 220, 39.

Colin, P., Valenzuela, O., Klypin, A., 2005, astro-ph/0506627.

Contopoulos, G., Grosbl, P., 1989, AAR, 1, 261.

Debattista, V. P., Sellwood, J. A., 2000, ApJ, 543, 704.

Diemand, J., Zemp, M., Moore, B., Stadel, J., Carollo, M., 2005, astro-ph/0504215.

Hasan, H., Norman, C., 1990, ApJ, 361, 69.

Hasan, H., Pfenniger, D., Norman, C., 1993, ApJ, 409, 91.

Hernquist, L., Weinberg, M., 1992, ApJ, 400, 80.

Kalnajs, A. J., 1971, ApJ, 166, 275.

Kandrup, H. E., Eckstein, B. L., Bradley, B. O., 1997, AA, 320, 65.

Lynden-Bell, D., Kalnajs, A. J., 1972, MNRAS, 157, 1.

Navarro, J. F., Frenk, C. S., White, S. D. M., 1997, ApJ, 490, 493.

Martinez-Valpuesta, I., Shlosman, I., 2004, ApJ, 613, L29.

Martinez-Valpuesta, I., Shlosman, I., Heller, C., 2005, ApJ, in press and astro-ph/0507219.

Moore, B., Quinn, T., Governato, F., Stadel, J., Lake, G., 1999, MNRAS, 310, 1147.

O'Neill, J. K., Dubinski, J., 2003, MNRAS, 346, 251.

Shen, J., Sellwood, J. A., 2004, ApJ, 604, 614.

Skokos, Ch., Patsis, P. A., Athanassoula, E., 2002, MNRAS, 333, 847.

Valenzuela, O., Klypin, A., 2003, MNRAS, 345, 406.

A SAURON STUDY OF STARS AND GAS IN SA BULGES

J. Falcon-Barroso[1*], R. Bacon[2], M. Bureau[3], M. Cappellari[1], R. L. Davies[3], P. T. de Zeeuw[1], E. Emsellem[2], K. Fathi[4], D. Krajnovic[3], H. Kuntschner[5], R. M. McDermid[1], R. F. Peletier[6] and M. Sarzi[3]

[1] *Sterrewacht Leiden, The Netherlands*

[2] *CRAL - Observatoire, France*

[3] *University of Oxford, United Kingdom*

[4] *Rochester Institute of Technology, USA*

[5] *European Southern Observatory, Garching, Germany*

[6] *Kapteyn Astronomical Institute, Groningen, The Netherlands*

* jfalcon@strw.leidenuniv.nl

Abstract We present results from our ongoing effort to understand the morphological and kinematical properties of early-type galaxies using the integral-field spectrograph SAURON. We discuss the relation between the stellar and gas morphology and kinematics in our sub-sample of 24 representative Sa spiral bulges. We focus on the frequency of kinematically decoupled components and on the presence of star formation in circumnuclear rings.

Keywords: galaxies: structure - galaxies: kinematics and dynamics - stars: formation

1. Sa Bulges in the SAURON Survey

The starting point of our study is the SAURON survey of nearby, early-type galaxies (de Zeeuw et al. 2002). The full sample consists of 72 galaxies divided in three morphological groups: 24 ellipticals, 24 lenticulars, and 24 Sa bulges. Within each group, half of the galaxies are drawn from the field environment, and the remaining half are representative of the cluster population.

The main science driver for the survey is the study of the intrinsic shapes, velocity and metallicity distribution, and the relation between the stellar and gas kinematics to the underlying stellar populations. Most of the results of the survey up to now have focused on the 48 elliptical and lenticular galaxies (de Zeeuw et al. 2002, Emsellem et al. 2004, Cappellari et al. 2006, Sarzi et al. 2006). Here, we concentrate on the 24 Sa spiral bulges.

R. S. de Jong, Island Universes, 201–206.
© 2007 *Springer.*

A key question we want to address is whether secular evolution plays an important role in the formation of bulges (i.e., disk instabilities, Pfenniger & Norman 1990, Pfenniger & Friedli 1991), or whether they are scaled-down versions of ellipticals, as the main scaling relations suggest (e.g., Fundamental Plane, Jorgensen et al. 1996, Falcon-Barroso et al. 2002). A comprehensive description of the stellar and gas kinematics of the complete sample of 24 Sa spiral bulges is presented in Falcon-Barroso et al. (2005). We highlight some of the results here. Fathi et al. (2005) present an in depth study of an individual case (NGC 5448). Ganda et al. (2005) discuss similar SAURON observations of 18 later-type spiral galaxies.

2. Kinematically Decoupled Components

The stellar kinematic maps of our galaxies display a variety of substructures in the central regions, such as kinematically decoupled components. For example, Figure 1 (top panel) shows the stellar kinematics of NGC 5689. In that galaxy the component is clearly visible in the velocity map as a pinching of the isovelocities in the inner regions, which is also accompanied by a decrease of the velocity dispersion and an anti-correlated h_3 parameter at the same locations. In general this type of decoupled components appear to be aligned with the major axis of the galaxy and tend to be associated with dust disks or rings seen in unsharp-masked images. However, there are a few cases in our sample where the rotation axis of the decoupled component is misaligned with respect to the main rotation axis of the galaxy (e.g., NGC 4698, see Figure 1 bottom panel). In this case the decoupled component can be identified as a twist of the zero velocity curve in the inner regions. We find that 13 out of 24 galaxies (52%) display clear signatures of such structures. Despite the high number of kinematically decoupled components observed, the true fraction can be even higher as their detection can be hampered by inclination (i.e., as it is more difficult to detect them at low galaxy inclinations), but also by a limited spatial sampling.

The nature of these kinematically decoupled components is still uncertain, and there are different formation and evolution processes that can produce such a component in the inner regions of the galaxies. One of the most widely supported scenarios is that these objects formed by gas inflow towards the central regions of the galaxy which consequently induced star formation (Wozniak et al. 2003). The role of bars and dissipative processes, however, is not yet well understood in this context (Bureau & Athanassoula 2005, Heller & Shlosman 1994, Friedli & Benz 1995), as all these models are able to reproduce the observed velocities, inwards decrease of velocity dispersion and the h_3 anti-correlation. Under this scenario the kinematically decoupled component is formed from existing material in the galaxy.

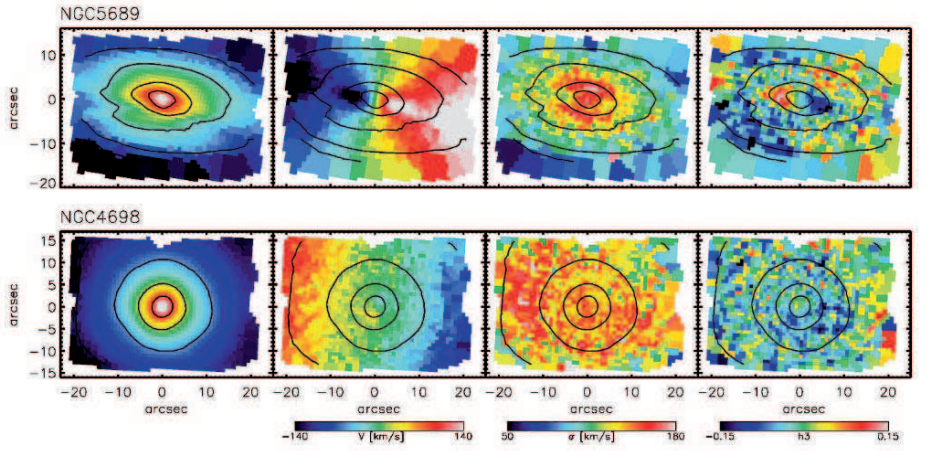

Figure 1. Stellar kinematic maps for NGC 5689 and NGC 4698. In each column (from left to right) we show the reconstructed intensity image from the SAURON datacube (in mag/arcsec^2), the stellar radial velocity, velocity dispersion (in km s^{-1}) and h_3 Gauss-Hermite moment.

An alternative possibility for the formation of these components is an interaction event. This model is preferred to explain the presence of misaligned components such as the one seeing in NGC 4698. This galaxy is a well-studied case in which the formation of the component is thought to be the result of an intermediate merger event (Bertola et al. 1999). In Figure 2, we present the case of NGC 5953, which offers a unique opportunity to study the effects that an on-going interaction has on the stellar and gas properties. The kinematical decoupling in the inner parts, together with the presence of large amounts of fresh gas, suggests that we might be witnessing the early stages in the formation of a kinematically decoupled component.

3. Global and Circumnuclear Star Formation

Several methods have been used in the past to trace star formation (SF) in galaxies. Given the little observational overhead, the emission of Balmer lines has become one of the most popular tracers (Kennicutt 1998). In addition to the Balmer lines, the [O III]/Hβ ratio can also serve as a diagnostic in situations where SF is intense and derives from pre-enriched material (Kauffmann et al. 2003). Here we use both diagnostics to investigate the importance of star formation in Sa galaxies.

The morphology of the star-forming regions in our sample appears to have multiple forms, although as expected in spiral galaxies, the bulk of SF is concentrated in the main disk. Within galaxies, we find that SF activity is more

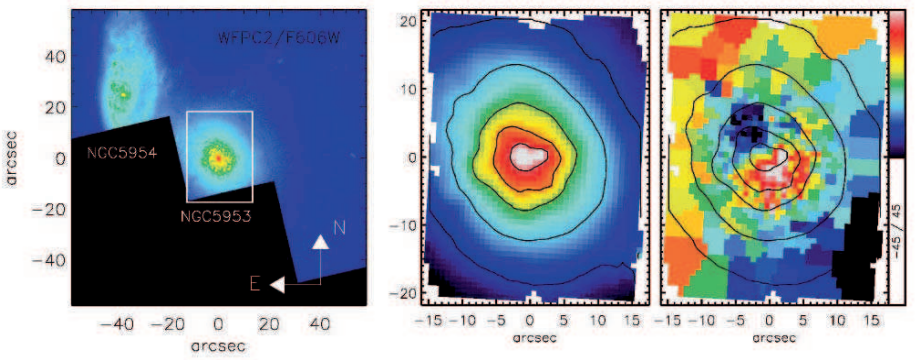

Figure 2. Interacting pair NGC 5953/NGC 5954. From left to right: i) HST/WFPC2 image of the pair of galaxies. Overlaid on NGC 5953 is the SAURON field-of-view. ii) SAURON reconstructed intensity image of NGC 5953, iii) stellar radial velocity of NGC 5953.

intense along dust lanes, has an amorphous morphology, or is confined in circumnuclear rings.

These rings represent one of the most spectacular forms of SF. The frequency of these circumnuclear regions in our sample is in good agreement with the most recent studies from Hα observations of larger samples (21$\pm$5%, Knapen 2005). In Figure 3, we present the cases of NGC 4245, NGC 4274, and NGC 4314 to illustrate the most common properties of the stars and gas in these SF regions. There is a remarkable correlation between the dust and the regions where SF is very intense (i.e., large Hβ flux). At the same time, the [O III]/Hβ ratio is very low at the same locations, confirming the presence of star formation. The velocity dispersion of the ionised gas is also low ($\sim$50 km s^{-1}) along the star-forming rings. We are thus seeing stars being formed from dynamically cold gas. A similar behaviour is also found in other galaxies in the sample with extreme SF activity.

As discussed in Section 2, star formation can produce the observed stellar velocity dispersion drops (also called 'sigma-drops'). In our sample we find that the presence of young stars does not necessarily relate directly to the stellar velocity dispersion (σ_*). In the examples shown in Figure 3, only NGC 4274 displays a sigma-drop at the location of the young stars. NGC 4245 shows a small decrease in σ_* only on the brightest Hβ knots along the ring. In NGC 4314, one of the galaxies with highest apparent SF activity, the presence of young stars hardly affects σ_*. In practice, these features strongly depend not only on the number of young stars present, but also on the inclination of the galaxy, as in face-on configurations (e.g., NGC 4314) the contribution of the young stars to the line-of-sight radial velocity is much smaller than that of the surrounding bulge.

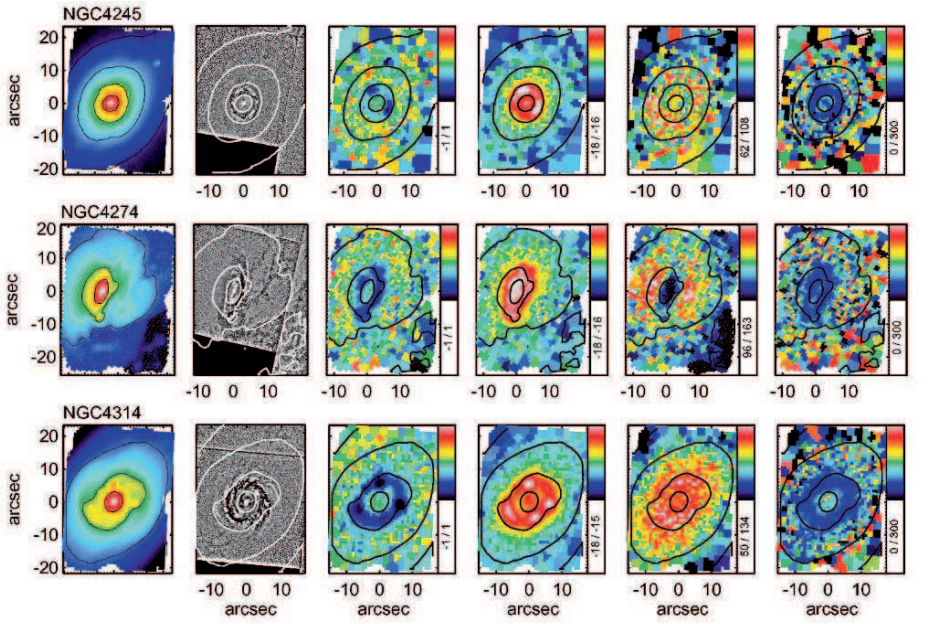

Figure 3. Stellar and gas maps for three star-forming ring galaxies NGC 4245, NGC 4274, NGC 4314. In each column (from left to right) we show i) the reconstructed intensity image from the SAURON datacube, ii) an HST unsharp-masked image, the iii) [O III]/Hβ ratio (logarithmic scale), Hβ flux (in units of ergs/cm^2/s, and logarithmic scale), iv) stellar velocity dispersion (in km s^{-1}), and v) ionised-gas velocity dispersion (in km s^{-1}).

The formation of star-forming rings is generally associated with bar-driven gas inflow towards the inner regions of galaxies (i.e., gas material gets trapped in rings as it approaches an important resonance). SF in the ring then begins once the gas density in the ring exceeds the limit set by the Toomre (1969) criterion. In our sample only three of the six galaxies with star-forming rings are known to be barred (NGC 4245, NGC 4274, NGC 4314). For the remaining three galaxies with rings (NGC 2844, NGC 5953, NGC 7742), the interacting scenario offers an alternative explanation (see Figure 2). Although the case of NGC 7742 is still unclear, as the presence of an oval (i.e., weak bar) could also explain the observed star-forming ring (see Figure 13 in de Zeeuw et al. 2002).

4. Conclusions

We are carrying out a comprehensive study of the kinematical properties of a sample of 24 Sa bulges drawn from the SAURON survey of representative galaxies. We find that kinematically decoupled components are present in half of our sample of galaxies (13/24). They are easily detected in the stellar velocity

maps, but often also leave an imprint in the stellar velocity dispersion and h_3 parameters. Despite the growing evidence that they are the result of star formation induced by bar-driven gas inflow towards the inner parts of galaxies, interactions as well as non-dissipative bar evolution models can also reproduce the observed kinematics.

Star formation in our sample displays different morphologies. The most striking cases appear in the form of circumnuclear rings. We find a good correlation between star formation and the velocity dispersion of the ionised gas in these rings, indicating that we are seeing young stars being formed from dynamically cold gas. The young stars in these rings often produce a decrease of the stellar velocity dispersion, although the presence of these sigma-drops strongly depends on the number of young stars, but more importantly on the inclination of the galaxy. While the presence and properties of circumnuclear rings can be easily explained in the context of bars, interactions can also reproduce the observed morphological and kinematic properties.

Acknowledgements JFB acknowledges support from the Euro3D Research Training Network, funded by the EC under contract HPRN-CT-2002-00305.

References

Bertola, F., Corsini, E. M., Vega Beltran, J. C., et al., 1999, ApJ, 519, L127
Bureau, M. and Athanassoula, E., 2005, ApJ, 626, 159
Cappellari, M., Bacon, R., Bureau, M., et al., 2006, MNRAS, 366, 1126
de Zeeuw, P. T., Bureau, M., Emsellem, E., et al., 2002, MNRAS, 329, 513
Emsellem, E., Cappellari, M., Peletier, R. F., et al., 2004, MNRAS, 352, 721
Falcon-Barroso, J., Peletier, R. F., and Balcells, M., 2002, MNRAS, 335, 741
Falcon-Barroso, J., Bacon, R., Bureau, M., et al., 2005, submitted to MNRAS.
Fathi K., van de Ven G., Peletier R. F., et al., 2005, MNRAS, 985
Friedli, D. and Benz, W., 1995, A&A, 301, 649
Ganda, K., Falcon-Barroso, J., Peletier, R.F., et al., 2005, MNRAS in press
Heller, C. H. and Shlosman, I., 1994, ApJ, 424, 84
Jorgensen I., Franx M., Kjaergaard P., 1996, MNRAS, 280, 167
Knapen J. H., 2005, A&A, 429, 141
Kauffmann G., et al., 2003, MNRAS, 346, 1055
Kennicutt, R. C., 1998, ApJ, 498, 541
Pfenniger, D. and Friedli, D., 1991, A&A, 252, 75
Pfenniger, D. and Norman, C., 1990, ApJ, 363, 391
Sarzi, M., Falcon-Barroso, J., Davies, R. L., et al., 2006, MNRAS, 366, 1151
Toomre A., 1964, ApJ, 139, 1217
Wozniak, H., Combes, F., Emsellem, E., and Friedli, D., 2003, A&A, 409, 469

A COOL GAS RING IN M100

Emma L. Allard[1], Reynier F. Peletier[2] and Johan H. Knapen[1]

[1] *University of Hertfordshire, UK*
[2] *University of Groningen, The Netherlands*

Abstract The SAURON integral field spectrograph was used to observe the central parts of the galaxy M100. We present here maps of Hβ emission and gas velocity dispersion. We focus on the discovery of a cold (low velocity dispersion) ring of gas, coinciding spatially with enhanced massive star formation as indicated here by Hβ emission and outlining the well known nuclear (pseudo) ring. Our SAURON fields also cover the dustlanes visible in M100's bar. Here we see cold gas and star formation offset from the leading edge of the dustlanes, indicative of the presence of shocks. This is further strong evidence that the nuclear ring of star formation is formed at the location of the Inner Lindblad resonance(s), fuelled by gas channelled inwards along the dustlanes through shocks.

Keywords: galaxies: spiral - ISM: kinematics and dynamics - galaxies: individual (NGC4321)

1. Introduction

Nuclear rings (or pseudo-rings) of star formation (SF) are seen commonly in spiral galaxies; recently Knapen (2005) found such rings in 20% of spiral galaxies and these occurred almost exclusively in barred hosts, supporting earlier findings by Buta & Combes (1996). They can be sites of massive SF; Kennicutt et al. (2005) estimate that nuclear rings contribute 3-5% to the overall current SF rate in the local universe. Nuclear rings are thought to lie at the position of the inner Lindblad resonances (ILRs), where gas driven in under the influence of the large bar slows down (Lynden-Bell & Kalnajs 1972; Shlosman 1999). Because nuclear rings turn inflowing gas into stars within the central region, they will contribute to secular evolution and pseudo-bulge formation. M100 (NGC 4321) is a prominent, relatively face-on spiral galaxy with a moderately strong bar, at a distance of 16.1 Mpc (Ferrarese et al. 1996) where 1 arcsec is equal to 70 pc. M100 hosts a well-known nuclear ring with prominent massive SF, which is located near a pair of ILRs induced by the bar (Knapen et al. 1995a). A detailed analysis of the optical and NIR morphology of the circumnuclear region of M100 has been given by Knapen et al. (1995a,b)

R. S. de Jong, Island Universes, 207–210.
© 2007 *Springer.*

and Ryder & Knapen (1999). Here we present integral field spectroscopic data of the bar and circumnuclear region of M100 and derive maps of the Hβ emission line intensity, and gas velocity dispersion. We report a ring of relatively cold gas within the circumnuclear region, which lies exactly at the location of the Hβ emission. Further analysis of the data including stellar kinematics and absorption line indices will be presented in a future paper (E. Allard et al., in preparation).

2. Observations and Analysis

The SAURON integral field spectrograph (Bacon et al. 2001) was used on the 4.2m William Herschel Telescope (WHT) on La Palma on 2003, May 2. The field of view was 33×41 arcsec^2, and contains 1431 square lenses of 0.94×0.94 arcsec^2 in size, each producing a spectrum. The wavelength range of 4760-5350Å is observed. To cover the complete bar and circumnuclear region of M100, three pointings were made (see Figure 1d).

The data were reduced using the specially developed XSauron software. The separate exposures were merged and mosaicked together to produce one final datacube. This was spatially binned using the Voronoi 2D binning method of Cappellari & Copin (2003) to achieve a minimum S/N across the field of 60 per angstrom for the extraction of the kinematics, and 100 for the line strength maps.

To determine the gas kinematics and emission line strengths we followed a 2-step approach (Sarzi et al. 2005): we first determined in each bin the stellar line of sight velocity distribution (LOSVD) using the Penalized Pixel Fitting Method (Cappellari & Emsellem 2004). We then fitted the full spectra using a linear combination of single age, single metallicity models from Vazdekis (1999), convolved with the previously determined LOSVD.

3. Results

By measuring the flux of the Hβ emission line for each spectrum in the datacube, we can reconstruct an intensity map and this is shown in Figure 1a. The emission is brightest in the pseudo-ring and HII regions, where it traces massive SF. The HII regions at the end of the bar are connected to the ring by a thin arc of emitting material which lies along the bar. The gas velocity dispersion map (Fig. 1b) shows a value of $\sigma = 140\pm10$ km s^{-1} averaged over the central 5 arcsec. A ring of considerably lower velocity dispersion, $\sigma = 51\pm8$ km s^{-1}, is seen at a distance of 7 arcsec from the centre. It has a thickness of 7 arcsec, and is surrounded by a zone where $\sigma = 102\pm30$ km s^{-1}. Regions of low σ are correlated spatially with enhanced Hβ emission, such as the pseudo-ring and the arc of material seen in the western side of the bar. This suggests we are detecting the cold gas from which young stars are being created. To see how

this arc of Hβ emitting, low dispersion material is connected to the dustlanes seen in optical images (i.e. Fig 1d), we overlaid the Hβ emission contours on a *B–R* image of the region (Fig. 1c). This shows that the low dispersion material is *offset* by some 700 pc from the dark dustlanes in the bar. The dustlanes are thought to be associated with shocks in the gas flow (Prendergast 1964; Athanassoula 1992) and we expect strong shear at this position and so little SF. Immediately after the shock however we may expect a pile up of gas, leading to an increase in SF, and so an offset between the SF and the dustlanes is to be expected.

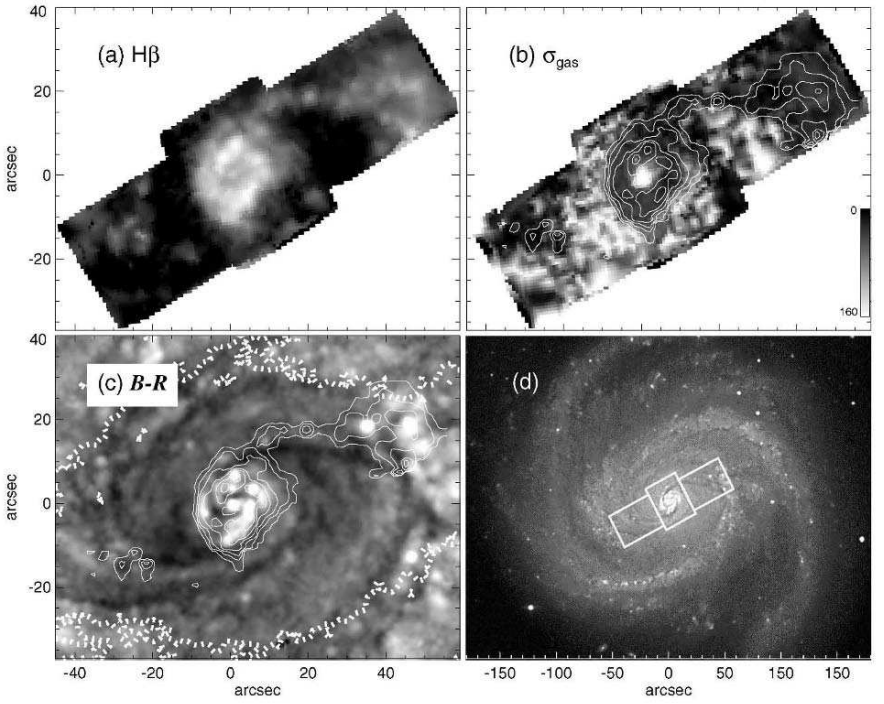

Figure 1. SAURON maps of the central and bar region of M100. (a) Hβ emission line intensity. (b) Gas velocity dispersion (in km s^{-1}); overlaid are Hβ contours at relative levels [0.0.05,0.1,0.2,0.5,1,2,3]. (c) *B–R* image from Knapen et al. (2004); the location of the bar is indicated by a K_s-band contour (thick dashed line) at 18.3 mag arcsec^{-2}; Hβ contours as in Figure 1b. (d) Optical image of M100 with approximate locations of the SAURON pointings. North is up and East is to the left.

4. Conclusions

We have obtained integral field spectroscopic data of the central region of the barred spiral galaxy M100. The Hβ emission shows the well-known bright ring, broken into hotspots of emission. In the gas velocity dispersion map, the ring is clearly colder than the underlying disk. Significantly lower dispersion occurs exactly where the strongest Hβ emission occurs, both within the ring and aligned and offset from the dustlanes in the bar. The low gas dispersion suggests that cold gas flows into the area through the dustlanes, and accumulates into a ring under the influence of the ILRs. Instabilities within this gas then trigger significant massive SF.

Acknowledgements Based on observations obtained at the WHT, operated on the island of La Palma by the Isaac Newton Group in the Spanish Observatorio del Roque de los Muchachos of the Instituto de Astrofísica de Canarias. We thank the SAURON team for making the instrument and the associated software available for this collaborative project. The optical image of M100 was kindly provided by Nik Szymanek. EA is supported by a PPARC studentship.

References

Athanassoula, E., 1992, MNRAS, 259, 345

Bacon, R., et al. 2001, MNRAS, 326, 23

Buta, R. & Combes, F. 1996, FCPh, 17, 95

Cappellari, M. & Copin, Y. 2003, MNRAS, 342, 345

Cappellari, M. & Emsellem, E. 2004, PASP, 116, 138

Ferrarese, L., et al. 1996, ApJ, 464, 568

Kennicutt, R.C., Janice, C.L., Funes, J.G., Sakai, S., & Akiyama, S. 2005, ASSL 329, 187

Knapen, J. H. 2005, A&A, 429, 141

Knapen, J. H., Beckman, J. E., Heller, C. H., Shlosman, I., & de Jong, R. S. 1995a, ApJ, 454, 623 (K95)

Knapen, J. H., Beckman, J. E., Shlosman, I., Peletier, R. F., Heller, C. H. & de Jong, R. S. 1995b, ApJ, 443, L73

Knapen, J. H., Stedman, S., Bramich, D. M., Folkes, S. L. & Bradley, T. R. 2004, A&A, 426, 1135

Lynden-Bell, D. & Kalnajs, A. J. 1972, MNRAS, 157, 1

Prendergast, K. H. 1964, Astron J, 111, 1566

Ryder, S. D. & Knapen, J. H. 1999, MNRAS, 302, L7

Sarzi, M., et al. 2005, MNRAS, submitted

Shlosman, I. 1999, ASPC, 187, 100

Vazdekis, A. 1999, ApJ, 513, 224

BOXY EDGE-ON PROFILES

Comparing orbital structures with the underlying galactic morphology

P.A. Patsis[1*] and E.M. Xilouris[2**]

[1]*Research Center for Astronomy, Athens, Greece*

[2]*Institute of Astronomy and Astrophysics, National Observatory of Athens, Greece*

* patsis@academyofathens.gr, ** xilouris@astro.noa.gr

Abstract The vertical profiles of disk galaxies are built by the material trapped around stable periodic orbits, which form their "skeletons". Thus, the knowledge of the evolution of the stability of the orbits of the main families as a function of the various parameters of a model, gives the possible morphologies that can be observed in a disk galaxy when viewed edge-on. The orbital structures which lead to the appearance of boxy "bulges" and "X"-like features are compared with edge-on profiles of disk galaxies. There is a direct correspondence between the orbital profiles and the main morphological features encountered in the images after a model subtraction or after applying a simple unsharp-masking technique.

Keywords: galaxies: structure - galaxies: kinematics and dynamics - stellar dynamics

Introduction

In Patsis et al. (2002a,b) we have presented boxy orbital profiles of 3D, time-independent, models of disk galaxies. They have been built by combinations of stable, 3D, orbits belonging mainly to families of periodic orbits (p.o.) bifurcated from x1 at the vertical $n/1$ resonances. This has been done in a set of typical 3D models of disk galaxies. A profile of a single family includes stable orbits in a range of "energies" (Jacobi constants - E_j). Combinations of the profiles of several families of a model form a model profile. The three basic conclusions of these papers are:

(a) The morphology supported by the composite orbital profile of a family may differ from the morphology of the individual periodic orbits.

R. S. de Jong, Island Universes, 211–214.
© 2007 *Springer.*

(b) The radial extent of the profile of an orbital 3D family is usually confined within a radius defined by an E_j value. Orbits with a Jacobi constant larger than this E_j, increase their size by increasing almost only in the vertical dimension, and this leads to models with edge-on stair-type profiles.

(c) It is the presence of the vertical resonances and not the kind of perturbation in the models that shapes the orbital profiles.

In the present paper we apply simple image processing techniques on the images of three edge-on disk galaxies with rather boxy "bulges" in order to detect structures similar to those predicted by the orbital theory. Here we focus our attention to the structures observed in the central regions of IC 2531, NGC 4013, and UGC 2048.

1. Observations

The observations and the data reduction of the galaxies analyzed in this study are presented in Xilouris et al. (1997).

Observations of the galaxies UGC 2048 and NGC 4013 were made at Skinakas observatory in Crete, using the 1.3 m telescope. IC 2531 was observed with the 1 m Australian National University telescope (ANU) at the Siding Spring Observatory. The I-passband we use is comparable to that of the Cousin's photometric system, while standard photometric procedures, described in detail in Xilouris et al. (1997), were applied to the data.

2. Reduction Techniques

The first technique we applied is the subtraction of an axisymmetric model from the image of the galaxy. What it left, the residuals, will indicate all these structures that mainly have to do with either the non-uniform distribution of the dust (seen as absorption features) or the non-uniform distribution of the stars (seen as excess of starlight). The deviations seen in excess could be due to non-axisymmetric stellar components.

The model that we use is described in great detail in Xilouris et al. (1997). The stellar emissivity (luminosity per unit volume) consists of an exponential (in both radial and vertical directions) disk and a bulge described by the $R^{1/4}$ law. For the extinction coefficient we use a double exponential law. The radiative transfer model is that described by Kylafis & Bahcall (1987) (see also Xilouris et al. 1997).

Our task has been to find those values of the parameters which create images of the model galaxies as close as possible to the images of the observed galaxies. For the model fitting techniques, the reader is referred to Xilouris et al. (1997, 1999).

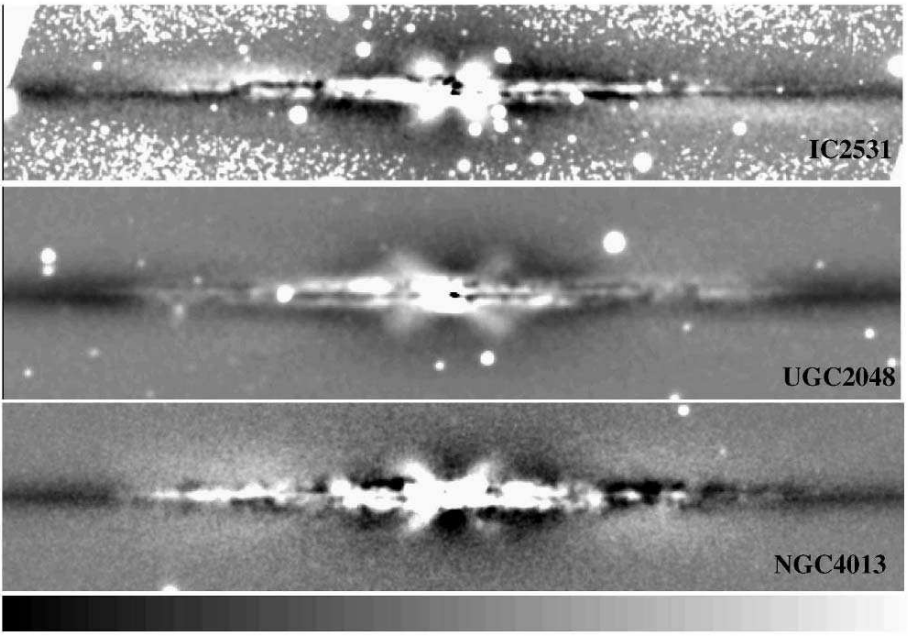

Figure 1. Residual images for IC 2531 (a), UGC 2048 (b) and NGC 4013 (c). From the original images a best fitting axisymmetric profile is subtracted according to the models of Xilouris et al. (1997). An "X"-shaped feature embedded in the boxy "bulge" is conspicuous in all three cases.

Another simple image processing technique that has been applied in addition is a standard Gaussian unsharp masking of the images.

3. Results

In Fig. 1 we give the model subtracted images for IC 2531 (a), UGC 2048 (b), and NGC 4013 (c). In the latter we have overplotted contours that help better understand the features of the residual images. Under the assumption of a constant M/L ratio this reflects excess in the surface density. The main characteristic feature is an "X" shape revealed in the central parts of the galaxies.

The images after unsharp masking show a kind of "X" shape in the central stellar component as well. This can be seen in Fig. 2 for the same galaxies. Characteristic contours underline the features we study.

4. Summary - Conclusions

Simple image processing techniques were applied to three edge-on galaxies with boxy profiles and revealed structures predicted by the orbital models. According to these models the features we see in Figs. 1 and 2 indicate the

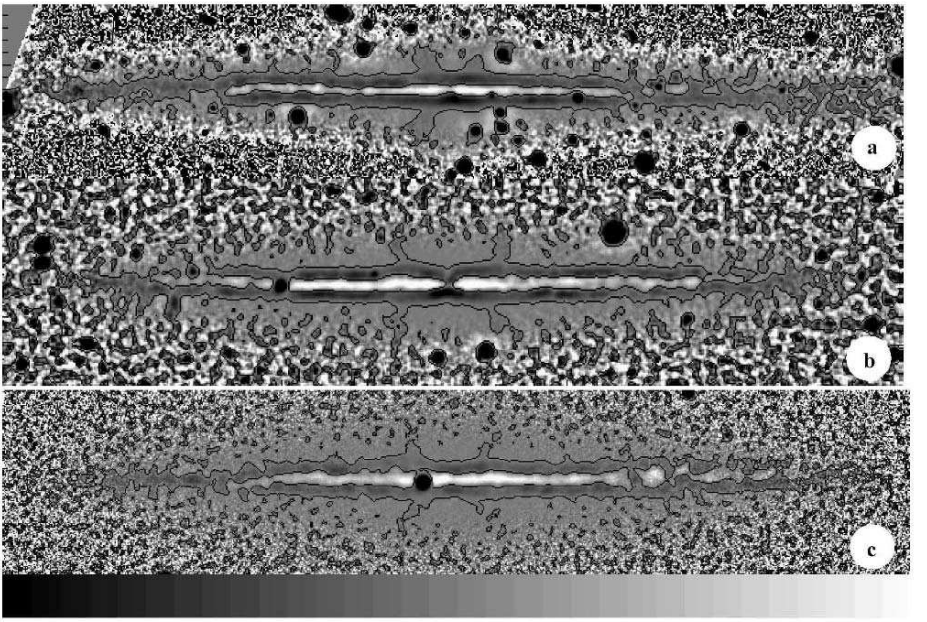

Figure 2. The result of unsharp masking in the images of IC 2531 (a), UGC 2048 (b) and NGC 4013 (c). "X" shape features similar to the structures foreseen by the orbital models can be found in all three cases.

presence of vertical resonances and a large percentage of orbits trapped by 3D families, mainly bifurcations of x1. The reader may compare these features with Figs. 3b, 7a, 9a, 14b, and 18a in Patsis et al. (2002a).

References

Kylafis, N. and J.N.Bahcall, 1987, ApJ 317, 637

Patsis, P.A., Skokos, Ch., and E. Athanassoula, 2002a, MNRAS 337, 578

Patsis, P.A., Athanassoula, E., Grosbol P., and Ch. Skokos, 2002b, MNRAS 335, 1049

Xilouris E. M., Kylafis N. D., Papamastorakis J., Paleologou, E. V. and G. Haerendel, 1997, A&A 325, 135

Xilouris, E.M., Byun, Y.I, Kylafis, N.D., Paleologou, E.V. and J. Papamastorakis, 1999, A&A, 344, 868

RESONANCES AND EXTENT OF SPIRAL ARMS IN DISK GALAXIES

Preben Grosbøl[1*] and Philippe Héraudeau[2**]

[1] *European Southern Observatory, Germany*

[2] *Kapteyn Astronomical Institute, Groningen, The Netherlands*

* pgrosbol@eso.org, ** P.Heraudeau@astro.rug.nl

Abstract The distribution of visual matter in 84 spiral galaxies was estimated from NIR K-band maps observed with SOFI/NTT, ESO. Decomposing the maps into standard axisymmetric components (e.g. disk and bulge) and using HI line width data with a maximum disk assumption for the halo, synthetic rotation curves were estimated for each galaxy. The extent of the main spiral pattern measured on the K maps of galaxies was compared with the distance between major resonances (i.e. ILR, 4:1, CR and OLR) as obtained from the synthetic rotation curves assuming that the start of the spiral corresponded to either ILR or CR.

The first preliminary analysis indicated that 1/3 of the disk galaxies have a main, symmetric spiral structure with a radial extent consistent with that of the ILR-4:1 distance in a maximum disk, rotation curve model. Another 1/3 of the sample show better agreement with the CR-OLR resonances. The extent of the spirals does not agree with distances estimated for neither ILR-CR nor ILR-OLR. Sub-maximum disk rotation curve models (e.g. 60%) show larger scatter.

Keywords: galaxies: spiral - galaxies: structure - galaxies: kinematics and dynamics

1. Introduction

The existence of spiral density waves (Lin & Shu 1964) in disks of spiral galaxies is well documented through NIR surface photometry. The pattern speed of such waves has shown to be very difficult to determine by direct measurements and only for a few early type barred galaxies it has been possible (see e.g. Merrifield & Kuijken 1995). Most pattern speeds are estimated by associating a morphological feature (e.g. end of bar) with a specific resonance (e.g., see Roberts et al. 1975). This provides no simple way of verification.

[1] Based on observations collected at the European Southern Observatory, La Silla, Chile

R. S. de Jong, Island Universes, 215–218.
© 2007 *Springer.*

The current paper compares the extent of the main spiral pattern in disk galaxies with predictions from synthetic rotations curves derived from their NIR surface photometry. Since two resonances are involved, it is possible to check which assumptions are the best to fit the measured extent if any.

2. Data and Reductions

A sample of 84 nearby, spiral galaxies with deep K′ surface photometry were used to study the morphology of spiral patterns. It consisted of the galaxies studied by Grosbøl et al. (2004; hereafter GPP) and a set of spirals for which recent SNIa's were detected. Both sets were observed with the same technique at SOFI/NTT, ESO. All the galaxies had intermediate inclination angles and recession velocities $<$5000 km/s. All observations and reductions were done as described in GPP.

After removing obvious foreground stars and determining the sky projection parameters for the galaxies, the K maps were decomposed. The outer parts, where the spiral structure was located, were fitted with a flat exponential disk while the central parts were allowed to consist of a central point source, a spherical, modified Hubble law bulge and a steep, inner exponential disk.

3. Synthetic Rotation Curves and Extent of Spiral

The synthetic rotation curves were based on the decomposition of the K-maps adding a dark matter halo with a logarithmic potential. All visual components for a galaxy were assumed to have the same mass-to-light ratio Υ. Since contributions from disk and halo masses to the rotation curve are almost degenerate (Barnes et al. 2004), Υ was determined by specifying a maximum disk solution and deriving the total rotation speed from the HI line width.

The distance between major resonances was estimated by assuming that a morphological feature corresponded to a given resonance, e.g. start of main spiral pattern indicated location of Inner Lindblad Resonance (ILR) or co-rotation (CR). Then, one can derive distances between any combination of resonances assuming a constant angular speed for the spiral. The distances will vary somewhat depending on the explicit receipt used, however the general behavior will not change significantly as it relates to the flatness of rotation curves.

Radii of three morphological features were measured for each galaxy that is a) end of bar, b) start of main spiral, and c) end of symmetric part of the spiral pattern. Due to smooth transitions, the radii are frequently uncertain by up to 3-5″. The extent d_s of the main spiral pattern was then defined as the radial distance between its start and end. The resonance associated to the start of the spiral was assumed to be between its start and bar termination.

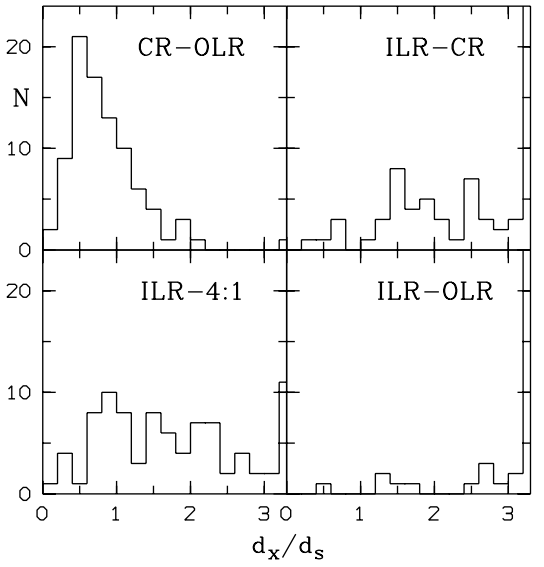

Figure 1. Histograms of the ratio of radial distance between major resonances d_x estimated from the synthetic rotation curves relative over actual measured extent d_s of the main, symmetric spiral pattern. Four set of distances between major resonances are shown namely ILR-4:1, ILR-CR, ILR-OLR and CR-OLR.

4. Results and Discussion

Four major resonances (i.e., ILR, 4:1, CR and OLR) were considered for either start or termination of the main spiral with the region d_x occupied by the pattern being ILR-4:1, ILR-CR, ILR-OLR or CR-OLR. Histograms for these four cases are given in Fig. 1 where d_x was divided by the actual measured extent d_s. The exact location of the peak will depend on the procedure for deriving the synthetic rotation curve. It is clear that only the pairs ILR-4:1 and CR-OLR display peaks around 1.0 while both ILR-CR and ILR-OLR do not agree with the actual extent.

For the current models the ratio between ILR-4:1 and CR-OLR is roughly 1:2. Thus, the peak around 1.0 in the ILR-4:1 histogram ($\sim$30 galaxies) would be located around 0.5 in the CR-OLR histogram leaving a peak of $\sim$30 galaxies close to 1 for which the extent of their spiral agree well with the predicted CR-OLR distance.

The detailed distribution of d_{I4}/d_s (for ILR-4:1) as function of the relative bar length r_b/h_d is shown in Fig. 2 where also the morphological class is indicated. For relative short bars (often weak bars) most galaxies seems to have the main spiral in the region ILR-4:1 while for larger values of r_b/h_d a significant fraction have d_{I4}/d_s close to 2 corresponding to CR-OLR. Normal SA spiral

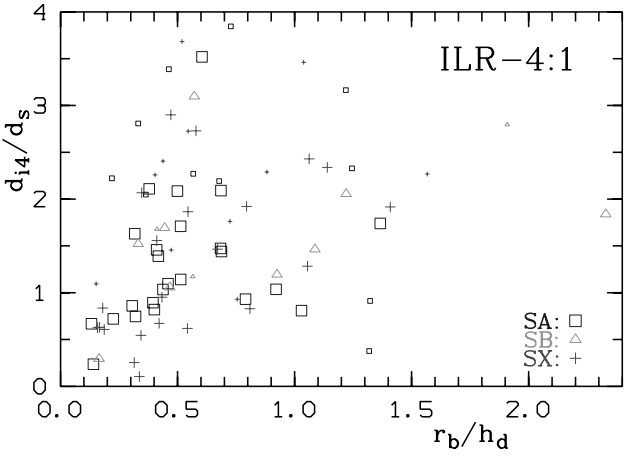

Figure 2. Distribution of the relative distance d_{I4}/d_s between resonances ILR-4:1 divided by the actual, measured extent of the main, symmetric spiral pattern as function of the relative bar length r_b/h_d where h_d is the scale length of the main exponential disk. The general spiral class is shown by different symbols where the larger marks are for luminosity class <3.

galaxies show a wide distribution as could be expected since many have bars in the NIR (see GPP). The following preliminary conclusions are suggested:

- 1/3 of the sample agree with the main, symmetric spiral being located between ILR-4:1 resonances while another 1/3 seems to be in the range of the CR-OLR.
- galaxies with short relative bars (i.e. $r_b < 0.3h_d$) are more likely to agree with the ILR-4:1 region while galaxies with long bars (i.e. $1.1h_d < r_b$) mostly correspond to CR-OLR.
- most of galaxies morphologically classified as barred in the optical have spiral extents which corresponds to the CR-OLR distance.

Nearly 1/3 of the sample does not have an extent of their spiral matching one of the 4 main cases. This may be due to special morphological features which introduced erroneous estimates of the radii. Also the procedure for generating synthetic rotation curves may not be valid for all galaxies.

References

Barnes, E.I., Sellwood, J.A. & Kosowsky, A. 2004, AJ, 128, 2724
Grosbøl, P., Patsis, P. A. & Pompie, E. 2004, A&A, 423, 849
Lin, C.C. & Shu, F.H. 1964, ApJ, 140, 646
Merrifield, M.R. & Kuijken, K. 1995, MNRAS, 274, 933
Roberts, W.W., Roberts, M.S. & Shu, F.H. 1975, ApJ, 196, 381

DYNAMICS OF LOCALIZED PACKETS OF SPIRAL DENSITY WAVES IN GASEOUS DISKS

George R. Mamatsashvili* and George D. Chagelishvili

Abastumani Astrophysical Observatory, Tbilisi, Georgia

* g.mamatsashvili@astro-ge.org

Abstract We study the linear dynamics of spiral density wave packets (localized both in physical and wavenumber planes) in gaseous disks by the shearing sheet approximation using nonmodal approach combined with numerical calculations. The dynamics is determined by the disk flow non-normality and is well comprehended not in the physical, but in the wavenumber plane. Consequently, we do not use the classical characteristics of spectral analysis – corotation, Lindblad resonance – for the comprehension.

Keywords: galaxies: kinematics and dynamics - galaxies: spiral - galaxies: ISM

Introduction

The wave theory of spiral structure of galaxies with the rare exception is developed on the basis of the spectral/modal theory of hydrodynamic stability. The very exception represents works (Goldreich & Lynden-Bell 1965; Goldreich & Tremaine 1978; Nakagawa & Sekiya 1992) using so-called *nonmodal approach*. The advantage of this approach became even more obvious in the 1990s after the recognition by the hydrodynamic community of the imperfection of canonical/modal analysis in the study of smooth shear flows (see Reddy, Schmidt & Hennington 1993, and references therein). This imperfection is connected to the non-normality of the linear eigenvalue problem. The latter is the basis of transient extraction of the background shear flow energy by perturbations despite the exponential stability of all the normal modes of a system (Reddy & Hennington 1993). This transient growth of perturbations is well described by the nonmodal approach. Due to this it has become extensively used in recent years (see Criminale & Drazin 1990, and references therein). This approach is highly productive when accompanied by numerical calculations.

Following this path we apply the nonmodal approach in combination with numerical calculations to the study of the dynamics of localized (both in

R. S. de Jong, Island Universes, 219–224.
© 2007 *Springer.*

wave-number and in ordinary planes) packets of spiral density waves in gaseous galactic disks, since disks of this kind represent an example of shear flows. The packet dynamics is determined by the disk flow non-normality. Therefore, we comprehend the dynamics in terms of the nonmodal approach in the wavenumber plane. We present just one complex demonstrative picture that is difficult to understand by means of the classical characteristics of the spectral analysis, e.g. corotation and Lindblad resonances. An extensive investigation of the linear dynamics for different values of the system parameters will be presented elsewhere.

1. Physical Model and Nonmodal Approach

Our model of study is a thin differentially rotating gas sheet whose unperturbed two-dimensional pressure P_0 and surface density Σ_0 are taken to be homogeneous. Adopting the shearing sheet approximation we write the linearized Euler and continuity perturbation equations in the local co-moving Cartesian coordinate frame (x, y) (Goldreich & Lynden-Bell 1965; Goldreich & Tremaine 1978):

$$\frac{Du}{Dt} - 2\Omega_p v = -\frac{\partial \chi}{\partial x}, \quad \frac{Dv}{Dt} + 2Bu = -\frac{\partial \chi}{\partial y}, \quad \frac{D\sigma}{Dt} + \Sigma_0 \left(\frac{\partial u}{\partial x} + \frac{\partial v}{\partial y} \right) = 0,$$

where $D/Dt = \partial/\partial t + 2Ax\partial/\partial y$, $\chi = c_{\rm s}^2 \sigma/\Sigma_0 + \psi$, $c_{\rm s}^2$ is the sound speed. All other notations are the same as in Goldreich & Tremaine (1978). In our case $A < 0$ and $\Omega_p > 0$. This set of equations is completed by Poisson's equation:

$$\left(\frac{\partial^2}{\partial x^2} + \frac{\partial^2}{\partial y^2} + \frac{\partial^2}{\partial z^2} \right) \psi = 4\pi G \sigma \delta(z).$$

Following the standard method of nonmodal analysis we introduce the spatial Fourier harmonics (SFH) of perturbations with a time dependent phase (Bodo et al. 2005):

$$F(\mathbf{r}, t) \sim F(k_x(t), k_y, t) \exp[{\rm i}k_x(t)x + {\rm i}k_y y]; \;\; k_x(t) \equiv k_x - 2Ak_y t.$$

where $F \equiv (u, v, p, \sigma, \psi)$. The stream cross/radial wavenumber varies at a constant rate. One can say that in the linear approximation SFH "drifts" along the k_x axis in $\mathbf{k}$-plane (wavenumber plane).

For the further analysis it is convenient to use the non-dimensional quantities (henceforth, we omit the hats): $t\kappa \equiv \tau$, $K_y \equiv c_{\rm s} k_y/\kappa$, $K(\tau) = [K_x^2(\tau) + K_y^2]^{1/2} \equiv c_{\rm s} k(t)/\kappa$, $\hat{\Omega}_p \equiv \Omega_p/\kappa$, $\hat{A} \equiv A/\kappa$, $\hat{B} \equiv B/\kappa$, $1/Q \equiv \pi G \Sigma_0/c_{\rm s}\kappa$, $\hat{u} \equiv u/c_{\rm s}$, $\hat{v} \equiv v/c_{\rm s}$, $\hat{\sigma} \equiv \sigma/\Sigma_0$, $\hat{\psi} \equiv \psi/c_{\rm s}^2$, where Q is the local Toomre's parameter. To demonstrate our results most clearly we take marginally stable disks ($Q = 1$). Of course, stable/unstable disks can be considered in a similar manner. In our presentation $A = -0.75$, $B = 0.25$,

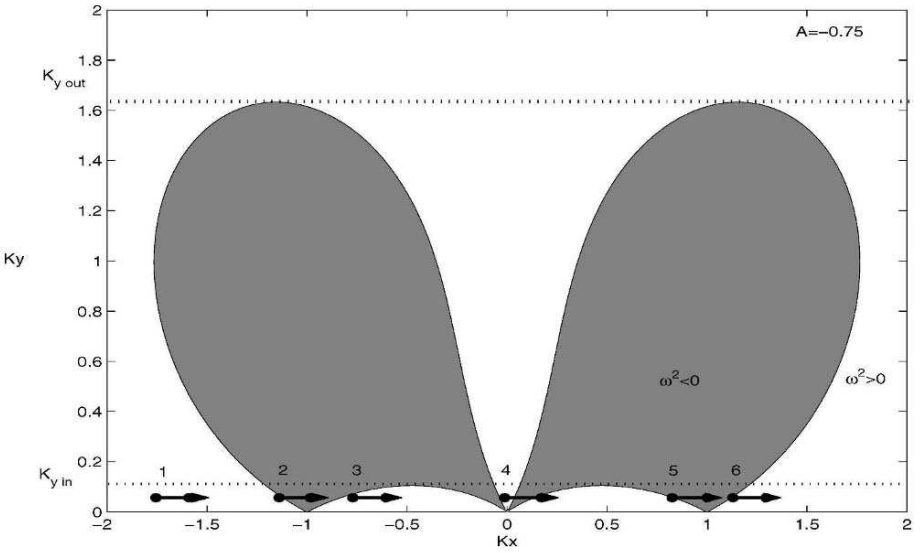

Figure 1. Stable and unstable (shaded) regions in **K**-plane for $K_y > 0$. The role of the shear (A) is significant: contrary to the case $A = 0$, when $\omega^2 > 0$ at all K except for $K_x^2 + K_y^2 = 1$, shear leads to the appearance of the wide unstable regions and there remains only the narrow central stable region at small K_y. The arrows $1 \to 2 \to 3 \to 4 \to 5 \to 6 \to$ indicate the drift of the considered SFH situated initially at the point 1.

$\Omega_p = 1$. Such a situation is realized, for example, in our Galaxy at distances greater than 16 kpc from the galactic center.

The considered system admits two types of solutions/modes (Goldreich & Lynden-Bell 1965; Goldreich & Tremaine 1978): vortex and (spiral density) wave. We confine ourselves to the latter one. In order to carry out this analysis we derive a single second order differential equation for $\psi(K_x(\tau), K_y, \tau)$ that applies only to the wave mode SFH (Goldreich & Tremaine 1978):

$$\psi''(\tau) + \omega^2(K_x(\tau), K_y)\psi(\tau) = 0,$$

$$\omega^2(K_x(\tau), K_y) = K^2(\tau) - \frac{2}{Q}K(\tau) + 1 + 12A^2\frac{K_y^4}{K^4(\tau)} + 8\Omega_p A\frac{K_y^2}{K^2(\tau)}.$$

The dynamics of the wave SFH is mainly determined by the sign and value of $\omega^2(K_x(\tau), K_y)$. We define stable (where $\omega^2 > 0$) and unstable (where $\omega^2 < 0$) regions in **K**-plane. This regions for $K_y > 0$ are presented in Fig. 1.

2. Packet Dynamics

Now we present the results of the numerical study of the dynamics of localized both in physical and wavenumber planes packets of spiral density waves.

We perform numerical calculations in **K**-plane for each SFH and then by means of inverse Fourier transform find the location and appearance of a packet as it evolves with time. For the surface density perturbations in **K**-plane at the initial moment of time we take the following form:

$$\sigma(K_x, K_y, 0) =$$

$$= \epsilon_p e^{-iK_x x_0 - iK_y y_0} \left(e^{-\left(\frac{K_x - K_{x0}}{\Delta K_x}\right)^2 - \left(\frac{K_y - K_{y0}}{\Delta K_y}\right)^2} + e^{-\left(\frac{K_x + K_{x0}}{\Delta K_x}\right)^2 - \left(\frac{K_y + K_{y0}}{\Delta K_y}\right)^2} \right)$$

This packet consists of two oval shaped localization areas in wavenumber plane with sizes defined by ΔK_x and ΔK_y and centers situated at (K_{x0}, K_{y0}) and $(-K_{x0}, -K_{y0})$. The quantities x_0 and y_0 specify the initial position of the packet in physical plane. ϵ_p is the amplitude of the perturbation (In the presented simulations $\epsilon_p = 0.1,\ K_{x0} = -4,\ K_{y0} = 0.04,\ \Delta K_x = 0.14,\ \Delta K_y = 0.00316$). We can express SFH of other perturbed quantities $u,\ v,\ \psi$ by $\sigma(K_x, K_y, 0)$ assuming that only waves with the negative frequency are considered at the initial moment (Nakagawa & Sekiya 1992).

In the following we examine the peculiarities of a localized packet originally composed of short leading (with $K_x(0)/K_y < 0$) waves, since a packet of short trailing (with $K_x(0)/K_y > 0$) waves has quite simple and predictable dynamics – it propagates without splitting and its group velocity never changes sign. By our choice the initial group velocity of the packet is directed towards the galactic center. We use the quantity $E(x, y, \tau) = [u^2(x, y, \tau) + v^2(x, y, \tau) + \sigma^2(x, y, \tau)]/2$, called the packet energy density, as a measure of the packet intensity. The dynamics of $E(x, y, \tau)$ in the considered case is followed in Fig. 2. In our calculations the initial short leading wave packet's Fourier transform (PFT) (more precisely Fourier transform of the packet energy density) is characterized by $K_{y0} \pm \Delta K_y < K_{y\,in} = 0.125$. For simplicity in the following we describe/trace the PFT dynamics in the upper ($K_y > 0$) part of **K**-plane as it crosses different, relative to the $\omega^2 = 0$ curve, regions of the upper **K**-plane.

In the beginning the packet in physical **r**-plane propagates towards the galactic center as a whole. In order to get into the physics of the subsequent evolution we further refer to Fig. 1, because the PFT moves/drifts (as $K_x(\tau) \equiv K_x - 2AK_y(\tau)$) along the K_x axis alongside the propagation of the packet in **r**-plane (see $1 \rightarrow 2 \rightarrow 3 \rightarrow 4 \rightarrow 5 \rightarrow 6 \rightarrow$). As we will see below, *the peculiarities of the dynamics in physical plane stem from this "drift" of PFT in* **K***- plane*. During the linear drift PFT crosses two unstable regions (where $\omega^2 < 0$) and one intermediate stable region (where $\omega^2 > 0$) in **K**-plane. At the time when the PFT enters the first unstable region in **K**-plane (point 2 in Fig. 1, where ω^2 first becomes negative) the packet gradually stops in physical plane, since the group velocity becomes zero as $\omega^2 < 0$. From this moment

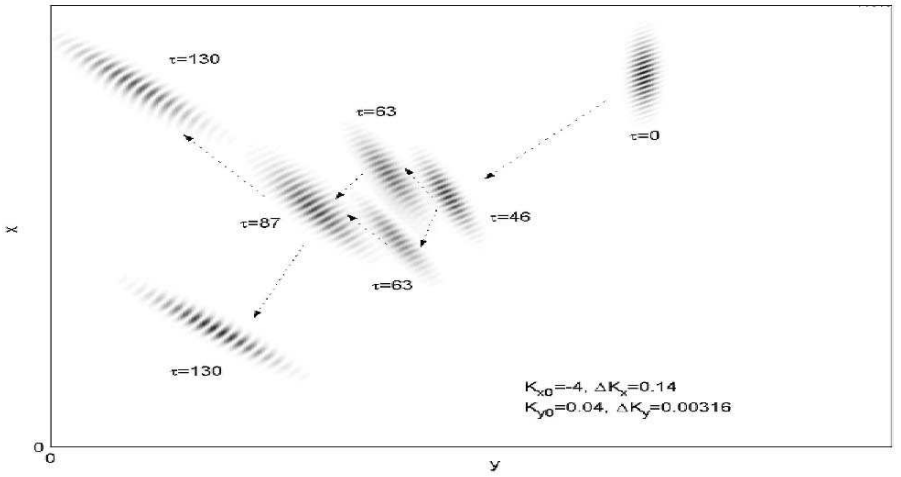

Figure 2. Evolution of the packet energy density $E(x, y, \tau)$ (shaded)in **r**-plane for the various values of τ : $\tau = 0, 46, 63, 87, 130$. In the beginning the packet propagates as a whole, then in **r**-plane splits into two parts as its FT enters the intermediate stable region and then these two parts join when PFT leaves this region. After that the packet splits again when PFT moves into another stable region throughout which ω^2 is positive. Movies of the above dynamics can be viewed at **http://www.mamacashvili.pochta.ru**

the first amplification of the packet energy takes place. Then PFT leaves this area (point 3) and the first act of over-reflection occurs. After this PFT starts to cross the relatively long intermediate stable region where $\omega^2 > 0$. The crossing takes quite a long time, as the drift velocity (that is equal to $1.5K_y$) is small at small K_y. $K_x(\tau)$ of each SFH decreases here and constituent waves become long leading. The initial incident PFT is made up of SFHs with just negative frequency, but now there appear also SFHs with positive frequency. This fact is reflected in the splitting of the packet into two parts in physical plane. These two split fragments of the enhanced packet propagate along different trajectories as they consist of SFH with opposite signs of frequency. They move away from each other ($\tau = 63$ in Fig. 2). This intermediate stable region contains point $K_x = 0$, therefore constituent waves of each split packet change from long leading to long trailing ($K_x(\tau)/K_y > 0$) after crossing the line $K_x = 0$ (point 4). As a result, at the same time both split parts change the sign of their group velocity, begin to near each other and merge ($\tau = 87$). The merger happens when PFT enters the second unstable region of wavenumber plane (point 5). However, this merger is temporal, it lasts until PFT is in the unstable region. The resultant packet stops in physical plane until PFT leaves this region. At this time an amplification of the packet energy happens again. On leaving the unstable region (point 6) PFT finally gets into the region with $\omega^2 > 0$ and never leaves it. I.e., on leaving the unstable region the second final act of the

over-reflection happens: the packet splits again ($\tau = 130$) in **r**-plane and two split parts never merge. As in the first case the splitting is related to the presence of SFHs with positive and negative signs of frequency in the PFT. Now the split parts are composed of short trailing waves and have different group velocities.

3. Summary

We have presented the peculiarities of the dynamics of a localized packet of spiral density waves using the nonmodal approach combined with numerical calculations. From the performed analysis it is obvious that the transient growth of the wave perturbations – a manifestation of the non-normality of the differentially rotating flow systems – determines the energetic (amplification) and spatial (splitting) characteristics of the wave packet dynamics. We can judge about the subsequent behavior of the packet from the analysis of its Fourier transform in the wavenumber plane. The main purpose of our study has been to gain a better insight into the dynamics of density waves so important for the spiral structure of galaxies.

Acknowledgement G.M. would like to acknowledge financial support from the Organizing Committee of the Island Universes Conference.

References

Bodo, G., Chagelishvili, G., Murante, G., Tevzadze, A., Rossi, P., Ferrari, A., 2005, A&A, 437, 9

Criminale, W.O., Drazin, P.G., 1990, Studies in Appl. Math., 83, 123

Farrell, B.F., Ioannou, P.J., 1991,. Phys. Fluids A, 5, 1390

Goldreich, P., Lynden-Bell, D., 1965, Mon. Not. R. astr. Soc., 130, 125.

Goldreich, P., Tremaine, S., 1978, Ap.J. 222, 850.

Nakagawa, Y., Sekiya, M., 1992, Mon. Not. R. astr. Soc., 256, 684.

Reddy, S.C., Henningson, D.S., 1993, J. Fluid Mech. 252, 209.

Reddy, S.C., Schmidt, P. J., Henningson, D.S., 1993, SIAM J. Appl. Math., 53, 15.

IV

THE OUTSKIRTS AND ENVIRONMENT OF DISK GALAXIES

James Bullock.

DYNAMICAL EVOLUTION OF ACCRETED DWARF GALAXIES

James S. Bullock[1*] and Kathryn V. Johnston[2]

[1] *Center for Cosmology, University of California, Irvine, USA*

[2] *Van Vleck Observatory, Wesleyan University, Middletown, USA*

* bullock@uci.edu

Abstract We model accretion histories of 11 Milky-Way size dark matter halos set within an LCDM context and focus on the accreted dwarfs that survive until $z = 0$ as dwarf satellites ($\sim$ 120 satellites in all). We evolve each galaxy as a two-component system (dark matter + stars) using a basis-function expansion code with 10^5 particles per satellite. In agreement with previous results, we show that the dark matter halos of satellites evolve rapidly and continuously after accretion. However, the stellar material is much more resistant to tidal stripping and experiences more complicated evolution. The circular velocity profiles ($V^2 \equiv GM(r)/r$) of orbiting satellites decrease in normalization as a function of time, but maintain a roughly constant *central* slope, $V \propto r^{0.5}$. The outer parts of halos are stripped more rapidly than the inner parts such that the maximum circular velocity $V_{\rm max}$ decreases more slowly than the radius where the circular velocity peaks, $r_{\rm max}$. This means that subhalos become less dense but *more concentrated* at fixed $V_{\rm max}$ than halos in the field and that dwarfs of fixed stellar velocity dispersion inhabit *less massive* subhalos than might naively be expected. Moreover, the central *stellar* velocity dispersion of satellites, σ_*, often remains quite stable even as the *dark matter* velocity dispersion decreases. As a result, the ratio of $V_{\rm max}/\sigma_*$ is always *larger* before accretion than at $z = 0$. In addition, the stellar surface brightness distributions physically expand with time. Their half-light radii often grow by a factor of ~ 2 or more without any associated stellar mass loss. This result may be important for explaining the observed size difference between the dwarf galaxy populations of M31 and the Milky Way: the M31 dwarfs are bigger by a factor of ~ 2 because their halos have been more significantly stripped, perhaps because they were accreted ~ 4 Gyr earlier than the Milky Way's population.

Keywords: Local Group - galaxies: general - galaxies: dwarf - galaxies: fundamental parameters - galaxies: structure - galaxies: interactions

R. S. de Jong, Island Universes, 227–238.
© 2007 *Springer.*

Introduction

Galaxies accreted onto larger dark matter halos are expected to experience significant tidal interactions and mass loss. The evolution of dwarf galaxy halos within host halos of Milky-Way size objects are especially important for interpreting the the abundances of dwarf galaxies in the Local Group and for predictions related to gravitational lensing by substructure (Zentner and Bullock 2003; Metcalf 2005 and references therein). The evolution of *stellar* material within those subhalos is of related interest. Indeed quantifying how stars are expected to deviate in their evolution compared to the dark matter may be essential for interpreting an array of dwarf galaxy observations (e.g., McConnachie and Irwin (2006) and references therein).

In this work we use a set of idealized N-body simulations set within the standard LCDM cosmology. We use cosmologically determined merger histories for 11 Milky Way size halos to investigate the expected evolutionary history of dwarf satellite galaxies. The methods we use follow those outlined in Bullock and Johnston (2005) (BJ05, hereafter), where we focused on accreted satellites that were *destroyed* to form the stellar halo. Here we focus on the minority of accretion events that survive until $z = 0$ as satellites.

1. Simulations

We set the mass accretion and satellite accretion histories of our host halos using Extended-Press-Schechter (Lacey and Cole 1993) and employ the merger tree algorithm proposed by Somerville and Kolatt (1999). We demand that the hosts at $z = 0$ have a mass of $1.4 \times 10^{12} M_{\odot}$. The merger tree provides an account of how the mass of the host halo varies with time, and we use the results of Wechsler et al. (2002) to track the evolution of its density profile and corresponding gravitational potential. The luminosities of each accreted system are set using a semi-analytic method described in BJ05, which includes the effects of cosmological reionization (Bullock et al. 2000) and inefficient star formation in dwarf galaxies in order to solve the dwarf satellite problem (Klypin et al. 1999). Our models match the luminosity function of surviving dwarf galaxies *and* the total mass of the stellar halo today. No dark matter halos with *initial* maximum circular velocities $V_{\rm max} < 15 {\rm km\,s^{-1}}$ host dwarf galaxies because of the effects of reionization.

For each luminous accretion event we run a high-resolution N-body simulation that tracks the evolution of the dark matter component of a satellite disrupting within an analytic, time-dependent, parent galaxy + host halo potential (see BJ05). The dark matter is initialized as an NFW density profile using the appropriate concentration parameter for the epoch of accretion (Bullock et al. 2001) and an NFW phase-space distribution (see also Kazantzidis et al. 2004). We use our model stellar mass for each satellite to assign a King density

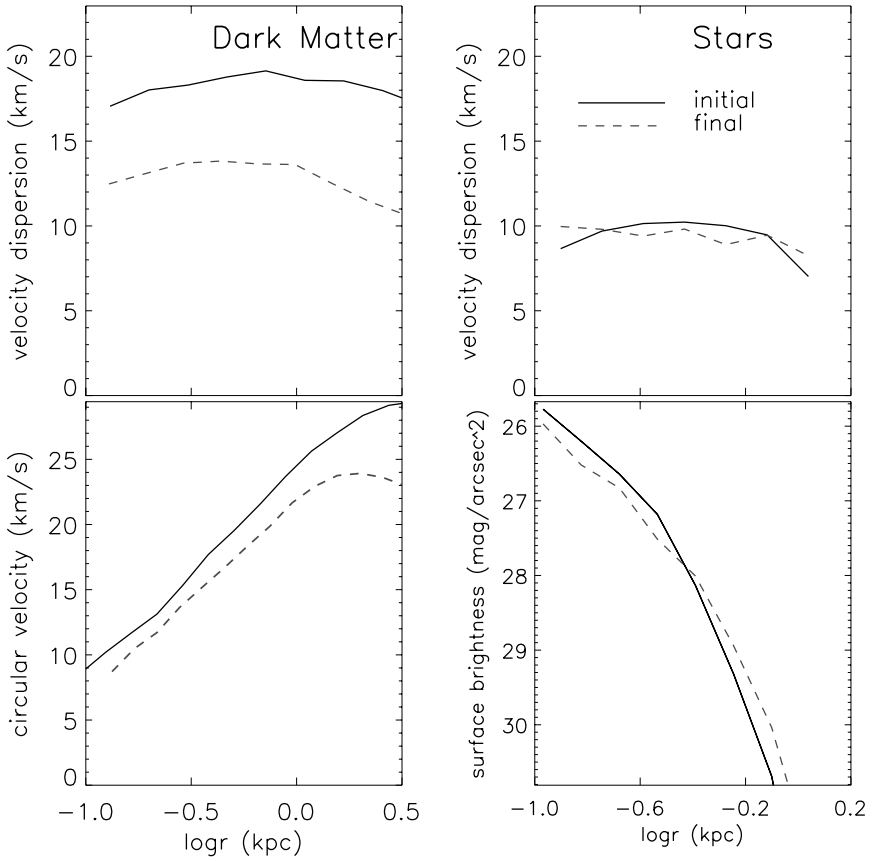

Figure 1. Example evolution for one of our surviving satellite galaxies accreted onto its Milky-Way size host 4 Gyr ago. *Left:* The dark matter velocity dispersion profile is shown in the top panel and the total circular velocity profile is shown on the bottom. The solid lines depict the satellite before accretion and dashed lines show the satellite at $z = 0$. *Right:* The *stellar* velocity dispersion (top) and surface brightness profile (bottom) for the same satellite before accretion (solid) and at $z = 0$ (dashed). Note that its stellar velocity dispersion has evolved much less than its dark matter velocity dispersion. Dark matter is preferentially stripped, while the more tightly bound stellar particles have expanded nearly isothermally.

profile and we "tag" stellar particles by assigning a variable mass-to-light ratio to each particle based on its initialized energy. This method allows us to track the evolution of mass weighted and luminosity weighted particles separately. When we use the term "stellar" below we are referring to luminosity-weighted measurements. The results we present below include all of the surviving satellites with more than 3000 particles at $z = 0$ for the 11 halo accretion histories presented in BJ05.

2. Results

Before presenting results for our full population of model satellite galaxies we illustrate these trends using an example accretion event. Figure 1 shows the evolution of the dark matter and stellar matter distributions for one of our surviving satellites. This particular satellite was accreted at a lookback time of 4 Gyr and is a member of "Halo 1" as described in BJ05. The upper left panel shows the initial (solid) and final (dashed) projected velocity dispersion profile (as seen from the "Galactic center" of the "Milky Way" host). The lower left panel shows the circular velocity profile, $V(r) \equiv \sqrt{GM(r)/r}$, before accretion (solid) and at $z = 0$ (dashed). The initial (solid) and final (dashed) projected velocity dispersion profiles of the stars for this satellite are shown in the upper right panel along with the initial and final projected surface brightness profiles in the lower right panel.

Observe that while the central velocity dispersion of the dark matter has decreased by $\sim 30\%$ since accretion, the *stellar* velocity dispersion has shown very little evolution. This is because the highest energy (fastest moving) dark matter particles are preferentially stripped, while the lower energy (more slowly moving) star particles remain bound. The unstripped stars now feel a more shallow potential well and expand as a result (nearly self-similarly, as seen in the lower right panel of Figure 1). We also point out that the circular velocity profile (bottom left) is most significantly affected in the outer parts: the radius where the rotation curve peaks, $r_{\rm max}$ has decreased by a factor of ~ 2, while the value of the maximum rotation velocity $V_{\rm max}$ itself has decreased by only $\sim 20\%$. The slope of the inner velocity curve remains unchanged from that in the initial halo, $V(r) \propto r^{0.5}$. We find the same result for the inner slopes in all of our accreted satellites, for a range of masses, as long as the halo particle number remains greater than 3000 (at which point numerical effects become important, as we conclude base on convergence studies). We note that this result on inner halo slopes and the result on the evolution of $r_{\rm max}$ and $V_{\rm max}$ agree with the results of Kazantzidis et al. (2004).

We now illustrate how these trends manifest themselves within the larger population of satellites.

Dark Halo Evolution

Figure 2 shows the relationship between $V_{\rm max}$ and $r_{\rm max}$ for all of our surviving satellites before accretion (open circles) and at $z = 0$ (solid circles). The line running through the open points reflects the mean relationship expected

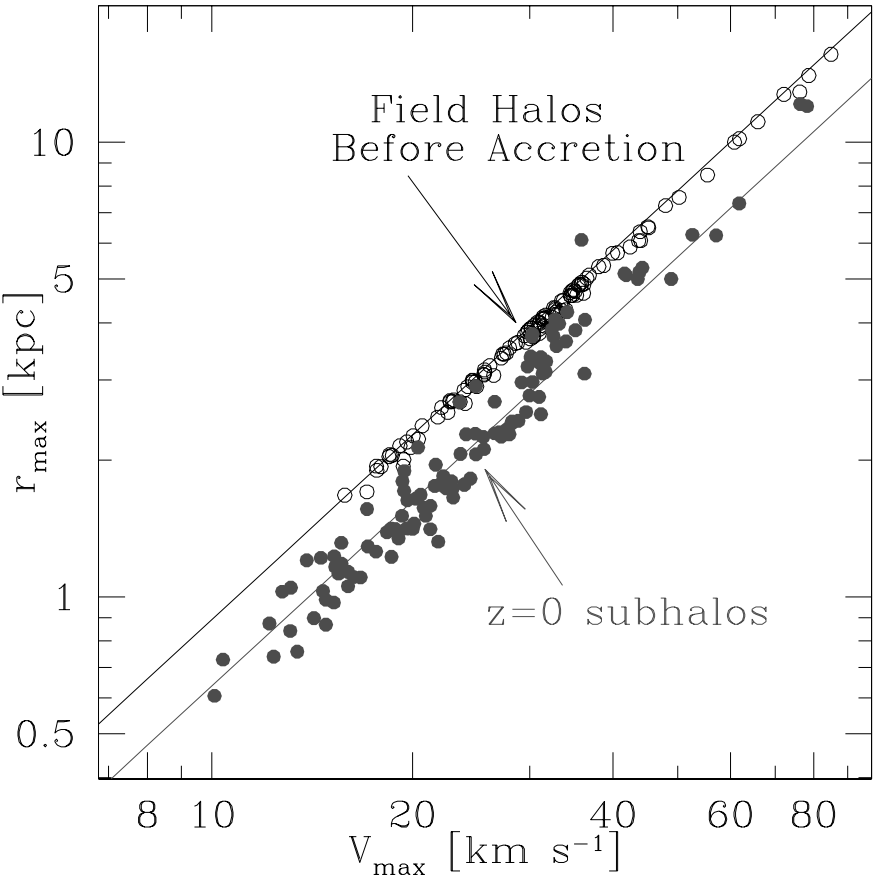

Figure 2. Open circles show the radius of the maximum rotation velocity, $r_{\rm max}$ versus the maximum rotation velocity $V_{\rm max}$ for our ensemble of ("field") dwarf galaxies before they were accreted onto the host halo. These points include only those systems that survive until $z = 0$ without being destroyed. Solid circles show the same satellites at $z = 0$, after each dwarf had undergone significant orbital evolution. The lines show power-law relations $r_{\rm max} \propto V_{\rm max}^{1.35}$. The line fitting the $z = 0$ subhalo points has a normalization lower by a factor of 1.4 compared to the field dwarf line.

for "field" halos of this size, $r_{\rm max} \propto V_{\rm max}^{1.35}$, from Bullock et al. (2001)[1]. Our initial satellites fall on this line by design. The line characterizing the $z = 0$

[1]The predicted evolution in NFW concentration at fixed mass tends to counter-act the redshift evolution in virial velocity at fixed mass in such a way that the $V_{\rm max} - r_{\rm max}$ relation is roughly invariant with redshift (Bullock et al. 2001).

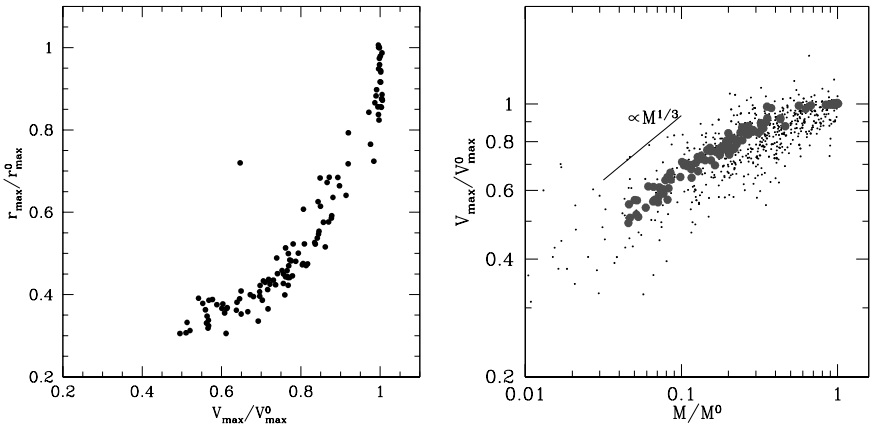

Figure 3. *Left:* The ratio of final to initial maximum circular velocity ($V_{\rm max}/V^0_{\rm max}$) is plotted along the horizontal axis and the ratio of final to initial *radius* of maximum circular velocity is plotted along the vertical axis ($r_{\rm max}/r^0_{\rm max}$). *Right:* Large filled circles show the ratio of final to initial maximum circular velocity ($V_{\rm max}/V^0_{\rm max}$) as a function of final to initial halo mass (M/M^0) for our ensemble of surviving satellites. The small dots show simulation data provided by A. Kravtsov from Kravtsov et al. (2004) which rely on full cosmological simulations with fewer particles per halo than our own idealized simulations.

subhalos has the same slope but is a factor of 1.4 lower at fixed $V_{\rm max}$. In this sense the subhalo distribution is *more concentrated* than the initial (field) distribution of halos. Interestingly, this is consistent with the conclusion of Bullock et al. (2001) who used cosmological simulations to investigate the difference between field halo and subhalo concentrations.

The left panel of Figure 3 shows a more detailed view of the evolution of the $V_{\rm max}$-$r_{\rm max}$ relation. Here we plot the ratio of final to initial $r_{\rm max}$ as a function of final-to-initial $V_{\rm max}$ for all of our surviving satellites. We sample a range of $V_{\rm max}/V^0_{\rm max}$ ratios, which we can think of as an evolutionary sequence from very little orbital evolution (upper right corner of the figure) to significant orbital evolution (lower left corner). We see that $V_{\rm max}$ evolves significantly only after the outer part of the rotation curve is truncated by tidal stripping.

In the right panel of Figure 3 the large solid circles show the final-to-initial $V_{\rm max}$ ratio as a function of final-to-initial bound mass, M for our surviving satellites. Here we see a result quite similar to that reported by Hayashi et al. (2003), Kazantzidis et al. (2004), and Kravtsov et al. (2004): the maximum circular velocity tends to decrease with stripped mass as $V_{\rm max} \propto M^{1/3}$ (straight line). One difference is that we find that some initial mass loss occurs without any significant reduction in halo $V_{\rm max}$. For $(M/M^0) \gtrsim 0.5$, we find $V_{\rm max}$ remains relatively constant, while for $(M/M^0) \lesssim 0.5$ the standard scaling ($V_{\rm max} \propto M^{1/3}$) occurs. This may be related to the fact that we sample

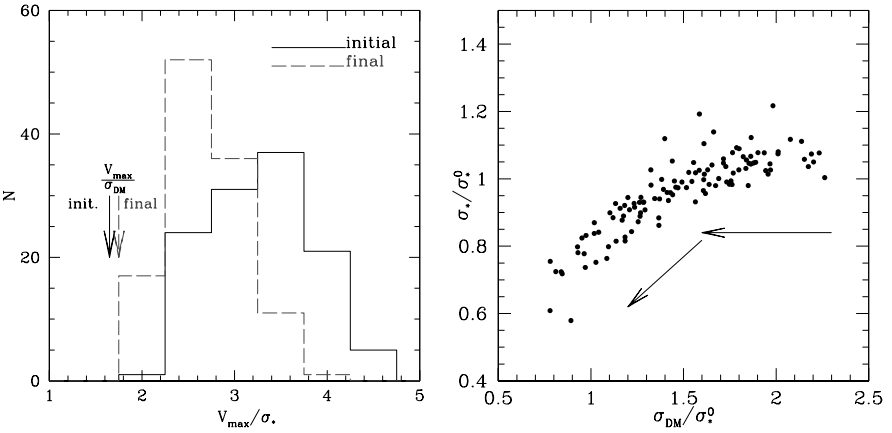

Figure 4. *Left:* Histogram of the ratio of satellite halo $V_{\rm max}$ to central stellar velocity dispersion σ_* for satellites before accretion (solid) and as subhalos at $z = 0$ (dashed). For reference the characteristic ratios of halo $V_{\rm max}$ to central *dark matter* velocity dispersions are indicated by the arrows. Note that dwarfs evolve in such a way that the mapping between σ_* and $V_{\rm max}$ was always larger before accretion. *Right:* Stellar velocity dispersion of $z = 0$ dwarfs as a function of central dark matter velocity dispersion, both normalized by the central stellar velocity dispersion that each satellite had before accretion (σ_*^0). Arrows indicate a qualitative evolutionary trend: the stellar velocity dispersion remains roughly constant until the dark matter is stripped to a point where $\sigma_{DM} \lesssim 1.5\sigma_*^0$, after which the stellar material is stripped along with the dark matter.

finer stepping in orbital evolution than some of the previous authors. For comparison, the small dots in the right panel of Figure 3 reproduce the results of Kravtsov et al. (2004), who used cosmological simulations to investigate the same phenomena. The results are broadly in agreement, although the cosmological simulation results show significantly more scatter. It is possible that the limited particle number in those simulations is responsible for the increased scatter. It is also possible that the idealized nature of our work produces a smaller scatter than would otherwise be expected.

Evolution of the Stellar Component

As discussed in conjunction with Figure 1, the stellar material in accreted dwarfs is more tightly bound than the dark matter and (even at a fixed radius) samples a different distribution function. For example, the central projected stellar velocity dispersions, σ_* of our model dwarf galaxies remain quite stable even as the dark matter is stripped. This effect is illustrated in Figure 4 where the left panel shows the histogram of the ratio of $V_{\rm max}/\sigma_*$ for satellite halos before accretion (solid) and at $z = 0$ (dashed). Note that because the total mass (represented by $V_{\rm max}$) tends decrease more quickly than than σ_*, the

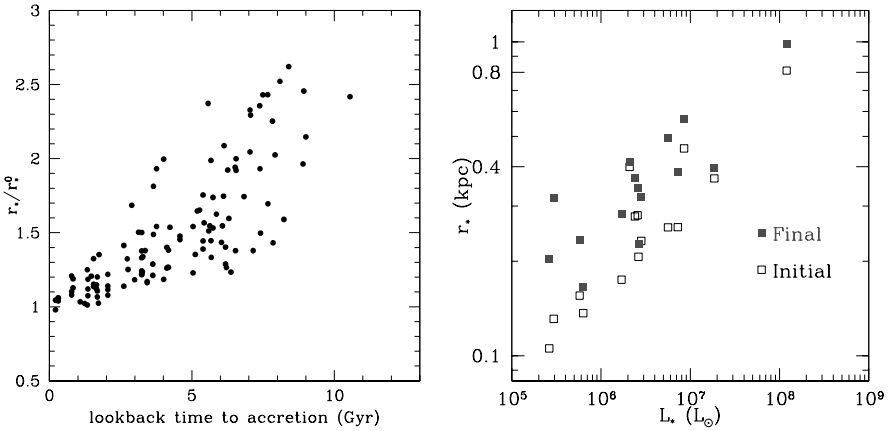

Figure 5. *Left:* The ratio of projected half-light radius at $z = 0$ to projected half-light radius before accretion (r_*/r_*^0) as a function of the lookback time to each satellites accretion. *Right:* Projected half-light radius (r_*) of dwarf galaxies for one of our halo realizations before accretion (open) and at $z = 0$ (solid) as a function of satellite luminosity. Note that the stellar distributions expand significantly without significant stellar mass loss.

ratio ($V_{\rm max}/\sigma_*$) is always larger before accretion than at the current epoch. We expect this trend to be true regardless of the galaxy formation scenario adopted. Indeed, in our models the stellar velocity dispersion start off much smaller than the central dark matter velocity dispersions (solid arrow) and the halos evolve to bring the stellar and dark matter velocity dispersions towards similar values (dashed arrow).

The velocity dispersion of the *dark matter* falls monotonically as the satellites evolve and mass is stripped. The right panel of Figure 4 shows the *final* central stellar velocity dispersion of our satellite galaxies in units of their *initial* stellar velocity dispersion, σ_*/σ_*^0, plotted as a function of the central *dark matter* velocity dispersion in the same units, σ_{DM}/σ_*^0. The arrows guide the following qualitative interpretation: the stellar velocity dispersion remains relatively constant until stripping reduces the dark matter velocity dispersion to $\sigma_{DM} \lesssim 1.5\sigma_*$. After this, the stellar material becomes stripped along with the dark matter.

If dark matter mass loss occurs while the stellar velocity dispersion remains relatively constant, a natural expectation is that the radial distribution of stellar material will expand. The left panel of Figure 5 illustrates that this is indeed the case. Here we plot the ratio of the projected half-light radius, r_*, to the initial half-light, r_*^0, as a function of the lookback time of each satellite's accretion. We see the general trend that more evolved satellites (larger lookback time to

accretion) tend to have larger half-light radii. In some cases, the satellites have expanded by more than a factor of ~ 2.

The predicted expansion of our dwarf satellites is quite interesting in light of the work of McConnachie and Irwin (2006) who showed that the dwarf satellites of M31 have scale radii that are at least a factor of 2 bigger at fixed magnitude compared to the population of the Milky Way. In the right panel of Figure 5 we show that such a trend may result from the physical processes just described. Here we show r_* as a function of satellite luminosity, L_* for one of our Milky-Way size halos (Halo 2 from JB05). The solid points reflect our satellite galaxies at $z = 0$ and the open points show the same galaxies before accretion. It is clear from this figure that the systems have expanded *without significant stellar mass loss*. This result, in conjunction with evolutionary trends highlighted in the left hand panel of Figure 5 suggest that the satellites of M31 may have been accreted much earlier ($\gtrsim 4$ Gyr) than those of the Milky Way. Indeed, any set of physical processes which would have increased the likelihood of their halos to be stripped of material would cause this kind of expansion. If the phenomena we describe is indeed the cause of the mismatch, one prediction is that the relation between luminosity and stellar velocity dispersion should be nearly *identical* between the satellites of M31 and the Milky Way, even though the size - luminosity relation is different.

3. Discussion

Our main results may be summarized as follows:

- Upon accretion into larger dark matter halos, satellite galaxy halos evolve in such a way that they become smaller (less massive) but *more concentrated* with time: for a fixed maximum circular velocity $V_{\rm max}$, the radius where the rotation curve peaks decreases by $\sim 40\%$ compared to the "field" relation.

- As satellite halos evolve and lose mass within their background potentials, the *slope* of their inner rotation curves remain relatively constant, $V(r) \propto r^{0.5}$ for an initial NFW halo.

- Stellar velocity dispersions in accreted dwarfs remain roughly constant for the first several Gyr even while the dark matter mass decreases. Only when tidal stripping reduces the *dark matter* velocity dispersion to a value similar to that of the initial *stellar* velocity dispersion do stars begin to be lost. The result is that the ratio $(V_{\rm max}/\sigma_*)$ is always larger before accretion than it is at $z = 0$.

- The surface brightness profiles in accreted dwarf galaxies tend to expand as their dark matter halos are stripped. In many cases $z = 0$ satellites

will have expanded by a factor of ~ 2 or more from their "original" size (prior to accretion).

- Recent indications that the dwarf satellites of M31 are a factor of ~ 2 larger than the dwarf population of the Milky Way (McConnachie and Irwin 2006) may be explained by the tendency for dwarf galaxies to expand during their orbital evolution. Our results suggest that the M31 dwarfs are more significantly affected by their tidal environment, perhaps because they were accreted, on average, much earlier than the dwarf satellites around the Galaxy.

Our results regarding the evolution of the dark matter halos of dwarf galaxies are qualitatively in line with those of Kazantzidis et al. (2004), however our results rely on a much larger number of simulated systems whose initial conditions (orbits, accretion times, NFW concentrations) were set by cosmological expectations for the merger histories of Milky Way type halos.

Indeed, understanding the LCDM expectation for the shape of subhalo circular velocity curves is essential for interpreting the mismatch between the predicted velocity function of subhalos and the *inferred* number of dwarf satellites (Klypin et al. 1999; Moore et al. 1999). In order reasonably compare the number of dwarf galaxies observed to the predicted velocity function, one must infer each dwarf satellite's subhalo $V_{\rm max}$ using the observed *stellar* central velocity dispersion σ_*. This mapping depends sensitively on the precise shape of each satellite's rotation velocity curve. If a dwarf galaxy sits in a dark halo with a very slowly rising rotation curve then the multiplicative factor that converts σ_* to $V_{\rm max}$ can be quite large (see Zentner and Bullock 2003 and references therein). Stoehr et al. (2002) have suggested that substructure halos experience significant mass redistribution in their centers as a result of tidal interactions and that they are therefore less concentrated than comparable halos in the field. They argue that when this is taken into account, the dwarf satellite problem may be explained by a sudden onset of "dark" halos at a fixed *current* $V_{\rm max}$ value. Our results suggest that this is incorrect. The rotation curves of subhalos retain their initial central slope and they peak at a *smaller* radius than do halos in the field (for fixed $V_{\rm max}$). This implies that the multiplicative factor that converts an observed σ_* to a halo $V_{\rm max}$ should be *smaller* than otherwise expected. Indeed these conclusions are in line with those of Kazantzidis et al. (2004).

Whatever one believes the *current* ratio of $(V_{\rm max}/\sigma_*)$ is, our results on the evolution of *stellar* material in an orbiting subhalo suggest that this ratio must have been *larger* in the past. If one believes, for example, that Draco ($\sigma_* \simeq 9{\rm km\,s^{-1}}$) sits in a fairly massive dark matter halo today (e.g., $V_{\rm max} \simeq 35{\rm km\,s^{-1}}$, from Stoehr et al. 2002) then it is quite likely that it formed and was accreted within an even more massive dark matter halo ($V_{\rm max} \simeq 70{\rm km\,s^{-1}}$?).

In this case one might argue that this makes the "dwarf satellite problem" even worse, because now one must explain why this fairly substantial halo has retained only $\lesssim 1\%$ of its baryons, while a similarly sized system, the LMC, seems to have retained a fairly large fraction of its baryons in comparison. Kravtsov et al. (2004) have explored the role of interactions in explaining the abundances of dwarf satellite galaxies in a related context. Including the expected evolution of of stellar material in this analysis may prove to be an important step in future work on the issue, especially in any attempt to identify "fossils of reionization" as discussed by Gnedin and Kravtsov (2006).

Acknowledgements The authors wish to thank Brant Robertson, Andreea Font, and Andrey Kravtsov for useful discussions. KVJ's contribution was supported through NASA grant NAG5-9064 and NSF CAREER award AST-0133617. JSB is supported by the Center for Cosmology at UC Irvine. We would like to thank Piet van der Kruit, Roelof de Jong, and the rest of the organizers for an enjoyable and productive conference.

References

Bullock, J. S. and Johnston, K. V. 2005, ApJ 635, 931

Bullock, J. S., Kravtsov, A. V., and Weinberg, D. 2000, ApJ 539, 517.

Bullock, J. S., Kolatt, T. S., Sigad, Y., Somerville, R. S., Kravtsov, A. V., Klypin, A. A., Primack, J. R., and Dekel, A. 2001, MNRAS 321, 559

Gnedin, N. Y. and Kravtsov, A. V. 2006, astro-ph/0601401

Hayashi, E., Navarro, J. F., Taylor, J. E., Stadel, J., and Quinn, T. 2003, ApJ 584, 541

Kazantzidis, S., Mayer, L., Mastropietro, C., Diemand, J., Stadel, J., and Moore, B. 2004, ApJ 608, 663

Klypin, A., Kravtsov, A. V., Valenzuela, O., and Prada, F. (1999). Where Are the Missing Galactic Satellites? ApJ 522, 82

Kravtsov, A. V., Gnedin, O. Y., and Klypin, A. A. 2004, ApJ 609, 482

Lacey, C. and Cole, S. 1993, MNRAS 262, 627

McConnachie, A. W. and Irwin, M. J. 2006, MNRAS 365, 1263

Metcalf, R. B. 2005, ApJ 622, 72

Moore, B., Ghigna, S., Governato, F., Lake, G., Quinn, T., Stadel, J., and Tozzi, P. 1999, ApJL 524, L19

Somerville, R. S. and Kolatt, T. S. 1999, MNRAS 305, 1

Stoehr, F., White, S. D. M., Tormen, G., and Springel, V. 2002, MNRAS 335, L84

Wechsler, R. H., Bullock, J. S., Primack, J. R., Kravtsov, A. V., and Dekel, A. 2002, ApJ 568, 52

Zentner, A. R. and Bullock, J. S. 2003, ApJ 598, 49

James Bullock and Annette Ferguson.

RESOLVING THE STELLAR OUTSKIRTS OF M31 AND M33

Annette Ferguson[1], Mike Irwin[2], Scott Chapman[3], Rodrigo Ibata[4], Geraint Lewis[5] and Nial Tanvir[6]

[1]*Institute for Astronomy, University of Edinburgh, UK*
[2]*Institute of Astronomy, University of Cambridge, UK*
[3]*California Institute for Technology, Pasadena, USA*
[4]*Observatoire de Strasbourg, Strasbourg, France*
[5]*Institute of Astronomy, University of Sydney, Australia*
[6]*Centre for Astrophysics Research, University of Hertfordshire, UK*

Abstract Many clues about the galaxy assembly process lurk in the faint outer regions of galaxies. The low surface brightnesses of these parts pose a significant challenge for studies of diffuse light, and few robust constraints on galaxy formation models have been derived to date from this technique. Our group has pioneered the use of extremely wide-area star counts to quantitatively address the large-scale structure and stellar content of galaxies at very faint light levels. We highlight here some results from our imaging and spectroscopic surveys of M31 and M33.

Keywords: galaxies: halos - galaxies: stellar content - galaxies: structure -

1. Introduction

The study of galaxy outskirts has become increasingly important in recent years. From a theoretical perspective, it has been realised that many important clues about the galaxy assembly process should lie buried in these parts. Cosmological simulations of disk galaxy formation have now been carried out by several groups and have led to testable predictions for the large-scale structure and stellar content at large radii – for example, the abundance and nature of stellar substructure (e.g., Bullock & Johnston 2005, Font et al. 2005), the ubiquity, structure and content of stellar halos and thick disks (e.g., Abadi et al. 2005, Governato et al. 2004, Brook et al. 2005) and the age distribution of stars in the outer regions of thin disks (e.g., Abadi et al. 2003).

Bullock & Johnston (2005) find that Milky Way-like galaxies will have accreted 100-200 luminous satellites during the last 12 Gyr and that the

R. S. de Jong, Island Universes, 239–244.
© 2007 *Springer.*

signatures of this process should be readily visible at surface brightnesses of $V \sim 30$ magnitudes per square arcsec and lower. Although traditional surface photometry at such levels (roughly 9 magnitudes below sky) remains prohibitive, star count analyses of nearby galaxies have the potential to reach these effective depths (e.g., Pritchet & van den Bergh 1994). The requirement of a large survey area (to provide a comprehensive view of the galaxy) and moderate-depth imagery can now be achieved in a relatively straightforward manner using wide-field imaging cameras attached to medium-sized telescopes.

2. The INT WFC Surveys of M31 and M33

In 2000, we began a program to map the outer regions of our nearest large neighbour, M31, with the Wide-Field Camera equipped to the INT 2.5m. The success of this program led us to extend our survey to M33 in the fall of 2002. To date, more than 45 and 7 square degrees have been mapped around these galaxies respectively. Our imagery reaches to V$\sim$24.5 and $i\sim$23.5 and thus probes the top 3 magnitudes of the red giant branch (RGB) in each system. The raw data are pipeline-processed in Cambridge and source catalogues are produced containing positions, magnitudes and shape parameters. The M31 survey currently contains more than 7 million sources, and the M33 survey more than 1 million. Magnitude and colour cuts are applied to point-like sources in order to isolate distinct stellar populations and generate surface density maps (see Figure 1). The faint structures visible by eye in Figure 1 have effective V-band surface brightnesses in the range 29-30 magnitudes per square arcsec. Early versions of our M31 maps have been discussed in Ibata et al. (2001), Ferguson et al. (2002) and Irwin et al. (2005).

Results for M31

The left-hand panel of Figure 1 shows the distribution of blue (i.e. presumably more metal-poor) RGB stars in and around M31. A great deal of substructure can be seen including the giant stream in the south-east, various overdensities near both ends of the major axes, a diffuse extended structure in the north-east and a loop of stars projected near NGC 205.

Origin of the Substructure: Do the substructures in M31 represent debris from one or more satellite accretions, or are they simply the result of a warped and/or disturbed outer disk? We are addressing these issues with deep ground-based imagery from the INT and CFHT, Keck-10m spectroscopy and deep HST/ACS colour-magnitude diagrams (CMDs). Our findings to date can be summarized as follows:

- M31 has at least 12 satellites lying within a projected radius of 200 kpc. The bulk of these systems, the low-luminosity dwarf spheroidals, are

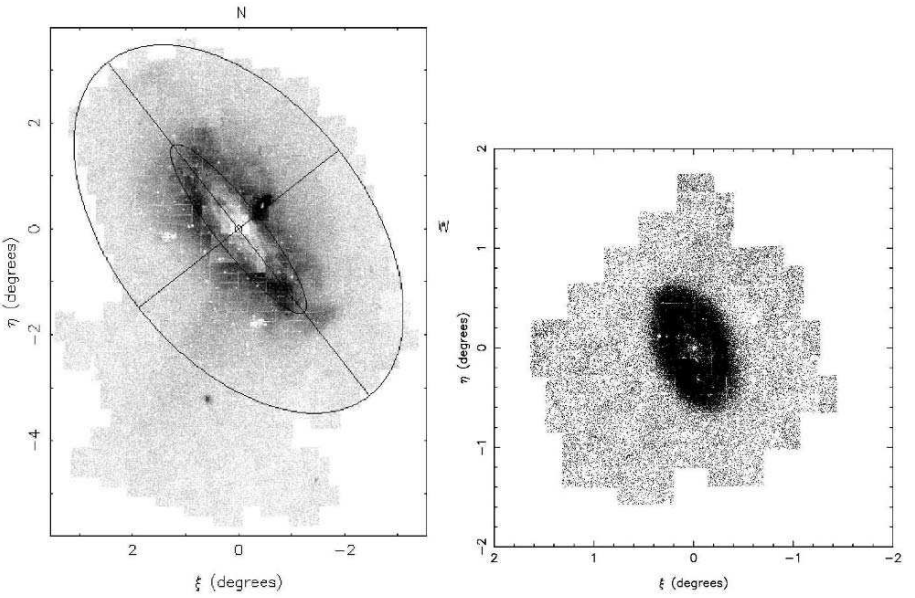

Figure 1. INT/WFC RGB star count maps of M31 (left panel) and M33 (right panel).

unlikely to be associated with the stellar overdensities since their RGB stars are much bluer than those of the substructure (Ferguson et al. 2002).

- The combination of line-of-sight distances and radial velocities for stars at various locations along the giant stellar stream constrains the progenitor orbit (e.g., McConnachie et al. 2003, Ibata et al. 2004). Currently-favoured orbits do not connect the more luminous inner satellites (e.g., M32, NGC 205) to the stream in any simple way however this finding leaves some remarkable coincidences (e.g., the projected alignment on the sky, similar metallicities) yet unexplained.

- Deep HST/ACS CMDs reaching well below the horizontal branch reveal different morphologies between most substructures in the outskirts of M31 (Ferguson et al. 2005, see Figure 2). These variations reflect differences in the mean age and/or metallicity of the constituent stellar populations. Analysis is underway to determine whether multiple satellite accretions are required, or whether consistency can be attained with a single object which has experienced bursts of star formation as it has orbited M31. The giant stream is linked to another stellar overdensity, the NE shelf, on the basis of nearly identical CMD morphologies and

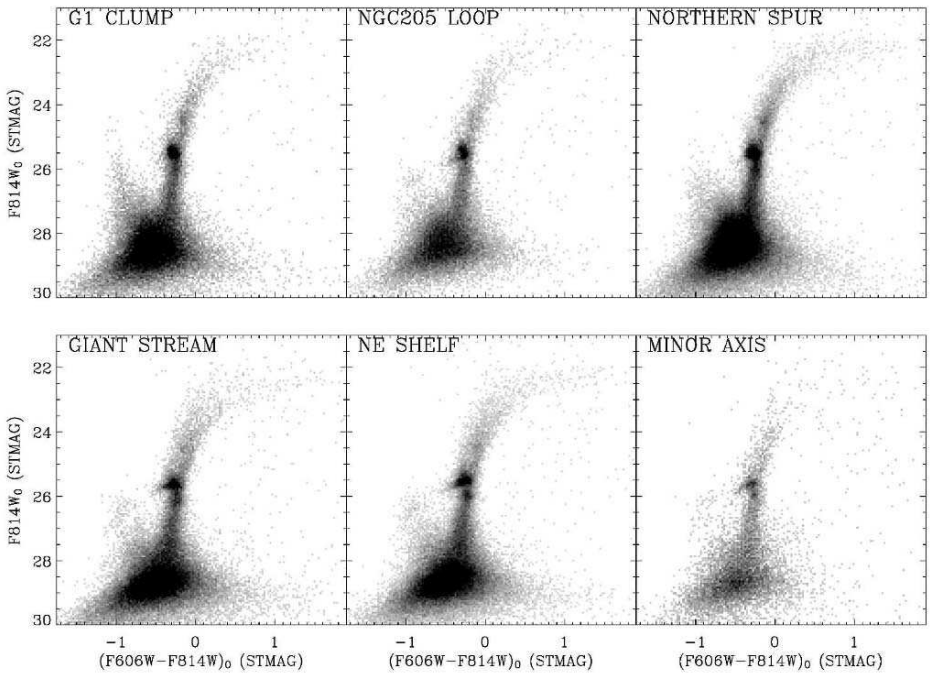

Figure 2. HST/ACS Hess diagrams of six halo fields in M31. Clear differences are apparent between most CMDs, indicating genuine stellar population variations between the substructures.

RGB luminosity functions; indeed, this coupling seems likely in view of progenitor orbit calculations (e.g., Ibata et al. 2004).

Smooth Structure: The INT/WFC survey provides the first opportunity to investigate the smooth underlying structure of M31 to unprecedented surface brightnesses. We have used the dataset to map the minor axis profile from the innermost regions to $\gtrsim 55$ kpc (Irwin et al. 2005). Figure 3 shows how the combination of inner diffuse light photometry and outer star count data can be used to trace the effective *i*-band surface brightness profile to ~ 30 magnitudes per square arcsec. The profile shows an unexpected flattening (relative to the inner $R^{1/4}$ decline) at large radius, consistent with the presence of an additional shallow power-law stellar component (index ≈ -2.3) in these parts. This component may extend out as far as 150 kpc (Guhathakurta, this conference). Taken together with our knowledge of the Milky Way halo, this finding supports the ubiquitous presence of power-law stellar halos around bright disk galaxies (see also Zibetti et al. 2004, Zibetti & Ferguson 2004).

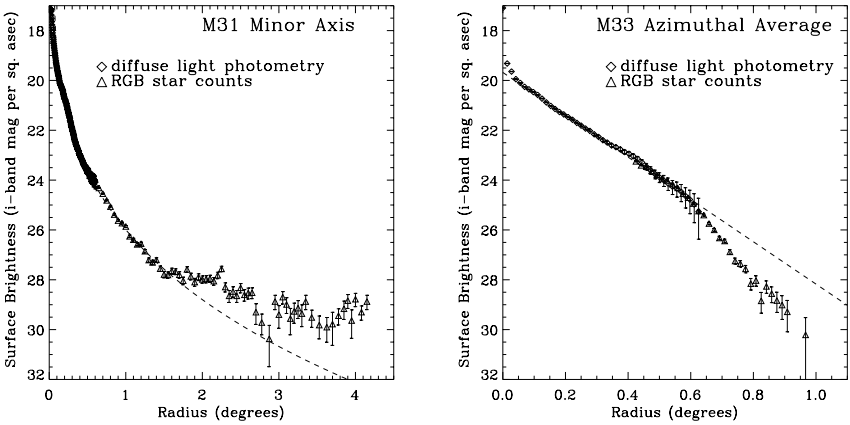

Figure 3. Effective *i*-band surface brightness profiles for M31 (left) and M33 (right). The inner points are derived from surface photometry and the outer ones from RGB star counts. Overplotted are a de Vaucouleurs $R^{1/4}$ law with $r_e = 0.1$ degrees (left panel) and an exponential profile with $r_0 = 0.1$ degrees (right panel).

The kinematics of M31's outer regions are being probed with Keck DEIMOS spectroscopy (e.g., Ibata et al. 2005). Two surprising results have emerged from our program so far. Firstly, there is a high degree of rotational support at large radius, extending well beyond the extent of M31's bright optical disk. Secondly, the overall coherence of this kinematic component is in striking contrast to its clumpy substructured appearance in the star count maps. Further work is underway to understand the nature and origin of this rotating component.

Results for M33

The right-hand panel of Figure 1 shows the RGB map of the low mass system, M33. Although it has the same limiting absolute depth as the M31 map, the stellar density distribution is extremely smooth and regular (Ferguson et al. 2006, in preparation). To a limiting depth of ~ 30 magnitudes per square arcsec (readily visible by eye here), the outer regions of M33 display no evidence for stellar substructure (c.f. the simulations of Bullock & Johnston 2005). Equally surprising, our analysis of the isophote shape as a function of radius indicates no evidence for any twisting or asymmetries. M33 appears to be a galaxy which has evolved in relative isolation.

The radial *i*-band profile of M33 has been quantified via azimuthally-averaged photometry in elliptical annuli of fixed PA and inclination (Figure 3). The

inner parts of the profile are constructed from diffuse light photometry, whereas the outer regions are derived from RGB star counts. The luminosity profile displays an exponential decline out to ~ 8 kpc (roughly 4.5 scalelengths) beyond which it significantly steepens. This behaviour is reminiscent of the "disk truncations" first pointed out by van der Kruit in the 80's, but until now not seen directly with resolved star counts. The steep outer component dominates the M33 radial light profile out to at least 14 kpc and limits the contribution of any shallow power-law stellar halo component in M33 to be no more than a few percent of the disk luminosity (Ferguson et al. 2006, in preparation).

3. Future Work

Quantitative study of the faint outskirts of galaxies provides important insight into the galaxy assembly process. The outskirts of our nearest spiral galaxies, M31 and M33, exhibit intriguing differences in their large-scale structure and stellar content. While M31 appears to have formed in the expected hierarchical fashion, M33 shows no obvious signatures of recent accretions. Observations of the outer regions of additional galaxies are required to determine which of these behaviours is most typical of the general disk population.

References

Abadi, M. G., Navarro, J. F., Steinmetz, M., & Eke, V. R. 2003, ApJ, 597, 21

Abadi, M. G., Navarro, J. F., & Steinmetz, M. 2005, astro-ph/0506659

Brook, C. B., Veilleux, V., Kawata, D., Martel, H., & Gibson, B. K. 2005, astro-ph/0511002

Bullock, J. S., & Johnston, K. V. 2005, astro-ph/0506467

Ferguson, A. M. N., Irwin, M. J., Ibata, R. A., Lewis, G. F., & Tanvir, N. R. 2002, AJ, 124, 1452

Ferguson, A. M. N., Johnson, R. A., Faria, D. C., Irwin, M. J., Ibata, R. A., Johnston, K. V., Lewis, G. F., & Tanvir, N. R. 2005, ApJL, 622, L109

Font, A. S., Johnston, K. V., Bullock, J. S., & Robertson, B. 2005,astro-ph/0507114

Governato, F., et al. 2004, ApJ, 607, 688

Ibata, R., Irwin, M., Lewis, G., Ferguson, A. M. N., & Tanvir, N. 2001, Nature, 412, 49

Ibata, R., Chapman, S., Ferguson, A. M. N., Irwin, M., Lewis, G., & McConnachie, A. 2004, MNRAS, 351, 117

Ibata, R., Chapman, S., Ferguson, A. M. N., Lewis, G., Irwin, M., & Tanvir, N. 2005, ApJ, 634, 287

Irwin, M. J., Ferguson, A. M. N., Ibata, R. A., Lewis, G. F., & Tanvir, N. R. 2005, ApJL, 628, L105

McConnachie, A. W., Irwin, M. J., Ibata, R. A., Ferguson, A. M. N., Lewis, G. F., & Tanvir, N. 2003, MNRAS, 343, 1335

Pritchet, C. J., & van den Bergh, S. 1994, AJ, 107, 1730

Zibetti, S., & Ferguson, A. M. N. 2004, MNRAS, 352, L6

Zibetti, S., White, S. D. M., & Brinkmann, J. 2004, MNRAS, 347, 556

CHEMICAL ABUNDANCE CONSTRAINTS ON GALAXY FORMATION

K.A. Venn

University of Victoria
kvenn@uvic.ca

Abstract According to current structure formation scenarios, dwarf galaxies are the fundamental building blocks of galactic evolution. The surviving systems thereby provide a unique laboratory for detailed study of the generic galactic assembly process and the chemo-dynamical evolution of the low-mass end of the galaxy distribution. In this proceedings, I will outline important differences in the chemistry of the stars in the dwarf satellite galaxies versus those of the stellar populations in the Galaxy, and discuss some pros and cons of various formation scenarios for the Galactic halo and thick disk.

Keywords: Galaxy: formation - Galaxy: abundances - galaxies: abundances - Galaxy: stellar content - galaxies: dwarf - Galaxy: halo

1. Introduction

How did the Galactic halo form? Is the outer halo filled with tidal streams from disrupted dwarf galaxies that remain coherent in phase space? (e.g., Bullock & Johnston 2005; Bullock et al. 2002; Font et al. 2001, 2005; Abadi et al. 2005)

How did the Galactic thick and thin disks form? Is the thick or thin disk a result of the merger of a dwarf galaxy (or a few dwarfs), particularly at intermediate epochs? (e.g., Abadi et al. 2003; Steinmetz et al. 2002; Navarro et al. 2004a, 2004b; Robertson et al. 2005)

One observational constraint for Galaxy formation via dwarf accretions is to determine the chemistry of the stars (especially. the old stars) in the Local Group dwarf galaxies. We have compared stellar abundances in seven nearby dSph systems to chemistry of nearby stars from various stellar populations in the Galaxy (see Venn et al. 2004, and data references therein). These stellar populations include the halo, thick disk, thin disk, and highly elliptical/extreme retrograde orbit stars; see Fig. 1.

R. S. de Jong, Island Universes, 245–252.
© 2007 *Springer.*

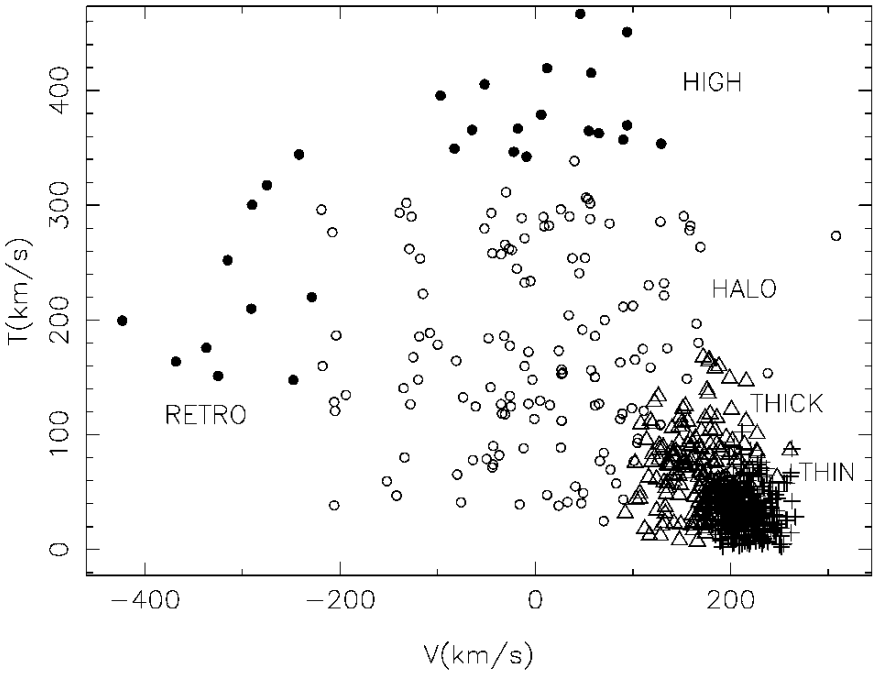

Figure 1. Toomre diagram showing stellar identifications using kinematic probabilities from velocity ellipsoids; thin disk (+), thick disk (empty triangles), halo (circles), highly elliptical and extreme retrograde orbits (filled circles). Adapted from Venn et al. (2004).

2. Galactic Halo and Dwarf Galaxies

A comparison of the [alpha/Fe] ratios of stars in the nearby dSph galaxies shows very little in common with similar metallicity stars in the Galactic halo (see Fig. 2). The alpha-elements are considered an average of the magnesium, calcium, and titanium abundances; all elements formed through alpha capture in massive stars (either in the CO-burning cores, or alpha-rich interior zones). The [alpha/Fe] ratio is important because it samples the relative contributions of SN II/ (SN II + SN Ia) which depends on the star formation history, the initial mass function, and also the retention of the SN products by the host galaxy. Thus, for stars in the same metallicity range in the Galaxy and its dwarf satellites, and with the same old ages, these stars do not have the same [alpha/Fe] ratios.

One subset of Galactic halo stars, those on true retrograde orbits relative to the 1 sigma Gaussian velocity distribution of the halo ($V \leq -200$ km/s) do overlap the low [alpha/Fe]of the dSphs. However, this may be a coincidence and represent small number statistics because high resolution spectroscopic

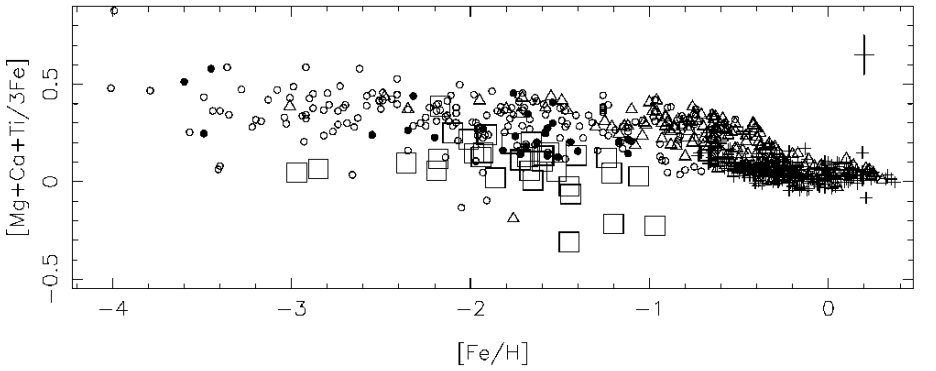

Figure 2. [alpha/Fe] abundances for Galactic stars and those in seven nearby dSph galaxies (large squares). The Galactic stellar populations are defined in Fig. 1. with additional metal-poor stars without kinematics assigned to the halo. Adapted from Venn et al. (2004).

analyses provide other elemental abundance ratios (next paragraph) that do not overlap as well.

The s- and r-process abundances are also sensitive to the star formation history in a galaxy. While there is ongoing debate on the number of r-processes, their sites, and their precise yields, r-process enrichment is linked to massive star evolution. Similarly, there is debate as to the s-process yields (particularly how they vary with the metallicity of the progenitor star), however the s-process enrichment is generally linked to intermediate mass stars through nucleosynthesis in the AGB phase. Thus, determination of the s- and r-process ratios is another unique way to fingerprint and ideally determine the conditions in a host galaxy during the formation of the stars we now see as red giants.

Some s- and r-process ratios, e.g., [Ba/Fe], [Eu/Fe], are in very good agreement between the Galactic halo stars and stars in the dSph galaxies. This implies that their r-process contributions are similar. However, the [Y/Eu] and [Ba/Y] ratios are not in good agreement. Yttrium, produced by the weak r-process and in the s-process, is significantly underabundant in the dSph stars (see Fig. 3). The s-process contribution to Y in the dSphs is probably due to a larger fraction of contributions from metal-poor AGB stars. During the s-process, if there is a lack of seed Fe atoms in a storm of neutrons, then it is thought that they will continue to collect neutrons and overproduce the second and/or third s-process peak elements (like Ba and Pb) at the expense of the first s-process peak elements (like Y); e.g., Travaglio et al. (2003). To confirm that the dSph have been enriched by metal-poor AGB stars requires determination of the lead (Pb) abundance in the red giants; however, there are no Pb I transitions available in our VLT UVES spectra (Shetrone et al. 2003). Nevertheless,

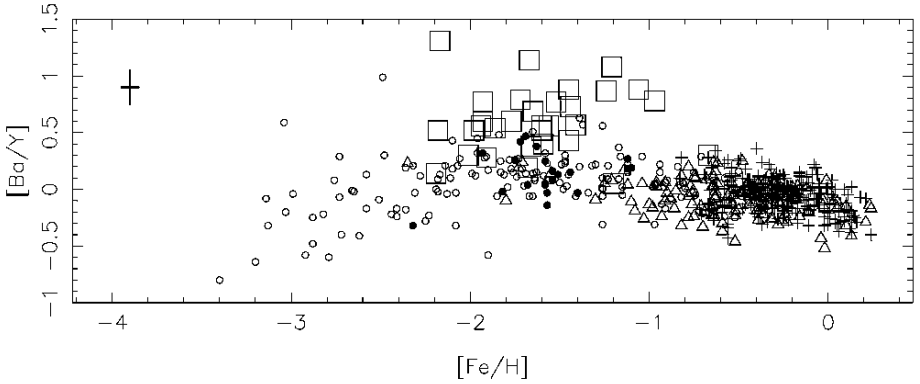

Figure 3. A sample of r- and s-process abundance ratios. The [Ba/Y] in Galactic stars is clearly offset from the values seen for most of the stars analysed in the dSph galaxies. Adapted from Venn et al. (2004).

it is clear that the stars in the dSph do not resemble those of any kinematic subset of stars in the Galactic halo.

3. Why are the dSph Stars Chemically Different from those in the Galactic Halo?

Since the CDM model is very successful in explaining structure in the Universe, then how is it that the dwarf satellites around the Galaxy have stars with unique chemistries from the Galactic halo?

LMC sized satellites dominate? One possibility is that larger dwarf galaxies (like the dIrr's, or the LMC) dominated the formation of the Galaxy. In this case, the chemistry of the old stars in the dIrrs needs to be determined. With current equipment, the old red giants in the (more distant) dIrr's in the Local Group are too faint for high resolution spectroscopic analyses. Only stars in the Magellanic Clouds are accessible. Analysis of $\sim$100 red giants in various fields in the LMC is currently underway (e.g., Pompeia et al. 2005), with preliminary results suggesting that the [alpha/Fe] ratios in these stars are low like in the dSphs, even in the most metal-poor of the target stars. Also, the ratio of the light s- and r-process elements again seem lower than similar stars in the Galaxy.

Merging dominated at early epochs? A second possibility is that all of the merging to form the Galaxy happened at very early epochs; before significant star formation occurred in the dwarf galaxies. If so, then the oldest stars (presumably the most metal-poor stars) in the dSph galaxies should have similar abundances. Our work on the Sculptor dSph may show some agreement (Hill et al. 2005), with [alpha/Fe] ratios reaching the Galactic halo plateau values

near metallicities of [Fe/H]$= -1.8$. It is not yet clear if other dSph galaxies will show a similar pattern.

Surviving satellites different from protogalactic fragments? A third possibility is that the protogalactic fragments that formed the Galactic halo were fundamentally different from the surviving dwarf galaxies that we see as the nearby dSphs today. This is usually attributed to an environmental effect; that the fragments that merged into the Galaxy were located deeper within the Galactic potential, and therefore would have had a different SFH and chemical evolution relative to the more isolated (surviving) dwarf galaxies that we see today. The only way to address this question is to ascertain the effects of environment on several of the star formation properties of dwarf galaxies (the IMF, feedback, effects of outflows, etc); general questions that interest many astronomers.

4. Galactic Thick Disk and Dwarf Galaxies

Chemically the thick disk of the Galaxy is unusual. Thick disk stars have higher [alpha/Fe] ratios than thin disk stars at similar metallicities, and have higher metallicities than most Galactic halo stars; see Fig. 2. This observational result is most compelling from the differential analyses (e.g., Bensby et al. 2003; Reddy et al. 2003; Brewer & Carney 2005). This is an important observational constraint since it implies that the thick disk reached a fairly high metallicity with $\sim$only SN II products. Thus, star formation had to be rapid so that SNIa did not lower the [alpha/Fe] ratios by contributing only [Fe/H] (iron, without alpha-elements).

While there are currently several excellent and improving N-body and semi-analytical simulations to form the thick disk, there seems to be at least one scenario that can be ruled out from the stellar chemical abundances. This would be the scenario that the thick disk stars are the stellar remnant of the merger of a dwarf galaxy, one like those currently analysed in the Local Group (i.e., dSphs, dIrrs, and the LMC), at intermediate epochs. Ancient mergers, or mergers of dwarf galaxies unlike those currently examined (chemically) in the Local Group, are not ruled out (e.g., Gilmore et al. 2002).

Examination of the estimated [alpha/Fe] ratios in Fig. 4 show that the thick disk does not resemble the chemistry of the stars in the dSph galaxies (Shetrone et al. 2001, 2003; Geisler et al. 2005, Bonifacio et al. 2004; Monaco et al. 2005), nor the available and preliminary abundances in the LMC (Hill et al. 2000, 2004; Pompeia et al. 2005). Examination of young, massive stars in the more distant and isolated dIrr galaxies also do not resemble the thick disk. This includes abundances from A-type supergiants in NGC 6822, WLM, and Sextans A (Venn et al. 2001, 2003; Kaufer et al. 2004).

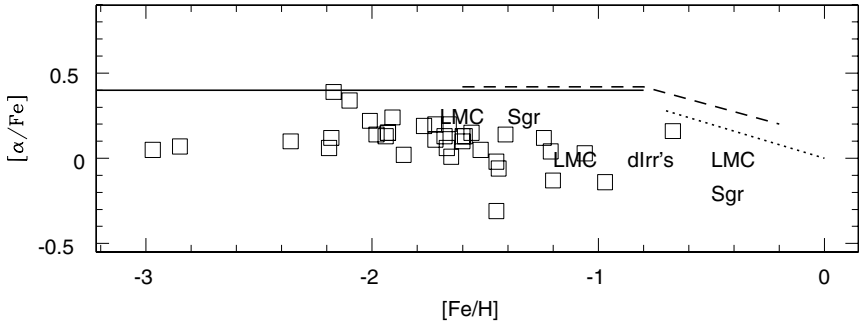

Figure 4. Cartoon showing estimated [alpha/Fe] ratios for Galactic halo (solid line), thick disk (dashed line), and thin disk (dotted line) stars. Also, the positions of the stars in seven dSph galaxies, and estimated locations of stars and clusters in the LMC, the Sgr dwarf, and for massive stars in the dIrr galaxies (see text for references).

The connections between the formation of the thick disk and that of the thin disk are also unusual since stars in the thin disk have lower [alpha/Fe] ratios at similar metallicities. While there are several models to explain this, a common theme, and from a purely chemical view, is that the thick disk gas is diluted by alpha-poor and iron-poor gas, e.g., more pristine, less chemically evolved gas, and flattens into the thin disk with later star formation. If so, then to explain the offset found in the differential analyses comparing thin and thick disk stars, $\geq 30\%$ of the thin disk gas would need to be pristine.

5. Summary

The chemistry of stars in the Local Group dwarf galaxies has allowed us to address questions related to the formation of the Milky Way. Stars in the Galactic halo appear to be chemically distinct from the current data for stars in the dwarfs. This suggests either that merging happened at very early epochs before significant chemical evolution occurred in the dwarfs, or that the protogalactic fragments were different from the remaining (surviving) dwarf galaxies, possibly due to their environment. Stars in the Galactic thick disk also appear to be chemically distinct from those in the dwarf galaxies. This suggests that the thick disk is not the stellar remnant of the merger of a dwarf galaxy at intermediate epochs, at least not a dwarf galaxy that had a similar chemical evolution to any of those we currently see in the Local Group.

Acknowledgements Many thanks to the DART team for an exciting project and inspiring collaborators, especially Eline Tolstoy. KAV thanks the National Science Foundation for support through a CAREER award, AST 99-84073.

References

Abadi M.G., Navarro J.F., Steinmetz M., Eke V.R., 2003, ApJ, 597, 21

Abadi M.G., Navarro J.F., Steinmetz M., 2005, MNRAS, submitted (astro-ph/0506659)

Bensby T., Feltzing S., Lundström I., 2003, A&A, 410, 527

Brewer M., Carney B.W., 2005, AJ, in press (astro-ph/0509267)

Bonifacio P., Sbordone L, Marconi G., Pasquini L., Hill V., 2004, A&A, 414, 503

Bullock J.S., Johnston K.V., 2005, ApJ, submitted, (astro-ph/0506467)

Bullock J.S., Wechsler R.H., Somerville R.S., 2002, MNRAS, 329, 246

Font A.S., Johnstone K.V., Bullock J.S., Robertson B., 2005, ApJ, submitted (astro-ph/0507114)

Font A.S., Navarro J.F., Stadel J., Quinn T., 2001, ApJL, 563, 1

Gilmore G., Wyse R.F.G., Norris J.E., 2002, ApJ, 574, 39

Geisler D., Smith V.V., Wallerstein G., Gonzalez G., Charbonnel C., 2005, AJ, 129, 1428

Hill V., Francois P., Spite M., Primas F., Spite F., 2000, A&A, 364, 19

Hill V., 2004, in "Origin and Evolution of the Elements" from the Carnegie Observatories Centennial Symposia, Cambridge University Press, Eds. A. McWilliam and M. Rauch, p. 205

Hill V., Venn K.A., Tolstoy E., et al., 2005, A&A, in prep.

Kaufer A., Venn K.A., Tolstoy E., Pinte C., 2004, AJ, in press (astro-ph/0401411)

Monacoo L, Bellazini M., Bonifacio P., Ferraro F.R., Marconi G., Pancino E., Sbordone L., Zaggia S., 2005, A&A, 441, 141

Navarro J.F., Helmi A., Freeman K.C., 2004a, ApJL, 601, 43

Navarro J.F., 2004b, in "Penetrating Bars through Masks of Cosmic Dust", astro-ph/0405497

Pompeia L., 2005, in "From Lithium to Uranium: Elemental Tracers of Early Cosmic Evolution", IAU Symp. 228, eds. V. Hill, P. Francois, F. Primas.

Reddy B.E., Tomkin J., Lambert D.L., Allende-Prieto C., 2003, MNRAS, 340, 304

Robertson B., Bullock J.S., Font A.S., Johnstone K.V., Hernquist L., 2005, ApJ, 632, 872

Shetrone M.D., Côté P., Sargent W.L.W., 2001, ApJ, 548, 592

Shetrone M.D., Venn K.A., Tolstoy E., Primas F., Hill V., Kaufer A., 2003, AJ, 125, 684

Steinmetz M., Navarro J.F., 2002, New A, 7, 155

Travaglio C., Gallino R., Arnone E., Cowan J., Jordan F., Sneden C., 2003, ApJ, 601, 864

Venn K.A., Lennon D.J., Kaufer A., McCarthy J.K., Przybilla N., Kudritzki R.P., Lemke M., Skillman E.D., Smartt S.J., 2001, ApJ, 574, 765

Venn K.A., Tolstoy E., Kaufer A., Skillman E.D., Clarkson S., Smartt S.J., Lennon D.J., Kudritzki R.P., 2003, AJ, 126, 1326

Venn K.A., Irwin M.J., Shetrone M.D., Tout C., Hill V., Tolstoy E., 2004, AJ, 128, 1177

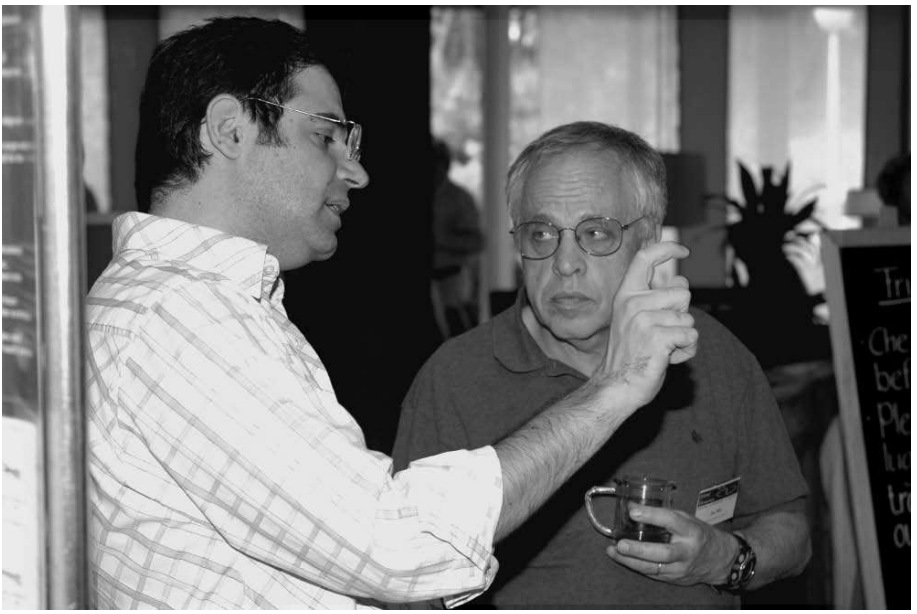

To tea or

to coffee?
Top: João Alves and Joe Silk. *Bottom:* Ignacio Trujillo and Michael Pohlen.

THE OUTER DISKS OF GALAXIES: "TO BE OR NOT TO BE TRUNCATED?"

Michael Pohlen[1] and Ignacio Trujillo[2]

[1]*Kapteyn Astronomical Institute, University of Groningen, The Netherlands*
[2]*Max–Planck–Institut für Astronomie, Heidelberg, Germany*

Abstract We have in recent years come to view the outer parts of galaxies as having vital clues about their formation and evolution. Here, we would like to briefly present our results from a complete sample of nearby, late-type, spiral galaxies, using data from the SDSS survey, especially focused on the stellar light distribution in the outer disk. Our study shows that only the minority of late-type galaxies show a classical, exponential Freeman Type I profile down to the noise limit, whereas the majority exhibit either downbending (stellar truncation as introduced 1979 by Piet van der Kruit) or upbending profiles.

Keywords: galaxies: structure - surveys

1. Historical Introduction

Why study outer disks? The structure of galactic disks is of fundamental importance for observationally addressing the formation and evolution of spiral galaxies. Especially the *outer edges* of disk galaxies are of interest, since substructure, the so called fossil evidence, is expected to be imprinted by the galaxy formation process. Recent formation and evolution scenarios suggest for example that galaxies continue to grow from the accretion and tidal disruption of satellite companions.

What is their shape? The general shape of the surface brightness profile of galactic disks is currently one of our favourite paradigms, namely a pure exponential disk. Its success is based solely on empirical evidence (albeit dating back now nearly 50 years) and has in fact never been fully physically motivated.

> In view of the great variety of structures among spirals ... there is good evidence, however, that at least in ordinary spirals the smoothed radial luminosity distribution is approximately exponential in the outer parts (de Vaucouleurs 1959)

R. S. de Jong, Island Universes, 253–258.
© 2007 *Springer.*

Eleven years later the nature of the disk was finally settled by Ken Freeman in his 1970 paper.

> Almost every disk-like galaxy with measured $I(R)$ shows an exponential disk ... and its origin is certainly a significant cosmogonic problem. (Freeman 1970)

However, only nine years later Piet van den Kruit indicated that the exponential nature does not hold to infinity, but

> [..] at the edges of the disk the decrease in apparent surface brightness is exceedingly steep. This sharp drop implies that galaxies do not retain their exponential light distribution to such faint levels. (van der Kruit 1979)

This marked the detection of truncations at a safe distance of ~ 4.5 times the radial scalelength, so the paradigm of the exponential disk was not in real danger at the time.

Where are they truncated? After van der Kruit and Searle's seminal papers about the structure of galactic disks (e.g., van der Kruit & Searle 1981), the matter of imperfectly exponential disks was rather ignored for some more ten years, until Barteldrees & Dettmar (1994) confirmed their existence using for the first time modern CCD equipment, but placed the cut-off closer to the center, for some galaxies at a disturbing close < 3 times the scalelength.

Finally starting from the year 2000 several groups (e.g., Pohlen et al. 2000; de Grijs et al. 2001; Florido et al. 2001; Kregel et al. 2002; Pohlen et al. 2002; Erwin et al. 2005a) followed up the question of where the disks are truncated, how the shape of the profile in the very outer parts looks like, and if all disks have a truncation. For a recent review see Pohlen et al. (2004).

To keep a long story short our answer is that we know now that not all galaxies are truncated, but those which are, are now believed to be truncated 'early' (at $\sim 3h$), often abruptly (but not completely) and the profiles are best described as a broken exponential and so probably better called *breaks* than *cut-offs*. The prototypical break is recently observed for M 33 by Ferguson et al. (2006) using the star-count method as an independent approach compared to the so far purely surface photometric measurements. The currently favoured origin for these breaks are global star-formation thresholds as described by Martin & Kennicutt (2001) or Schaye (2004), although this does not explain the origin of the material beyond the break (see Pohlen et al. 2004).

What next? What we still need is a complete census of the outer disk structure in the local universe extending the work done by Courteau (1996) and de Jong (1996) including a detailed discussion of the light profile in the outer region to answer our famous question: "To be or not to be (truncated)?". This is now done and will be presented briefly here and later in detail in Pohlen & Trujillo (2005, in prep.) for late-type galaxies and in Erwin et al. (2005b, in prep.) for early-type galaxies.

2. Sample

We used the LEDA online catalogue (the richest, most complete and up-to-date catalogue with homogeneous parameters of galaxies for the largest available sample) to select our initial galaxy sample using the following selection criteria: $2.99 < T < 8.49$ (Sb-Sdm), $\log r_{25} < 0.301$, $v_{\rm vir} < 3250$ km/s, $|b2| > 20^\circ$, and $M_{\rm abs} < -18.4$ B-mag. This leaves us with an unbiased, volume limited sample of late-type, face-on ($i \lesssim 60\,{\rm deg}$), nearby (local) disk galaxies (avoiding the Milky Way). Our sample complements the CCD imaging sample of $\sim$ 65 early-type SB0-SBb galaxies by Erwin et al. (2005b, in prep.). The actual data we use for our present study come from the Sloan Digital Sky Survey (SDSS, data release 2) providing images of $\sim 15\%$ (98/655) of the galaxies in our original LEDA sample.

3. Results

SDSS profiles: To convince the reader, and first of all ourselves, that SDSS images with a rather short exposure time of only $\sim$ 60s are indeed deep enough to trace the outer disk, we compared for three galaxies the SDSS images with deep surface photometry. The deep data is presented in Pohlen et al. (2002) and was obtained at the CAHA 2.2m telescope using CAFOS. The total exposure time of these images is about 3 hours reaching reliably down to $\mu_{\rm lim} = 27.2\,R$-mag arcsec^{-2}. As shown in Fig. 1 (for two of the galaxies) the agreement is astonishingly good, allowing us to safely use SDSS images to study the profile clearly beyond the break radius.

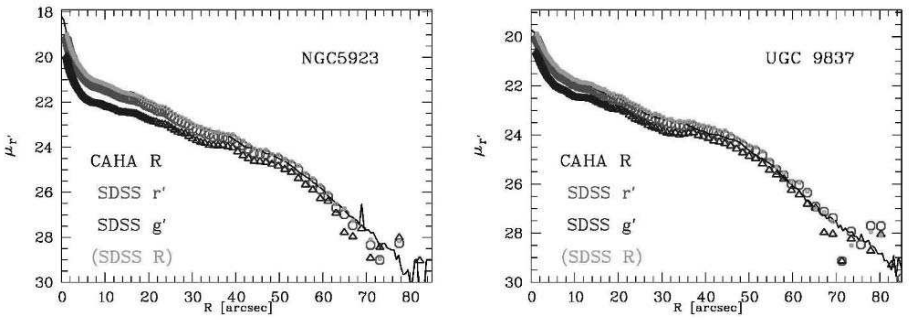

Figure 1. Comparison of the azimuthally averaged, radial surface brightness profiles from SDSS images with much deeper imaging by Pohlen et al. (2002). The small, green squares are produced by using the transformation to convert SDSS g' and r' into standard Johnson R-band following Smith et al. (2002).

Classification: We classify each galaxy profile by eye according to the following nomenclature. If there is no indication for any obvious break in the profile the galaxy is classified as Type I following Freeman (1970). In the same sense, galaxies showing a profile better described as a broken exponential with a clear break and a *downbending*, steeper outer region are defined here as Type II:

> Type II has $I(R) < I_0 \exp(-\alpha R)$ in an interval $R_1 < R < R_2$ not far from the center. (Freeman 1970)

This definition includes the class of truncated galaxies shown by Pohlen et al. (2002). Although "not far from the center" may suggest to exclude truncated galaxies (where the break is at several radial scalelengths) from this class, thus following quote allows us to generalise Ken's definition:

> It is worth pointing out that for the [...] galaxies in which the Type II characteristic is most prominent [e.g. NGC 7793], the exponential disk begins outside the main region of the spiral-arm activity. (Freeman 1970)

Finally, following Erwin et al. (2005a), galaxies showing a broken exponential profile with a break, but followed by an *upbending*, shallower outer region, are called Type III. Three proto-typical cases are shown in Fig. 2.

Frequencies and parameter distribution: The Type II class is split into several sub classes (discussed in detail by Pohlen & Trujillo, 2005, in prep.) but the majority, about $32.9\% \pm 5.1\%$ of the total sample, are what we call now *classical truncations* (Type CT), associated with those having a star formation threshold origin. An equal amount of galaxies (also 32.9%) are in fact *anti-truncated* and fall into the Type III class. Finally, only the minority ($15.3\% \pm 3.9\%$) of galaxies is barely consistent with being pure exponential disks of Type I.

We find indications for a trend with Hubble Type: Early-type galaxies (Sb-Sc) are more commonly Type III while Type CTs seem to be significantly more frequent in later types. Counting the neighbouring galaxies around each galaxy reveals the fact that Type III galaxies statistically prefer a high density, Type CT galaxies a low density environment. However, this relation is far from being clear-cut.

The break radius for galaxies with classical truncations, the ones discovered by Piet van der Kruit in 1979, happens in the r'-band at $R_{\rm break} = 2.5 \pm 0.6\, h_{\rm inner}$ ranging between 1.4 and 4.2. Since we can follow the profile of the Type I galaxies down to $\sim 6 - 8$ times their scalelength, they seem to be genuinely untruncated galaxies.

While the scalelength varies with filter (being larger in g' compared to r') as known before, we do not find a systematic difference for the break radius. We do, however, find that the distribution of the surface brightness at the break radius ($\mu_{\rm break}$) for galaxies with a classical truncation is peaked around a mean

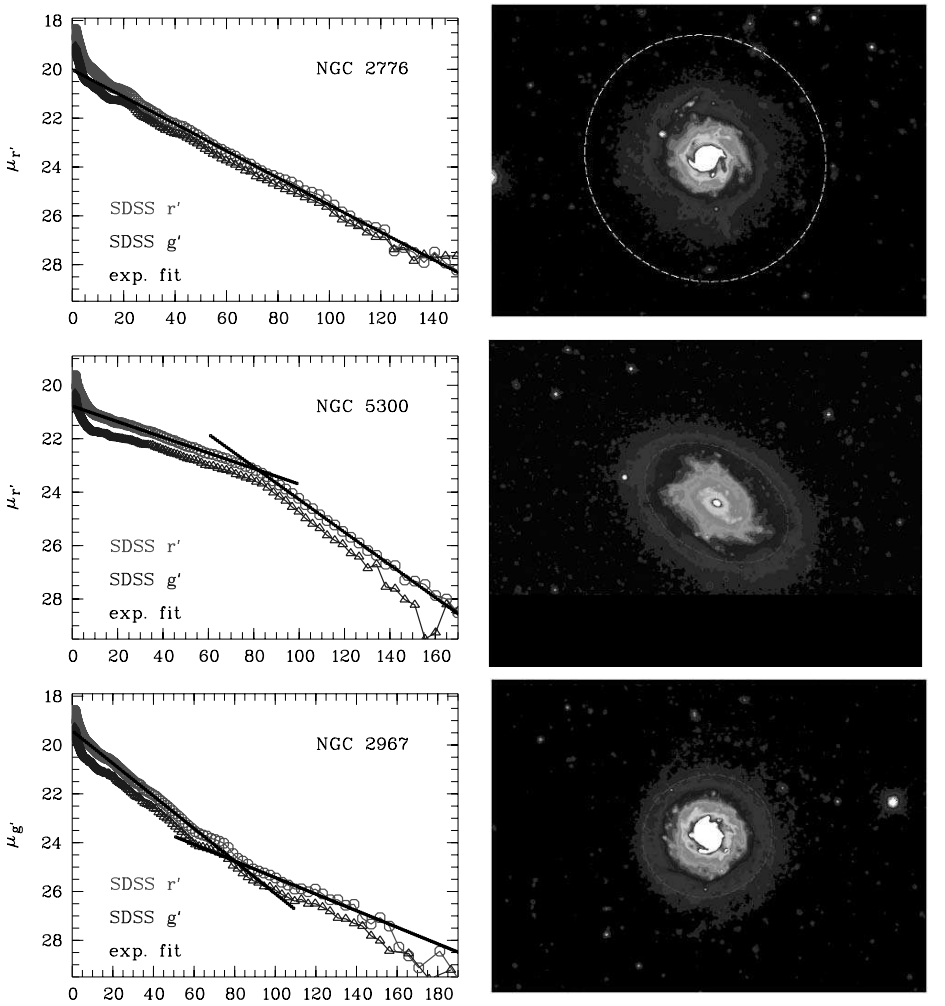

Figure 2. The three main disk types: Type I, Type CT, and Type III *(from top to bottom)*. Left column: Azimuthally averaged, radial (in units of [″]) SDSS surface brightness profiles in the g' and r'-band overlayed by r'-band exponential fits to the individual regions: single disk; inner and outer disk. Right column: r'-band images with the break radius marked as a red ellipse. The white ellipse for the first Type I galaxy corresponds to roughly the noise limit at $\sim 140''$.

value. Together with the absence of a relation between $R_{\rm break}/h_{\rm inner}$ and mass (rotational velocity), this favours a star formation threshold scenario for its origin.

4. Stellar Disks Truncations at High-z

Pérez (2004, 2006) showed that it is possible to detect truncations even out to high redshift ($z\sim1$). So we carefully defined a complete sample of high redshift galaxies (Trujillo & Pohlen, 2005) using the ACS data of the Hubble Ultra Deep Field. From the final sample of 36 galaxies, 21 show truncations. Now, using the position of the truncation as a direct estimator of the size of the stellar disk it becomes possible to outright observe inside-out growth of galactic disks comparing the ACS to our local SDSS sample. The results suggest that the radial position of the truncation has increased with cosmic time by $\sim$1–3 kpc in the last $\sim$8 Gyr indicating a small to moderate ($\sim$25%) inside-out growth of the disk galaxies since $z\sim1$ (see Trujillo & Pohlen, 2005).

Acknowledgements M.P. would like to thank Peter Erwin and John Beckman for their stimulating discussions and useful suggestions during this work. Part of this work was supported by a Marie Curie Intra-European Fellowship within the 6th European Community Framework Programme.

References

Barteldrees, A., & Dettmar, R.-J. 1994, A&AS, 103, 475
Courteau, S. 1996, ApJS, 103, 363
de Grijs, R., Kregel, M., & Wesson, K. H. 2001, MNRAS, 324, 1074
de Jong, R. S. 1996, A&A 313, 45
de Vaucouleurs, G. 1959, Handbuch der Physik, 53, 311
Erwin, P., Beckman, J. E., & Pohlen, M. 2005a, ApJ, 626, L81
Ferguson et al. 2006, these proceedings, p. 239
Florido, E., Battaner, E., Guijarro, A., Garzón, F., & Jiménez-Vicente, J. 2001, A&A, 378, 82
Freeman K. C. 1970, ApJ, 160, 811
Kregel, M., van der Kruit, P. C., & de Grijs, R. 2002, MNRAS, 334, 646
Martin, C. L., & Kennicutt, R. C., Jr. 2001, ApJ, 555, 301
Pérez, I. 2004, A&A, 427, L17
Pérez, I. 2006, these proceedings, p. 259
Pohlen, M., Dettmar, R.-J., & Lütticke, R. 2000, A&A, 357, L1
Pohlen, M., Dettmar, R.-J., Lütticke, R., & Aronica, G. 2002, A&A, 392, 807
Pohlen, M., Beckman, J. E., Hüttemeister, S. H., Knapen, J. H., Erwin, P., & Dettmar, R.-J. 2004, In Penetrating Bars through Masks of Cosmic Dust: The Hubble Tuning Fork Strikes a New Note, ed. D. L. Block, I. Puerari, K. C. Freeman, R. Groess, & E. K. Block (Dordrecht: Springer), 713
Schaye, J. 2004, ApJ, 609, 667
Smith, J.A., Tucker, D.L., Kent, S.M., et al. 2002, AJ, 123, 2121
Trujillo, I., & Pohlen, M. 2005, ApJ, 630, L17
van der Kruit, P. C. 1979, A&AS, 38, 15
van der Kruit, P. C., Searle, L., 1981, A&A 95, 105

RADIAL PROFILES OF STELLAR DISKS IN GALAXIES AT z≈1 FROM THE UDF AND THE GOODS FIELDS

Isabel Pérez

Kapteyn Astronomical Institute, University of Groningen, The Netherlands
isa@astro.rug.nl

Abstract Following the finding that a number of stellar disks at redshift ≈1 show radial profiles best fit by a double exponential (Pérez 2004), we have carried out a campaign to derive the radial profiles of a sample of galaxies from the Ultra Deep Field (UDF). Of the 19 UDF galaxies, six show double exponential profiles. The results are compatible with the previous study and there is no clear evidence for disk evolution. However, we do not detect any galaxy with a break radius larger than 2.5 scale-lengths, unlike the local galaxies where breaks are found up to around 4 scale-lengths. The colours of the truncated galaxies seem to be bluer than those of 'untruncated' galaxies, suggesting a younger population. The ratio between the inner and the outer scale-length is 2.0±0.5 in agreement with the results from the previous sample from GOODS data.

Keywords: galaxies: structure - galaxies: high-redshift - galaxies: evolution

1. Introduction

The new deep surveys carried out from space (i.e. GOODS, UDF) have opened the Pandora box in the study of the morphology of galaxies at high redshift. Disk galaxies are clearly recognised up to unprecedented redshifts and internal features such as bars can be clearly distinguished up to redshifts of about one. These new surveys have motivated us to study the shape of the radial disk profiles at high redshift and compare it to the observed profiles in nearby systems (Pérez 2004). The finite size of stellar disks was first reported by van der Kruit (1979), who showed that disks were sharply truncated at around 4 scale-lengths. Recently, evidence has arisen that this truncation does not occur sharply, but instead there is a break in the exponential radial profile, which is best fit by a double exponential shape (de Grijs et al. 2001; Pohlen et al. 2002). Recent work (Pohlen & Trujillo 2006) has shown, using the a sample of galaxies from the Sloan Digital Sky Survey (SDSS), that the

R. S. de Jong, Island Universes, 259–264.
© 2007 *Springer.*

R_{br}/h_{in} in the r' band is 2.5±0.6 with a range $1.4 - 4.2$; where R_{br}, the break radius, is the radius where the slope changes and h_{in} is the inner disk scale-length. A recent work by Hunter & Elmegreen (2006), shows that irregular galaxies also show this double exponential profile with a R_{br}/h_{in} ranging between 1.5 and 2.2. Different hypothesis for the origin of the double exponential have been proposed; origin related to a surface density threshold for star formation (Kennicutt 1989), related to the maximum specific angular momentum of the sphere from which the disk collapsed (van der Kruit 1987) or to the galactic magnetic force (Battaner et al. 2002). A study of the evolution of the truncation radius can help to discern among the different hypothesis for the formation of the double exponential. Such a project was carried out as a pilot survey using HST archival data (Pérez 2004). In Pérez (2004), double exponential galaxies were found (6 out of 12) with R_{br}/h_{in} of 1.8 ± 0.5. However, there was no conclusive result about the evolution of the break radius with redshift, due to the small number statistics and the uncertainties in the values found for the local galaxies. It was, however, clear that double exponential disks existed at $z \approx 1$. Other groups that have been working on the shape of disks galaxies at high redshift since then have been obtaining similar results (Trujillo & Pohlen 2005; Tamm & Tenjes 2005). The limiting magnitude of 26.7 in the z-band for the GOODS allows us to detect (with the criterion for detection of truncation used in this work, see below) breaks occurring at around $3 \times h_{in}$. The use of the UDF sample increases this detection to around $4 \times h_{in}$. Therefore, if there are some profiles with breaks similar to the local galaxies with $R_{br}/h_{in} \approx 4$ in the high-z sample, we ought to see them.

2. Sample and Profile Fitting

The new UDF sample was chosen similarly to the initial GOODS sample. The cosmological dimming ($\propto(1+z)^4$) determined our choice of the maximum redshift to reach the outermost isophotes ($\mu_B \approx 27.5$ mag arcsec^{-2}). The lower redshift limit was chosen to ensure a reasonable number of objects in the final sample, at a redshift where evolutionary effects should still be significant (Mao et al. 1998). A range of $0.6 < z < 1.0$ was finally chosen. This range implies a dimming between $2-3$ magnitudes with an isophotal threshold range between $27.5 - 26.5$ mag arcsec^{-2}. The z-band images were used for the analysis to ensure that the rest frame of the above galaxies (V and B-band) corresponds to the wavelength of widely observed local samples. The redshifts for the UDF fields were obtained from the ESO/VLT GOODS (Vanzella et al. 2004) and the COMBO 17 projects (Wolf et al. 2004). The galaxies were visually selected to be relatively symmetric and not strongly interacting. Hubble types range from Sa to Sc (our visual classification of the HST/ACS z-band images) and galaxy inclination angles (derived from the ellipticity of the

outermost isophote) are all less than 35°. Finally, a sample of 19 galaxies were selected. For statistic purposes, both samples were combined making a total of 35 galaxies.

Ellipse fitting to the light distribution was performed using the ELLIPSE task within IRAF. All the galaxies showed point-like nuclear regions. So, the centre was fixed using the coordinates obtained by fitting a Gaussian to the nucleus. The position angle (PA) and the ellipticity (e) were left as free parameters in the fitting. Profiles with fixed PA and e were also obtained, no influence in the break radius was found. The free PA$-e$ fitting profiles were chosen to determine whether there were any systematic relation between the position of morphological features with the truncation radius. No attempt was made to do a bulge-disk decomposition, and the disk was assumed to dominate the light profile beyond $\approx$ 1 scale-length, a good assumption for Sb and later types (de Jong 1996); see Pérez (2004) for a discussion on the implications of this fitting procedure. The sky background was subtracted by taking the mean value of boxes placed around the galaxies in regions far from the target galaxies. The standard deviation of the median of the distribution in the different boxes was adopted as the error in the background determination.

We then fit to the 1-D azimuthally averaged profile two exponential functions of form $I(\mathrm{R})^{\mathrm{in/out}} = I_0^{\mathrm{in/out}} e^{(-\mathrm{R}/\mathrm{h}_{\mathrm{in/out}})}$ (in refers to the inner disk and out to the outer exponential disk). The criterion used for detection of truncation was that the outer exponential should extend to at least $2 \times \mathrm{h}_{out}$ before reaching the noise level. The break radius was first visually determined, with an error around 12%. This value was used to separate the fitting regions for the inner and the outer exponentials; excluding the bulge region. The final break radius is defined as the radius where the two fitted exponential profiles cross. While the error in the inner scale-length is dominated by the effect of the bulge, the outer scale-length error is dominated by the determination of the break radius and the sky-subtraction.

3. Results

Of the 19 UDF galaxies, six show a double exponential profile, with a $\mathrm{R_{br}/h_{in}}$ of 1.8 ± 0.7. This result is similar to that found in the GOODS sample, where 6 out of 12 galaxies showed a double exponential profile with an average $\mathrm{R_{br}/h_{in}}$ of 1.8 ± 0.5. When the first study came out on the shape of radial profiles on galaxies at high-z, the comparison with the local data showed that the "early" truncated galaxies were missing in local samples. The new results on the shape of radial profiles of local galaxies by Pohlen & Trujillo (2006) shows that, in fact, locally the $\mathrm{R_{br}/h_{in}}$ in the r' band is 2.5 ± 0.6 with a range $1.4 - 4.2$. Therefore, it seems that local galaxies also show the early truncation detected at high-z. However, we do not observe any high-z galaxy truncated

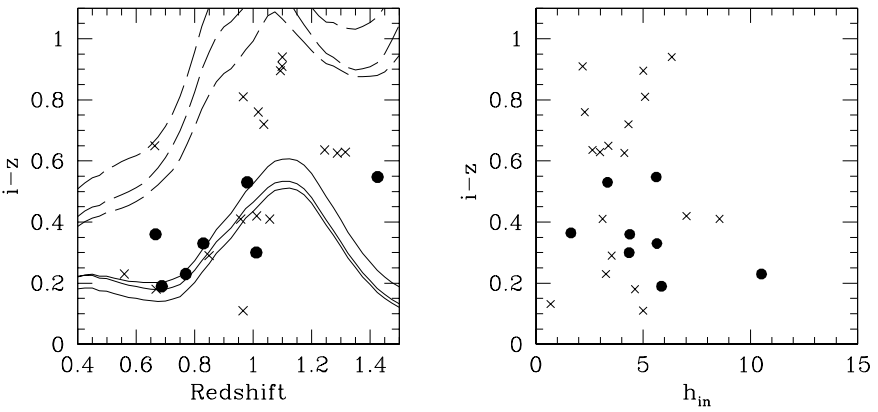

Figure 1. The right panel shows the i-z colour as a function of the disk scale-length for the sample galaxies, the full dots are the galaxies with a double exponential profile and the crosses are the 'untruncated' galaxies. The left panel shows the i-z colour as a function of redshift with the same coding as before. Over-plotted on the data, the dashed lines represent the colour evolution with redshift for the Bruzual & Charlot single burst models (2003) with different metallicities and the full lines represent the declining in time SFR models.

beyond 2.5 scale-lengths; unlike in the local universe where the break location distribution extends to around 4 scale-lengths. In many of the cases, the break could have been detected if it occurred at around 4 scale-lengths (for the UDF galaxies). Further investigation of the biases involved in the sample selection is needed to conclude whether the distribution of break radii at high-z differs from that found in local galaxies.

Frequency of the double exponential profiles

For nearby objects the frequency of 'classical' truncation (following the notation of Pohlen & Trujillo in this volume) from a sample of SDSS galaxies is about 32.9%±5.1%. In the first high-z sample from GOODS, six of 16 galaxies showed a two-slope profile. From the UDF sample (19 galaxies), 6 showed double exponentials. Around 34% of the galaxies at high-z show a truncation. Although this is not a complete sample, the percentage is indicative of the frequency of double exponential profiles at high-z.

Colour of the sample galaxies and comparison with stellar population models

We computed the colour at different redshifts using population synthesis models (Bruzual & Charlot 2003) adopting the Chabrier IMF (Chabrier 2003). The star formation rate (SFR) ranges from single burst at different metallicities

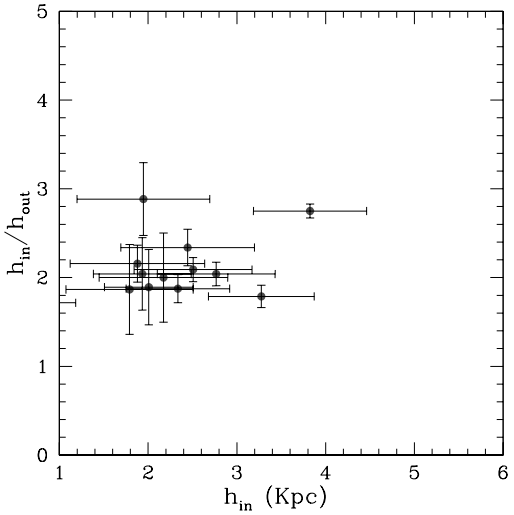

Figure 2. The plot shows the ratio between the inner and the outer exponential scale-lengths as a function of the inner scale-length. Notice that the ratio between the inner and the outer scale-length seems to remain basically unchanged around a value of 2.

to continuous star formation or formation declining with time. We then compared the observed colours of the sample with the modelled colours. The truncated galaxies show a smaller range of colours than the untruncated galaxies, the truncated galaxies being bluer on average than the untruncated galaxies. Most of the truncated galaxies colours are compatible with a continuous or declining star formation history. However, the single burst models are not compatible with the observed data within the whole parameter range (see Fig. 1).

Ratio between the inner and the outer exponential scale-length

It is interesting to notice that the ratio between the inner and the outer scale-length seems to remain unchanged for the high-z sample compared to the low-z sample. The R_{br}/h_{in} is around 2 for both the GOODS and the UDF sample (see Fig. 2). This value is remarkably similar to the value obtained by Pohlen et al. (2002), where they found a value of 2 ± 0.2, although the sample only consisted of three local galaxies. It needs to be further investigated whether for a larger sample of nearby objects this ratio remains the same; however, there is further evidence that this is the case. The study by Hunter & Elmegreen (2006) shows that for a sample of Im and Sm galaxies the R_{br}/h_{in} is around 2. This result suggests that the dust does not make R_{br}/h_{in} appear smaller at higher redshifts.

4. Conclusions

To complement and improve the study of galaxy radial profiles at high-z started by Pérez (2004), we have used UDF data to search for double exponential profiles at z $\approx$ 1. Of the 19 UDF galaxies, six show a double exponential profile. The UDF data allows us to reach the location of the break up to 4 $\times$ h_{in}. The average break radius happens at R_{br}/h_{in} of 1.8 $\pm$ 0.7, never reaching a value of R_{br}/h_{in} greater than 2.5. However, the distribution of the break radius goes to around 4 $\times$ h_{in} for local galaxies. We need to further investigate the possible biases involved in the sample selection to be able to conclude whether the distribution of break radii at high-z differs from that found in local galaxies. The colours of the truncated galaxies seem to be bluer than those of 'untruncated' galaxies, suggesting a younger population. Computing the colour at different redshifts using population synthesis models, we find that most of the truncated galaxies colours are compatible with a continuous or declining in time star formation history. Single burst models are not compatible with the observed data within the whole parameter range. Finally, we find that the ratio between the inner and the outer scale-length is 2.0$\pm$0.5 in agreement with the Peérez (2004) sample. This result is remarkably similar to the value found for nearby objects, implying that the dust does not make R_{br}/h_{in} appear smaller at higher redshifts.

References

Battaner, E., Florido, E., and Jimenez-Vicente, J. 2002, A&A, 388, 213

Bruzual, G. and Charlot, S. 2003, MNRAS, 344, 1000

Chabrier, G. 2003, ApJ, 586, 133

de Grijs, R., Kregel, M., and Wesson, H. 2001, MNRAS, 324, 1074

de Jong, R.S. 1996, A&A, 313, 45

Hunter, D.A. and Elmegreen, B.G. 2006, ApJ Suppl, 162.

Kennicutt, R.C. 1989, ApJ, 344, 685

Mao, S., Mo, H.J., and White, D.M. 1998, MNRAS, 297, 71

Pérez, I. 2004, A&A, 427, 17

Pohlen, M., Dettmar, R.J., Lutticke, R., and Aronica, G. 2002, A&A, 392, 807

Pohlen, M., and Trujillo, I. 2006, these proceedings, p. 253

Tamm, A. and Tenjes, P. 2005, A&A, 433, 31

Trujillo, I. and Pohlen, M. 2005, ApJ, 630, 17

van der Kruit, P.C. 1979, A&A, 38, 15

van der Kruit, P.C. 1987, A&A, 173, 59

Vanzella, E., Christiani, S., Dickinson, M., Kuntschner, H., Moustakas, L.A., and Nonino, M. 2004, submitted to A&A (astro-ph/0406591)

Wolf, C., Meisenheimer, K., Kleinheinrich, M., Borch, A., Dye, S., Gray, M., Wisotzki, L., and Bell, E.F. 2004, submitted to A&A (astro-ph/0403666)

THE OUTER BANKS OF GALAXY DISKS

Dennis Zaritsky[1] and Daniel Christlein[2]

[1]*Steward Observatory, University of Arizona, USA*
[2]*Yale University and Universidad de Chile*

Abstract We discuss the nature of the outer disks of galaxies ($R > R_{25}$) with a focus on the presence of dust at these radii and the kinematics of $H\alpha$ knots.

Keywords: stars: formation - galaxies: kinematics and dynamics - galaxies: structure - galaxies: spiral

1. Introduction

At ever larger radii in disk galaxies we expect to probe material that is more directly connected to the most recent accretion events. As such, the study of the extended disk (that which lies beyond the standard R_{25} isophote) and even beyond the realm of neutral hydrogen, into what we here refer to as the outer banks (Figure 1), may provide new clues as to how disks assemble. What probes can we identify at such large galactocentric radii? Certainly HI extends beyond the high surface brightness optical disk, but it too ends before we reach a region where disks are no longer well organized. Whether this edge represents the edge of the disk or simply the edge of the neutral hydrogen is an open question.

There have been several developments that have revitalized the study of the outer disk. First, GALEX images have been used to identify numerous knots of young star formation well beyond the optical radii (Thilker et al. 2005; de Paz et al. 2005). Second, extended stellar disks have been found to be ubiquitous (Erwin et al. 2005). Third, the study of resolved stellar populations is finding unexpected structures in both the Milky Way and M31 (Newberg et al. 2002; Ferguson et al. 2002). Here we focus on the interstellar component of extended disks.

The probe we explore within these extended disks are Hα and UV knots of recent or ongoing star formation out to radii $\sim 2R_{25}$ and diffuse Hα emission. Whether these knots extend, at least in some cases, beyond the HI disks is also an open question (certainly the bulk of these would be expected to lie within

R. S. de Jong, Island Universes, 265–270.
© 2007 *Springer.*

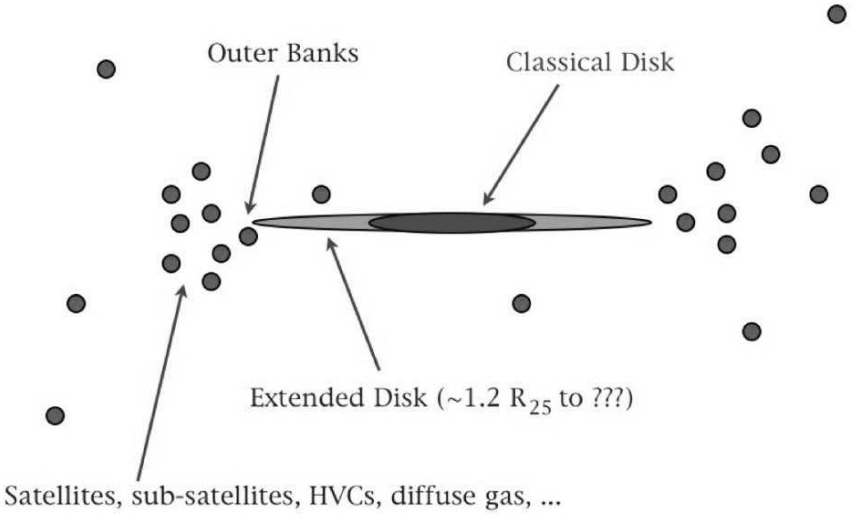

Figure 1. A cartoon illustrating our view of disk galaxies. Our conservative aim is to probe the extended disk and our ambition is to probe the outer banks.

the HI disk, as seen for NGC 628, see Figure 2). These knots can be used as kinematic tracers, and also provide information on the physical state of the gas, the latter of which we explore in our program, but not in this contribution. Here, we focus on the existence of dust at these radii and present kinematic information. The ultimate, perhaps unattainable, goal of this work is to identify knots and ionized diffuse gas at radii beyond the HI edge. These detections would present a bridge between the inner disk kinematics and the outer halo satellite kinematics.

Figure 2 shows the distribution of GALEX sources surrounding NGC 628. These sources have the colors and magnitudes of young clusters at the distance of NGC 628. There is a clear excess of sources, and therefore these are associated sources. Although the background level is high, and we cannot identify which sources are true NGC 628 young clusters, there is an evident abundance of sources out to $2R_{25}$. Whether some of the sources beyond this radius belong to NGC 628 as well will require spectroscopy to measure redshifts.

Some of these sources have been identified in Hα as well. One such source at R = 28 kpc in NGC 628, identified by Ferguson et al. (1998), is nearly at $2R_{25}$. The presence of HII regions enables the study of abundance gradients, which so far appear to extend fairly smoothly out to these radii (Ferguson et al. 1998; Christlein, Bland-Hawthorn, & Zaritsky 2005). Between the presence of UV knots and Hα, it is evident that the outer disk is a significant component

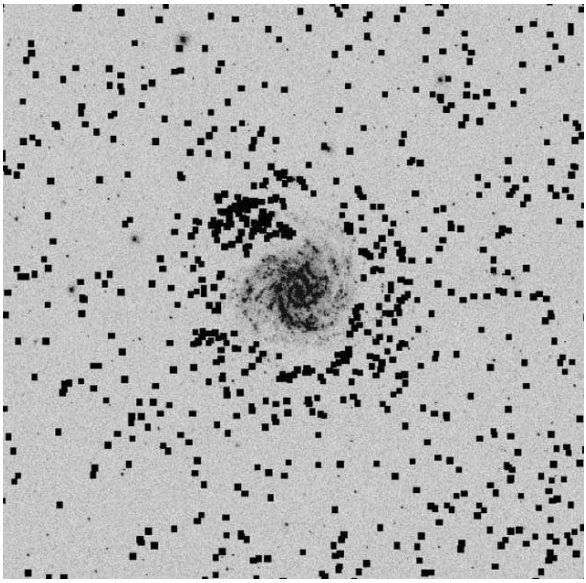

Figure 2. An optical image of NGC 628 with highlighted GALEX UV sources that have colors and magnitudes consistent with the sources being young (age $<$ few hundred Myr). Note the excess of source to about 2 optical radii. Sources are missing from the interior region due to their exclusion from the public catalogs.

of at least this one galaxy. While the existence of neutral gas at large radii has been long established, these recent results indicate that stars, in particular star formation, and ionized gas are present as well.

To examine whether dust is present in general out to large radii in galaxies, Nelson et al. (1998) examined IRAS 100 μm images. They stacked images, using the optical parameters to reorient the IRAS images, and found an excess of far IR emission out to $\sim R_{25}$, consistent with the identification of neutral and ionized gas (Figure 4). Extended dust emission has also been identified from deep observations of a targeted galaxy, NGC 891 (Popescu et al. 2004). Therefore, all components that have been identified in the classical disk are present in the extended disk as well.

2. Spectroscopic Data

To measure the kinematics of material in the extended disk, and perhaps probe the outer banks, we have embarked on a spectroscopic program observing nearly edge-on galaxies. These galaxies were selected to be of a few arcmin in angular size so that the slit length and spatial resolution allowed us to explore a large range of radii with reasonable angular resolution, of a certain

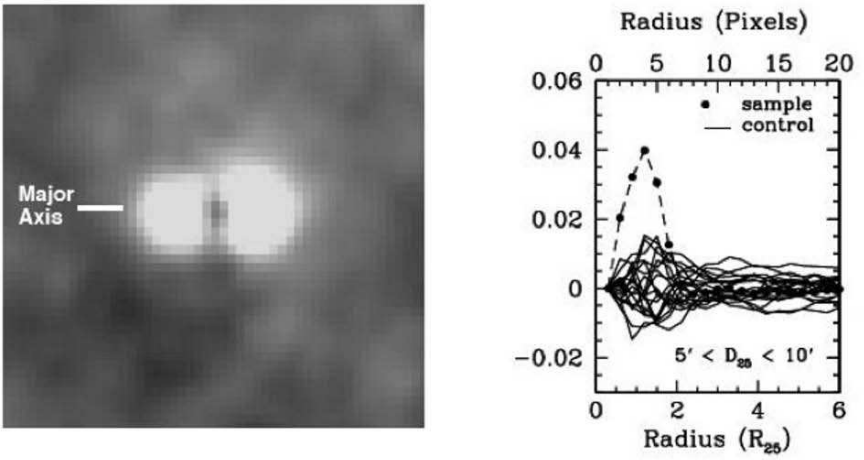

Figure 3. Results from Nelson et al. (1998). The left panel shows the sum 100μm image from IRAS of a sample of nearby galaxies. The images were rotated before summation so that the optical major axes line up. A central point source was fitted and subtracted to highlight the flux beyond that due to a point source. Notice that the excess flux is along the disk major axis. The panel on the right presents a cut through the image, showing the excess flux in comparison to a set of Monte Carlo realizations of summed stars.

redshift (typically around 4000 to 7000 km/sec) to place the Hα line between night-sky lines, and edge on, so that a single slit position had a larger likelihood of intersecting some outer disk ionized gas.

The observations we present were carried out on Magellan (with the B&C spectrograph), the MMT (with the Red Channel spectrograph), VLT (with the FORS1 spectrograph), and Gemini-South (with GMOS). Typical velocity resolutions are less than a few tens of km/sec (enough to resolve well the rotation curve of these galaxies). Typical exposure times are between 4 and 8 hours.

In Figure 4 we show both a section of the 2-D spectra (sky subtracted) and our measurements for the radial velocities, the Hα fluxes, and the disk surface brightness. The extended spectroscopic exposures allow us to detect Hα knots that have fluxes of a few time 10^{35} erg s^{-1}, two orders of magnitudes below the detections presented by Ferguson et al. (1998) and at least a magnitude fainter than those at the nominal edge of the Hα disk. However, these knots are exactly on the rotation curve. This result is repeated in almost every case where we identify knots between 1 and 1.5 R_{25}, which happens about 1/3 of the time. We find no evidence for substantial kinematic disturbances out to at least $1.5R_{25}$.

On a couple of occasions we find an Hα knot at larger radius with a radial velocity much more like the systemic velocity of the galaxy rather than of the rotation (see Figure 5). It is these cases, with non-circular motions, that may

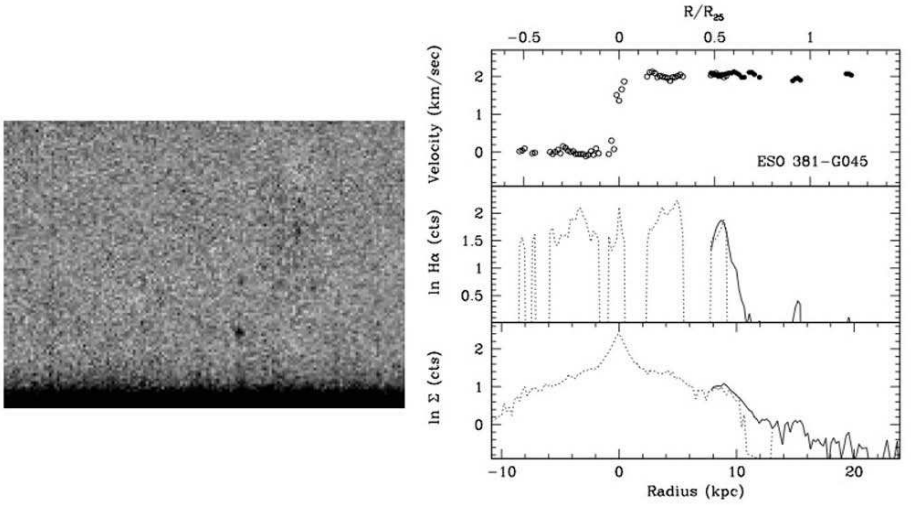

Figure 4. Results from deep long-slit spectroscopy. The panel on the left shows the sky-subtracted spectra around Hα with the spectral direction corresponding to the x-axis and the spatial direction corresponding to the y-axis. The dark band at the bottom is the edge of the optical disk, two faint knots are visible above the band which correspond to Hα emission regions. The panel on the right shows the rotation curve (upper panel, with the dark points highlighting the results obtained from the image on the left), Hα counts (middle panel, with the solid line highlighting the data from the shown image), and surface brightness (lower panel).

indicate that we have reached beyond the edge of the disk. One problem in interpreting these velocities is that for nearly edge-on galaxies, the line-of-sight velocity is not necessarily the circular velocity (and hence observing a low value may simply indicate that one has not caught the object at the tangent point). The difficulty with this interpretation is that these knots are already at $\sim 2R_{25}$, so increasing its velocity even by a factor of two would require moving it out to $4R_{25}$, which would be an even more extreme radius at which to have an object following the disk rotation curve. In such a case, our observations would demonstrate that the disk is highly clumped at these radii.

In conclusion, we are finding that the extended disk, out to $\sim 1.5R_{25}$ exhibits very standard kinematics. Beyond this radius, we have only identified a couple of knots, but these exhibit non-standard kinematics. The subsequent challenge is to identify more tracers at these larger radii and identify the smooth transition, if it exists, between disk and halo. These regions should be where the disk is growing, if it grows from inside out, and will be, in the ocean of accreting material, the outer banks of galaxy disks.

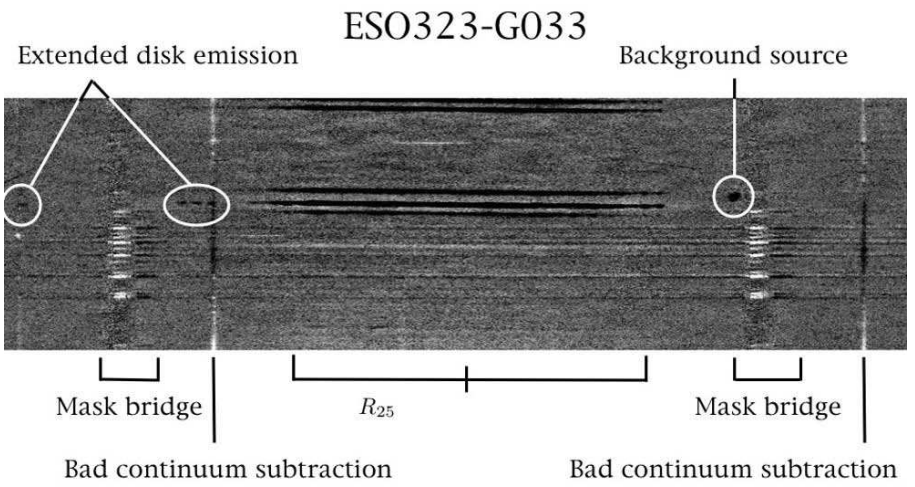

Figure 5. Continuum-subtracted long-slit spectroscopy. The centrally located horizontal dark bands are Hα and [NII]. The circles highlight outer disk knots of Hα emission (and in one case a background galaxy). The rightmost knot has a velocity consistent with the systemic velocity rather than the extrapolation of the rotation curve.

References

Christlein, D., Bland-Hawthorn, J., & Zaritsky, D. 2005, in prep.

Gil de Paz, A. et al. 2005, ApJL, 627, L29

Erwin, P., Beckman, J. E., and Pohlen, M. 2005, ApJ, 626, L81

Ferguson, A. M. N., Gallagher, J. S., and Wyse, R. F. G. 1998, AJ, 116, 673

Ferguson, A. M. N., Irwin, M. J., Ibata, R. A.,Lewis, G. F. and Tanvir, N. R. 2002, AJ, 124, 1452

Nelson, A. E., Zaritsky, D., and Cutri, R. M. 1998, AJ, 115, 2273

Newberg, H.J. et al. 2002, ApJ, 569, 245

Popescu, C. C., Tuffs, R. J., Kylafis, N. D., and Madore, B. F. 2004, A&A, 414, 45

Thilker, D.A. et al. 2005, ApJL, 619, L79

THE GASEOUS HALOES OF DISC GALAXIES

F. Fraternali[1], T. Oosterloo[2], J.J. Binney[1] and R. Sancisi[3,4]

[1]*Theoretical Physics, University of Oxford, UK*
[2]*ASTRON, Dwingeloo, The Netherlands*
[3]*INAF-Osservatorio Astronomico, Bologna, Italy*
[4]*Kapteyn Astronomical Institute, University of Groningen, The Netherlands*

Abstract The study of gas outside the plane of disc galaxies is crucial to understanding the circulation of material within a galaxy and between galaxies and the intergalactic environment. We present new H I observations of the edge-on galaxy NGC 891, which show an extended halo component lagging behind the disc in rotation. We compare these results for NGC 891 with other detections of gaseous haloes. Finally, we present a dynamical model for the formation of extra-planar gas.

Keywords: galaxies: kinematics and dynamics - galaxies: ISM - intergalactic medium

1. Introduction

Gas plays a vital role in the evolution of disc galaxies. The collapse of gas produces star formation; stars enrich gas, expel it via winds and supernova explosions and create a circulation called the galactic fountain (e.g. Shapiro & Field 1976). Outflows of gas from galactic discs with velocities of the order of $100\,\mathrm{km\,s^{-1}}$ are indeed observed both in the neutral (Kamphuis, Sancisi & van der Hulst 1991) and the ionised phase (Fraternali, Oosterloo & Sancisi 2004). On the other hand, disc galaxies also seem to acquire a substantial amount of gas from their surroundings. Accretion of unpolluted material from the Intergalactic Medium (IGM) is predicted by chemical evolution models of the Milky Way (e.g. Rocha-Pinto & Maciel 1996) and the low metallicities of some of the High Velocity Clouds (HVCs) (e.g. Tripp et al. 2003) suggest that cold material is indeed accreted by spiral galaxies like our own (Oort 1970).

In recent years, a new and important fact has emerged. Observations at various wavelengths have shown the presence of a considerable amount of gas in the haloes of disc galaxies (extra-planar or halo gas). Deep $\mathrm{H}\alpha$ observations have revealed the presence of extended layers of diffuse ionised gas (DIG) around edge-on spiral galaxies (Hoopes, Walterbos & Rand 1999). X-ray observations have shown the presence of hot plasma at distances of tens of kpc

R. S. de Jong, Island Universes, 271–276.
© 2007 *Springer.*

from the plane of galactic discs (e.g. Strickland et al. 2004). H I observations have revealed extended thick layers surrounding the galactic discs (Swaters, Sancisi & van der Hulst 1997; Fraternali et al. 2001; Matthews & Wood 2003). The origin and the nature of this halo gas are still unknown. However, it is a unique probe to study the exchange of gas within a galaxy and between galaxies and the IGM.

2. NGC 891

NGC 891 is one of the best known and studied nearby edge-on galaxies. It is at the distance of 9.5 Mpc, classified as a Sb/SBb, and it is often referred to as very similar to the Milky Way (e.g. van der Kruit 1981).

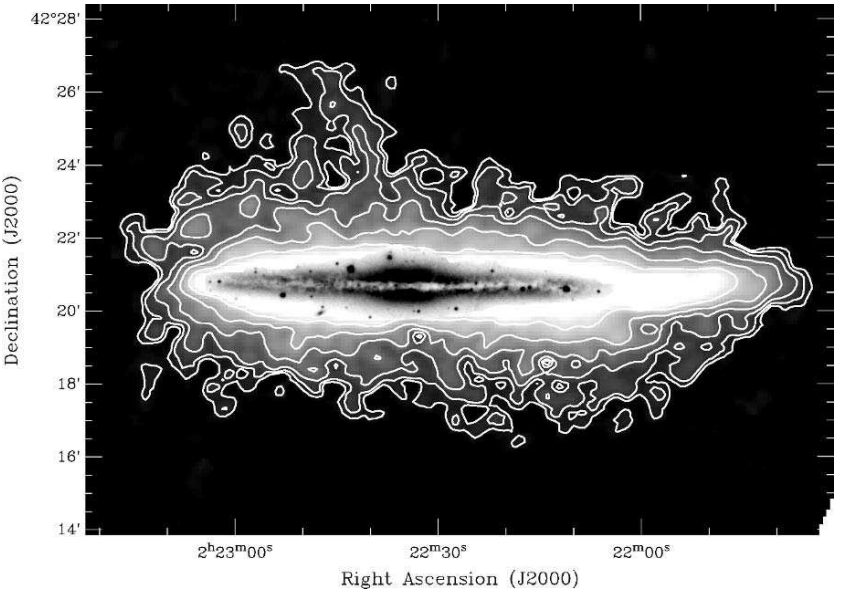

Figure 1. Optical DSS image (grey-scale) and total H I map (contours+negative grey-scale) of NGC 891, the latter obtained from the new WSRT observations (Oosterloo, Fraternali & Sancisi 2005). H I contours are: 1.7, 4.5, 9, 18.5, 37, 74, 148, 296.5, 593 $\times$ 10^{19} atoms cm^{-2}. The beam size is $28''$; $1' = 2.8$ kpc.

NGC 891 has been the subject of numerous studies at different wavelengths that have led to the detection of various halo components: an extended radio halo (Allen, Sancisi & Baldwin 1978), a thick layer of diffuse ionised gas (DIG) (e.g. Dettmar 1990), and diffuse extra-planar hot gas (Bregman & Pildis 1994). Also "cold" ISM components have been detected in the halo such as H I (Swaters, Sancisi & van der Hulst 1997), dust (Howk & Savage 1999) and CO (Garcia-Burillo et al. 1992).

New H I observations of NGC 891 have been obtained with the Westerbork Synthesis Radio Telescope (WSRT) with a total integration time of about 200 hrs (Oosterloo, Fraternali & Sancisi 2005). Figure 1 shows the new total H I map of NGC 891 in contours overlaid on a grey-scale DSS optical image. This H I halo is remarkably extended with a spur of gas reaching a distance of 15 kpc from the plane. The H I disc of NGC 891 is lop-sided, more extended on the S-W side of the galaxy (right in Fig. 1) and possibly $truncated$ on the N-E (left) side (see also Sancisi & Allen 1979; Swaters, Sancisi & van der Hulst 1997).

The halo gas in NGC 891 rotates more slowly than the gas in the plane (Swaters, Sancisi & van der Hulst 1997). This is a common property of gaseous haloes (e.g., Fraternali et al. 2001; Heald et al. 2005a). Our new data allow us to study the kinematics of the halo gas in detail and derive rotation curves at different heights from the plane (Fraternali et al. 2005; Fraternali, in preparation). The measured gradient in rotation velocity is $\Delta_{\rm v_{rot}} \sim -15\,{\rm km\,s^{-1}kpc^{-1}}$ for 1.3<z<5.2 kpc. This value agrees with the velocity gradient measured in the ionised gas (Heald et al. 2005b).

3. Halo Gas in Other Disc Galaxies

How common are gaseous haloes? Until now, neutral extra-planar gas has been studied in 6 disc galaxies. The H I data for these galaxies are among the deepest ever obtained and this may indicate that halo gas is a common feature that has escaped detection because of a lack of sensitivity.

Table 1. Observations of halo gas in disc galaxies

Galaxy	Type	Distance (Mpc)	$M_{\rm halo}$ H I ($10^8\ M_\odot$)	$M_{\rm halo}/M_{\rm total}$ (%)	L(FIR) ($L_\odot$)	Ref.
NGC 253	Sc	3.9	0.8	3	2.63×10^{10}	1
NGC 891	SBb	9.5	6	15	1.25×10^{10}	2
NGC 6946	Scd	6.0	>3.5	>5.8	9.79×10^{9}	3
NGC 4559	Scd	9.7	5.9	11.5	1.91×10^{9}	4
NGC 2403	Scd	3.2	3	11.0	1.13×10^{9}	5
UGC 7321	Sd	10.0	$\gtrsim 0.1$	$\gtrsim 1$	7×10^{7}	6

[1] Boomsma et al. 2005a; [2] Swaters, Sancisi & van der Hulst 1997; [3] Boomsma et al. 2005b; [4] Barbieri et al. 2005; [5] Fraternali et al. 2002; [6] Matthews & Wood 2003.

Table 1 summarizes the 6 halo gas detections sorted by their FIR luminosity (which is a measure of the star formation rate, SFR). A relation between the amount of halo gas and the SFR may be expected if the halo gas has a galactic fountain origin. It is possible that a trend is indeed present for low luminosity galaxies. Note that the mass of halo gas estimated for NGC 6946 is a lower

limit due to the low inclination ($\sim 30^\circ$) of the galaxy that does not allow an efficient separation of the halo component (Boomsma et al. 2005b). However, the starburst galaxy NGC 253 is totally anomalous, having very little extra-planar H I compared to the other galaxies. This may be an indication that in the most actively star forming galaxies most of the halo gas is ionised.

In addition to these galaxies, there are indications of the presence of halo gas in several others (e.g. NGC 5055, Battaglia et al. 2005; UGC 1281, Kamphuis et al., this conference; UGC 12632, Oosterloo, private communication) and extra-planar features have been observed in NGC 2613 (Chaves & Irwin 2001). Moreover, it is very likely that this halo gas is analogous to the Intermediate and High Velocity Clouds (IVCs/HVCs) of the Milky Way (Wakker & van Woerden 1997) and of external galaxies (M31 and M33, Westmeier, Braun & Thilker; M83 and M51, Miller & Bregman 2005).

4. A Dynamical Model for Extra-planar Gas

What is the origin of these gaseous haloes? Some authors have tried to explain them using ballistic galactic fountain models and compared them with Hα observations of ionised gas (Collins, Benjamin & Rand 2002; Heald et al. 2005a). They found a general disagreement between the kinematics and distribution of the halo gas predicted by the models and those shown by the data. Other authors have tried to model the halo gas as a stationary medium in hydrostatic equilibrium (Benjamin 2002; Barnabè et al. 2005). This approach leads to solutions that can reproduce the observed gradient in the rotation velocity (Barnabè et al. 2005), however the temperatures of the extra-planar (hydrostatic) gas are of the order of 10^5 K and it is unclear how this medium can be related to cold neutral gas.

We have developed a model for the formation of the neutral extra-planar gas that takes into account internal and external processes. At the current stage (Fraternali & Binney 2005) the model tries to reproduce the halo gas as a continuous flow of collision-less particles from the disc into the halo region. The particles are stopped at the passage through the plane. The output of the models are particle-cubes that can be directly compared to the H I data-cubes. The idea behind this approach is to start from a basic model, study its failures and improve it progressively to match the data more and more closely.

Figure 2 shows three representative channel maps of NGC 891 (left column) compared with those produced by two dynamical models. The two models are for maximum and minimum disc (maximum DM halo) potentials. The channel maps shown here have velocities far from systemic, i.e. they show the gas that rotates the fastest. The data show that this gas is mostly located in the disc (the channel maps are thin) whilst the models predict much thicker channel maps, i.e. fast rotating extra-planar gas. This is a failure of the fountain model and

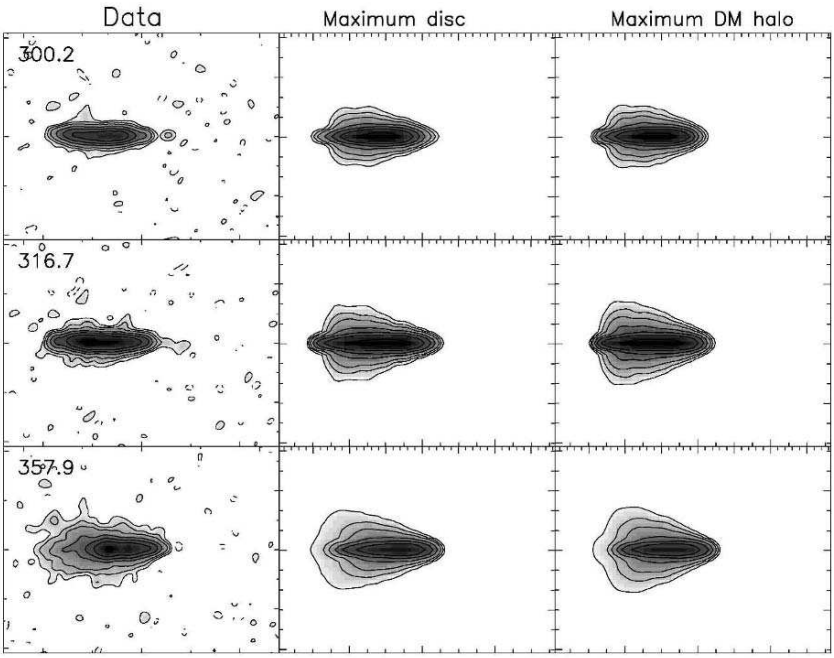

Figure 2. Comparison between three observed channel maps of NGC 891 (Oosterloo, Fraternali & Sancisi 2005) and those produced with the two dynamical models. The first column shows the data, heliocentric radial velocities are reported in the upper left corner.

this problem cannot be removed by allowing the particles to cross the disc or by considering that they are ionised as they leave the plane and become visible at 21 cm at some point on their orbits (phase change). There is an intrinsic and unavoidable need for low angular momentum material, which suggests that one has to take into account interactions between the fountain flow and a hot gaseous halo and/or accretion material (Fraternali & Binney, in preparation).

5. Conclusions

The new H I observations of NGC 891 show the presence of extended neutral gas halo reaching up the distance of 15 kpc from the plane. This halo gas rotates more slowly than the gas in the plane (with a gradient of -15 $\mathrm{km\,s^{-1}kpc^{-1}}$). These kinematic properties cannot be explained by an isolated galactic fountain; they require that interactions with a hot halo and/or gas accretion from the IGM must play an important role.

References

Allen R.J., Sancisi R., Baldwin J.E., 1978, A&A, 62, 397

Barbieri C.V., Fraternali F., Oosterloo T., Bertin G., Boomsma R., Sancisi R., 2005, A&A, 439, 947

Battaglia G., Fraternali F., Oosterloo T., Sancisi R. 2005, A&A, in press

Barnabe' M., Ciotti L., Fraternali F., Sancisi R., 2005, A&A, in press

Benjamin R.A., 2002, in Seeing Through the Dust ed. A.R. Taylor, T.L. Landecker, and A.G. Willis, ASP Conference Series, Vol. 276, 201

Boomsma R., Oosterloo T.A., Fraternali F., van der Hulst J.M., Sancisi R. 2005b, A&A, 431, 65

Boomsma R., Oosterloo T., Fraternali F., van der Hulst J.M., Sancisi R., "Extra-planar Gas", Dwingeloo, ASP Conf. Series, ed. R. Braun

Bregman, J.N.; Pildis, R.A., 1994, ApJ, 420, 570

Chaves T.A., Irwin J.A. 2001, ApJ, 557, 646

Collins J.A., Benjamin R.A., Rand R.J., 2002, ApJ, 578, 98

Dettmar, R.J. 1990, A&A, 232, L15

Fraternali F., Oosterloo T., Sancisi R., van Moorsel G., 2001, ApJ, 562, 47

Fraternali F., van Moorsel G., Sancisi R., Oosterloo T., 2002, AJ, 123, 3124

Fraternali F., Oosterloo T., Sancisi R., 2004, A&A, 424, 485

Fraternali F., Oosterloo T., Sancisi R., Swaters R., 2005, "Extra-planar Gas", Dwingeloo, ASP Conf. Series, ed. R. Braun (astro-ph/0410375)

Fraternali F. & Binney J.J. 2005, MNRAS, submitted

Garcia-Burillo, S., Guelin, M., Cernicharo, J., Dahlem, M. 1992, A&A, 266, 21

Heald G.H., Rand R.J., Benjamin R.A., Collins J.A., Bland-Hawthorn J., 2005a, ApJ, in press, (astro-ph/0509225)

Heald G.H., Rand R.J., Benjamin R.A., Bershady M.A. 2005b, these proceedings, p. 295 (astro-ph/0508559)

Hoopes C.G., Walterbos R.A.M., Rand R.J., 1999, ApJ, 522, 669

Howk J.C., Savage B.D. 1999, AJ, 117, 2077

Kamphuis J., Sancisi R., van der Hulst T., 1991, A&A, 244, 29

van der Kruit P.C., 1981, A&A, 99, 298

Matthews L.D., Wood K., 2003, ApJ, 593, 721

Miller E.D., Bregman J.N. 2005, ASPC, 331, 261

Oort J.H., 1970, A&A, 7, 381

Oosterloo T., Fraternali F., Sancisi R., 2005, in preparation

Rocha-Pinto H.J., Maciel W.J., 1996, MNRAS, 531, 279, 447

Sancisi R., Allen R.J., 1979, A&A, 74, 73

Shapiro P.R., Field G.B., 1976, ApJ, 205, 762

Strickland D.K., Heckman T.M., Colbert E.J.M., Hoopes C.G., Weaver K.A. 2004, ApJS, 151, 193

Swaters R.A., Sancisi R., van der Hulst J.M., 1997, ApJ, 491, 140

Tripp T.M., Wakker B.P., Jenkins E.B., Bowers C.W., Danks A.C., Green R.F., Heap S.R., Joseph C.L., Kaiser M.E., Linsky J.L., Woodgate B.E., 2003, AJ, 125, 3122

Wakker B.P, van Woerden H., 1997, ARA&A, 35, 217

Westmeier T., Braun R., Thilker D. 2005, A&A, 436, 101

GASEOUS HALOS AND THE INTERSTELLAR DISK-HALO CONNECTION

Ralf-Jürgen Dettmar

Astronomical Institute, Ruhr-University Bochum, Germany

Abstract The presence of diffuse ionized gas (DIG) in the halos of spiral galaxies is discussed in the framework of the disk-halo interaction. The halo DIG is typically correlated with the presence of other components of the ISM in the halo including X-ray hot gas, cosmic rays, and magnetic fields. All these tracers of an extraplanar ISM correlate well with star formation in the disk thus corroborating the paradigm of an ISM driven by multiple and clustered supernovae.

Keywords: galaxies: ISM - ISM: structure - ISM: bubbles - galaxies: spiral

1. Introduction

Various components of the interstellar medium (ISM) – from neutral and molecular hydrogen to diffuse ionized or X-ray hot gas – are found in halos and disk-halo interfaces of spiral galaxies. The structure of these components perpendicular to the galactic plane, i.e. in the main direction of the gradient of the gravitational potential, can be viewed as a very good indicator for the physical state of the dynamical interstellar medium. Galactic as well as extragalactic observations corroborate the picture of an interstellar medium driven by multiple and clustered supernova causing the so-called disk-halo interaction. Within the circuit of matter in a star forming disk galaxy the gaseous halos can be considered as important as the tideland (or wadden sea) – surrounding the island of Terschelling where the conference summarized in these proceedings took place – for the evolution of life.

The scenario of the disk-halo connection predicts outflows and this is well supported by observations in the case of nuclear starbursts (see, e.g., Strickland 2004a, b). However, we have little direct evidence for the required outflows of hot gas into the halos of more normal (i.e. non-starburst) galaxies and here the mass exchange between disk and halo is still a (well) working hypothesis, while some recently published galaxy formation models rather predict H^+

R. S. de Jong, Island Universes, 277–282.
© 2007 *Springer.*

halos of spiral galaxies as being a cooling component of X-ray hot halos from the formation process (e.g., Toft et al. 2002).

To look specifically at extraplanar DIG is a good start from the observational point of view since it is of all tracers of halo gas the easiest to observe with regard to sensitivity and resolution (Dettmar 1992, 1998). Observational evidence of the widespread diffuse ionized medium in external galaxies thus proofs helpful since it allows us to study the influence of the energy released by young and massive stars into the ISM and its feedback process.

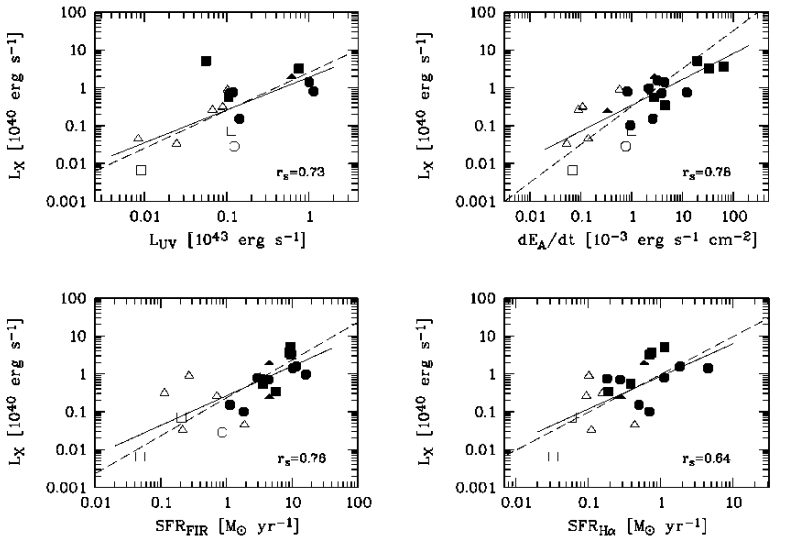

Figure 1. Correlation of the X-ray luminosity of spiral galaxies and the presence of halo DIG indicated by filled symbols with various indicators for the SFR or energy input per unit area for a sample of edge-on galaxies (adopted from Tüllmann et al. 2005).

2. DIG in the Disk-halo Interface and Star Formation in the Disk

A halo component of DIG for external galaxies was first discovered in Piet van der Kruit's favorite galaxy, the proto-typical edge-on spiral NGC 891, by Rand et al. (1990) and Dettmar (1990). A few small samples have been studied since then (e.g., Pildis et al. 1994, Rand 1996; Rossa & Dettmar 2000). In Rossa & Dettmar (2003a, b) a survey of a larger sample is presented that demonstrates the correlation of halo gas properties with the star formation rate (SFR) in the disk (see also Miller & Veilleux 2003 for comparison). This survey covers a broad range in SFR extending the observations to less active galaxies. Up to now emphasis was mainly given to galaxies with high SFR or even starburst

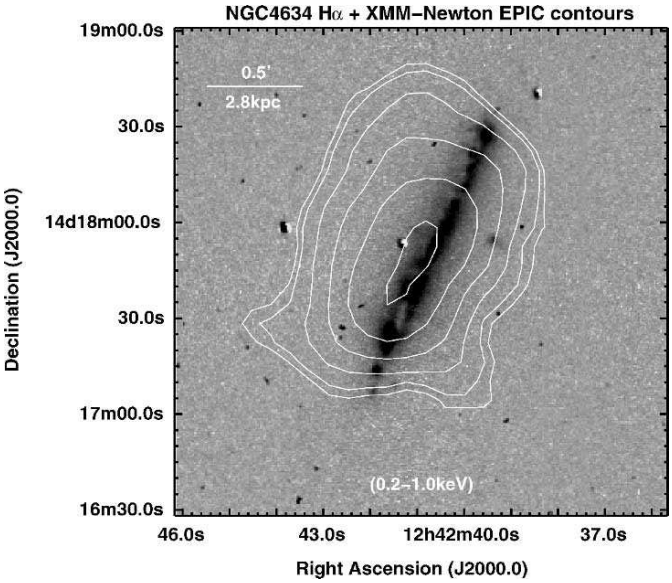

Figure 2. The radial extent of the X-ray halo of NGC 4634 from integrated EPIC XMM/Newton observations (adopted from Tüllmann et al. 2005) demonstrates the correlation with the star formation in the disk.

galaxies (Lehnert and Heckman 1995). In Rossa & Dettmar (2003a) we have chosen a sample of galaxies such that it supplements the previously studied "starburst" objects at the low activity end. If the starformation rate per unit area is low as determined by the FIR luminosity normalized to the disk surface the presence of DIG halos indeed diminishes. The FIR luminosity per unit area therefore allows us to derive a minimum SFR per area required to drive the disk-halo interaction. Given the known large uncertainties in the normalization of SN-rates from FIR-fluxes a reasonable estimate for the local break-out condition is in the order of $\sim$15 SNe over the lifetime of an OB association. An obvious shortcoming of this analysis lays in the use of global measurements for the FIR luminosities and future observations with higher angular resolution, e.g. with the Spitzer-satellite, will allow a much better comparison of the local SFR with halo gas properties.

High resolution ground-based (see, e.g. Howk and Savage 2000) and HST imaging (Rossa et al. 2004) studies of the DIG distribution in edge-on galaxies do not reveal the number and specific morphology of "chimney" like structures predicted by some models (Norman and Ikeuchi 1989). With only one or two cases found in the Milky Way the number of "chimneys" also falls short by an order of magnitude and more. This gives the impression that current global ISM models may not handle the very different physical scales – from star formation sites to galactic halos – well enough to allow us a detailed comparison.

For a solution we may have to await the next generation of numerical models for better predictions concerning the disk-halo interaction.

3. The Hot Interstellar Medium in Halos

As mentioned above, for nucleated starburst the disk-halo connection is described by theory and numerical modeling (e.g., MacLow & Ferrara 1999) and resulting predictions for outflows and winds from X-ray emitting hot gas are generally in good agreement with observations (Cecil et al. 2002, Strickland et al. 2004a, b). An attempt to relate the presence of X-ray halos in spiral galaxies to their star formation in the disk as derived from various indicators such as far infrared (FIR) fluxes is shown in Fig. 1. A correlation of the global X-ray emission with the SFR in the disk was also found for a sample including more normal disk galaxies by Ranalli et al. (2003). With the current generation of X-ray satellites it is now possible to extend the X-ray studies from the starbursting and luminous galaxies to less active cases. One first result of a small survey with XMM/Newton is shown in Fig. 2 (Tüllmann et al. 2005).

4. Large-scale Magnetic Field Structure in Halos

The diffuse halo gas is in most of the observed cases also associated with radiocontinuum halos and a break-out condition for cosmic rays as a function of star formation rate per unit area is discussed by Dahlem et al. (1995). A compilation of observations of edge-on galaxies in Hα, radio continuum, and X-rays is given in Dettmar (1998) and Rossa and Dettmar (2003 a, b) and the multiphase halo ISM is discussed by Tüllmann et al. (2005). A large scale magnetic field structure in the halo is of particular interest for the interpretation in terms of a global dynamo theory for the enhancement of magnetic fields in galaxies. This aspect is discussed in more detail by, e.g., Beck et al. (1996).

5. Dust in the Halo

Since the star formation process in the disks will also locally enhance the radiation field it was suggested more than a decade ago that dust could be elevated by radiation pressure from the disk into the halo (Franco et al. 1991). Ferrara (1997) modeled the evolution in time of the dust distribution under the influence of the radiation field caused by an OB association and showed that the dust would be dispersed into a large volume. This, however, is in contrast to the observed dust distribution in several galaxies. Sofue et al. (1994) demonstrate that the dust in the disk of NGC 253 is highly structured in large scale arches much resembling solar prominences in shape. Also the dust distribution in the edge-on galaxy NGC 891 studied, e.g., by Howk and Savage (1997) is organized in long filaments reaching from the disk into the halo. These filaments end in a level of dust sheets high above the disk plane.

The possible influence of magnetic fields on the charged dust particles as an additional process to structure the dust distribution in galactic halos was put forward by Shchekinov et al. (1999). In the presence of large scale organized magnetic fields in galactic halos as demonstrated for the case of NGC 5775 (Tüllmann et al. 2000) such processes have to be discussed in more detail in the future.

6. Summary

Gaseous DIG halos are found in galaxies with sufficiently high SFR per unit area. Typically these layers of extraplanar DIG can be traced out to distances of $z \leq 1$–2 kpc – sometimes even up to 5 kpc or more – from the mid-plane of the disk. These H^+ halos seem to be associated with halos of cosmic rays and X-ray plasma as expected if caused by the disk-halo interaction of the ISM. The polarized radiocontinuum emissions indicates an ordered magnetic field in the halo and also the highly structure dust distribution in the halos of some galaxies could be influenced by magnetic fields due the coupling of charged dust to both the radiation and magnetic fields.

Acknowledgements Work at Ruhr-University Bochum in this field is supported through DFG SFB 591 and through Deutsches Zentrum für Luft- und Raumfahrt. I am very greatfull to my students and collaborators for their support and contributions.

References

Beck, R., Brandenburg, A., Moss, D., Shukurov, A., Sokoloff, D. 1996, ARA&A 34, 155 437
Cecil, G., Bland-Howthorn, J., Veilleux, S. 2002, ApJS 576, 745
Dahlem, M. 1997, PASP 109, 1298
Dahlem, M., Liesenfeld, U., Golla, G. 1995, ApJ 444, 119
Dettmar, R.-J. 1990, A&A 232, L15
Dettmar, R.-J. 1992, Fund. Cosmic Phys. 15, 143
Dettmar, R.-J. 1998, in The Local Bubble and Beyond, eds. Breidtschwerdt, D. et al., Springer LNP 506, p. 527 112, 256
Ferrara, A. 1997, in: The Physics of Galactic Halos, eds. H. Lesch et al., Akademie Verlag, p. 189
Franco, J. et al. 1991, ApJ 366, 443
Haffner, L. M., Reynolds, R. J., & Tufte, S. L. 1999, ApJ 523, 223
Hoopes, C. G., Walterbos, R. A. M., Greenawalt, B. E. 1996, AJ 112, 1429
Howk, J. C. & Savage, B. D. 1997, AJ 114, 2463
Lehnert, M. D. & Heckman, T. M. 1994, ApJ 426, L27
Lehnert, M. D. & Heckman, T. M. 1995, ApJS 97, 89
Miller, S. T. & Veilleux, S. 2003 ApJS, 148, 383
MacLow, M. M. & Ferrara, A. 1999, ApJ 513, 142
Norman, C. A. & Ikeuchi, S. 1989, ApJ 345, 372
Pildis, R. A., Bregman, J. N., & Schombert, J. M. 1994, ApJ 427, 160
Ranalli, P., Comastri, A. & Setti, G. 2003, A&A 399, 39

Rand, R. J. 1996, ApJ 462, 712
Rand, R. J., Kulkarni, S. R., & Hester, J. J. 1990, ApJ 352, L1
Reynolds, R. J., Haffner, L. M., & Tufte, S. L. 1999, ApJ 525, L21
Rossa, J. & Dettmar, R.–J. 2000, A&A 359, 433
Rossa, J. & Dettmar, R.–J. 2003a, A&A 406, 493
Rossa, J. & Dettmar, R.–J. 2003b, A&A 406, 505
Rossa, J., Dettmar, R.–J., Walterbos, R. A. M., Norman, C. A. 2004, AJ 128, 674
Shchekinov, Y. A. & Dettmar, R.-J. 1999, Proceedings 26th ICRC, session OG, Vol. 4, p.298
Sofue, Y., Wakamatsu, K.-I., Malin, D. F. 1994, AJ 108, 2102
Strickland et al. 2004a, ApJS 151, 193
Strickland et al. 2004b, ApJ 606, 829
Toft, S., Rasmussen, J., Sommer-Larsen, J., & Pedersen, K. 2002, MNRAS 335, 799
Tüllmann, R., et al. 2000, A&A 364, L36
Tüllmann, R., et al. 2005, astro-ph/0510079

Enjoying the views: Jerry Sellwood and Donald Lynden-Bell.

GEOMETRODYNAMICAL DISTANCES TO CLOUD STREAMS

Donald Lynden-Bell and Shoko Jin

Institute of Astronomy, Cambridge, UK

Abstract Two methods are given for determining distances to streams of high-velocity-clouds in orbit about the Galactic Centre. Both rely on the parallax generated by the offset of the Sun from the stream's orbital plane. The distances to all points of the Magellanic Stream are found without use of the Magellanic Cloud distances.

Keywords: intergalactic medium - galaxies: kinematics and dynamics - galaxies: halos - Magellanic Clouds

1. Introduction

Distances to high-velocity-clouds have remained unknown or uncertain ever since they were discovered (Davies 1960; Dieter 1965; Hulsbosch & Raimond 1966; Oort 1970). Here we show that distances to long streams to such clouds can be determined if they are in orbit about the galactic centre and we give a test to decide whether they are in orbit. We give two methods the first of which assumes less but can only work well at distances less than $\sim$25 kpc. The second method works best at greater distances and is used on the Magellanic Stream.

Method I: Nearby Streams

Let v_l be the line of sight radial velocity to a cloud in direction[1] $\hat{\mathbf{l}}$ which is part of a stream. We use the symbol v_l to stand for this velocity **after** its reduction to the **galactic** system of rest. Following around the stream we find the point Z at which v_l is zero. At this point the stream must move perpendicularly to the line of sight $\hat{\mathbf{l}}_z$. If the apparent direction of the stream there in the plane of the sky is $\hat{\mathbf{s}}_z$, then the vector $\hat{\mathbf{s}}_z$ lies in the orbital plane of the stream. If d_z

[1]hats denote unit vectors, $\hat{\mathbf{l}} = (\cos l \cos b, \sin l \cos b, \sin b)$

R. S. de Jong, Island Universes, 283–286.
© 2007 *Springer.*

is the unknown distance to Z and $\mathbf{d}_o = (R_o, 0, 0)$ is the vector from the Sun to the galactic centre then $\hat{\mathbf{n}}$, the unit normal to the orbital plane will be along

$$(d_z \hat{\mathbf{l}}_z - \mathbf{d}_o) \times \hat{\mathbf{s}}_z$$

For any chosen value of d_z the points on the stream can be projected from the Sun until they hit the plane through the galactic centre whose normal is $\hat{\mathbf{n}}$. The orbital stream of clouds can then be drawn in that plane. The angle made by the stream to the line of sight is then known so the observed v_l can be deprojected to give the full vector velocity of the stream at each point. It is then possible to check whether energy and angular momentum are conserved along the stream for this particular choice of d_z. By varying d_z we discover what distance to Z gives angular momentum conservation but it is more powerful to use vectorial mathematics. If $\hat{\mathbf{s}}$ is the apparent direction of the stream in the plane of the sky (in direction $\hat{\mathbf{l}}$) then angular momentum conservation along the stream leads to the relationship

$$Y = DX + \text{const} \tag{1}$$

where D is the unknown d_z/R_o, $\hat{\mathbf{d}}_o = (1, 0, 0)$

$$X = \frac{(\hat{\mathbf{l}}_z \times \hat{\mathbf{s}}_z).\hat{\mathbf{s}}}{\hat{\mathbf{d}}_o.(\hat{\mathbf{l}} \times \hat{\mathbf{s}}) v_l} \quad , \quad Y = \frac{(\hat{\mathbf{d}}_o \times \hat{\mathbf{s}}_z).\hat{\mathbf{s}}}{\hat{\mathbf{d}}_o.(\hat{\mathbf{l}} \times \hat{\mathbf{s}}) v_l} \quad .$$

A graph of Y against X for the different points of the stream has gradient D so d_z can be determined. The plane of the stream is then known so the distances to all points of the stream can be deduced. Conservation of energy then provides a check as does the linearity of the graph of Y against X. While this method should work well for streams at less than 25 kpc from us, it fails for more distant streams because the projections from the Sun are at a small angle to the orbital plane so that the line of the stream in that plane is ill-determined.

Method II: Distant Streams

For distant streams the observed v_l is nearly equal to $\dot{r}$ the velocity radially away from the galactic centre. We start by neglecting the difference and correct later. We also use the potential $V_c^2 \ln r$ suitable for an extensive halo. Then

$$\frac{\dot{r}^2}{2} + \frac{h^2}{2r^2} + V_c^2 \ln r = E \quad . \tag{2}$$

At some point H the radial velocity squared $v_l^2 \sim \dot{r}^2$ will have a maximum so differentiating this energy equation

$$-\frac{h^2}{r^3} + \frac{V_c^2}{r} = 0$$

so at H, $r = r_h = h/V_c$.

Subtracting the energy equation at a general point from that at $r = r_h$ and multiplying the result by $2V_c^{-2}$ we find

$$\frac{(\dot{r}^2)_{\max} - \dot{r}^2}{V_c^2} + 1 = \frac{r_h^2}{r^2} - \ln \frac{r_h^2}{r^2} \quad . \tag{3}$$

We know the left hand side from the observed velocities and $V_c = 220$km/s so we may solve for r/r_h. Although the distances are still unknown this gives us distance ratios to the clouds the stream. We now take three points which lie on the centre line of the observed stream. Knowing their lines of sight $\hat{\mathbf{l}}_1,\ \hat{\mathbf{l}}_2,\ \hat{\mathbf{l}}_3$ any choice of r_h leads to distances to the clouds along those lines of sight. However the plane through the tips of the resulting vectors will not in general lie through the galactic centre. We choose that value of r_h which achieves this. With r_h so determined the distances to the clouds of the stream follow from their velocities (used as $\dot{r}$ in equation (3)). Refinements correct them for projection before use there. We now know both the plane of the orbit and the distances to all the clouds so we project the cloud positions not radially from the Sun but **orthogonally** onto the plane of the orbit. We can then determine accurately the angle that the stream makes to any line of sight, so v_l can be deprojected and angular momentum conservation can be checked.

2. Application to the Clouds of the Magellanic Stream

The Magellanic Stream has been a well studied phenomenon for many years (Wannier & Wrixon 1972; Mathewson et al. 1974; Braun & Thilker 2004; Bruns et al. 2005). An orbit in a Keplerian potential has its maximum $\dot{r}^2$ perpendicular to the line to pericentre. For a $V_c^2 \ln r$ potential nearly circular orbits give only $90/\sqrt{2} = 64^\circ$ for this angle, but for the eccentricity that we deduce for the Magellanic Stream this angle increases to 70.5°. The measured angle along the Magellanic Stream is about 77°. Is this evidence for a significant halo between 45 and 150kpc from the galactic centre? Despite the difference between 70.5 and 77 we use our very simple halo potential and method II.

We take the 3 points central to the stream to be those at $l, b, v_l = 290, -60, +22; 0, -83, -70; 83, -60, -167$. We take $(\dot{r}^2)_{\max} = (205\mathrm{km/s})^2$ and $V_c = 220\mathrm{km/s}, R_0 = 8.5\mathrm{kpc}$. These values lead to a normal to the plane of the stream with direction cosines $\hat{\mathbf{n}} = (.993, .097, -.074)$ and a distance to H of 74kpc. In the 3 directions above the distances to the stream are $d = 43, 45$ and 53kpc respectively while d_z=74kpc. The pericentric and apocentric distances from the galactic centre are then 43 and 170kpc.

The above determination of $\hat{\mathbf{n}}$ has nothing to do with the satellites of the Milky Way, nevertheless Sculptor lies very precisely ($< 0.1^\circ$) in this plane of the Magellanic Stream through the Galactic Centre and Draco lies only 0.5°

from that plane. The mass centre of the Magellanic Clouds lies only 1.2° from it. In these calculations we took the directions to satellites in the galactocentric sky given by Lynden-Bell & Lynden-Bell (1995), which were based on distances used there.

3. Conclusion

Application of Method II to the Magellanic Stream has given distances good to about 10%. This encourages us to apply these methods to other high-velocity-cloud streams whose distances are unknown or uncertain.

Acknowledgements We dedicated this talk to Renzo Sancisi who recently retired from Groningen and who has shown us many interesting observations of galaxies with enthusiastic delight (Baldwin, Lynden-Bell & Sancisi 1980). We thank Steve Majewski for challenging us to determine distances to cloud streams from the parallax due to the Sun's offset from the Galactic Centre (Majewski 2004).

References

Baldwin J.E., Lynden-Bell D & Sancisi R. 1980, MNRAS 193, 313.
Braun R. & Thilker D.A. 2004, A&A 417, 421.
Bruns C, Kerp J, Staveley-Smith L., Mebold U., Putman M.E., Haynes R.F., Kalberla, P.M.W., Muller E. & Filpovic M.D. 2005, A&A 432, 45.
Davies R.D. 1960, MNRAS 120, 483.
Dieter N.H. 1965, ApJ 70, 552.
Hulsbosch A.N.M. & Raimond E 1966, Bull astr Inst Netherl 18, 413.
Lynden-Bell D. & Lynden-Bell R.M. 1995, MNRAS 275, 429.
Majewski S.R. 2004, ASP Conference Series 327, 63.
Mathewson D.H., Cleary M.N. & Murray J.D. 1974, ApJ 190, 291
Oort J.H. 1970, A&A 7, 381.
Wannier, P. & Wrixon G.T. 1972, ApJ 178, 623.

MORPHOLOGY OF GALACTIC GLOBULAR CLUSTERS

C. W. Chen* and W. P. Chen**

Institute of Astronomy, National Central University, Taiwan

* awei@outflows.astro.ncu.edu.tw, ** wchen@astro.ncu.edu.tw

Abstract We study shapes and sizes of 110 Galactic globular clusters (GCs) with the 2MASS Point Source Catalog. In general, Galactic GCs have spherical halos, with a median flattening of 0.1. GCs closer to the bulge show more circularized shapes and have smaller physical sizes. Intrinsically more luminous clusters, hence perhaps more massive, tend to be more circularized. Six GCs are highly flattened with flattening ≥ 0.3 Arp 2 and Pal 12 are known to be associated with the streamer of the Sagittarius dwarf galaxy. Pal 5 is being cannibalized by the Milky Way, UKS 1 and NGC 6355 are bulge globular clusters suffering strong tidal distortion. NGC 2419 is a halo member with a Galactocentric distance 90 kpc. Its flattened shape can not be accounted for. It may well be the remnant core of an already dissolved dwarf galaxy.

Keywords: globular clusters : tidal distortion : morphology

1. Introduction

The destruction of globular clusters (GCs) are crucial to the evolution of the host galaxy. The initial population of GCs must be substantially higher than the current one but the clusters close to the bulge should have particularly higher mortality due to bulge shocking. Stars from disintegrated GCs were accreted to, and likely now dominate the stellar populations of, the bulge and halo of the Milky Way galaxy Gnedin & Ostriker 1997. Nordquist et al. (1999) investigated the effect of the tidal force from a bulge on the shape of a GC in a close encounter, and concluded that a typical GC passing within several hundred pc from the bulge would suffer substantial distortion. They suggested the effect to be detectable in the bulge GCs NGC 6293 and NGC 6440.

Meylan & Mayor (1986) noticed that 47 Tuc and ω Cen are flattened, likely due to their overall rotation. White & Shawl (1987) determined the axial ratios and orientations of 100 GCs with blue sensitive plates, and found a mean axial ratio of 0.93 ± 0.01, which they attributed to the rotation of the clusters

R. S. de Jong, Island Universes, 287–290.
© 2007 *Springer.*

rather than to Galactic tidal interactions. We used the Two Micron All Sky Survey (2MASS) infrared data to determine the shapes and sizes of the halos of GCs, in order to investigate how the stellar distribution changes with cluster evolution and passage through Galactic environments, e.g., by tidal interactions from the Galactic bulge or the Sagittarius dwarf. In every GC field, stars brighter than $K_s \sim 15.6$ mag, i.e., the 3-σ detection of 2MASS are selected. Without membership information, we analyze the morphology of a star cluster with a star counting method Chen et al. 2004. The clustering parameter is defined as $P_i = (N_t - N_f)/N_t = 1 - N_f/N_t$, where N_t is the total number of neighbors within a specific angular region around the ith star and N_f is the average field star number in the same area. The area used is a circular region which contains 50 field stars. The clustering parameter gives a measure of the local stellar density enhancement ranging from $P_i \sim 0$ in a field region to $P_i \sim 1$ in a cluster. Thus it behaves like a probability of cluster membership.

The stellar surface number density is estimated by summing up the clustering parameters of all the stars within a sky-coordinate grid. The core of a GC naturally is not resolved by 2MASS. We focus on the halo of a GC, defined as where the density drops to 5 times the background fluctuations. The boundary of the halo is then fitted with an ellipse whose flattening ($f = 1 - b/a$, where a and b are semi-major and semi-minor axes respectively) and average size ($r = (a + b)/2$) could be derived. The typical error of f is a few percent. Figure 1 shows our analysis on the bulge GC NGC 6355.

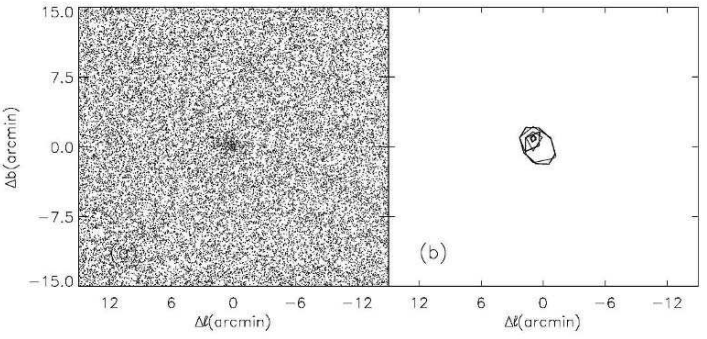

Figure 1. *Left*: The spatial distribution of 2MASS stars in the NGC 6355 field; *Right*: The computed effective stellar density contours.

2. Morphology of Globular Clusters

A total of 110 GCs selected from Harris (1996) with high enough density contrast ($\geq$ 5 times the background fluctuation) have been analyzed. The results are shown in Fig. 2. In general GC halos are circular/spherical (median f $\sim$ 0.12). The fraction of non-circular GCs is higher in our sample than in

White & Shawl (1987), who studied the cores of GCs, perhaps because the core of a GC tends to circularize by internal stellar encounters and the halo is more vulnerable to distortion by external perturbation. We also found that GCs closer to the bulge tend to be smaller and more circular. Intrinsically more luminous clusters, hence likely more massive, have more circular halos.

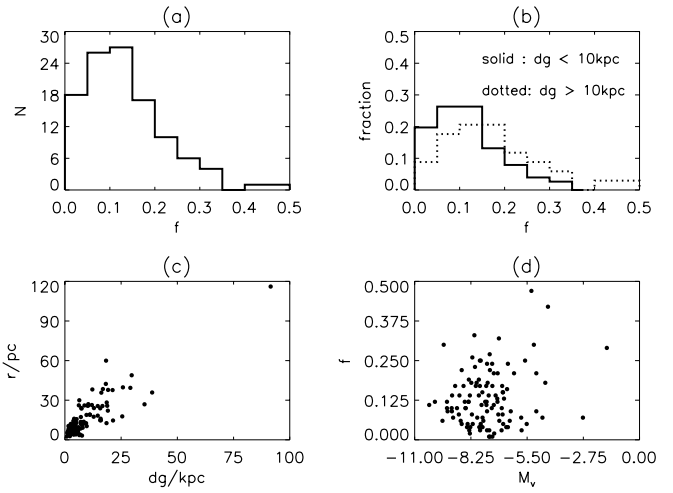

Figure 2. a) Distribution of flattening of GCs. b)Flattening for GCs close to and away from the bulge. c) The physical size vs Galactocentric distance d) Flattening vs absolute visual magnitude

None of the two bulge GCs, NGC 6293 and NGC 6440, suspected by Nordquist et al. (1999) to have distorted shapes, show detectable elongation in our analysis. We note 6 GCs with highly flattened shapes, $f \geq 0.3$. These 6 GCs, together with NGC 6293 and NGC 6440 are listed in Table 1, for which the first 5 columns give, respectively, the name of the cluster, its coordinates, heliocentric (d_s) and Galactocentric (d_g) distances, and the absolute magnitude, all taken from Harris (1996). The last 3 columns list the derived average angular radius (θ), physical size (r) and flattening (f) from our analysis.

Arp 2 and Pal 12, both known to be associated with the Sagittarius tidal stream van den Bergh & Mackey 2004 show significant elongation. Pal 12 is elongated roughly toward the direction of the tidal stream but Arp 2 points orthogonal to it. Odenkirchen et al. (2003) found a tidal tail associated with Pal 5 which extends more than 10 deg. They deduced that the cluster, being cannibalized by the Milky Way galaxy, is presently near the apocenter but has undergone several disk crossings, resulting in strong tidal shocks. Our data on Pal 5 are limited by the 1 deg field of view set by the 2MASS database interface, thus detect flattening only for the inner part of the cluster. UKS 1 and NGC 6355 are both bulge GCs, with the projected elongation in either

Table 1. Morphological Parameters of Globular Clusters

Name	(l,b) (deg,deg)	d_s (kpc)	d_g (kpc)	M_V	θ (arcmin)	r (pc)	f
NGC 6293	(357.62, +07.83)	8.8	1.4	-7.77	2.60	6.7	0.05
NGC 6440	(007.73, +03.80)	8.4	1.3	-8.75	2.54	6.2	0.06
Arp 2	(008.55, -20.78)	28.6	21.4	-5.29	1.76	14.6	0.47
Pal 12	(030.51, -47.68)	19.1	15.9	-4.48	2.88	16.0	0.42
Pal 5	(000.85, +45.86)	23.2	18.6	-5.17	4.19	28.3	0.30
UKS 1	(005.12, +00.76)	8.3	0.8	-6.88	1.02	2.3	0.32
NGC 6355	(359.58, +05.43)	9.5	1.8	-8.08	1.89	5.2	0.33
NGC 2419	(180.37, +25.24)	84.2	91.5	-9.58	4.74	116.1	0.30

case pointing to the direction of the Galactic bulge, a clear manifestation of tidal distortion. NGC 2419 is a halo member, away from the Galactic disk (35.9 kpc) and the bulge (90 kpc). It is one of the five most luminous Galactic globular clusters, and among the most metal-poor Galactic GCs, with [Fe/H] ~ -2.4 (Harris et al. 1997). There is no obvious cause for its flattened shape. It may well be in a late stage of disintegration or as the remnant core of a dissolved dwarf galaxy.

References

Chen W.P., Chen C.W. & Shu C.G. 2004, AJ 128, 2306
Gnedin O.Y. & Ostriker J.P. 1997 ApJ 474, 223
Harris W.E. 1996, AJ 112, 1487
Harris W.E. et al. 1997, AJ 114, 1030
Nordquist H.K., Klinger R.J., Laguna P. & Charlton J. C. 1999, MNRAS 304, 288
Meylan G. & Mayor M. 1986, A&A 166, 122
Odenkirchen M. et al. 2003 AJ 126, 2385
White R.E. & Shawl S.J. 1987, ApJ 317, 246
van den Bergh S. & Mackey A.D. 2004, MNRAS 354, 713

OBSERVATIONS OF STRIPPED EDGE-ON VIRGO CLUSTER GALAXIES

Hugh H. Crowl[1], Jeffrey D.P. Kenney[1], J.H. van Gorkom[2] and Bernd Vollmer[3]

[1]*Department of Astronomy, Yale University, New Haven, USA*
[2]*Department of Astronomy, Columbia University, New York, USA*
[3]*CDS, Observatoire Astronomique de Strasbourg, France*

Abstract We present observations of highly inclined, HI deficient, Virgo cluster spiral galaxies. Our high-resolution VLA HI observations of edge-on galaxies allow us to distinguish extraplanar gas from disk gas. All of our galaxies have truncated Hα disks, with little or no disk gas beyond a truncation radius. While all the gas disks are truncated, the observations show evidence for a continuum of stripping states: symmetric, undisturbed truncated gas disks indicate galaxies that were stripped long ago, while more asymmetric disks suggest ongoing or more recent stripping. We compare these timescale estimates with results obtained from two-dimensional stellar spectroscopy of the outer disks of galaxies in our sample. One of the galaxies in our sample, NGC 4522 is a clear example of active ram-pressure stripping, with 40% of its detected HI being extraplanar. As expected, the outer disk stellar populations of this galaxy show clear signs of recent (and, in fact, ongoing) stripping. Somewhat less expected, however, is the fact that the spectrum of the outer disk of this galaxy, with very strong Balmer absorption and no observable emission, would be classified as "k+a" if observed at higher redshift. Our observations of NGC 4522 and other galaxies at a range of cluster radii allow us to better understand the role that clusters play in the structure and evolution of disk galaxies.

Keywords: galaxies: clusters - galaxies: ISM - galaxies: evolution

1. Introduction

The morphology-density relationship (Oemler 1974; Melnick & Sargent 1977; Treu et al. 2003) is one of the clearest examples of the effect that clusters have on their member galaxies. There are several cluster processes that may contribute to this observed effect (Treu et al. 2003). ISM-ICM stripping (which includes both ram-pressure stripping and turbulent viscous stripping) may be among the most important processes in the transformation of late-type cluster spirals into Sa's and S0's. This process, which removes gas from the

R. S. de Jong, Island Universes, 291–294.
© 2007 *Springer.*

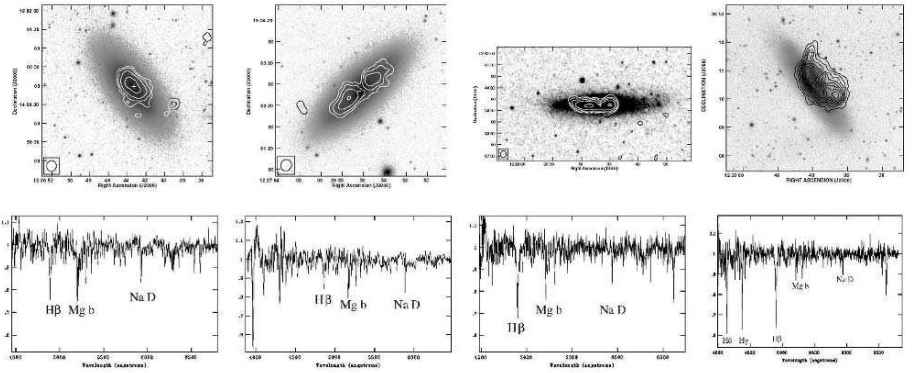

Figure 1. HI maps (top) and outer disk spectra (bottom) for (from left to right) IC 3392, NGC 4419, NGC 4388, and NGC 4522. The HI disks of the galaxies become more asymmetric from left to right, a trend that is accompanied by an increase in the strength of the Hβ line.

galaxy but leaves the stars unperturbed, results in galaxies with truncated gas and star-forming disks (Koopmann & Kenney 2004a;b). Simulations of ICM-ISM interactions (e.g., Schulz & Struck 2001; Vollmer et al. 2001) have shown that a smooth, uniform ISM can be stripped from the outer regions of galaxies in clusters via ram pressure. Some of this gas and dust will escape from the galaxy and become part of the ICM, while some will fall back onto the galaxy (Vollmer et al. 2001). In either scenario, simulations show large amounts of extraplanar material near the disk of the galaxy during ISM-ICM stripping. Therefore, by studying the details of ISM-ICM stripping events, we can gain a better understanding of the structure and dynamics of galaxy clusters.

2. HI Imaging and Optical Spectroscopy

As part of a larger VLA survey of Virgo Cluster spiral galaxies (Chung et al. 2006, in preparation), we have observed several edge-on spiral galaxies to allow us to distinguish potential extraplanar gas from disk gas. In at least one case (NGC 4522; described in detail in the next section), there has been the unambiguous detection of extraplanar gas. Figure 1 shows HI maps of the outer disks of four of the sample edge-on galaxies. The HI morphologies range from very symmetric, truncated disks (IC 3392 and NGC 4419) to NGC 4522, with extraplanar gas making up 40% of the measured HI.

In order to better characterize the stellar population of the outer disks of these galaxies, we observed them with the SparsePak Integral Field Unit (Bershady et al. 2004) on the WIYN 3.5m telescope. SparsePak allows us to take simultaneous spectra of many positions in the disk. Through averaging of several positions, we have obtained high signal-to-noise spectra of the outer stellar disks just beyond the gas truncation radius (Figure 1). The outer disk integrated

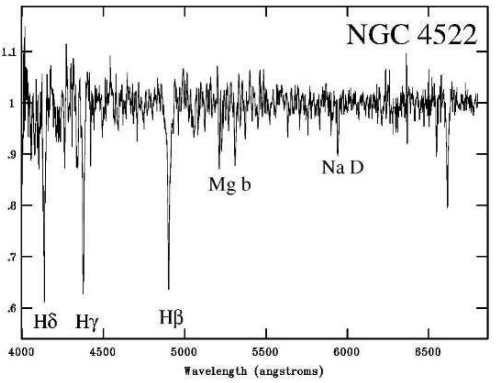

Figure 2. SparsePak spectrum of outer disk (the average of fibers at radii between 50" and 60" (4-5 kpc)) of NGC 4522. The lack of Hα emission and strong higher-order Balmer line absorption lead us to classify this as a k+a or a+k spectrum.

spectra of these galaxies also show a notable trend: an increase in strength of the Hβ line from IC 3392 (EW(Hβ)=3.8 Å) and NGC 4419 (EW(Hβ)=2.7 Å) to NGC 4388 (EW(Hβ)=6.5 Å) and NGC 4522 (EW(Hβ)=8.2 Å). Taken together, these data seem to suggest an evolutionary sequence. Galaxies with very symmetric disks (i.e. NGC 4419 and IC 3392) have outer disks with older stellar populations and, as the gas disks become more asymmetric and irregular (i.e. NGC 4388 and NGC 4522), the age of the stellar population is younger.

3. NGC 4522: A Local Analog to k+a Galaxies

NGC 4522 is a highly inclined, $0.5L_*$, spiral galaxy in the southern part of the Virgo Cluster, $0.6\ r_{100}$ from M87 at the center of the cluster, and only $0.3\ r_{100}$ from M49, which is at center of subcluster B. There is strong evidence, both from HI (Kenney et al. 2004) and radio continuum (Vollmer et al. 2004) observations that it is currently being stripped of its gas by interaction with an ICM. In a galaxy stripped of its gas such as this, we expect rapid cessation of star formation as the raw materials for forming stars are removed from the disk. Indeed, Koopman & Kenney (2004a;b) find many such galaxies in the Virgo cluster: galaxies with normal stellar disks, but truncated Hα disks.

The spectrum of NGC 4522 (Figure 2) shows no signs of active star formation and, indeed, the Hα line shows moderately strong absorption. The higher order indices show extraordinarily strong absorption: EW(Hδ)=5.3 Å, EW(Hγ)=5.5 Å, and EW(Hβ)=8.2 Å. Models have suggested that rapid truncation of star formation will leave distinct spectral signatures, most notably a sharp rise in strength of the higher order Balmer line indices (Couch & Sharples 1987; Shioya et al. 2002). In their models of a simple stellar population, Shioya et al. 2002 show that Hδ equivalent width rises by ~ 5 Å on

very short timescales as the O and B stars die and the A stars, with very strong Balmer lines, begin to dominate the integrated light. Such galaxies, with no active star formation but strong Balmer absorption lines have been observed in clusters and are commonly called "k+a" galaxies, in reference to their mix of stellar populations. Galaxies with a k+a spectral signature were first discovered in high-z clusters (Dressler & Gunn 1982,1983) but have been since discovered as nearby as the Coma cluster (Poggianti et al. 2004). Our observations of NGC 4522 imply the outer disk is similar in stellar population to the k+a galaxies at higher redshift (as described by Dressler et al. 1999). While we are studying only one region of a galaxy, it appears possible to create a k+a spectrum with ram pressure stripping.

4. Summary

There is little doubt that cluster processes play an important role in the evolution of their member galaxies. The relative importance of specific processes, however, has yet to be fully understood. Recent work (Shioya et al. 2004) has suggested a convergent evolutionary scheme; that different processes that lead to the same morphological endpoint. By studying galaxies in the nearby Virgo cluster, we can hope to better understand the details of cluster galaxy evolution processes. It appears that ram pressure stripping must play an important role in the transformation of galaxies in clusters and that k+a spectra of galaxies observed at higher redshift can plausibly be caused by ram pressure stripping of gas-rich spirals.

References

Bershady, M. A., Andersen, D. R., Harker, J., Ramsey, L. W., & Verheijen, M. A. W. 2004, PASP, 116, 565

Couch, W. J., & Sharples, R. M. 1987, MNRAS, 229, 423

Dressler, A., & Gunn, J. E. 1982, ApJ, 263, 533

Dressler, A., & Gunn, J. E. 1983, ApJ, 270, 7

Kenney, J.D.P., van Gorkom, J.H., & Vollmer, B. 2004, AJ, 127, 3361

Koopmann, R.A. & Kenney, J.D.P. 2004a, ApJ, 613, 851

Koopmann, R.A. & Kenney, J.D.P. 2004b, ApJ, 613, 866

Melnick, J. & Sargent, W.L.W. 1977, ApJ, 215, 401

Oemler, A. 1974, ApJ, 194, 1

Schulz, S. & Struck, C. 2001, MNRAS, 328, 185

Shioya, Y., Bekki, K., Couch, W. J., & De Propris, R. 2002, ApJ, 565, 223

Shioya, Y., Bekki, K., & Couch, W. J. 2004, ApJ, 601, 654

Treu, T., Ellis, R.S., Kneib, J-P., Dressler, A., Smail, I, Czoske, O., Oemler, A. & Natarajan, P. 2003, ApJ, 591, 53

Vollmer, B., Cayatte, V., Balkowski, C., & Duschl, W.J. 2001, ApJ, 561, 708

SPARSEPAK OBSERVATIONS OF DIFFUSE IONIZED GAS HALO KINEMATICS IN NGC 891

George H. Heald[1], Richard J. Rand[1], Robert A. Benjamin[2] and Matthew A. Bershady[3]

[1] *Univ. of New Mexico, USA*
[2] *Univ. of Wisconsin – Whitewater, USA*
[3] *Univ. of Wisconsin – Madison, USA*

Abstract We present WIYN SparsePak observations of the diffuse ionized gas (DIG) halo of NGC 891. Preliminary results of an analysis of the halo velocity field reveal a clear gradient of the azimuthal velocity with z which agrees with results for the neutral gas. The magnitude of the gradient has been determined, using two independent methods, to be approximately 15 km s^{-1} kpc^{-1}.

Keywords: galaxies: kinematics and dynamics - galaxies: individual (NGC891) - galaxies: ISM

1. Observations and Data Reduction

Data were obtained during the nights of 10–12 December 2004 with the SparsePak IFU (see Bershady et al. 2004; 2005). We used the 860 l/mm grating at order 2, which provides a spectral resolution $\lambda/\Delta\lambda \sim 4{,}900$, and the 316 l/mm grating at order 8, which provides a spectral resolution $\sim 10{,}000$. In the latter mode, the wavelength coverage includes the Hα, [N II] $\lambda\lambda$6548,6583 and [S II] $\lambda\lambda$6716,6731 emission lines. The higher spectral resolution data are presented and discussed in this paper. The data were reduced in IRAF. Figure 1 shows the SparsePak pointings on an Hα image of NGC 891.

2. Azimuthal Velocities from Envelope Tracing

To analyze the kinematic structure of the DIG halo of NGC 891, position-velocity (PV) diagrams have been constructed from the spectra of all 82 fibers in pointing 'H' (cf. Fig. 1). To enhance signal-to-noise, several fibers were averaged together for each major axis distance R at the highest z. Figure 1 indicates which fibers were included in each z-range. Because a bright sky line interferes with several of the Hα profiles, and to increase signal-to-noise,

R. S. de Jong, Island Universes, 295–298.
© 2007 *Springer.*

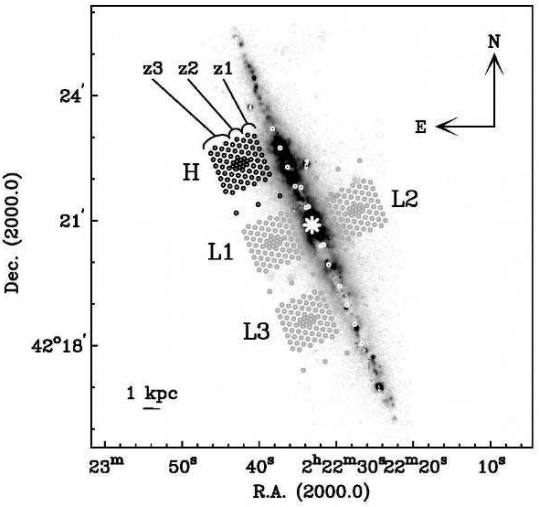

Figure 1. Hα image of NGC 891 from Rand et al. 1990, with the positions of the SparsePak fibers during the higher spectral resolution observations (H) overlaid as black circles. Lower spectral resolution pointings (L1, L2, and L3), to be presented in a future paper, are plotted with gray circles. Fibers on the major axis are plotted in white for clarity. Ranges of z used to construct PV diagrams (see text) are labeled z1, z2, and z3. The rotation center is marked with a white star. The receding side is to the south.

PV diagrams were constructed of the sum of the [N II] λ6583 + [S II] λ6716 emission lines. Contour plots of the PV diagrams are included in Fig. 3.

Rotation curves were derived for each PV diagram using the envelope tracing method (e.g., Sofue & Rubin 2001). Because NGC 891 is nearly edge-on ($i > 88°$; Swaters 1994), the edge of each line profile furthest from the systemic velocity (the "envelope") corresponds to gas at the line of nodes; this velocity is thus approximately the azimuthal velocity at that R. The azimuthal velocity is found by (Sofue & Rubin 2001):

$$v_{\rm az} = (v_{\rm env} - v_{\rm sys})/\sin(i) - \sqrt{\sigma^2_{\rm inst} + \sigma^2_{\rm gas}}, \qquad (1)$$

where $v_{\rm env}$ is the velocity at the location of the envelope, $\sigma_{\rm inst}$ is the velocity resolution of the instrument, and $\sigma_{\rm gas}$ is the velocity dispersion of the gas. Azimuthal velocity curves were constructed from the PV diagrams, and are shown in Fig. 2. Extinction in the midplane prevented reliable velocities from being found for $z \approx 0''$.

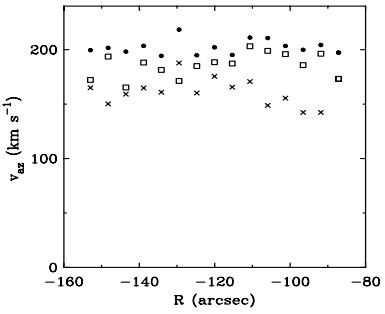

Figure 2. Azimuthal velocity curves, derived from the PV diagrams shown in Fig. 3 using the envelope tracing method. Velocities are shown for $25'' < z < 45''$ (z1; *filled circles*), $45'' < z < 65''$ (z2; *open squares*), and $z > 65''$ (z3; *crosses*), and are relative to $v_{\rm sys} = 528$ km s^{-1}.

It is clear from Fig. 2 that the derived azimuthal velocities decrease with height. A close inspection of the PV diagrams shows that this is not an effect of signal-to-noise variations with height. An average azimuthal velocity gradient of 0.80 km s^{-1} arcsec^{-1} (17 km s^{-1} kpc^{-1}) was calculated. Similar results were obtained by following this procedure for the [N II] λ6583 emission line alone (14 km s^{-1} kpc^{-1}). These values are in agreement with that measured by Fraternali et al. 2005 for the neutral component, 15 km s^{-1} kpc^{-1}.

3. Azimuthal Velocities from PV Diagram Modeling

The envelope tracing method is sensitive to the changing signal-to-noise ratio of the data with z. To account for this effect and the radial gas distribution, we have generated galaxy models. The Hα image presented in Fig. 1 was used to obtain estimates of the radial density profile at each of the heights considered in the model. Because the distribution of the DIG is not axisymmetric, the profiles were modified by hand to better match the shape of the data PV diagrams. The amplitude of the radial density profile was chosen such that the signal-to-noise in the model approximately matched that in the data.

We then created model galaxies with these derived radial profiles using a version of the GIPSY task GALMOD, modified to allow for a vertical gradient in azimuthal velocity which begins at a height z_0 above the midplane:

$$v(R,z) = v(R, z \leq z_0) - \frac{dv}{dz}\,[|z| - z_0]\,, \tag{2}$$

where dv/dz has units of [km s^{-1} arcsec^{-1}], and for the models considered here, the major axis rotation curve is flat [$v(R, z \leq z_0) = 200$ km s^{-1}]. The inclusion of the parameter z_0 was motivated by the results of Fraternali et al. 2005, who find that the gradient in the neutral component of NGC 891 starts at approximately $z = 1.3$ kpc (though that result may be a consequence of beam smearing). That value of z_0 was used for the models shown here, but we note that the appropriate value cannot be determined for our data (we lack data below $z \approx 1.2$ kpc). Artificial SparsePak observations were made of the models to create PV diagrams, and compared to the data (Fig. 3).

The model that appears to best match the data has $dv/dz = 15$ km s^{-1} kpc^{-1}. A statistical analysis of difference images suggests that the best match occurs at $dv/dz = 12 - 14$ km s^{-1} kpc^{-1}, but because the model cannot perfectly reproduce the shape of the PV diagrams, comparing by eye is the most reliable way to determine the gradient. To ensure that our results are not influenced by an incorrect specification of the radial density profile, we also consider models with a flat radial density profile, and find that the same gradient yields the best match. We conclude that the vertical gradient in azimuthal velocity for the DIG halo of NGC 891 is approximately 15 km s^{-1} kpc^{-1}.

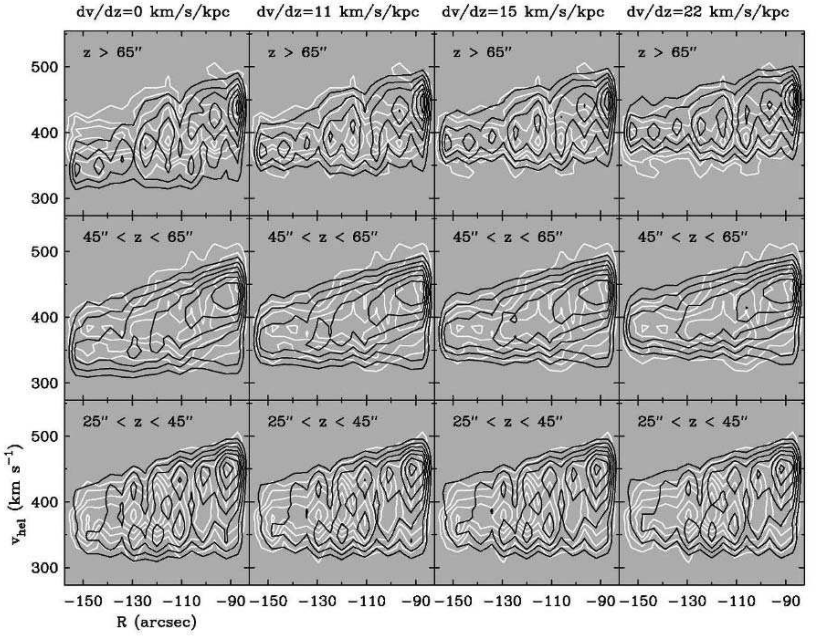

Figure 3. Comparison between data (*white*) and model (*black*) PV diagrams for different values of dv/dz, at the indicated heights. Contour levels for data and models are 10, 15, 20, 25, 30, 35, and 40σ for $25'' < z < 45''$ (z1); 5, 8, 11, 14, 17, and 20σ for $45'' < z < 65''$ (z2); 3, 4.5, 6, 7.5, 9, 10.5, and 12σ for $z > 65''$ (z3). The systemic velocity is $v_{\rm sys} = 528$ km s^{-1}.

4. Future Work

To attempt to understand the origin of the azimuthal velocity gradient derived in this paper, the kinematic data will be compared with the results of an entirely ballistic model of disk–halo flow (cf. Collins et al. 2002). Further information regarding the kinematic structure will be obtained once the lower spectral resolution pointings are reduced and analyzed. Results from these efforts will be presented in a forthcoming paper.

Acknowledgements This material is based on work partially supported by the National Science Foundation under Grant No. AST 99-86113.

References

Bershady, M. A., et al. 2004, PASP, 116, 565

Bershady, M. A., et al. 2005, ApJS, 156, 311

Collins, J. A., Benjamin, R. A., & Rand, R. J. 2002, ApJ, 578, 98

Fraternali, F., et al. 2005, in ASP Conf. Proc. 331, Extra-Planar Gas, ed. R. Braun (San Francisco: ASP), 239

Rand, R. J., Kulkarni, S. R., & Hester, J. J. 1990, ApJ, 352, L1

Sofue, Y. & Rubin, V. 2001, ARA&A, 39, 137

Swaters, R. 1994, Doctoraal Scriptie, Univ. Groningen

STELLAR POPULATIONS IN THE OUTER REGIONS OF M31

Rachel Johnson[1*], Daniel Faria[2] and Annette Ferguson[3]

[1] *University of Oxford, UK*
[2] *Lund Observatory, Sweden*
[3] *IfA, Edinburgh, UK*
* raj@astro.ox.ac.uk

Abstract The stellar populations of nearby galaxies are accessible for detailed analysis, and can provide constraints on galaxy formation scenarios. We have obtained deep HST ACS images of several fields in the outer regions of M31, three of which are presented here. The intermediate age populations in these fields appear very similar, whereas the contribution of young stars varies from field to field.

Keywords: galaxies: stellar content - galaxies: individual (M31) - galaxies: halos

Introduction

Ground based observations of red giant stars in M31 (e.g., Ferguson et al. 2002) have shown that its outer regions contain considerable structure. We have obtained HST ACS observations of 8 fields at various locations in the outer regions of M31, principally targetting substructures seen in the ground-based images. Our initial analysis (Ferguson et al. 2005) found differences between the colour-magnitude diagrams (CMDs) from the various fields, in particular in the morphology of the red clump, the strength of the red giant branch and asymptotic giant branch bumps and the presence of a blue plume.

Here we compare 3 fields located close to the major axis of M31 - the G1 clump, the stellar warp, and the northern spur. These fields all lie well outside the bright inner disk of M31 (the inner disk scale length is 5.9 kpc), at projected distances of 29.6 kpc (G1 clump), 25.5 kpc (warp) and 25.7 kpc (spur). The warp and the G1 clump are at the southern end of the major axis and the warp is at the northern end.

R. S. de Jong, Island Universes, 299–302.
© 2007 *Springer.*

All fields were observed with ACS in the two filters F606W and F814W. Exposure times were ≈10000 s (F606W) and ≈15000 s (F814W) for the warp field, and 2500 s (F606W) and 5000 s (F814W) for the spur and clump fields.

Results & Discussion

Figure 1 shows the colour magnitude diagrams for the 3 fields. The data in the CMDs are calibrated in Vegamag and have been de-reddened (E(B-V)≈0.06 for these fields).

The lines in the G1 clump CMD show 90% and 50% completeness limits and error bars determined from artificial star tests. The completeness limits and errors in the spur CMD should be similar, while the warp CMD is somewhat deeper. The lines in the warp CMD show the region used to create the red giant branch luminosity function.

The main features of the CMDs are labelled on the G1 clump CMD. All show a broad red giant branch (RGB), and a prominent round red clump (RC). Two additional bumps, above and below the red clump, are also seen in the CMDs, most obviously in the spur field. These are most likely the AGB (above) and RGB (below) bumps.

The ages and metallicities of the old and intermediate stars can be constrained from the locus and width of the RGB, in conjunction with the position and morphology of the RC. Comparison of the RGB locus with the overplotted isochrones shows that the isochrones are a reasonable fit, although no single isochrone fits the RGB well along its whole length.

Figure 2 shows the normalised RGB luminosity functions. The magnitude of and relative number of stars in the red clump are very similar in all fields, as is the colour. Comparison of the red clump colour and magnitude to the models of Girardi & Salaris (2001) gives an estimate of the age and metallicity of the stellar population of ∼5 Gyr and [M/H]=–0.4. Using artificial CMDs created using the StarFISH software (Harris & Zaritsky 2001) we modelled the G1 clump field and found that an age spread of at least a few Gyr is required to produce the vertical extent of the red clump.

The spur and warp fields have an additional feature in the luminosity function at m_{814}≈23.1, which we associate with the AGB bump. Comparison of the distance between the AGB bump and the RC to the models of Alves and Sarajedini (1999) again gives a population age of 4-5 Gyr for the metallicity found above.

The CMD features due to younger populations do not look so similar. A prominent blue plume is seen in the G1 clump and the warp fields, but not in the spur field. The youngest stars in the G1 clump model have ages of 250 Myr. The warp field also has an additional prominent feature at m_{606}-m_{814}≈0.3.

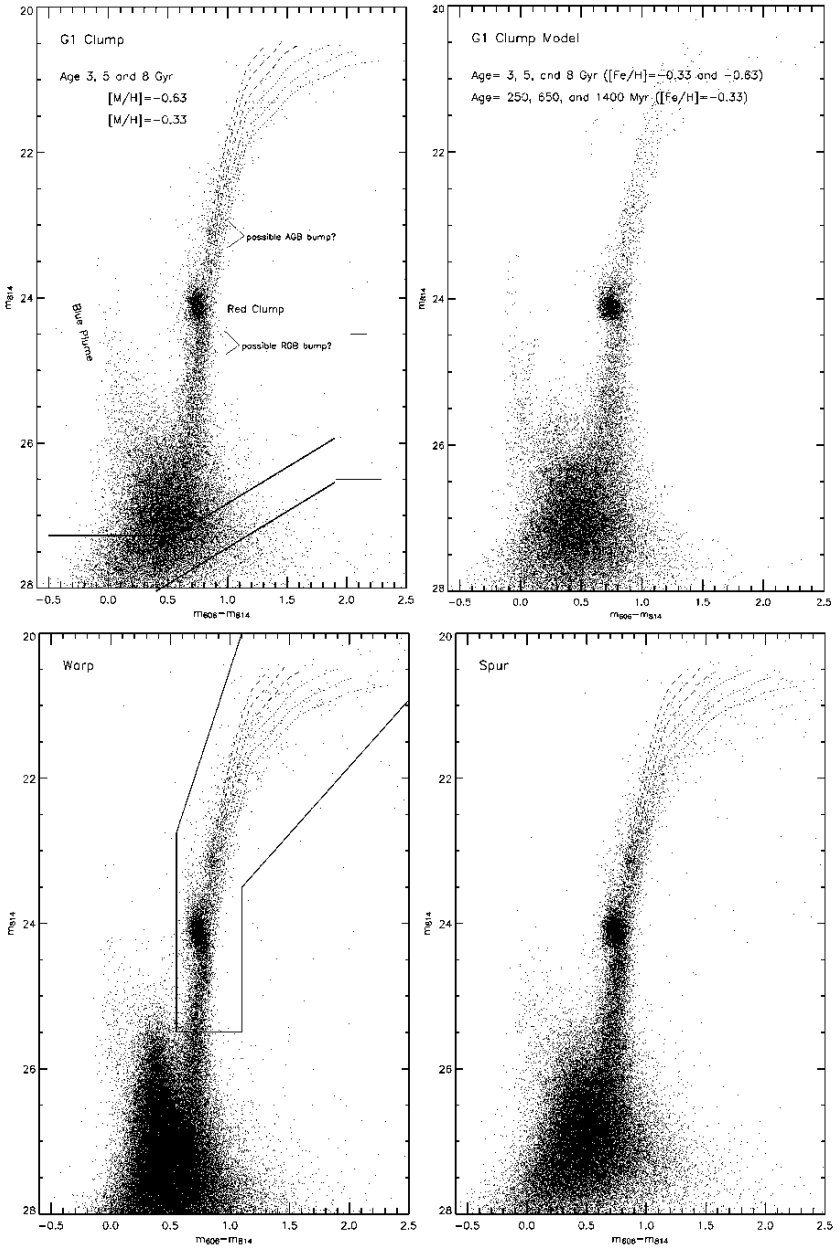

Figure 1. Colour magnitude diagrams of the G1 Clump, Warp and Spur fields. Also shown is the CMD of our model G1 clump population. The lines in the G1 clump CMD give the 90% and 50% completeness limits from artificial star tests. The lines in the Warp CMD delineate the region used to create the RGB luminosity function.

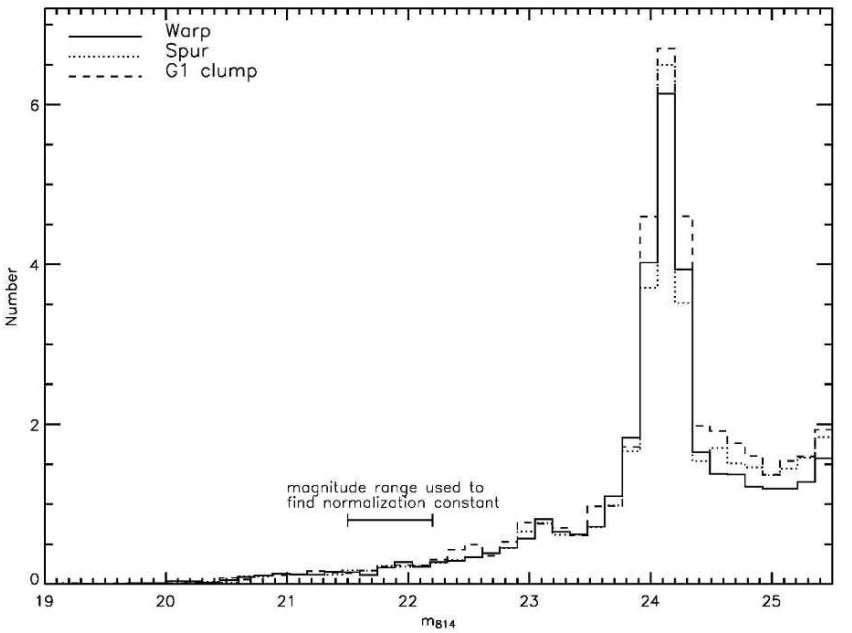

Figure 2. Normalized RGB luminosity functions in m_{814} for the three fields.

It seems that these fields, on opposite sides of M31, experienced a similar star formation history a few Gyr ago. The resolution with which we can distinguish different stellar population ages is ∼1-2 Gyr at ∼6 Gyr. The age, age spread, and relatively high metallicity in these fields appear similar to those in a field studied by Brown et al. (2003), which is at 11 kpc along the minor axis, or at a de-projected radius in the disk of 51 kpc. Whether any of these populations were produced by the same mechanism, and what that mechanism might be, is still unclear, and will be investigated using our full data-set of imaging and spectroscopy.

References

Alves D.R. & Sarajedini A. 1999, ApJ, 511, 225

Brown T.M., Ferguson H.C., Smith E., Kimble R.A., Sweigart A.V., Renzini A., Rich R.M., VandenBerg D.A. 2003, ApJL, 592, 17

Ferguson A.M.N., Irwin M.J., Ibata R.A., Lewis G.F., Tanvir N.R. 2002, AJ, 124, 1452

Ferguson A.M.N., Johnson R.A., Faria D.C., Irwin M.J., Ibata R.A., Johnston K.V., Lewis G.F., Tanvir N.R. 2005, ApJL, 622, 109

Girardi L. & Salaris M. 2001, MNRAS, 323, 109

Harris J. & Zaritsky D. 2001, ApJS, 136, 25

A STUDY OF EXTRA-PLANAR HI GAS

NGC 7814 and UGC 1281

P. Kamphuis[1*], R.F. Peletier[1], P.C. van der Kruit[1], T.A. Oosterloo[2] and R. Sancisi[1,3]

[1] *Kapteyn Astronomical Institute, University of Groningen, The Netherlands*

[2] *ASTRON, Dwingeloo, The Netherlands*

[3] *INAF - Osservatorio Astronomico di Bologna, Italy*

* kamphuis@astro.rug.nl

Abstract The origin of HI at anomalous velocities and at large distances above the disk, detected in a few spiral galaxies, is still a puzzle. To improve on our understanding of this extra-planar gas, we have started a study of a representative sample of nearby edge-on galaxies. In this paper we present the observations and a preliminary analysis of the extra-planar gas of UGC 1281 and NGC 7814. These galaxies were observed with the WSRT for 4 $\times$ 12 hours. In the dwarf galaxy UGC 1281, there are clear indications of a gaseous halo. A preliminary analysis of NGC 7814 shows no halo; however, we have detected extra-planar gas, at velocities higher than the maximal rotational velocity, above and below the plane. The origin of this gas is unclear.

Keywords: galaxies: individual (UGC 1281, NGC 7814) - galaxies: ISM - galaxies: halos - galaxies: kinematics and dynamics - ISM: structure

Introduction

The picture of the vertical HI gas distribution in spiral galaxies emerging from recent deep HI observations of a number of galaxies (NGC 891, Fraternali et al. 2003, NGC 2403; Fraternali et al. 2002 and UGC 7321, Matthews et al. 2003) is that of a cold thin disk surrounded by a thick layer of more slowly rotating gas (halo gas). In NGC 891 this halo extends up to 15 kpc ($\sim$40$\times$ optical scale height) from the plane of the disk. 3D-modeling shows that this gas rotates more slowly than the gas in the disk (see Fig. 4 in Swaters et al. 1997). In UGC 7321 gas has been found in the halo up to 2.4 kpc ($h_{z,\mathrm{H}} \sim 140$ pc). This high latitude HI material might be analogous to the Galactic High Velocity Clouds (HVCs) (Fraternali et al. 2002), and might provide an answer to the question of the origin of the HVCs.

R. S. de Jong, Island Universes, 303–306.
© 2007 *Springer.*

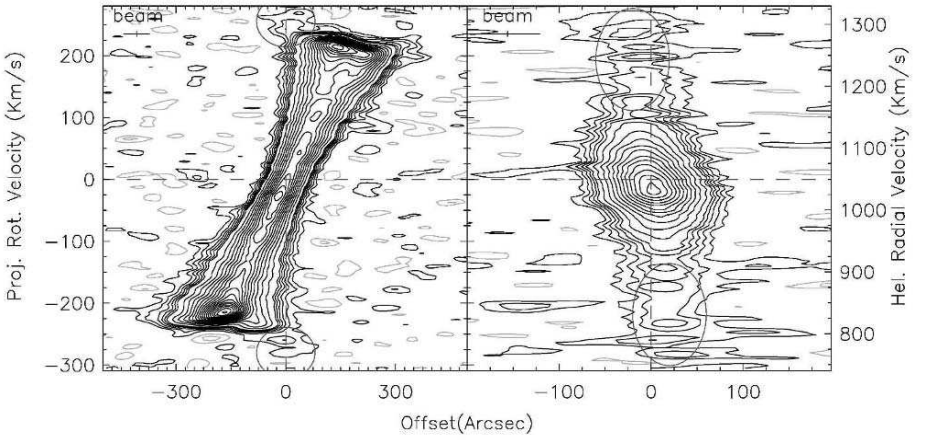

Figure 1. Position-Velocity diagrams of the HI along the major axis (left panel) and along the minor axis (right panel) in NGC 7814. The circles and ellipses indicate the anomalous gas. Contours are from -3σ (grey) to +6σ (black) in steps of 1.5σ (σ = 0.5 mJy/beam); the 0 contour is omitted. After +6σ the contours are from 4.2 mJy/beam, increasing with steps of 2.5 mJy/beam.

To study the phenomenon of HI halos we constructed a sample of spiral galaxies with a range of luminosities, morphological types and star formation properties. The first, central question is that of the origin of the HI halos. The study of the presence and of the density distribution and kinematical properties of the halos for such a range of different systems should provide the basis for understanding the physical mechanisms at the origin of the phenomenon. Here we present a preliminary analysis of two galaxies observed with the Westerbork Synthesis Radio Telescope (WSRT).

1. The Observations

We observed the edge-on galaxies NGC 7814 and UGC 1281 for 4 × 12 hours with the WRST in the 21 cm line. The data were reduced in the standard way with MIRIAD (Sault & Killeen 2004).

NGC 7814

NGC 7814 is a very massive ($V_{\rm max}$ = 240 km/s) early type spiral (Sa) with a flattened bulge (axis ratio 0.57)(van der Kruit & Searle 1982). The distance to the galaxy is 15 Mpc. Its systemic velocity is 1050 ±8 km/s.

During our inspection of the natural weighted data, we found two features extending out from the plane (Fig. 2). They appear at the highest rotational velocities observed in this galaxy. They have a small velocity dispersion (± 15 km/s). The origin and dynamics of this gas are a puzzle. There are indications

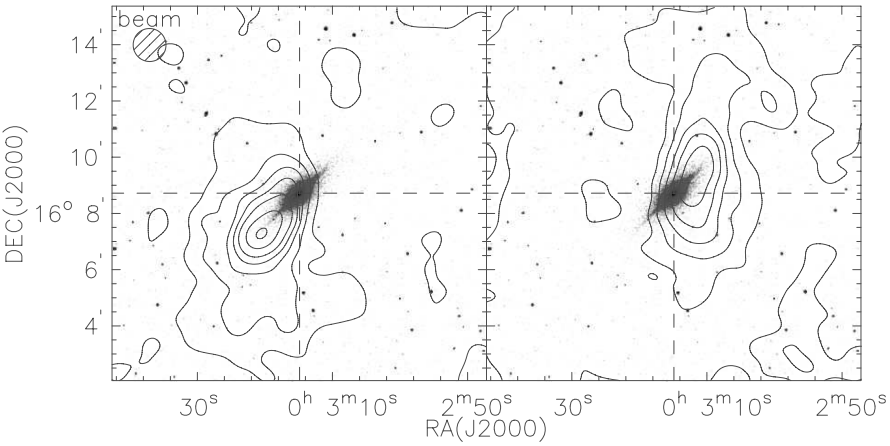

Figure 2. NGC 7814 contour plots showing the extra-planar HI features (3 channels stacked) overlaid on an optical image. Contours are from -3σ (grey) to +6σ (black) in steps of 1.5σ ($\sigma = 1.6$ mJy/beam), the 0 contour is omitted. After +6σ the contours run from 12.5 mJy/beam increasing with steps of 5 mJy/beam. The left (right) panel shows the feature at 1285$\pm$8 km/s (804$\pm$8 km/s). These are the highest (lowest) velocity channels. The systemic velocity is 1050 $\pm$ 8 km/s.

that there is a bar in the inner region (from the subtraction of an axisymmetric model to the light). The features are situated at the edges of the optical bulge (Fig. 2) and may be connected with the bar.

UGC 1281

The other galaxy observed at 21 cm was the Low Surface Brightness (LSB) dwarf galaxy UGC 1281. Here we find a halo, extending 700 pc on both sides of the plane at column densities $N_H = 4.2 \times 10^{19}(3\sigma)$. UGC 1281 is a quiescent galaxy, forming fewer stars per unit of mass than NGC 891, the classical example of a galaxy with a halo, indicating that the amount of star formation itself is not the only parameter determining the presence of a gaseous halo in spiral galaxies.

The 'Position-Velocity diagrams' (PV diagrams) parallel to the minor axis (Fig. 3) indicate a thickening on the side of the systemic velocity (156 $\pm$ 1 km/s), suggesting the presence of halo gas lagging in velocity with respect to the disk. As in the case of the superthin galaxy UGC 7321 (Matthews & Wood 2003) the origin of such a lagging HI halo in a LSB (low star formation) dwarf galaxy is difficult to explain.

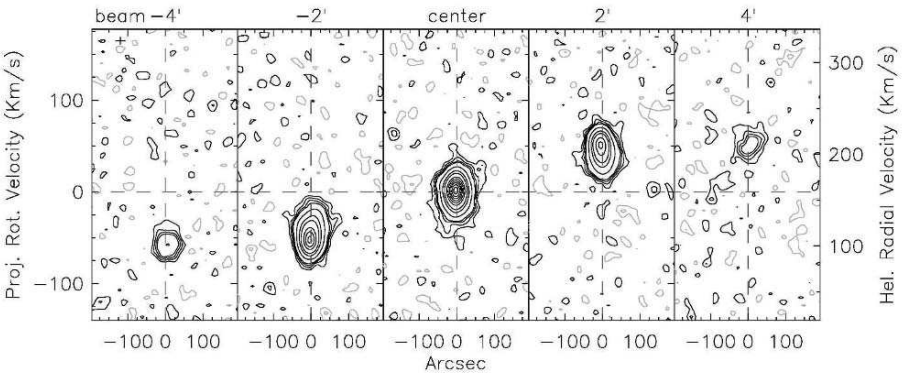

Figure 3. PV diagrams parallel to the minor axis of UGC 1281 at a distance of -4, -2, 0, 2 and 4 arcmin from the center. Contours are from -3σ (grey) to +6σ (black) in steps of 1.5σ ($\sigma = 0.33$ mJy/beam), the 0 contour is omitted. After +6σ the contours are from 5 mJy/beam to 20 mJy/beam increasing with steps of 6 mJy/beam and from 30 mJy/beam on increasing with 10 mJy/beam.

2. Future Work

For NGC 7814 a model analysis of the data is necessary to investigate the presence of the non-circular motion and the peculiar z-extent. For UGC 1281 we are still trying to improve the observational picture with additional data. Also, Hα observations of UGC 1281 are needed to obtain a better estimate of the star formation in this galaxy. In the end, it is our goal to analyse the properties of 16 edge-on galaxies and to determine how common HI halos are and which factors (e.g., mass, star formation, morphological type, luminosity) play a role in the formation of these halos.

References

Fraternali, F., van Moorsel, G., Sancisi, R., Oosterloo, T., 2002, AJ, 123, 3124

Fraternali, F., Oosterloo, T., Boomsma, R., Swaters, R., & Sancisi, R. 2004, IAU Symposium, 217, 136 (astro-ph/0310799)

van der Kruit, P. C., Searle, L. 1982, A&A 110, 79

Matthews, L. D., Wood, K. 2003, ApJ, 593, 721

Sault, B., Killeen, N. 2004, Miriad User Guide, http://www.atnf.csiro.au/computing/software/miriad/

Swaters, R. A., Sancisi, R., van der Hulst, J. M. 1997, ApJ, 491, 140

UNEXPECTED YOUNG STAR CLUSTERS IN THE TIDAL DEBRIS OF NGC 2782

Karen Knierman

Steward Observatory, University of Arizona, Tucson, USA
kknierman@as.arizona.edu

Abstract We report on a study of a nearby minor merger, NGC 2782, which is the result of a merger between two disk galaxies with a mass ratio of 0.25 occurring $\sim$ 200 Myr ago. This merger produced an HI-poor, optically bright Eastern tail and an HI-rich, optically faint Western tail. Deep optical images reveal the presence of blue ($B - V \sim 0.0$) clusters along both tails, suggesting that they are young ($<$100 Myr) and possibly formed within the tail. The presence of young clusters in the Western tail is unexpected due to the lack of molecular gas observed in previous studies. These results suggest that star cluster formation is a common outcome of minor mergers regardless of molecular gas content in the tidal debris.

Keywords: galaxies: star clusters - galaxies: interactions - galaxies: individual (NGC 2782)

1. Introduction

Does the tidal debris of minor mergers contribute significantly to structures in spiral galaxy halos or the IGM? Though major mergers are known to create structures ranging from star clusters to tidal dwarf galaxies in their debris (Duc et al. 2000; Knierman et al. 2003), minor mergers are more common and were likely to be important in the early universe. Structures in minor mergers' tidal debris may be captured by the parent galaxy and create structure in the galaxy's halo like those found in the Milky Way (Ibata et al. 1997), or contribute to the pollution of the IGM. Tidal debris can also give insight into unusual environments of star formation and how gas behaves in galaxy interactions. Studying the formation of structure in the tidal debris of minor mergers can help us understand a common process in galaxy formation, particularly spiral galaxies.

2. Minor Mergers and NGC 2782

Not much is known about minor mergers (mass ratios between a dwarf galaxy and a disk galaxy of $<$0.3) and their tidal debris. Previous work (e.g., Bastian et al. 2005; Tran et al. 2003; de Grijs et al. 2003) found the tidal debris

R. S. de Jong, Island Universes, 307–310.
© 2007 *Springer.*

to contain blue star clusters ($B-V\sim-0.2$; de Grijs et al. 2003) with young ages indicating they were formed within the tail.

The peculiar spiral, NGC 2782, is the result of a merger between a two disk galaxies with a mass ratio of 0.25 occurring ∼200 Myr ago. This merger produced two tidal tails: an HI-rich, optically faint Western tail ($M_{HI}=14\times10^8M_\odot$, $M_{mol}<0.06\times10^8M_\odot$) and an Eastern tail which has a concentration of HI and CO at its base ($M_{HI}=6.6\times10^8M_\odot$, $M_{mol}=6\times10^8M_\odot$), but a gas-poor optical knot at the tip (see Figure 1; Smith 1994). Non-detection of CO at the location of HI knots in the Western tail led Braine et al. (2001) to argue that the HI is not gravitationally bound and "has presumably not had time to condense into H_2 and for star formation to begin." However, if this tail was pulled from the outer region of the spiral galaxy, it may have a low metallicity which may affect the conversion factor between CO and H_2.

3. Star Cluster Candidates in the Tidal Tails of NGC 2782

Using deep *UBVR* images from the VATT, 57 star cluster (SC) candidates in the Eastern tail and 47 star cluster candidates in the Western tail (with 5 overlapping candidates) were detected by eye from the surrounding tail (see Figure 1). SC candidates in the Eastern tail are clustered mainly around the base of the tail where CO was detected and not in the gas-poor optical knot. SC candidates in the Western tail are located along the tail length.

Photometry for the SC candidates in *UBVR* was plotted on color-color diagrams with Charlot, Worthey & Bressan (1996) single stellar population models for a Salpeter IMF with $Z_\odot$ and 0.4 $Z_\odot$ (see Figure 2). From the models, there is seen to be a population of SC candidates in both tails with colors consistent with ages <100 Myr. Since the interaction age is ∼200 Myrs, these clumps likely formed within the tail. Narrowband Hα observations yielded a detection of one SC candidate in the Western tail and two SC candidates in the Eastern tail (see Figure 1). Two Hα clumps are very blue ($B-V\sim0.0$) and have ages consistent with $\sim$ 10 Myr. The Hα clump in the Eastern tail closest to the central galaxy has slightly redder colors ($B-V=0.5$), but may be contaminated with dust. The HI clump in the Western tail that yielded a non-detection in CO, has blue colors ($B-V=-0.11$) consistent with an age of ∼10 Myr.

4. Discussion and Conclusions

Consistent with previous observations, the Eastern tail has a population of young, star forming clusters with ages <100 Myr. Unexpectedly, the molecular gas-poor Western tail also has a population of young, star forming clusters with ages <100 Myr indicating that star formation has occurred in this tail. Perhaps the lack of molecular gas is due to evacuation by the star formation since the

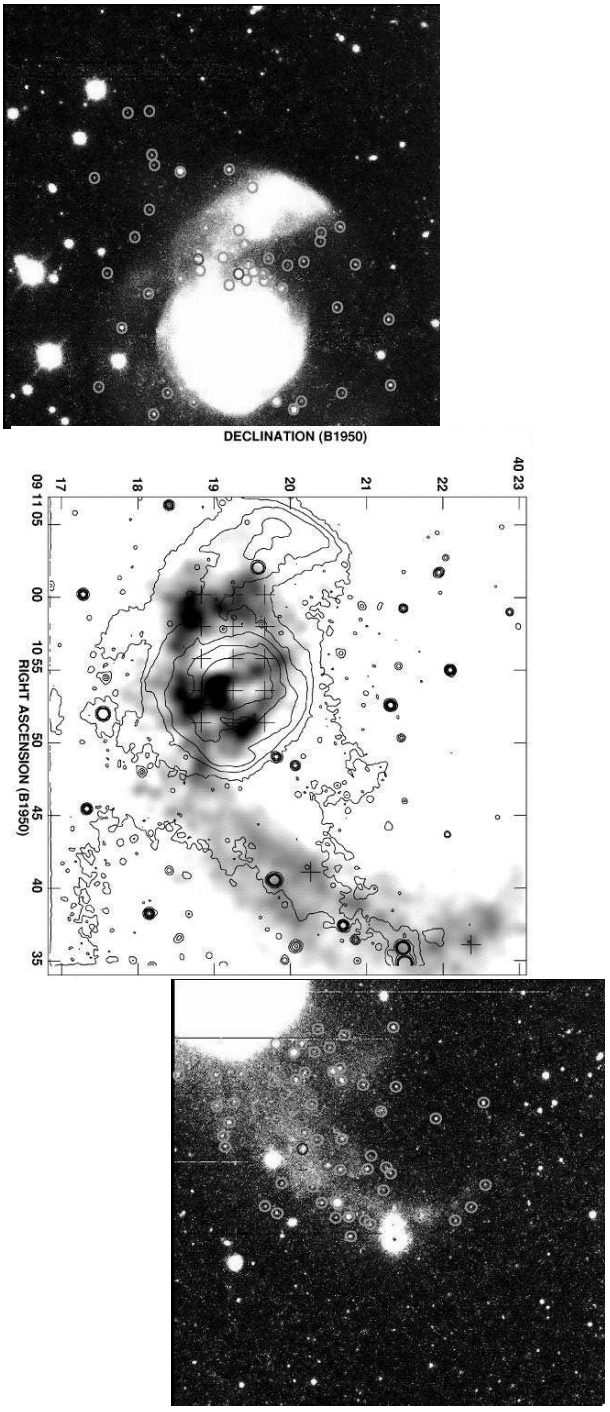

Figure 1. Center: B-band optical contours overlaid on HI greyscale. Crosses mark the location of 12m CO observations (Smith 1994; Smith et al. 1999). *Top-left:* B-band image of Eastern tail from VATT with star cluster candidates marked. *Bottom-right:* B-band image of Western tail.

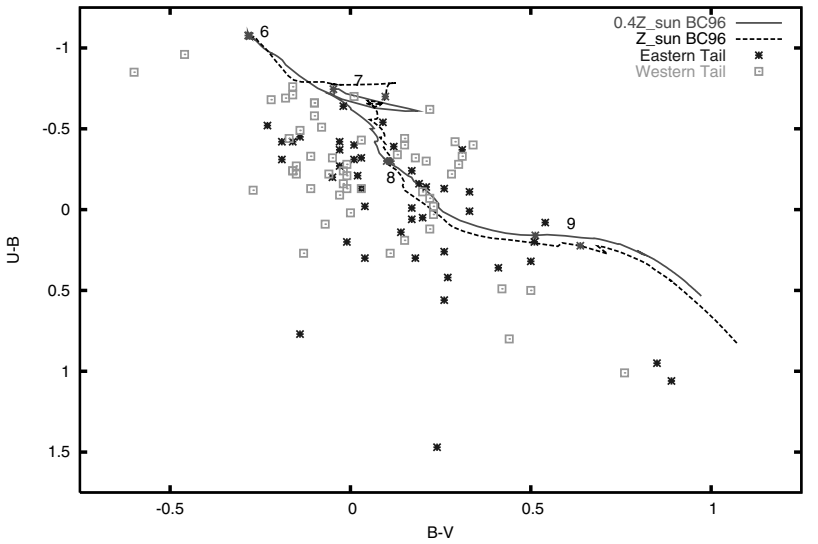

Figure 2. $U-B$ vs. $B-V$ color-color diagram of star cluster candidates in the tidal debris of NGC 2782. Candidates from the Eastern tail are indicated by stars while those in the Western tail are indicated by boxes. The solid line shows a Charlot et al (1996) single stellar population model with 0.4 $Z_{\odot}$ while the dotted line shows $Z_{\odot}$. Log(age) is indicated by the numerals.

less massive HI clumps in NGC 2782 have lower gravity as compared to larger tidal dwarf galaxies found in major mergers. *Though the gas properties of the tails are different, star formation still occurs in each perhaps indicating that star formation is a common occurrence in tidal debris.*

Acknowledgements K. Knierman was supported by the Arizona Space Grant Graduate Fellowship.

References

Bastian, N., et al. 2005, A&A, 435, 65.

Braine, J., et al. 2001, A&A, 378, 51.

Charlot, S., Worthey, G., & Bressan, A. 1996, ApJ, 457, 625.

de Grijs, R. et al. 2003, New Astronomy, 8, 155.

Duc, P.-A.,et al. 2000, AJ, 120, 1238.

Hibbard, J. E., Guhathakurta, P., van Gorkom, J. H., & Schweizer, F. 1994, AJ, 107, 67.

Ibata, R. A., et al. 1997, AJ, 113, 634.

Jogee, S. Kenney, J. D. P., & Smith, B. J. 1998, ApJ, 494, L185.

Knierman, K. A., Hunsberger, S. D., Gallagher, S. C., Charlton, J. C., Whitmore, B. C., Kundu, A., Hibbard, J. E., & Zaritsky, D. 2003, AJ, 126, 1227

Smith, B. 1994, AJ, 107, 1695.

Smith, B. et al. 1999, AJ, 117, 1237.

Tran, H.D. et al. 2003, ApJ, 585, 750.

INFALL OF SUBSTRUCTURES ONTO A MILKY WAY-LIKE DARK HALO

Yang-Shyang Li* and Amina Helmi**

Kapteyn Astronomical Institute, University of Groningen, The Netherlands

* ysleigh@astro.rug.nl, ** ahelmi@astro.rug.nl

Abstract We analyze properties of subhalos/substructures resolved in a dark matter simulation of a Milky Way-like halo in a ΛCDM cosmology. We explore possible links between subhalos and the Galactic satellites and find: 1) The infall patterns of subhalos are slightly elongated along the major axis of the galaxy halo and are clumpy on smaller scales. 2) The Great disk defined by MW satellites (Kroupa et al. 2005) is easily reproduced in our simulations without recurring to sophisticated galaxy formation recipes and is purely due to their highly centrally concentrated distribution around the Galaxy.

Keywords: dark matter - Galaxy: formation - galaxies: dwarf - galaxies: kinematics and dynamics - methods: numerical

1. Introduction

The relation between resolved substructures/subhalos in N-body dark matter simulations and the luminous satellites in galaxy halos is still unclear. The two populations differ in number ("the missing satellite problem") by factors of a hundred or more (Kauffmann, White & Guiderdoni 1993; Klypin et al. 1999; Moore et al. 1999); and also in their spatial density distributions (Gao et al. 2004). Recently, it has been argued that the MW satellites define a disk-like structure, that is so highly flattened (*rms* thickness of $10-30$ kpc) that it appears to be inconsistent with the expectations of CDM models (Kroupa et al. 2005). Sophisticated semi-analytic galaxy formation recipes have been used to identify "luminous" satellites in dark matter simulations (Kang et al. 2005; Zentner et al. 2005; Libeskind et al. 2005). This modelling has produced results that are consistent with observations. However, major uncertainties associated to the modelling of star formation and feedback processes in galaxies of the dwarf scale (Bullock, Karvtsov & Weinberg 2001) limit their predictive power.

R. S. de Jong, Island Universes, 311–314.
© 2007 *Springer.*

In this contribution, we explore the possible links between the subhalos found in a dark-matter simulation of a galaxy halo and the satellites of the Milky Way. Our approach is simpler than the above-mentioned semi-analytic models and aims at finding the similarities and differences between the two populations of objects, mostly from a dynamical point of view. To this end, we use a high-resolution dark matter simulation from the GA series (Stoehr et al. 2002), that models the formation of a MW-like halo in a ΛCDM cosmology. Throughout this article we focus on an experiment (GA2new) with 5,953,033 particles of mass $1.93 \times 10^6 M_\odot$, which results in the smallest resolved substructures (10 particles) to be $\sim 2 \times 10^7 M_\odot$. Gravitationally bound subhalos have been identified using the SUBFIND algorithm (Springel et al. 2001). In the simulation we present here, there are 505 subhalos at the present time.

2. Ghostly Streams and the Infall of Dark Matter Substructures

Figure 1 shows the distribution of subhalos in their principal axes reference frame, at the epoch when they were accreted onto the MW-like halo (top) and at the present day (bottom). The projections show the edge-on view. This distribution is slightly elongated along the direction of the major axis of the MW-like halo at each epoch (indicated with a dashed line in each panel). Notice that there are clumps of subhalos often sharing similar velocities indicating that infall does not occur in isolation but in groups.

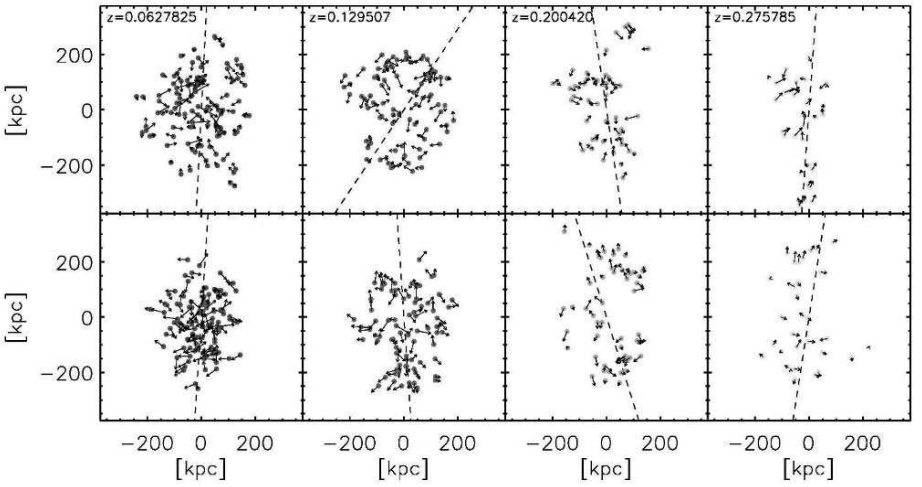

Figure 1. Several clusters of subhalos can be identified on the infall patterns (top). Each subhalo is assigned an arrow representing its velocity: the length corresponds to 0.15 of the magnitude while the arrow is oriented in the direction of motion.

This grouping may well be the origin of the ghostly streams reported by Lynden-Bell & Lynden-Bell 1995: a few satellites and globular clusters appear to be sharing a common orbital planes. If some of the luminous satellites are embedded in dark (sub)halos that fell in together, such coherent structures would be naturally expected.

3. On the Great Disk of Milky-Way Satellites

The subhalos in our GA simulation show at least two differences in their distributions in comparison to the Galactic dwarfs: 1) their spatial distribution is much less anisotropic (Figure 3 Left); 2) their density distribution is much shallower (Figure 2 Left). However, if we randomly select sets of 11 subhalos according to the MW satellites density profile, we can easily reproduce their elongated configuration. About $1/3$ of our random realizations give configurations as flattened as those of the MW dwarfs, as indicated by the shaded area of the histogram showing the fraction of experiments with a given intermediate-to-major axis ratio (Figure 2 Right).

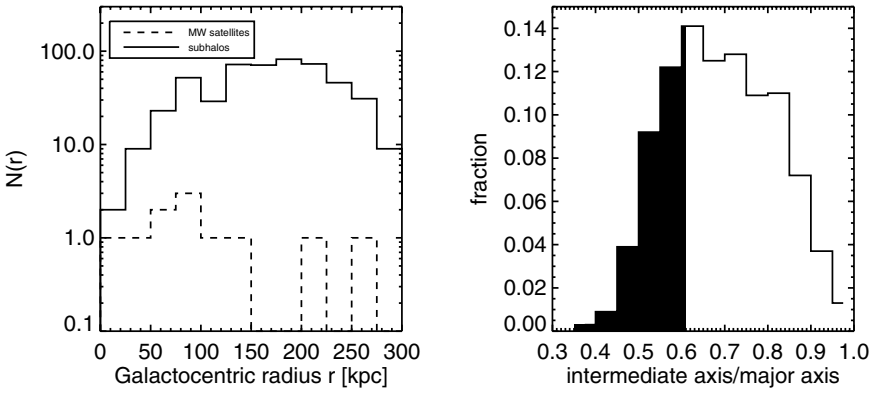

Figure 2. Left: Density distribution of MW satellites and subhalos. Right: Histogram of fractions of a given structure defined by subhalos selected according to the Galactic satellites density distribution of 1,000 realizations.

Figure 3 shows the distribution of the MW satellites (left), one random realization of a set of 11 subhalos selected to follow the density distribution of the satellites (centre) and the full sample of subhalos (right) in their principal axes frame.

These results show that the disk-like configuration of the MW satellites is driven by their strongly centrally concentrated density distribution around the Galaxy. This suggests that their 3D distribution is solely the result of dynamical processes (possibly associated to mass at the time of infall), and that there is no need to recur to sophisticated galaxy formation tools and recipes to explain the characteristics of the satellite distribution around the Galaxy.

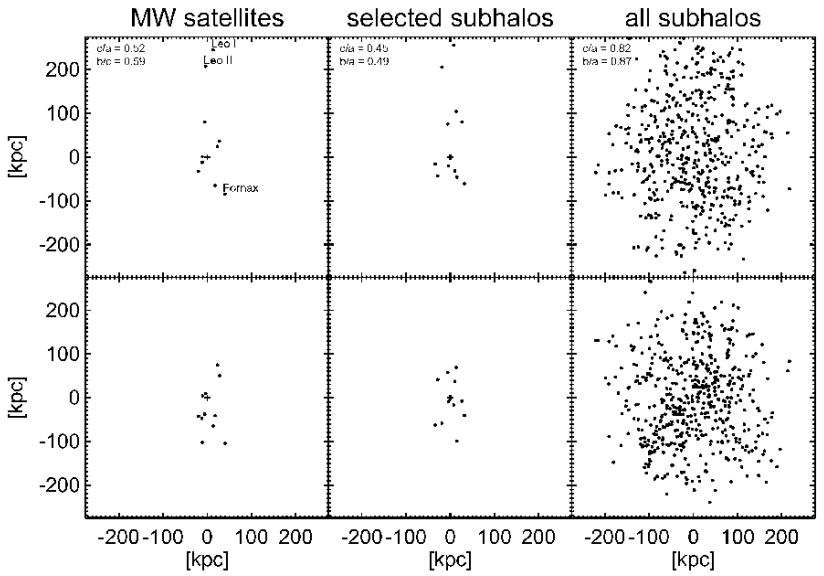

Figure 3. The spatial distribution of the MW satellites (left), one random realization of a set of 11 selected subhalos (centre) and the full sample of subhalos (right). Top: edge-on view; bottom: face-on view.

Furthermore, we note that the "highly" anisotropic MW satellites distribution is actually biased by the presence of 2-3 outliers (Leo I, Leo II & Fornax) located at very large distances, and which, inevitably, give rise to a planar configuration. Therefore, it transpires that the current MW satellites distribution tells us very little about the shape of the dark matter distribution around our Galaxy.

Acknowledgements Y.S. Li thanks Felix Stoehr for the great help on the GAnew datum manipulations and Simon White for stimulating discussions.

References

Bullock J.S., Kravtsov A.V. & Weinberg D.H. 2001, ApJ, 548, 33
Gao L. et al. 2004, MNRAS, 352L, 1
Kang X., Mao S., Gao L. & Y.P. Jing 2005, A&A, 437, 383
Kauffmann G., White S.D.M. & Guiderdoni B. 1993, MNRAS, 264, 201
Klypin A. et al. 1999, ApJ, 522, 82
Kroupa P., Theis C. & Boily M. 2005, A&A, 431, 517
Libeskind N. et al. astro-ph/0503400
Lynden-Bell D. & Lynden-Bell R.M. 1995, MNRAS, 275, 429
Moore B. et al. 1999, ApJ, 524L, 19
Springel V., White S.D.M., Tormen G. & Kauffmann G. 2001, MNRAS, 328, 726
Stoehr F. et al. 2002, MNRAS, 335L, 84
Zentner A.R. et al. 2005, ApJ, 629, 219

THE FAR-INFRARED PROPERTIES OF THE MOST ISOLATED GALAXIES

U. Lisenfeld[1,2], L. Verdes-Montenegro[2], S. Leon[2] and J. Sulentic[3]

[1]*Dept. Física Teórica y del Cosmos, Universidad de Granada, Spain*
[2]*Instituto de Astrofísica de Andalucía, Granada, Spain*
[3]*Department of Astronomy, Univ. of Alabama, Tuscaloosa, USA*

Abstract Although it is widely accepted that galaxy interactions stimulate secular evolutionary effects (e.g. enhanced star formation), the amplitude of this effect and the processes for accomplishing them are not well quantified. The goal of the project AMIGA (Analysis of the Interstellar Medium of Isolated Galaxies) is to provide a sizable reference sample (n=1050) of the most isolated galaxies as a basis for the study of the influence of the environment on galaxy properties. Here, we present the far-infrared (FIR) properties of 1030 galaxies of the sample for which IRAS data are available. We improved the detection rate and accuracy of the IRAS data with respect to the Point Source and Faint Source Catalog by redoing the data reduction with the IPAC utility ADDSCAN/SCANPI. Comparing the FIR to the blue luminosities, we find a slightly non-linear relation. Furthermore, we find that interacting galaxies tend to have an enhanced FIR emission.

Keywords: infrared: galaxies - surveys - galaxies: ISM - galaxies: interactions

1. The AMIGA Project

A key question in astrophysics is the relative role of nurture versus nature in galaxy evolution. In order to make progress, studies need to be based on a well-defined sample of isolated galaxy which has been lacking so far. We are compiling and analysing data for the first complete unbiased control sample of the most isolated galaxies in the northern sky (Leon & Verdes-Montenegro 2003, Verdes-Montenegro et al. 2005). To compare and quantify the properties of different phases of the interstellar medium, as well as the level of star formation, we are building a multiwavelength database (far-infrared, near-infrared, optical, Hα, radio continuum, HI and CO) for this sample. The data will be publicly available from www.iaa.es/AMIGA.html.

Our sample is based on the Catalogue of Isolated Galaxies (CIG, 1050 galaxies, Karatchenseva 1973) assembled with the requirement that no

R. S. de Jong, Island Universes, 315–318.
© 2007 *Springer.*

similarly sized galaxies with diameter d (where d is between 1/4 and 4 times diameter D of the CIG galaxy) lie within 20d. We chose the CIG as a basis because this sample presents various advantages: (i) It is selected using a powerful criterium, so that the CIG contains a large fraction of the most isolated nearby galaxies in the northern hemisphere. Since the selection criterium does not take into account redshift, it actually excludes some galaxies which have only apparent companions that lie in reality at a very different redshift. This is however not a problem for our purpose because (ii) the sample is large enough to be statistically significant. It furthermore covers a large enough volume to be almost (80%) optically complete up to a Zwicky magnitude of 15 mag (Verdes-Montenegro et al. 2005). (iii) Finally, the fact that the galaxies in the CIG are nearby (the bulk of the galaxies have recession velocities below 10 000 km/s) enables us to determine the morphologies in a reliable way (Sulentic et al. 2006). Since furthermore all morphological types are found in CIG, we are able to study galaxy properties as a function of galaxy type.

As a first step, we are performing a number of refinements to the CIG: a) We are carrying out a computational revision and quantification of the degree of isolation using SExtractor and LMORFO to the POSSI plates (Verley et al., in prep.), b) we are revising the morphologies with the help of POSSII and our optical images (Sulentic et al. 2006), and c) we have checked the positions and accumulated new redshifts available in the literature (Leon & Verdes-Montenegro 2003, Verdes-Montenegro et al. 2005).

2. Reprocessing of IRAS Data

We obtained the IRAS fluxes at 12, 25, 60 and 100 μm using the utility ADDSCAN/SCANPI at IPAC. We followed the recommendation for the calculation of the total fluxes and visually inspected all spectra in order to check for (i) the presence of cirrus emission, (ii) confusing with neighboring galaxies and (iii) the significance of the detection (e.g. confusing with noise spikes). A more detailed description of the data processing will be presented in Lisenfeld et al. (in prep.). This reprocessing yielded:

- An increase in the number of data points in comparison to the IRAS Point Source Catalog (PSC) and Faint Source Catalog (FSC): Whereas there are only 524 galaxies of the 1050 CIG galaxies in the PSC/FSC, the ADDSCAN/SCANPI reduction provided data for 1031 objects.
- An improvement of the signal-to-noise-ratio by a factor of 2-5. In particular, (55, 70, 9, 81) galaxies at (12, 25, 60, 100)μm were only upper limits in the PSC/FSC but changed to detections after our reprocessing.
- An improved accuracy of the fluxes, because ADDSCAN/SCANPI is able to measure the total flux of extended objects, as long as their size is not above a few arcmin. We found a trend of the ratio of the flux

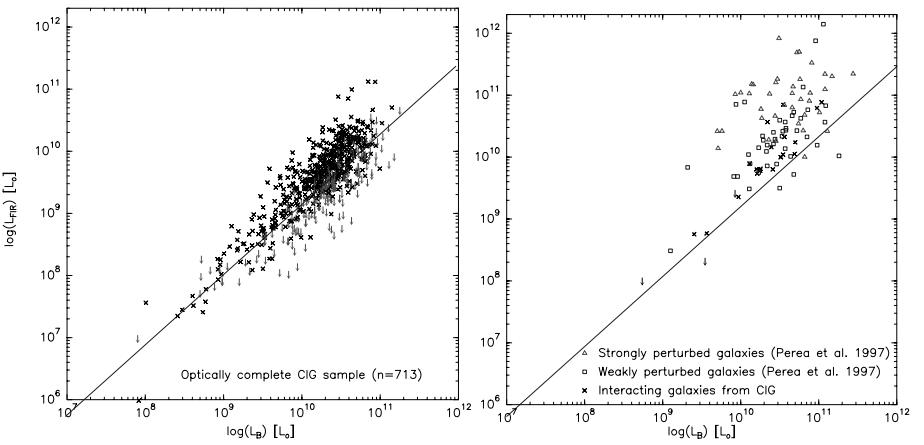

Figure 1. The relation between the FIR and blue luminosity for an optically complete subsample of the CIG, excluding 23 interacting CIG galaxies **(left)** and for different samples of interacting galaxies **(right)** The line is in both panels the regression found for the CIG (eq. 1).

derived with ADDSCAN/SCANPI to the flux from the PSC/FSC to increase with source diameter, especially at short wavelengths, suggesting that the fluxes in the PSC/FSC indeed underestimate the correct fluxes for large object. Furthermore, our visual inspection of the spectra allowed us to reject dubious cases. In fact, we classified (29, 21, 5, 3) galaxies at (12, 25, 60, 100)μm as non-detection that were listed as detection in the PSC/FSC.

3. Relation Between $L_{\rm FIR}$ and $L_{\rm B}$

As a first result, we show in Fig. 1 a comparison of the FIR luminosity, $L_{\rm FIR}$, (calculated from the 60 and 100 μm fluxes) to the blue luminosity, $L_{\rm B}$, derived from the corrected Zwicky magnitudes (see Verdes-Montenegro et al. 2005). A more detailed analysis of the data, including the full presentation of the characteristics of the FIR luminosities and colours will be presented in Lisenfeld et al. (in preparation). We limit the sample to 736 galaxies with optical magnitudes between 11 and 15 mag, representing an 80% complete subsample of the CIG (Verdes-Montenegro et al. 2005). Furthermore, based on the morphological revision of the sample we exclude 23 galaxies which are judged to be interacting (Sulentic et al. 2006).

We fit the correlation, taking into account the upper limits by applying survival methods from the package ASURV (Feigelson & Nelson 1985, Isolbe, Feigelson & Nelson 1986) and obtain for the relation (adopting $L_{\rm B}$ as the

independent variable).

$$\log(L_{\rm FIR}) = (1.13 \pm 0.03)\log(L_{\rm B}) - (2.1 \pm 0.3) \quad (1)$$

The slope obtained for the sample of the 23 clearly interacting CIGs was considerably higher, 1.46 $\pm$ 0.14. The difference is due to an increase in $L_{\rm FIR}$: Whereas the average $L_{\rm B}$ of both samples are basically the same ($< L_{\rm B} > = 10.22 \pm 0.02$ for the 713 CIG galaxies and $< L_{\rm B} > = 10.23 \pm 0.11$ for the 23 interacting CIG galaxies) the FIR luminosity is increased for the interacting galaxies ($< L_{\rm FIR} > = 9.18 \pm 0.08$ for the 713 CIG galaxies and $< L_{\rm B} > = 9.75 \pm 0.17$ for the 23 interacting CIG galaxies).

In Fig. 1 (left) we show different samples of interacting galaxies compared to the slope of the CIG (eq. 1). The interacting galaxies clearly lie above this slope, indicating an enhancement of the FIR emission compared to $L_{\rm B}$.

Acknowledgements UL, LVM and SL are partially supported by DGI (Spain) AYA 2002-03338, AYA2004-08251-CO2-02 (UL), the Junta de Andalucía and the Universidad de Granada.

References

Feigelson, E.D., & Nelson, P.I., 1985, ApJ, 293, 192
Karatchenseva, V.E., 1973, Comm. Spec. Ap. Obs, USSR 8, 1
Isobe, T., Feigelson, E.D., Nelson, P. I, 1986, ApJ, 306, 490
Verdes-Montegnegro, L., Leon, S., A&A, 411, 391
Perea, J., del Olmo, A., Verdes-Montenegro, L., 1997, ApJ, 490, 166
Sulentic, J., Verdes-Montegnegro, L., Bergond, G., et al., 2006, A&A submitted
Verdes-Montegnegro, L., Sulentic, J. Lisenfeld, U., et al., 2005, A&A, 436, 443

STUDYING GALAXY FORMATION IN LOOSE GALAXY GROUPS

D.J. Pisano[1,2*], D.G. Barnes[3], B.K. Gibson[4], L. Staveley-Smith[5], K.C. Freeman[6] and V.A. Kilborn[4]

[1]*Naval Research Laboratory, Washington, DC, USA*

[2]*National Research Council Research Fellow*

[3]*School of Physics, University of Melbourne, Australia*

[4]*Centre for Astrophysics & Supercomputing, Swinburne University, Hawthorn, Australia*

[5]*Australia Telescope National Facility, Epping, Australia*

[6]*RSAA, Mount Stromlo Observatory, Weston, Australia*

* pisano@nrl.navy.mil

Abstract We present the results of our HI survey of six loose groups of galaxies analogous to the Local Group. The survey was conducted using the Parkes telescope and the Australia Telescope Compact Array to produce a census of all the gas-rich galaxies and analogs to the high-velocity clouds (HVCs) within these groups down to $M_{HI} < 10^7$ $M_\odot$ as a test of models of galaxy formation. We present the HI mass function and halo mass function of the loose groups and show that they are consistent with those of the Local Group. We discuss the possible role of HVCs in solving the "missing satellite" problem and discuss the implications of our observations for models of galaxy formation.

Keywords: intergalactic medium - radio lines: galaxies - galaxies: formation - galaxies: dwarf

1. Introduction

The majority of "island universes", 60%, reside in galaxy groups (Tully 1987), including the Milky Way. Loose groups of galaxies, like our Local Group, are collections of a few large, bright galaxies and tens of smaller, fainter galaxies. The large galaxies are typically separated by a few hundred kiloparsecs from each other and spread over an extent of approximately a megaparsec. They represent the most diffuse components of large scale structure and a laboratory for studying galaxy formation. Loose groups are almost certainly still in the process of collapsing (Zabludoff & Mulchaey 1998) and they may also contain the gaseous remnants of galaxy formation in the form of the high-velocity

R. S. de Jong, Island Universes, 319–322.
© 2007 *Springer.*

clouds (HVCs; Blitz et al. 1999). They also illustrate one of the major challenges to current models of cold dark matter (CDM) galaxy formation. CDM models predict that the Local Group should contain ∼300 low mass dark halos, while there are only ∼20 luminous dwarf galaxies known. While this may imply that we lack a complete census of the luminous galaxies in the Local Group, it may also be uniquely deficient in dwarf galaxies. Or, perhaps, the HVCs may populate these dark matter halos and solve the "missing satellite" problem. In order to address this question and to better understand the properties of loose groups, we have conducted an HI survey of six groups analogous to the Local Group.

2. Observations

We selected our groups from the optical catalog of Garcia (1993). The resulting groups are between 10.6 and 13.4 Mpc distant, contain between 3–9 bright galaxies which are separated, on average, by ∼550 kpc, and have diameters of ∼1.6 Mpc. Their masses, as estimated by the virial theorem and the projected mass estimator (Heisler et al. 1985), of $\sim 10^{11.7-13.6} M_{\odot}$ are comparable to the mass of the Local Group $\sim 10^{12.4} M_{\odot}$ (Courteau & van den Bergh 1999).

We used the Parkes Multibeam and Australia Telescope Compact Array (ATCA) to survey the entire area of each group down to a M_{HI} sensitivity of $5\text{–}8 \times 10^5 M_{\odot}$ per 3.3 km s^{-1}. All Parkes detections in the groups were confirmed to be real by the follow-up ATCA observations. A total of 64 HI-rich galaxies were detected in the six groups, almost twice the number of optically cataloged group galaxies (Garcia 1993) and 50% more galaxies than were detected by HIPASS in the same fields (Meyer et al. 2004). All of our detections are associated with optical counterparts and have properties consistent with typical spiral, irregular, or dwarf irregular galaxies. No analogs to the HVCs were detected. Examples of two typical new detections are shown in Figure 1.

3. Is the Local Group Missing Dwarf Galaxies?

We wish to know if our sample of loose groups has a significantly different population of dwarf galaxies as compared to the Local Group in order to determine if the Local Group is unique in some fashion. To do this we constructed an HI mass function (HI MF) and a cumulative circular velocity distribution function (CVDF), both shown in Figure 2. The CVDF is an effective surrogate for a halo mass function as traced by luminous matter. After correcting for the incompleteness of our survey, using both the detection rate of fake sources inserted into our data and by scaling the HIPASS completeness function (Zwaan et al. 2004) to our survey parameters, we derive a flat HI MF similar to that for the Local Group as shown on the left panel of Figure 2. This result is

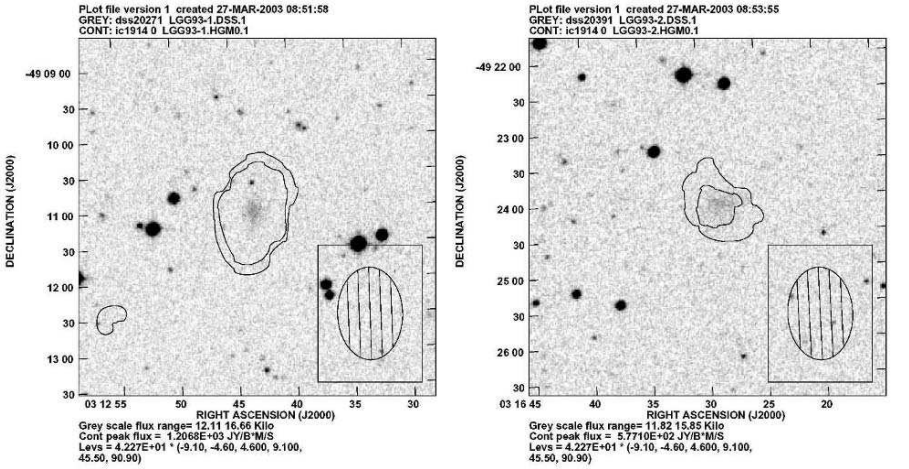

Figure 1. An overlay of the HI total intensity contours on the optical images of LGG 93-1 (left) and LGG 93-2 (right) also known as AM 0311-492 and LSBG F200-023, respectively. The ATCA beam is indicated by the hatched oval in the lower left of both images.

consistent with the results for the HI MF presented by Zwaan et al. (2005), who find the HI MF flattens in low density environments, and the results of Tully et al. (2002), who find a similar behavior for the optical luminosity function. Similarly, the six loose groups have an identical CVDF to the Local Group with both falling below the predictions of CDM around $V_{circ} \sim 50 \mathrm{km\,s^{-1}}$. This demonstrates that the lack of a large population of dwarf galaxies is not unique to the Local Group.

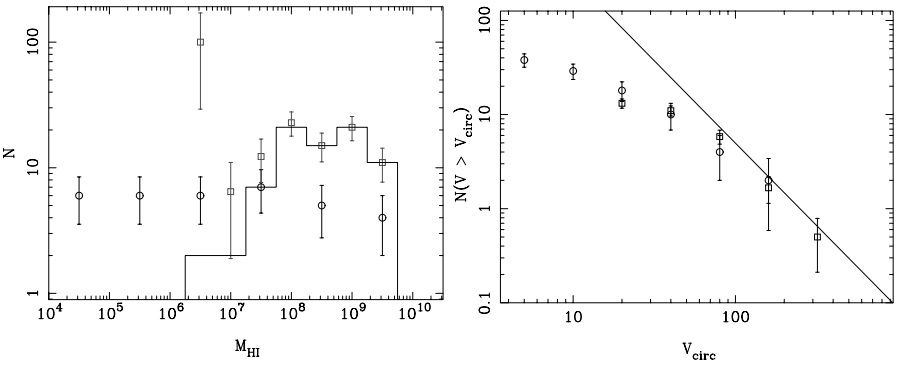

Figure 2. Left: The HI mass function (HI MF) of the Local Group (circles) and the sum of the six loose groups (solid histogram) corrected for incompleteness (squares). Right: The cumulative velocity distribution function for the Local Group (circles), and the average of the six loose groups (squares). The solid line represents the CDM model of Klypin roughly normalized to the second data point.

4. Are the High-Velocity Clouds the "Missing Satellites"?

Blitz et al. (1999) and Braun & Burton (1999) suggested that the HVCs seen around the Milky Way may be embedded within the low mass dark matter halos that are predicted by CDM models of galaxy formation. Our non-detection of any HVC analogs in these six loose groups suggests that if this is the case, then they must be relatively low mass HI clouds, $M_{HI} \sim 10^{5-6} M_{\odot}$, and be within $\sim$150 kpc of the Milky Way (Pisano et al. 2004). These constraints are consistent with limits found by others through a variety of methods (e.g., Zwaan 2001, de Heij et al. 2002), but does not necessarily imply that HVCs are associated with the CDM dark matter halos (e.g., Maller & Bullock 2004). Deeper HI surveys of individual galaxies are still necessary to better constrain the nature and origin of HVCs.

Acknowledgements This research was performed while D.J.P. held a National Research Council Research Associateship Award at the Naval Research Laboratory. Basic research in astronomy at the Naval Research Laboratory is funded by the Office of Naval Research. D.J.P. also acknowledges generous support from the ATNF via a Bolton Fellowship and from NSF MPS Distinguished International Research Fellowship grant AST 0104439.

References

Blitz, L., Spergel, D.N., Teuben, P.J., Hartmann, D., & Burton, W.B., 1999, ApJ, 514, 818
Braun, R., & Burton, W. B. 1999, A&A, 341, 437
Courteau, S., & van den Bergh, S. 1999, AJ, 118, 337
de Heij, V., Braun, R., & Burton, W. B. 2002, A&A, 392, 417
Garcia, A.M., 1993, A&AS, 100, 47
Heisler, J., Tremaine, S., & Bahcall, J. N. 1985, ApJ, 298, 8
Maller, A. H., & Bullock, J. S. 2004, MNRAS, 355, 694
Meyer, M. J., et al. 2004, MNRAS, 350, 1195
Pisano, D. J., Barnes, D. G., Gibson, B. K., Staveley-Smith, L., Freeman, K. C., & Kilborn, V. A. 2004, ApJ, 610, L17
Tully, R.B., 1987, ApJ, 321, 280
Tully, R. B., Somerville, R. S., Trentham, N., & Verheijen, M. A. W. 2002, ApJ, 569, 573
Zabludoff, A.I., & Mulchaey, J.S., 1998, ApJ, 498, L5
Zwaan, M. A. 2001, MNRAS, 325, 1142
Zwaan, M. A., et al. 2004, MNRAS, 350, 1210
Zwaan, M. A., Meyer, M. J., Staveley-Smith, L., & Webster, R. L. 2005, MNRAS, 359, L30

THE ENVIRONMENT OF LOW SURFACE BRIGHTNESS GALAXIES FROM SDSS

Stefan Dominik Rosenbaum* and Dominik J. Bomans**

Astronomisches Institut der Ruhr-Universitaet Bochum, Germany

* dominik.rosenbaum@astro.rub.de, ** dominik.bomans@astro.rub.de

Abstract Using the public data releases of the Sloan Digital Sky Survey (SDSS), we investigated the galaxy density around Low Surface Brightness (LSB) galaxies in comparison to High Surface Brightness (HSB) galaxies. Our results show significantly lower galaxy densities in the vicinity of LSBs compared to HSBs on scales between 2 and 8 Mpc. On scales below 2 Mpc, the galaxy densities in the neighbourhood of LSBs are systematically (but only with a slight significance) below that of HSBs. In pie slice diagrams LSBs favour the outer rims of the filaments of the Large Scale Structure (LSS). Some LSBs are even found inside voids.

Keywords: galaxies: distances and redshifts - galaxies: evolution - galaxies: statistics

Introduction

The existence of gas-rich disk-galaxy-like LSB galaxies with central surface brightnesses of $\mu_B > 22.5\,\mathrm{mag/arcsec^2}$ has been established over the last 15 years, but their formation and evolution scenarios are not well understood so far (e.g., Impey & Bothun 1997). However, in these gas-rich LSBs the HI surface densities stay systematically below the Kennicutt (1998) criterion for sufficient star formation (e.g., van der Hulst et al. 1993, Pickering et al. 1997). One way of understanding the properties of these galaxies might be found in the nature of the small- and large-scale environments in which LSB galaxies are embedded, since the lack of star formation can only occur if these galaxies were formed in low density regions of the initial universe. Only a scenario involving low density regions for the formation of those galaxies can warrant that neither tidal encounter with companions nor infall of massive gas clouds could have taken place and have triggered a sufficient star formation which would have gradually brightened the stellar disk. Evidence for the stronger isolation of LSBs in comparison to HSBs was found before by Bothun et al. (1993) and Mo et al. (1994). A lack of nearby ($r < 0.5\,\mathrm{Mpc}$) companions of LSB

R. S. de Jong, Island Universes, 323–326.
© 2007 *Springer.*

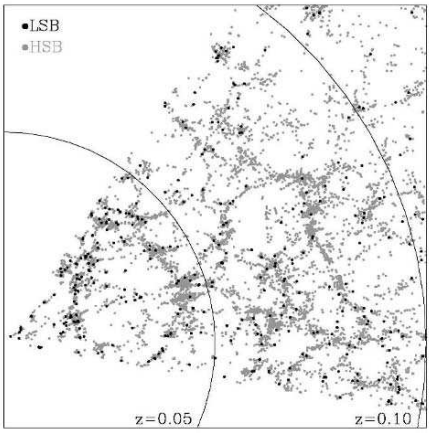

Figure 1. The distribution of LSB galaxies (black) in comparison to HSB galaxies (green / grey) obtained from one of the equatorial strips of the SDSS DR3 is shown in a so called pie slice diagram. The diagram suggests that in a redshift range between 0 < z <0.05 the projected distribution of the mostly dwarf-like LSB galaxies (see Figure 1) follows that of the HSB galaxies. For the redshift interval 0.05 < z <0.1 the situation changes. There, the due to the selection function (Fig. 3) mostly large LSB galaxies reside in the outer parts of the filaments and some of them are even found in voids of the large scale structure.

galaxies was detected by Zaritzky & Lorrimer (1993). Starting with the public data releases of the Sloan Digital Sky survey (SDSS, York et al. 2000) we are now able to test the isolation of large, mass rich LSB galaxies on intermediate scales between 2 Mpc and 8 Mpc (see also, Rosenbaum & Bomans 2004).

Data Analysis

We retrieved LSB candidates and a HSB comparison sample from the main galaxy sample of the Sloan Digital Sky Survey's Data Release 3 (DR3, Abazajian et al. 2005). The sample was limited to a redshift of $0.01 \leq z \leq 0.1$ and in order to minimize the uncertainty of the redshift a z-confidence greater than 90% was demanded.

We distinguished between LSB galaxies with a central surface brightness $\mu_B > 22.5\,\mathrm{mag/arcsec}^2$ and HSB galaxies. The environmental galaxy density for each sample LSB and HSB was statistically measured using a software we developed for counting the number of galaxies within a sphere of a certain radius around the scrutinised galaxy. The radius of the sphere was a fixed parameter during each run. In several runs the radius of the sphere was varied between $r = 0.8\,\mathrm{Mpc}$ and $r = 8.0\,\mathrm{Mpc}$ in steps of 0.6 Mpc. In order to avoid biasing of the sample due to boundary effects, edge correction was applied. For a detailed description of the data analysis procedure see Rosenbaum & Bomans (2004).

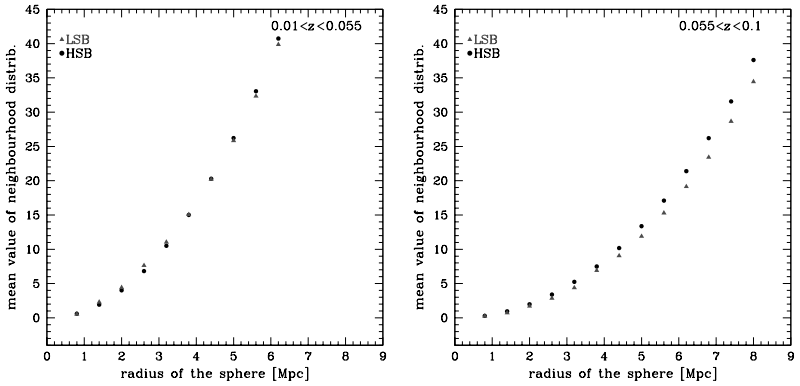

Figure 2. Left panel shows the mean numbers of neighbours for the LSB sample (triangles) and the HSBs (dots) from number counting with spheres in connection to the corresponding sphere radii. The redshifts are within the interval $0.0 < z < 0.05$. Due to the selection function (see Fig. 3) the environment of mostly dwarf-like LSBs are probed. Note that the LSB distribution follows that of HSBs. Right panel shows the same as left panel, but for the redshift interval of $0.05 < z < 0.1$. This means that mostly large, Malin-like LSBs were probed due to the SDSS selection function (see Fig. 3). Note that the mean values of the LSB sample are systematically below that of the HSB distribution (the error bar corresponds to the size of the triangles).

Results

The pie slice diagram (Fig. 1) shows that LSB galaxies are located in the filaments of the Large Scale Structure (LSS) traced by the distribution of HSB galaxies. Further investigations of the plot lead to the impression that the LSB galaxies within the redshift interval of $0.055 < z < 0.1$ show the tendency to be located more often at the edges of these filaments than in the center and some LSB galaxies are even found in void regions. This is not the case for the LSBs within the redshift interval of $0.01 < z < 0.055$. Their distribution follows the LSS indicating that in this redshift interval LSBs and HSBs possess the same clustering properties.

In Fig. 2 the mean number of neighbours in dependence of the corresponding sphere radius is plotted for LSBs as well as for HSBs. Thereby, a division into two symmetric redshift bins was performed (left panel: $0.01 < z < 0.055$; right panel: $0.055 < z < 0.1$). The plots indicate that for the $0.01 < z < 0.055$ redshift bin the galaxy density around LSBs is the same as around HSBs. For a redshift range of $0.055 < z < 0.1$ the situation is different. There, LSB galaxies are more isolated than HSBs. Taking into account the LSB selection function (Fig. 3) this indicates that large, Malin-like LSBs are more isolated than HSBs, but small dwarf-like LSBs are embedded in the LSS traced by HSBs.

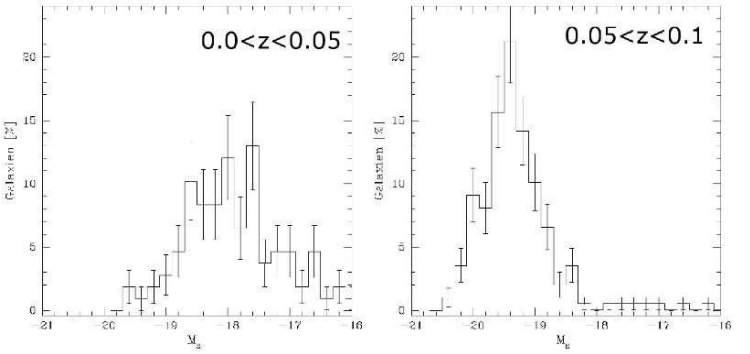

Figure 3. Left panel shows the g-band luminosity distribution of the LSBs from SDSS DR3 in the redshift interval of $0.01 < z < 0.055$. The distribution has a mean value of $M_g = 17.57 \pm 0.11$ mag indicating that the SDSS selection function has selected a LSB population mostly consisting of dwarfish galaxies. Right panel is the same as left panel, but for a redshift interval of $0.055 < z < 0.1$. The LSB luminosity distribution in this case has a mean value of $M_g = 19.25 \pm 0.06$ mag. This means that the population selected by the SDSS routines as spectroscopic targets mainly consists of large LSB galaxies in this redshift interval.

Summary and Conclusions

Large LSB galaxies seem to favour the outer parts of the filaments of the LSS and there are a few of extremely isolated LSB galaxies located in voids. Based on our results presented here, we conclude that the large LSB galaxies formed in voids of the LSS and have drifted to the outer parts of the filaments. This scenario is also discussed in Rosenbaum & Bomans (2004). The isolation of these LSB galaxies on intermediate and small scales must have effected their evolution since tidal encounters acting as triggers for star formation would have been rarer in these LSB galaxies than for HSB galaxies. We also found evidence that small, dwarf-like LSB galaxies possess different environments and hence a different formation history.

References

Abazajian, K. et al. 2005, AJ 129, 1755
Bothun, G. D. et al. (993, AJ 106, 530
Impey, C. D. & Bothun, G. D. 1997, ARA&A 35, 267
Kennicutt, R. C. 1998, ARA&A 36, 189
Mo, H. J. et al. 1994, MNRAS 267, 129
Pickering, T. E. et al. 1997, AJ 114, 1858
Rosenbaum, S. D. & Bomans, D. J. 2004, A&A 422, L5
van der Hulst, J. M et al. 1993, AJ 106, 548
York, D. G. 2000, AJ 120, 1579
Zaritsky, D. & Lorrimer, S. J. 1993, Evolution of Galaxies and their Environment, 82

V

INTERSTELLAR MATTER

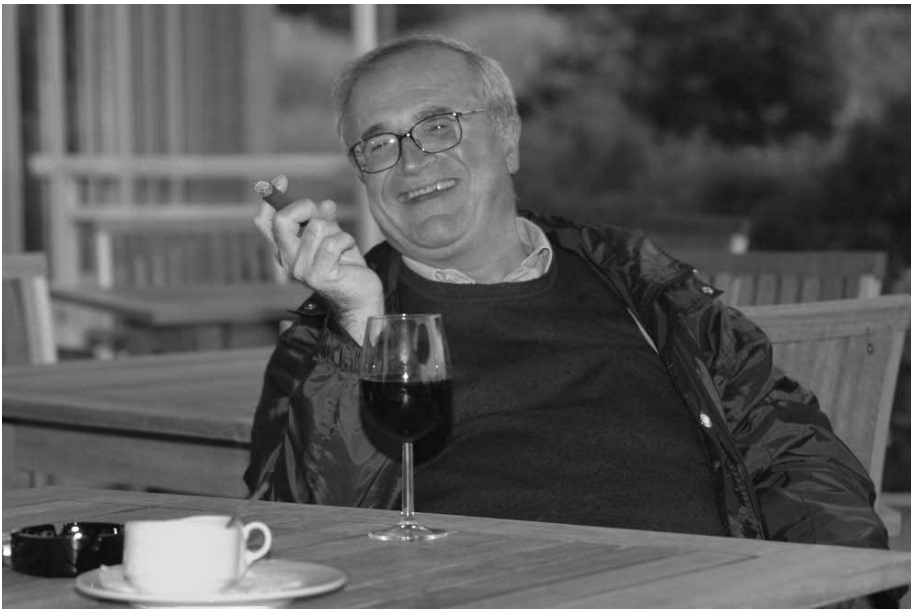

Renzo Sancisi enjoying his 65^{th} at Island Universes while creating molecular clouds.

STAR FORMATION, INTERSTELLAR PHYSICS & THE SED OF GAS-RICH GALAXIES

Michael A. Dopita

Research School of Astronomy & Astrophysics, The Australian National University, Australia
Michael.Dopita@anu.edu.au

Abstract Star-forming regions in galaxies consist of a number of components, the evolving young stellar clusters with their associated HII regions, isolated OB stars embedded in compact HII regions, older, non-ionizing stars, and the pre-existing old stellar populations. All of these are surrounded by a complex, turbulent and fractal screen of gas and obscuring dust. Here, I describe how self-consistent dynamical and radiative transfer modeling of these various components is leading to synthetic pan-spectral energy distributions ranging from the Lyman Limit up to millimetre wavelengths. These models provide excellent fits to real objects, and furnish the diagnostic tool needed to derive the fundamental parameters of star-forming galaxies in both the local and distant universe.

Keywords: stars: formation - galaxies: high-redshift - ISM: galaxies - HII regions

1. Introduction

All of our current knowledge of the physical conditions in the interstellar medium (ISM) of galaxies derives ultimately from spectroscopy. The presence and nature of the interstellar dust is deduced from the way it absorbs and scatters the light of stars, and how it re-radiates this absorbed energy into the infrared. A study of the emission lines permits us to measure temperatures and densities and determine chemical abundances in the gas phase. In addition, the spectral energy distribution (SED) of galaxies encodes information about the current and past star formation rate and the presence and relative importance of any embedded active nucleus. Each wavelength region in the galaxian SED is sensitive to a different combination of these parameters. The purpose of of theoretical modelling of the pan-spectral SED is to learn to decode and quantify this information, and so probe the history of both nearby and distant galaxies.

The star formation history of the universe is a fundamental indicator of galaxy evolution. The famous Lilly-Madau Plot (Madau et al. 1996) provides this quantity on a global scale. However, as shown notably by Ascasibar

R. S. de Jong, Island Universes, 329–340.
© 2007 *Springer.*

et al. (2002), an unacceptable scatter attaches not only to the observational estimates, and also to theoretical estimates based on the ΛCDM cosmology. For the observational data, much of this scatter results from uncertain corrections for the absorption by dust, and from the application of different methods with different observational biases and uncertainties. For the theoretical curves the uncertainties are mostly due to cosmic variance, the choice of the "prescription" of star formation which has been adopted, and to the treatment of feedback between the star formation and the interstellar medium.

Beyond the global picture of the star formation history of the universe provided by the Madau Plot, there is increasing interest in deriving the star formation rates of individual galaxies. At high redshift this information is used to determine how galaxies were assembled as a function of environment and of time. At low redshift, the interest is in seeing how star formation depends on the local environment, and for this purpose, spatially dependent SED information is being increasing used, as shown by *Spitzer Space Observatory*, GALEX and ground-based observations being made by the SINGS collaboration, and reported at this conference (Kennicutt 2006; Murphy et al. 2006). Apart from normal galaxies, the nearby star-bursting objects such as Arp 220 in which we can resolve the structure of a starburst region, and for which we frequently have much better quality data over more wavebands than we have for most high-redshift objects also provide much needed insight. Once modeled and their SEDs fully understood, such objects can be used to gain physical insight into star formation processes in the early universe.

In order to successfully model the SED we must bring together in one theoretical package a wide range of physics. This package requires a quantification of the stellar populations including stellar structure, stellar evolution, and atmospheric transfer modeling. It needs ISM physics including the physics of ionized plasmas, and a good understanding of interstellar dust. We need to understand the geometry of the dust with respect to the stars, since this determines the shape and peak of the far-IR re-emission. Ideally we should seek to develop an understanding of this geometry from the constraints offered by the other physics of the problem. Finally, the radiative transfer problem must be solved for the complex multi-phase nature of the interstellar medium. The various types of models used to compute broad-band SEDs have been recently reviewed by Dopita (2005). Few, if any, models have all these physical elements included at the same time, and so fully self-consistent models are still lacking. This hampers the predictive power of the SED modeling that has been done up to the present. We will now briefly survey the state-of-the-art in the incorporation of these various physical elements into SED modelling.

2. The Physical Elements of SED Modelling

Stellar Spectral Energy Synthesis. There are a number of publicly available codes which give consistent results on the SED of the stellar component, for whatever choices of the IMF are preferred. These include the Starburst 99 code (Leitherer et al. 1999), the Pégase code (Fioc & Rocca-Volmerange 1997), the Bruzual & Charlot, (2003) code and the Kodama & Arimoto (1997) code. These codes differ mainly on their predictions in the EUV, since here they rely on theoretical atmospheric and mass-loss models in which a good deal of progress has been made recently. In this respect the Starburst 99 code is probably the state of art (Smith, Norris, & Crowther 2002). The major strength of the Bruzual and Charlot code is in the synthesis of the older stellar populations.

Ionized Gas Physics. For the ionized plasma, two major codes have been used in SED modelling, the Cloudy code (Ferland 1996), and the Mappings III code (Sutherland & Dopita 1993; Dopita et al. 2000a; Dopita et al. 2000b). Both of these include all relevant gas-phase physics and a complete model for the absorption and re-emission of radiation by dust grains in the nebula. These codes provide both the emission line SFR diagnostics discussed above, as well as giving estimates of both the chemical abundance and the ionization parameter in the ionized gas (Dopita et al. 2000a; Kewley et al. 2002b). The ionization parameter provides us with an independent physical constraint on the geometry of the gas and dust with respect to the central stars.

Grain Composition and Size Distribution. Most models use a dust model consisting of both a carbonaceous and siliceous component. Apart from composition, the grain size distribution and the grain composition are the principal factors which determine the wavelength-dependence of the absorption and scattering processes. Most models use a grain size distribution and a composition which yield results consistent with observations of the extinction curve, and which also attempts to match the constraints on the cosmic abundances of the atomic species locked up the the grains in local and Magellanic Cloud environments. Examples include the older Desert et al. (1990) model, the more recent Weingartner & Draine(2001a, 2001b) model or the models of Dwek and his collaborators (Dwek, 2005). The simplest successful grain models have "astronomical silicates", an idealized (amorphous) material which has no laboratory counterpart, but has elements of many types of siliceous material, PAH molecules about 10Å across, and larger graphitic species. More complex models allow for other grain types such as iron or other materials, and includes "ices" in molecular cloud environments, notably CO_2, water and ammonia ice mantles on other grain materials.

The Survival of PAHs. The question of the survival of PAHs in the ISM is a problem which has received very little attention in the literature. Owing to the importance of this molecule in the *Spitzer Space Observatory* observations, we here investigate this problem in a little more detail.

The most recent and comprehensive study on the survival, dehydrogenation, and charge state of PAHs is by LePage, Snow & Bierbaum (2003), which shows that PAH survival in a UV radiation field is highly size-dependent. The smallest PAHs are stripped of their peripheral hydrogen atoms through photo-detachment reactions, because of the low number of degrees of freedom available to store internal energy subsequent to the absorption of a UV photon. In larger PAHs, photo-detachment is less likely, and this process may be balanced by radiative association reactions. Size also determines the PAH charge state and photo-dissociation rate. The photo-dissociation rate is very high in regions in which H-ionizing photons can penetrate, so PAHs are largely confined to the un-ionized regions, and are strongly photo-excited to emit in their characteristic IR molecular bands in the molecular photo-dissociation regions (PDRs) around HII regions. This is very clearly seen in the stunning images coming out of the *Spitzer Space Observatory* (e.g., Whitney et al. 2004.

Because the 2200Å absorption feature is a characteristic of the resonance of the $\pi-$electrons in carbon rings, both PAH molecules and graphite are carriers of this feature. However, the size of the graphitic platelets cannot be too large, since this would shift and broadens the feature. Photo-destruction of PAHs in the ionized and (possibly) the diffuse phases of the ISM will largely remove the 2200Å bump from the UV attenuation curve. Such weakness is observed in the attenuation curve of the light of starburst galaxies Calzetti (2001), and in low-metallicity systems such as the SMC in which the weakness of this feature may be rather a metallicity effect.

The fact that strong PAH emission is seen in the infrared spectra in almost all classes of disk galaxies, as well as in violently starbursting galaxies, coupled with the fact that PAH molecules are rapidly destroyed in ionized regions demands an effective PAH formation process in the interstellar medium. Stellar sources of PAH fail by orders of magnitude to maintain the PAH concentration against the destruction rate. We can estimate this destruction rate from the volume of gas, V, ionized by HII regions produced by $1.0 M_\odot$ $\mathrm{y}r^{-1}$ of star formation. If ρ is the density in the ISM, then the mass of interstellar gas processed through HII regions each year is then $dM_{ISM}/dt = \rho V/\tau_{HII}$ where τ_{HII} is the mean age of the HII regions, taken to be 5Myr; the period over which the central stars produce appreciable ionizing flux. Substituting values taken from the results of spectral synthesis modelling given in output of the Starburst 99 code (Leitherer et al. 1999), we find:

$$\left[\frac{M_{ISM}}{M_\odot \mathrm{yr}^{-1}}\right] = 45 \left[\frac{M_*}{M_\odot \mathrm{yr}^{-1}}\right] \left[\frac{n}{\mathrm{cm}^{-3}}\right]^{-1} \quad (1)$$

This implies that large fraction of the carbon in the molecular cloud has to be be processed into PAHs in order to maintain this molecular species. If this is the case, then equation (1) shows that, if the fraction of molecular mass converted into stars, or the efficiency of star formation is given by $\epsilon_{\rm SFR}$, then PAHs will disappear from the interstellar medium when:

$$\left[\frac{n}{\rm cm^{-3}}\right] \leq \left[\frac{\epsilon_{\rm SFR}}{0.025}\right] \tag{2}$$

This equation predicts a sharp edge in the PAH emission in the outer regions of galaxies when the density or pressure in the ISM falls below a threshold value.

The Dust Attenuation Curve. The destruction of PAHs in the ionized and diffuse phases of the ISM will largely remove the 2200Å bump from the UV attenuation curve. In order to compute this attenuation we have to take account the turbulent fractal structure of the ISM dust screen, *see* Fischera et al. (2003); Fischera et al. (2004) and the review by Fischera (2005). This produces a log : normal distribution in both the local density and in the column density, as has been demonstrated in the case of translucent and molecular clouds in this conference (Alves 2006). The cloudy fractal nature of the foreground screen flattens the attenuation curve in the way that was first derived observationally by Calzetti (2001) in the case of starburst galaxies. In these objects, we cannot observe the extinction curve directly, since we do not possess the resolution to make measurements of the extinction in lines of sight to individual stars.

The Dynamical Evolution of HII Regions. As emphasized above, the strength of the local radiation field, and the geometry of the dust relative to the gas determines the distribution of dust grain temperatures, and therefore the shape of the SED at IR wavelengths. In starburst galaxies, the OB stars are born in molecular clouds as compact or ultra-compact (UC) HII regions. If the local star formation rate densities are high enough, these join up to form a cluster-driven HII region which expands, driven by the over-pressure produced by the collective mass-loss from the cluster stars. In this phase the molecular clouds are engulfed, shredded and dispersed. In addition, the OB stars in the cluster will diffuse away from their point of birth, and may outrun the expansion of the HII region as a whole. Eventually the cluster stars expire as supernovae and the pressure driving the continued expansion of the HII will drain away, the shell will become momentum-conserving, and eventually break up into generalized interstellar turbulence.

The challenge to SED modelling is to describe these various phases sufficiently well to provide realistic constraints for the disposition of the gas and dust relative to the radiation field produced by the exciting stars. Before we can do this, however, we must establish whether the radiative transfer problem must be treated as a global problem (as is usually done) or whether the

various components can be treated as local radiative transfer problems, in which case the global SED can be determined by the sum of the various components present in a galaxy.

The vast majority of the far-IR emission arises from absorption of the UV radiation field in a relatively thin dust layer, the classical photo-dissociation region (PDR). These have an optical depth corresponding to $A_{\rm V} \sim 3$, and a thickness $dR \sim 300/n_{\rm H}$ pc. In the molecular regions surrounding normal galactic HII regions, densities are typically $100 - 1000$ cm^{-3}, implying that much of the far-IR which they produce comes from a layer of parsec or sub-parsec dimensions. In starburst galaxies, interstellar pressures may range up to a factor of 100 higher than this, producing correspondingly thinner PDR zones. Indeed, the ISM pressures are so great that a large fraction of the light not directly incident on molecular clouds can also be absorbed in distances short or comparable to the dimensions of the ionized plasma bubble. In such galaxies, the diffuse interstellar medium is also dense enough to locally absorb much of the light produced by the lower mass young stars which have diffused from their parent molecular cloud complexes as well as the UV and visible light produced by the older stellar populations. Indeed, the amount of dust obscuration is observed to increase both with galaxian mass (Kewley et al. 2002a), and with the absolute rate star formation (Buat et al. 1999; Adelberger & Steidel (2000); Dopita et al., 2002; Vijh et al., 2003). Largely, this arises by the operation of the Schmidt (1959) law of star formation. This couples the star formation rate per unit area to the gas surface density, and therefore, for a given dust to gas ratio, to the total dust obscuration. In normal spiral as well as in starburst galaxies, the surface rate of star formation is observed to follow such a Schmidt Law over several decades; $\Sigma_{\rm SFR} \propto \Sigma_{\rm gas}^{1.4}$, *see* Kennicutt (1998).

It is therefore clear that in starburst galaxies the radiative transfer problem can be treated as a local problem (except at low metallicity, where the gas-to-dust ratio becomes high), but that in more normal galaxies, some regions in spiral arms will require a local radiative transfer solution, whereas in the inter-arm and diffuse components a global radiative transfer approach is definitely required. This can be clearly seen in the *Spitzer Space Observatory* results presented at this conference (Kennicutt 2006; Murphy et al. 2006), where individual HII regions and HII region complexes appear prominently on the 25μm (hot dust) maps, while the inter-arm medium is relatively much more prominent at longer wavelengths in the cooler dust emission.

The work of Dopita et al. (2005) drew on the theory of the size distribution of HII regions by Oey & Clark (1997a,b). In this, the HII regions are assumed to expand and evolve as stellar mass-loss and supernova driven bubbles for as long as their internal pressure exceeds the ambient pressure in the ISM. When this condition is no longer met, the HII region is assumed to "stall". Of course, on reaching the stall condition, the HII region does not abruptly stop

expanding, but a momentum-conserving expansion continues until interstellar turbulence (about 10 km s^{-1}, van der Kruit & Shostak 1982) destroys the integrity of swept-up shell. The time taken to reach the stall radius turns out to be proportional to the stall radius, and the mass of the OB star cluster is important in determining the stall radius; HII regions with low mass clusters stall early and at small radius for a given pressure or density in the ISM.

The Excitation Conditions in HII Regions. The emission line spectrum of an HII region depends upon three parameters, the gas-phase chemical abundances, the effective temperature of the central star(s), and the ionization parameter $\mathcal{U} = \mathcal{Q}_*/nc$, which is the ratio of the photon density to the atomic density. For a fixed IMF, the ionization parameter will determine the excitation or the mean ionization state of the plasma.

We might expect that the excitation would depend sensitively upon the state of evolution of the HII region, or upon the size of the exciting cluster. In fact, for clusters of a given age and metallicity, there is a unique value of the ionization parameter in the HII region. This is because the pressure in the stellar winds at the outer boundary of the mass-loss bubble, $P_{\rm w}$, determines the equilibrium pressure in the HII region plasma, $P_{\rm HII}$. Thus, $P_{\rm w} = L_{\rm mech}/4\pi R_{\rm w}^2 v_{\rm w} = P_{\rm HII} = n_{\rm HII} k T_{\rm HII}$, where $v_{\rm w}$ is the mean stellar wind velocity measured at the radius of termination of the free-wind region $R_{\rm w}$. In general we can take $R_{\rm w} = \alpha R$ with $\alpha \sim 0.3$. Thus:

$$\mathcal{U} = \alpha^2 k T_{\rm HII} N_* v_{\rm w}/cL_{\rm mech} \tag{3}$$

Since the HII region temperature is always $T_{\rm HII} \sim 10^4$K, then, for any central star cluster at a particular time in its evolution, the ionization parameter is determined solely by the instantaneous ratio of $N_* v_{\rm w}/L_{\rm mech}$. For coeval clusters which are massive enough so that stochastic variations in these quantities are unimportant, the ionization parameter will be essentially independent of cluster mass and is only a function of cluster age. All quantities needed to compute the ionization parameter, are given in the STARBURST99 output.

Since the extended atmosphere of the exciting stars absorb a greater and greater fraction of the ionising photons as the metallicity increases, and at greater metallicity a greater fraction of the momentum flux in the radiation field is converted to mechanical energy in the winds, the ratio of $N_* v_{\rm w}/L_{\rm mech}$ strongly decreases as the metallicity increases. The ionization parameter also strongly decreases with cluster age due to the decrease in N_*. The effect of these variations on $\mathcal{U}$ is shown in Fig 1.

3. The SEDs of Starburst Galaxies

Dopita et al. (2005) showed that the main factor controlling the shape of the far-IR SED in starburst galaxies is the pressure in the ISM (which is the same

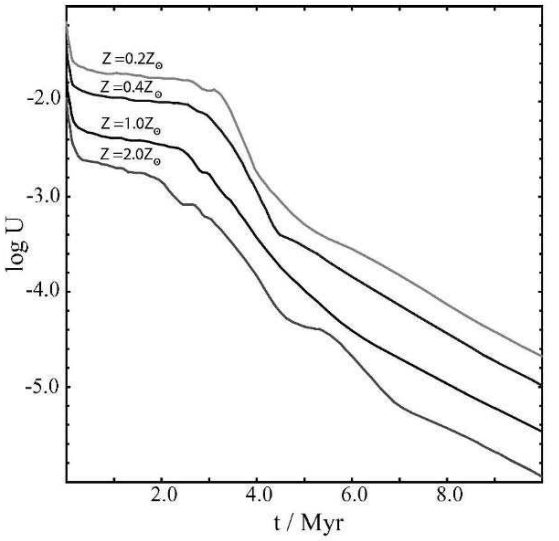

Figure 1. The ionization parameter of HII regions as a function of metallicity and time computed for a cluster of mass $3 \times 10^3 M_\odot$ from the STARBURST99 output. These computations include the evaluation of the self-consistent size evolution of the HII regions.

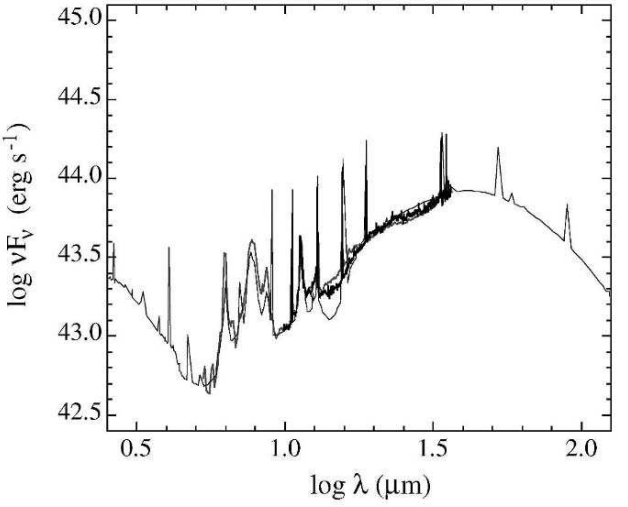

Figure 2. A composite starburst SED model fit (light thin blue line) to the IRS high-resolution and IRS low-resolution *Spitzer Space Observatory* spectra (thick lines) for NGC7714 (Brandl et al. 2004). The model has an ISM pressure of $P/k \sim 10^7$ cm^{-3}K, and the current mean star formation rate (SFR) given by the sum of the rate of single-star SFR and the cluster SFR is $10 M_\odot$ yr^{-1}. It assumes that single stars have their own HII region for a total of 3 Myr, and that the clusters are characterized by a dissipation timescale $\tau = 8$ Myr.

as the pressure in the HII region in the case of stalled HII regions). In high pressure environments, the HII regions stall sooner, are smaller, and the dust temperature distribution peaks at shorter wavelengths. This forms the basis of an understanding of the empirical behavior noted by Dale et al. (2001, 2002) and Lagache et al. (2003), in which more violent starbursts and intrinsically more luminous galaxies were observed to have stronger far-IR bumps in the SEDs peaking at shorter wavelengths.

The effect of compact or ultra-compact (UC) HII regions becomes increasingly important in dense, high pressure starburst environments (Dopita et al. 2006). In this case, the expansion of the HII regions stalls at very small radii (typically less than one parsec), allowing a very high rate of star formation rate per unit volume to be maintained along with a very small porosity of the ionized component. This apparently counter-intuitive situation is assisted by the fact that the dust in the ionized zones of the HII regions competes very successfully for the ionizing photons, making the HII region even smaller than would be predicted by Strömgren theory.

UC HII regions are likely to provide provide an important fraction of the bolometric flux in such environments. Such regions will be characterized by their hot dust temperatures, and a small equivalent width of the far-IR nebular lines relative to the dust continuum. In addition, the excitation as measured by far-IR lines will be systematically reduced, For example, Rigby & Rieke (2004) find that the [NeIII] 15.5μm / [NeII] 12.8μm ratio is systematically lower in starburst galaxies than would be predicted on a simple model. Their preferred solution is that massive stars in high-metallicity starbursts spend much of their lifetimes embedded within UC HII regions, in which the foreground dust screen serves to quench the line emission. This is true. However, the absorption of the ionizing photons by dust within the HII region itself is much more effective in quenching the line emission.

The amount of foreground dust extinction around the starburst can be estimated by the depth of the absorption in the 10 μm , and in some cases even the 20 μm silicate features. Generally, the silicate absorption can be used to measure the total extinction when the extinction in the circum-starburst dust screen has a visual extinction exceeding $A_{\rm v} \sim 3$–5 mag.

The computed SEDs provide good fits to both the line and continuum shapes of starburst galaxies, as can be seen in Fig. 2, where we compare the IRS high-resolution and IRS low-resolution *Spitzer Space Observatory* spectra (thick lines) for NGC7714 (Brandl et al. 2004) with our model.

When a complete grid of models has been computed for starbursts, we expect to be able to derive not only fraction of star formation in UC HII regions, and the total star formation rate, but also the mean pressure in the interstellar medium of the starburst region, the rate at which molecular clouds are destroyed and the metallicity. In addition, the excitation state of the gas and the

equivalent width of the emission lines relative to the dust continuum in the mid- and far-IR will provide constraints upon the slope of the initial mass function at the high mass end. Finally, the near-IR spectrum can be used to quantify the luminosity contributed by the old stars, and the UV-visible spectrum provides a fit to the extinction of any foreground screen of dust surrounding both the starburst region and the region in which the older stars are found.

For high-redshift galaxies we are hampered by a relative scarcity of observations across the full spectrum. For the high redshift radio galaxies (HizRGs) and for the sub-mm galaxies however, we do have sub-mm observations sufficient to constrain the far-IR SED. For the HizRGs, we now have 450μm and 850μm surveys of Archibald et al. (2001) and Reuland et al. (2004) covering 69 sources over the redshift range $z = 1 - 5$, and the data on the sub-mm galaxies (SMGs) has been recently summarized by Blain et al. (2004). These data are sufficient to fit a modified Black Body to derive a "dust temperature". In fact, such fitting has very little physical significance, because the far-IR and sub-mm portion of the SED is actually produced by a superposition of a wide range of dust temperatures. These depend locally on both the radiation field intensity, spectral distribution, grain composition and size (particularly for the larger grains), and the SED is the integral of these parameters through the star-forming region. Nonetheless, the modified Black-Body fits are still useful as a convenient parameterization of the SED beyond about 100 μm .

In the compilation by Blain et al. (2004), the "dust temperature" inferred from these modified Black-Body fits in the starburst galaxies and the ultra-luminous galaxies (ULIRGSs) in the local universe is observed to correlate with the absolute luminosity. Because these galaxies are dominated in a bolometric sense by their star forming populations, the correlation can be interpreted as a correlation between dust temperature and star formation rate. This is in agreement with what we inferred above, namely that high star formation rates should also correlate with high mass-specific star formation rates and high star formation rate densities, which are associated with regions of high ISM pressures.

The high-redshift SMGs provide a similar correlation, but shifted to higher luminosity. At a given luminosity, the dust in SMGs is about 20K cooler than in ULIRGs in the local universe, and at a given dust temperature, the SMGs are typically 30 times as luminous as their ULIRG counterparts. Takagi et al. (2003a,b) found that most ULIRGS have a constant surface brightness of order $10^{12} L_{\odot}\mathrm{kpc}^{-2}$. Our results show that this corresponds to an ISM with a pressure of order $P/k \sim 10^7$ cm^{-3}K . These parameters probably characterise "maximal" star formation, above which gas is blown out into the halo of the galaxy and star formation quenched. Only mergers, which provide an additional ram-pressure confinement of the star formation activity may exceed this surface brightness. Thus, in order to scale the star formation up to the rates

inferred for SMGs ($\sim 1000 - 5000 M_{\odot}\mathrm{yr}^{-1}$), we must involve a greater area of the galaxy in star formation, rather than trying to cram more star formation into the same volume. For a typical value of $10^{13} L_{\odot}\mathrm{kpc}^{-2}$, we require "maximal" star formation over an area of $\sim 10\mathrm{kpc}^2$, and the most luminous SMGs require star formation to be extended over an area of at least $\sim 100\mathrm{kpc}^2$.

We can therefore conclude that SMGs are truly starbursts extended on a galaxy-wide scale, rather than the more confined or nuclear starbursts which characterise ULIRGs in the local or moderate-redshift universe and that the modelling parameters we have derived for local ULIRGS — pressure, molecular gas dissipation timescales, and line of sight attenuations — can probably be directly applied to modelling the SEDs of SMGs in the distant universe. It remains to be ascertained whether the dust parameters are similar in these very different environments, but this too can be inferred from the pan-spectral SED.

Acknowledgements M. Dopita acknowledges the support of both the Australian National University and of the Australian Research Council (ARC) through his ARC Australian Federation Fellowship, and the financial support of the ARC through Discovery project grant DP0208445.

References

Adelberger, K.L., & Steidel, C.C. 2000, ApJ, 544, 218.
Alves, J. 2006, these proceedings, p. 417
Archibald, E. N., Dunlop, J. S., Hughes, D. H., et al. 2001, MNRAS, 323, 417
Ascasibar, Y., Yepes, G., Gottlöber, S., & Müller, V. 2002, A&A, 387, 396.
Blain, A. W., Chapman, S. C., Smail, I. & Ivison, R. 2004, ApJ, 611, 52.
Brandl, B.R., Devost, D., Higdon, S. J., U. et al, 2004, ApJS, 154, 188.
Bruzual, G. & Charlot, S. 2003, MNRAS, 344, 1000.
Buat, V., Donas, J., Milliard, B. & Xu, C. 1999, A&A, 352, 371.
Burton, M. G. et al. 2000, ApJ 542, 359
Calzetti, D. 2001, PASP, 113, 1449.
Dale, D. A., Helou, G., Contursi, A., Silberman, N. A., & Kolhatkar, S. 2001, ApJ, 549, 215
Dale, D. A., & Helou, G. 2002, ApJ, 576, 159.
Desert, Boulanger & Petit 1990, A&A, 237, 215.
Dopita, M. A., Kewley, L. J., Heisler, C. A., & Sutherland, R. S. 2000a, ApJ, 542, 224.
Dopita, M. A & Sutherland, R. S. 2000, ApJ, 539, 742.
Dopita, M. A., Pereira, M. Kewley, L. J. & Capaccioli, M. 2002, ApJS, 143, 47.
Dopita, M. A., Groves, B. A., Sutherland, R. S., & Kewley, L. J. 2003,ApJ, 583, 727
Dopita, M. A., et al. 2005, ApJ 619, 755
Dopita, M. A. 2005, *"The Spectral Energy Distribution of Gas Rich Galaxies: Confronting Models with Data"*, Heidelberg, Oct. 4-8, 2004, eds. C. C. Popescu & R. J. Tuffs, AIP Conf. Ser., 761, 203
Dopita, M. A., et al. 2006, ApJ (submitted)

Dwek, E. 2004, *"The Spectral Energy Distribution of Gas Rich Galaxies: Confronting Models with Data"*, Heidelberg, Oct. 4-8, 2004, eds. C. C. Popescu & R. J. Tuffs, AIP Conf. Ser., 761, 103

Ferland, G. J. 1996, Internal Report, Dept. of Physics & Astronomy, University of Kentucky

Fioc, M. & Rocca-Volmerange, B. 1997, A&, 326, 950

Fischera,J., Dopita,M. A., & Sutherland,R. S., 2003, ApJL, 599, L21

Fischera,J., Dopita,M. A. 2004, ApJ, 611, 919.

Fischera, J. 2005, *"The Spectral Energy Distribution of Gas Rich Galaxies: Confronting Models with Data"*, Heidelberg, Oct. 4-8, 2004, eds. C. C. Popescu & R. J. Tuffs, AIP Conf. Ser., 761, 283

Kennicutt, R.C. Jr. 1998,Ann.Rev.A&A, 36, 189.

Kennicutt, R. C. Jr. 2006, these proceedings, p. 397

Kewley, L. J. & Dopita, M. A. 2002, ApJS, 142, 35-52

Kewley, L. J., Geller, M. J., Jansen, R. A. & Dopita, M. A. 2002, AJ, 124, 3135.

Kodama, T. & Arimoto, N. 1997, A&A, 320, 41.

van der Kruit, P. C. & Shostak, G. S. 1982,A&A, 105, 351

Lagache, G., Dole, H. & Puget, J-L. 2003, MNRAS, 338, 555

LePage, V., Snow, T. P., & Bierbaum, V. M., 2003, ApJ, 584, 316

Leitherer, C. et al. 1999, ApJS, 123, 3.

Madau, P. et al. 1996, MNRAS, 283, 1388.

Murphy, E. J. et al. 2006, these proceedings, p. 409

Oey, M. S., & Clarke, C. J. 1997, MNRAS, 289, 570.

Oey, M. S., & Clarke, C. J. 1998, AJ, 115, 1543.

Reuland, M., Röttgering, H., van Breugel, W., & De Breuck, C. 2004, MNRAS, 353, 377

Rigby, J. R., & Rieke, G. H. 2004, ApJ, 606, 237

Schmidt, M. 1959, ApJ, 129, 243

Smith, L. J., Norris, R. P. F., & Crowther, P. A. 2002, MNRAS, 337, 1309

Sutherland, R. S. & Dopita, M. A. 1993 ApJS, 88, 253.

Takagi, T., Vansevius, V. & Arimoto, N. 2003, PASJ, 55, 385

Takagi, T., Arimoto, N. & Hanami, H. 2003, MNRAS, 340, 813

Vijh, U. P., Witt, A. F. & Gordon, K. D. 2003, ApJ, 587, 533.

Weingartner,J. C. & Draine, B. T. 2001a, ApJ, 548, 296.

Weingartner, J. C. & Draine, B. T. 2001b, ApJS 134, 263

Whitney, B. A. et al. 2005, ApJS, 154, 315

SINGS OBSERVATIONS OF SPIRAL GALAXIES

Evidence for secular evolution

Michael Regan[1*], Michele D. Thornley[2], Stuart N. Vogel[3], Kartik Sheth[4], Bruce T. Draine[5], David J. Hollenbach[6], Martin Meyer[1], Daniel A. Dale[7], Charles W. Engelbracht[8], Robert C. Kennicutt, Jr.[8], Lee Armus[4], Daniela Calzetti[1], Karl D. Gordon[8], George Helou[9], Claus Leitherer[1], Sangeeta Malhotra[1], George H. Rieke[8] and Marcia J. Rieke[8]

[1] *Space Telescope Science Institute, Baltimore, USA*
[2] *Department of Physics, Bucknell University, USA*
[3] *Department of Astronomy, University of Maryland, USA*
[4] *Spitzer Science Center, Caltech, Pasadena, USA*
[5] *Princeton University Observatory, USA*
[6] *NASA Ames Research Center, USA*
[7] *Department of Physics & Astronomy, University of Wyoming, USA*
[8] *Steward Observatory, University of Arizona, Tucson, USA*
[9] *Caltech, Pasadena, USA*
* mregan@stsci.edu

Abstract One process in the secular evolution of galaxies is the formation of pseudo-bulges. The formation of these pseudo-bulges requires the inflow of gas to smaller radii. If the inflow rate is faster than the rate of star formation, a central concentration of gas will form. In this paper we present radial profiles of stellar and 8 micron emission from Polycyclic Aromatic Hydrocarbons (PAHs) for 11 spiral galaxies to investigate whether the interstellar medium in these galaxies contains a central concentration above that expected from the exponential disk. We find that in five of the 11 galaxies there is a central excess in the 8 micron and CO emission above the inner extrapolation of an exponential disk. In particular, all four barred galaxies in the sample have strong central excesses in both 8 micron and CO emission. This correlation suggests that the excess seen in the CO profiles is, in general, not simply due to a radial increase in the CO emissivity.

Keywords: galaxies: structure - galaxies: ISM - dust, extinction - infrared: galaxies

R. S. de Jong, Island Universes, 341–346.
© 2007 *Springer.*

Introduction

While interactions, mergers, and accretion are clearly important in galaxy evolution, galaxies can also evolve significantly by internally-driven processes that redistribute angular momentum using stellar bars, spiral arms, or triaxial halos. Such processes are known collectively as secular evolution (see review by Kormendy & Kennicutt 2004 and references therein). As galaxies evolve, gas loses angular momentum to the stars and falls to a smaller radius. The gas may then form new stars and create a region of enhanced stellar surface density in the center of the disk known as a pseudobulge (see references in Kormendy & Kennicutt 2004). A pseudobulge is primarily distinguished from a true bulge by the fact that it has an exponential light profile rather than an $\exp(-const\ r^{\frac{1}{4}})$ light profile. A central excess of gas is strong evidence that gas is forming a pseudobulge, and thus serves as a marker for current secular evolution.

In this paper we look at 11 spiral galaxies that are common to a previous CO survey (Regan et al. 2001) and the Spitzer Infrared Nearby Galaxies Survey (SINGS). SINGS is a Spitzer Legacy project to observe 75 nearby galaxies, using all three instruments of Spitzer, to investigate the relationship between star formation and the ISM in galaxies (Kennicutt et al. 2003). For the 11 galaxies in common, we compare the radial distribution of the 3.6 micron IRAC images, which primarily trace the stellar component in the galaxy, to the 8 micron PAH images and the BIMA SONG CO 2.6 mm CO (1−0) images, both of which trace the ISM in the galaxy. We find that the images of 8 micron diffuse emission are highly correlated with the CO images, providing more evidence that the PAH emission is a good tracer of the ISM. We also find that in five out of 11 galaxies there is a central excess in the PAH emission, suggesting that the gas is being driven inward faster than it is forming stars. This net inflow of gas into the central region is an expectation of secular evolution.

1. Results

Figure 1 shows the wealth of information which is present in IRAC images of nearby spirals. As extinction from starlight is virtually absent in the mid-infrared at 3.6 micron, all galaxies look more symmetric than they do in optical light. The 3.6 micron images show the stellar surface density through the emission from stellar photospheres, including the prominent strong bar in NGC 3351. At 8 microns, the spiral structure is more prominent than at 3.6 micron emission, and a variety of complicated local structures can be seen, e.g., supershells along the spiral arms (in NGC 628).

Figure 2 shows that we can detect both the stellar and 8 micron light well beyond R_{25} in many of the galaxies. In all of the galaxies we can accurately measure the average disk stellar surface brightness to a radius of at least $1.5R_{25}$,

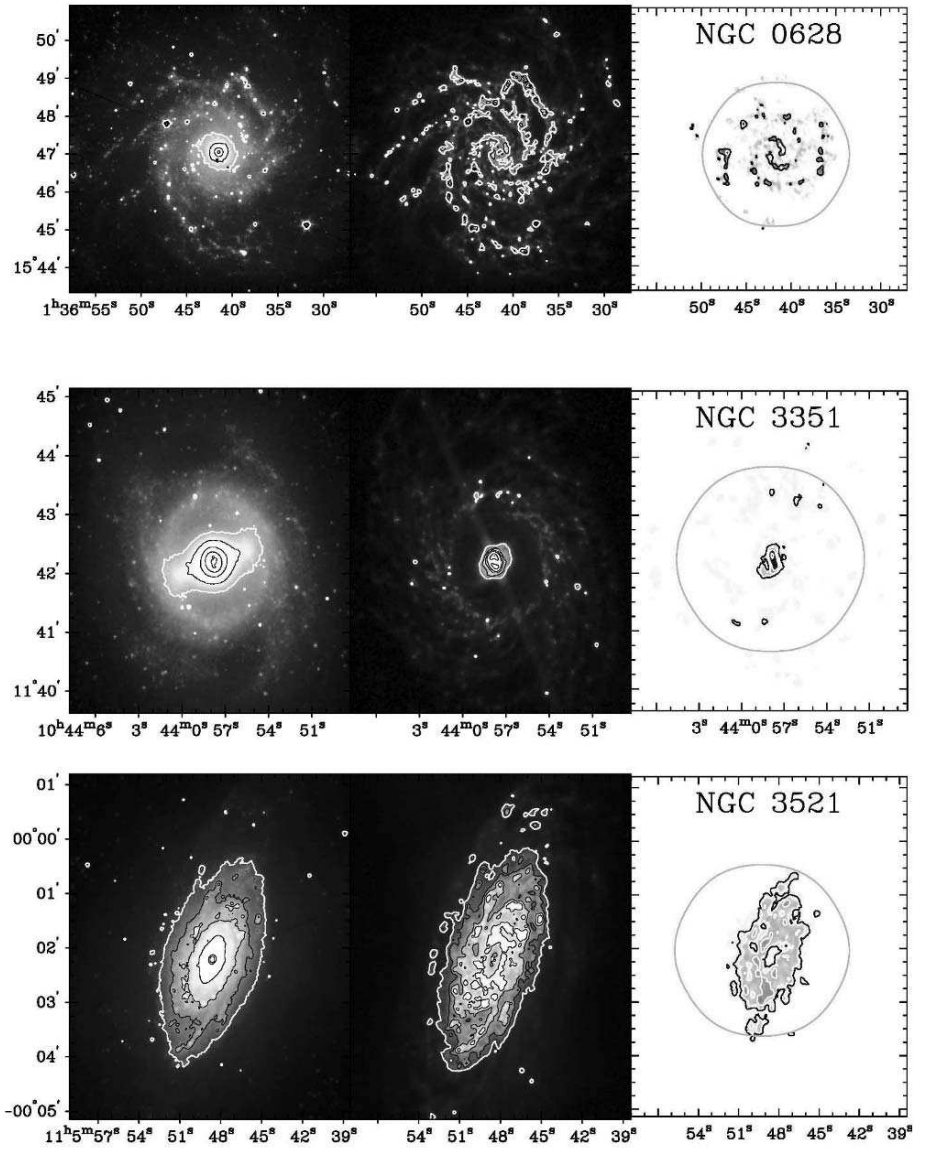

Figure 1. (Left Column) 3.6 micron images of the some of the sample galaxies. At this wavelength the emission is dominated by photospheric emission from red giant stars. The contours are at 1, 2, 4, 8, 32 and 64 MJy sr^{-1}. (Center Column) Stellar continuum subtracted 8 micron images of the same galaxies, primarily tracing the emission from PAHs (see text). The contours are at 3, 6, 12, 24, 96 and 192 MJy sr^{-1}. (Right Column) Total CO (1−0) emission from BIMA SONG (Regan et al. 2001) of the same galaxies. The cyan contour represents the effective limit of the CO mosaic (the 50% gain level). The contours are at 20, 40, 80, and 160 K km s^{-1}.

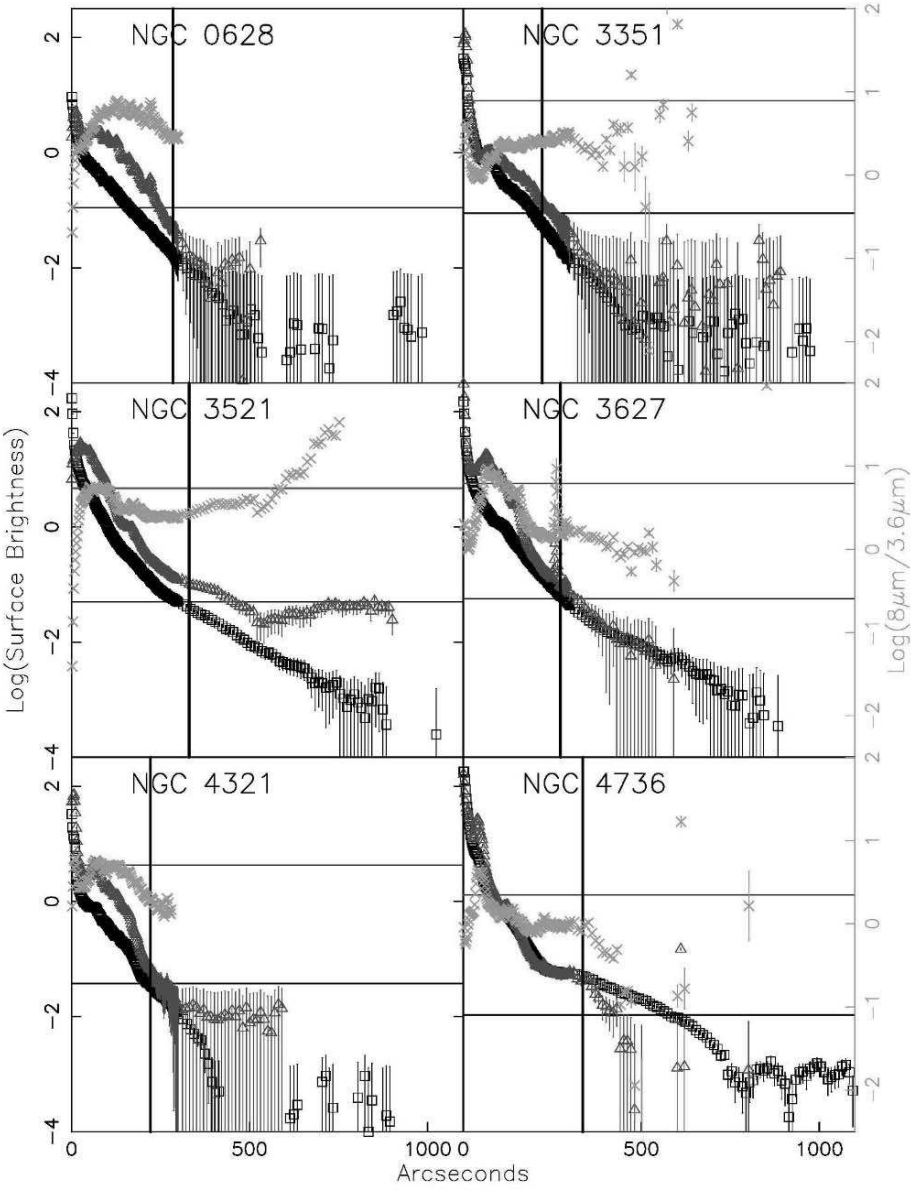

Figure 2. The radial profiles of the 3.6 micron stellar (black squares) and 8 micron PAH emission (red triagles) for some of the sample galaxies. In addition, the green crosses represent the ratio of the surface brightnesses (right scale). The surface brightness is measured in MJy sr^{-1}. The values plotted are the median for the 3.6 micron emission and mean for the 8 micron emission in each elliptical annulus, and the error bars are the uncertainty in the sky level. A vertical bar shows the R_{25} radius for each galaxy. The horizontal bar shows the average sky level for the 3.6 micron and 8 micron emission in each galaxy.

and in some galaxies we can detect it beyond $2R_{25}$. In most of the galaxies we do not detect any "edge" of the stellar disks; there does not seem to be any sharp drop in the stellar surface brightness as the surface brightness reaches our detection limit due to uncertainties in the sky level.

In five of the 11 galaxies (NGC 3351, NGC 3627, NGC 4321, NGC 4826, and NGC 6946) there is a central component of the 8 micron PAH emission that is brighter than the inner extrapolation of the exponential disk. We also see this central excess in the CO emission profiles of these galaxies. In the remaining six galaxies, five galaxies show no central excess in either PAH or CO emission. Only one galaxy in this sample, NGC 5055, exhibits an excess in CO emission which is not echoed in 8 micron PAH emission.

2. Conclusions

In all but one of the 11 galaxies we examined, the central excess or hole seen in the CO emission is also seen in 8 micron emission. This confirmation of the excess in a different tracer makes it unlikely that the CO excess is due to a variation in the relationship between CO flux and molecular gas mass. This excess is what is expected if the gas is flowing inward as part of the secular evolution of the galaxy.

References

Kennicutt, R. C., et al. 2003, PASP, 115, 928

Kormendy, J. & Kennicutt, R. C. 2004, ARA&A, 42, 603

Regan, M. W., Thornley, M. D., Helfer, T. T., Sheth, K., Wong, T., Vogel, S. N., Blitz, L., & Bock, D. C.-J. 2001, ApJ, 561, 218

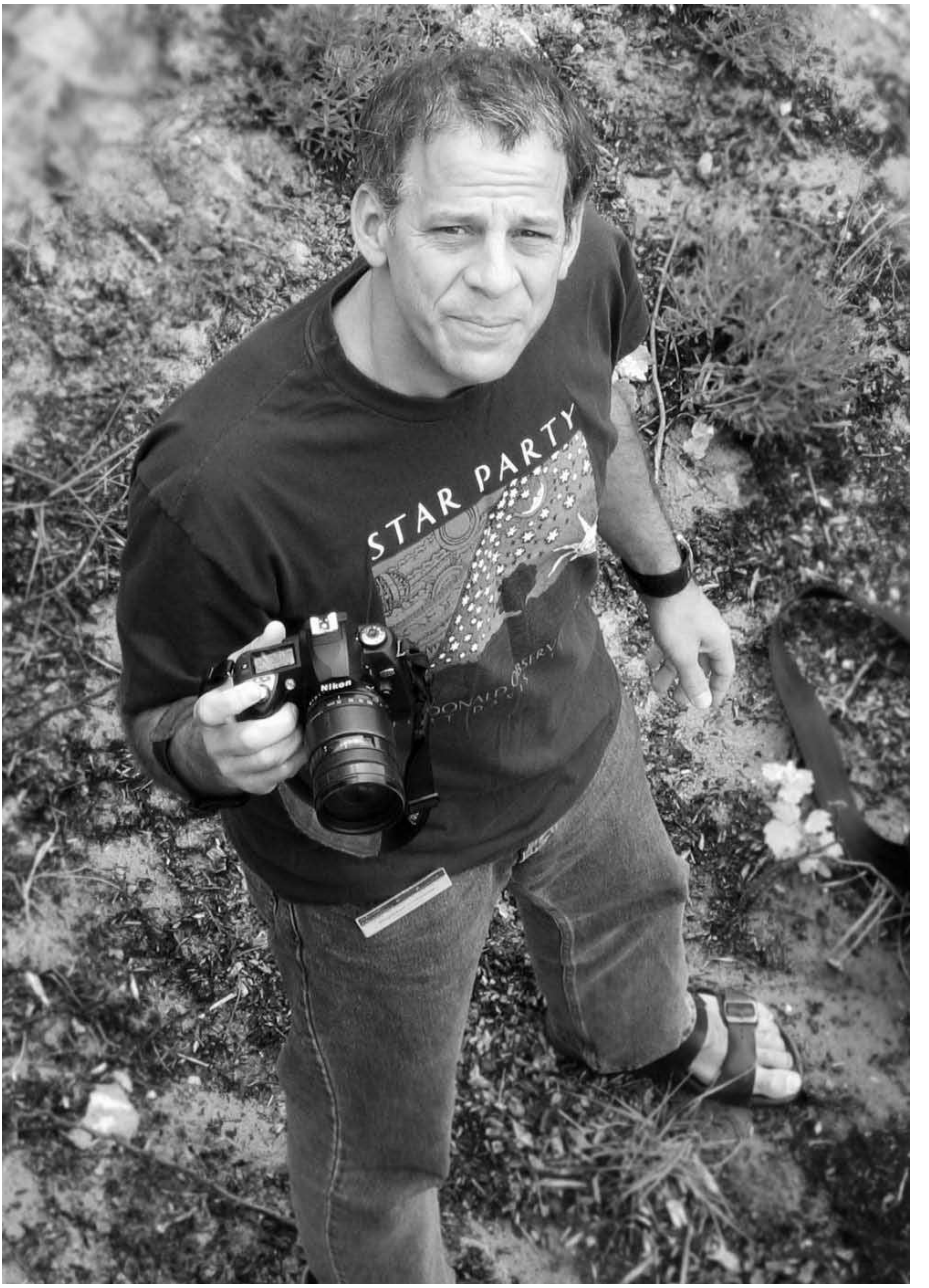

Stéphane Courteau, who took most of the pictures, but obviously not this one.

THE MOLECULAR ISM OF LOW SURFACE BRIGHTNESS SPIRAL GALAXIES

L. D. Matthews

Harvard-Smithsonian Center for Astrophysics, Cambridge, MA USA
lmatthew@cfa.harvard.edu

Abstract I summarize some results from the recent CO survey of late-type, low surface brightness (LSB) spiral galaxies by Matthews et al. (2005). We have now detected CO emission from six late-type, LSB spirals, demonstrating that despite their typical low metallicities and low mean gas surface densities, some LSB galaxies contain a molecular medium that is traced by CO. We find that the CO-detected LSB spirals adhere to the same $M_{\rm H_2}$-FIR correlation as brighter galaxies. We also find a significant drop-off in the detectability of CO among low-to-intermediate surface brightness galaxies with $V_{\rm rot} \lesssim$90km s^{-1}, pointing toward fundamental changes in the physical conditions of the ISM with decreasing disk mass.

Keywords: ISM: molecules - galaxies: general - galaxies: ISM - galaxies: spiral - radio lines: galaxies

1. Background

Low surface brightness (LSB) spiral galaxies are defined as having central disk surface brightnesses $\mu(0)_B \gtrsim$23 mag arcsec^{-2}, indicating low stellar surface densities. However, despite their faint optical appearances, the majority of LSB spirals show evidence for ongoing star formation, including blue colors, Hα emission and/or resolved populations of young stars (e.g., Schombert et al. 1992; Gallagher & Matthews 2002). Signatures of star formation are frequently coupled with large atomic gas fractions ($M_{\rm HI}/L_B \sim$1), underscoring that LSB spirals are not the faded remnants of brighter galaxies. In a number of cases, evidence is also seen for stellar populations spanning a wide range of ages (e.g., van den Hoek et al. 2000), implying that LSB spirals have been forming stars for a significant fraction of a Hubble time—but with low efficiency.

Lingering questions regarding the evolutionary history of LSB spirals are *why* their star formation has remained suppressed, and what physical processes

R. S. de Jong, Island Universes, 347–352.
© 2007 *Springer.*

regulate the type of low-level star formation that is observed in these systems. Given that LSB spirals comprise a significant fraction ($\sim$50%) of the local disk galaxy population (e.g., Minchin et al. 2004), answers to these questions are crucial for our overall understanding of the star formation history of the universe. In addition, they are relevant to understanding star formation in other low-density and/or low-metallicity environments, including protogalaxies, the outskirts of giant galaxies, and damped Lyα absorption systems.

2. Studies of the ISM of LSB Spirals

Past Results

Key to understanding the process of star formation in LSB spirals is an improved knowledge of the composition and structure of their interstellar medium (ISM). To date, most of our knowledge of the ISM in LSB spirals comes from studies of their H I gas, which appears to be by far the dominant component of their ISM ($\gtrsim$95% by mass). H I studies have shown that while H I is typically present throughout the stellar disk of LSB spirals, H I surface densities often fall below the critical threshold for instability-driven star formation throughout most of all of their disks (e.g., van der Hulst et al. 1993; de Blok et al. 1996).

In a broad sense, the low H I densities of LSB spirals seem to account naturally for their inefficient star formation. However, this explanation is not entirely satisfactory for several reasons. First, important ISM parameters including the gas scale height, volume density, and turbulent velocity remain poorly constrained. Secondly, we know some star formation is occurring in LSB spirals in spite of subcritical H I surface densities. Furthermore, it is ultimately from the molecular, not the atomic gas that stars form. It is clear that a more comprehensive picture of star formation in LSB spirals requires a more complete knowledge of their multi-phase ISM.

Unfortunately, direct searches for molecular gas in LSB spirals have proved to be challenging. Indeed, initial searches for CO emission from late-type, LSB spirals failed to yield any detections (Schombert et al. 1990; de Blok & van der Hulst 1998), leading to the suggestions that the metallicities of typical LSB spiral may be too low for the formation of CO molecules or efficient cooling of the gas, that the interstellar pressures may be insufficient to support molecular clouds, or that star formation may occur directly from the atomic medium (Schombert et al. 1990; Bothun et al. 1997; Mihos et al. 1999).

New Results from Deep CO Surveys

To partially circumvent the challenges of detecting CO emission from LSB spirals, my collaborators and I began surveying examples of LSB spirals viewed *edge-on*, using observations 2-3 times deeper than previous studies. Our targets

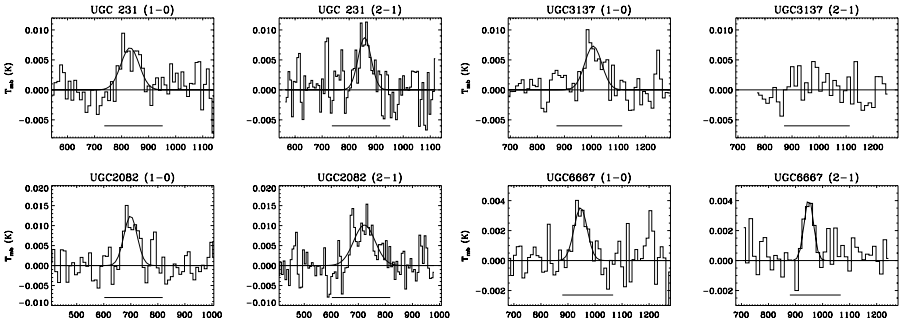

Figure 1. CO(1-0) and (2-1) spectra of four late-type, LSB spiral galaxies detected by M05.

comprised extreme late-type (Scd-Sm) LSB spirals with redshifts V_r $\leq$2000 km s^{-1}. Two advantages of our approach are: (1) the column depth of the molecular gas is enhanced for an edge-on geometry; and (2) an edge-on viewing angle allows complementary studies of the vertical structure of various ISM and stellar components of the galaxies at other wavelengths.

In a pilot survey with the NRAO 12-m telescope, we detected for the first time ^{12}CO(1-0) emission from three late-type, LSB spiral galaxies (Matthews & Gao 2001). More recently, we followed up with a more extensive survey of 15 LSB spirals in both the ^{12}CO(1-0) and ^{12}CO(2-1) lines using the IRAM 30-m telescope (Matthews et al. 2005; hereafter M05). In this latter survey, we detected CO emission from the nuclear regions of four LSB spirals, one of which was previously detected by Matthews & Gao (2001; Fig. 1). For the galaxies detected in these two surveys, we estimate the molecular hydrogen content of the nuclear regions (central 1-3 kpc) to be $M_{\rm H_2} \approx (0.3 - 2) \times 10^7\ M_\odot$, assuming a standard Galactic CO-to-H_2 conversion factor. While the conversion of CO flux to H_2 mass in low-density, low-metallicity galaxies can be rather uncertain, *these observations have clearly established that at least some bulgeless, late-type, LSB spirals contain modest amounts of molecular gas in their nuclear regions, and that CO traces at least some fraction of this gas.* In addition, our results establish that a bulge is not a prerequisite for the presence of molecular gas at the centers of low-density LSB galaxies. Therefore our surveys extend the realm of CO-detected LSB spirals from the giant, bulge-dominated LSB systems detected by O'Neil et al. (2000,2003) and O'Neil & Schinnerer (2004) to the more common, low-mass, pure-disk LSB systems.

While the samples of late-type, LSB spirals surveyed in CO are still small, already some interesting trends are emerging. Here I briefly describe two of our key findings. For further results and discussion, I refer the reader to M05.

LSB Spirals and the FIR-H_2 Correlation. For bright, massive spiral galaxies, there is a well-established correlation between far-infrared (FIR)

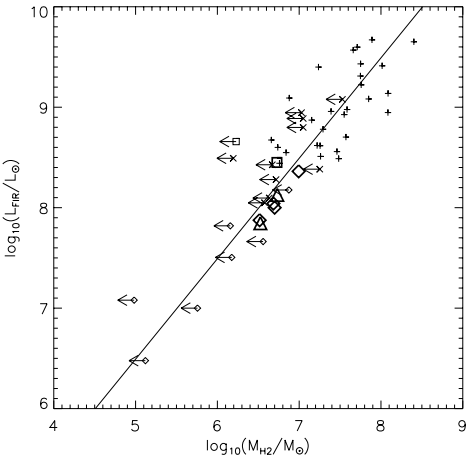

Figure 2. Log of the far-infrared luminosity versus log of the nuclear H_2 mass for extreme late-type spiral galaxies. M_{H_2} was derived from a single measurement with a telescope beam subtending ∼0.2-2 kpc toward each galaxy's center. Open symbols are LSB spirals taken from three different sources: triangles (Matthews & Gao 2001); diamonds (M05); squares (B03). '+' symbols are HSB spirals and 'X' symbols are ISB spirals, both taken from B03.

luminosity and H_2 mass (or CO luminosity; e.g., Young & Scoville 1991). This correlation is assumed to arise from heating of dust grains embedded in giant molecular clouds (GMCs) by hot young stars. There are a number of reasons why this correlation might break down for LSB spirals; for example, if molecular gas in LSB spirals resides primarily outside GMCs, if their stellar mass function is biased toward low-mass stars (Lee et al. 2004), or if the appropriate CO-to-H_2 conversion factor for these galaxies is very different from what we have assumed.

Figure 2 shows a plot of the nuclear H_2 masses (or 3σ upper limits) for our CO survey galaxies, versus the FIR luminosity derived from *IRAS* data. Also plotted is a sample of extreme late-type spirals recently surveyed in CO by Böker et al. (2003; hereafter B03). The B03 sample comprises the same range of redshifts and Hubble types as our LSB spiral CO surveys, but covers a wide range in surface brightness, including two LSB spirals [$\mu_I(0) \geq 21.4$ mag arcsec^{-2}], 15 intermediate surface brightness (ISB) spirals [$18.7 \leq \mu_I(0) < 21.4$ mag arcsec^{-2}], and 25 high surface brightness (HSB) spirals. Also overplotted as a solid line on Fig. 2 is the H_2-FIR relation derived by B03 for a sample of brighter, more massive galaxies.

Figure 2 reveals that the CO-detected LSB spirals delineate a remarkably tight extension of the H_2-FIR defined by brighter galaxies. Only a handful of the LSB/ISB galaxies undetected in CO show evidence of possible deviation from this correlation. Our findings suggest that as in brighter galaxies, the CO

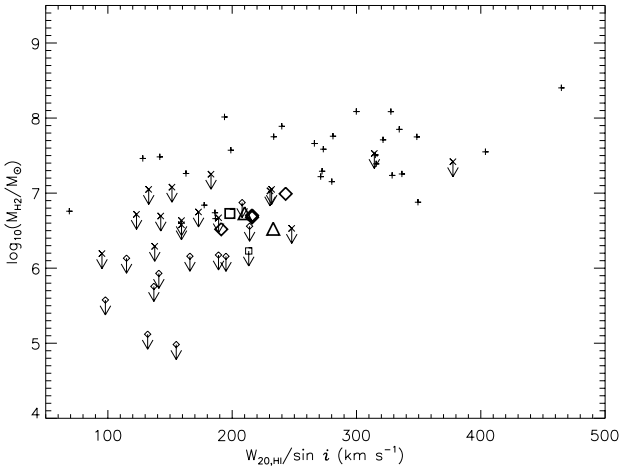

Figure 3. Log of the nuclear molecular hydrogen mass versus inclination-corrected total H I linewidth for extreme late-type spirals. Symbols are as in Figure 2.

detected in LSB spirals is associated with dense molecular clouds and sights of massive star formation rather than a more diffuse molecular medium.

A Link between Disk Rotational Velocity and the Detectability of CO in Low-Mass Galaxies. Figure 3 plots the nuclear H_2 mass versus the inclination-corrected total H I linewidth ($W_{20}/\sin i$) for the same samples shown in Fig. 2. W_{20} is related to the maximum rotational velocity of disk galaxies as $V_{\rm rot} \approx 0.5(W_{20} - 20)/(2\sin i)$ (see M05).

We see that for larger rotational velocities ($W_{20}/\sin i > 250$ km s^{-1}), the quantities plotted on Fig. 3 shows a nearly flat correlation. However, for galaxies with $W_{20}/\sin i < 200$ km s^{-1} (corresponding to $V_{\rm rot} \lesssim 90$ km s^{-1}), the inferred nuclear H_2 mass (i.e., the CO detectability) begins to drop significantly, and no ISB or LSB spirals below this limit have so far been detected in CO. As discussed by M05, it appears that neither decreasing mean H I surface density, nor decreasing metallicity among the lower mass galaxies can fully account for this trend. Figure 3 therefore points toward a decreasing concentration of molecular gas in the inner regions of galaxies with decreasing rotational velocity. This trend seems to depend only weakly on optical central surface brightness in the sense that both LSB and ISB galaxies show similar declines in CO detectability with $V_{\rm rot}$, although a few HSB systems with low $V_{\rm rot}$ do have CO detections.

It is interesting to note that the characteristic velocity, $V_{\rm rot} \approx 90$ km s^{-1}, below which we see a decline in the detectability of CO among late-type spirals is similar to the velocity characterizing a slope change in the optical Tully-Fisher relation for H I-rich, extreme late-type disks found by Matthews et al. (1998)

($V_{\rm rot} \sim 90$ km s^{-1}), the characteristic rotational velocity below which star formation appears to have been suppressed at high redshift ($V_{\rm rot} \sim 100$ km s^{-1}; Jimenez et al. 2005), and the rotational velocity below which galaxy dust lanes are seen to disappear ($V_{\rm rot} \sim 120$ km s^{-1}; Dalcanton et al. 2004). *All of these results are consistent with fundamental changes in some key parameter(s) governing the ISM conditions and the regulation of star formation in low-mass galaxies*. Possible causes could include: a decreasing fraction the disk unstable to GMC formation (e.g., Li et al. 2005), a change in the characteristic velocity for turbulence (Dalcanton et al. 2004), an increasing fraction of the disk below the critical pressure needed for the existence of a cold ISM phase (Elmegreen & Parravano 1994), the increasing dominance of gas relative to stars in the underlying disk potential, and/or decreasing effects of rotational shear (e.g., Martin & Kennicutt 2001). We are presently undertaking additional multiwavelength observations of our CO survey sample to better constrain the importance of these various effects.

References

Böker, T., Lisenfeld, U., & Schinnerer, E. 2003, A&A, 406, 87 (B03)

Bothun, G., Impey, C., & McGaugh, S. 1997, PASP, 109, 745

Dalcanton, J. J., Yoachim, P., & Bernstein, R. A. 2004, ApJ, 608, 189

de Blok, W. J. G., McGaugh, S. S., & van der Hulst, J. M. 1996, MNRAS, 283, 18

de Blok, W. J. G. & van der Hulst, J. M. 1998, A&A, 336,49

Elmegreen, B. G. & Parravano, A. 1994, ApJ, 435, L121

Gallagher, J. S., III & Matthews, L. D. 2002, in Modes of Star Formation and the Origin of Field Populations, ASP Conf. Series, Vol. 285, ed. E. K. Grebel and W. Brandner (ASP: San Francisco), 303

Jimenez, R., Panter, B., Heavens, A. F., & Verde, L. 2005, MNRAS, 356, 495

Lee, H.-c., Gibson, B. K., Flynn, C., Kawata, D., & Beasley, M. A. 2004, MNRAS, 353, 113

Li, X., Mac Low, M.-M., & Klessen, R. S. 2005, ApJ, 620, L19

Martin, C. L. & Kennicutt, R. C. Jr. 2001, ApJ, 555, 301

Matthews, L. D., Gallagher, J. S., & van Driel, W. 1998, AJ, 116, 2196

Matthews, L. D. & Gao, Y. 2001, ApJ, 549, L191

Matthews, L. D., Gao, Y., Uson, J. M., & Combes, F. 2005, AJ, 129, 1849 (M05)

Mihos, J. C., Spaans, M., & McGaugh, S. S. 1999, ApJ, 515, 89

Minchin, R. F., et al. 2004, MNRAS, 355, 1303

O'Neil, K., Hofner, P., & Schinnerer, E. 2000, ApJ, 545, L99

O'Neil, K. & Schinnerer, E. 2004, ApJ, 615, L109

O'Neil, K., Schinnerer, E., & Hofner, P. 2003, ApJ, 588, 230

Schombert, J. M., Bothun, G. D., Impey, C. D., & Mundy, L. G. 1990, AJ, 100, 1523

Schinnerer, E. & Scoville, N. 2002, ApJ, 577, L103

van den Hoek, L. B., de Blok, W. J. G., van der Hulst, J. M., de Jong, T. 2000, A&A, 357, 397

van der Hulst, J. M., Skillman, E. D., Smith, T. R., Bothun, G. D., McGaugh, S. S., & de Blok, W. J. G. 1993, AJ, 106, 548

Young, J. S. & Scoville, N. Z. 1991, ARA&A, 29, 581

THE KINEMATICS AND PHYSICAL CONDITIONS OF WARM IONIZED GAS IN SPIRAL DISKS

Matthew A. Bershady[1] and David R. Andersen[2]

[1]*University of Wisconsin, USA*
[2]*Herzberg Institute of Astrophysics, Canada*

Abstract We present integral-field echelle observations of the warm, ionized phase of the interstellar medium (ISM) of many, nearly face-on spiral galaxies. Luminosities and line-widths of Hα, [SII] and [NII] reveal several distinct trends in the conditions of the ionized gas. In principle these measures yield estimates for temperature, density, and energy sources of the kinematic heating. The emergent picture is complex: we find variations of the line-widths between galaxies and with galactic radius, and correlations between line-widths and emission-line luminosity and line-ratio. Two related bimodalities appear in line-ratio distributions and in the radial distribution of Hα luminosity. We briefly contrast ISM observations of nearby galaxies to the Milky Way and high-z galaxies.

Keywords: galaxies: ISM - galaxies: kinematics and dynamics - HII regions

1. Introduction

What drives gas velocity dispersions in star-forming galaxies is still an open question. In dynamically-cold disks it is unclear whether gas moves primarily in response to the local gravitational potential of the disk, cloud-cloud interactions, or is largely driven by a combination of photon-heating and (gravitational and wind-driven) shocks. The situation is complicated by a wide range of physical conditions and surface-brightness, and the need to disentangle geometric effects. The vertical dispersion-component of the ionized gas, which we focus on here, is observationally well-defined (projection issues are minimized in face-on systems), and easily obtained with optical spectroscopy. Understanding the variations of vertical line-widths in dynamically quiescent disks may tell us, in a broader context, what drives line-widths in more extreme systems. One underlying goal is to understand how well random motions of the ionized gas can be used as a dynamical tracer, as has often been used in studies of nearby and distant, star-forming galaxies.

R. S. de Jong, Island Universes, 353–358.
© 2007 *Springer.*

The earliest line-width measurements of the vertical dispersion component in disks were made of HI (van der Kruit & Shostak, 1982, 1984). Their small amplitudes ($\sigma_{HI} \sim$ 6-12 km/s) and near-constancy with galactocentric radius led to the suggestion that these motions were driven by photon heating. However, Combes & Bequaert (1997) observed similar values of $\sigma_{CO} \sim$ 6-9 km/s for cold, molecular gas, while Hα Fabry-Perot studies of ionized gas in HII regions yield median values of $\sigma_{H\alpha} \sim$ 14-25 km/s – again, nearly constant with radius (e.g., Rozas et al. 2000). Corrected for thermal broadening, Jimenez-Vicente et al. (1999) found $\sigma_{H\alpha}$ as low as $\sim$ 11 km/s. This suite of observations seems to rule out a purely thermal origin for the vertical heating, but the nature of the "heating" mechanisms and their dependence on gas-phase remains quite unclear. Hints include the density-dependence of the observed HI line-widths from the work of van der Kruit & Shostak, and the well-known luminosity-dependence of the observed HII line-widths.

Past studies encompass only a handful of nearly face-on galaxies. Optical studies have sampled small filling-factors with long-slit spectrographs, or were limited to emission surface-brightness typically above that of the diffuse component of the warm ionized medium. Here, we take a first step toward understanding the range of ionized-gas vertical velocity dispersions using full, two-dimensional maps of a large sample of normal, nearly face-on disks.

2. DensePak Survey

A sample of 39 nearly face-on spiral galaxies spanning a range of type and luminosity were selected for Hα-region echelle observations with the DensePak integral field unit (IFU) on the WIYN telescope. This survey (Andersen et al. 2001, 2003, 2005 and these proceedings) is a precursor to the Diskmass Survey (Verheijen et al., these proceedings), and has the desirable attribute of high spectral resolution ($\lambda/\Delta\lambda$ = 14,500) with 3 arcsec spatial sampling.

Gaussian line-fits were made to Hα and [NII]$\lambda\lambda$6548,6583 in $\sim$5500 fiber spectra. [SII]$\lambda\lambda$6716,6730 were also measured in most galaxies. Few spectra appear to have multi-component, or significantly non-Gaussian lines. Fibers sample $1.1^{+0.4}_{-0.2}$ kpc (median and quartile) diameter footprints for this sample ($H_0 = 70$ km/s/Mpc used throughout). Line-fluxes were well-calibrated by matching the spectral continuum level to calibrated R-band surface-photometry. Effects of beam smearing (<5 km/s) and instrumental broadening ($\sim$9 km/s) are small (<18%; 12% typical), and well calibrated. The following analysis is based on measured line-widths corrected for these effects.

3. Results and Discussion

We find a median vertical dispersion of $\sigma_{H\alpha} \sim 18$ km/s, with a sample distribution that appears constant with radius. However, individual galaxies

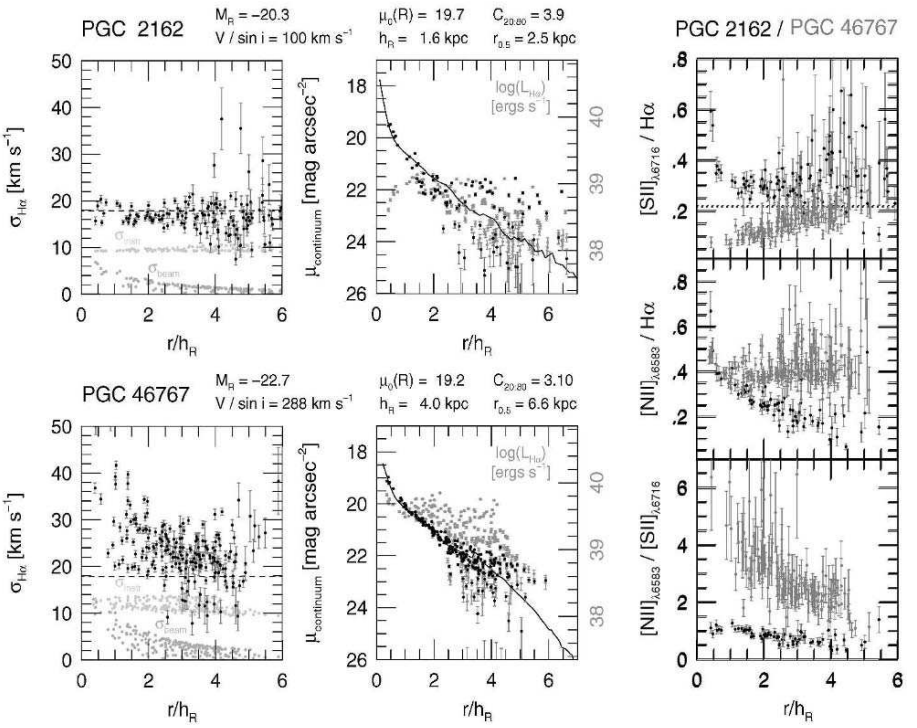

Figure 1. **Left Panels:** Hα velocity dispersion vs radius for each fiber observed in two galaxies (marked). Radii are normalized by the disk radial scale length, h_R. Sample median dispersion of 18 km/s is marked by the horizontal, dashed line. Beam-smearing and instrumental resolution for each fiber, also plotted, lie well below most corrected data points. Note differences in mean and radial trends of σ between these two galaxies. These galaxies are otherwise typical of the survey which contains systems with $i < 30$ and sizes ($45'' < D_{25} < 75''$) well-matched to the IFU foot-print, such that maps (typically covering 0.4-1 arcmin^2) sample out to several disk scale-lengths. **Central Panels:** Continuum fiber flux (dark points; left scale) and Hα fiber luminosity (light points; right scale) are over-plotted for the same two galaxies. Solid curves represent the calibrated R-band surface-brightness profiles used to calibrated the spectral continuum flux. Note the increase in Hα luminosity in the inner two scale-lengths of PGC 46767, while PGC 2162 plateaus at, or below, $10^{39.2}$ ergs/s, and in fact drops in the very center. In general, this behavior is correlated with the amplitude and radial trend of $\sigma_{H\alpha}$, with $10^{39.2}$ ergs/s in a $\sim$1.1 kpc diameter beam being a dividing threshold, as shown in Fig. 2 and 3. **Right Panels:** Line-ratios vs radius for both galaxies are over-plotted to show dramatic differences in mean values and radial trends for these two galaxies. These line-ratio differences correlate with differences in σ and $L_{H\alpha}$ in our sample. These two galaxies are roughly representative of the extremes in the range of galaxies observed. The dashed, horizontal line in the top-right panel at [SII]/Hα = 0.22 is roughly where Reynolds (1988) notes there is a distinction between HII-like regions and the diffused, ionized gas (DIG) of the Milky Way. There is a bimodality in the distribution of [SII]/Hα for the entire sample, with a correlation to the luminosity and rotation speed of the system. This is akin to the results noted by Rubin, Ford, & Whitmore (1984). However, there are galaxies in our sample (e.g., PGC 32638), which straddle this division, and transition from HII-like to DIG-like as a function of radius.

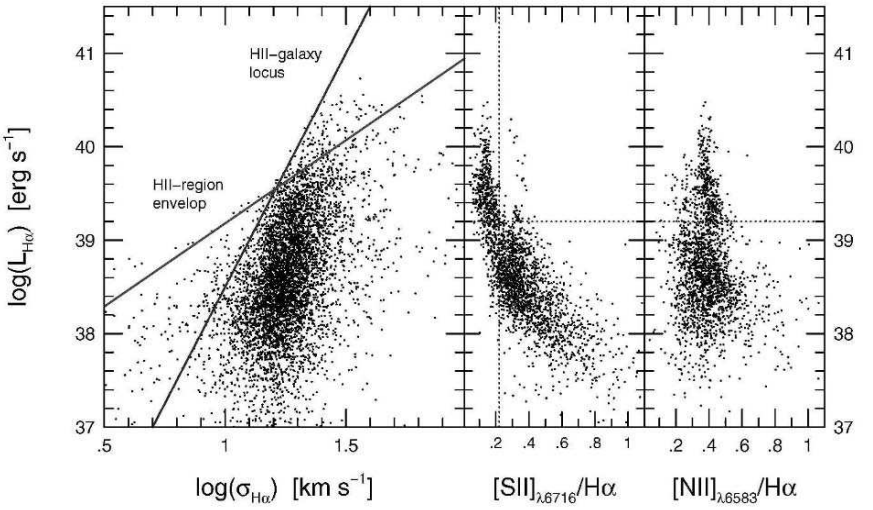

Figure 2. **Left Panel:** Hα luminosity vs velocity dispersion for each fiber for all galaxies in our survey. Lines for HII regions and HII galaxies (described in text) bound different portions of the distribution observed in $\sim$1.1 kpc diameter apertures. **Right Panels:** Hα luminosity vs line-ratios of [SII] and [NII] to Hα. The strong trend of [SII]/Hα with $L_{H\alpha}$ is seen in MW ISM studies (e.g., Haffner et al. 1999), but the lack of correlation of [NII]/H with $L_{H\alpha}$ is not. Both distributions appear bimodal about log($L_{H\alpha}$)=39.2 ergs/s (dotted horizontal line).

have different median $\sigma_{H\alpha}$, and some show strong radial trends. These differences correlate with line-strength and line-ratio. Galaxies with low $\sigma_{H\alpha}$ tend to have constant dispersion with radius, weak Hα emission, and high [SII]/Hα flux ratios. Galaxies with strong radial gradients in $\sigma_{H\alpha}$ have larger $\sigma_{H\alpha}$ values and stronger emission, significantly lower [SII]/Hα, and somewhat higher [NII]/Hα. Two extreme examples are shown Fig. 1. Sample correlations of line-widths and line-ratios with $L_{H\alpha}$ are shown in Fig. 2.

One puzzle to resolve is why Hα Fabry-Perot studies find a much shallower envelop in the σ-$L_{H\alpha}$ distribution for HII regions of individual galaxies (a slope of 1.5-3 in dex; e.g., Relano et al. 2005) than the σ-$L_{H\alpha}$ correlation found for low- and high-redshift HII-galaxies as an ensemble (a slope of ~ 5 in dex, e.g., Melnick et al. 1987; Siegel et al. 2005). Our L-σ distribution (Fig. 2) for all points within all galaxies is well bounded by the HII-region envelop at low sigma ($<$16 km/s) and by the HII-galaxy locus at high sigma ($>$16 km/s). However, the majority of points fall on a locus which is closer to the HII-galaxy relation although perhaps somewhat steeper. Aperture and selection effects must be considered - something we can model for our survey.

The above correlations produce a strong trend in [SII]/Hα along the L-σ locus: Regions of higher σ and $L_{H\alpha}$ have lower [SII]/Hα. This line-ratio trend with luminosity agrees qualitatively with studies of the DIG in the MW

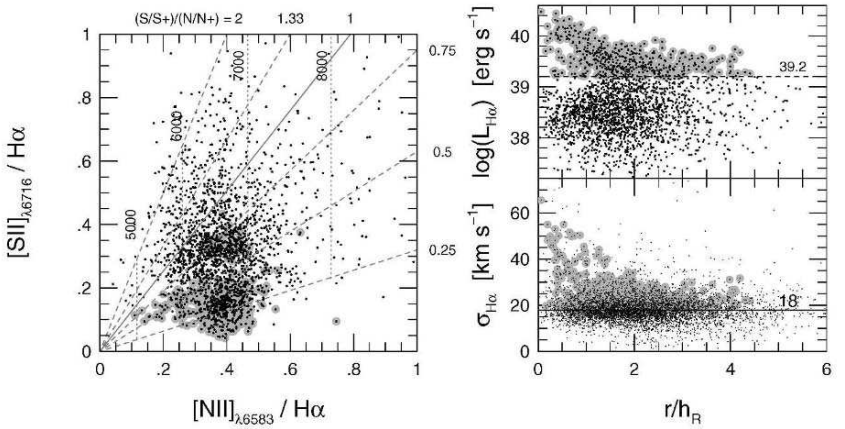

Figure 3. **Left Panel:** Line-ratios of [SII] and [NII] to Hα. Lines represent an extrapolation of the ionization-ratio model of Haffner et al. (1999), with vertical lines representing constant temperature (labeled). adopted from the model of Haffner et al. (1999). Note the bimodal distribution split roughly by [SII]/Hα = 0.22. **Right Panels:** Hα luminosity (top) and velocity dispersions (bottom) vs radius for each fiber for all galaxies in our sample. Radii are normalized as in Figure 1. Note the bifurcation in luminosity at small radii. Fibers containing more than log($L_{H\alpha}$)>39.2 are marked as larger, grey dots. These appear primarily at above-median σ and at low [SII]/Hα.

(Haffner et al. 1999). Unlike the MW ISM, however, [NII]/Hα does *not* appear to be correlated with $L_{H\alpha}$ overall (although this correlation is seen in some individual galaxies). Consequently, [NII]/[SII] correlates positively with line-strength and line-width.

We also find the bivariate distributions of any two of [SII]/Hα, [NII]/Hα and $L_{H\alpha}$ are bimodal about $L_{H\alpha} \sim 10^{39}$ ergs/s/kpc^2 or [SII]/H$\alpha \sim 0.2$ (Fig. 2 and 3). However, there is no bimodality in the distribution of any one of these parameters alone. While the physical interpretation of the range and bimodality in these line-ratios is unclear with extant data, Reynolds notes that a value of [SII]/H$\alpha \sim 0.22$ is roughly the demarcation between MW HII-regions and the DIG, and [NII]/[SII] ~ 1.6 gives a similar division (e.g., Haffner et al. 1999). Large values of [SII]/Hα are typically indicative of shock heating in the diffuse gas, consistent with the lower $L_{H\alpha}$ in these regions. The bimodality, then, may be loosely interpreted as a physical division between HII-like regions and diffuse, DIG-like regions.

Variation in [NII]/Hα is interpreted as arising from variations in metallicity or ionization parameter, with the latter favored by MW ISM studies of the DIG, and the former favored for HII regions in external galaxies. Without additional line diagnostics, given the coverage and sensitivity of our data, and hence the range of physical conditions likely sampled, it is unclear which interpretation applies. Even if [NII]/Hα is a reasonable metallicity index for luminosity-weighted measurements in systems dominated by HII regions, it should be

applied with caution to the data considered here, particularly because [NII]/[SII] has a much wider range than seen in the MW DIG (cf. Haffner et al. 1999). Whether this range represents variations in abundance, temperature, or ionization is subject of future inquiry. In this context, adding resolved measurements of HII galaxies into this analysis would be particularly useful, since Melnick et al. (1987) have long pointed out that these systems appear to be metal-poor versions of giant HII regions found in nearby, large galaxies.

Finally, we point out a bifurcation exists in $L_{H\alpha}$ vs radius (Fig. 3). Galaxies with steeply rising $L_{H\alpha}$ at small radii have strong σ gradients and $L_{H\alpha}$ above 10^{39} ergs/s/kpc^2. Consequently, these regions mostly have small [SII]/Hα and large [NII]/[SII]. Further, it is these points that are found in the most rapidly rotating systems, such that V_{rot}/σ is lower even though σ is larger. Our line-ratio correlations with rotation are in general agreement with the long-slit measurements of Rubin, Ford, & Whitmore (1984). They argued their findings in terms of abundance variations due to a global-mass-dependent chemical enrichment history. Here, however, the trends are not based on means of individual galaxies or their luminosity-class, but on the conditions at a specific location within any given galaxy. The presence of radial gradients, and a quantitative threshold in $L_{H\alpha}$ on scales of $\sim$1 kpc within individual galaxies, imply line ratios arise from local conditions within, rather than global properties of, galaxies. That this statement of locality and luminosity-dependence appears also to apply to ionized-gas line-widths may be a strong indication they have significant non-virial components.

Acknowledgements This research was supported by NSF/AST-0307417 and enriched by discussion with M. Haffner, R. Reynolds, and the Diskmass group.

References

Andersen, D. R. et al. 2001, ApJ, 551, L131
Andersen, D. R., & Bershady, M. A. 2003, ApJ, 599, L79
Andersen, D. R. et al. 2005, submitted to AJ
Combes, F. & Bequaer, J.-F. 1997, A&A, 326, 554
Haffner, M., Reynolds, R. J., Tufte, S. L. 1999, ApJ, 523, 223
Jimenez-Vicente, J., et al. 1998, A&A, 342, 417
Melnick, J. Terlevich, R., Moles, M. 1988, MNRAS, 235, 297
Reynolds, R. J. 1988, ApJ, 333, 341
Relano, M. et al. 2005, A&A, 431, 235
Rozas, M. et al. 2000, A&A, 386, 42
Rubin, V. C., Ford, W. K., Whitmore, B. C. 1984, ApJ, 281, L21
Siegel et al. 2005, MNRAS, 356, 1117
van der Kruit, P. C., & Shostak, G. S. 1982, A&A, 105, 351
van der Kruit, P. C., & Shostak, G. S. 1984, A&A, 134, 258

GLOBAL LINE PROFILE ASYMMETRIES IN DISK GALAXIES

David R. Andersen[1] and Matthew A. Bershady[2]

[1]*NRC Herzberg Institute for Astrophysics, Canada*
[2]*University of Wisconsin, Madison, USA*

Abstract We analyze and compare global line-profiles of 39 disk galaxies with HI and HII data. We find good agreement between the first and second moments of the profiles and recession and rotation velocities, respectively. The shapes of HI and HII profiles differ markedly, however, as the line profile asymmetries are not correlated. Asymmetry in neither HI nor HII profiles is correlated with rotation curve asymmetry which suggests that differing distributions of gas, and not kinematic asymmetries, dominate the global profile asymmetries of normal disk galaxies.

Keywords: galaxies: ISM - galaxies: kinematics and dynamics

1. Introduction

Global line-profiles, such as those obtained from single dish HI observations, provide no direct spatial information, yet contain a wealth of information about disk galaxies that have been used to develop the Tully-Fisher scaling relation, to map out large scale structure, and to establish that a large fraction of disk galaxies are asymmetric.

Kinematic asymmetries were first noted in HI velocity fields (Baldwin, Lynden-Bell & Sancisi 1980). Richter & Sancisi (1994), using the asymmetry index as defined by Tifft & Cocke (1989), first established that $\sim$50% of disk galaxies have asymmetric HI line profiles. They conjectured that since some of the galaxies with asymmetric line profiles were disturbed optically, line-profile asymmetry was most likely due to kinematic asymmetries. Since then, different methods have been developed for measuring line-profile asymmetry, but results have been similar (c.f. Haynes et al. 1998). The large fraction of asymmetric galaxies implies that these asymmetries are long-lived. However, evidence suggests photometric and kinematic asymmetries may not be related to global profile asymmetries (cf. Verheijen 1997; Swaters et al. 1999).

R. S. de Jong, Island Universes, 359–362.
© 2007 *Springer.*

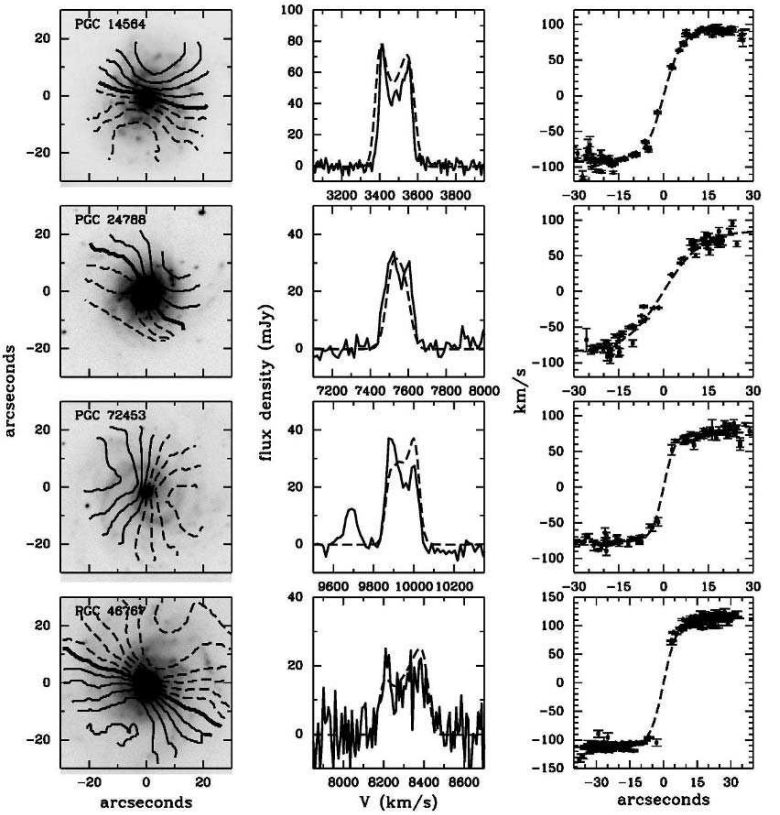

Figure 1. **Left Panels:** Velocity fields of four galaxies. **Central Panels:** HI(dashed) and HII(solid) profiles scaled to the radio flux. **Right Panels:** Rotation curves extracted from the Hα data. Asymmetries in the rotation curves are not usually apparent in the profiles.

Here, we compare moments obtained from HI and HII global line profiles and show these moments are precise and accurate measures of recession velocities, linewidths, and asymmetries. We then explore differences between the HI and HII asymmetries in our sample and comment on the physical causes of line profile asymmetries.

2. Data

Hα integral field spectroscopy was obtained for 39 nearby, nearly face-on disk galaxies using DensePak. From this data we created integrated HII (i.e., Hα) linewidth profiles. HI 21-cm line-profiles for 25 of these galaxies were observed using the Nançay radio telescope. The reduction and basic analysis of these HI and HII data are presented in Andersen et al. (2005). The lower signal to noise of the HI data, combined with some bad baseline determinations mean that we were only able to measure HI linewidths for 14 of these galaxies.

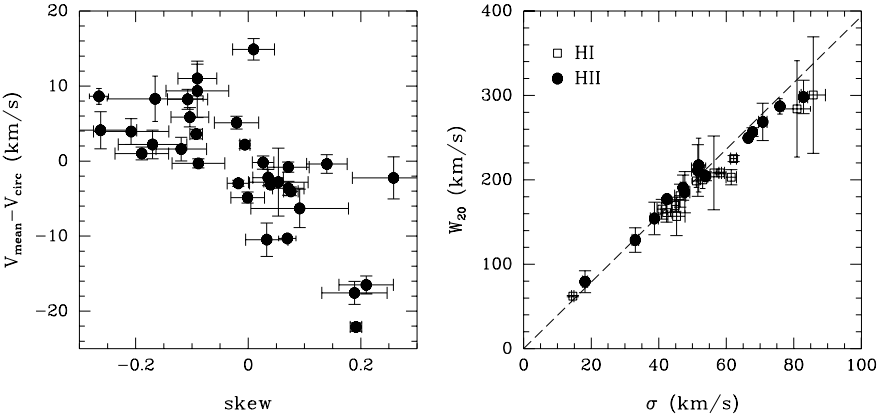

Figure 2. **Left Panel:** The difference between recession velocities measured from profiles and velocity field modeling are strongly correlated with skew, implying the third moment can improve estimates of the first. **Right Panel:** The second moment, σ, is highly correlated with the modeled velocity width, W_{20}. Only at low recession velocities do the two quantities deviate due to the intrinsic Hα linewidth.

We also constructed and modeled the Hα velocity field data to find rotation and recession velocities and rotation curve asymmetries (Andersen et al. *in preparation*). Four examples of the Hα velocity fields, HII and HI global line profiles and Hα rotation curves are shown in Figure 1.

3. Line Profile Moments and Asymmetries

We have established a moments-analysis method that is a simple, accurate and precise alternative for extracting recession velocities, velocity widths and asymmetry from line-profiles (Andersen & Bershady 2005). Figure 2 shows that the first moment is a good surrogate for velocity-field modeled recession velocity (especially if the third moment, skew, is used to correct the first moment), and the second moment, σ, is strongly correlated with disk rotation velocity.

The third moment, skew, is highly correlated with other measures of line profile asymmetry (Figure 3). Roughly half our sample showed significant asymmetries consistent with Richter & Sancisi (1994), but surprisingly, the HI and HII skew measures were decidedly un-correlated. Since the HI gas is present at much larger radii, the non-correlation of asymmetry suggests that the difference is either related to kinematic asymmetries present at different physical scales, or that the distribution of HI and HII phases differ significantly. To shed light on this question, we studied the kinematic asymmetries of the Hα rotation curves. Neither HI nor HII profile asymmetries are correlated with rotation curve asymmetry, which suggests that asymmetries in the global profiles are not related to kinematic asymmetries.

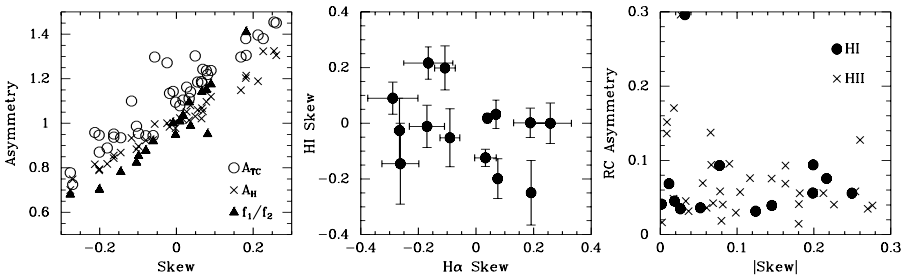

Figure 3. **Left Panel:** Skew is highly correlated with the ratio of peak fluxes and asymmetries as measured by Haynes et al. (1998) and Tifft & Cocke (1988). **Central Panel:** Skew measured from HI and HII profiles may be anti-correlated, one hint that the shape of the profiles is more closely related to differences in the distribution of the gas than to kinematic asymmetries. **Right Panel:** Skew is not correlated with rotation curve asymmetry (Dale et al. 2001); skew does not appear to measure kinematic asymmetry for normal disk galaxies.

4. Summary

A moment analysis of 39 normal, nearly face-on disk galaxies with global HI and HII profiles shows that the first and second moments are correlated with recession and rotation velocities respectively. Even better estimates of recession velocities can be made from the first moment if the third moment, skew, is considered as well. Skew is highly correlated with measures of global profile asymmetry. Skew measured for HI and HII global line profiles are uncorrelated, which suggests that the distribution of the different phases of hydrogen gas, not kinematic asymmetries, is responsible for most global profile asymmetries. Further evidence supporting this suggestion is that global line profile asymmetries are uncorrelated with asymmetries in the Hα rotation curves.

References

Andersen, D.R. et al. 2005, Submitted to ApJ Supplement Series
Andersen, D.R. & Bershady, M.A. 2005, Submitted to ApJ
Baldwin, J.E., Lynden-Bell, D., Sancisi, R. 1980, MNRAS, 193, 313
Dale, D.A. et al. 2001, AJ, 121, 1886
Haynes, M.P. et al. 1998, AJ, 115, 62
Richter, O.-G., & Sancisi, R. 1994, A&A Letters, 290, 9
Swaters, R.A., et al. 1999, MNRAS, 304, 330
Tifft, W.G. & Cocke, W.J. 1988, ApJS, 67, 1
Verheijen, M.A.W. 1997, Ph.D. Thesis, University of Groningen, The Netherlands

EXTRAGALACTIC MOLECULAR CLOUDS

Yuri Beletsky and João Alves

European Southern Observatory, Garching, Germany

Abstract We report the results of our study of 436 giant molecular clouds (GMCs) in NGC5128 using dust extinction. The proposed technique allows us to probe the extinction up to 10 magnitudes in this galaxy. The clump mass spectrum, derived by a clumpfind algorithm, is consistent with a power law, $dN/dM \propto M^{-\alpha}$, with α = 2.3.

Keywords: galaxies: ISM - dust, extinction - ISM: structure

1. Introduction

The physics of the formation of Giant Molecular Clouds (GMC) is one of the major unsolved problems of the interstellar medium. Although much work have been done on the subject it is not yet known what the dominant formation mechanism is, or even what the relative importance of gravity, shocks, and magnetic fields are in the cloud formation process. A study of GMCs in external galaxies can address the fundamental questions of whether the molecular ISM in external galaxies is organized differently than in the Milky Way and whether GMCs play the same central role in massive star formation as in the Milky Way, and are then responsible for galaxy evolution. Using the technique of mapping of dust column density through a molecular cloud in the nearby radio-galaxy NGC5128 (Centaurus A) we easily disentangle molecular clouds and assess their basic properties and star forming status, as opposed to the confused "inside view" of Galactic molecular clouds.

2. Observations

The observations were made on the 5th and 6th of March 2001 using the near-infrared imager/spectrometer SOFI (J ($1.25\,\mu$m), H ($1.65\,\mu$m), and Ks ($2.162\,\mu$m) bands) on the 3.5 m NTT telescope in La Silla, Chile. The SOFI detector is a Hawaii HgCdTe 1024×1024 array. We used the SOFI large-field mode, with a pixel scale 0.29 arcsec per pixel. Conditions during the observations were generally clear with a typical seeing better than 0.7 arcsec. The

R. S. de Jong, Island Universes, 363–366.
© 2007 *Springer.*

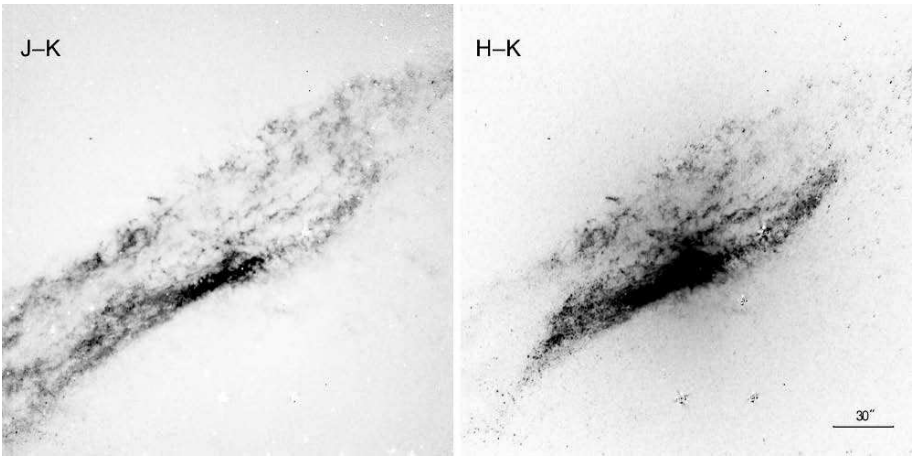

Figure 1. $J-K$ (left) and $H-K$ (right) color maps of Centaurus A. North is up, and East is to the left.

integration times were 30×10 s, 77×10 s, 60×10 s for the J, H and Ks band respectively. The observations were carried out using the "jitter" technique. Jittering was controlled by the automatic jitter template, which produce a set of dithered frames. Offsets are generated randomly within a box of 40×40 arcsec centered on the galaxy center.

3. The Technique

We are extending the successful idea of mapping dust column density through a molecular cloud (NICE method) proposed by Lada et al. (1994) to extragalactic GMCs. Instead of measuring the color of thousands of background stars to molecular clouds, we measure the average color of the unresolved thousand stars that fall on a pixel of a near-IR detector. Briefly, the color excess is given by:

$$E(J-K_s) = (J-K_s)_{\rm observed} - (J-K_s)_{\rm intrinsic} \qquad (1)$$

where $(J-K_s)_{\rm intrinsic}$ is the average color of the background stars. We convert color excesses to equivalent visual extinction adopting a reddening law from Rieke & Lebofsky (1985):

$$A_V = 5.88\, E(J-K_s) \qquad (2)$$

We measure the near-IR diffuse galaxy light seen through GMCs, in a simple analogy to our Galactic work (Alves et al. 2001). The technique allows one to derive the basic characteristics (morphology, mass, statistics) for this population and compare the dust extinction results with published molecular line data, in particular with CO interferometric data having almost the sub-arcsec resolution that is achievable in the extinction maps. The $J-K$ and $H-K$ maps of Centaurus A are shown in Figure 1. One of the major concerns in our analysis is to determine which fraction of the observed signal is due to some foreground contaminant (mainly due to presence of unresolved stars). However, we note that this factor should not significantly affect the derived parameters of molecular clouds, and in particular it should have no effect on the slope of the power-law derived for the Centaurus A GMC mass spectrum.

4. Cloud Mass Spectrum

Molecular cloud observations often show a complicated, self similar structure over a wide range of spatial scales. A main problem is the quantitative description of these structures. We extracted clouds from the $J-K$ color map using a 2D-version of the $clumpfind$ Williams et al. (1994) automatic routine for analyzing the clumpy structure. The algorithm works by first contouring the data at a multiple of the rms noise of the observations, then searches for local maxima in the data which locate the clumps, and then follows them down to lower intensities. The clouds were defined as regions containing more than 25 pixels, each with a value greater than 5 σ_{rms}. Using this algorithm we identified 436 molecular clouds.

The size of the clump is defined as the effective circular radius:

$$\Delta R = \sqrt{A/\pi},$$

where A is the projected area of the clump on the sky.

5. Results and Conclusions

Histogram of the mass distribution of GMCs in our catalog and the mass-size relationship are presented in Figure 2. The mass distribution of molecular clouds in Centaurus A is comparable with that found in M33 (α = -2.6, Engargiola et al. 2003) and steeper than that found in the inner Milky Way (α = -1.5, Scoville et al. 1987). A full analysis of these data should appear soon in the literature (Beletsky et al 2005).

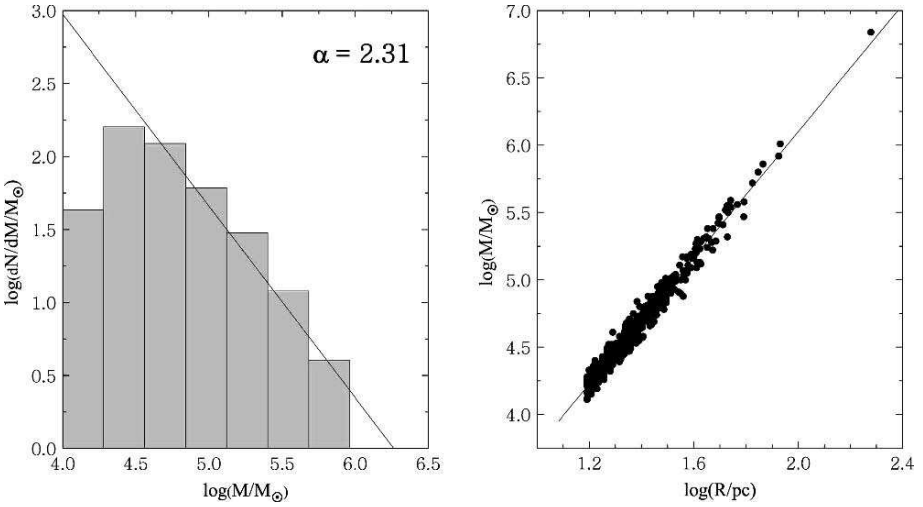

Figure 2. Clump mass spectrum (left) and mass-size relationship (right) for the GMC catalog. Both the mass spectrum the mass-size relationship are fitted by a power law function $dN/dM \propto M^{-\alpha}$.

References

Alves, J. F., Lada, C.J., & Lada, E.A. 2001, Nature, 409, 159

Lada, C.J., Lada, E.A., Clemens, D.P. & Bally, J. 1994, ApJ, 429, 694

Beletsky, Yu., Alves, J. 2005, in preparation

Engargiola, G., Plambeck, R. L., Rosolowsky, E., & Blitz, L. 2003, ApJS, 149, 343

Rieke, M. J. & Lebofsky, L. A. 1985, ApJ, 288, 618

Scoville, N. Z., Yun, Min Su, Sanders, D. B., Clemens, D. P., & Waller, W. H. 1987, ApJS, 63, 821

Williams, J.P., de Geus, E.J., Blitz, L. 1994, ApJ, 428, 693

THE FORMATION OF MOLECULAR CLOUDS IN SPIRAL GALAXIES

Clare Dobbs* and Ian Bonnell**

Dept. of Physics and Astronomy, University of St Andrews, Scotland

* cld2@st-and.ac.uk, ** iab1@st-and.ac.uk

Abstract We investigate, through numerical hydrodynamical calculations, the behaviour of a galactic disk subject to an external spiral potential. In particular, we focus on the evolution of inter-arm structure such as spurs, the formation of molecular clouds, and the generation of velocity dispersion as gas passes through the spiral arms.

Keywords: galaxies:spiral, hydrodynamic, ISM:clouds, ISM:molecules, stars:formation

Introduction

Molecular clouds are the sites of star formation in spiral galaxies, and are largely confined to the spiral arms. Their properties, including kinematics and internal structure, have been widely studied. However, the properties and distribution of molecular clouds are less well understood in relation to their formation and evolution. We identify molecular hydrogen in galactic simulations of spiral galaxies and display the location of molecular clouds.

Our calculations also reveal detailed inter-arm structure, including spurs and feathering. These features arise in purely hydrodynamical simulations providing the temperature of the gas is low ($\approx$ 100K).

1. Simulations of Spiral Galaxies

Calculations

Gas is passed through a spiral galactic potential (including spiral [Cox & Gomez 2002], logarithmic [Binney & Tremaine 1994] and halo [Caldwell & Ostriker 1981] components), which produces a 4-armed spiral pattern. Particles are located in a galactic disk, with radius 5kpc < r < 10kpc, scale height 100pc and mass $5 \times 10^8 M_{\odot}$. In all calculations the gas is isothermal, with temperatures of 10, 100, 10^3 or 10^4K. All calculations use SPH (smoothed

R. S. de Jong, Island Universes, 367–370.
© 2007 *Springer.*

particle hydrodynamics) code. These results include only the potential and gas pressure.

Formation of Molecular Clouds

The evolution of molecular hydrogen has been determined in our calculations (post process) using an algorithm from Bergin et al. (2004). For the lower temperature calculations, gas becomes sufficiently dense to become molecular when compressed by a shock. The locations of molecular 'clouds' are displayed in Figure 1 as they form in the spiral arms. In this simulation, the disk temperature is 100K and there are 4×10^6 particles. At the time in Figure 1 (100Myrs), approximately 10% of the gas is molecular $(5 \times 10^7 M_\odot)$.

Most of the molecular clouds are subsequently destroyed by photo-dissociation, although a few survive and emerge into inter-arm regions. A peak in the total H_2 mass was observed at $\approx$ 100K. At higher temperatures (10^3 or 10^4K), the lower density spiral shocks produce less H_2 which is more readily converted back to atomic gas.

Inter-Arm Structure

As the gas passes through the potential, shocks occur in the spiral arms, and significant secondary perturbations of the disk develop. Feathering of the spiral arms and spur-like structures evolve which extend over arm and inter-arm regions (Figure 1). These features arise solely from the kinematics of the gas and are only present at low (100K) temperatures. At higher sound speeds, the arm/inter-arm density contrast is less and the gas is largely smoothed with higher pressures. Correspondingly, there is little secondary structure present in the 10^4K temperature simulation. Previous spiral galaxy simulations have generally assumed a much higher sound speed. Wada & Koda (2001) and Gittins (2004) use temperatures of $\approx 10^4 K$ and describe much smaller instabilities. Kim & Ostriker (2001) describe the formation of more significant spurs when magnetic fields are applied. From our simulations it is apparent that fluid instabilities arise at low temperatures (corresponding with the colder part of the ISM which necessarily forms GMCs) without magnetic fields or self gravity.

2. Velocity Dispersion in GMCs

A consistent velocity dispersion law is observed across many GMCs, and on multiple scales (Heyer & Brunt 2004). We have been considering how such a velocity dispersion relation can be generated through a clumpy shock. Bonnell et al. (2005) show that a velocity dispersion-sizescale dependence comparable to the observed $\sigma v \propto r^{0.5}$ law is obtained when non-uniform gas passes through a spiral arm shock. Calculations for a simpler scenario are also described in Bonnell et al. (2005). Gas is passed through a simple 1D sinusoidal

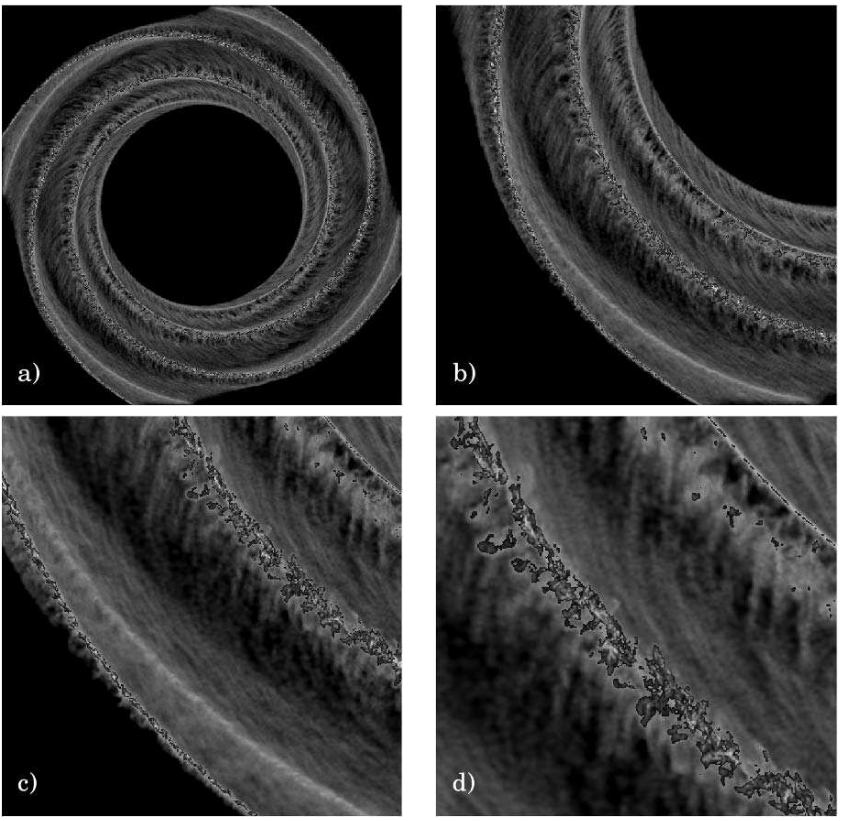

Figure 1. Column density plots showing density of molecular hydrogen (red) against overall density (black and white). The time in these images is 100Myrs. Length-scales of plots are a) 20kpc $\times$ 20kpc, b) 10kpc $\times$ 10kpc, c) 5kpc $\times$ 5kpc, d) 3kpc $\times$ 3kpc. The overall density shows the formation of spurs, feathering and widespread instabilities.

potential, and self-shocks as it climbs out of the potential. SPH calculations have been performed for a uniform shock in comparison to a clumpy shock, both with 2×10^5 particles, and the resulting velocity dispersions calculated. The velocity dispersion relation is largely flat and subsonic for the smooth shock. By contrast a supersonic velocity dispersion is induced in the shocked clumpy gas (Figure 2). This dispersion arises due to the inhomogeneity of the medium - gas encountering denser areas of the shock will decelerate more compared to empty regions. Thus a range of velocities occur in the shocked material.

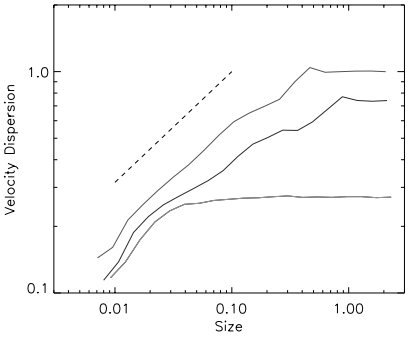

Figure 2. One dimensional velocity dispersion vs size-scale of post shock gas: uniform (bottom, green), clumps radii 0.2 (middle, blue), clumps radii 0.1 (top, red), $\sigma v \propto r^{0.5}$ (dashed). The sound speed is 0.3.

References

Bergin, E.A., Hartmann L.W., Raymond, J.C., Ballesteros-Paredes, J., 2004, ApJ, 612, 921
Binney, J., Tremaine, S., 1994, *Galactic Dynamics*
Bonnell, I.A., Dobbs, C.L., Robitaille, T.P., Pringle, J.E., 2005, MNRAS, submitted
Caldwell, J.A.R., Ostriker, E.C., 1981, ApJ, 251, 61
Cox, D.P., Gomez, G.C., 2002, ApJ, 142, 261
Gittins, D.M., 2004, PhD thesis, Univ. of Cambridge
Heyer, M.H., Brunt, C.M., 2004, ApJ, 615, 45
Kim, W.T., Ostriker, E.C., 2002, ApJ, 570, 132
Wada, K., Koda, J., 2004, MNRAS, 349, 270

CLOUD MASS FUNCTION IN A DISK GALAXY

Asao Habe[1*] and Takayuki Saitoh[2**]

[1]*Hokkaido University, Sapporo, Japan*

[2]*National Observatory of Japan, Mitaka, Japan*

* habe@astro1.sci.hokudai.ac.jp, ** saitoh.takayuki@nao.ac.jp

Abstract In order to study formation and evolution of interstellar clouds, we simulate the multi-phase interstellar matter in a disk galaxy using an SPH code, considering radiative cooling, cloud formation, star formation and heating by supernovae. By calculating various cases of total interstellar mass and strength of UV background radiation, we study how cloud mass function depends on theses parameters. We show that the power index, α, of the cloud mass function is small when there is a large amount of interstellar medium or strong UV radiation. Our results suggest that cloud mass function is a good indicator of these interstellar processes.

Keywords: ISM: clouds - ISM: structure- galaxy: spiral - stars: formation

1. Introduction

Star formation has a very important role in galaxy formation and evolution. Cloud formation and evolution are important to understand star formation process in galaxies. Molecular clouds are especially important for star formation, since they are star formation sites. Star formation is expected to depend on cloud properties. In massive molecular clouds both low mass and high mass star formation is expected, while in low mass molecular clouds only low mass star formation is expected. It is obvious that molecular clouds are closely related to star formation processes. Thus, the cloud mass function is closely related to star formation properties.

We study star formation processes in disk galaxy and the evolution of interstellar medium (e.g., the formation of molecular clouds, the star formation in gravitational instable clouds, and the back reaction of supernovae on interstellar medium) using the tree-GRAPE-SPH code of Saitoh et al. (2005). We derive the cloud mass functions from our numerical simulations.

R. S. de Jong, Island Universes, 371–374.
© 2007 *Springer.*

Recent high resolution observations have resolved molecular cloud components in galaxies and the theoretical study of cloud mass functions is very timely.

2. Model

We assume a small disk galaxy for detailed calculations. Total mass of a model galaxy is $2 \times 10^9 M_\odot$, and total gas mass is $2.5 - 5 \times 10^8 M_\odot$. The galaxy radius is 4 kpc. Initially, gas is uniformly distributed in the disk of the model galaxy. In the SPH simulation we use 50,000 SPH particles, and include cooling, heating by SN and diffuse UV in our calculations. We employ a wide range cooling function (20K $<$T $<$ 10^8K) as used in high resolution simulations of inter-stellar medium (e.g., Wada & Norman 2001). Star formation and feedback are modeled as in cosmological galaxy formation models (Katz 1992).

3. Numerical Results

Self-gravitational instability of gas occurs in the disk, since the gas temperature decreases by the radiation cooling. As a result, a filamentary structure develops in the cooled gas and many clouds are formed. In these clouds, star formation occurs and supernova explode after the massive stars evolve. The supernova explosions heat the gas and many cavity are formed as shown in Figs. 1 and 2.

We determine the cloud masses and find that the cloud mass function is approximated by a power law form with power index -α,

$$\frac{dN}{dM} = k(\frac{M}{M_0})^{-\alpha}.$$

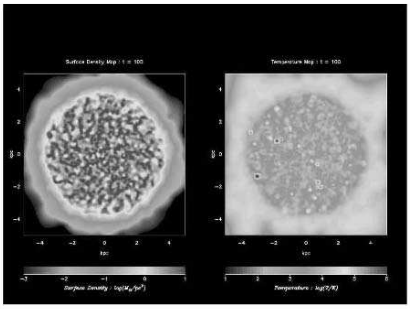

Figure 1. Face-on view of the disk galaxy. Surface density (the left panel) and gas temperature (the right panel).

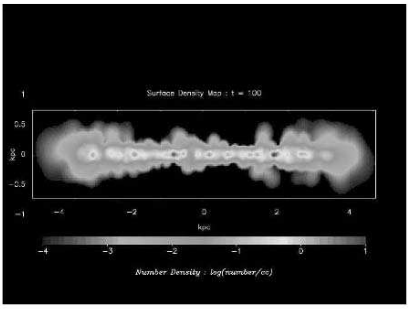

Figure 2. The edge-on view of gas in the disk galaxy.

We find that α ranges from about 1.6 to 3, depending on total gas mass and UV strength as shown in Figs. 3 and 4. In our simulations, small α is realized in the strong UV radiation case and in massive gas case. These results agree well with the following observational results : $\alpha \sim 1.6$ - 1.9 (Milky way : Solomon et al. 1987, Heyer et al. 2001), α $\sim$1.9 (LMC : Fukui et al. 2001), α $\sim$2.6 (M33: Engargiola et al. 2003). These results show that α is not common and depends on galaxy properties. Our results indicate that observed values of α depend on the environment of the interstellar gas.

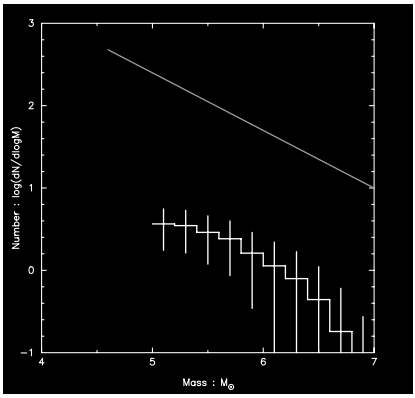

Figure 3. The cloud mass function in the gas rich case in our simulation. The solid line shows the cloud mass function with power index $\alpha = 1.6$ for comparison.

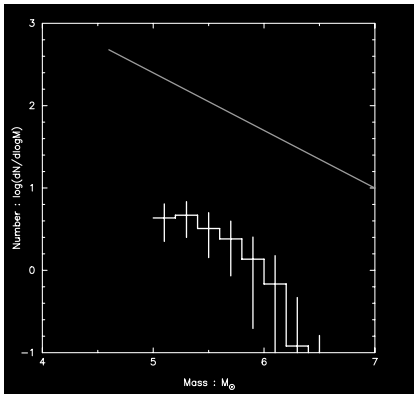

Figure 4. The same as Fig. 3, but for small gas case in our simulation. The cloud mass function is steeper than in Fig. 3.

4. Summary

We simulate the evolution of the multi-phase interstellar gas of small disk galaxy using a tree-GRAPE SPH code. We consider radiative cooling of gas, cloud formation by self-gravitational instability, star formation and heating by supernovae explosion of newly formed massive stars. Our numerical results show that the cloud mass function depends on gas mass and UV background. In our numerical results, the cloud mass function is well approximated by a power law function, and small power index is realized in a gas rich environment and large power index is realized in a gas deficient or a strong UV environment.

We suggest that high resolution observation of molecular clouds in nearby galaxies with for example ALMA will allow us to measure cloud mass functions, which will provide important constraints on the evolution of ISM and star formation in these galaxies.

Acknowledgements The authors wish to thank Drs. M. Fujimoto, K. Sorai, and H. Kuno for valuable discussions. This work is supported in part by Grant-in-Aid for Scientific Research (14340058) of Japan Society for the Promotion of Science.

References

Engargiola, G.; Plambeck, R. L.; Rosolowsky, E.; Blitz, L., 2003, ApJS 149, 343.
Fukui, Yasuo; Mizuno, Norikazu; Yamaguchi, Reiko; Mizuno, Akira; Onishi, Toshikazu, 2001, Pub. Astron. Soc. Japan 53, L41.
Heyer, Mark H.; Carpenter, John M.; Snell, Ronald L., 2001, AJ 551, 852.
Katz, N. 1992, AJ 391, 502.
Solomon, P. M.; Rivolo, A. R.; Barrett, J.; Yahil, A., 1987, AJ 319, 730.
Wada, K. & Norman, C., 2001, AJ 547, 172.

Albert Bosma, Peter Barthel, and Ken Freeman at the beach.

TRACING MOLECULAR HYDROGEN WITH ATOMIC HYDROGEN IN M81 AND OTHER NEARBY GALAXIES

Jonathan S. Heiner[1,2*], Ronald J. Allen[1**] and Pieter C. van der Kruit[2***]

[1] *Space Telescope Science Institute, Baltimore, USA*

[2] *Kapteyn Astronomical Institute, University of Groningen, The Netherlands*

* heiner@stsci.edu, ** rjallen@stsci.edu, *** vdkruit@astro.rug.nl

Abstract We present our progress on a detailed study of M81 in the radio, ultraviolet and infrared wavelengths, in which we attempt to use HI produced in photodissociation regions (PDRs) as a tracer for molecular hydrogen. Radio (VLA), UV (Galex) and IR (Spitzer) data are all available at about 6 arcsec resolution or better, corresponding to a linear scale of little over 100 parsec. We expect to pursue the viability of the use of HI as a tracer for H_2 across a variety of nearby galaxies, including NGC2403, M33 and M83, using VLA and GALEX data as a major extension to the existing studies of e.g. M101 and M81 in this context.

Keywords: galaxies: individual (M81) - galaxies: ISM - ISM: molecules - ISM: atoms - infrared: ISM - ultraviolet: ISM - radio continuum: ISM

1. Introduction

By assuming that HI is a photodissociation product of star formation, it can be used independently from the popular CO(1-0) tracer. In many instances, patches of HI are found close to bright FUV-sources, as is expected for PDRs. These complexes of young, hot stars create a 'blanket' of dissociated HI around them. Together with the incident ultraviolet flux on the HI, and the local dust-to-gas ratio, the associated volume density of molecular hydrogen can be derived from the local HI column density. How do we know that the HI is being produced in PDRs? Recent publications suggest that 8 μm PAH emission from star-forming regions can be used to trace PDRs. Matching regions of HI emission to PAH emission would support our approach. We aim to extend this project to other nearby galaxies in the coming year.

R. S. de Jong, Island Universes, 375–378.
© 2007 *Springer.*

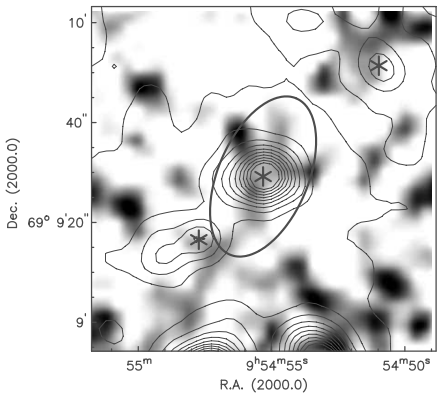

Figure 1a. A $70'' \times 70''$ field in a spiral arm of M81, with FUV sources (asterisks and contours) and radio emission (grayscale).

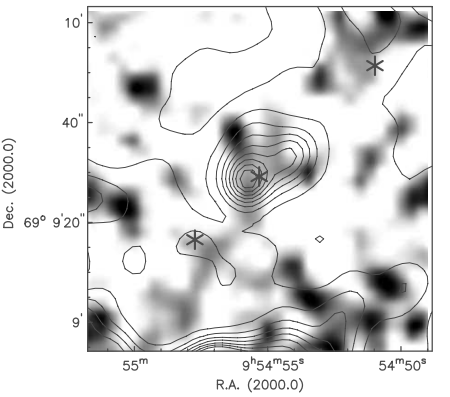

Figure 1b. The same region as in 1a, but with 8μm PAH contours. Note the PAHs away from the FUV source, associated more closely with the HI.

2. Hydrogen Cycle - Primordial or Product

The familiar hydrogen cycle takes us from atomic hydrogen to molecular hydrogen, catalyzed by dust grains, and back to atomic hydrogen by photodissociation, through photons in the ultraviolet range. Using the formula below describing the photodissociation process allows the use of HI as a tracer of molecular hydrogen.

$$N_{HI} = \frac{7.8 \cdot 10^{20}}{\delta/\delta_0} \ln \left[1 + \frac{106 G_0}{n_{H_2}} \left(\delta/\delta_0\right)^{-1/2} \right] cm^{-2} \qquad (1)$$

In the picture of large scale photodissociation regions (PDRs), at a linear scale of a few hundred parsec, a large fraction of interstellar atomic hydrogen could have been formed by photodissociation. It would be a product of star formation instead of being primordial and inert. So what was first? The presently observed atomic hydrogen or the molecular hydrogen? Note that the model formula is heavily dependent on the dust-to-gas ratio δ, scaled to the solar neighborhood value.

3. Method

Figure 1a shows the method to determine the local H_2 volume density. First, one determines the source flux (central asterisk), then the distance to any surrounding patches of HI (grayscale) - using a spherical model corrected for M81's inclination and position angle, hence the ellipse. The incident flux on the HI patches is computed using the radius to the central source. Finally one

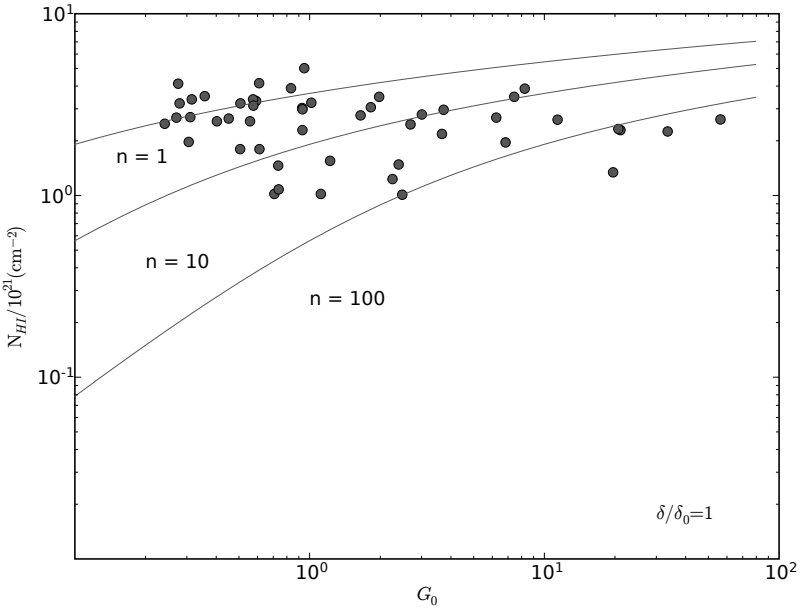

Figure 2. Incident flux G_0 vs HI column density with fitted molecular hydrogen volume densities.

takes maximum local HI column density as an estimate of the true local column density. Together with the dust-to-gas ratio at the appropriate galactocentric radius from the literature, these are the required input parameters to the model formula yielding the local H_2 volume density.

4. PAH Overlay

Figure 1b shows an example of how the PAH emission coincides more with the presence of HI then with the location of the FUV source. The source of FUV emission is clearly surrounded by PAH emission and atomic hydrogen patches, which would be in the PDR surrounding the OB complex. We are planning to compile statistics on how often this occurs, although preliminary qualitative results for the PAH/HI overlay indicate that this happens for the majority of cases.

5. Tentative Results

Determining the HI column density and the flux at about two dozen specific regions gives the plot shown in Fig. 2. Simply matching the flux and column density of each suspected PDR does not yield much of a correlation. However, correcting for the distance between FUV source and HI patch, calculating the

incident flux G_0 as shown here, gives better results. Fitting the model equation 1 indicates a molecular hydrogen volume density of the order 10^2. Varying the dust-to-gas ratio would tilt the fitted curves.

6. Why use HI as a Tracer?

Advantages include: it being an independent alternative to the popular CO tracer, the desired FUV and radio data is readily available and the 21cm emission is insensitive to excitation conditions, making for reliable HI maps.

Among the disadvantages are a strong dependence on δ/δ_0 - which is not always available from the literature, the geometry of the gas remains unknown and one needs to assume a certain FUV extinction correction

7. Plans for the Next Year

We aim to finish our detailed analysis of M81, including utilizing the Spitzer IRAC data. At the same time, we're starting a similar analyis of M83 with FUV data from the Galex SUNGG team. We are planning to obtain high-resolution ($6''$) HI data from THINGS, aiming to get additional data on other nearby galaxies like M33, NGC 2403, NGC 7793, LMC... Finally we can also do global modeling instead of detailed modeling to determine the total H_2 content of various nearby galaxies.

8. Summary

Preliminary results indicate a detectable correspondence of HI regions being located close to many FUV sources. The observed quantities can be fitted by the photodissociation model. Also, PAH emission often coincides with the locations of the HI regions, which is expected to be an indication that these regions are really PDRs.

References

Braun, R., 1995, A&AS, 114, 409
Willner, S.P., et al. 2004, ApJS, 154, 222W

CENTRAL STRUCTURE OF MOLECULAR GAS IN MAFFEI 2

Nario Kuno[1,4], Koichiro Nakanishi[1], Kazuo Sorai[2] and Toshihito Shibatsuka[3]

[1]*Nobeyama Radio Observatory, Minamimaki-mura, Minamisaku-gun, Nagano, Japan*

[2]*Hokkaido University, Sapporo, Hokkaido, Japan*

[3]*The University of Tokyo, Hongo, Bunkyo-ku, Tokyo, Japan*

[4]*SOKENDAI, Shonan Village, Hayama, Kanagawa, Japan*

Abstract We present results of CO observations of the barred spiral galaxy Maffei 2 with Nobeyama Millimeter Array (NMA). The distribution of the molecular gas in the central region shows elongated structure with two peaks as shown in the previous data. We found that the elongated structure resolved into spiral arms that continue from the offset ridges along the bar to a radius of less than 50 pc.

Keywords: galaxies: ISM - galaxies: kinematics and dynamics - galaxies: structure - galaxies: individual (Maffei 2)

1. Introduction

Fueling of molecular gas is necessary for central starburst and AGN activities in galaxies. Bar structure is one of the possible mechanisms for the gas fueling toward a galactic center. Observations of nearby barred spiral galaxies with high angular resolution are required to understand the mechanism of the gas fueling by bar.

Maffei 2 is one of the nearest barred spiral galaxies (D=2.8 Mpc: Karachentsev et al. 2003). The central region is undergoing a starburst (e.g., Turner & Ho 1994). Therefore, Maffei 2 is a good example to study the mechanism of gas fueling by a bar and to investigate the relation between a bar structure and a starburst. We present the results of observations of molecular gas in Maffei 2 with Nobeyama Millimeter Array (NMA).

2. Observations

Observations in CO(1–0) and CO(2–1) were made with Nobeyama millimeter Array (NMA). CO(1–0) were observed with antenna configurations AB,C, and D, while only C and D were used for CO(2–1). We achieved $1.7'' \times 1.5''$

R. S. de Jong, Island Universes, 379–382.
© 2007 *Springer.*

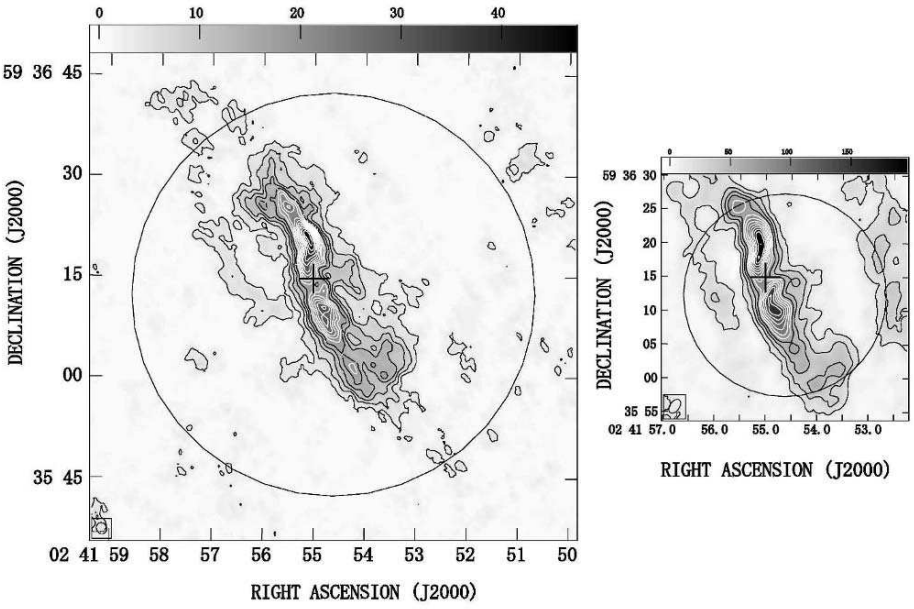

Figure 1. Integrated intensity maps in CO(1–0) (left) and CO(2–1) (right). Circles indicate the field of view of NMA. Crosses indicate the 2MASS center.

beam in CO(1–0) and $2.3'' \times 1.4''$ beam in CO(2–1). The beam sizes correspond to 23 pc $\times$ 20 pc and 31 pc $\times$ 19 pc at the distance of Maffei 2.

3. Central Structure of Molecular Gas

Figure 1 shows the integrated intensity maps of CO(1–0) and CO(2–1). In the bar region, the offset ridge along the leading edge of the bar can be seen. The width of the ridge (FWHM) is about $4''$ which corresponds to 54 pc at the distance of Maffei 2. The offset ridges are truncated at about $20''$ from the center in both sides. The offset ridges connect to a strong peak at about $5''$ ($\sim$ 70 pc) north and south from the center derived from 2MASS image (Jarrett et al. 2003). The distribution of CO(2–1) emission is consistent with CO(1–0) emission. Although the size of the peaks are about the same as that in CO(1–0), they are closer to the center than in CO(1–0). The center is weak in both lines.

Figure 2 shows the position-velocity diagram of CO(2–1) parallel to the major axis. The diagrams show complicated velocity structure. It is apparent that the central structure is separated into two parallel components in the P-V diagram. It means that there are two components along the line of sight. These structures weakly connect each other and make oval feature in the P-V diagram. The radial velocities at the center of both components are not at the

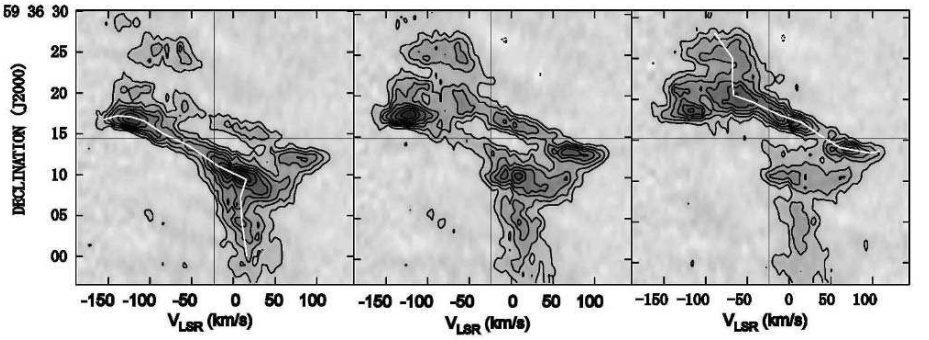

Figure 2. Position–Velocity diagrams along the major axis (middle) and parallel to the major axis (The offset is $\pm 0.9''$) in CO(2–1). The horizontal line is the position of the minor axis. The vertical lines are the systemic velocity of Maffei 2. White curves trace the spiral arms shown in Figure 3.

systemic velocity of Maffei 2. Since the feature in the P-V diagram is symmetric against the 2MASS center, it seems that the 2MASS center coincides with the dynamical center. When we trace gas stream from the offset ridge as shown by white curves in Figure 2, the radial velocity at the offset ridge is almost constant. For the northern side (upper side in Figure 2), blue-shift of the radial velocity from the systemic velocity means inward motion of the gas along the offset ridges toward the center. Then, the radial velocity increases with a constant velocity gradient closing to the center. The radial velocity changes from blue-shift to red-shift before the minor axis, while the point should be on the minor axis for a circular motion. We can see that after the northern component crosses the line of sight to the center, the radial velocity increases rapidly and closes to the center again. The symmetric feature can be seen for the southern component.

We made integrated intensity map of each component of the parallel feature separately (Figure 3). The map shows that the offset ridges connect toward the center as two-arm spiral structure. The spiral structure is symmetric against the 2MASS center. The spiral structure can explain the complicated velocity structure seen in the P-V diagram. Furthermore, the oval structure seen in the P-V diagram indicates that there is an oval structure overlapped on the spiral structure. The schematic face-on view is shown in Figure 3.

We can measure the size of the spiral structure using the P-V diagrams along the major and minor axes and the channel maps. Here, we assume the inclination angle (67°) and the position angle (26°) derived for the galactic disk. The sizes are determined by the following ways and shown in Figure 3.

1. The separation along the major axis between the spiral arms can be measured in the P-V diagram along the major axis.

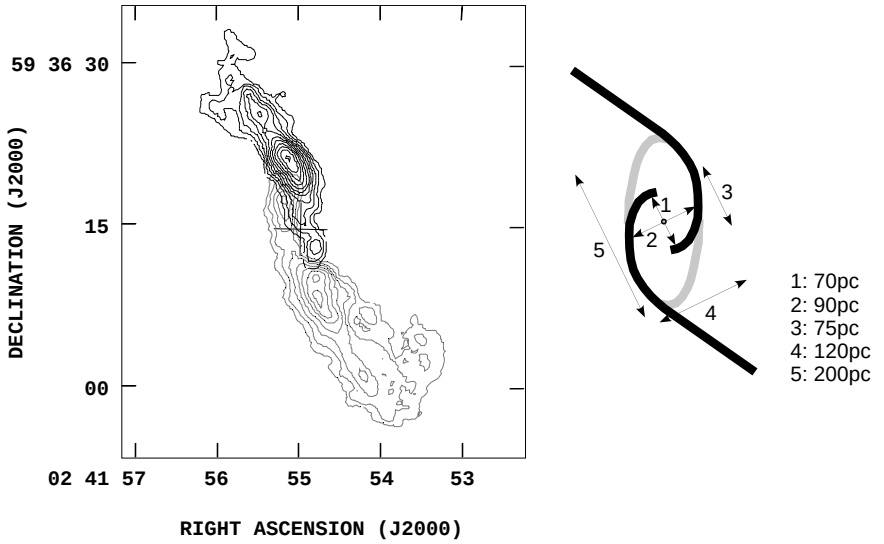

Figure 3. (Left) The integrated intensity map of the spiral arms. The cross is the 2MASS center. (Right) Schematic face-on view of the molecular gas distribution. The sizes derived from the observational data are indicated.

2. The separation along the minor axis between the spiral arms can be measured in the P-V diagram along the minor axis.

3. The separation along the major axis direction between the positions where radial velocity equals to the systemic velocity. If we assume that most of the gas moves along the spiral arms, the spiral arms are perpendicular to the line of sight there. It can be measured in channel map at the systemic velocity of Maffei 2.

4. The separation along the minor axis direction between the positions where radial velocity equals to the systemic velocity. It can be measured in channel map at the systemic velocity.

5. The length of the oval structure along the major axis can be measured in the P-V diagram along the major axis.

The formation mechanisms of the spiral structure are discussed in Kuno et al. (2005).

References

Jarrett, T. H., Chester, T., Cutri, R., Schneider, S. & Huchra, J. P. 2003, AJ, 125, 525
Karachentsev, I. D., Sharina, M. E., Dolphin, A. E. & Grebel, E. K. 2003, A&A, 408, 111
Kuno, N., Nakanishi, K., Sorai, K. & Shibatsuka, T. 2005, in preparation
Turner, J. L. & Ho, P. T. P. 1994, ApJ, 421, 122

THE DUSTY DISK OF THE EARLY-TYPE GALAXY NGC 3656

Lerothodi L. Leeuw[1], Jacqueline Davidson[2], C. Darren Dowell[3], Roger H. Hildebrand[1] and Henry E. Matthews[4]

[1]*University of Chicago, USA*
[2]*USRA-SOFIA, USA*
[3]*Caltech-JPL, USA*
[4]*NRC-HIA, Canada*

Abstract SHARC II 350 μm continuum and archival *HST* $J-H$ band maps are presented of NGC 3656, the brightest of our sample of six elliptical galaxies for which resolved CO gas disks have recently been detected with $7''$-spatial-resolution, interferometry mapping. These gas disks confirm the conclusions of earlier results showing optical dust lanes and unresolved CO that implied the common existence of molecular gas in ellipticals and the disk-like structure of this gas. The presented SHARC II mapping results provide the best-to-date resolved FIR-submm extent of NGC 3656 and of any elliptical galaxy >40 Mpc, showing that dust of 29 K exists out to at least $\sim$1.8 kpc in this galaxy. These new data are used in conjunction with the archival *HST* maps and other published data to determine dust properties and associations with galactic structures, including dominant heating sources such as star-formation or diffuse-stellar radiation.

Keywords: galaxies: elliptical and lenticular, cD - galaxies: individual (NGC 3656) - galaxies: ISM - galaxies: structure - infrared: galaxies - submillimeter

1. Introduction

Cold gas and dust in nearby elliptical galaxies was discovered only about 15 years ago. Compared to the cold ISM in spirals, the cold gas and dust is present in relatively small amounts and is seen in 50% to 80% of nearby ellipticals. The source and content of the cold ISM in these galaxies is still uncertain, with optical and far-infrared dust-mass estimates differing by $\sim$10 to 100. Therefore, the present study aims to map and analyze emission from the cold dust of elliptical galaxies in order to probe and better constrain the dust and evolutionary properties of ellipticals.

R. S. de Jong, Island Universes, 383–386.
© 2007 *Springer.*

We begin with a small sample of far-infrared (FIR) bright, nearby (less than 70 Mpc) ellipticals for which gas disks of CO emission have recently been resolved with interferometry of 7″ spatial resolution (e.g., Young 2002; see *left* panel of Figure 1). Our observational study exploits the latest very sensitive submm array detectors (e.g., SHARC II at 350 μm on the CSO) with a goal of providing the best submm (cold dust) distribution maps to date for our sample of galaxies (and for most in the sample the very first detections beyond 100 μm); dust temperature maps; gas-to-dust mass ratios; dust grain properties; dust association with other galactic structures; and constraints for models of dust evolution and generation in elliptical galaxies.

2. NGC 3656 and Other Elliptical Galaxies in the Sample

The six galaxies in our sample are all ellipticals in that their luminosity profiles follow the de Vaucouleur law; however, they represent a spread of merger traces or ages, from galaxies that have been classified as on-going or early-age major merger (e.g., NGC 3656, Balcells et al. 2001) to very-late accretion or quiescent system (e.g., NGC 807, Murray et al. 2000). The FIR and submm mapping results (e.g. dust content) will be compared between the sample galaxies as a probe of not only dust, but also of local merger-formation and evolutionary history of elliptical galaxies in general.

NGC 3656 is the far-infrared (FIR)-brightest elliptical in our sample. It has an optical elliptical body with an obscuring north-south, galactic minor-axis, edge-on gaseous dust lane (see *right* panel of Figure 1), two tidal tails, a system of shells and counter-rotating cores. These features together have been interpreted as evidence that the NGC 3656 system is an early major-merger remnant of disk galaxies (cf. Balcells 1997, 2001). Central structures that are seen in unsharp-masked and residual galaxy-model K-band images of NGC 3656 have recently been interpreted as qualitative evidence that phase-mixing, since the disk-disk merger and subsequent violent relaxation of this galaxy, is incomplete (Rothberg & Joseph 2004).

3. Archival *HST* and CSO Observations of NGC 3656

The *right* panel in Fig. 1 shows an *HST* F110W image with F110W-F160W ($\sim J$–H band) contours that demonstrate that the dust lane of NGC 3656 has the most extinction in a north-south region of radius $\sim 5''$ with east-west asymmetry and a peak that is centered about 1″ east of the galactic nucleus (or the center of the dust lane). The asymmetry is consistent with the dust lane being seen edge-on and its nearside being on the galaxy's eastern part.

Figure 2 shows a map of NGC 3656 from our exploratory CSO/SHARC II observations, during which we detected spatially-resolved, 350 μm continuum emission. The submm continuum of NGC 3656 has an unresolved core and

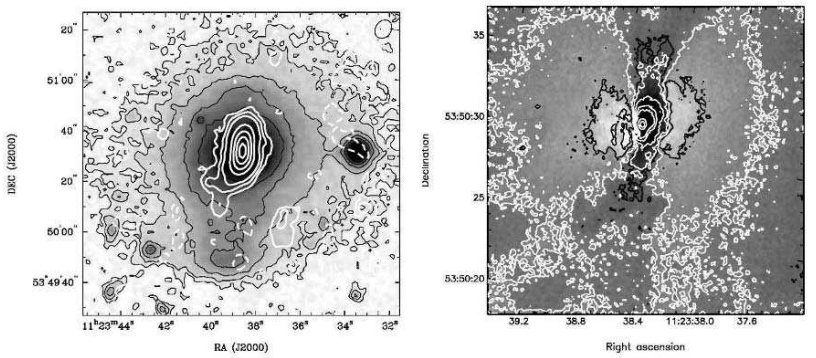

Figure 1. *Left:* Total integrated CO(1-0) intensity map (white contours) of NGC 3656 with CO diameter of $34''$ overlaid on optical data (gray scale and black contours) adopted from by Young 2002. The white contours are in units of -5%, -2%, 2%, 5%, 10%, 20%, 30%, 50%, 70%, and 90% of 81.1 Jy $\mathrm{beam}^{-1}\mathrm{kms}^{-1} = 4.7 \times 10^{22}\mathrm{cm}^{-2}$ CO integrated intensity or column densities peaks (Young 2002). *Right:* An archival *HST* F110W image overlayed with F110W-F160W contours to depict the dust extinction in NGC 3656.

extended emission that is slightly elongated north-to-south down to the 50% contour level and within a radius of $\sim 5''$. Beyond this it is detected with less certainty and has a generally bulging S-shape in the similar sense as seen in CO (1-0) and Hα images of the same region (see, e.g., *left* panel in Figure 1).

The extent of the resolved 350 μm emission down to the 50% contour level in NGC 3656 is consistent with a de-convolved Gaussian of FWHM of $8''.1$. This is about half the extent of the CO (1-0) emission observed in this galaxy. If one assumes the 350 μm emission is associated with the same dust as measured by *IRAS* at 60 and 100 μm, then our CSO results imply 29 K dust with an emissivity index of 1.6 and angular size of 1.5×10^{-9} steradians (see Figure 3). Using the distance of 45 Mpc (e.g., Young 2002) and 350 μm dust absorption value of 0.192 m^2/kg (Draine 2003), a dust mass of 1.4×10^8 solar masses is calculated for the temperature of 29 K and 350 μm integrated flux of 0.64 Jy.

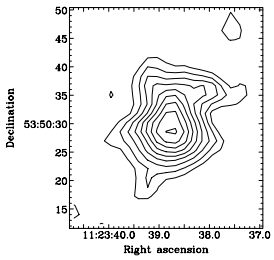

Figure 2. SHARC II 350 μm continuum map of NGC 3656 obtained with a CSO beam of $9''$. The submm contours are in units of 0.06, 0.1, 0.14, 0.18, 0.22, 0.26, 0.3, 0.34, 0.38 Jy beam^{-1}.

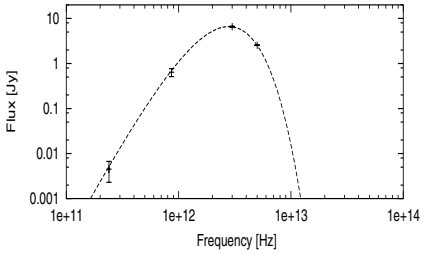

Figure 3. Weighted, single-temperature greybody of 29 K and emissivity index of 1.6 fit to *IRAS* 60 μm and 100 μm, SHARC II 350 μm and IRAM 1250 μm data of NGC 3656.

4. Implications of the CSO and *HST* Results of NGC 3656

Both the flux level and extent of the submm emission show that our 350 μm map of NGC 3656 cannot represent all the dust associated with the CO gas as resolved in this galaxy by Young 2002, if the normal gas-to-dust ratio (100) is used to estimate the dust flux level expected at 350 μm. The high extinction region of radius $\sim 5''$ seen in the *HST* colour map is roughly co-spatial with the high-brightness submm and radio regions respectively presented in this paper and by Mollenhoff et al. 1992, and probably represents a star-formation site and thus warmer and/or denser dust in NGC 3656. Our SHARC II data constrain the temperature of the remainder, more extended, dust distribution (associated with the more extended CO emission) to be less than 20 K. The current submm observations do not resolve the compact-core and extended-dust in NGC 3656; however, the fluxes of these components could be of comparable magnitude, originate from very distinct emission mechanisms, and thus impact their submm SED analysis, as is the case in the easier to spatially resolve, nearest merger-remnant elliptical Centaurus A (Leeuw et al. 2002).

The above results imply: (1) 350 μm observations are not just tracing cold dust, but also star-formation heating sources; (2) longer, but achievable 350 μm SHARC II integrations are required to detect the cold dust emission at lower flux contours more closely associated with the CO and less heated by star-formation sites; (3) future mapping sampling *colder* and *warmer* dust respectively using SCUBA II/JCMT at 850 μm and HAWC/SOFIA at 88 and 155 μm or MIPS/*Spitzer* at 24 and 70 μm will be useful in de-convolving the star-formation heating effects from the dust distribution; (4) follow-up interferometry at submm, mm or high-frequency radio respectively with instruments such as SMA, CARMA, or VLA could also resolve the components of the cold dust, star-forming, and compact core (if it is distinct) at spatial resolutions comparable to the *HST* maps. Though our SHARC II observations are preliminary, the results already provide the best spatially resolved FIR-submm extent of this galaxy and of any elliptical >40 Mpc to date, showing that dust of 29 K, probably heated by star-formation, exists out to at least $\sim$1.8 kpc in NGC 3656.

Acknowledgements This work was supported in part by NSF grant number AST 0204886. LLL received travel grants from the AAS and RAS.

References

Balcells, M. 1997, ApJ, 486, L87
Balcells, M., van Gorkom, J.H., Sancisi, R., & del Burgo, C. 2001, AJ, 122, 1758
Draine, B.T. 2003, ARA&A, 41, 241
Leeuw, L.L, Hawarden, T.G., Matthews, H.E., Robson, E.I., Eckart, A. 2002, ApJ, 565, 131
Mollenhoff, C., Hummel, E., & Bender R. 1992, A&A, 255, 35
Murray, C.M., Oosterloo, T.A., & Morganti, R. 2000, AAS, 1971, 1103
Rothberg, B. & Joseph, R.D. 2004, AJ, 128, 2098
Young, L.M. 2002, AJ, 124, 788

SUPERMASSIVE BLACK HOLE BINARY AND NUCLEAR STAR BURST

Hidenori Matsui[1*], Asao Habe[1**] and Takayuki R. Saitoh[2***]

[1]*Division of Physics, Hokkaido University, Sapporo, Japan.*

[2]*National Astronomical Observatory of Japan, Mitaka, Tokyo, Japan.*

* hidenori, ** habe@astro1.sci.hokudai.ac.jp, *** saitoh.takayuki@nao.ac.jp

Abstract We study influence of a galactic central supermassive black hole (SMBH) binary on gas dynamics and star formation activity in the galactic central region by making three-dimensional Tree+SPH simulations. Due to orbital motion of SMBHs, there are various resonances between gas motion and SMBH binary motion. We have shown that these resonances trigger gas concentrations and filaments in the galactic central region and the formation of small gaseous spiral arms around the SMBH binary. In these regions, star formation becomes very active. As the result, a nuclear star burst occurs in the galaxy.

Keywords: hydrodynamics - black hole physics - galaxies: nuclei - galaxies: starburst

1. Introduction

Nuclear star bursts are important for the formation of medium-sized black holes and in connection to AGN activity (Matsushita et al. 2000). To trigger a nuclear star burst, gas fueling into the galactic central region is needed. However, to fuel gas into the galactic central region, angular momentum must be removed from disk gas, which is a difficult problem.

Recently, supermassive black hole (SMBH) binaries have been detected in the galactic centers, e.g., in NGC6240 (Komossa et al. 2003), Arp 220 (Clements et al. 2002), and 3C 66B (Sudou et al. 2003). Particularly, NGC 6240 has been well observed in the wide range of wave lengths (e.g., Tacconi et al. 1999). In the hard X-ray observation, two strong peaks are detected in the galactic center and this is the strong evidence for a SMBH binary (Komossa et al. 2003). Moreover, indications of a nuclear star burst have been found in the radio continuum, near-infrared, and soft X-ray observations of this galaxy (e.g., Lira et al. 2002; Pasquali et al. 2004). The SMBH binary may play an important role in the nuclear star burst.

R. S. de Jong, Island Universes, 387–390.
© 2007 *Springer.*

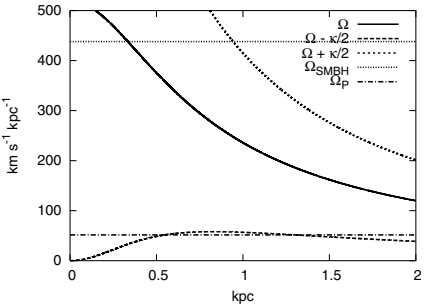

Figure 1. The resonances as function of radius. We show the Ω, $\Omega - \kappa/2$, $\Omega + \kappa/2$, Ω_{SMBH}, and Ω_p, where Ω is the gas angular velocity, κ is epicycle frequency, Ω_{SMBH} is the angular velocity of SMBH, and Ω_p is the angular velocity of major axis of the binary orbit in the elliptical orbit case.

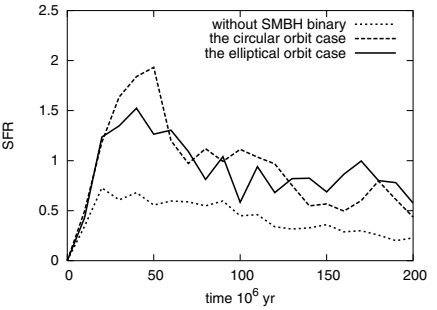

Figure 2. The star formation rate (SFR) within the galactic central region of $500\,\mathrm{pc}$ as function of time since the start of the calculation for models without and with a SMBH binary on circular and elliptical orbits.

The gravity of a SMBH binary has a non-axisymmetric component like a barred galaxy. As in a barred galaxy, change of gravitational potential due to orbital motions of SMBHs in a binary can induce resonance phenomena in nuclear gas disk, which are detected in the merging galaxies (Tacconi et al 1999; Scoville et al. 2002). If the resonances occur between a SMBH binary and gas motion, we expect that the gas motion is influenced and gas concentrations are induced similar to barred galaxies (Athanassoula 1992; Fukuda et al. 1998). In this way, a SMBH binary may trigger a nuclear star burst by these resonances.

In this paper, we study the influence of a galactic central SMBH binary on galactic gas motion using 3-dimensional Tree+SPH hydrodynamics simulations. We show that the resonances due to a SMBH binary trigger gas concentrations in the galactic central region and a nuclear star burst.

2. Result

The circular orbit case

We show the result of the model with the SMBH binary, with the SMBHs moving in their circular orbits. Each SMBH has a mass of $5 \times 10^8 M_\odot$. In this case, the gravitational potential will change with pattern speed $\Omega_{\rm SMBH}$, which is the orbital angular velocity of the SMBH. The expected resonances between gas motion and SMBH binary motion are shown in Fig. 1.

In the left panel of Fig. 3 we show the gas surface density and star formation sites in this model at $t = 5 \times 10^7$ yr, which is in the active star formation stage. Gas within the 900 pc radius is highly disturbed by the SMBH binary and most of the gas is accumulated into an elongated region. In the elongated region

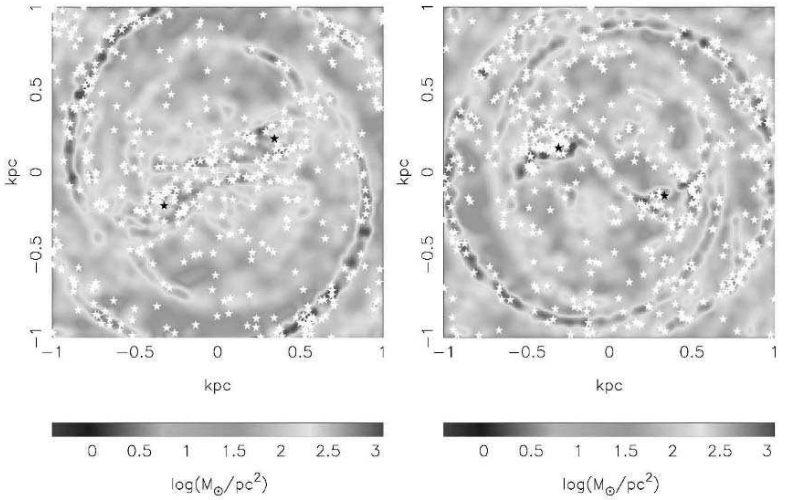

Figure 3. The surface density and star formation site at 5×10^7 yr. The left panel is the result of the circular orbit case and the right panel is one of the elliptical orbit case. The color represent surface density. The positions of SMBHs are represented by symbols of black stars. Newly formed stars are shown by symbols of white stars.

many clumps are formed. Star formation occurs in these clumps and become very active. Gaseous spiral arms are excited. In these arms star formation is also very active. These features are very different from the case without a SMBH binary, in which gas surface density is axisymmetric, gas does not concentrate, spiral arms are not formed, and star formation is not active in the galactic central region.

The time variation of the star formation rate (SFR) within the 500 pc radius is shown in Fig. 2. The active star formation has continued from 3 to 6×10^7 yr and the mean SFR in this stage is about $1.4 M_\odot$ yr^{-1}, which is much higher than that without SMBH binary.

The elliptical orbit case

We now discuss the results of the model with a SMBH binary on elliptical orbits with an eccentricity of 0.82. Again each SMBH has a mass of 5×10^8 $M_\odot$. In this case, the major axis of the elliptical orbit shifts with time and we denote the angular velocity of the shift as Ω_p. If we approximate this mean potential as rigid rotating one, an additional resonance is expected as shown in Fig. 1.

In the right panel of Fig. 3, we show the gas surface density and star formation sites during active star formation stage in this model. High density cores and filaments are formed and star formation is very active in these regions, although the SFR is similar to that of the circular orbit case as shown in Fig. 2.

However, the regions of active star formation are more compact than in the circular orbit case.

3. Summary

We study the influence of a galactic central SMBH binary on gas dynamics by numerical simulations. We have shown that a SMBH binary has a large influence on gas motion. Due to a SMBH binary, gas clumps and spiral arms are formed in the galactic central region. In these regions, star formation becomes very active and a star burst is triggered. Especially, in the case of an elliptical orbit SMBH binary, gaseous filaments and dense clump structures are formed and active star formation occurs in the dense and compact regions. These features can be strong evidence of existence of a SMBH binary. It is very interesting to compare these features to high resolution observations of galaxies which are suggested to have a SMBH binary.

Acknowledgements This work has been supported by the Nukazawa Science Foundation, Grant-in-Aid for the 21st Century COE Scientific Research Programme on "Topological Science and Technology" from the Ministry of Education, Culture, Sport, Science, and Technology of Japan (MECSST), and in part by Grant-in-Aid for Scientific Research (14340058) of Japan Society for the Promotion of Science.

References

Athanassoula, E., 1992, MNRAS, 259, 328
Clements, D. L., et al., 2002, Apj, 581, 974
Fukuda, H., Wada, K., & Habe, A., 1998, MNRAS, 295, 463
Komossa, S., Burwitz, G., et al., 2003, Apj, 582, L15
Lira, P., Ward, M. J., Zezas, A., & Murray, S. S., 2002, MNRAS, 333, 709
Matsushita, S., et al. 2000, Apj, 545, L107
Pasquali, A., Gallagher, J. S., & de Grijs, R., A&A, 2004, 415, 103
Scoville, M. S., Yun, M. S., & Bryant, P. M., 1997, Apj, 484, 702
Sudou, H., Iguchi, S., Murata, Y., & Taniguchi, Y., 2003, Science, 300
Tacconi, L. J., Genzel, R., Tecza, M., & Gallimore, J. F. 1999, Apj, 524, 732

RADIO CONTINUUM, CO, AND THERMAL INFRARED EMISSION IN NEARBY STAR-FORMING GALAXIES

T. Wong[1,2*], A. Hughes[3], R. Ekers[1], R. Paladino[4], M. Murgia[4,5], L. Blitz[6], T.T. Helfer[6], L. Moscadelli[4], L. Gregorini[5], L. Staveley-Smith[1], M. Filipovic[7], Y. Fukui[8] and N. Mizuno[8]

[1] *CSIRO ATNF, Australia*

[2] *School of Physics, UNSW, Sydney, Australia*

[3] *Swinburne University of Technology, Hawthorn, Australia*

[4] *INAF-Cagliari, Loc. Poggio dei Pini, Italy*

[5] *Istituto di Radioastronomia del CNR, Bologna, Italy*

[6] *Radio Astronomy Laboratory, University of California, Berkeley, USA*

[7] *University of Western Sydney, Penrith South DC, Australia*

[8] *Dept. of Astrophysics, Nagoya University, Chikusa-ku, Nagoya 464-8602, Japan*

* Tony.Wong@csiro.au

Abstract The correlation between far-infrared and radio emission in galaxies is remarkably strong considering the very different emission mechanisms which are thought to be responsible for the two. We have examined this correlation in the LMC on scales ranging from 40 pc to 4 kpc, finding that the FIR-radio correlation remains extremely tight down to $<$100 pc, whereas correlations of either FIR or radio with HI or CO degrade considerably below 1 kpc. However, in nearby spiral galaxies the mid-infrared (MIR) and radio emission begin to decorrelate even on scales of $<$2 kpc. The difference in behaviour from the LMC may be due to the larger fraction of synchrotron flux in more massive galaxies.

Keywords: Magellanic Clouds - infrared: galaxies - radio continuum: galaxies

1. Motivation

Among the tightest correlations between galaxy properties is that between the far-infrared (FIR) and radio luminosities, which exhibits a scatter of less than a factor of 2 over more than 4 orders of magnitude (Yun et al. 2001). The correlation persists when normalizing by mass (Xu et al. 1994) and is significantly better than correlations between other star formation tracers (Cram

R. S. de Jong, Island Universes, 391–394.
© 2007 *Springer.*

et al. 1998). Indeed, the correlation has been used as a redshift indicator (Carilli and Yun 1999) and to identify high-redshift submillimeter galaxies using cm synthesis radio imaging to determine positions. What makes the FIR-radio correlation surprising is that it couples a thermal process (IR dust emission) with a largely non-thermal process (synchrotron emission), the latter of which should depend on the magnetic field strength and cosmic ray density. Since the radio continuum appears only weakly correlated with FIR emission on scales below a few hundred pc in our Galaxy (Boulanger and Perault 1988), its close association with FIR emission on global scales requires explanation.

Several theoretical models have been proposed, which generally fall into one of two categories: (1) **Calorimetric** models in which relativistic electrons and UV photons are produced by massive stars in proportional numbers, then converted independently to radio and FIR photons (Völk 1989), and (2) **Magnetic field-gas density coupling** models, as might arise if dynamo effects and field-line stretching amplify B to yield equipartition with the gas density (Groves et al. 2003). Yet strong observational constraints are still lacking, which motivates us to use spatially resolved data for the LMC and nearby spirals to examine the correlations in detail. A similar approach is being undertaken by the SINGS team (Murphy et al. 2006).

2. Wavelet Cross-correlation Analysis

The most common way of comparing images of the same field taken at different wavelengths is a pixel correlation analysis. This allows maximum flexibility in choosing which regions to compare, but can often obscure the size scales on which correlations change. For a scale-dependent correlation analysis, we have instead adopted the wavelet cross-correlation method described by Frick et al. (2001). Essentially, both images are Fourier transformed, filtered through an annulus in the Fourier domain, and then transformed back. The wavelet cross-correlation, at the scale defined by the annulus, is simply the product of the two filtered images normalised by their individual powers. We choose as our analysing wavelet the "Pet Hat" function (Frick et al. 2001), for its relatively good resolution in the Fourier domain.

3. LMC Results

A comparison of the wavelet cross-correlation functions for different pairs of images is shown in Figure 1*a*. By far the best correlations are among the classical "star formation tracers": far-infrared (60 μm), Hα, and radio continuum (20 cm). These correlations are extremely strong down to scales of $<$0.1 kpc ($6'$). Correlations between the gas tracers CO and HI decline significantly on scales of $<$1 kpc, and correlations of the star formation tracers with the gas tracers are even poorer. This result calls into question models for the FIR-radio

correlation that rely on coupling the magnetic field to the gas density, as the radio emission would be expected to correlate strongly with the gas. On the other hand, a large fraction ($\sim$50%) of the 1.4 GHz flux from the LMC has been attributed to thermal emission (Haynes et al. 1991), which may reflect enhanced cosmic ray escape (Chi and Wolfendale 1990). Thus, the strong correlation of radio continuum with other star formation tracers—and its poor correlation with gas tracers—may not be surprising. Furthermore, the global FIR-radio correlation is dominated by the bright region around 30 Doradus, which may not be typical of the LMC. A more detailed analysis, including comparison of different subregions of the LMC, is currently underway (Hughes et al., in preparation).

4. Nearby Spirals

Relatively few spiral galaxies have had FIR data at adequate spatial resolution to examine image correlations internally. This has changed with the Spitzer Nearby Galaxies Survey (SINGS; Kennicutt et al. 2003), which has produced 24μm and 70μm images of 75 nearby galaxies. We focus here on a subset of 7 galaxies for which the SINGS 24μm mid-infrared (MIR) images provide a comparable angular resolution ($\sim$6$''$) to CO and 1.4 GHz radio images we have recently analysed (Murgia et al. 2005). The results of that analysis had indicated a strong correlation between the radio and CO emission, both on a pixel-by-pixel basis and when azimuthally averaged. Although the MIR generally traces warmer dust than the FIR, the global MIR-radio correlation is nearly as tight as the FIR-radio correlation (Gruppioni et al. 2003), and the MIR appears to be a good tracer of massive star formation (Roussel et al. 2001).

Visual inspection reveals a strong similarity of the MIR and radio images, which is reinforced by a pixel correlation analysis. However, the wavelet cross correlation shows a significant breakdown in the MIR-radio correlation on scales of $<$2 kpc in most of the sample (Figure 1*b*). Notable exceptions include NGC 4826 and NGC 6946, which show a good correlation down to scales of a few hundred pc. The CO-radio correlation tends to break down on similar scales as the MIR-radio. The presence of a diffuse radio component at intermediate scales that has no counterpart in the MIR or CO may be responsible. However, further work is required to remove artifacts in the VLA images due to the presence of a radio nucleus or insufficient coverage of the visibility plane. Somewhat better correlations are generally found between MIR and CO emission, although still breaking down on scales of $<$1 kpc. This may reflect a general spatial correlation between molecular clouds and HII regions.

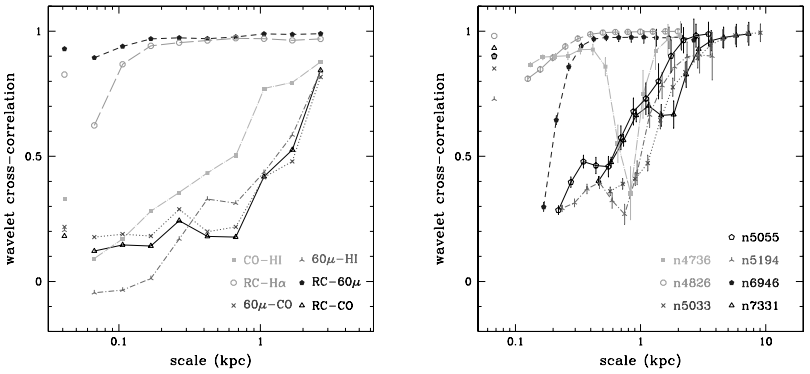

Figure 1. Wavelet cross-correlations, as a function of scale size, for (a) different pairs of images covering the LMC; (b) 20cm and 24μm images for seven different spiral galaxies. The coefficient is constrained to line between -1 and 1. The points on the far left of each panel represent the usual linear correlation coefficient.

References

Boulanger, F. and Perault, M., 1988, ApJ, 330, 964

Carilli, C. L. and Yun, M. S., 1999,
ApJ, 513, L13

Chi, X. and Wolfendale, A. W., 1990, MNRAS, 245, 101

Cram, L., Hopkins, A., Mobasher, B., and Rowan-Robinson, M., 1998, ApJ, 507, 155

Frick, P., Beck, R., Berkhuijsen, E. M., and Patrickeyev, I., 2001, MNRAS, 327, 1145

Groves, B. A., Cho, J., Dopita, M., and Lazarian, A., 2003, PASA, 20, 252

Gruppioni, C., Pozzi, F., Zamorani, G., Ciliegi, P., Lari, C., Calabrese, E., La Franca, F., and Matute, I., 2003, MNRAS, 341, L1

Haynes, R. F., et al., 1991, A&A, 252, 475

Kennicutt, R. C. et al., 2003, PASP, 115, 928

Murphy, E.J. et al., 2006, these proceedings, p. 409

Murgia, M., Helfer, T. T., Ekers, R., Blitz, L., Moscadelli, L., Wong, T., and Paladino, R., 2005, A&A, 437, 389

Roussel, H., Sauvage, M., Vigroux, L., and Bosma, A., 2001, A&A, 372, 427

Völk, H. J., 1989, A&A, 218, 67

Xu, C., Lisenfeld, U., Volk, H. J., and Wunderlich, E., 1994, A&A, 282, 19

Yun, M. S., Reddy, N. A., and Condon, J. J., 2001, ApJ, 554, 803

VI

(EVOLUTION OF) STAR FORMATION IN GALACTIC DISKS

Lauren MacArthur, Torsten Böker, Johan Knapen, Rob Kennicutt, Mike Fall, Lisa Kewley, a bit of Tim de Zeeuw, and Amanda Bauer at the dinner table.

Coffee/tea break near the posters.

THE MULTIWAVELENGTH VIEW OF STAR-FORMING DISKS

Robert C. Kennicutt, Jr.

Steward Observatory, University of Arizona, Tucson, USA

Institute of Astronomy, University of Cambridge, United Kingdom[*]
robk@ast.cam.ac.uk

Abstract Our understanding of star formation in disks is in the midst of an observational revolution, with *Spitzer, GALEX*, and a host of groundbased surveys providing complete inventories of star formation in nearby galaxies, and the first truly multiwavelength spatially-resolved datasets. The same data provide detailed information on the structure of the cold interstellar medium on «100 pc scales, and thus offer the promise of understanding the complex interplay between the star formation rate and the ISM, down to the physical scales where star formation events are triggered. This talk will present a few highlights and insights that have emerged from the surveys.

Keywords: galaxies: ISM - galaxies: structure - stars: formation

Introduction

These are truly exciting times for those who study star formation and the interstellar medium in galaxies. The bulk of the energy emitted by young stars in galaxies is radiated in the ultraviolet and the mid- to far-infrared, and thanks the *GALEX* and *Spitzer* space telescopes we are now able to obtain imaging and spectra of nearby galaxies in these wavelength regions with unprecedented depth and completeness. The combination of these data with groundbased observations in the visible, near-infrared, and radio is allowing us to obtain pixel-resolved SED maps of galaxies covering virtually the full electromagnetic spectrum. This in turn is allowing us to test the various single-wavelength star formation rate (SFR) tracers that have served as the backbone of our field for the past 3 decades, to treat the systematic effects of dust extinction and the stellar IMF with unprecedented rigor, and gradually develop improved,

[*]Current address

R. S. de Jong, Island Universes, 397–408.
© 2007 *Springer.*

multi-wavelength diagnostics of SFRs. In turn the applications of these methods are revealing new information on the distributions of star formation, the structure and physical conditions in the surrounding ISM, and the complex physical interplay between star formation and its parent ISM.

In short this subject is in the early stages of an observational revolution. I will begin this talk by reviewing the full extent of the new datasets that are being obtained on nearby galaxies, and the new capabilities that they are enabling. I will then focus on the early results from the *Spitzer* telescope, with emphasis on the SINGS Legacy Project (*Spitzer* Infrared Nearby Galaxies Survey). Many of the data presented have been obtained only in the past few months, so I will emphasize generic capabilities and preliminary results. Other results from SINGS are presented by Mike Regan and Eric Murphy elsewhere in this volume.

1. The Observational Revolution

The opening of the ultraviolet and infrared regions with *GALEX* and *Spitzer* is only part of an avalanche of information emerging on nearby star-forming galaxies. The first wave of new data has come from the Sloan (SDSS) and 2dF digital sky surveys, which have provided semi-integrated spectra of hundreds of thousands of galaxies out to $z \sim 0.5$, with the statistical power to characterize even rare objects and phenomena, and study environmental dependencies with unprecedented robustness (e.g., Brinchmann et al. 2004). The limited spatial sampling of these fiber spectra introduces some systematic uncertainties into the interpretation of the data, but this problem is being addressed head-on with a series of truly integrated spectrophotometric surveys of galaxies, including the Nearby Field Galaxy Survey (NFGS; Jansen et al. 2000), and a large survey of local normal, starburst, and interacting galaxies at Arizona (Moustakas & Kennicutt 2005). At the same time several large Hα imaging surveys (e.g., GoldMine, HαGS, SINGG, SINGS, STARFORM, AMIGA, MOSAIC, 11HUGS) are providing deep, high-resolution maps of the massive star formation in thousands of galaxies with $z \leq 0.05$, and publicly-available image libraries in most cases. These supplement a number of prism-based volume-limited SFR surveys (e.g., UCM, KISS), which provide emission-line selected SFR statistics for the local cosmological volume.

These new surveys bring with them several new capabilities, especially when data from two or more of the datasets are combined. For the first time one can obtain SFRs for samples of thousands to millions of galaxies (*GALEX* alone is expected to detect $>10^7$ galaxies out to $z = 1$) over large areas of sky and with well-defined completeness properties (Martin et al. 2005). This is essential for removing the various luminosity, surface brightness, and inclination biases that afflicted earlier datasets, and for studying problems such as

the cosmic SFR density and the temporal properties of star formation, where a solid grasp of the observational selection effects is critical. Perhaps the most important new capability comes from being able to map galaxies with complete UV-to-FIR wavelength coverage. Extinction by dust is the overwhelming contributor to the systematic error budget in nearly all UV and optical SFR measurements of galaxies. Most of the energy that is absorbed by this dust is re-emitted in the infrared, and by mapping galaxies across this wavelength range one can effectively construct bolometric energy maps of galaxies and recover all of the luminosity from the young stars, and use the spectral energy distribution (SED) maps to measure this extinction. In this regard the spatial resolutions of *GALEX* and *Spitzer* ($\sim$5–6$''$ at 0.15 and 24 μm, respectively) are important because for nearby galaxies ($d \leq 30$ Mpc) this corresponds to the linear scale over which dust redistributes the radiation, and it also is roughly the subkiloparsec scale over which the collapse of large interstellar clouds and subsequent star formation is initiated.

2. The SINGS Project

The observational foundation of SINGS is a complete and homogeneous set of 3.5–160 μm imaging and low-resolution 10–100 μm SED maps for 75 nearby galaxies ($d \leq 30$ Mpc), chosen to span the range of types, luminosities, and infrared/optical properties of normal galaxies in the local universe. In addition, spectral maps at 5–14 μm and high-resolution maps at 10–37 μm are being obtained for 150 infrared sources in these galaxies, including the nuclear regions, and 75 extranuclear targets that again are selected to span the range of star formation and ISM properties found in the local universe. The Spitzer observations are being complemented by a wide array of ancillary observations including $BVRIJHK$ and Hα imaging, GALEX imaging at 1500 Å and 2300 Å, CO, HI, and radio continuum mapping, Pα and H-band imaging with HST, and optical spectroscopy. The dataset enables studies of star formation and the ISM in the galaxies themselves, and provides a toolbox of local spectral energy distributions (SEDs) and spectra for modeling more distant galaxies.

The primary astrophysical objectives of SINGS derive from the new observational capabilities that Spitzer brings to this field, in this case its unprecedented angular resolution and sensitivity. The spatial resolution of $\sim$2$''$ at 8 μm corresponds to a linear resolution of 100 pc at the median distance of the SINGS sample (10 Mpc), and 35 pc at the distance of the M81 group (incorporated as a complete subset of the SINGS sample). Even at 70 μm near the peak of the infrared energy distribution of galaxies, the diffraction limit maps to less than a kiloparsec at the median distance of the sample.

The core science program of SINGS is focussed on exploring this complex interplay between star formation and the ISM. By combining infrared, ultraviolet, and visible (e.g., Hα) maps we are able to map the star formation across the full range of evolutionary stages and gas densities, linking seamlessly the high-density "starburst" and "normal" quiescent disk star-forming regimes. The multi-wavelength data also are enabling us to test the reliability and applicability ranges of ultraviolet, visible, and infrared star formation rate (SFR) diagnostics, and eventually to develop improved, composite SFR calibrations, along with a deeper physical understanding of how dust influences the observed properties of galaxies. The IRS spectra trace virtually all of the relevant ISM phases (HII regions, shocks, PDRs, molecular gas, X-ray ionized gas) and thus provide constraints on the physical conditions in the star-forming disks, and insights into the physical origins for the observed trends in SEDs and infrared properties observed across the sample.

3. A Case Study: M81

The main empirical product of the SINGS imaging observations of a galaxy is an SED cube, i.e., imaging in $\sim$14 $-$ 17 bands between 0.15 $-$ 160 μm, often with several other bands extending to 20 cm in the radio continuum and 10 keV in X-rays, as well as in the 21 cm HI and 1.3 mm CO J = 1$\rightarrow$0 lines. This provides pixel-resolved SED maps of the galaxies over the energy range over which the bulk of the luminosity from young stars is emitted.

Within this SED four spectral regions are especially useful as diagnostics of the star formation and gas density distributions, and these are illustrated in Figure 1 for M81 (NGC 3031), the first SINGS target observed with Spitzer. The far-ultraviolet (top left panel, in this case a composite of 1500 Å FUV and 2300 Å NUV images) directly traces the photospheric emission of mainly massive stars, but attenuated by a patchy distribution of interstellar dust. The top right panel shows an Hα image of the same region; in this case one is observing ionizing ultraviolet radiation from the same stars reprocessed by the surrounding interstellar hydrogen, again attenuated by dust.

The imaging bands of *Spitzer* sample three distinct spectral components. At the shortest wavelengths ($<$5 μm, not shown) the IR emission is dominated by photospheric radiation from red giants and supergiants. The IRAC 3.5 μm and 4.5 μm imaging provides valuable information on the distribution of stellar mass in galaxies, but little information on the gas and star formation. At mid-infrared wavelengths (7 – 20 μm) the emission at most wavelengths is dominated by band emission from aromatic molecules, the so-called PAH grains. Finally at longer wavelengths ($>$20 μm) the emission is dominated by silicate dust grains at lower temperatures (T = 10 – 100 K), which radiate the bulk of the reprocessed stellar emission.

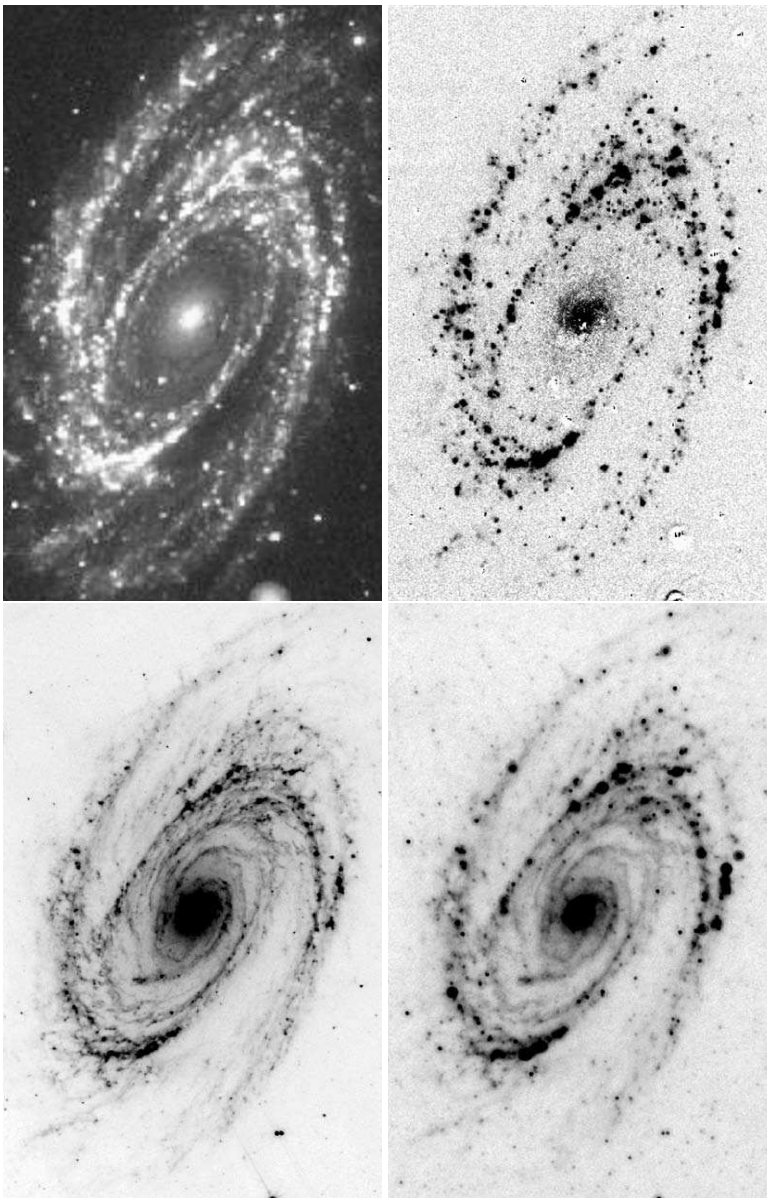

Figure 1. The nearby Sab spiral M81 (NGC 3031) observed at four wavelengths that provide complementary tracers of massive star formation and the associated ISM. Top left: Ultraviolet (1350 − 2800 Å), imaged with the GALEX satellite. Top right: M81 in Hα, observed with the Burrell Schmidt telescope, courtesy R. Walterbos. Lower Left: 8 μm with the IRAC camera on Spitzer. Lower right: 24 μm, as imaged with the MIPS instrument on Spitzer. Note the dramatic change in the structure and the clumpiness of the infrared emission between 8 μm (PAH dominated) and 24 μm (silicate dust dominated), and the presence of diffuse “cirrus" emission at both infrared wavelengths.

Although the PAH and silicate grains are presumed to be well mixed through most of the ISM, the structures of the disks as traced by the species is quite distinct, as shown for M81 in Figure 1. The lower left panel shows an IRAC image in the 8 μm band, which is dominated by a strong set of PAH features. The emission is highly filamentary, and upon detailed examination is found to consist of discrete sources, usually surrounding bright star forming regions, along with diffuse dust in the general ISM being heated by the general interstellar radiation field (Helou et al. 2004, Willner et al. 2004). These bright filaments closely trace the dark dust lanes and clumps seen in visible-wavelength images. The lower right panel of Figure 1 shows the MIPS 24 μm image, with a very distinct structure (Gordon et al. 2004). The 24 μm emission also consists of two distinct components, bright knots that are coincident with HIIregions, and a background diffuse component (see for example the smooth spiral arm emission in the very inner disk). This latter component is related to the "cirrus" emission discovered by IRAS and inferred from decomposition of the integrated SEDs of galaxies. *Spitzer* resolves these components spatially as well. As one moves to longer wavelengths the diffuse component becomes stronger. This change is real, even after accounting for the decreased angular resolution of *Spitzer* at the longer wavelengths (Engelbracht et al. 2004, Hinz et al. 2004).

Most of these basic features already had been observed prior to Spitzer with the ISO mission and in some instances IRAS (e.g., Helou 2000). However Spitzer is providing much higher sensitivity and spatial resolution, especially in the far-infrared, which will enable a direct empirical (and thus less model-dependent) separation of the components and their heating components. As one example, detailed analysis of the structure of the FIR emission in M33 as a function of wavelength strongly suggests that the heating source for the coldest dust is quite distinct from that of the warm dust associated with star-forming regions (Hinz et al. 2004).

4. Assessment and Calibration of Star Formation Tracers

Since the days of *IRAS* the far-infrared luminosities of galaxies have been applied as quantitative measures of the SFR (see Kennicutt 1998a and references therein). This diagnostic is especially useful in extreme starburst galaxies, where the dust re-emits virtually all of the luminosity of the galaxy and young stars dominate the dust heating; thus making the infrared luminosity essentially a bolometric measure of the SFR. However in normal galaxies all of these conditions are broken; dust only absorbs a fraction of the young stellar luminosity, and older stellar populations can contribute significantly (and sometimes dominantly) to the dust heating. As a result considerable efforts have been made with both *ISO* and *Spitzer* to find other infrared measures that more closely trace the SFR, locally, globally, or ideally over all scales.

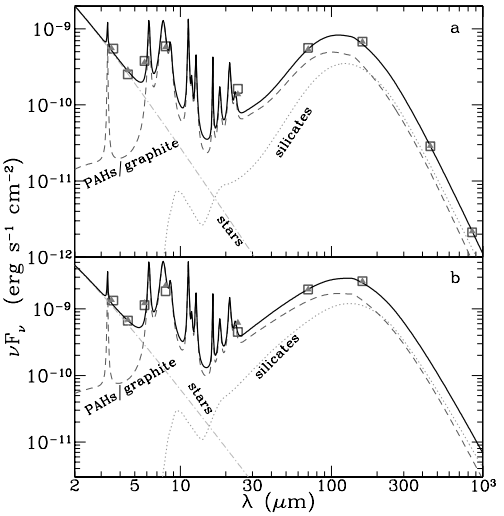

Figure 2. Model infrared spectral energy distribution (solid line) fit to the observed broadband fluxes of NGC 7331, from Regan et al. (2004). The dashed and dotted lines designate different emission components, as described in the text. The lower plot is for the integrated fluxes of NGC 7331, while the upper plot is a fit to the inner star-forming ring only. Reproduced with the permission of the AAS.

Such infrared measures of the SFR are urgently needed to interpret the observations of high-redshift galaxies from *Spitzer*, so we have made this area an early priority in the SINGS science program. Dale et al. (2005) have used integrated SEDs of the galaxies to assess global SFR measures, while Calzetti et al. (2005) and Dale et al. have carried out spatially-resolved measurements of 3 SINGS galaxies, M51, M81, and NGC 7331.

One of the early surprises that emerged from the imaging observations was the remarkable correlation between the locations and brightnesses of the 24 μm infrared emission and Hα emission from the ionized gas. Readers can gain some feel for this by comparing the two righthand panels of Figure 1. Prior to obtaining these data many of us expected that anywhere from 20–50% of the bright IR-emitting star forming regions would be virtually invisible in Hα or the ultraviolet, because many current models of star formation suggest that massive stars will remain deeply embedded in their natal molecular clouds, for periods of order 1–2 Myr or even longer (e.g., Dopita et al. 2005 and references therein). Since the lifetimes of the HII regions themselves are only of order 5 Myr, one would expect to see a large number of deeply obscured regions. However in most of the galaxies we have studied to date, the fraction of such objects is of order 1% (Prescott et al. 2005), suggesting that either the excavation time for the OB stars is of order 10^5 years or less, or alternatively that channels for escape of ionizing radiation are present even in the youngest

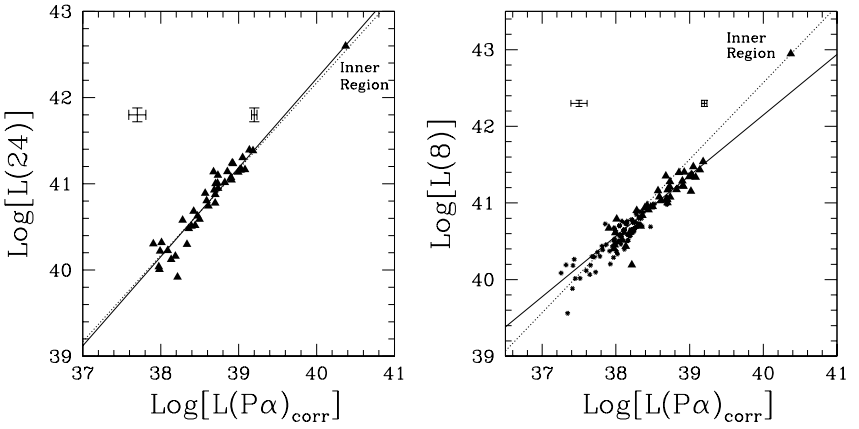

Figure 3. Left: Correlation between 24 μm fluxes and extinction-corrected Paschen-α fluxes of 42 HII regions in the central disk of M51. Right: Same comparison but with continuum-subtracted 8 μm PAH fluxes. Figures taken from Calzetti et al. (2005), reproduced with permission of the AAS.

cluster/GMC complexes. The correspondence of the infrared and nebular emission also implies that most of the 24 μm emission from these regions arises from dust mixed with the ionized gas itself. This is in marked contrast to the cooler dust and the PAH emission, which shows a much stronger diffuse component, presumably arising from starlight that has propagated well outside of the star-forming regions into the general ISM. The strong association of the bright infrared sources with HII regions also implies a fairly rapid timescale for dispersal of the gas and dust around star-forming regions, comparable to the ionization lifetimes of the HII regions ($\sim$10 Myr).

The tightness of this correspondence is illustrated in Figure 3 (left panel), which compares 24 μm fluxes and Pα fluxes of 42 HII regions in the inner disk of M51, from Calzetti et al. (2005). The HII regions in M51 are highly extincted ($A_V = 2-4$ mag), so the dust re-emits $\sim$90% of the stellar luminosity. Of course the typical 24/Pα or 24/Hα ratio varies widely across the HII regions in the SINGS sample (Prescott et al. 2005), but the close correspondence between the 24 μm and *obscured* ionizing luminosities is allowing us to use the combination of infrared and Hα fluxes to derive an extinction-corrected total ionizing flux and SFR (Kennicutt et al. 2005).

The right panel of Figure 3 shows a similar comparison between extinction-corrected Pα and 8 μm fluxes for the same 42 regions in M51. As can be seen from Figure 1, the PAH emission is less strongly correlated spatially with the HII regions, but previous studies of ISO data by Roussel et al. (2001) and Forster-Schreiber et al. (2004) have shown that there is a good empirical correlation between SFR as traced by Hα and PAH luminosity, at least among active

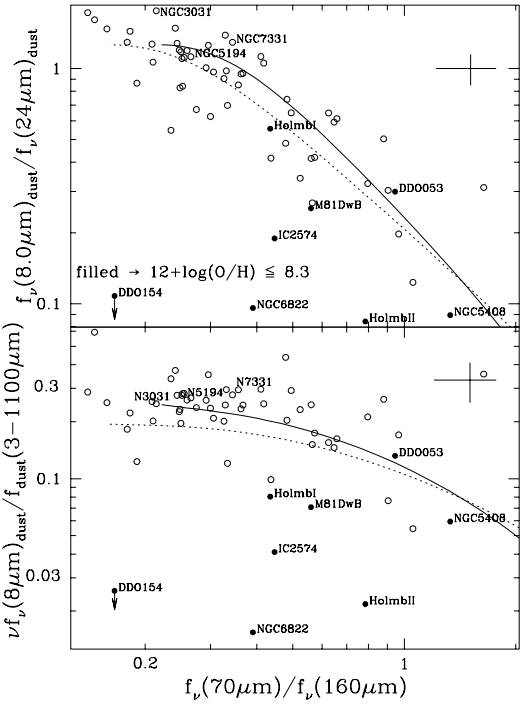

Figure 4. Behavior of the integrated (continuum-subtracted) 8 μm luminosities of the SINGS galaxies, with the fluxes normalized to their integrated 24 μm fluxes (top) and total IR luminosities (bottom). Both are plotted as a function of far-infrared SED shape, as measured by the MIPS 70/160 μm flux ratio. Solid points denote metal-poor dwarf galaxies. Figure taken from Dale et al. (2005), reproduced with the permission of the AAS.

starburst galaxies. In M51 there is a good correlation between the fluxes but with more scatter than at 24 μm and with a curious nonlinear slope ($\sim$0.8). However subsequent analysis of 8 μm, 24 μm, and Pα measurements of a larger galaxy sample is showing that the two infrared tracers are linearly correlated with Pα luminosity, with roughly comparable scatter when the measurements are restricted to metal-rich actively star-forming galaxies (Calzetti et al., in preparation). However, the PAH tracers break down entirely in two regimes: in metal-poor galaxies or HII regions ($Z < 0.2 - 0.3Z_\odot$), where the PAH emission weakens or disappears, or in regions with a bright interstellar radiation field, where the emission can be excited in the absence of star formation (e.g., the inner dust lanes in M81– see Fig. 1).

Some of these results can be seen in Figure 4, which displays the behavior of the *integrated* continuum-subtracted 8 μm emission in the SINGS sample. In the top panel the 8 μm fluxes are normalized to the integrated 24 μm emission, while in the bottom panel they are normalized to the total infrared luminosities. There is a relatively narrow dispersion in SED shapes among the

luminous, actively star-forming spiral and irregular galaxies, though the scatter in ratios is still significant, a factor of 3–5 overall, which can be reduced to factors of 2–3 if some information on the SED shape at longer wavelengths is available. However metal-poor galaxies, shown as solid points in Figure 4, deviate systematically, and in those cases the 8 μm emission will systematically underestimate the SFR if a standard calibration (derived from more luminous galaxies) is applied. Moreover, in such galaxies the rest 8 μm flux will not be dominated by PAH emission at all, but rather by stellar photospheric emission or hot silicate dust, in which case the derived "SFR" would be meaningless. However, it is likely that most of the galaxies that are luminous enough to be detected by Spitzer at high redshift probably exceed the metallicity threshold for significant PAH emission.

5. Summary, Applications, and Implications

Out of these studies a consistent physical picture for the infrared emission of galaxies is clearly emerging. The warm silicate dust that is traced by *Spitzer* at 24 μm is strongly associated with the youngest star forming regions and HII regions, and can be used as a robust measure of the dust-obscured SFR, in the same way that Hα traces the unobscured component. The colder dust emission (including a diffuse component at shorter wavelengths) appears to be largely heated by the "older" O and B stars, as well as by the general interstellar radiation field, to produce the "cirrus" component seen by *IRAS*. The PAH emission (including the component traced in 8 μm IRAC images) is more complex, including a PDR component around young star-forming regions, and a diffuse component closely associated with the colder cirrus emission that probably dominates in most normal galaxies. Giving credit where credit is due, most of this picture was already in place from *ISO* studies (Tuffs & Popescu 2005), and the *Spitzer* data, with their spectacular sensitivity and resolution, are providing strong confirmation, extending over a wider range of galaxy types and local physical conditions.

For high-redshift applications the most pressing questions are the reliability of the rest 24 μm and 8 μm *Spitzer* fluxes (the latter of which redshifts into the 24 μm band at $z = 2$). As we have seen the 24 μm flux is probably a more reliable tracer of the current SFR than the total infrared flux, good news given the much higher spatial resolution at that wavelength relative to the 70 μm and 160 μm channels. The applicability of the PAH emission is more problematic, but so long as most applications are restricted to luminous, dusty starburst galaxies it probably provides as good an indicator as total FIR luminosity. A common liability of all infrared tracers is that they miss entirely star formation that is not attenuated by dust. However this opens the prospect of using hybrid Hα+infrared or UV+infrared methods to fully sample the star formation.

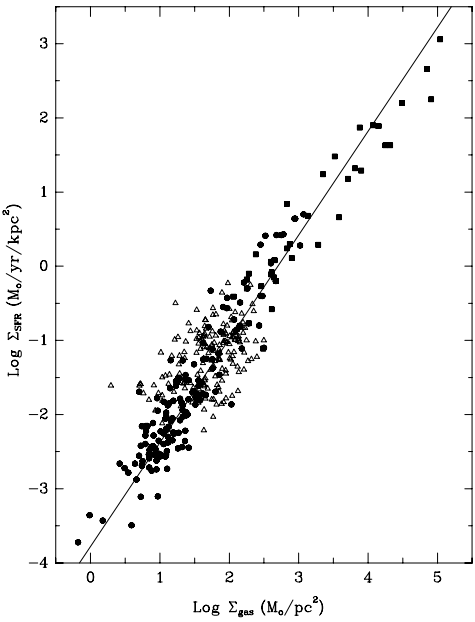

Figure 5. A comparison of the local SFR density vs total gas density relationship in M51 (open triangles) with the integrated relation found in normal and starburst galaxies (solid symbols). The line is the Kennicutt (1998b) $N = 1.4$ power law for reference.

Figure 5 shows an example of an early application of these results. Until recently most measurements of the form of the SFR vs gas density law in galaxies (Schmidt law) have been limited to integrated measurements of galaxies, where disk-averaged SFR densities and gas densities are correlated for a sample of galaxies. However the advent of *Spitzer* along with high-resolution HI and CO surveys such as the THINGS HI survey (Walter et al. 2005)) and the BIMA SONG CO survey (Helfer et al. 2003) now make it possible to study the local behavior of the star formation law within galaxies, on a point-by-point basis. We have carried out such a pilot study of M51, using a combination of THINGS and SONG data to map the gas density, and a combination of Hα, Pα, and 24 μm *Spitzer* data to map the corresponding extinction-corrected SFRs. The correlation in M51 is shown by the dark triangles, while the integrated relation found for galaxies (an update of the Kennicutt 1998b analysis) is shown by the gray symbols underneath (Kennicutt et al. 2005). The scatter of the local relation is larger, which is not surprising given the smaller scales that are being probed (300–550 pc). But I find it remarkable that the general form of the correlation still appears to hold on these scales. This is but a taste of what is to come as we begin to apply these powerful multi-wavelength diagnostics to the longstanding problems of star formation in galaxies near and far.

Acknowledgements I am deeply indebted to my collaborators on the SINGS team: Lee Armus, George Bendo, Brent Buckalew, Daniela Calzetti, John Cannon, Danny Dale, Bruce Draine, Chad Engelbracht, Karl Gordon, Al Grauer, George Helou, David Hollenbach, Tom Jarrett, Lisa Kewley, Claus Leitherer, Aigen Li, Sangeeta Malhotra, Martin Meyer, Eric Murphy, Moire Prescott, Mike Regan, George Rieke, Marcia Rieke, Helene Roussel, Kartik Sheth, JD Smith, Michele Thornley, and Fabian Walter. We are also grateful to Sanae Akiyama, Janice Lee, and John Moustakas at Arizona and Megan Sosey and Matt Mutchler at STScI for their expert help in processing the SINGS data. Support for the SINGS project, part of the Spitzer Space Telescope Legacy Science Program, is provided by NASA through Contract Number 1224769 issued by JPL, Caltech, under NASA contract 1407. I also gratefully acknowledge the support of NASA grant NAG5-8426.

References

Brinchmann, J. et al. 2004, MNRAS, 351, 1151
Calzetti, D. et al. 2005, ApJ, in press (astro-ph/0507427)
Dale, D.A. et al. 2005, ApJ, in press (astro-ph/0507645)
Dopita, M. A., et al. 2005, ApJ, 619, 755
Engelbracht, C. et al. 2004, ApJS, 154, 248
Engelbracht, C. et al. 2005, ApJ, 628, L25
Förster-Schreiber, N.M., Roussel, H., Sauvage, M., & Charmandaris, V. 2004, A&A, 419, 501
Gordon, K.D. et al. 2004, ApJS, 154, 215
Helfer, T.T. 2003, ApJS, 145, 259
Helou, G. 2000, in Infrared Space Astronomy, Today and Tomorrow, ed. F. Casoli, J. Lequeux, F. David, Berlin: Springer, p337
Helou, G.. et al. 2004, ApJS, 154, 253
Hinz, J.L. et al. 2004, ApJS, 157, 259
Jansen, R.A., Fabricant, D., Franx, M., & Caldwell, N. 2000, ApJS, 126, 331
Kennicutt, R.C. 1998a, ARA&A, 36, 189
Kennicutt, R.C. 1998b, ApJ, 498, 541
Kennicutt, R.C. 2003, PASP, 115, 928
Kennicutt, R.C. et al. 2005, in preparation
Li, A., & Draine, B.T. 2001, ApJ, 554, 778
Li, A., & Draine, B.T. 2002, ApJ, 576, 762
Lonsdale, C.J. et al. 2003, PASP, 115, 897
Martin, D.C. et al. 2005, ApJ, 619, 1
Moustakas, J., & Kennicutt, R.C. 2005, ApJS, in press
Prescott, M.K.M. et al. 2005, in preparation
Regan, M.W. et al. 2004, ApJS, 154, 204
Roussel, H., Sauvage, M., Vigroux, L., & Bosma, A. 2001, A&A, 372, 427
Tuffs, R.J., & Popescu, C.C. 2005, in The Spectral Energy Distributions of Gas-Rich Galaxies: Confronting Models with Data, ed. C.C. Popescu, R.J. Tuffs, New York: AIP Conf Proc, 761, p344
Walter, F. et al. 2005, in Extraplanar Gas, ed. R. Braun, San Francisco: ASP Conf Ser, 331, p269
Willner, S.P. et al. 2004, ApJS, 154, 222

VAN DER KRUIT TO SPITZER: A NEW LOOK AT THE FAR-INFRARED–RADIO CORRELATION

E.J. Murphy[1], R. Braun[2], G. Helou[3], L. Armus[3], J.D.P. Kenney[1] and the SINGS team

[1]*Department of Astronomy, Yale University, New Haven, USA*

[2]*ASTRON, Dwingeloo, The Netherlands*

[3]*California Institute of Technology, Pasadena, USA*

* murphy@astro.yale.edu

Abstract We present an initial look at the far-infrared–radio correlation within the star-forming disks of four nearby, nearly face-on galaxies (NGC 2403, NGC 3031, NGC 5194, and NGC 6946). Using *Spitzer* MIPS imaging and WSRT radio continuum data, we are able to probe variations in the logarithmic 70 μm/22 cm (q_{70}) flux density ratios across each disk at sub-kpc scales. We find general trends of decreasing q_{70} with declining surface brightness and with increasing radius. We also find that the dispersion in q_{70} within galaxies is comparable to what is measured *globally* among galaxies at around 0.2 dex. We have also performed preliminary phenomenological modeling of cosmic ray electron (CRe^-) diffusion using an image-smearing technique, and find that smoothing the infrared maps improves their correlation with the radio maps. The best fit smoothing kernels for the two less active star-forming galaxies (NGC 2403 and NGC 3031) have much larger scale-lengths than that of the more active star-forming galaxies (NGC 5194 and NGC 6946). This difference may be due to the relative deficit of recent CRe^- injection into the interstellar medium (ISM) for the galaxies having largely quiescent disks. A more complete discussion of this proceedings article can be found in Murphy et al. (2006).

Keywords: infrared: galaxies - radio continuum: galaxies - cosmic rays: galaxies

1. Introduction

Soon after the Westerbork Radio Synthesis Telescope (WSRT) went online, van de Kruit (1971) made the first report of a correlation between 1415 MHz radio and 10 μm mid-infrared luminosities for a sample of Seyfert galaxy nuclei. This discovery was soon extended to the nuclei of normal spirals, though the dispersion was found to be smaller in the correlation for the original sample of Seyferts (van der Kruit 1973). It was not until the coming of IRAS

R. S. de Jong, Island Universes, 409–415.
© 2007 *Springer.*

that the optically thin radio continuum emission from galaxies was found to be better correlated with the far-infrared (FIR) dust emission of galaxies *without* an active galactic nucleus (AGN) (de Jong et al. 1985; Helou, Soifer, & Rowan-Robinson 1985).

The connection between radio and infrared emission from galaxies is that they are both powered by massive stars, as pointed out originally for starbursts by Harwit & Pacini (1975). Young massive stars, which heat up dust to provide the FIR emission, are the same stars which end as supernovae (SNe) and bring about the synchrotron emission observed at radio wavelengths. If this general picture is correct, the fact that the mean free path of UV photons ($\sim$100 pc) which heat the dust is much less than the diffusion length for a CRe^- ($\sim$1-2 kpc) suggests that the radio image should resemble a smeared version of the infrared image. This idea was first introduced by Bicay & Helou (1990), who attempted to model the propagation of CRe^-s by smearing IRAS data of galaxies using parameterized kernels containing the physics of the CRe^- propagation and diffusion, to better match the morphology of the corresponding radio data.

In an attempt to better understand the FIR-radio correlation, we are using MIPS infrared data from the *Spitzer* Infrared Nearby Galaxies Survey (SINGS) legacy science project (Kennicutt et al. 2003). In this initial study, we examine the variations of the FIR-radio correlation on sub-kpc scales within four of the nearest face-on galaxies in the SINGS sample: NGC 2403, NGC 3031 (M81), NGC 5194 (M51a), and NGC 6946. Using high resolution *Spitzer* imaging, we are also able to test the smearing model of Bicay & Helou (1990) with greater accuracy, at higher spatial resolution, and in more galaxies, with the aim of gaining better insight into CRe^- diffusion and confinement within galaxy disks. For a complete discussion, we direct the reader to Murphy et al. (2006).

2. Results

q_{70} Maps

In Figure 1 we plot $q_{70} \equiv \log\left(\frac{f_\nu(70\,\mu\mathrm{m})[\mathrm{Jy}]}{f_\nu(22\ \mathrm{cm})[\mathrm{Jy}]}\right)$ for each galaxy. We find that elevated q_{70} ratios are associated with bright structures in the infrared and radio images of each galaxy. The most obvious cases are seen for the bright spiral arms of NGC 3031, NGC 5194 and NGC 6946. All three galaxies show enhanced q_{70} ratios along their arms, with local peaks centered on HII regions, and depressed ratios located in the quiescent inter-arm and outer-disk regions of each galaxy. For NGC 2403, which does not have a grand-design spiral morphology, we still see q_{70} peaks associated with HII regions.

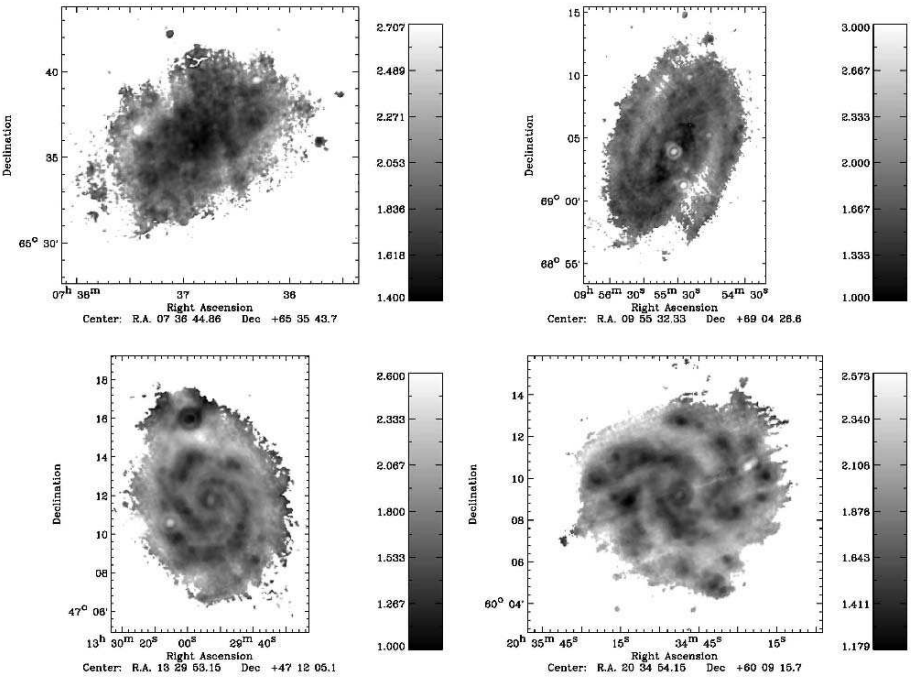

Figure 1. q_{70} maps for pixels having a 3-σ detections in both the input radio and 70 μm maps. The q_{70} ratios are enhanced along spiral arms and on HII regions due to 70 μm emission being more strongly peaked than the 22 cm emission. Top: NGC 2403 and NGC 3031. Bottom: NGC 5194 and NGC 6946.

To quantify radial variations in q_{70}, along with any dependencies of q_{70} on the 70 μm surface brightness within each galaxy, we perform aperture photometry using apertures having diameters equal to the FWHM of the MIPS 70 μm PSF (i.e. 17″). The measured dispersion of q_{70} within each galaxy is less than $\sim$0.25 dex. We find a general trend of increasing q_{70} ratios with increasing 70 μm surface brightness and decreasing radius. The residual dispersion around the trend of q_{70} with increasing radius is found to be larger than the residual dispersion around the trend of q_{70} with increasing 70 μm surface brightness by $\sim$0.1 dex. This suggests that the star formation sites within the disk are more important in determining the overall appearance of the q_{70} maps compared to the exponential profiles of the disks themselves.

Infrared/Radio Relations Inside and Among Galaxies

In Figure 2 we show our local sub-kpc q_{70} ratios together with global q_{70} values for 1752 galaxies from the study of Yun et al. (2001). Using their

cataloged 1.4 GHz NRAO VLA Sky Survey (NVSS) and 60 and 100 μm IRAS data, we converted IRAS based q_{60} values to *Spitzer* q_{70} values using the SED models of Dale & Halou (2002). We find that the dispersion in the local sub-kpc q_{70} ratios within our sample galaxies is comparable to that of global ratios. In the Yun et al. (2001) sample, q_{70} appears to be roughly constant with increasing galaxy luminosity, while, within each disk, q_{70} ratios clearly increase with the 70 μm luminosity. This difference in the observed trend between q_{70} and luminosity within and among galaxies can be explained by the diffusion of CRe^- within the galaxy disks.

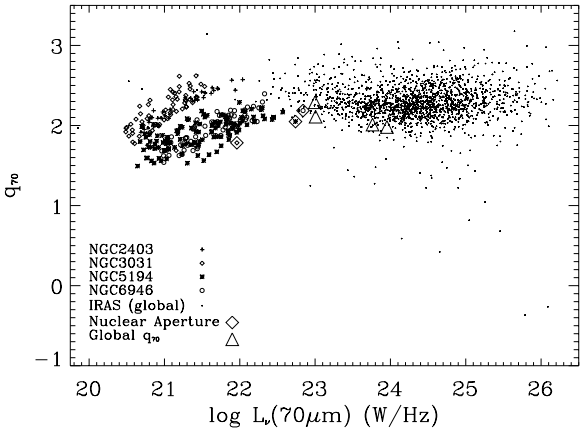

Figure 2. Matched 1.5 kpc aperture measured q_{70} ratios for each sample galaxy plotted with global q_{70} ratios estimated from the data presented by Yun et al. (2001). While the global q_{70} ratios are constant with 70 μm luminosity, the local sub-kpc q_{70} ratios are not.

3. Image-Smearing and Cosmic Ray Diffusion

To help understand the underlying physics of the correlation, we look to see whether the image-smearing model works to improve the correlation between the infrared and radio morphologies of galaxies. Determining the functional form of the best fit smearing kernel provides insight into the propagation and diffusion characteristics of cosmic rays within galaxy disks. In this study we examine the behavior for Gaussian and exponential kernels oriented in the planes of the sky and each galaxy disk.

We define the residuals between the smeared 70 μm map ($\tilde{I}(t,p,l)$: t =shape, p = orientation, and l = scale-length) and the observed 22 cm map (R) by,

$$\phi(Q,t,p,l) = \frac{\sum[Q^{-1}\tilde{I}_j(t,p,l) - R_j]^2}{\sum R_j^2}, \quad (1)$$

where $Q = \frac{\sum \tilde{I}_j(\mathbf{r})}{\sum R_j(\mathbf{r})}$ and j indexes each pixel. In Figure 3 we plot $\log(\phi)$, as a function of the scale-length (l), for each galaxy and find that the image-smearing technique improves the overall correlation between the radio map and the 70 μm image by an average of $\sim$0.2 dex. Unlike Marsh & Helou (1998), we find exponential kernels are preferred, independent of projection, over Gaussian kernels, suggesting that additional processes such as escape and decay appear necessary to describe their evolution through the galaxy disks.

We find distinct behavior between our active and less active star-forming galaxies. Figure 3 shows that scale-lengths $<$1 kpc work best to improve the correlation for the more active star-forming galaxies (NGC5194 and NGC6946: SFR$\geq$4 $M_\odot$/yr), while scale-lengths $>$1 kpc work best for the less active star-forming galaxies (NGC 2403 and NGC 3031: SFR $<$1$M_\odot$/yr). We also find that by smearing the 70 μm images, we are able to reduce the slope of the observed non-linearity in q_{70} with 70 μm surface brightness by $>$25% for each galaxy. This suggests that the non-linearity may be due to the diffusion of

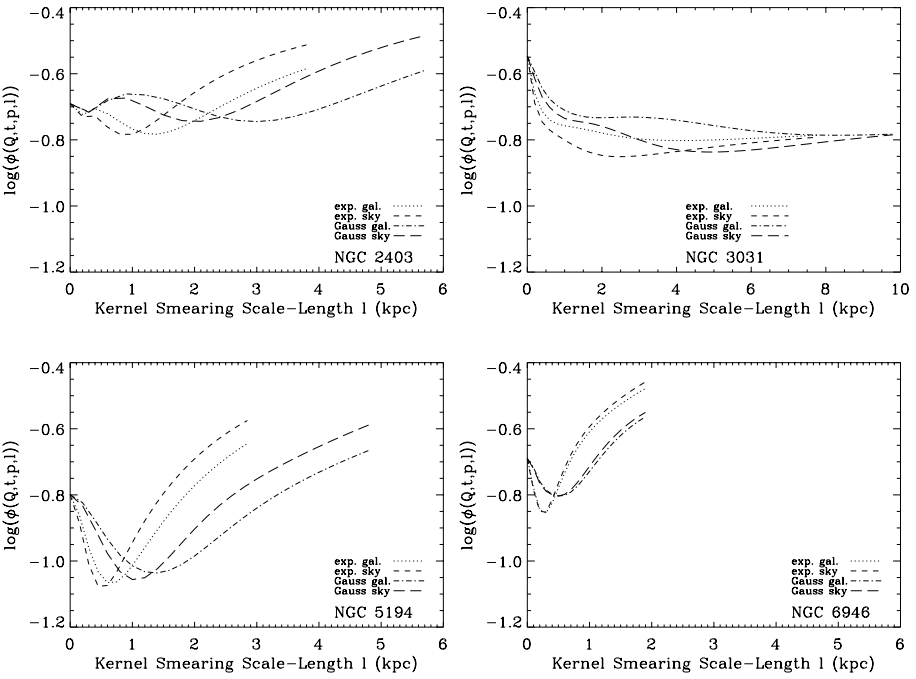

Figure 3. Residuals of observed radio maps with smeared 70 μm images, defined by $\phi(Q,t,p,l)$, as a function of smearing scale-length shown for each kernel per galaxy. Residuals for the active star-forming galaxies are minimized by kernels having $<$1 kpc scale-lengths, while the less active star-forming galaxies are better fit by those with scale-lengths $>$1 kpc.

CRe^-s and is not expected to be found in the *global* correlation when integrating the flux over entire galaxies.

4. Conclusion

In examining the behavior of q_{70} within the disks of our sample galaxies, along with our image-smearing analysis, we find:

1 An empirical trend of q_{70} decreasing with declining 70 μm surface brightness and increasing radius to be a general property within the galaxies. However, the dispersion measured in q_{70} at constant 70 μm surface brightness is found to be smaller than at constant radius by $\sim$0.1 dex, suggesting that star formation sites are more important in determining the q_{70} disk appearance than the underlying exponential disks.

2 The dispersion in the *global* FIR-radio correlation is comparable to the dispersion for q_{70} on sub-kpc scales within the galaxy disks. Also, the trend of increasing q_{70} ratio with increasing 70 μm luminosity within each galaxy is not observed in the *global* correlation.

3 The phenomenological modeling of cosmic ray electron (CRe^-) diffusion using an image-smearing technique is successful as it both decreases the measured dispersion in q_{70} and reduces the slope of the observed non-linearity in q_{70} with 70 μm surface brightness. The latter suggests that the non-linearity may be due to the diffusion of CRe^-s from star-forming regions.

4 Exponential kernels work marginally better to tighten the correlation than Gaussian kernels, independent of projection. This result suggests that CRe^- evolution is not well described by a pure random-walk diffusion and requires additional processes such as escape and decay.

5 Our two less active star-forming galaxies require kernels having larger scale-lengths to improve the correlation, while our two more active galaxies require smaller scale-lengths. This difference may be due to time-scale effects in which there has been a deficit of recent CRe^- injection into the ISM of the two less active star-forming galaxies, thus leaving the underlying diffuse disk as the dominant structure in the morphology.

References

Bicay M. D. and Helou, G. 1990, ApJ, 362, 59
Dale, D. A. and Helou, G. 2002, ApJ, 576, 159
de Jong, T., Klein, U., Wielebinski, R., and Wunderlich, E. 1985, A&A, 147, L6
Harwit, H, and Pacini, F 1975, ApJL, 200, L127
Helou, G., Soifer, B. T., and Rowan-Robinson, M. 1985, ApJL, 298, L7
Kennicutt, R. C. Jr., et al. 2003, PASP, 115, 928
Marsh, K. A. and Helou, G. 1998, ApJ, 493, 121

Murphy, E. J., et al. 2006, ApJ, 638, 157
van der Kruit, P.C. 1971, A&A, 15, 110
van der Kruit, P.C. 1973, A&A, 29, 263
Yun, M. S., Reddy, N. A., and Condon, J. J. 2001, ApJ, 554, 803

THE ORIGIN OF THE INITIAL MASS FUNCTION IS IN THE CLOUD STRUCTURE

João Alves[1*], Marco Lombardi[1**] and Charles Lada[2***]

[1] *European Southern Observatory, Germany*

[2] *Harvard-Smithsonian Center for Astrophysics, USA*

* jalves@ese.org, ** mlombard@eso.org, *** clada@cfa.harvard.edu

Abstract Detailed knowledge of the initial distribution of stellar masses at birth (known as the initial mass function or IMF) is necessary to predict and understand the evolution of stellar systems, such as clusters and galaxies. Unfortunately, stellar evolution theory cannot predict the form of this critical function and the origin of the stellar IMF remains one of the major unsolved problems of modern astrophysics. Stars form in the cold dense cores of interstellar molecular clouds and the detailed knowledge of the spectrum of masses of such cores is clearly a key for the understanding of the origin of the IMF. To date, observations have presented somewhat contradictory evidence relating to this issue. Here we present a new and more robust determination of the dense core mass function. We find the core mass function to be surprisingly similar to the stellar IMF, modified by a uniform star formation efficiency of about 30%. This suggests that the distribution of stellar birth masses is a direct product of the fragmentation/coalescence process in a molecular cloud.

Keywords: dust, extinction - ISM: structure - ISM: clouds

1. Introduction

Typically only about 10% of the mass of a star-forming molecular cloud is in the form of dense (i.e., $n(\mathrm{H2}) \sim 10^4$ cm^{-3}) gas, yet it is within such dense gas that stars seem to exclusively form (Lada & Adams 1992). Knowledge of the structure of the dense gas component of molecular clouds is clearly important for understanding the formation of stars within it. Presumably the physical conditions that characterize these cores correspond to the initial conditions for star formation and must to some degree be responsible for the range of outcomes (e.g., masses, angular momenta, magnetic content, multiplicity, etc.) of the physical process of star formation. In particular the spectrum of masses of individual star forming cores must be related to some degree to the birth masses of the stars formed within them. Molecular spectral-line studies have long

R. S. de Jong, Island Universes, 417–422.
© 2007 *Springer.*

suggested that the mass spectrum of cloud cores is well described by a power-law (Blitz 1993; Kramer et al. 1998), specifically, $\mathrm{d}N(m)/\mathrm{d}m \sim m^{-1.7}$. This functional form differs from the form of the stellar IMF in two fundamental ways. First, the stellar IMF cannot be described by a single power-law (scale-free) function, instead it appears to consist of a series of power-law segments that overall is qualitatively similar to a log-normal function (Miller & Scalo 1979; Kroupa 2001; Muench et al. 2001). The stellar IMF has an associated scale or characteristic mass in the range between 0.20–0.50 solar masses. Second, above about a solar mass the slope of the stellar IMF is steeper (i.e., $\mathrm{d}N(m)/\mathrm{d}m \sim m^{-2.35}$) than the cloud mass spectrum. This latter difference implies a significant physical difference in the two distributions. For the stellar IMF, the bulk of the (stellar) mass is tied up in low mass objects while for clouds the bulk of the mass is tied up in the most massive objects. A consequence of this difference is that in order to produce the stellar IMF from the cloud mass spectrum, a transformation must take place during the process of star formation. It has been suggested that outflows generated during the protostellar stages of star formation provide a natural feedback to collapse/infall limiting the final mass of a protostellar object (Shu et al. 1987) and perhaps provides the mechanism for transforming the cloud mass spectrum into the stellar mass spectrum (Lada & Lada 2003). However it is not clear how such a process could produce a characteristic scale for stellar masses.

A different picture has been suggested by recent observations of the structure of dust emission in a few nearby star forming complexes. These studies have produced mass spectra of dense molecular cores that above about 0.5 solar masses have a relatively steep slope (-2.1 to -2.3) similar to the stellar IMF (Motte et al. 1998; Testi & Sargent 1998; Johnstone et al. 2000; Johnstone et al. 2001; Beuther & Schilke 2004). Moreover, in one example, the ρ Ophiuchi cloud, the core mass spectrum exhibited a flattening or break near a mass of about 0.5 solar masses, also similar to the stellar IMF. In another cloud, measurements of dust emission produced a core mass spectrum between 0.1 and 0.5 solar masses with a slope of approximately -1.4 (Sandell & Knee 2001), consistent with the flatter slope suggested by the Ophiuchus observations for core masses less than 0.5 solar masses, but also consistent with the apparently universal functional form derived from molecular-line studies of cores, independent of mass. Nevertheless these studies of the dust emission from cores suggest that the individual cores are the direct precursors of new stars and that the stellar IMF is completely specified by the fragmentation process in molecular clouds. In addition these studies also suggest a high efficiency (about 100%) of star formation in dense gas. In this case the characteristic scale of stellar mass is set by the fundamental physics of cloud fragmentation (Shu et al. 2004; Larson 2005). Which picture is correct? At present the question of the

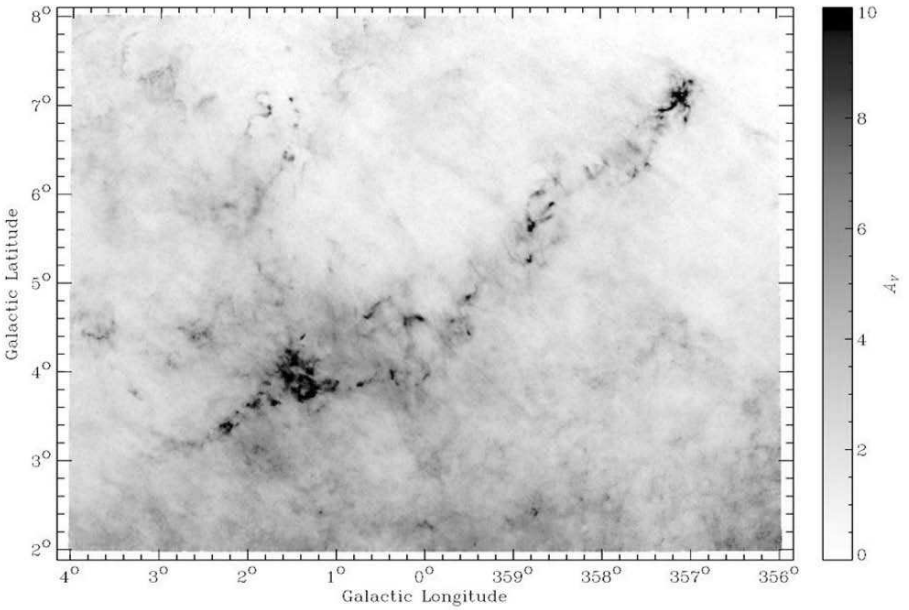

Figure 1. Dust extinction map of the Pipe nebula molecular complex. This map was constructed from near-infrared observations (1.25 μm, 1.65 μm, 2.2 μm) of about 4 millions stars in the background of the complex. Approximately 170 individual cores were identified within the cloud. Most of these cores appear as distinct, well separated entities facilitating the measurements of their basic physical parameters. We find the peak extinctions of the cores to range from 3.5 to 27 visual magnitudes with sizes (radii) between about 0.1 to 0.4 pc and masses ranging between 0.5 to 28 $M_\odot$.

distribution of core masses and its relation to the stellar IMF is uncertain with somewhat contradictory observational results.

In order to bring new insight to this issue we used an independent method of measuring cloud structure and masses that uses precise infrared measurements of dust extinction toward stars background to a molecular cloud (the NICE method (Lada et al. 1994; Alves et al. 1998; Alves et al. 2001)). Such measurements are free from many of the complications and systematic uncertainties that plague molecular-line or dust emission data and thus enable robust maps of cloud structure to be constructed.

2. The Pipe Nebula

We applied a 3-band (1.25 μm, 1.65 μm, 2.2 μm) optimized version of this method, the NICER method (Lombardi & Alves 2001), to about 4 million background stars to the Pipe nebula complex to construct a $6^\circ \times 8^\circ$ dust column

density map of this complex [1]. The Pipe nebula is a virtually unstudied nearby molecular cloud complex (Onishi et al. 1999; Lombardi et al. 2005), at a distance of about 120 pc and with a total mass of $\sim 10^4$ $M_\odot$. This molecular complex was selected because 1) this is the closest to Earth complex of this size and mass, which allowed us to achieve spatial resolutions of ~ 0.03pc, or about 3 times smaller the typical dense core size, and 2) it is particularly well positioned along a relatively clean line of sight to the rich star field of the Galactic bulge. The resulting extinction map is presented in Figure 1. Regarding the extraction of sources from this map, a dense core is defined as a 10σ contrast enhancement to its local surrounding background ($\sigma \sim 0.2$ mag). Because of the high dynamic range of column density achieved, traditional automatic source extraction algorithms were found inadequate and a custom-made semi-automatic procedure, with a better handling of large scale smooth column density gradients, was used instead. Approximately 170 individual cores were identified within the cloud. Most of these cores appear as distinct, well separated entities facilitating the measurements of their basic physical parameters. We find the peak extinctions of the cores to range from 3.5 to 27 visual magnitudes with sizes (radii) between about 0.1 to 0.4 pc and masses ranging between 0.5 to 28 $M_\odot$.

The dense core mass function, presented in Figure 2, is surprisingly similar in shape to the stellar IMF. Specifically, both distributions are characterized by power-law (or Salpeter law, Salpeter 1955) functional forms that rise with decreasing mass until they reach a distinct break point, this is then followed by a broad peak, and finally a steady decline toward the lowest mass objects. Although similar in shape, the stellar and core mass functions are however significantly offset in mass, corresponding to a scale change (in mass) of about a factor of 3: the break from the Salpeter slope occurs at around 2 $M_\odot$ for the cloud cores instead of the 0.6 $M_\odot$ for the stellar case (Muench et al. 2002). This offset, estimated for several data binnings, is physically quite significant since it implies that a characteristic star formation efficiency of about 30% ($27\pm5\%$) exists for the dense gas, independent of stellar mass. This efficiency is very similar to the maximum measured for young embedded clusters (Lada & Lada 2003) and individual dense cores where it is also found to be relatively independent of stellar mass (Jijina et al. 1999).

It is well known that the generation of a powerful outflow is a natural consequence of the formation of a protostar in a dense core (Lada 1985). It has been long suspected that such outflows could be very disruptive to surrounding material and could play an important role in limiting the mass which can accrete onto a protostar (Shu et al. 1987; Shu et al. 1991). Matzner & McKee

[1] The near-infrared data used was taken from the 2MASS All Sky Survey (Kleinmann et al. 1994).

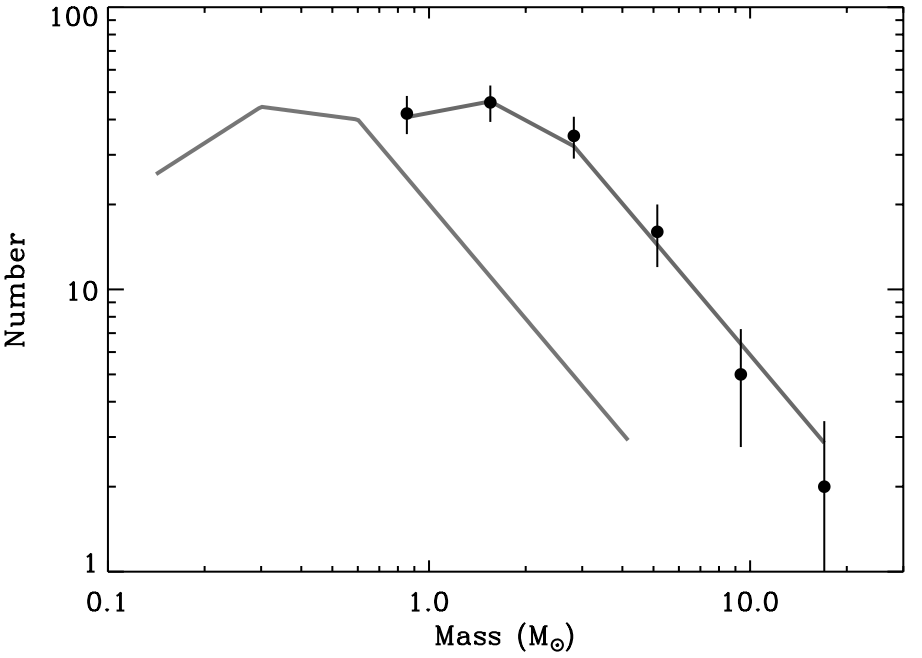

Figure 2. Mass function of dense molecular cores (filled circles). The line on the left represents the stellar IMF [with the form $\mathrm{d}N(m)/\mathrm{d}m \sim m^{-2.35}$ for masses above 0.6 $M_\odot$, $\mathrm{d}N(m)/\mathrm{d}m \sim m^{-1.15}$ for masses between 0.6 $M_\odot$ and 0.12 $M_\odot$, and $\mathrm{d}N(m)/\mathrm{d}m \sim m^{1.7}$ for masses below 0.12 $M_\odot$ (Kroupa 2001; Muench et al. 2002)]. The line on the right represents the stellar IMF binned to the resolution of the data and shifted to higher masses by about a factor of 3. The dense core mass function is essentially the same as the stellar IMF function, apart from a uniform star formation efficiency factor. The lowest mass bin is estimated to be 90% complete.

2000 have theoretically investigated the disruption of dense cores by protostellar outflows and have concluded that outflow disruption of individual cores can produce star formation efficiencies in the range of 25–75%. They further argued that because this efficiency is independent of stellar mass, the stellar and core mass functions should be of similar overall functional form. Recently, Shu, Li & Allen 2004 have presented an outline for a self-consistent theory for the origin of the stellar IMF. In this picture cores are formed from magnetized turbulent gas and are also similarly disrupted by outflows with a resulting star formation efficiency predicted to be $\approx 33\%$. Thus, the core mass spectrum we derive for the Pipe Nebula may implicate outflows as the key mechanism for core disruption and for setting the final masses of protostellar objects. Shu et al. also predict both a slope for the power-law portion of the core mass function and a location of the break from the power-law form that are very similar to the

core mass function of the Pipe Nebula. Thus, apart from a uniform efficiency factor, the birth mass of a star appears to be completely predetermined by the mass of the dense core in which it is born.

The results of this paper suggest that the distribution of stellar birth masses over essentially the entire range of stellar mass is a direct product of the fragmentation/coalescence process in a molecular cloud and a uniform star formation efficiency of about 30%.

References

Alves J., Lada C.J., Lada E.A. 2001, Nature 409, 159
Alves J., Lada C.J., Lada E.A., Kenyon S.J., Phelps R. 1998, *ApJ* 506, 292
Beuther H., Schilke P. 2004, *Science* 303, 1167
Blitz L. 1993, In: *Protostars and Planets III*, pp. 125–161
Jijina J., Myers P.C., Adams F.C. 1999, *APJS* 125, 161
Johnstone D., Fich M., Mitchell G.F., Moriarty-Schieven G. 2001, *ApJ* 559, 307
Johnstone D., Wilson C.D., Moriarty-Schieven G., et al. 2000, *ApJ* 545, 327
Kleinmann S.G. et al. 1994, *Astrophysics & Space Science* 217, 11
Kramer C., Alves J., Lada C., et al. 1998, *A&A* 329, L33
Kroupa P. 2001, *MNRAS* 322, 231
Lada C.J. 1985, *ARAA* 23, 267
Lada C.J., Adams F.C. 1992, *ApJ* 393, 278
Lada C.J., Lada E.A. 2003, *ARAA* 41, 57
Lada C.J., Lada E.A., Clemens D.P., Bally J. 1994, *ApJ* 429, 694
Larson R.B. 2005, *MNRAS* 359, 211
Lombardi M., Alves J. 2001, *A&A* 377, 1023
Lombardi M., Alves J., Lada C.J. 2005, *A&A* in press
Matzner C.D., McKee C.F. 2000, *ApJ* 545, 364
Miller G.E., Scalo J.M. 1979, *ApJS* 41, 513
Motte F., Andre P., Neri R. 1998, *A&A* 336, 150
Muench A.A., Alves J.., Lada C.J., Lada E.A. 2001, *ApJL* 558, L51
Muench A.A., Lada E.A., Lada C.J., Alves J. 2002, *ApJ* 573, 366
Onishi T., Kawamura A., Abe R., et al. 1999, *PASJ* 51, 871
Salpeter E.E. 1955, *ApJ* 121, 161
Sandell G., Knee L.B.G. 2001, *ApJL* 546, L49
Shu F.H., Adams F.C., Lizano S. 1987, *ARAA* 25, 23
Shu F.H., Li Z.Y., Allen A. 2004, In: *ASP Conf. Ser. 323: Star Formation in the Interstellar Medium: In Honor of David Hollenbach*, p. 37
Shu F.H., Ruden S.P., Lada C.J., Lizano S. 1991, *ApJL* 370, L31
Testi L., Sargent A.I. 1998, *ApJL* 508, L91

MODES OF STAR FORMATION ALONG THE HUBBLE SEQUENCE AND BEYOND

Richard de Grijs

Department of Physics & Astronomy, The University of Sheffield, UK

Abstract I assess the similarities and differences between the star-formation modes in quiescent spiral galaxies versus those in violent starburst regions. As opposed to the quiescent star-formation mode in spiral galaxies, current empirical evidence on the star-formation processes in the extreme, high-pressure environments induced by galaxy encounters strongly suggests that star *cluster* formation is an important and perhaps even the dominant mode of star formation in such starburst events. The sizes, luminosities, and mass estimates of the young massive star clusters (YMCs) are entirely consistent with what is expected for young Milky Way-type globular clusters (GCs). Recent evidence lends support to the scenario that GCs, which were once thought to be the oldest building blocks of galaxies, are still forming today. One of the key unanswered questions in this field relates to their possible survival chances for a Hubble time, and thus to the potential evolutionary connection between YMCs and GCs.

Keywords: galaxies: star clusters - galaxies: starburst - galaxies: evolution

1. Quiescent Versus Violent Modes of Star Formation

Star formation plays a major role in the evolution of galaxies. However, despite this, it is still rather poorly understood. In fact, on galaxy-wide scales, we do not have much more than a few scaling relations – such as the Schmidt-Kennicutt law (Schmidt 1959, Kennicutt 1998) – at our disposal. The process of star formation itself, while central to galaxy astrophysics, is one of the remaining "dark corners of the evolutionary process" (e.g., O'Connell 2005).

The Schmidt-Kennicutt law, in one of its modern guises relating the (galactic) star formation density to the gas surface density (e.g., Kennicutt 1998), is remarkably successful in describing the star-formation properties of galaxies ranging from quiescent spirals (such as the Milky Way), via circumnuclear and localised star-forming environments (e.g., M83, NGC 6946), to major, galaxy-wide bursts of star formation (e.g., M82, the "Antennae" system) and – in the extreme – the ultraluminous infrared galaxies (ULIRGs) thought to be the

R. S. de Jong, Island Universes, 423–428.
© 2007 *Springer.*

remnants of major galaxy-galaxy interactions. The global star-formation rates in these wide-ranging environments correlate very closely with the local gas surface density over at least 5 orders of magnitude.

While this suggests very strongly that star formation is indeed driven by the local gas surface density, I point out that in order to maintain the high star-formation rates seen in starburst environments, the star-formation *efficiency* needs to be maintained at moderate to high levels for a significant length of time. Star-formation efficiencies, defined here as the total mass in stars with respect to the total available gas mass in a given environment, range from $0.1-3$ per cent for quiescent spiral and irregular galaxies, as well as for dwarf starbursts, to $\gtrsim 10-30$ per cent in the more extreme environments of major interactions and the most violently star-forming areas in ULIRGs (e.g., Gao & Solomon 2004a,b).

2. Star Formation in Interacting Galaxies

Perhaps not surprisingly, the highest star-formation efficiencies are generally found in the context of gravitationally interacting galaxies. [For the purpose of this discussion I ignore any possible connection between active galactic nuclei and starbursts.] Many authors have pointed out that such major star-forming episodes are difficult, if not impossible, to sustain for any cosmologically significant length of time, as the high star-formation efficiencies will deplete the available gas reservoir on short time-scales (generally, $\lesssim 10^7$ yr), quickly lead to massive supernova explosions, and thus quench the ongoing starburst (e.g., Chevalier & Clegg 1985; Doane & Mathews 1993; see also, e.g., Schweizer et al. 1996). The limitations on the duration of most starburst events imposed by the available gas content imply that most ongoing starbursts cannot have sustained their high levels of active star formation for significant lengths of time. These considerations naturally suggest that galaxy interactions (or equivalent events) and enhanced levels of active star formation are intimately linked; conversely, starburst events are often (but not exclusively) linked to ongoing or recent (generally within the last $\sim 10^{8-9}$ yr) galaxy mergers or interactions.

The importance of star *cluster* formation

It is becoming increasingly clear that a major fraction of the star formation in interacting galaxies likely takes place in the form of dense, massive star clusters (e.g., de Grijs et al. 2001, 2003d, and references therein). In de Grijs et al. (2003d) we analysed the *Hubble Space Telescope (HST)*/ACS Early Release Observations of the "Mice" and the "Tadpole" interacting systems, using a pixel-by-pixel approach. In both systems we found more than 40 young massive star-forming regions (possibly star clusters, although the distances to

these galaxies of ~ 100 Mpc precluded us from concluding so more robustly) – we noted that these most likely represented the proverbial "tip of the iceberg" because of observational selection effects. Overall, we found that more than 35 per cent of the active star formation in these galaxies occurred in the dense star-forming regions; in the tidal tails and spiral arms, at least 75 per cent of the blue (B-band) flux originated from these areas.

This preponderance of dense star-forming "clusters" can be understood easily in the context of the previous discussion. Elmegreen & Efremov (1997) showed, for instance, that in order to produce a massive star "cluster" – for a give ambient pressure – a high star-formation efficiency is required. Their figure 4 clearly shows that the more massive progenitor molecular clouds, with masses in excess of $\sim 10^7$ M$_\odot$, are more conducive to high star-formation efficiencies than their lower-mass counterparts. In the presence of significant external pressure (as in the case of interacting galaxies), and high star-formation efficiencies (as found, once again, in interacting galaxies), the resulting star formation through cloud collapse is therefore expected to occur predominantly in the form of massive star-forming regions.

Decoupled star and cluster formation

This scenario is qualitatively supported by the detailed star and star cluster formation histories that have been derived for a number of nearby galaxies. In M82's fossil starburst region "B", for instance, we found a clear and dominant peak in the star cluster formation history around 10^9 yr ago (de Grijs et al. 2001, 2003a). However, star cluster formation declined rapidly (within a few $\times 10^8$ yr) after this burst episode, while quiescent star formation in the galaxy's disk continued until at least 20 to 30 Myr ago (de Grijs et al. 2001). This indicates a physical decoupling between the star and star cluster formation modes in M82 B, implying special conditions as prerequisite for star cluster formation (see also Ashman & Zepf 1992; Elmegreen & Efremov 1997).

This situation is, in fact, similar to that in the Large Magellanic Cloud (LMC), and also to that in the nearby starburst dwarf galaxy NGC 5253. In the LMC, the star cluster population consists of a dozen old, globular cluster (GC)-like objects with ages of ~ 13 Gyr, and a large complement of "populous" clusters, all younger than $\sim 3 - 4$ Gyr. With the exception of a single object, ESO 121-SC03, there are no known populous clusters in the LMC with robustly confirmed ages in the "age gap" between about 3 and 13 Gyr (see, however, Rich et al. 2001, and references therein). The LMC's field star population, on the other hand, does not show any such marked absence of star-formation activity in this period, in neither the central bar region nor the outer disk field (see, e.g., Holtzman et al. 1999).

Tremonti et al. (2001) obtained high-resolution *Hubble Space Telescope*/ STIS spectroscopy of both a number of young massive star clusters (YMCs) and the diffuse field population in the disk of NGC 5253. Their composite cluster spectrum shows strong O-star signature (P Cygni profiles associated with massive stellar winds) that are not seen in the composite field-star spectrum. This raises the question, once again, whether star formation might operate differently in the field than in the clusters. They concluded that a fair fraction of the field star population might consist of dissolved star clusters. If this is the correct interpretation, this would imply that most of the YMCs in NGC 5253 dissolve on time-scales of ~ 10 Myr. It has recently been pointed out that this type of "infant mortality" might be plausible in other interacting galaxies such as the Antennae (Whitmore 2004) and M51 (Bastian et al. 2005) as well.

3. Fate of the Young Massive Star Clusters

Despite the infant mortality process observed in some of the nearest interacting systems, significant fractions of star clusters induced by the interactions survive to become bound objects. This is supported, e.g., by the existence of ~ 1 Gyr-old clusters in M82 B (de Grijs et al. 2001, 2003a), thought to have been triggered by its last tidal encounter with M81, and other galaxies containing star clusters older than a few $\times 10^7$ yr.

In many cases, these clusters resemble young *globular* clusters based on their current sizes, luminosities and photometric (and sometimes spectroscopic) mass estimates. The question remains, however, whether at least a fraction of these young objects will survive to ages of $\gtrsim 10$ Gyr. GCs have long been thought to be the oldest building blocks of galaxies, formed at or before the time of galaxy formation. Yet, the discovery of YMCs resembling GC progenitors begs the question whether we are witnessing the formation of proto-GCs in the most violent star-forming regions. If we can prove this conclusively, one way or the other, the answer to this crucial question will have far-reaching consequences for our understanding of a wide range of astrophysical issues, with bearing on the key issues of the nature of star formation, galaxy assembly and evolution.

There are a number of approaches to address this question. Here, I will focus on the use of the cluster luminosity (or mass) function (CLF; i.e., the number of clusters in a population within a given luminosity or mass range). The seminal work by Elson & Fall (1985) on the young LMC cluster system (with ages $\lesssim 2 \times 10^9$ yr) seems to imply that the CLF of YMCs is well described by a power law of the form $N_{\rm YSC}(L){\rm d}L \propto L^{\alpha}{\rm d}L$, where $N_{\rm YSC}(L){\rm d}L$ is the number of YSCs with luminosities between L and $L + {\rm d}L$, with $-2 \lesssim \alpha \lesssim -1.5$ (see de Grijs et al. 2003c for a review). On the other hand, for old GC systems with ages $\gtrsim 10^{10}$ yr, the CLF shape is well established to be roughly Gaussian (or

log-normal), characterized by a peak (turn-over) magnitude at $M_V^0 \simeq -7.4$ mag and a Gaussian FWHM of ~ 3 mag (e.g., Whitmore et al. 1995; Harris et al. 1998).

This type of observational evidence has led to the popular, but thus far mostly speculative theoretical prediction that not only a power-law, but *any* initial CLF (or cluster mass function; CMF) will be rapidly transformed into a Gaussian (or log-normal) distribution because of (i) stellar evolutionary fading of the lowest-luminosity (and therefore lowest-mass) objects to below the detection limit; and (ii) disruption of the low-mass clusters due both to interactions with the gravitational field of the host galaxy, and to internal two-body relaxation effects leading to enhanced cluster evaporation (e.g., Elmegreen & Efremov 1997; Gnedin & Ostriker 1997; Ostriker & Gnedin 1997; Fall & Zhang 2001).

The M82 B cluster population: initial conditions revealed?

In de Grijs et al. (2003a,b) we reported the discovery of an approximately log-normal CLF (and CMF) for the roughly coeval star clusters at the intermediate age of ~ 1 Gyr in M82 B. This provided the first deep CLF (CMF) for a star cluster population at intermediate age, which thus serves as an important benchmark for theories of the evolution of star cluster systems. Recently, we further investigated whether the most likely initial CMF in M82 B was more similar to either a log-normal or a power-law distribution (de Grijs et al. 2005), by taking into account the dominant evolutionary processes (including stellar evolution, and internal and external gravitational effects) affecting the mass distributions of star cluster systems over time-scales of up to ~ 1 Gyr in the presence of a realistic underlying gravitational potential.

From our detailed analysis of the expected evolution of CMFs, we conclude that our observations of the M82 B CMF are inconsistent with a scenario in which the 1 Gyr-old cluster population originated from an initial power-law mass distribution. This applies to a range of characteristic disruption time-scales. Our conclusion is supported by arguments related to the initial density in M82 B, which would be unphysically high if the present cluster population were the remains of an initial power-law distribution.

In a static gravitational potential, which is a good approximation to the M82 B situation despite its recent encounter with M81 (see de Grijs et al. 2005), Vesperini (1998) shows conclusively that there exists a particular CMF of which the initial mean mass, width and radial dependence remain unaltered during the entire evolution over a Hubble time. In fact, the mean mass and width of *any* initial log-normal CMF tends to evolve towards the values for this equilibrium CMF, which is very close (within the 1σ uncertainties) to the current parameterisation of the M82 B CMF. By extension, this may imply that we are

indeed witnessing the formation of proto-globular clusters in M82 – provided that a fraction of them survive for a Hubble time.

Acknowledgements I thank, in particular but in no particular order, Uta Fritze–v. Alvensleben, Geneviève Parmentier, Peter Anders, Henny Lamers and Nate Bastian for their valuable comments on and contributions to various aspects of the studies highlighted in this article. This work has been partially supported by the International Space Science Institute in Berne (Switzerland).

References

Ashman K.M., Zepf S.E., 1992, ApJ, 384, 50

Bastian N., Gieles M., Lamers H.J.G.L.M., Scheepmaker R., de Grijs R., 2005, A&A, 431, 905

Chevalier R.A., Clegg A.W., 1985, Nature, 317, 44

de Grijs R., O'Connell R.W., Gallagher J.S. III, 2001, AJ, 121, 768

de Grijs R., Bastian N., Lamers H.J.G.L.M., 2003a, MNRAS, 340, 197

de Grijs R., Bastian N., Lamers H.J.G.L.M., 2003b, ApJ, 583, L17

de Grijs R., Anders P., Lynds R., Bastian N., Lamers H.J.G.L.M., O'Neill E.J., Jr., 2003c, MNRAS, 343, 1285

de Grijs R., Lee J.T., Mora Herrera M.C., Fritze–v. Alvensleben U., Anders P., 2003d, New Astron., 8, 155

de Grijs R., Parmentier G., Lamers H.J.G.L.M., 2005, MNRAS, submitted

Doane J.S., Mathews W.G., 1993, ApJ, 419, 573

Elmegreen B.G., Efremov Y.N., 1997, ApJ, 480, 235

Fall S.M., Zhang Q., 2001, ApJ, 561, 751

Gao Y., Solomon P.M., 2004a, ApJ, 606, 271

Gao Y., Solomon P.M., 2004b, ApJS, 152, 63

Gnedin O.Y., Ostriker J.P., 1997, ApJ, 474, 223

Harris W.E., Harris G.L.H., McLaughlin D.E., 1998, AJ, 115, 1801

Holtzman J.A., et al., 1999, AJ, 118, 2262

Kennicutt R.C., Jr., 1998, ARA&A, 36, 189

O'Connell R.W., 2005, in: Starbursts – from 30 Doradus to Lyman break galaxies, Astrophysics & Space Science Library, de Grijs R., González Delgado R.M., eds., Springer: Dordrecht, ASSL, 329, 333

Ostriker J.P., Gnedin O.Y., 1997, ApJ, 487, 667

Rich R.M., Shara M.M., Zurek D., 2001, AJ, 122, 842

Schmidt M., 1959, ApJ, 129, 243

Schweizer F., Miller B.W., Whitmore B.C., Fall, S.M., 1996, AJ, 112, 1839

Tremonti C.A., Calzetti D., Leitherer C., Heckman T.M., 2001, ApJ, 555, 322

Vesperini E., 1998, MNRAS, 299, 1019

Whitmore B.C., Sparks W.B., Lucas R.A., Macchetto F.D., Biretta J.A., 1995, ApJ, 454, L73

Whitmore B.C., 2004, in: The Formation and Evolution of Massive Young Star Clusters, ASP Conf. Ser., vol. 322, Lamers H.J.G.L.M., Smith L.J., Nota A., eds., ASP: San Francisco, p. 419

SPIRAL SHOCK TRIGGERING OF STAR FORMATION

Ian A. Bonnell* and Clare L. Dobbs

Dept. of Physics and Astronomy, University of St Andrews, Scotland

* iab1@st-and.ac.uk

Abstract We present numerical simulations of the passage of clumpy gas through a galactic spiral shock and the subsequent formation of giant molecular clouds (GMCs) and the triggering of star formation. The spiral shock forms dense clouds while dissipating kinetic energy, producing regions that are locally gravitationally bound and collapse to form stars. In addition to triggering the star formation process, the clumpy gas passing through the shock naturally generates the observed velocity dispersion size relation of molecular clouds. In this scenario, the internal motions of GMCs need not be turbulent in nature. The coupling of the clouds' internal kinematics to their externally triggered formation removes the need for the clouds to be self-gravitating. Globally unbound molecular clouds provides a simple explanation of the low efficiency of star formation. While dense regions in the shock become bound and collapse to form stars, the majority of the gas disperses as it leaves the spiral arm.

Keywords: galaxies:spiral, hydrodynamic, ISM:clouds, ISM:molecules, stars:formation

1. Introduction

Star formation has long been known to occur primarily in the spiral arms of disc galaxies (Baade 1963). Spiral arms are denoted by the presence of young stars, HII regions, dust and giant molecular clouds, all signatures of the star formation process (Elmegreen & Elmegreen 1983; Ferguson et al. 1998). What is still unclear is the exact role of the spiral arms in inducing the star formation. Is it simply that the higher surface density due to the orbit crossing is sufficient to initiate star formation, as in a Schmidt law, or do the spiral arms play a more active role? Roberts (1969) first suggested that the spiral shock that occurs as the gas flows through the potential minima triggers the star formation process in spiral galaxies. Shock dissipation of excess kinetic energy can result in the formation of bound structures which then collapse to form stars.

R. S. de Jong, Island Universes, 429–434.
© 2007 *Springer.*

Giant molecular clouds (GMCs) are observed to contain highly supersonic motions and a wealth of structure on all length scales (Larson 1981; Blitz & Williams 1999). The supersonic motions are generally thought to be 'turbulent' in nature and to be the cause of the density structure in GMCs (Mac Low & Klessen 2004; Elmegreen & Scalo 2004). We propose an alternative scenario whereby it is the passage of the clumpy interstellar medium through a galactic spiral shock that not only produces the dense environment in which molecular clouds form (Cowie 1981; Elmegreen 1991), but also gives rise at the same time to their supersonic internal motions (Bonnell et al. 2005).

2. Simulations of Spiral Shocks

We use high resolution Smoothed Particle Hydrodynamics (SPH) (Monaghan 1992) simulations to follow the passage of interstellar gas through a spiral arm. The galactic potential is a combination of a two-armed spiral potential and a logarithmic potential that provides a flat rotation curve ($v = 200$ km/s). The initial conditions, from a test particle simulation, are of 10^6 $M_\odot$ of isothermal, 100K gas with a surface density of $1 M_\odot$ pc^{-2}. The gas is chosen such that it forms a dense cloud of 100 pc once in the spiral arm. Star formation is modeled by the inclusion of sink-particles (Bate, Bonnell & Price 1995).

3. Triggering of Star Formation in the Spiral Shock

The evolution of the gas over 34 million years as it passes through the spiral potential is shown in Figure 1. The initially clumpy, low density gas ($\rho \approx 0.01$ $M_\odot$pc^{-3}) is compressed by the spiral shock as it leaves the minimum of the potential. The shock forms some very dense ($> 10^3$ $M_\odot$pc^{-3}) regions, which become gravitationally bound and thus collapse to form regions of star formation. Further accretion onto these regions, modeled with sink-particles, raises their masses to that of typical stellar clusters (10^2 to 10^4 $M_\odot$). Star formation occurs within 2×10^6 years after molecular cloud densities are reached. The total spiral arm passage lasts for $\approx 2 \times 10^7$ years. The gas remains globally unbound throughout the simulation and re-expands in the post-shock region. The star formation efficiency is of order 10 % and should be taken as an upper limit in the absence of any form of stellar feedback.

The star forming clouds that form in the spiral shocks are generally unbound and thus disperse once they leave the spiral arm. Numerical simulations of unbound clouds (Clark & Bonnell 2004; Clark et al. 2005) have recently shown that they can form local subregions which are gravitationally unstable and thus form stars. In contrast, the bulk of the cloud does not become bound and thus disperses without entering into the star formation process. The resultant star formation efficiencies are of order 10 per cent, even without the presence of the

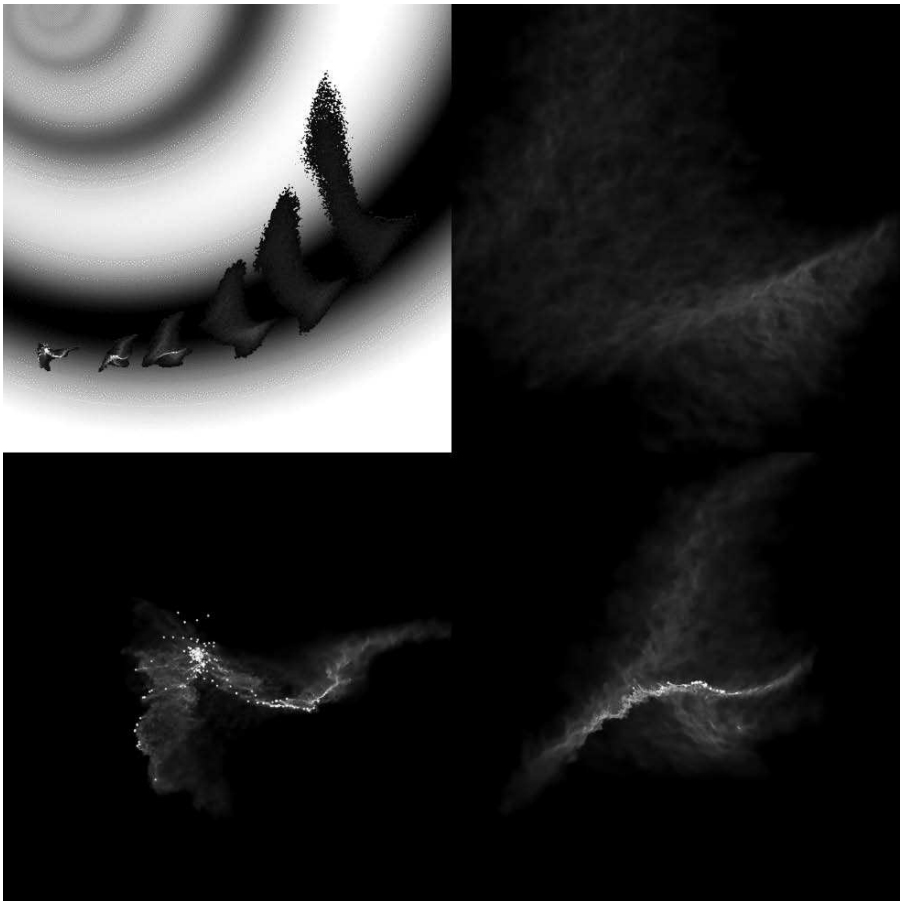

Figure 1. The evolution of cold interstellar gas through a spiral arm is shown relative to the spiral potential of the galaxy (upper left-panel). The minimum of the spiral potential is shown as black and the overall galactic potential is not shown for clarity. The 3 additional panels, arranged clockwise, show close-ups of the gas as it is compressed in the shock and subregions become self-gravitating. Gravitational collapse and star formation occurs within 2×10^6 years of the gas reaching molecular cloud densities. The cloud produces stars inefficiently as the gas is not globally bound.

divergent flows of gas leaving a spiral arm. This then offers a simple physical mechanism to explain the low star formation efficiency in our Galaxy.

In addition to forming dense clouds in which star formation occurs, the spiral shock forms structures which resemble the observed structures in GMCs. Detailed images of the GMCs formed in a spiral shock are shown in Figure 2. The projections of the dense gas along a length of 50 pc, viewed from above the disc of the galaxy, is taken just after star formation has been initiated. We

Figure 2. The internal structure of a 50 pc molecular cloud is shown as projected onto the plane of the galaxy. The gas has fragmented into many quasi-periodically-spaced dense regions with on-going star formation.

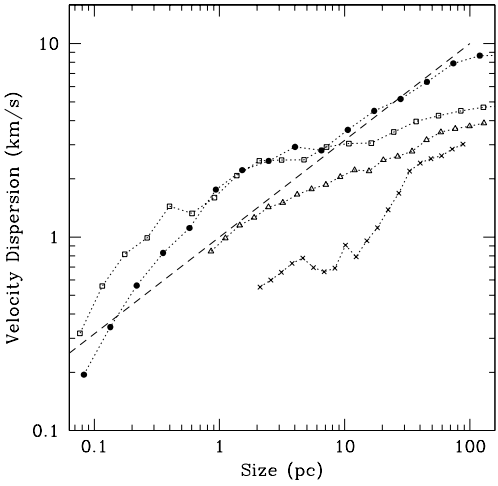

Figure 3. The velocity dispersion is plotted as a function of size at 5 different times during the passage of the gas through a spiral shock. The velocity dispersion is plotted at 4.2, 14, 18, 23, and 27×10^6 years after the start of the simulation. Star formation is initiated at $\approx 23 \times 10^6$ years. The dashed line indicates the Larson relation for molecular clouds where $\sigma \propto R^{-1/2}$ (Larson 1981; Heyer & Brunt 2004).

see significant amounts of substructure as the dense gas breaks up into many components of several parsecs in size and separation. The dense regions have column densities typical to GMCs. This structure can be understood as being due to the combination of the clumpy nature of the pre-shock gas along with Rayleigh-Taylor like instabilities which occur as gas continues to flow into the shock.

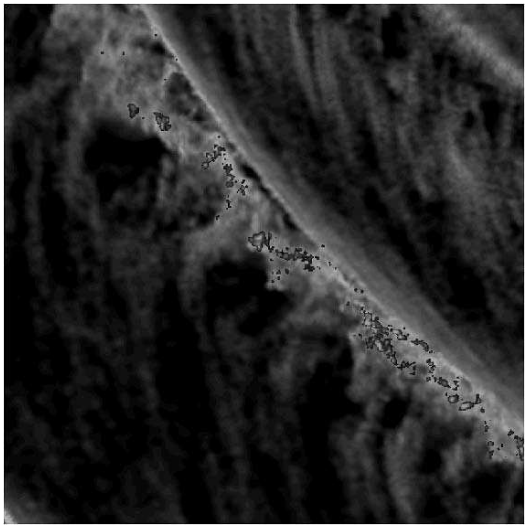

Figure 4. The formation of spurs and feathering from structure leaving the spiral arms is shown in this global simulation.

4. The Generation of the Internal Velocity Dispersion

In addition to triggering star formation, we must be able to explain the origin of the internal velocity dispersion and how it depends on the size of the region considered (Larson 1981; Heyer & Brunt 2004). The evolution of the velocity dispersion as a function of the size of the region considered is shown in Figure 3. The initially low velocity dispersion, of order the sound speed $v_s \approx 0.6$ km/s, increases as the gas passes through the spiral shock. At the same time, the velocity dispersion increases more on larger scales, producing a $v_{\rm disp} \propto R^{0.5}$ velocity dispersion size-scale relation. The basic idea is that when structure exists in the pre-shocked gas, the stopping point of a particular clump depends on the density of gas with which it interacts. Thus, some regions will penetrate further into the shock, broadening it and leaving it with a remnant velocity dispersion in the shock direction. Smaller scale regions in the shock are likely to have more correlated momentum injection as well as mass loading and thus small velocity dispersions. Larger regions will have less correlation in both the momentum injection and mass loading such that there will be a larger dispersion in the post-shock velocity.

5. Global Simulations

Recent global simulations of gas dynamics in spiral galaxies (see Dobbs, this proceedings) show that the spiral shocks can account for the formation of molecular gas from cold atomic gas and generate the large scale distribution

of molecular clouds in spiral arms. Structures in the spiral arms arise due to the shocks that tend to gather material together on more similar orbits. Thus, structures grow in time through multiple spiral arm passages. These structures present in the spiral arms are also found to form the spurs and feathering in the interarm region as they are sheared by the divergent orbits when leaving the spiral arms. The velocity dispersion in the gas undergoes periodic bursts during the spiral arm passage as the clumpy shock drives supersonic random motions into the gas. Such bursts in the internal gas motions are likely to be observable and would give support for a spiral shock origin of giant molecular clouds and the triggering of star formation.

6. Conclusions

The triggering of star formation by the passage of clumpy gas through a spiral arm can explain many of the observed properties of star forming regions. The clumpy shock reproduces the observed kinematics of GMCs, the so-called 'Larson' relation. There is no need for any internal driving of the quasi-turbulent random motions. The shock forms dense structures in the gas which become locally bound and collapse to form stars. The clouds are globally unbound and thus disperse on timescales of 10^7 years, resulting in relatively low star formation efficiencies. Global simulations provide a mechanism to study molecular cloud formation and the generation of the observed spurs and feathering in spiral galaxies.

References

Baade, W., 1963, Evolution of stars and Galaxies, Harvard University press (Cambridge), p 63.

Bate M. R., Bonnell I. A., Price N. M., 1995, MNRAS, 277, 362.

Blitz, L. & Williams, J., 1999, *The origin of stars and planetary systems*, eds C.J.Lada, N.D. Kylafis, (Kluwer:Dordrecht), 3

Bonnell, I.A., Dobbs, C.L., Robitaille, T.P., Pringle, J.E., 2005, MNRAS, submitted

Clark, P.C., Bonnell, I.A., 2004 MNRAS, **347**, L36

Clark, P.C., Bonnell, I.A., Zinnecker, H., Bate, M.R., 2004 MNRAS, **359**, 809

Cowie L. L., 1981, ApJ, 245, 66

Elmegreen B. G., 1991, ApJ, 378, 139

Elmegreen B. G., Elmegreen D. M., 1983, MNRAS, 203, 31

Elmegreen B., Scalo, J., 2004, ARA&A, **42**, 211

Ferguson A. M. N., Wyse R. F. G., Gallagher J. S., Hunter D. A., 1998, ApJ, 506, L19

Heyer M. H., Brunt C. M., 2004, ApJ, 615, 45

Larson R. B., 1981, MNRAS, 194, 809.

Mac Low, M.M., Klessen, R.S., 2004, RvMP, **74**, 125

Monaghan J. J., 1992, ARA&A, 30, 543.

Roberts, W.W., 1969, ApJ, **158**, 123

THE METALLICITY HISTORY OF DISK GALAXIES

Evolution between $0 < z < 3$

Lisa Kewley[1*] and Henry A. Kobulnicky[2**]

[1] *Institute for Astronomy, University of Hawaii, USA*

[2] *University of Wyoming, USA*

* kewley@ifa.hawaii.edu, ** chipk@uwyo.edu

Abstract We present results of our investigation into the metallicity history of disk galaxies between redshifts 0<z<3. Theory predicts that metallicity changes less rapidly than star formation rate as a function of redshift, but until now, there has been no observational foundation for the metallicity history of star-forming galaxies. Our local comparison samples include the Nearby Field Galaxy Survey (NFGS) and an objectively selected sample of galaxy pairs. We find that the central metallicities in close pairs are affected by gas flows triggered by an interaction. We compare the metallicity properties of our local field galaxies with a large sample of galaxies from the GOODS Field North and the Lyman Break Galaxies. In our preliminary analysis, we observe metallicity evolution of 0.15 dex per unit redshift.

Keywords: galaxies: starburst - galaxies: abundances - galaxies: high-redshift - galaxies: evolution

Introduction

To learn how galaxies in the early universe evolved into those that we see today requires a solid understanding of the chemical and star formation history of galaxies. The star formation history of galaxies has been studied extensively, but our understanding of the metallicity history of galaxies is still largely theoretical. Theory predicts that the mean stellar metallicity of galaxies rises as the galaxies undergo chemical enrichment from generations of star formation (e.g., Nagamine et al. 2001).

Observational investigations into the metallicity history of galaxies were difficult in the past because most studies focused on absorption line systems observed in quasar spectra. Obtaining an absolute representative galaxy

R. S. de Jong, Island Universes, 435–440.
© 2007 *Springer.*

metallicity by this method is difficult because only a single line of sight is available through these systems. Fortunately, alternative metallicity estimates are now possible for star-forming galaxies out to $z \sim 3$ thanks to new efficient spectrographs on 8-10m telescopes and emission-line diagnostics from state-of-the-art stellar evolution and photoionization models (e.g., Kobulnicky & Kewley 2004, Lilly, Carollo, & Stockton 2003, Kobulnicky et al. 2003, Shapley et al. 2004). In this paper, we present results from our ongoing study into the metallicity evolution of star-forming galaxies between redshifts $0 < z < 3$.

1. Sample Selection and Metallicity Measurements

The aim of this project is to investigate the *relative* change in the mean metallicity and the difference in the spread of metallicities between local galaxies and those at higher redshift in the same mass range. For this preliminary study, we use B-band luminosity as a surrogate for mass.

We chose two local samples; the Nearby Field Galaxy Survey (NFGS) and an objectively selected sample of galaxy pairs. A detailed discussion of the NFGS sample selection is given in Jansen et al. (2000). The 198-galaxy NFGS sample spans the full range of Hubble type and absolute magnitude present in the CfA1 redshift catalog. The NFGS is the only objectively selected sample for which integrated (global) long-slit spectra are available. The integrated spectra cover $\sim$80% of the B-band galaxy light.

The galaxy pairs sample is based on the 502-galaxy sample of Barton, Geller, & Kenyon (2000). Nuclear optical spectra were obtained by Barton et al. These optical spectra cover $\sim$ 10% of the B-band galaxy light. A total of 212/502 pair members contain emission lines suitable for classification. We investigate possible dynamical effects on the central metallicities of the pair members in the following section.

AGN were removed from the sample using the theoretical optical classification scheme of Kewley et al. (2001). We corrected the Balmer emission-lines for underlying stellar absorption as described in Kewley et al. (2002). The emission-line ratios were corrected for extinction using the Balmer decrement and the Clayton, Cardelli & Mathis (1989) attenuation curve. We calculated metallicities for the local samples following the prescription outlined in Kewley & Dopita (2002).

Estimates of metallicities for intermediate-redshift ($0 < z < 1$) galaxies have recently been made by Kobulnicky & Zaritsky (1999), Kobulnicky et al. (2003), Lilly, Carollo, & Stockton (2003), Kewley & Kobulnicky (2004), Maier et al. (2004), Maier et al. (2005) and Savaglio et al. (2005). In Kobulnicky & Kewley (2004), we calculated metallicities for 204 $0.3 < z < 1$ galaxies in the GOODS-North field using spectra from the Team Keck Redshift Survey (TKRS; Cowie et al. 2004, Wirth et al. 2004). We combined the TKRS

metallicities with measurements from the DEEP Groth Strip Survey (Kobulnicky et al. 2003), and additional objects from the Canada-France Redshift Survey (Lilly et al. 2003, Corollo & Lilly 2002). Note that metallicities for the TKRS and DEEP galaxies are based on equivalent widths because the survey spectra were not flux calibrated. For galaxies at redshifts between $0.4 < z < 1$, the red emission-lines are redshifted out of the optical regime. In this case, metallicities must be obtained using [OII] $\lambda 3727$, [OIII] $\lambda 5007$ and Hβ using the R_{23} diagnostic where R_{23}=([OII] $\lambda 3727$+[OIII] $\lambda\lambda 5007, 4959$)/H$\beta$ (see Kewley & Dopita 2000, for a review of R_{23}). The major problem with the R_{23} method for our study is that the ratio R_{23} is degenerate or double-valued with metallicity, giving both a high and a low metallicity estimate. We assume that the $0.4 < z < 1$ galaxy metallicities are high, but further observations of additional emission-lines are required for more reliable metallicity estimates.

Our high redshift sample consists of emission-line galaxies from Pettini et al. (2001), Kobulnicky & Koo (2000), and Shapley et al. (2004). The metallicities from Shapley et al. were derived using the [NII]/Hα ratio, which is sensitive to the (unconstrained) ionization parameter of the gas. Metallicities for the remaining galaxies were calculated by Pettini et al. and Kobulnicky & Koo using the R_{23} diagnostic.

2. Metallicity and Gas Flows in Galaxy Pairs

Before we use the local galaxy pair sample in our metallicity history study, we must first check whether there are any dynamical effects on the central metallicities which would complicate correction for aperture effects. In Figure 1 we show the luminosity-metallicity relation for our galaxy pairs (filled circles) as a function of projected separation. Galaxy pairs with close projected separations $s < 20$ kpc/h have systematically lower metallicities (~ 0.2 dex) than either the field galaxies (unfilled circles) or the more widely separated pairs. There are 10 close pairs with metallicities lower than any field galaxy at the same luminosity. The R-band luminosity-metallicity relation produces almost identical results. In Kewley, Geller, & Barton (2005), we show that there is a tight anti-correlation between nuclear metallicity and the strength of the central starburst in the galaxy pairs, such that lower metallicity pairs have greater central burst strengths. This anti-correlation is stronger than that expected from the luminosity-metallicity relation alone. All five galaxies in the pairs sample with extremely high central burst strengths have close companions and lower metallicities than the field galaxies. This result provides strong circumstantial evidence that gas infall has plays an important role in the low metallicity galaxy pair members. This gas infall may carry more pristine gas from the outskirts of the galaxy into the central regions, diluting the central metallicity. Comparison with hydrodynamic merger models supports this

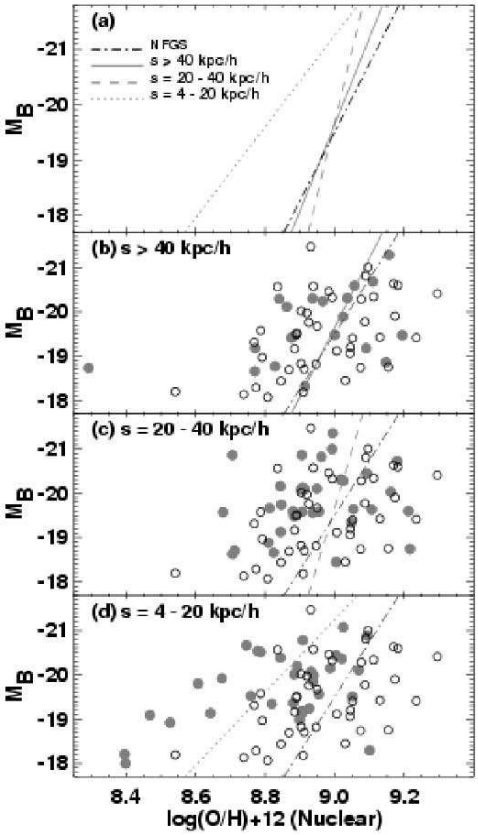

Figure 1. (a) The least squares best-fit to the B-band luminosity metallicity relations for the field galaxies (dot-dashed line), and the pair members with projected separations (s) between 4-20 kpc/h (dotted line), 20-40 kpc/h (solid line), and >40 kpc/h (dashed line), (b-d) comparison between the luminosity-metallicity relation of the field galaxies (unfilled circles) and the galaxy pairs (filled circles) for the three groups of projected separation. The close pairs have a luminosity-metallicity relation shifted more towards lower metallicities than the field galaxies and the more widely separated pairs.

scenario (see Kewley et al. 2005 for more details). Because gas infall appears to affect the central metallicities of galaxy pairs, we cannot simply make an aperture correction to convert our central metallicities into global metallicities needed for our metallicity history study.

3. Metallicity History between $0 < z < 3$

In Figure 2 we give preliminary results of our study into the metallicity history of star-forming galaxies between $0 < z < 3$. The grey rectangle indicates the maximum error range in the intermediate-redshift sample metallicities. This error range is determined by the range in metallicities that could be

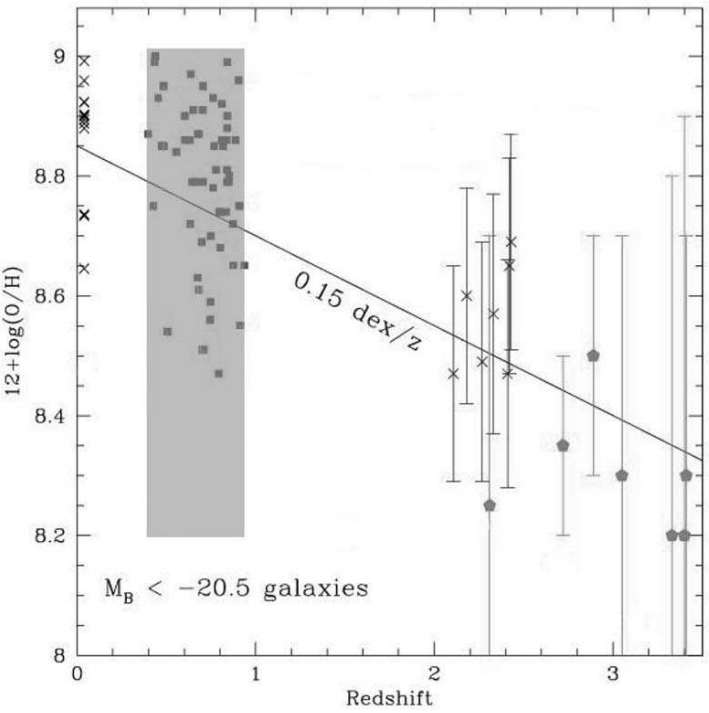

Figure 2. Metallicity evolution for star-forming (emission-line) galaxies between $0 < z < 3$. Crosses, squares, asterixes and hexagons represent the local NFGS sample, the intermediate redshift sample, the high redshift [NII]/Hα sample, and the high redshift R_{23} sample respectively. The grey square indicates the potential error range of the metallicities in the intermediate redshift sample.

derived using the degenerate R_{23} diagnostic. The metallicities for the high redshift sample are shown as asterixes and hexagons on Figure 2. The hexagons indicate that the metallicities were calculated using the R_{23} method while the asterixes indicate that the metallicities were calculated using the [NII]/Hα line ratio.

Figure 2 shows that the mean metallicity decreases with redshift, as anticipated by chemical evolution models of stellar metallicities (e.g., Nagamine et al. 2004, among many others). The line of best-fit to the data in Figure 2 gives a mean change in metallicity of 0.15 dex/z. This estimate should be used with caution: many of the intermediate-redshift galaxy metallicities require confirmation with upcoming observations of a larger number of emission-lines. In our future investigations we will consider emission-line and photometric selection effects which could potentially alter both the mean and spread of the metallicities observed in the intermediate and high redshift samples.

4. Summary

We find that the central metallicities in our close galaxy pairs are systematically lower than metallicities of field galaxies or more widely separated pairs at the same luminosity. This result holds regardless of whether B or R-band luminosities are used. These results support a merger scenario where galaxy interactions cause gas flows towards the central regions, carrying less enriched gas from the outskirts of the galaxy into the central regions, as described in detail in Kewley et al. (2005).

We have provided an initial view of the metallicity history of star-forming galaxies between $0 < z < 3$. In future, we aim to obtain a solid observational understanding of the metallicity history of star-forming galaxies as a function stellar mass.

References

Cardelli, J. A., Clayton, G. C., & Mathis, J. S. 1989, ApJ, 329, 33
Cowie, L. L., Barger, A. J., Hu, E. M., Capak, P., Songaila, A, 2004, AJ, 127, 3137
Davis, M. & Peebles, P. J. M. 1983, ApJ, 267, 465
Jansen, R. A., Franx, M., Fabricant, D., & Caldwell, N. 2000, ApJS, 126, 271
Kewley, L., Dopita, M., Sutherland, R., Heisler, C., & Trevena, J. 2001, ApJ, 556, 121
Kewley, L. J., Geller, M. J., Jansen, R. A., & Dopita, M. A. 2002, AJ, 124, 3135
Kewley, L. J., & Dopita, M. A., 2002, ApJS, 142, 35
Kewley, L. J., Jansen, R. A., & Geller, M. J. 2005, PASP, 117, 227
Kewley, L. J., Barton, E. J., & Geller, M. J. 2005, AJ, *submitted*
Kobulnicky, H. A., & Kewley, L. J. 2004, ApJ, *in press* astro-ph/0408128
Kobulnicky, H., et al. 2003, ApJ, 599, 1009
Kobulnicky, H. A., Koo, D. C. 2000, ApJ, 545, 712
Kobulnicky, H. & Zaritsky D. 1999, ApJ, 511, 908
Lilly, S., Carollo, C., & Stockton, A., 2003, ApJ, 597, 730
Maier, C., Meisenheimer, K., & Hippelein, H. 2004, A&A, 418, 475
Maier, C., Lilly, S., & Carollo, C. M. 2005, astro-ph/0509114
Nagamine, K., Fukugita, M., Cen, R., Ostriker, J. 2001, ApJ, 558, 497
Osterbrock, D. E. 1989, Astrophysics of Gaseous Nebulae and Active Galactic Nuclei (Mill Valley; University Science Books)
Pettini, M., et al. 2001, ApJ, 554, 981
Savaglio, S. et al. 2005, astro-ph/0508407
Shapley, A. E., Erb, D. K., Pettini, M., Steidel, C. C., Adelberger, K. L. 2004, ApJ, 612, 108
Wirth, G. D. et al. 2004, AJ, 127, 3121

THE 11 MPC Hα AND ULTRAVIOLET GALAXY SURVEY

José G. Funes, S.J.[1], Robert C. Kennicutt, Jr.[2], Janice C. Lee[2], Shoko Sakai[3], Christy Tremonti[2] and Liese van Zee[4]

[1] *Vatican Observatory Research Group, University of Arizona, USA*
[2] *Steward Observatory, University of Arizona, USA*
[3] *Division of Astronomy and Astrophysics, UCLA, USA*
[4] *Astronomy Department, Indiana University, USA*

Abstract We introduce 11HUGS (11Mpc Hα and Ultraviolet Galaxy Survey), an outgrowth of the recently completed 11MPC Survey, a ground-based Hα and R-band imaging program of a volume-limited sample of 367 spiral and irregular galaxies within a distance of 11 Mpc. As such, the 11HUGS galaxies are a complete subset of the 11MPC Survey catalog which avoid the Galactic plane ($|b| > 30^{\circ}$) and are observable by GALEX. The goal of 11HUGS is to characterize the demographics and star formation properties of nearby galaxies, with an emphasis on the dwarf galaxies which dominate the sample population. The data also provide a foundation for follow-up studies of the HII region populations, star formation, chemical abundance, and ISM properties of the galaxy sample. The combination of Hα imaging, which provides snapshots of the ongoing star formation, and UV imaging, which traces star formation over a much longer timescale, will yield powerful constraints on the systematic errors in the inferred star formation related quantities.

Keywords: stars: formation - galaxies: dwarf - galaxies: statistics - surveys

1. Introduction

Most of our present knowledge of the star formation properties of nearby galaxies has been derived from imaging, photometry, and spectroscopy of galaxies in the Hα emission line (e.g., Kennicutt 1998 and references therein). However, datasets of complete samples with sufficient sensitivity to trace the full population of star-forming galaxies are lacking and cannot be sewn together from the patchwork of existing Hα surveys. Most of the published studies are biased toward bright, face-on, and/or high-surface brightness systems (Bongiovanni et al. 2005, Gallego et al. 1997, Salzer et al. 2001). A

R. S. de Jong, Island Universes, 441–444.
© 2007 *Springer.*

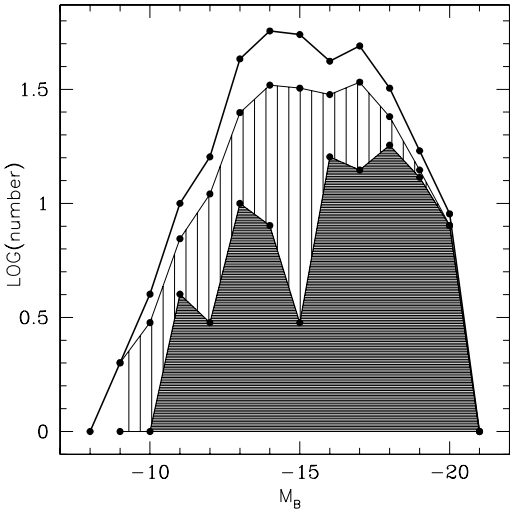

Figure 1. **The 11 HUGS Sample.** The top line shows the distribution of galaxy luminosities for the 11MPC parent sample. The filled histogram shows the coverage of this volume by the GALEX PI team GANGS (GALEX Nearby Galaxies Survey) survey and illustrates the roughly 5-fold under-representation of galaxies fainter than M_B=-17 (note the logarithmic vertical scale). The middle histogram shows the total GALEX coverage of the 11 Mpc local volume galaxy population when our new 11HUGS observations are combined with data from the GANGS survey.

considerable fraction of spiral and irregular galaxies are not detected, and a considerable fraction of star formation is missed.

To address the problem of incompleteness and sensitivity, we have undertaken an Hα and R-band imaging program of the local 11Mpc volume (11MPC Survey, Kennicutt et al., in preparation), with the goal of constructing a more representative dataset for characterizing the distributions of absolute and mass-normalized star formation rates, star formation distributions and intensities, and HII region populations in the local volume.

11HUGS (the 11Mpc Hα and Ultraviolet Galaxy Survey) is an outgrowth of the recently completed 11MPC Survey which will complement the Hα dataset with GALEX UV imaging at 1500Å and 2300Å for a complete subsample of the local 11 Mpc volume. The composite dataset provides a foundation for follow-up studies of star formation, chemical abundance, and ISM properties of the galaxy sample. The combination of Hα imaging, which provides snapshots of the ongoing star formation, and UV imaging, which traces star formation over a much longer timescale ($\sim 10^7$ vs. $\sim 10^8$ yr), will yield powerful constraints on the systematic errors in the inferred star formation related quantities.

2. Sample and Observations

To construct a sample which most closely approximates a volume limited sample, we selected all known spiral and irregular galaxies with $d < 11$Mpc, $|b| > 20^{\circ}$, $B < 15.0$ and a flow-corrected velocity $v < 820km/s$ from the Tully Nearby Galaxies Catalog (Tully 1988, NBG), the Kraan-Korteweg catalog (1986), and the NASA/IPAC Extragalactic Database (NED). After excluding probable Virgo Cluster and Coma Group members and collecting all available direct distance estimates, our resulting catalog contains 367 galaxies within 11 Mpc, where H_o = 75 km/s/Mpc has been adopted to convert flow-corrected velocities to distances for galaxies without direct distance estimates.

Hα+[N II] and R-band imaging for the sample was obtained in 2001 - 2004 using direct imagers on the Steward Observatory Bok 2.3 m telescope on Kitt Peak, the 1.8 m Vatican Advanced Technology Telescope (VATT), and 0.9 m telescope at Cerro Tololo Interamerican Observatory (CTIO).

The galaxies for which GALEX UV imaging will be obtained are a complete subset of the 11MPC Hα Survey catalog which avoid the Galactic plane ($|b| > 30^{\circ}$) and are observable by GALEX (Galaxy Evolution Explorer). GALEX UV observations for approximately half of these objects have been taken by GANGS (GALEX Nearby Galaxies Survey), but dwarf galaxies are underrepresented in the existing data. Our survey will remedy this by obtaining comparably deep (1.5k sec) images for the remaining galaxies in the 11 Mpc volume-limited sample as demonstrated in Fig. 1. The HUGS sample consists of 123 galaxies and the majority of them (84 galaxies) are dwarfs with $M_B \geq -16$. Thus our sample represents a full inventory of spiral and irregular galaxies in the local 11 Mpc volume.

3. A Complete Star-Formation Inventory of the Local Universe

Since the equivalent width (EW) of the observed Hα+[N II] lines, is a measure of the star formation rate per unit (red) luminosity (Kennicutt 1998), the histogram in Fig. 2 shows the range of observed star formation activities for the 11 Mpc limited volume, spanning from EW(Hα+[N II]) $\sim$0 to 580 Å. The distribution has a median of 28 Å.

The 11HUGS archive will provide the most complete dataset ever assembled on the star formation properties of the local universe. All 11HUGS FUV, NUV, Hα and R-band imaging data, as well as a integrated flux and EW catalog, will be made publicly available.

The immediate goal of our program is to study the temporal and spatial properties of starbursts in dwarf galaxies (Janice Lee's PhD Thesis). A complete set of star formation rates for a volume-limited sample can be used to constrain the burst properties of the dwarf population. In addition, our 11MPC

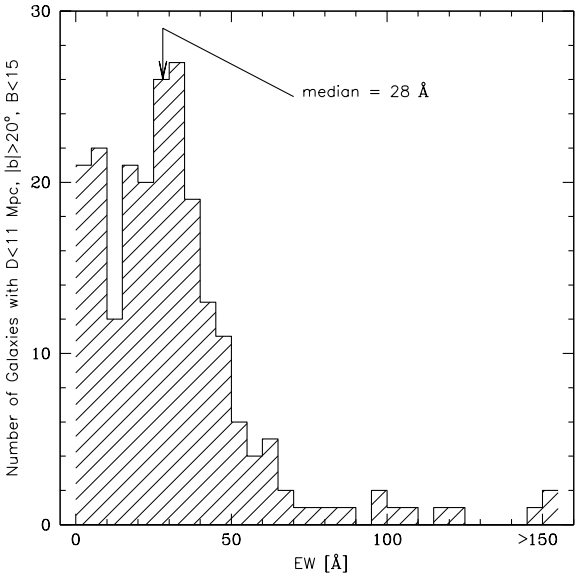

Figure 2. The distribution of observed EW(Hα+[N II]) in the 11MPC sample

and other Hα surveys can be used to explore the demographics of star-forming galaxies and the contribution of starbursts to the cosmic star formation budget (Kennicutt et al. 2005).

Finally, most determinations of the cosmic star formation rates and its evolution with redshift are based on UV or emission-line selected surveys which systematically exclude galaxies with relatively weak or spatially-extended star formation. Our complete inventory will allow to quantify the incompleteness in low-redshift surveys, and model the likely incompleteness at higher redshifts.

References

Bongiovanni, A., Bruzual, G., Magris, G., Gallego, J., Garcia-Dabo, C. E., Coppi, P., & Sabbey, C., 2005, MNRAS, 359, 930

Gallego, J., Zamorano, J., Rego, M., & Vitores, A. G., 1997, ApJ, 475, 502

Kennicutt, R. C., 1998, ARA&A, 36, 189

Kennicutt, R. C., Lee, J. C., Funes, J. G., Sakai, S., & Akiyama, S. 2005, ASSL Vol. 329: Starbursts: From 30 Doradus to Lyman Break Galaxies, 187

Kennicutt, R.C., Lee, J.C., Funes, J.G., Sakai, S., Akiyama, S., in preparation

Kraan-Korteweg, R. C., 1986, A&AS, 66, 255

Salzer, J.J., Gronwall, C., Lipovetsky, V.A., Kniazev, A., Moody, J.W., Boroson, T.A., Thuan, T.X., Izotov, Y.I., Herrero, J.L., & Frattare, L.M., 2001, AJ, 121, 66

Tully, R.B., 1988, Nearby Galaxies Catalog, Cambridge: CUP

CONTINUOUS STAR CLUSTER FORMATION IN THE SPIRAL NGC 45

Marcelo Mora[1], Søren S. Larsen[2] and Markus Kissler-Patig[1]

[1]*ESO Garching, Germany*
[2]*ESO / ST-ECF, Germany*

Abstract We determined ages for 52 candidate star clusters with masses $\leq 10^6\ M_\odot$ in the low surface brightness spiral galaxy NGC 45. Four of these candidates are old globular clusters located in the bulge. The remaining ones span a large age range. The cluster ages suggest a continuous star/cluster formation history without evidence for bursts, consistent with the galaxy being located in a relatively unperturbed environment in the outskirts of the Sculptor group.

Keywords: galaxies: star clusters - galaxies: evolution - galaxies: starburst - galaxies: dwarf

1. Introduction

Star clusters are an ideal tool to study star formation histories in nearby galaxies. Historically, star clusters have been studied in the Milky Way, Local Group, ellipticals, mergers and starbursts. But there are only few studies in low luminosity galaxies. The closest examples with similar luminosity to NGC 45 are LMC, SMC, and M33 (e.g., Côté et al. 1997). Star clusters in these galaxies show different star formation histories. The LMC shows 3 bursts of star formation (Pietrzynski & Udalski 2000), while the SMC shows a more uniform star cluster formation history. M33 also shows a continuous star cluster formation (Chandar et al. 1999). But beyond the Local Group, the properties of cluster populations and star formation in general are poorly known in normal galaxies. NGC 45 is an interesting galaxy: it is an outlying member of the Sculptor group with (m-M)=28.42 ± 0.41 (Freedman et al. 1992), it is located in an unperturbed environment, and it has a low luminosity of M_B=-17.13 (Bottinelli et al. 1985). In the presented work in progress, we study the star formation history of this spiral galaxy by looking at the NGC45 star cluster system.

R. S. de Jong, Island Universes, 445–448.
© 2007 *Springer.*

2. Observations

In our study we used HST ACS and WFPC2 data. We acquired the images using the filters F435W (∼B), F555W (∼V), F814W (∼I) and F336W (∼U). The object detection was performed using SExtractor. The aperture photometry of 6 pixels radius was done using the IRAF/PHOT task. We selected our cluster candidates by looking at the physical object sizes. For this purpose we used two criteria. We selected cluster candidates as objects with extended FWHM according to SExtractor and as well as with extended FWHM according to BAOLAB ISHAPE (Larsen 1999). Fiftytwo "round", extended objects satisfied the criteria and were treated as star clusters.

3. Color Magnitude Diagram

The color-magnitude diagram (Figure 1) shows two main cluster populations: a red one around F435W−F555W∼0.7 (likely globular clusters) and another, broader distribution around F435W−F555W∼0, which are likely young cluster candidates.

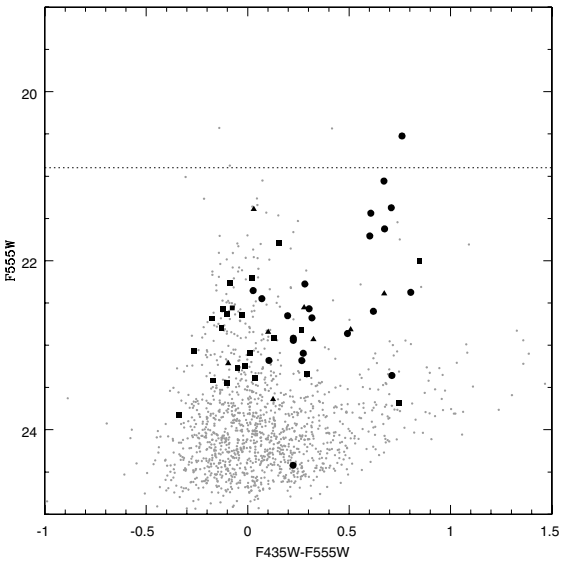

Figure 1. NGC 45 color magnitude diagram. Here we plot objects with *UBVI* photometry. Approximately 3400 stars are shown (black dots) and 52 star cluster candidates. Filled squares correspond to a 1-10 Myr cluster population, filled triangles to cluster age 10-100 Myr and filled circles to cluster age 100-1000 Myr (for age derivation see below). The dashed line is the TO of the old MW globular cluster system $M_{VTO} \sim -7.4$.

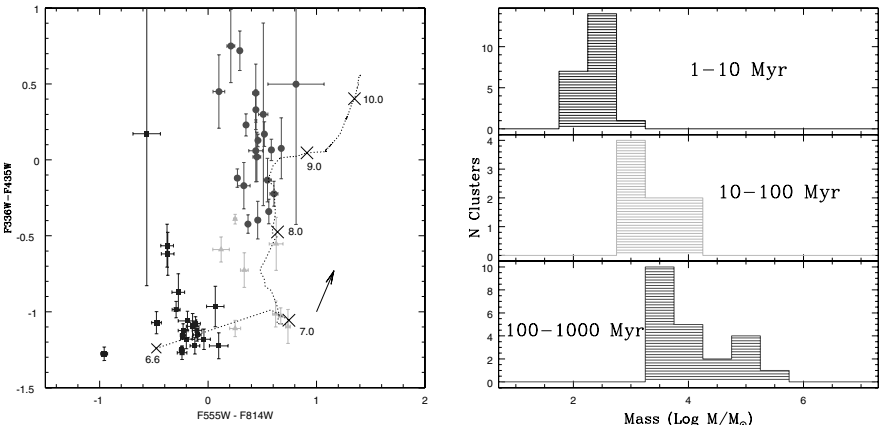

Figure 2. Left: color-color diagram of the cluster candidates . Filled circles are clusters with ages 100 Myr -1 Gyr. Triangles are the clusters with intermediate ages: 10 to 100 Myr. And the third group (filled squares) is younger than 10 Myr. The dashed line is the SPP GALEV model for a Salpeter IMF and a solar metallicity (Z=0.02), for ages 1 Myr to 10 Gyr (The crosses indicates the log of the age). Right: Mass distribution as a function of age. Each bin corresponds to 0.5 Log $M/M_{\odot}$.

4. Color-Color Diagram: Ages and Masses

One of the principle problems in deriving ages, metallicities and masses for star clusters in spirals, is the fact that we do not know the extinction towards the individual objects. Bik et al. (2003) proposed a method known as the 3D fitting method to solve this problem. It consists in minimizing the extinction, mass and age for each single cluster using a SSP model (in our case: GALEV, Anders & Fritze-v. Alvensleben 2003) assuming a fixed metallicity. We apply this method to our dataset assuming a solar metallicity for all clusters.

The color-color diagram in Figure 2 (left plot) shows all the star clusters corrected for reddening. We use the same symbols as in Figure 1. The arrow indicates the reddening corresponding to a 1 magnitude extinction in *V*. A theoretical SSP model track for ages between 1 Myr and 10 Gyr and a solar metallicity is also shown in dashed line. The clusters are distributed across the theoretical track and show an age distribution without signatures of discrete bursts. The estimated masses of the clusters are shown in the right part of Figure 2 for three age bins. The upper part shows 22 clusters between 1–10 Myr old, the middle part 8 clusters between 10–100 Myr and the lower part shows 22 clusters between 100–1000 Myr. Before drawing conclusions about the mass distributions, it is necesary to take size-of-sample effects into account (Larsen 2002; Whitmore 2003). Due to the small number of clusters in each age bin, the likelihood of sampling the cluster mass distributions to significantly higher masses than those observed is low. This makes it

difficult to tell whether a physical upper mass limit exists. Furthermore, the ages of the clusters in the oldest bin are particularly uncertain because of the age-metallicity degeneracy in optical broad-band colors. This also translates into an uncertainty on the derived masses. Here we have used solar-metallicity SSP models, but the colors of the reddest clusters are also consistent with an old, metal-poor GC population. A more detailed discussion of these issues will be given in Mora et al. (in preparation). Considering this, we can say that younger clusters are in general less massive than older ones and there are no massive young clusters. There are more massive clusters at intermediate and old ages when compared to the youngest bin. No clusters more masive than 10^6 $M_\odot$ are observed.

5. Summary and Conclusions

The color magnitude diagram shows two main cluster populations, which are in concordance with an old (≥ 1 Gyr) globular cluster-like population and younger objects more similar to the open clusters in the Milky Way. Most of the latter have young (≤ 100 Myr) ages. This age distribution is possibly due to cluster disruption and fading.

The existence of intermediate-age clusters is deducted from the color-color diagram. This shows that NGC 45 is a galaxy with continuous star formation history.

The mass distribution as a function of age shows that more massive clusters are in general older than the less massive. This is also observed in M33 and both galaxies also show similar cluster mass ranges (between 10^2 $M_\odot$ up to $10^5 M_\odot$) (Chandar et al. 1999).

The role of size-of-sample effects needs to be further investigated.

Finally NGC 45 provides evidence that unperturbed low luminosity spiral galaxies can show continuous cluster formation.

References

Anders, P. & Fritze-v. Alvensleben, U. 2003, A&A 401, 1063

Bik, A., Lamers, H. J. G. L. M., Bastian, N., Panagia, N. & Romaniello, M. 2003, A&A 397, 473

Bottinelli, L., Gouguenheim, L., Paturel, G.& de Vaucouleurs, G. 1985, ApJS 59, 293

Chandar, R., Bianchi, L. & Ford, H.C. 1999, ApJ 517, 668

Côté, S., Freeman, K.C., Carignan, C., & Quinn, P. J. 1997, AJ 114, 1313

Freedman, W., Wendy L., Madore B.F., et al., 1992 ApJ 396,80

Larsen, S.S. 1999, A&A 354,836

Larsen, S.S. 2002, AJ 124,1393

Pietrzynski, G. & Udalski, A. 2000, AcA 50, 337

Whitmore, B.C. 2001 STScI Symp. 14 A Decade of *HST* Science, ed. M.Livio, K.Noll, & M. Stiavelli

HST / STIS RESULTS ON NUCLEAR STAR CLUSTERS IN SPIRAL GALAXIES

Joern Rossa[1], Roeland P. van der Marel[1], Torsten Böker[2], Joris Gerssen[3], Luis C. Ho[4], Hans-Walter Rix[5], Joseph C. Shields[6] and Carl-Jakob Walcher[5]

[1]*Space Telescope Science Institute, Baltimore, USA*

[2]*Astrophysics Division, ESTEC, Noordwijk, The Netherlands*

[3]*Department of Physics, University of Durham, United Kingdom*

[4]*Observatories of the Carnegie Institution of Washington, Pasadena, USA*

[5]*Max-Planck-Institut fuer Astronomie, Heidelberg, Germany*

[6]*Department of Physics and Astronomy, Clippinger Research Laboratories, Ohio University, Athens, USA*

Abstract Recent HST imaging surveys have revealed the presence of central star clusters in a majority of spiral galaxies. These nuclear clusters (NCs) may provide important clues to the central structure and secular evolution of disk galaxies. However, their origin and nature are not entirely understood. We therefore performed a spectroscopic survey with HST/STIS of NCs in 40 early- and late-type spiral galaxies. To study the ages and physical properties of the clusters we performed stellar population synthesis modeling using Bruzual-Charlot template spectra. The luminosity-weighted NC ages are almost always less than a Hubble time, indicating that star formation is an ongoing process in spiral galaxy centers. We find that NCs in late-type spirals are younger and less massive than those in early-type spirals.

Keywords: galaxies: spiral - galaxies: star clusters - galaxies: nuclei - galaxies: evolution

1. Introduction

Previous HST/WFPC2 imaging surveys have revealed that many spiral galaxies harbor nuclear star clusters (NCs) in their central regions (Böker et al. 2002; Carollo et al. 1998). These NCs have typical effective radii of 2.4 to 5 pc (Böker et al. 2004) with typical luminosities of 10^6 to $10^7\,L_\odot$. NCs are thought to form from gas inflows into galactic centers. Their origin and evolution thus must be tightly linked to phenomena of secular evolution (Kormendy & Kennicutt, 2004) and to the growth of supermassive black holes. Therefore, NCs provide an exciting new perspective in the study of galaxy centers.

R. S. de Jong, Island Universes, 449–452.
© 2007 *Springer.*

We present new results of a spectroscopic survey of NCs in both early- and late-type spirals based on HST/STIS observations. We observed 40 galaxies of Hubble T-type 1-9 (Sa to Sm) to determine the ages and masses of their NCs. While previous ground-based spectroscopic observations with higher S/N have already been applied in similar studies (Walcher et al. 2005b), HST's spatial resolution decreases the contamination from disk light compared to ground-based studies. This is particularly important in early-type spirals with prominent bulges.

2. Sample Selection and Observations

The spectroscopic sample comprises galaxies from previous HST/WFPC2 imaging surveys. Fifteen early-type spirals were selected from the survey of Carollo e al. (1998), which used the following selection criteria: T=1-6, $v \leq 2500\,\mathrm{km\,s^{-1}}$, $i \leq 75^\circ$, and $d \leq 1'$. In addition, 25 late-type spirals were selected from the survey of Böker et al. (2002), which used the selection criteria: T=6-9, $v \leq 2000\,\mathrm{km\,s^{-1}}$, $i \leq 51^\circ$. We only observed those galaxies with known NCs, and selected only those NCs believed to be bright enough for useful spectroscopy.

Our observations were performed with the HST/STIS G430L grating, using the $52'' \times 0.2''$ slit, and with a pixel scale of $0.05071''$. The covered wavelength range is $\lambda\lambda$2888.6-5703.2 Å. The pixel scale is 2.73 Å. The exposure times varied from 900-2340 seconds. Some representative spectra are shown in Figure 1.

3. Results and Conclusions

We performed stellar population synthesis by fitting a linear sum of single-age population templates of Bruzual & Charlot (2003) to those NC spectra with sufficiently high S/N ≥ 5 per pixel (see Figure 1). The fractions of NCs which were fitted was 10/15 (early-type) and 9/25 (late-type). The fits yield luminosity-weighted ages and M/L values. Combined with the observed luminosity L, also calculated from the STIS spectra, we infer the cluster mass M. The analysis also yields the best-fit metallicity (Z) and dust extinction (A_V). Tests show that the derived ages are relatively insensitive to possible systematic uncertainties in Z and A_V.

The distributions of the inferred population ages and NC masses are shown separately for the early- and late-type spirals in Figure 2. The mean luminosity-weighted age of the NCs is 2.3×10^8 years for the late-type sample and 1.7×10^9 years for the early-type sample. This is younger than the galaxies themselves, indicating that star formation is an ongoing process in the nuclei of spiral galaxies, especially those of late-type. The NC differences as a function

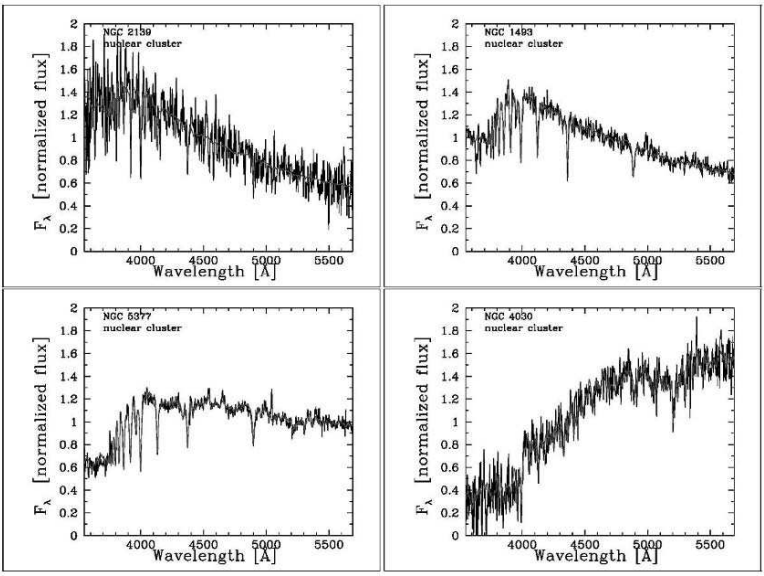

Figure 1. HST/STIS spectra of the NCs (black), overlaid with the best spectral-population synthesis fits (red). The spectra are sorted (from left to right and from top to bottom) in order of increasing luminosity-weighted age $\langle \log \tau \rangle_L$ (6.97, 7.74, 8.63, 9.83, respectively). The galaxy names are indicated in the individual sub-panels.

of Hubble type are not unexpected, given that late-type spirals generally have larger gas reservoirs and more star formation than early-type spirals.

The derived NC masses are consistent with those inferred dynamically from VLT velocity dispersion measurements, for those four late-type galaxies in common between our STIS sample and the Walcher et al. (2005a) VLT sample. The mean mass of the NCs is $1.8 \times 10^6\,\mathrm{M}_\odot$ for our late-type sample and $4.3 \times 10^7\,\mathrm{M}_\odot$ for our early-type sample. The fact that NCs in early-type spirals tend to be more massive than those in late-type spirals suggests a possible correlation with bulge mass. This is intriguing, especially given the fact that such a correlation is known to exist for black holes in galaxy centers.

We have also derived broadband magnitudes from our STIS spectra, and calculated $B-V$ colors. These allow us to gain some insight into the populations of NCs that are too faint for population synthesis. We find that faint clusters tend to be somewhat redder than bright clusters. This suggests that their populations may on average be older by up to 0.6 dex than the average ages inferred from the histograms in Figure 2. However, combined analysis of both the luminosities and colors of NCs does not indicate that faint clusters are necessarily less massive than bright clusters. Therefore, the mass distributions in Figure 2 are probably fairly representative for all NCs in spiral galaxies. More details of our STIS investigations of NCs will be presented in Rossa et al. (2006).

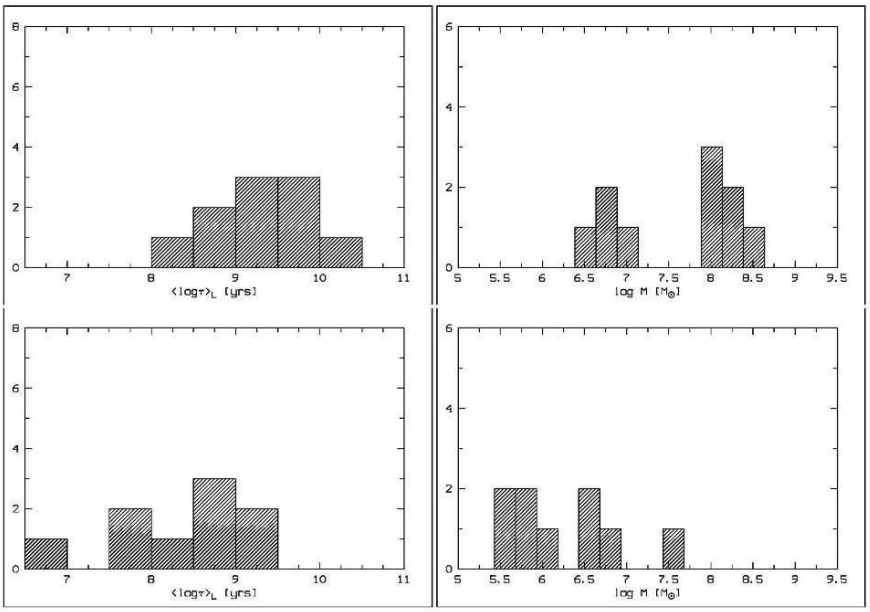

Figure 2. Histograms of the derived luminosity-weighted ages (left) and calculated masses (right). The top panels represent the early-type sample, whereas the bottom panels show the late-type sample.

Acknowledgements Support for proposals #9070 and #9783 was provided by NASA through a grant from the STScI, which is operated by the AURA, Inc., under NASA contract NAS 5-26555.

References

Böker, T., Laine, S., van der Marel, R. P., Sarzi, M., Rix, H.-W., Ho, L. C., & Shields, J. C. 2002, AJ, 123, 1389

Böker, T., Sarzi, M., McLaughlin, D. E., van der Marel, R. P., Rix, H.-W., Ho, L. C., & Shields, J. C. 2004, AJ, 127, 105

Bruzual, G., & Charlot, S. 2003, MNRAS, 344, 1000

Carollo, C. M., Stiavelli, M., & Mack, J. 1998, AJ, 116, 68

Kormendy, J., & Kennicutt, R. C., Jr. 2004, ARA&A, 42, 603

Rossa, J., van der Marel, R.P., Böker, T., Gerssen, J., Ho, L. C., Rix, H.-W., Shields, J. C., & Walcher, C. J. 2006, AJ, submitted

Walcher, C. J., van der Marel, R. P., McLaughlin, D., Rix, H.-W., Böker, T., Haering, N., Ho, L. C., Sarzi, M., & Shields, J. C. 2005a, ApJ, 618, 237

Walcher, C. J., Charlot, S., Rix, H.-W., Böker, T., Ho, L. C., van der Marel, R.P., Rossa, J., & Shields, J. C. 2005b, ApJ, submitted

ISLAND UNIVERSES COLLIDING

L. Snijders* and P.P. van der Werf**

Leiden Observatory, The Netherlands

* snijders@strw.leidenuniv.nl, ** pvdwerf@strw.leidenuniv.nl

Abstract Galaxies do not spend their whole lives in isolation. In fact, interactions and merger events are very important in galaxy evolution, even more so at high redshift, where the number-density of galaxies was considerably higher than it is today. These encounters often trigger a burst of star formation. We use high spatial resolution mid-infrared observations of nearby starburst galaxies to develop a detailed understanding of this starburst phenomenon and the resulting stellar populations. The issues addressed are the properties of superstarclusters, the nature of extreme star formation in (Ultra) Luminous Infrared Galaxies ((U)LIGs), and the characteristics of nuclear starburst rings in barred galaxies. In this paper we present the first mid-infrared imaging and spectroscopy obtained with VISIR at the ESO Very Large Telescope.

Keywords: galaxies: starburst - infrared: galaxies - galaxies: star clusters - galaxies: individual (NGC 4038/39)

1. Introduction

Starburst galaxies find themselves in a phase of rapid evolution. The rate at which their gas reservoir is turned into stars cannot be maintained for long, which makes the starburst phase per definition a transient one. The presence of bright coeval stellar populations makes starbursts unique laboratories for the study of star formation, stellar populations, and galaxy evolution, where it concerns the buildup of its stellar content.

Starbursts are generally dusty, hiding the most intense star-forming regions from view in the optical regime. For instance in the Antennae (NGC 4038/39), the ISO satellite revealed that a region that is totally inconspicuous in the HST images hosts spectacular star formation producing 15% of the 15 μm luminosity of the entire galaxy (Mirabel et al. 1998). The (mid-)infrared, in which one is less hindered by extinction, is therefore a suitable wavelength range to identify and study these obscured sites. We use the recently commissioned VLT Imager and Spectrometer for mid Infrared (VISIR) to study a sample of nearby starbursting systems. VISIR offers a large set of imaging filters and

R. S. de Jong, Island Universes, 453–456.
© 2007 *Springer.*

spectroscopic setups covering the N- and Q-band (8 – 13 and 16.5 – 24.5 μm respectively) and by combining imaging in diverse filters with spectroscopy we will be able to measure the properties of the star-forming regions in these galaxies.

2. Some Results: Heavily Embedded Star Formation in the Antennae

Most of the current massive star formation in NGC 4038/39 is known to occur in the overlap region (Mirabel et al. 1998). Imaging of this region in the [NeII] filter (see Fig. 1) directly shows the value of a ground-based mid-infrared instrument mounted on a large telescope. The extended structure of complex 1 (cluster 1a & 1b) has not been seen before. At shorter wavelengths only one of the clusters is visible, the other is hidden from view by extinction, and at longer wavelengths most instruments lack spatial resolution to separate the two clusters. Relative astrometry strongly suggests that cluster 1a can be associated with the bright south-eastern cluster in the overlap region seen in the near-infrared (Mengel et al. 2005) and with the reddened source WS95-80 in HST images (Whitmore & Schweizer 1995). Cluster 1b does not have a near-infrared or optical counterpart. This previously unidentified, heavily extincted cluster is probably responsible for a significant amount of the total infrared luminosity of the overlap region. This could explain why previous attempts to reconstruct the total infrared luminosity of this region based on near-infrared data did not succeed (Mengel et al. 2005). Convolving the [NeII] image with the VLA beam of the radio data by Neff (Neff & Ulvestad 2000) reproduces the location of the brightest radio peak, suggesting that both clusters contribute significantly to the radio emission.

The VISIR N-band spectra (see Fig. 1) look as one would expect for regions of massive star formation: strong fine structure lines, a rising continuum characteristic for thermal emission from hot dust, and silicate absorption indicating the presence of obscuring matter. Near-infrared data suggest that these clusters have ages younger than 6 Myr (Gilbert et al. 2000; Mengel et al. 2005). The presence of strong [SIV] emission in the mid-infrared spectra confirms that these clusters are young. An important question is whether the HII regions surrounding the clusters are hydrogen- or dust-bounded (i.e., a HII region so young and compact that dust absorbs most of the Lyman continuum). Assuming the regions to be hydrogen-bounded, line ratio's indicate an age of 6 Myr $\pm$ 1 Myr for cluster 1a and 5.5 $\pm$ 1 Myr for cluster 2 (assuming a standard IMF). In the dust-bounded scenario it is less straightforward to interpret the observed line ratio's. The actual age of the clusters is even younger in this case.

Besides obvious similarities there are some remarkable differences from previous observations of the same regions by ISO (Mirabel et al. 1998) and

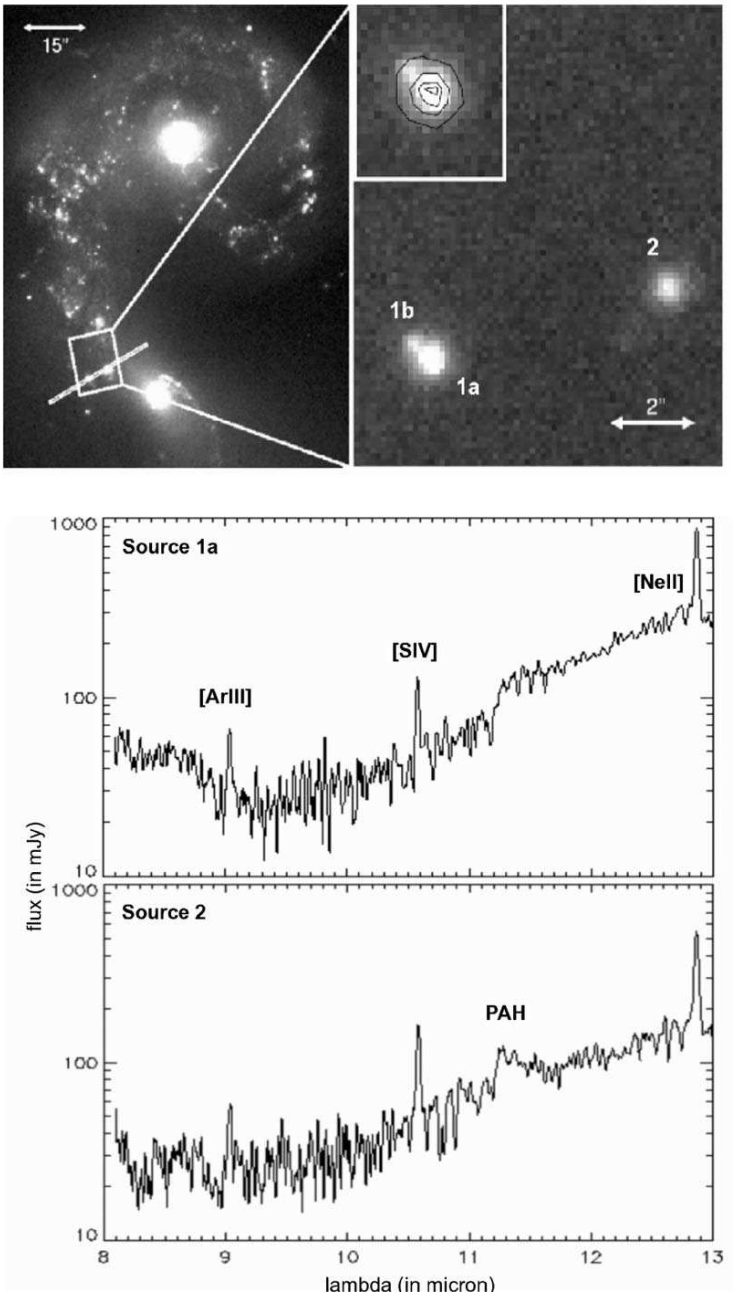

Figure 1. Images: left panel: SoFI Ks-band (2.16 μm); right panel: VISIR [NeII] 12.81 μm of the overlap region, inserted panel: cluster 1a and 1b in [NeII] with the contours of PAH 11.25 μm emission overlayed. Spectra: upper panel: low resolution N-band spectrum of cluster 1a; lower panel: idem cluster 2.

Spitzer (Brandl, private communication). The most striking difference is the strength of the PAH features. Where the ISO and Spitzer spectra of the region around cluster complex 1 show a pronounced 11.3 μm PAH-feature, the VISIR spectrum only shows a hint of it.

The absence of strong PAH emission is also confirmed by N-band imaging in the PAH 11.25 μm filter. The spectral slope derived from flux densities measured in the narrow-band PAH and [NeII] reference filters is consistent with the slope in the VISIR spectrum. We extrapolate this slope to derive the continuum flux level at the centre of the PAH filter. Subtraction of this continuum flux level from the measured flux density in the PAH imaging filter gives the contribution from PAH emission. Measured in an aperture with the same size as the spectrum extraction aperture, the value is consistent with having little to no PAH emission. Only in larger radii apertures some PAH emission is measured: within a region with a 100 pc radius the PAH emission adds up to $2.0 \pm 0.7 \cdot 10^{-13}$ erg/s/cm^2. This is roughly half of the flux measured in the Spitzer (5 arcsec) slit covering an area with a radius of 500 pc. Our preliminary conclusion is that the PAH emission does not trace the most massive, recent star formation, but the more diffuse material, illuminated by UV radiation from a slightly more evolved, less massive and possibly more widespread population of young stars. The preliminary results show that VISIR, due to the unprecedented spatial resolution in the mid-infrared, is an excellent tool to use in detailed studies of nearby star formation sites.

We will use our VISIR data combined with Spitzer mid- and far-infrared, SCUBA submm, and high resolution radio data to model the characteristics of the star-forming regions in these and other galaxies in detail and further investigate the issues mentioned here.

References

Gilbert, A. M., Graham, J. R., McLean, I. S., Becklin, E. E.; Figer, D. F., Larkin, J. E., Levenson, N. A., Teplitz, H. I., Wilcox, M. K, 2000, AJ, 533, L57

Mengel, S., Lehnert, M. D., Thatte, N., Genzel, R., 2005, A&A (astro-ph/0505445)

Mirabel, I. F., Vigroux, L., Charmandaris, V., Sauvage, M., Gallais, P., Tran, D., Cesarsky, C., Madden, S. C. & Duc, P.-A., 1998, A&A, 333, L1

Neff, S. G., Ulvestad, J. G., 2000, AJ, 120, 670

Whitmore, B. C. and Schweizer, F., 1995, AJ, 109, 960

ENVIRONMENTAL DEPENDENCE OF STAR FORMATION IN CLUSTER AND FIELD GALAXIES

Claire Thomas*, Phil James and Chris Moss

Astrophysics Research Institute, Liverpool John Moores University, UK

* cft@astro.livjm.ac.uk

Abstract The properties of local star forming galaxies, in both clusters and the field, can aid understanding of the environmental dependence of galaxy formation and evolution. We present initial results from an Hα survey of all Sa-Sc CGCG galaxies, with velocities within 3σ of the cluster mean, in six local Abell clusters, down to a limiting magnitude of M_B = -18.5. We also have a substantial field sample taken from the recent Hα Galaxy Survey (HαGS, James et al. 2004).

We confirm the result of Koopmann & Kenney (2004) that, compared to the field, cluster early-type spirals have a wider spread in bulge to disk ratio, with many having smaller such values. We see both enhanced and reduced star formation (SF) within our cluster sample; however, Hα emission is generally more concentrated in cluster galaxies than the field. We suggest that a significant effect of the cluster environment is an enhancement of SF in inner galaxy regions.

Keywords: stars: formation – galaxies: clusters: general – galaxies: evolution – galaxies: interactions – galaxies: spiral

1. Introduction

Comparison of the morphology-density relations at intermediate redshift and in the local Universe (e.g., Dressler 1997) shows an overabundance of spiral galaxies (by a factor of 2) and an underabundance of S0s (by a factor 2–3) in clusters at $z \gtrsim 0.4$ compared to today. This suggests that a large number of cluster spirals may have transformed into S0s in the past $\sim$5 Gyr.

A variety of possible physical mechanisms may be involved, which will have different effects on SF in spirals as they enter the cluster environment. For example, gas stripping (e.g., Gunn & Gott 1972), in particular ram-pressure stripping, should be most effective in the centres of rich clusters, leading to a rapid truncation of the star forming disk, but providing no obvious mechanism to promote circumnuclear SF. Strangulation (e.g., Larson, Tinsley & Caldwell 1980), on the other hand, is a more gradual process, and simulations by Bekki

R. S. de Jong, Island Universes, 457–460.
© 2007 *Springer.*

et al. (2002) have shown that this leads to anemic spirals rather than truncation. Tidal interactions with the cluster potential may induce SF across both bulge and disk, whereas interactions between galaxies, particularly at low relative velocities, may trigger SF in central regions (Kennicutt et al. 1998).

A study of the amount, distribution and morphological dependence of SF in local field and cluster spirals can help to disentangle these processes and provide a better insight into the influence of environment on galaxies today.

2. Data & Analysis

Our data consist of narrow-band Hα and broad R band CCD images for $\sim$ 240 CGCG galaxies selected from an Hα prism survey by Moss & Whittle (2000, 2005), to a limiting magnitude M_B = -18.5, and with velocities within 3σ of the cluster mean. We also have considerable field data taken from HαGS, covering the same range of galaxy morphologies as the cluster sample.

Here we present preliminary results from a complete sample of all Sa–Sc galaxies in six clusters (A400, 426, 569, 779, 1367, 1656). We restrict cluster galaxies to within 1 virial radius of the cluster centres, to reduce field contamination, and avoid the large errors associated with observations of highly inclined objects by restricting our sample to galaxies with a/b $\leq$ 4.0. We have also excluded known AGN from our analysis, as Hα emission does not provide a direct tracer of SF in these objects.

From our data we derive profiles of R band flux density, Hα flux and Hα equivalent width (EW) vs. semi-major axis for each galaxy, in both the cluster and field samples. Following the methods of Koopmann & Kenney (KK, 2004a,b), we define an outer isophotal radius, r_{24}, at 24 mag arcsec^{-2} in the R band, which allows us to normalise profiles of galaxies of different sizes and distances. We use an R band concentration index, C30, defined as

$$C30 = \frac{F_R(0.3r_{24})}{F_R(r_{24})} \tag{1}$$

which provides a quantitative measure of bulge to disk ratio, and an Hα concentration index, CHα, which is defined similarly as

$$CH\alpha = \frac{F_{H\alpha}(0.3r_{24})}{F_{H\alpha}(r_{24})} \tag{2}$$

We also use an effective radius, r_{eff}, which contains half of the R band flux of the r_{24} isophote.

3. Amount & Distribution of Star Formation

In Fig. 1 we have plotted total EW vs. T-type for field (a) and cluster (b) galaxies. Using a biweight estimator, we find the mean and standard deviation

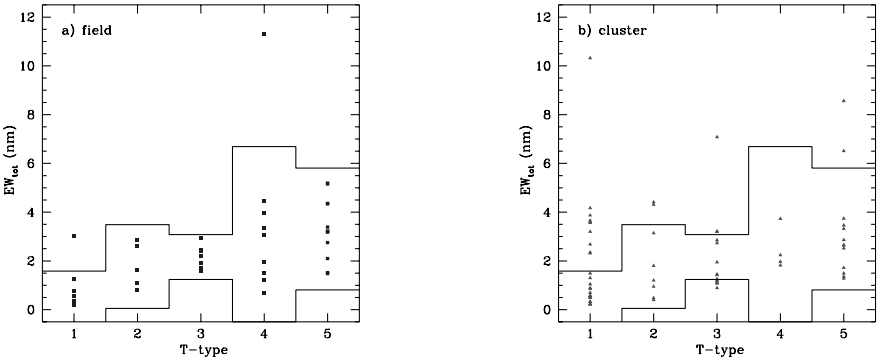

Figure 1. EW$_{tot}$ vs. T-type for full field (a) and cluster (b) samples. The solid lines show 2σ error bars for the field sample, calculated using a biweight estimator. 30% of the cluster sample lie beyond 2σ.

for the field sample and plot 2σ error bars. We would expect 5% of points to lie beyond 2σ, and this is the case for the field data. However, 30% of the cluster points lie beyond 2σ, suggesting different populations at the 4-5σ level.

The majority of the cluster points beyond 2σ have Hα EWs higher than those seen in the field. This suggests that, although cluster galaxy SF appears reduced in the median, the cluster environment is causing an enhancement of SF activity in some galaxies.

Figure 2 shows CHα vs. C30 for field and cluster galaxies. We find some evidence that SF may be more centrally concentrated in cluster galaxies than in the field, as suggested by KK, particularly at low values of C30 ($\lesssim 0.45$). 39% of our cluster sample have more than half of their Hα emission within 0.3 r_{24}, compared to only 20% of field galaxies. A KS test, however, suggests that the CHα distributions are different at only the 2σ level.

We find that C30, and therefore bulge to disk ratio, does not correlate well with T-type for our cluster sample, in agreement with the findings of KK, particularly for early type Sa-Sab galaxies, which span the full range of C30.

4. Cluster Galaxy Evolution

To try to understand how and where SF varies between field and cluster galaxies, we take a field galaxy at random and match it by T-type and absolute magnitude to a single cluster galaxy. We can then find the difference in EW$_{eff}$/EW$_{tot}$, a measure of the concentration of SF, and EW$_{tot}$, a measure of overall SF activity.

Figure 3 shows the results for field matched to cluster galaxies, with the dashed lines showing no change for each direction. Some 66% of the points lie above the no concentration change line, suggesting that star formation may generally be more concentrated in clusters. The majority of the field-cluster points lie within the 2σ ellipse shown, however, there is also a significant (>4σ)

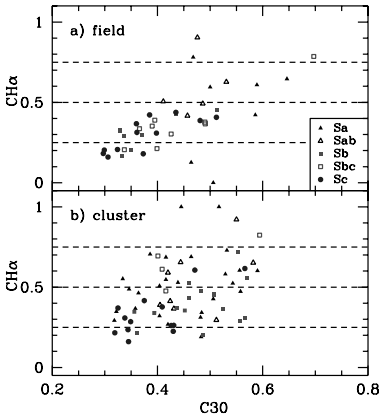

Figure 2. CHα vs. C30 for field and cluster galaxies. Dashed lines show $\frac{1}{4}$, $\frac{1}{2}$ and $\frac{3}{4}$ of Hα emission within 0.3 r_{24}.

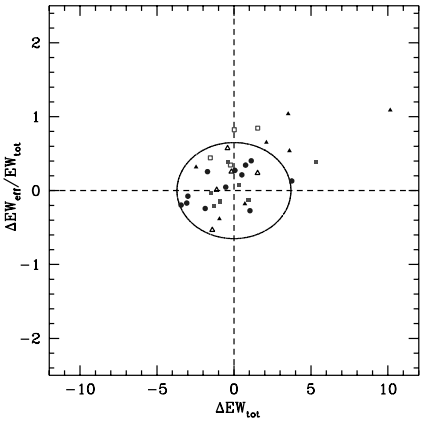

Figure 3. Difference in EW$_{eff}$/EW$_{tot}$ and EW$_{tot}$ for matched field-cluster galaxy pairs. Ellipse shows 2σ scatter for field-field sample.

population of cluster galaxies beyond 2σ, to the top right of the plot, which appear to be experiencing enhanced SF in their central regions.

5. Conclusions

We have a complete sample of Sa-Sc galaxies in six low redshift clusters, identified from an objective prism survey by Moss & Whittle, and a well matched comparison sample from HαGS. From these data we find that:

- C30, and therefore B/D, does not correlate well with T-type for cluster galaxies, with many early type galaxies having small B/D.
- Total EWs span a wider range for cluster galaxies, with both enhanced and reduced SF seen within our sample.
- Hα emission is generally more concentrated in cluster galaxies than the field. This is likely due to an enhancement of SF in inner galaxy regions.

References

Bekki K., Couch W. J. & Shioya Y., 2002, ApJ, 577, 651
Dressler A. et al., 1997, ApJ, 490, 577
Gunn J. E. & Gott J. R. I., ApJ, 1972, 176, 1
James P. A. et al., 2004, A&A, 414, 23
Kennicutt R. C., Schweizer F., Barnes J. E., Friedli D., Martinet L., Pfenniger D. 1998, Saas-Fee Advanced Course 26: Galaxies: Interactions and Induced Star Formation
Kennicutt R. C., 1998, ARA&A, 36, 189
Koopmann R. A. & Kenney J. D. P., 2004, ApJ, 613, 851
Koopmann R. A. & Kenney J. D. P., 2004, ApJ, 613, 866
Larson R. B., Tinsley B. M. & Caldwell C. N., 1980, ApJ, 237, 692
Moss C. & Whittle M., 2000, MNRAS, 317, 667
Moss C. & Whittle M., 2005, MNRAS, 357, 1337

VII

DISK GALAXIES THROUGH COSMIC TIME

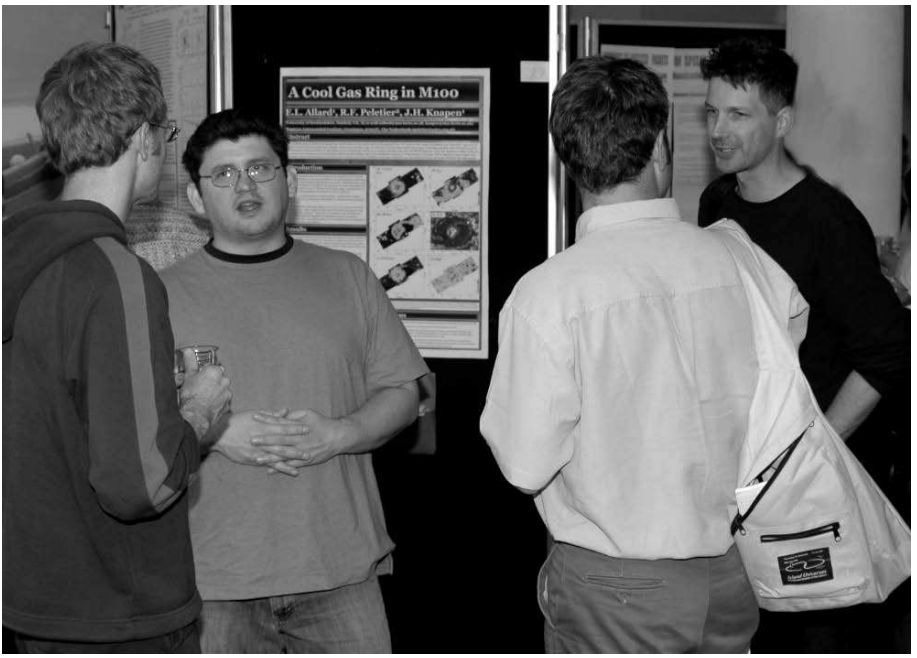

Scott Chapman, Bob Abraham, Benne Holwerda, and Roelof de Jong.

DISKS AT HIGH REDSHIFTS

What we see and when do we see it? What don't we see and why not?

Roberto G. Abraham

Department of Astronomy & Astrophysics, University of Toronto, Canada
abraham@astro.utoronto.ca

Abstract I review the observational evidence for massive disks at high redshifts. In an attempt to do something a little bit different, I will focus exclusively on galaxies at redshifts $z > 1$, where much of the action seems to be happening, but where our ignorance is particularly acute. To keep the discussion concrete, I pay particular emphasis to seven key papers (the 'Magnificent Seven') published in the last three years. Taken collectively, these papers do a fairly good job of describing what we see, and when we see it. I also use them as springboard to speculate about what we don't we see, and why not.

Keywords: galaxy formation - galaxy evolution - surveys

Buck: This could get ugly. And I do hate ugly.
Ezra: Well then, brace yourself, Buck. 'Cause here comes ugly.
— 'The Magnificent Seven' (1960, MGM Motion Pictures)

1. Introduction

'Cosmic downsizing' (Cowie 1996, Treu et al. 2005), the new dominant paradigm for galaxy evolution, tells us that star formation activity (and, very likely, black hole growth) shifts to lower and lower mass galaxies as the Universe evolves. We now know, from surveys like K20 (Cimatti et al. 2002), FIRES (Franx et al. 2003) and GDDS (Abraham et al. 2004) that roughly

R. S. de Jong, Island Universes, 463–474.
© 2007 *Springer.*

half the stellar mass density at $z = 1.8$ is in massive galaxies (Glazebrook et al. 2004; Fontana et al. 2004). Furthermore, as shown in Figure 1, the redshift range $1 < z < 3$ is clearly the range over which the rate of stellar mass growth in galaxies is changing most rapidly. Unfortunately, for technical reasons the redshift range $1.3 < z < 2$ has historically posed great challenges for observers, so that discovering the epoch of massive disk galaxy formation by observing the process occurring *in situ* has proven extraordinarily challenging. But if one is interested in reasonably massive systems (say, half the mass of the Milky Way) it is clear that the redshift range $z > 1$ is where the action is, and this review will focus exclusively on the evidence for massive disk galaxies over this redshift range.

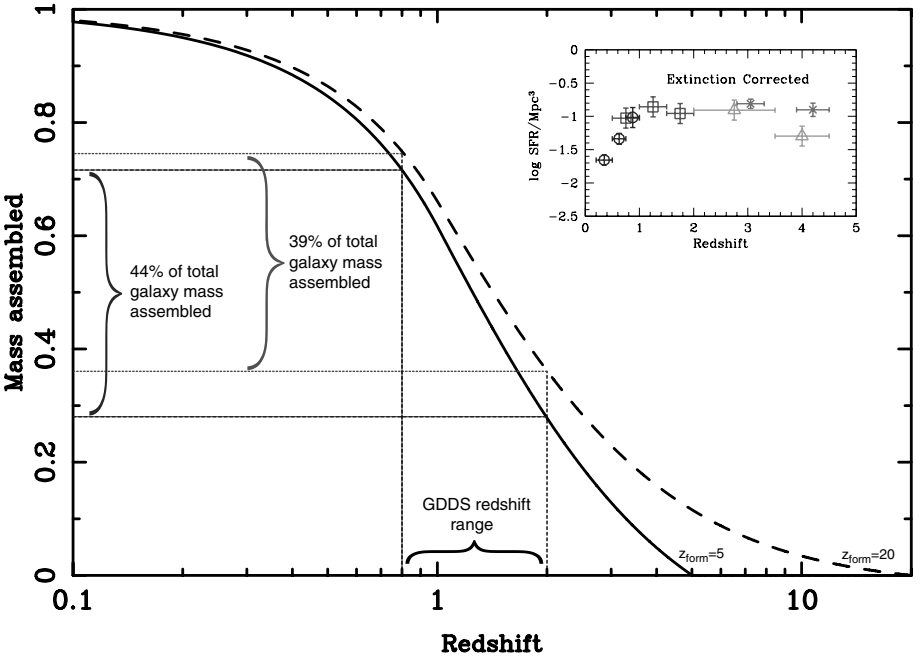

Figure 1. Total stellar mass assembled in galaxies as a function of redshift assuming a star-formation history $\Psi(z)$ given by $\Psi \propto (1+z)^3$ for $z < 1$ and a constant star-formation history for $z > 1$. This is consistent with the star formation history (taken from Steidel et al. 1999) shown as in inset in the top-right of the figure. Two possible epochs for initial galaxy formation are shown ($z = 5$ and $z = 20$), and the redshift range probed by the GDDS (Abraham et al. 2004) is indicated. Nearly half of all stars in the Universe form during the redshift interval $0.8 < z < 2$.

2. The Magnificent Seven

In preparing this review I tried to winnow the literature of $z > 1$ massive disk galaxies down to a minimal subset of fairly recent 'un-missable' or 'desert island' papers. Frankly, this process proved pretty dubious. In a number of cases similar papers came to similar conclusions at similar times, and elevating one paper above the rest seemed a bit invidious. But, in a spirit of making at least some progress, I did it anyway, even if in certain cases I effectively tossed a coin and chose a representative paper. (I will try to note such cases below). Also, I felt compelled to include a couple of 'ideas' or 'techniques' papers, even if these did not report earth-shattering results, simply because they seemed to me to be obvious harbingers of the future.

Here then (in alphabetical order) is the final outcome of this exercise, a set of papers I will refer to as The Magnificent Seven:

- Elmegreen & Elmegreen (2005): *"Stellar Populations in Ten Clump-Cluster Galaxies of the Ultra-Deep Field"*
- Erb et al. (2004): *"The Kinematics of Morphologically Selected $z \sim 2$ Galaxies in the GOODS-North Field"*
- Labbé et al. (2003): *"Large disklike galaxies at high redshift"*
- Papovich et al. (2005): *"The Assembly of Diversity in the Morphologies and Stellar Populations of High-Redshift Galaxies"*
- Stockton, Canalizo & Maihara (2004): *"A disk galaxy of old stars at $z \sim 2.5$"*
- Toft et al. (2005): *"Distant Red Galaxies in the Hubble Ultra Deep Field"*
- Trujillo et al. (2004): *"The Luminosity-Size and Mass-Size Relations of Galaxies out to $z \sim 3$"*

Three papers date from 2005, three are from 2004, and one is from 2003. Three use data from the Ultra Deep Field (UDF) which is a bit of a relief (given the number of HST orbits consumed by the UDF). Five are led by postdocs, which confirms what we already knew about who is really doing all the work in astrophysics (and tells us that the future is looking bright). As it turns out, Trujillo et al. (2004) has as much to say about $z < 1$ as it does about $z > 1$, and it is probably best reviewed in the context of lower redshift work by others, so I will omit detailed discussion of that paper here. The central theme underlying all the remaining papers is this: when do massive disk galaxies form?

3. When do Massive Disk Galaxies Form?

As noted earlier, we now know that roughly half the stellar mass density at $z = 1.8$ is in massive galaxies. But what fraction of these objects are disks?

Firstly, let me try to be a little more precise about what I mean by 'these objects' in the preceding sentence. For almost two decades we have known of the existence of a population of objects which appear redder than the expected colors of actively star-forming high-redshift galaxies. These objects, known as Extremely Red Objects (EROs), were first recognized as a distinct class on their own by Elston, Rieke, & Rieke (1988), with important follow-up work in papers by McCarthy, Persson, & West (1992), Graham et al. (1994), Hu & Ridgeway (1994), Soifer et al. (1994), Dey & Spinrad (1995) and Djorgovski et al. (1995). In the last decade, the field has basically exploded as the importance of this population has become clearer, and as instrumental sensitivities have improved[1]. But the question remains, what are these galaxies? In their early work, Elston, Rieke, & Rieke (1989) obtained spectra for some of the brightest of the EROs and identified them as early-type galaxies at moderate redshifts ($z \sim 0.8$). McCarthy et al. (1992) found several red galaxies with $R - K \sim 5 - 6$ at $z \sim 2$, and proposed that these red objects were evolved cluster members. So most of this early work concluded that relatively few of these red galaxies were massive evolved disks. However, beginning around 1998 a number of studies (e.g., Cimatti et al. 1998; Thompson et al. 1999; Dey et al. 1999) concluded that many of these systems were massive, young and dusty starburst galaxies or AGNs. Clearly spectroscopic and/or photometric studies on their own are unable to distinguish unambiguously between the two main possibilities (old early-type galaxies and dusty young galaxies, presumably a combination of mergers and active star-formation in fair-sized disks). Naturally, this set the stage for morphological work undertaken with the Hubble Space Telescope (HST).

Stiavelli & Treu (2001) used HST/NICMOS imaging to study the morphologies of ERO's, concluding that 60% of them are similar to E/S0 galaxies, 20% are similar to disk galaxies, and 15% have irregular morphologies. A sample of HST/WFPC2 and NICMOS images was used by Moriondo, Cimatti & Daddi (2000) to examine the morphologies of $R - K$ selected galaxies, and analogous result were found, with 50–85% of the objects appearing to be ellipticals,

[1] A confusing taxonomy for these systems has also developed, as additional classes have been added various authors to describe these red objects. These include: Hyper-Extreme Red Objects (HEROs) (Im et al. 2002) which are defined to be objects with $R-K > 7$; Very Red Objects (VROs) were also introduced to refer to objects with $5.3 < R - K < 6$ and $4 < I - K < 5$ (Alexander et al. 2002, Barger et al. 2003); Very Red Galaxies (VRGs) and Faint Red Outlier Galaxies (FROGs) (Moustakas et al. 1997). It is not obvious that there are bona-fide physical distinctions between these classes, and it is probably best (and certainly easiest) to refer to EROs in general, using the prescription given in McCarthy (2004) which defines this population as having $R - K > 5.3$ and $I - K > 4$ with $z > 1$.

with the rest being a mixed bag of disks and irregular galaxies[2]. However, Yan & Thompson (2003) took a similar approach (but complemented HST imagery with observations from the ground) and found almost the opposite result, namely that the EROs were comprised of 10% irregulars, 60% disks, and 30% E/S0s. Most recent studies have obtained similar numbers. For example, Cimatti et al. (2003) used HST/ACS imaging from the Great Observatories Origins Deep Survey (GOODS) to find the following fractions: 30–37% E/S0 galaxies, 24–46% disk galaxies, and 17–39% irregulars. Moustakas et al. (2004), also using GOODS data, found an E/S0 fraction of about 30-40%, a disky population of about the same fraction, and assigned the remaining 20-30% to a mixed bag of irregular, faint, and hard to classify objects. Gilbank et al. (2004) found similar results, reporting that about 30% of EROs are disks, 30% are early-type galaxies, 15% are irregulars, and the rest are unclassifiable. So, in summary, recent studies of ERO's based on samples defined in the near-infrared have converged upon a disk fraction of something like 30–40%.

So it seems there are surprisingly massive galaxies out there, and a lot of them seem to be big disks. This brings us to Labbé et al. (2003), the first paper in the Magnificent Seven collection. This paper is a head-on attempt to tackle the abundance of evolved disk systems at $z > 1.5$. These authors report the discovery of six systems that look a lot like big (scale sizes of order 10 kpc) high-redshift disks at $1.5 < z < 3.0$ in the Hubble Deep Field South. In spite of the morphological work on EROs described in the previous paragraph, this actually comes as quite a surprise, because over this redshift range no evolved big disk candidates are seen in the Hubble Deep Field North! Cosmic variance seems to be a significant factor in understanding these observations.

We now come face-to-face with the central problem plaguing all present investigations of high-redshift disks, and which we won't be able to do anything about soon. The problem is this: we now know that most of the action in terms of mass-building is happening at $z > 1$, but until JWST flies or advances are made in adaptive optics technology, one can only pick two out of the following three characteristics when defining a survey:

(1) A survey with sufficient area to militate against cosmic variance at $z > 1$.

(2) A survey with sufficient depth to probe more than just the brightest parts of galaxies at $z > 1$.

(3) A survey undertaken in the near-infrared, which is needed to probe more than just the youngest stellar populations at $z > 1$.

[2]The 50–85% range brackets the E/S0 fraction, because about one third of the original sample could not be classified due to low signal-to-noise in the HST images. If all of these uncounted objects are in fact disks or irregulars, the fraction of E/S0 could be as low as 50%. On the other hand if they have E/S0 morphologies, the total fraction would be 85%.

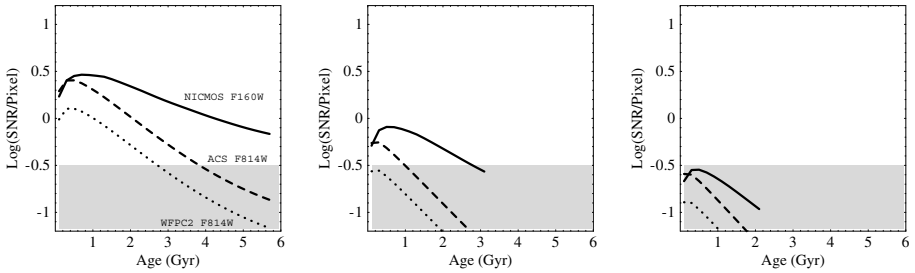

Figure 2. Spectral synthesis predictions for signal-to-noise/pixel (the appropriate figure of merit for work intended to probe resolved structures in galaxies) as a function of age for a 15ks ($\sim$ 5 orbit) exposure of a solar-neighborhood projected mass density seen at z=1 (left panel), z=2 (middle panel), and z=3 (right panel). Grey regions in this plot are unobservable due to low signal-to-noise. Another limit to accessible parameter space is the age of the Universe: curves shown are limited to ages less than that of the Universe at each epoch of observation. Tracks for various telescope/instrument combinations are shown. Dotted curves correspond to HST F814W imaging with the WFPC2 camera, dashed curves correspond to HST z' imaging with the Advanced Camera for Surveys, and solid curves correspond to HST F160W imaging with NICMOS. Calculations are based on a stellar population with an exponential star-formation history with an e-folding timescale of 1 Gyr. A Miller-Scalo IMF and 30% solar metallicity is assumed, as well as a common rebinned pixel scale of 0.1 arcsec/pixel for each instrument.

The discrepancy between what is seen in the HDF-N and what is reported by Labbé et al. in the HDF-S clearly highlights the desirability of the first of these characteristics. Figure 2 is an attempt to highlight the need for the other two. This figure shows the signal-to-noise/pixel as a function of age and redshift for HST observations of a projected stellar mass density corresponding to that of the Milky Way at the solar radius. A fairly long 5-orbit integration time is assumed. The region shown in gray is invisible even after a modest amount of binning. Figure 2 shows that at $z < 1$, there is relatively little bias in optical observations undertaken with HST. At this redshift, projected mass densities corresponding the intermediate regions of large disk galaxies are observable for around 70% of the maximum possible age for the galaxy (defined as the age of the Universe at the epoch of observation). However, the second panel in the figure shows that by $z = 2$ biases with optical HST imaging are severe: structural information at optical wavelengths comes only from the densest regions in galaxies (such as bulges), or from the youngest parts of galaxies (such as bright star-formation complexes with ages of less 1 Gyr). By $z = 2$ it is simply no longer possible to use optical data to compare fairly fundamental characteristics, such as the size and morphology of galaxies, with those of local objects, at least without much deeper imaging than is possible with 5 orbits on HST (highlighting the need for observations that go as deep

as the HDF). NICMOS allows mass densities comparable to those at the solar neighborhood to be probed at $z = 2$, but this instrument has a small field of view.

Given these problems, what is the best way forward? Of course, one approach is to simply wait a decade or so for JWST. Fortunately, there are good prospects for making real headway from the ground in the next couple of years using adaptive optics. The next paper in the Magnificent Seven collection, Stockton et al. (2004), was included in my list for this reason. This paper reports results from deep adaptive optics imaging of a single galaxy in the field of a $z = 2.48$ QSO, and concludes that this system is an evolved disk. Although AO imaging of a single object represents a fairly modest start, the conclusion of this paper reinforces the basic premise of Labbé et al. (i.e. big evolved disks are out there in reasonable abundance at $z > 2$). More importantly, the methodology is, I hope, a sign of things to come. Once Multi-Conjugate Adaptive Optics systems come on-line (in about a year, as of this writing), areal coverage at high image quality should be even larger than that of NICMOS. I am hoping that deep ground-based surveys of large numbers of putative disks at $z > 2$ will become possible, at better than HST resolution, by the end of 2007.

The nicest exploitation of high-resolution infrared imaging in the Magnificent Seven series is the paper by Papovich et al. (2005). I like this paper very much because the ethos it espouses is one I happen to share. Galaxies at high redshift may not resemble those seen nearby, so why do we place so much emphasis on trying to shoehorn them into familiar classes? Shouldn't we instead focus more on simply trying to understand the nature of their diversity, with a strong emphasis on their stellar populations, rather than on their transient morphology? A powerful tool in this context is internal color dispersion, which was first applied in this context by Abraham et al. (1999), but which is really applied much more effectively in Papovich et al. (2005). These authors show that at $z \sim 2$ surprisingly few galaxies have a high internal color dispersion, and those that do show signs of merging. Galaxies at $z \sim 1$ seem to show more diversity in their stellar populations. It is crucial to note that this analysis was undertaken using NICMOS observations, which probe the rest-frame at visible wavelengths. Papovich et al. conclude that star formation at high redshifts is 'dominated by discrete, recurrent starbursts, which quickly homogenize the galaxies' stellar content', and by comparing populations in two redshift bins conclude that a different mode of star-formation is occurring at lower redshift. The central conclusion is that there is a transition in the dominant mode of star formation that occurs at $z \sim 1.5$, which they associate with the emergence of Hubble-sequence.

It seems to me that the picture painted in Papovich et al. (2005) can be made to jibe very nicely with the cosmic downsizing, which also posits a transition in the mode of star-formation for massive galaxies at similar redshifts (see,

for example, Juneau et al. 2005). But on the other hand, it isn't so obvious that the picture of a non-diverse galaxy population at $z > 2$ is fully consistent with what other observations are telling us. The next paper in the Magnificent Seven collection, Toft et al. (2005), uses UDF observations to probe the rest-frame optical and UV morphologies of a set of distant red galaxies. The surface brightness distributions of the $z_{phot} > 2$ galaxies are better fit by exponential disks than by $R^{1/4}$ laws, but the rest-frame optical morphology of these objects is quite different from the rest-frame UV morphology. Generally speaking, all the galaxies have red central components that dominate the NICMOS imagery, coupled with off-center blue features that show up (and sometimes dominate) the ACS imagery. The rest-frame optical and UV morphological properties of the red galaxy population studied by Toft et al. seems rather diverse to me, and they seem to be pointing to complex stellar populations already in place at $z > 2$. Toft et al. (2005) note that a complex star-formation history is also implied by the broadband spectral energy distributions for these objects, which are best modeled using extended star formation histories and contributions from substantial quantities of dust.

While much of the work described so far supports the view that big disks are already in place at $z > 2$, my faith in this conclusion is somewhat shaken by the next Magnificent Seven paper, the dynamical study of Erb et al. (2004). These authors present near-IR Keck spectra of Hα emission from 13 $z \sim 2$ galaxies in the GOODS-N field, focusing primarily on very elongated systems so that slits could be aligned along the bodies of the galaxies to probe velocity shears most effectively. Because these galaxies are typically only a couple of arcseconds long, these kinds of observations are clearly very challenging from the ground in natural seeing. But Erb et al. (2004) focus only on the most straightforward of questions about these objects: are they linear because they are highly inclined disks, or because they are merging subunits? Amazingly, and in spite of quite good seeing, it turns out that aligning a slit along the major axis of one of these galaxies does not increase the probability of observing a tilted emission line. Furthermore, Erb et al. also find that the elongated subsample exhibits a significantly *lower* velocity dispersion than galaxies selected at random from the parent Hα sample, the opposite of what one expects if these linear objects were highly inclined disks. Erb et al. conclude that 'it is at least as likely that the galaxies' elongated morphologies are due to merging subunits'. So while earlier papers in the Magnificent Seven collection seem to be telling us that big disks are fairly abundant at $z \sim 2$, it seems that at least some things we thought were big disks may turn out not to be disks after all. I suspect that the Erb et al. (2004) paper is a first shot in what will probably be a long campaign of dynamical analyses of these systems, now that AO-fed near-infrared integral field units are on-line (e.g., OSIRIS on Keck, and SINFONI on the VLT) or coming on-line (e.g., NIFS on Gemini).

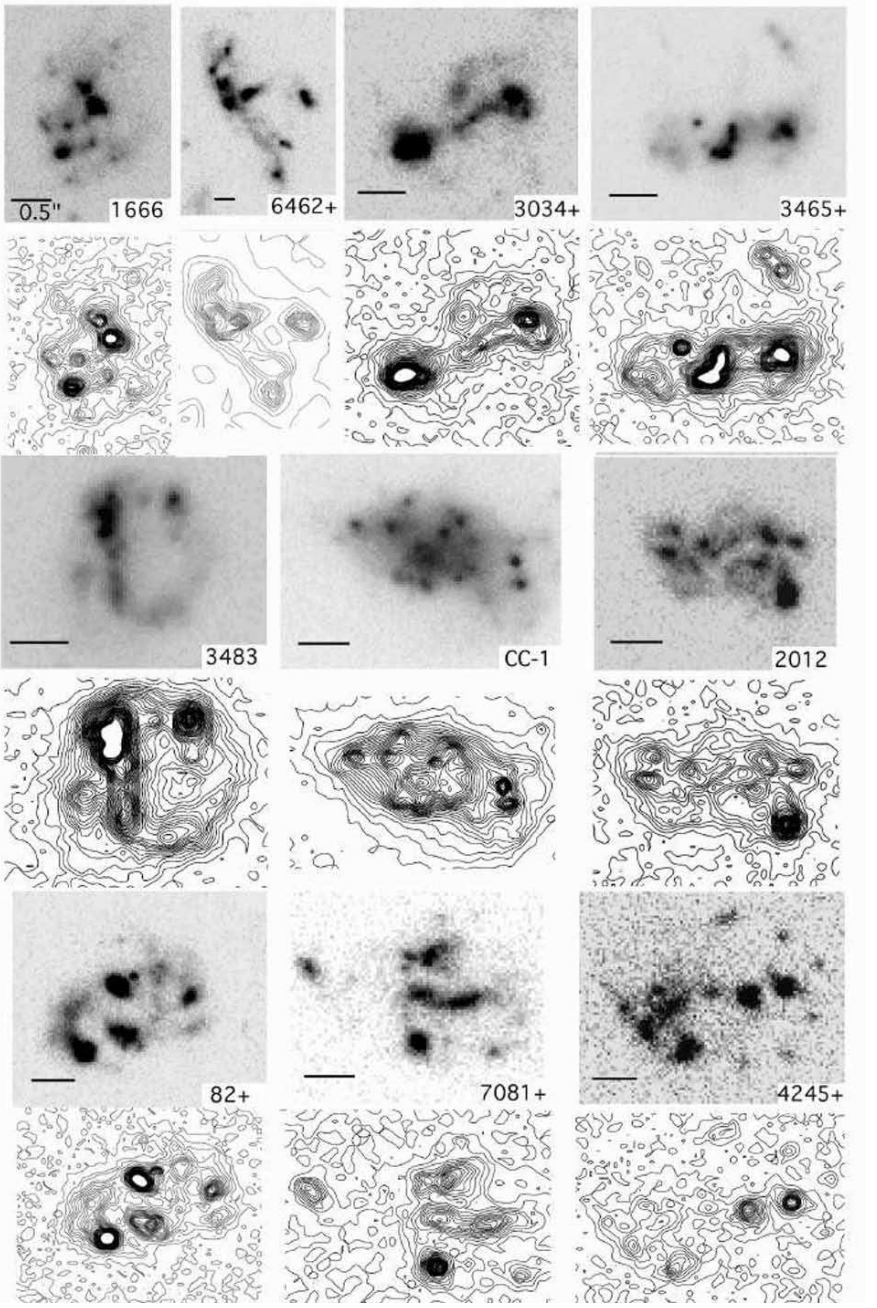

Figure 3. Ten clump clusters (figure taken from Elmegreen & Elmegreen 2005). The bar is 0.5 arcsec long, and the contour plots are in steps of 1σ sky noise, with the outermost contour at 26.8 mag arcsec^{-2}. Open question #1 is simple: what are these systems?

The final paper in the Magnificent Seven collection is a beautiful paper by Elmegreen & Elmegreen (2005) which, like Erb et al. (2004), seeks to determine whether or not a class of objects seen in HST data are (or are not) big disks at high redshift[3]. Like Papovich et al. (2005), Elmegreen & Elmegreen (2005) explore resolved colors, but the Elmegreens limit their focus to a set of peculiar galaxies in the Ultra-Deep Field that are marked by an irregular clumpy structure and no central bulge, referring to these objects as 'clump clusters' (see Figure 3, taken from their paper). Using B-band, V-band, i-band, and z-band images, these authors conclude clump clusters may well be related to the so-called 'chain galaxies' seen at high redshifts (van den Bergh 1996; Abraham et al. 1996), with both chains and clump clusters being early disks viewed at random angles with intrinsic axial ratios less than 0.2. The disks appear to be 'forming an early generation of stars in a small number of very large star complexes. If these galaxies evolve into today's disk galaxies, then we are observing a stage in which accretion and star formation are extremely clumpy and the resulting high velocity dispersions form thick disks.' In essence, the Elmegreens identify clump clusters with probable proto-disk systems[4]. Like Erb et al. 2004, they do not come to a definitive conclusion, leaving open the possibility that some of the clumps may merge into early-type systems. But the paper represents the closest anybody has come (so far) to using UDF data to try to take the bull by the horns and address the central question of whether or not the peculiar high-redshift galaxy population really are big disks caught in the process of forming.

References

Abraham, R. G., et al. 2004, AJ, 127, 2455

Abraham, R. G., Ellis, R. S., Fabian, A. C., Tanvir, N. R., & Glazebrook, K. 1999, MNRAS, 303, 641

Abraham, R. G., Tanvir, N. R., Santiago, B. X., Ellis, R. S., Glazebrook, K., & van den Bergh, S. 1996, MNRAS, 279, L47

Alexander, D. M., Vignall, C., Bauer, F. E., Brandt, W. N., Hornschmeier, A. E., et al., 2002, AJ, 123, 1149

Barger, A. J., Cowie, L. L., Capak, P., Alexander, D. M., Bauer, F. E., et al., 2003, AJ, 126, 632

Cimatti, A., Andreani, P., Rottgering, H., Tilanus, R., 1998, Nature, 392, 895

Cimatti, A., Daddi, E., Cassata, P., Pignatelli, E., fasano, G., et al., 2003, A&A, 412L, 1C

Cimatti, A., Daddi, E., Mignoli, M., Pozzetti, L., Renzini, A., et al., 2002, A&A, 381L, 68C

Cowie, L. L., Songaila, A., Hu, E. M., & Cohen, J. G. 1996, AJ, 112, 839

[3]Incidentally, Elmegreen & Elmegreen (2005) is actually the only paper in the Magnificent Seven collection that does not rely on infrared observations. The preponderance of near-IR papers in a 'greatest hits' collection does suggest to me that we've turned some kind of corner.

[4]Note that Sidney van den Bergh saw this all coming a decade ago; systems similar to clump clusters in the HDF are flagged as probable proto-disks in the van den Bergh et al. (1996) HDF morphological catalog paper.

Cowie, L. L., Gardner, J. P., Lilly, S. J., McLean, I., 1990, ApJ, 360, L1
Dey, A., Graham, J. R., Ivison, R., Smail, I., Wright, G., Lui, M., 1999, ApJ, 519, 610
Djorgovski, S., Soifer, B. T., Pahre, M. A., Larkin, J. E., Smith, J. D., et al., 1995, ApJ, 438, 13
Elmegreen, B. G., & Elmegreen, D. M. 2005, ApJ, 627, 632
Elston, R., Rieke, G. H., Rieke, M. J., 1988, ApJ, 331L, 77E
Elston, R., Rieke, G. H., Rieke, M. J., 1989, ApJ, 341, 80E
Erb, D. K., Steidel, C. C., Shapley, A. E., Pettini, M., & Adelberger, K. L. 2004, ApJ, 612, 122
Fontana, A., et al. 2004, A&A, 424, 23
Gilbank, D., Smail, I., Ivison, R., Packham, C., 2004, MNRAS, 346, 1125G
Glazebrook, K., et al. 2004, Nature, 430, 181
Graham, J. R., Dey, A., 1996, ApJ, 471, 720G
Griffiths, R. E., Ratnatunga K. U., Neuschaefer, L. W., Casertano, S., Im, M., et al., 1994, ApJ, 437, 67G
Hu, E., Ridgeway, S., 1994, AJ, 107, 1303
Im, M., Yamada, T., Tanaka, I., Kajisawa, M., 2002, ApJ, 578L, 191
Juneau, S., et al. 2005, ApJLett, 619, L135
Labbé, I., et al. 2003, ApJLett, 591, L95
McCarthy, P. J., 2004, Annu. Rev. Astron. Astrophys., 42, 477-515
McCarthy, P. J., Carlberg, R. G., Chen, W.-H., Marzke, R. O., First, A. E., et al., 2001, ApJ, 560L, 131M
McCarthy, P. J., Persson, S. E., West, S. C., 1992, ApJ, 386, 52M
Moriondo, G., Cimatti, A., Daddi, E., 2000, A&A, 364, 26M
Moustakas, L. A., Casertano, S., Conselice, C. J., Dickinson, M. E., Eisenhardt, P., et al., 2004, ApJ, 600L, 131M
Moustakas, L. A., Davis, M., Graham, J. R., Silk, J., Peterson, B. A., Yoshii, Y., 1997, ApJ, 475, 445M
Papovich, C., Dickinson, M., Giavalisco, M., Conselice, C. J., & Ferguson, H. C. 2005, ApJ, 631, 101.
Papovich, C., et al. 2006, ApJ, 640, 92
Pozzetti, L., Mannucci, F., 2000, MNRAS, 317, 17
Rudnick, G., et al. 2003, ApJ, 599, 847
Soifer, B. T., Matthews, K., Neugebauer, G., Armus, L., Cohen, J. G., et al., 1999, AJ, 118, 2065S
Spinrad, H., Dey, A., Stern, D., Dunlop, J., Peacock, J., et al., 1997, ApJ, 484, 581S
Stiavelli, M., Treu, T., 2001, In "Galaxy Disks and Disk Galaxies", ASP Conf. Ser., 230, pp. 603-6
Stockton, A., Canalizo, G., & Maihara, T. 2004,ApJ, 605, 37
Toft, S., van Dokkum, P., Franx, M., Thompson, R. I., Illingworth, G. D., Bouwens, R. J., & Kriek, M. 2005, ApJLett, 624, L9
Treu, T., Stiavelli, M., 1999, ApJ, 524L, 27
Treu, T., Ellis, R. S., Liao, T. X & van Dokkum, P. G., 2005, ApJ, 622, L5.
Trujillo, I., et al. 2004, ApJ, 604, 521
van den Bergh, S., Abraham, R. G., Ellis, R. S., Tanvir, N. R., Santiago, B. X., & Glazebrook, K. G. 1996, AJ, 112, 359
Yan, L., Thompson, D., 2003, ApJ, 586, 765Y

Explanations without pen and paper. *Top:* Roelof de Jong, Marc Verheijen, Matthew Bershady, Eric Bell, and Cris Brook. *Bottom:* Michael Pohlen, Ken Freeman, Martin Bureau, and Ignacio Trujillo.

EIGHT BILLION YEARS OF DISK GALAXY EVOLUTION

No galaxy is an island

Eric F. Bell[1], Marco Barden[1], Xianzhong Zheng[1], Casey Papovich[2], Emeric Le Floc'h[2], George Rieke[2], Christian Wolf[3] and the GEMS, MIPS Instrument, and COMBO-17 teams

[1] *Max-Planck-Institut für Astronomie, Heidelberg, Germany*
[2] *Steward Observatory, University of Arizona, Tuscon, USA*
[3] *University of Oxford, UK*

Abstract We present a brief discussion of the evolution of disk galaxy stellar masses, sizes, rotation velocities, and star formation rates over the last eight billion years. Recent observations have failed to detect significant evolution in the stellar mass Tully-Fisher relation, stellar mass–size relation, and the stellar mass function of disk galaxies. Yet, most $z < 1$ star formation is in disks, and this star formation would be expected to drive a rapid growth of the total stellar mass (and therefore mass function) of disks in the last eight billion years. Such a build-up is not seen; instead, a rapid build-up in the total stellar mass in non-star-forming spheroid-dominated galaxies is observed. Large numbers of disk-dominated galaxies are systematically shutting off their star formation and building up a spheroid (or losing a disk) in the epoch $0 < z < 1$.

Keywords: galaxies: evolution - galaxies: fundamental parameters - infrared : galaxies

The evolution of disk galaxy scaling relations — e.g., the luminosity–line-width (Tully-Fisher) relation, or the luminosity–size or stellar mass–size relations — give insight into the evolution of the masses, stellar populations and angular momentum contents of galaxy disks. Luminosity and stellar mass functions give yet deeper insight, as they show how galaxies populate these scaling relations. Here, we present a very brief overview of some recent insights into the evolution of disk galaxy scaling relations, their stellar mass function, and to explore the interplay between star formation and the growth of stellar mass. We will consider only $z < 1$, or the last eight billion years or so, given a concordance cosmology ($\Omega_{m,0} = 0.3, \Omega_{\Lambda,0} = 0.7, \mathrm{H}_0 = 70\,\mathrm{km\,s^{-1}\,Mpc^{-1}}$).

R. S. de Jong, Island Universes, 475–480.
© 2007 *Springer.*

1. (Non)-Evolution of Disk Galaxy Scaling Relations

The evolution of disk galaxy scaling relations has proven difficult to robustly determine, and some issues remain contentious. In some cases (the Tully-Fisher relation: Vogt et al. 1996 vs. e.g., Boehm et al. 2004) it is not clear where the source of the discrepancies lie. In other cases (the luminosity/stellar mass–size relations: e.g., Ravindranath et al. 2004 vs. Barden et al. 2005) the source of the discrepant interpretations has been resolved (see the discussion in Barden et al. 2005).

Barden et al. (2005) present an analysis of the evolution of the disk galaxy luminosity–size, and stellar mass–size relation over the epoch $0 < z < 1$ from the HST/GEMS (Galaxy Evolution from Morphology and SEDs; Rix et al. 2004) survey of the Extended Chandra Deep Field South. They chart the evolution of the distribution of disk sizes from $z = 0$ (using the SDSS) to gradually higher and higher redshift, carefully quantifying the effects of surface brightness dimming and incompleteness. At $z > 1.1$, the surface brightness limit of GEMS starts to significantly eat into the disk galaxy population, therefore they limited their study to $z < 1.1$. Using this sample of galaxies with well-understood and modest completeness corrections, they conclude that:

- there has been significant evolution in the luminosity–size relation, such that galaxies at $z = 1$ have roughly 1.5 mag arcsec^{-2} brighter rest-frame B-band surface brightnesses than galaxies of equivalent luminosity today; and
- that most of this evolution is attributable to the fading and reddening of stellar populations as they age from $z = 1$ to the present day, i.e., there is no detectable evolution in the stellar mass–size relation for galaxies with $M_* > 10^{10} M_\odot$.

The evolution of the Tully–Fisher relation remains a contentious issue. Nonetheless, important progress is still being made. A novel contribution was made recently by Conselice et al. (2005), who presented a study of the $z < 1$ evolution of the near-IR and stellar mass Tully-Fisher relations using a new sample of rotation velocities in conjunction with ground-based optical and near-IR data (for constructing optical/near-IR broad-band SED masses). Their analysis ruled out substantial evolution in the stellar mass Tully-Fisher relation[1].

Also recently, a number of groups have studied the evolution of the stellar mass function of galaxies split either by morphological type or color. These

[1]They then use this as an argument that the dark matter content and baryonic content of disks grow in lockstep, arguing that the stars were a good probe of baryonic mass and the rotation velocity was a good probe of dark mass. Yet, it is important to note that if the bulk of massive disks are maximum-disk (i.e., their baryonic content dominates their rotation velocity; e.g., Kassin et al. 2006, Kassin et al. this volume) then one also expects no evolution in the stellar mass Tully-Fisher relation.

cuts are, at a very general level, largely equivalent — most red galaxies are morphologically early-type and the bulk of blue galaxies are morphologically late-type out to $z = 0.7$ at least (Strateva et al. 2001; Bell et al. 2004). A general conclusion is that the stellar mass function of blue/disk galaxies does not evolve significantly since $z = 1$ (see Brinchmann & Ellis 2000 for first indications of this result; Bundy et al. 2006; Borch et al. 2006)[2].

It would appear that none of the scaling relations defining disk galaxy structure or dynamics, or indeed the space density of disk galaxies at a given mass, significantly change in the last eight billion years. *It is as if the disk galaxy population resolved to do nothing for the last eight billion years except age.*

Yet, there is one observational constraint that has not yet been brought to bear on the problem, which seems to give interesting and incisive insight: the evolution of disk galaxy star formation rates.

2. Eight Billion Years of Star Formation in Disks

With the advent of Spitzer, it has been possible to explore the star formation rates of galaxies at $z < 1$ with unprecedented accuracy: fully 50% of the $z = 1$ cosmic SFR has been resolved into individual galaxies with deep 24μm surveys (Le Floc'h et al. 2005; Zheng et al. 2006). One key result is that the bulk of $z < 1$ star formation is in disk galaxies: *the order-of-magnitude decline in cosmic SFR is the result of processes which are shaping the evolution of disk galaxies* (Bell et al. 2005; Melbourne et al. 2005; Wolf et al. 2005).

We explore this issue further in Fig. 1. Here, we show the contribution of different types of galaxy to the cosmic SFR and stellar mass budget at $z < 1$: such an analysis requires the assumption of a universally-applicable stellar IMF, and we adopt the parameterization of Chabrier (2003) in what follows. Full circles show the total SFR/stellar mass. Open diamonds show the estimated contribution from early-type galaxies. These were selected to be on the red sequence and have concentrated light profiles, with Sersic indices $n > 2.5$ derived from HST/ACS F850LP imaging data from GEMS. This selection is analogous to that used by McIntosh et al. (2005) for their study of the early-type galaxy stellar mass–size relation. Asterisks show the contribution all other galaxies, dominated by $n < 2.5$ galaxies (i.e., less concentrated, typically disk-dominated galaxies) with a small contribution from blue galaxies with $n > 2.5$ (which are often blue disks with significant bulges, or ongoing galaxy mergers). Other ways of splitting the sample — e.g., a pure $n = 2.5$ split, a pure

[2]The oft-cited ~ 1.5 magnitude fading of the characteristic luminosity L^* of the disk galaxy population from $z = 1$ to the present is more-or-less accounted for by the expected fading and reddening of the ageing stellar populations in blue star-forming disks: thus, the characteristic stellar mass of disks does not appear to evolve a large amount during the last 8 billion years (Lilly et al. 1995; Willmer et al. 2006; Borch et al. 2006; Blanton 2006)

blue/red split, or splits by visual morphology — produce qualitatively similar results to those shown in Fig. 1. The total stellar mass budget is derived from three COMBO-17 photometric redshift survey fields (see Borch et al. 2006); the type-split stellar mass and all SFR budgets used in the argument below were derived from only one field, the extended Chandra Deep Field South for which both HST/ACS data and Spitzer data were available. Uncertainties from cosmic variance have been estimated by exploring field-to-field variation in stellar mass budget of the red and blue galaxy populations (from COMBO-17). The $z = 0$ point is taken from the SDSS/2MASS (Bell et al. 2003).

In the upper panel of Fig. 1 we show the evolution of the cosmic star formation rate for all galaxies derived from Spitzer 24μm observations (solid circles; Le Floc'h et al. 2005; Bell et al. in prep.; and grey error bars show the compilation from Hopkins 2004). The asterisks show the evolution of the integrated SFR density in blue/disk-dominated galaxies; the diamonds the contribution from red, early-type galaxies. It is clear that the bulk of star formation is in blue and disk galaxies at all $z < 1$.

What do these SFRs predict for the build-up of stellar mass in disks? This is explored in the lower panels of Fig. 1, where we compare the evolution of the integrated stellar mass density with the integral of the star formation rate of different galaxy populations. The evolution of the integrated stellar mass density in all galaxies (solid circles), blue and disk galaxies (asterisks) and red spheroid-dominated galaxies (diamonds) is shown. The lines show the integral of the cosmic SFR: clearly, the evolution of the total cosmic SFR (solid line) is compatible with the observed build-up in cosmic stellar mass density from $z = 1$ to the present day, with some 40% of stars being formed in this epoch.

Disk galaxies contain the bulk of the star formation. Thus if one assumes that the disk galaxy population is a closed box (i.e., all stars ever formed in disks stay there) then one can predict the growth in the total disk stellar mass density. This result is shown by the dotted line. It is difficult to argue that this mismatch is some kind of catastrophic failure of the stellar mass/SFR estimation methodology: completely standard calibrations were used, and the integral of the cosmic SFR indeed reproduces well the build-up of stellar mass at $z < 1$. Instead, it is clear that *the disk galaxy population is not a closed box.* The key to understanding this issue lies in exploring the stellar mass growth in spheroid-dominated galaxies: the total stellar mass in spheroids increases significantly from $z = 1$ to the present day, while almost no star formation happens in the spheroid-dominated galaxy population. **Large numbers of disk-dominated galaxies are systematically shutting off their star formation and building up a spheroid (or losing a disk)** in the epoch $0 < z < 1$. The physical processes that are responsible for these transformations are as yet unclear, and might include bar-induced instabilities, merging with satellites or companions, or suppression of star formation by ram-pressure stripping or galactic winds.

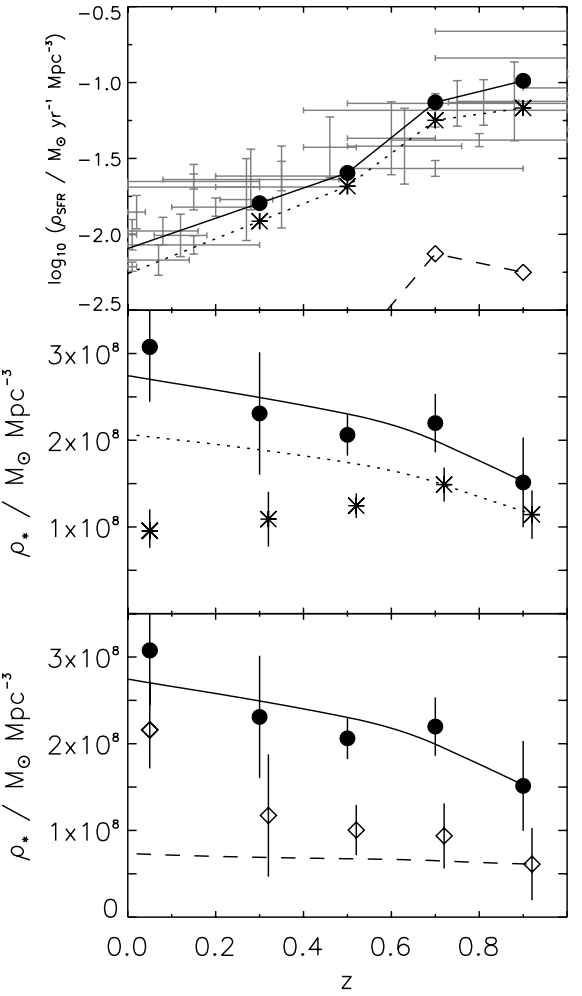

Figure 1. The cosmic evolution of star formation rate and stellar mass (filled circles and solid lines), split into contributions from the red, morphologically early-type galaxies (diamonds and dashed lines) and all other galaxies (asterisks and dotted lines; dominated by disk galaxies). In the uppermost panel, determinations of cosmic SFR are shown also in grey, adopted from Hopkins (2004). In the lower panels, the data points show the observed evolution of stellar mass as a function of redshift. The solid line shows the predicted build-up of stellar mass, assuming the star formation history shown by the solid line in the upper panel (assuming for gas recycling); it is clear that the integral of the cosmic star formation history predicts the cosmic evolution of stellar mass at $z < 1$ reasonably accurately. The dotted line shows the predicted evolution of total stellar mass assuming that all stars that form in blue/disk galaxies remain in blue/disk galaxies (i.e., if the blue cloud evolves like a closed box). The dashed line shows the corresponding evolution for early-type galaxies.

3. Discussion

This has important implications for how one interprets the non-evolution of disk galaxy scaling relations. Whereas one could have, without the measurement of the disk galaxy SFRs, postulated that disks were a non- or slowly-evolving population, the evolution of such (expected) rapid star formation-driven build-up in mass makes this interpretation meaningless. Instead, as low-mass disk galaxies are growing in mass (as they must, to replace the disks sacrificed for the ever-growing spheroid-dominated galaxy population), they must be growing also in rotation velocity (to preserve the non-evolving Tully-Fisher relation) and size (to preserve the non-evolving mass–size relation) — at least in an average sense. Furthermore, in this picture, the non-evolution of the stellar mass function of disks is a vital constraint: any mechanism which is transforming disks into spheroids must 'take' disks from the stellar mass functions at such a rate that they can be approximately replaced by star formation-related growth of lower-mass disks.

References

Barden, M., et al. 2005, ApJ, 635, 959
Bell, E. F., et al. 2003, ApJS, 149, 289
Bell, E. F., et al. 2004, ApJ, 608, 752
Bell, E. F., et al. 2005, ApJ, 625, 23
Blanton, M. 2006, submitted to ApJ (astro-ph/0512127)
Boehm, A., et al. 2004, A&A, 420, 97
Borch, A., et al. 2006, submitted to A&A
Brinchmann, J., & Ellis, R. S. 2000, ApJ, 536, 77L
Bundy, K., et al. 2006, submitted to ApJ (astro-ph/0512465)
Chabrier, G. 2003, ApJ, 586, L133
Conselice, C. J., et al. 2005, ApJ, 628, 160
Hopkins, A. M. 2004, ApJ, 615, 219
Kassin, S., et al. 2006, ApJ, in press (astro-ph/0602027)
Le Floc'h, E., et al. 2005, ApJ,632, 169
Lilly, S., et al. 1995, ApJ, 455, 108
McIntosh, D. H., et al. 2005, ApJ, 632, 191
Melbourne, J., et al. 2005, ApJ, 625, L27
Ravindranath, S., et al. 2004, ApJ, 604, 9L
Rix, H.-W., et al. 2004, ApJS, 152, 163
Strateva, I., et al. 2001, AJ, 122, 1861
Vogt, N., et al. 1996, ApJ, 465, L15
Willmer, C. N. A., et al. 2006, submitted to ApJ (astro-ph/0506041)
Wolf, C. et al. 2005, ApJ, 630, 771
Zheng, X. Z., et al. 2006, ApJ, in press (astro-ph/0512203)

SIZE EVOLUTION OF GALAXIES SINCE z∼3: COMBINING SDSS, GEMS AND FIRES

Ignacio Trujillo[1], Natascha M. Förster Schreiber[2], Gregory Rudnick[3], Marco Barden[1], Marijn Franx[4], Hans–Walter Rix[1], J. A. R. Caldwell[5], Daniel H. McIntosh[6], Andrew Zirm[4], Boris Häußler[1], Pieter G. van Dokkum[7], Ivo Labbé[8], Alan Moorwood[9], Huub Röttgering[4], Arjen van der Wel[4], Paul van der Werf[4] and Lottie van Starkenburg[4]

[1]*Max-Planck-Institut für Astronomie, Heidelberg, Germany*

[2]*Max-Planck-Institut für extraterrestrische Physik, Garching, Germany*

[3]*NOAO, Tucson, USA*

[4]*Leiden Observatory, Leiden, The Netherlands*

[5]*University of Texas, McDonald Observatory, Fort Davis, USA*

[6]*University of Massachusetts, Amherst, USA*

[7]*Yale University, New Haven, USA*

[8]*Carnegie Observatories, Pasadena, USA*

[9]*European Southern Observatory, Garching, Germany*

Abstract We present the evolution of the luminosity–size and stellar mass–size relations of luminous ($L_V > 3.4\times10^{10} h_{70}{}^{-2} L_\odot$) and of massive ($M_\star > 3\times10^{10} h_{70}{}^{-2} M_\odot$) galaxies in the last ∼11 Gyr. We use very deep near–infrared images of the Hubble Deep Field–South and the MS1054-03 field in the J_s, H and K_s bands from FIRES to retrieve the sizes in the optical rest–frame for galaxies with z>1. We combine our results with those from GEMS at 0.2<z<1 and SDSS at z∼0.1 to achieve a comprehensive picture of the optical rest–frame size evolution from z=0 to z=3. For less concentrated or disk–like objects, the galaxies at a given luminosity were typically ∼2.3±0.2 (±1 σ) times smaller at z∼2.5 than those we see today. The stellar mass–size relation has evolved significantly less: the mean size at a given stellar mass was ∼1.5±0.1 times smaller at z∼2.5. For disk galaxies, the weak redshift–dependence of the stellar mass–size relation would follow naturally if the individual galaxies grow inside–out, evolving "along" the relation.

Keywords: galaxies: fundamental parameters - galaxies: evolution - galaxies: structure - galaxies: high redshift

R. S. de Jong, Island Universes, 481–486.
© 2007 *Springer.*

1. Introduction

Over the last decades (starting with Fall & Efstathiou 1980 and Fall 1983) there has been a substantial effort on understanding, theoretically and through observations, how galaxies have reached their current sizes over cosmic time. The evolution of individual galaxies is not directly observable. However, look–back studies can provide extensive information on how the population properties of galaxies have changed with cosmic epoch.

As a result of the dearth of very deep near-infrared (NIR) images, most of the studies using the rest-frame optical have been limited in redshift up to z $\sim$1. To properly compare with local optically selected samples and to trace the size evolution in a consistent fashion at z$>$1 one needs to use very deep NIR data. On doing that any observed size evolution would then reflect true evolutionary changes not subject to the changing appearance of galaxies in different bandpasses. In addition to the use of rest-frame optical sizes, it would be of great help to facilitate a direct comparison with the theoretical expectations if the size evolution could be measured at a given mass rather than a given luminosity. An approach is to estimate the stellar masses from the rest-frame colors and spectral energy distributions (SEDs).

With the above ideas in mind we performed an exploratory work (Trujillo et al. 2004) to probe the evolution of the luminosity–size and stellar mass–size relations of the galaxies out to z$\sim$3. That work used very deep NIR images of the Hubble Deep Field–South (HDF–S) from the Faint Infrared Extragalactic Survey (FIRES; Franx et al. 2000). We found that the rest-frame V-band sizes of luminous galaxies ($<L_V>\sim 4\times10^{10}$ $h_{70}{}^{-2}L_\odot$) at 2$<$z$<$3 were 3 times smaller than for equally luminous galaxies today. In contrast, the mass–size relation had evolved relatively little: the size at mass ($<M_\star>\sim 4\times10^{10}h_{70}{}^{-2}M_\odot$), had changed by 20% ($\pm$20%) since z$\sim$2.5.

In the present work we add to the above data set the results from the analysis of the $\sim$ 4 times larger MS1054–03 FIRES field. In addition, we make a detailed comparison of our results with those found in the Sloan Digital Sky Survey (SDSS; York et al. 2000) at z$\sim$0.1 and in the Galaxy Evolution from Morphology and SEDs (GEMS; Rix et al. 2004) survey at intermediate redshift 0.2$<$z$<$1. This allows us to follow in detail the evolution of the luminosity–size and stellar mass-size relations of the luminous galaxies over the last $\sim$ 11 Gyr. All magnitudes in this work are given in the AB system unless otherwise stated. Throughout, we will assume a flat Λ-dominated cosmology (Ω_M=0.3, Ω_Λ=0.7 and H_0=70 km s^{-1} Mpc^{-1}).

2. FIRES: Data and Rest-frame Size Estimations

The data used were obtained as part of FIRES, a NIR survey of the HDF–S and MS 1054–03 fields carried out at the VLT. The NIR images were obtained

using ISAAC. The HDF–S was imaged for 33.6 hr in J_s, 32.3 hr in H, and 35.6 hr in K_s in a single $2.'5 \times 2.'5$. The NIR data were complemented with deep optical publicly available HST WFPC2 imaging. For the MS 1054–03 field, 77 hr of ISAAC integration time was obtained in a $5' \times 5'$ mosaic of four pointings. Already existing mosaics in the WFPC2 V_{606} and I_{814} bands were used. In addition, Bessel U, B, and V band imaging with the VLT FORS1 instrument were collected. The depth (3 σ) reached was 26.8 mag in J_s, 26.2 mag in H, and 26.2 mag in K_s for point sources in the HDF–S. The MS 1054–03 field surveys an area four times larger down to ~ 0.7 mag brighter magnitudes. The effective seeing in the reduced images is approximately $0.''47$ in all NIR bands in the HDF–S and $0.''49$ in the MS 1054–03 field.

Photometric redshifts z_{ph}, as well as the rest-frame optical luminosities, were estimated by fitting a linear combination of redshifted SEDs of galaxies of various types (Rudnick et al. 2001, 2003). Comparison with available spectroscopic redshifts z_{sp} implies an accuracy of $\delta z \equiv < |z_{sp} - z_{ph}|/(1+z_{sp}) > = 0.074$ for both fields. To ensure sufficient signal-to-noise ratio for the subsequent size determinations we selected only galaxies with $K_s \leq 23.5$ in the HDF–S and $K_s \leq 23$ in the MS 1054–03 field.

The stellar mass-to-light (M/L) ratio and hence the stellar masses of the objects are estimated using rest-frame (B–V) color and SEDs similar to that of Bell & de Jong (2001). The galaxy sizes used in this paper are measured in the observed band that is closest to the rest-frame V-band at every redshift; this means J_s for galaxies with $1<z<1.5$, H for galaxies with $1.5<z<2.6$ and K_s for galaxies with $2.6<z<3.2$. The structural properties of the galaxies are estimated from a Sérsic's $r^{1/n}$ model, convolved with the image point-spread function (PSF).

3. The Observed Luminosity/Stellar Mass vs Size Relations at High–z

In Figure 1 our sample is split in three different redshift bins: $1<z<1.4$, $1.4<z<2$ and $2<z<3.2$. This separation allows us to study the galaxies in roughly equal time intervals of $\sim$1.2 Gyr.

Overplotted on our observed distributions are the mean and dispersion of the distribution of the Sérsic half-light radii from the Sloan Digital Sky Survey (Shen et al. 2003) galaxies. We use the "local" SDSS sample for reference. The mean of the SDSS galaxies redshift distribution used for comparison is 0.1. We use the sizes and the shapes estimated in the observed r-band as this closely matches the V-band rest-frame filter at $z \sim 0.1$.

In the first row, our sample is compared to the total population observed by SDSS, whereas in the second row we compare with the galaxies classified by Shen et al. as late-type and in the third row with those classified as early-type.

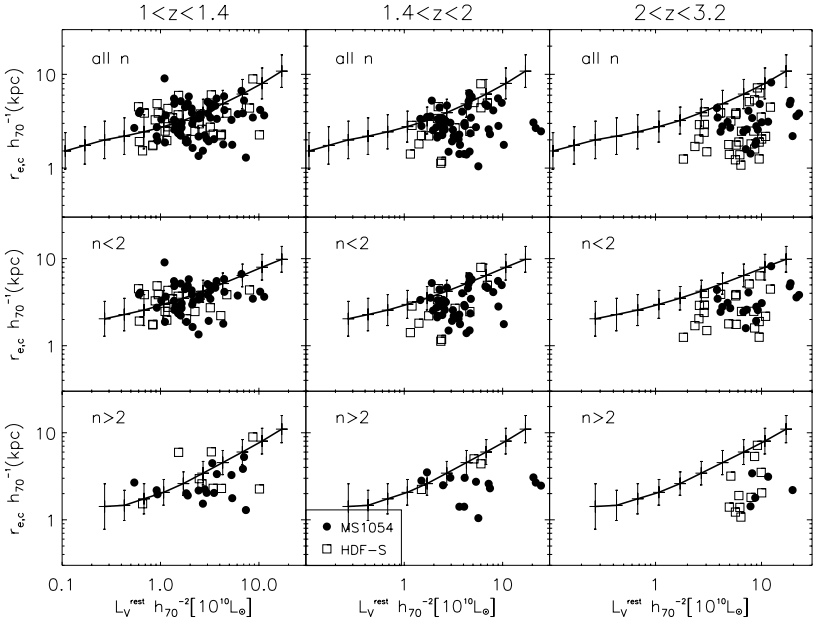

Figure 1. Distribution of the rest-frame optical sizes vs. the rest-frame V-band luminosities for all galaxies from FIRES. Galaxies from the HDF–S field are shown by open squares and galaxies from the MS1054 field by filled circles. The different rows show the galaxies separated according to their Sérsic index concentration parameter. Overplotted on the observed distribution of points are the mean and dispersion of the distribution of the Sérsic half-light radius of the SDSS galaxies (in the "V-band") as a function of the V-band luminosity. The second and third row show the SDSS distributions separating into late and early type respectively. For clarity individual error bars for the FIRES data are not shown; the mean size relative error is 30%.

Figure 1 shows that at a given luminosity, galaxies are progressively smaller at higher z. Of course, this evolution of the luminosity–size relation can be interpreted differently: at a given size, galaxies were more luminous at higher z.

To quantify the evolution of these relations as a function of redshift, we evaluate the ratio between the observed size and the expected size (at a given luminosity) from the SDSS distribution versus z. Galaxies at z$\sim$2.5 with $L_V > 3.4\times10^{10}\,h_{70}{}^{-2}\,L_\odot$ are $\sim$2.5 times smaller than for equally luminous galaxies today. We have also explored the relation between stellar mass and size for our sample (see Trujillo et al. 2005; Fig. 9). The stellar mass–size distribution evolves less than the luminosity–size relation at high-z. Galaxies with $M_\star > 3\times10^{10} h_{70}{}^{-2} M_\odot$ and z>1.5 have slightly smaller sizes than do equally massive galaxies today.

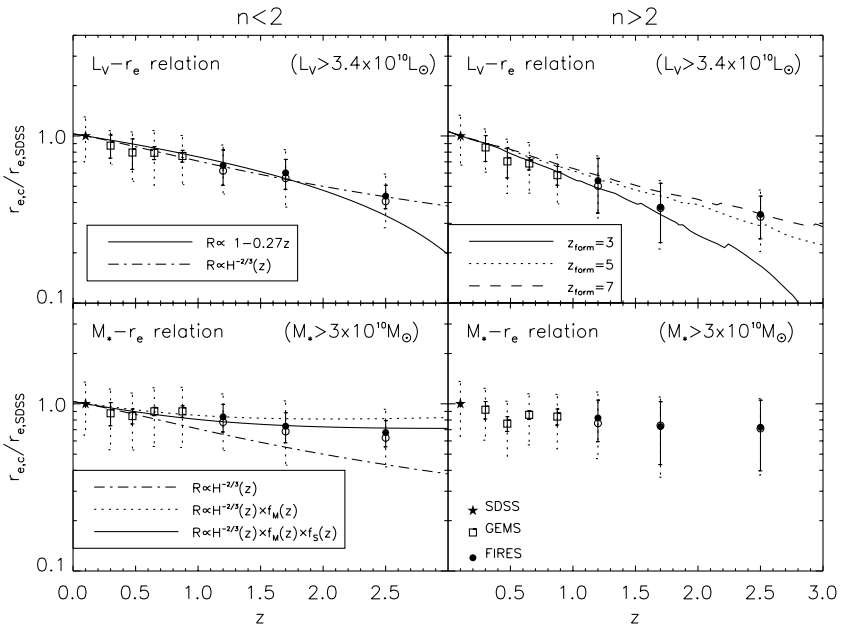

Figure 2. Redshift evolution of the ratio between the observed size and the present-day mean size at a given luminosity (upper panels), and the analogous ratio at a given mass (lower panels). The present-day values are derived from the SDSS sample (Shen et al. 2003). The comparison is restricted to the luminous ($L_V > 3.4\times10^{10} h_{70}{}^{-2} L_\odot$) and to massive ($M_\star\ 3\times10^{10} h_{70}{}^{-2} M_\odot$) galaxies. Open squares correspond to the GEMS sample (McIntosh et al. 2005; Barden et al. 2005) for galaxies with z<1 and solid points indicate the results from FIRES. The star indicates our local reference values from SDSS (mean $z\sim0.1$). We present the dispersion (dashed error bars) of the distribution and the uncertainty (2 σ) at the mean determination (solid error bars). The open circles correspond to a 7% correction of the sizes to model the size bias found through a comparison with NICMOS data (see Trujillo et al. 2005 for details). $Left\ column$: The dashed lines illustrate the expected evolution (Mo et al. 1998) at a fixed at fixed halo mass $R\propto H^{-2/3}(z)$ normalized to be 1 at z=0.1. The predicted size evolution at a given luminosity for Milky Way type objects (from the Bouwens & Silk 2002 infall model) is indicated with a solid line in the upper left panel. In the lower left panel we show (dotted line) the Mo et al. (1998) size evolution at a given halo mass corrected by the evolution of the stellar to halo mass $f_M(z)=(M_{halo}/M_\star)^{1/3}(z)$. The solid line accounts for the transformation of the gas settled in the disk into stars by multiplying the above correction for an extra factor $f_S(z)=R_\star/R_{disk}(z)$. $Right\ column$. The different lines illustrate the expected size evolution if the local luminosity–size relation for early-type galaxies is evolved in luminosity as expected for single-age stellar population models with different formation redshift [computed assuming a Salpeter (1955) IMF using the PEGASE (Fioc & Rocca-Volmerange 1997) code].

4. GEMS: Comparison of FIRES Data to the Evolution at z<1

In order to make a consistent comparison at lower redshifts with FIRES, we use the data from the largest sample currently available at intermediate redshift: the GEMS survey. The luminosity–size and stellar mass–size relations of this survey are presented in Barden et al. (2005; late-type galaxies) and McIntosh et al. (2005; early-type galaxies). Using their measurements of size, luminosity, mass, redshift and completeness we have repeated the same analysis as for the FIRES sample. To assure homogeneity with the FIRES sample we have only selected GEMS galaxies with $L_V > 3.4\times10^{10}\,h_{70}{}^{-2}\,L_\odot$ (in the case of the luminosity–size relation) and $M_\star > 3\times10^{10}\,h_{70}{}^{-2}\,M_\odot$ (in the case of the stellar mass–size relation). The resulting size evolution from both surveys together are shown in Fig. 2. From this comparison we see that the z<1 evolution (GEMS) and z>1 evolution (FIRES) derived from two independent analyses and data sets match very well. Comparison with different theoretical expectations is done in Fig. 2.

References

Barden, M. et al., 2005, ApJ, submitted, astro-ph/0502416
Bouwens, R. J. & Silk, J., 2002, ApJ, 568, 522
Bell, E. F. & de Jong, R. S., 2001, ApJ, 550, 212
Fall, S. M. & Efstathiou, G., 1980, MNRAS, 193, 189
Fall, S. M., 1983, in Athanassoula E., ed., Proc. IAU Symp. 100, Internal Kinematics and Dynamics of Galaxies. Reidel, Dordrecht, p. 391
Fioc, M., & Rocca-Volmerange, B., 1997, A&A, 326, 950
Franx, M. et al., 2000, "FIRES at the VLT: the Faint Infrared Extragalactic Survey", The Messenger 99, pp. 20
McIntosh, D. H., et al. 2005, ApJ, submitted, astro-ph/0411772
Mo, H. J., Mao, S. & White, S.D.M., 1999, MNRAS, 304, 175
Rix, H.-W. et al., 2004, ApJS, 152, 163
Rudnick, G. et al., 2001, AJ, 122, 2205
Rudnick, G. et al., 2003, ApJ, 599, 847
Shen, S., Mo, H.J., White, S.D.M., Blanton, M.R., Kauffmann, G., Voges, W., Brinkmann, J. & Csabai, I., MNRAS, 2003, 343, 978
Trujillo, I. et al., 2004, ApJ, 604, 521
Trujillo, I. et al., 2005, ApJ, submitted, astro-ph/0504225
York D. et al., 2000, AJ, 120, 1579

SPECIFIC STAR FORMATION RATES

A. E. Bauer*, N. Drory and G. J. Hill

Department of Astronomy, University of Texas at Austin, USA

* amanda@astro.as.utexas.edu

Abstract We present results from a study to determine how star formation contributes to galaxy growth since redshift $z = 1.5$. Using galaxies from the MUnich Near-Infrared Cluster Survey (MUNICS) and the FORS Deep Field (FDF), we investigate the specific star formation rate (SSFR, star formation rate [SFR] per unit galaxy stellar mass) as a function of galaxy stellar mass and redshift. We test the compatibility of our results with a sample drawn from a larger volume using the Sloan Digital Sky Survey. We find that the SSFR decreases as galaxy stellar mass increases, suggesting that star formation contributes more to the growth of low-mass galaxies than high-mass galaxies at all redshifts in this study. We also find a ridge in the SSFR that runs parallel to lines of constant SFR and decreases by a factor of 10 from $z = 1$ to today, matching the results of the evolution in SFR density seen in the "Lilly-Madau" diagram. The ridge evolves independently of galaxy stellar mass to a particular turnover mass at the high mass end. Galaxies above the turnover mass show a sharp decrease in SSFR compared to the average at that epoch, and the turnover mass increases with redshift.

Keywords: galaxies: evolution - galaxies: stellar content - surveys

Introduction

In an effort to study galaxy assembly, we look at the contribution of star formation (SF) to the growth of stellar mass in galaxies as a function of time. Stellar mass functions reveal that 50% of the local stellar mass density was in place by $z = 1$ (Drory et al. 2005). The stellar mass function describes the build up of stellar mass over cosmic time, but does not identify possible causes of growth for individual galaxies: mergers, tidal interactions, internal star formation, etc.

The well known "Lilly-Madau" diagram shows the star formation rate (SFR) density decreasing by a factor of 10 since $z = 1$ (Madau et al. 1996, Lilly et al. 1996), a result similarly concluded by measurements from SFR indicators covering nearly the full electromagnetic spectrum (e.g., Perez-Gonzalez

R. S. de Jong, Island Universes, 487–492.
© 2007 *Springer.*

et al. 2005). These results, however, give no indication of where the SF is taking place. Do all galaxies experience a factor of ten decrease in SFR? Is this trend dominated by high mass galaxies ending SF or by low mass galaxies initiating large amount of efficient SF? How and where are half of the local stars formed while the global SFR in decreasing by a factor of 10?

Cowie et al. (1996) used rest-frame K-band (2.2μm) luminosities and [OII] $\lambda 3727$ equivalent widths to show that galaxies with rapid SF decrease in K luminosity, and therefore mass, with decreasing redshift. A more direct measure of this association is the the specific star formation rate (SSFR, Guzman et al. 1997, Brinchmann & Ellis 2000), which measures the SFR per unit galaxy stellar mass, to study explicitly how SF contributes to galaxy growth for galaxies of different masses at different times in the history of the universe.

We combine two complementary redshift surveys to broaden the mass and redshift range that we can probe. The wide-area, medium deep MUNICS (Drory et al. 2001, Feulner et al. 2003) spectroscopic dataset provides intermediate to high mass galaxies typically in the mass range of $M_* \geq 10^{10}\mathrm{M}_\odot$. The FORS Deep Field (Heidt et al. 2003, Noll et al. 2004) covers a small portion of the sky very deeply, contributing $M_* < 10^{10}\ \mathrm{M}_\odot$ galaxies to the sample.

We adopt an $\Omega_M = 0.3$, $\Omega_\Lambda = 0.7$, $H_0 = 72\ \mathrm{km\ s^{-1}Mpc^{-1}}$ cosmology.

The Galaxy Data

The galaxies used in this study are gathered from the MUnich Near-Infrared Cluster Survey (MUNICS; Drory et al. 2001; Feulner et al. 2003) and the FORS Deep Field (FDF; Heidt et al. 2003; Noll et al. 2004). The MUNICS project is a wide-area, medium-deep, photometric and spectroscopic survey selected in the K-band, reaching $K \sim 19.5$, and including *BVRIJK*. Spectroscopy is complete to $K \sim 17.5$ over 0.25 square degrees and reaches $K = 19.5$ for 100 square arcmins. The spectra cover a wide wavelength range of $4000 - 8500$ Å at 13.2 Å (FWHM) resolution, sampling galaxies in the redshift range of $0.07 < z < 1$. Our MUNICS sample contains 202 objects, which are mostly massive ($M_* > 10^{10}\mathrm{M}_\odot$) field galaxies with detectable [OII]$\lambda 3727$ emission.

The FORS Deep Field (FDF) spectroscopic survey provides low-resolution spectra with detectable [OII]$\lambda 3727$ in the spectral window ($3300 - 10000$ Å at 23 Å (FWHM) resolution) to $z = 1.5$. The FDF survey is I-band selected reaching $I_{AB} = 26.8$ with spectroscopy to $I_{AB} = 24$. The FDF covers $7'$ x $7'$ in eight bands: $UBgRIzJK$. Our FDF sample includes 152 galaxies with detectable SF, and masses of mostly $M_* < 10^{10}\mathrm{M}_\odot$.

The trends seen among the FDF and MUNICS galaxy surveys exhibit similar evolution in their overlapping mass range around $M_* = 10^{10}\mathrm{M}_\odot$ and

are therefore suitable to analyze simultaneously to cover such a large range of galaxy stellar mass.

We developed an automated spectral measurement routine to consistently determine the fluxes of emission lines. We use the flux of the [OII] $\lambda 3727$ emission feature, which remains in the spectral window to $z = 1.5$, as a SFR indicator. We use the Kennicutt (1998, Equation 3) conversion from [OII] line luminosity to SFR in units of solar masses per year.

Stellar masses are determined for each galaxy by fitting a grid of composite stellar population models of varying age, star formation history, and dust extinction to multi-wavelength photometry to determine individual mass-to-light (M/L) ratios. This process is described in detail in Drory et al. (2004a).

Specific Star Formation Rates

Redshift and SFR distributions for both samples can be found in Figure 1 of Bauer et al. (2005). The majority of galaxies in the full samples (52% for MUNICS and 80% for FDF) have detectable SF, via the [OII]$\lambda 3727$ emission feature, and the closely matching redshift distributions indicating little redshift bias in sample selection. The maximum SFR increases with redshift, and is consistent between the two samples.

Figure 1 shows the SSFR versus galaxy stellar mass as a function of redshift, to $z = 1.5$. The open squares show MUNICS galaxies, the closed squares are FDF galaxies and the crosses in the lowest redshift bin are SDSS galaxies to be discussed in more detail later. Galaxies of low to intermediate stellar mass form a "ridge" in SSFR running parallel to lines of constant SFR in each redshift bin. The ridge exists in all redshift bins until, at some high "turnover" mass, the SSFRs drastically decrease, as expected for the higher mass, early-type, redder galaxies which tend to form fewer stars after $z = 1$. The turnover mass increases with redshift, showing higher SSFR for higher mass galaxies at earlier times, a process termed "downsizing" by Cowie et al. (1996).

A correlation exists between SSFR and mass (e.g., Brinchmann & Ellis 2000). Here we show this correlation evolves with redshift up to $z = 1.5$ independently of galaxy stellar mass. The ridge in the SSFR shifts downward as redshift decreases, indicating a steady decrease in the global SFR, from 10 $\mathrm{M}_\odot \mathrm{yr}^{-1}$ at $z = 1.5$ to 1 $\mathrm{M}_\odot \mathrm{yr}^{-1}$ at $z = 0$, agreeing with concurring trends in the "Lilly-Madau" diagram (Madau et al. 1996, Lilly et al. 1996) determined from a large variety of SFR indicators (see compilation by Hopkins 2004). Similar trends are also identified in the large sample of Feulner et al. (2005). While detecting the lowest SFRs at any epoch is affected by incompleteness, the evolution of the upper envelop is independent of selection effects.

In the present study we apply no corrections for extinction to the [OII] emission line fluxes. For the 10% of the galaxies where we have the necessary

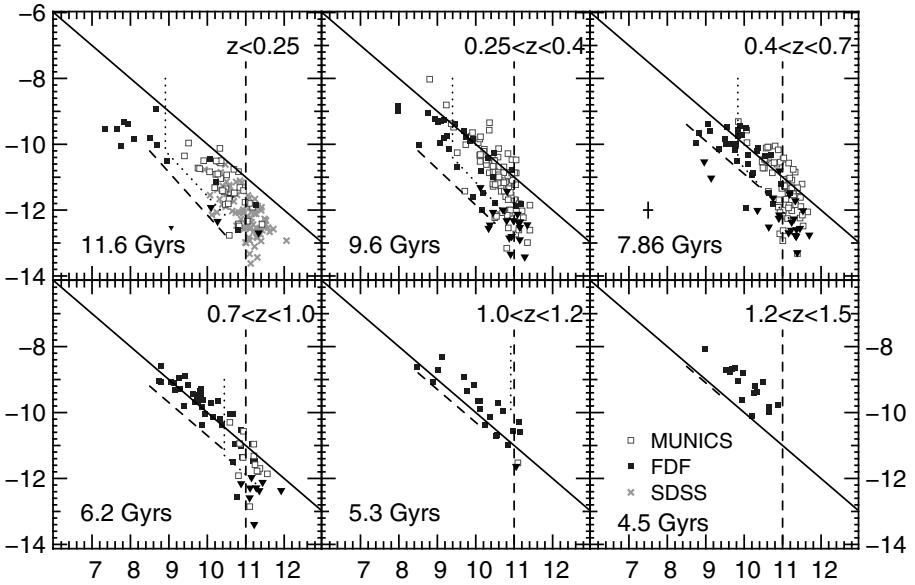

Figure 1. Specific Star Formation Rates versus Galaxy Stellar Mass. The open squares are MUNICS galaxies, filled squares represent FDF galaxies, the crosses show SDSS galaxies chosen to match the photometric limits of the MUNICS sample, and the triangles show 1 σ upper limits for SSFR. The solid diagonal line identifies a constant SFR = 1 $\mathrm{M}_{\odot}\mathrm{yr}^{-1}$. The dotted lines show the mass limits (vertical) and detectable star formation limits for the MUNICS survey while the dashed lines show the lower limits for detectable SSFR for FDF, derived from the spectroscopic sensitivity limits. Estimated error bars, appropriate for the majority of galaxies are shown in the $0.4 < z < 0.7$ bin.

Balmer emission lines to perform a proper dust correction, we find an average $E(B-V) = 0.2$, assuming a case B recombination. We feel it necessary to apply a unique dust correction to each galaxy (Maier et al. 2005) and consider a flat correction determined from a small sample of low redshift galaxies irrelevant to the differential SF studied here.

To ensure that the increase in SSFR at higher redshifts is not due to rarer objects being seen as larger volumes are probed, we investigate the trends in SSFR from the SDSS. We collected SDSS galaxies (Abazajian et al. 2004) selected to match the MUNICS magnitude limits as described in (Drory et al. 2004b), and determined stellar masses in the same way as the rest of our sample. We used the reported [OII]λ3727 emission line flux from the SDSS and followed the same Kennicutt (1998) conversion to SFR.

We chose a random sample of SDSS galaxies to match the number of galaxies in the lowest redshift bin from MUNICS and FDF and show them in Fig. 1 as crosses. The consistent SSFR between all galaxies samples, confirmed by

choosing several sets of SDSS galaxies, shows that our results are not due to volume effects in the low redshift bin.

Discussion

We present a study of the contribution of star formation (SF) to the growth of stellar mass in galaxies since $z = 1.5$ showing the SSFR versus galaxy stellar mass as a function of redshift over five decades in galaxy stellar mass. At all redshifts, the SSFR decreases as stellar mass increases. This indicates a higher contribution of SF to the growth of low mass galaxies since $z = 1.5$ and suggests that high mass galaxies formed the bulk of their stellar content earlier than $z = 1$.

Figure 1 shows evidence of a ridge in SSFR that runs parallel to lines of constant SFR. The ridge exists for all galaxy stellar masses $M_* = 10^7 - 10^{11}\mathrm{M}_\odot$ and increases uniformly, independent of mass as redshift increases. The first evidence for such a ridge and an upper bound in SSFR, moving to higher SFRs with increasing redshift was noted by Brinchmann & Ellis (2000). Our work moves beyond that study with spectroscopy of a mass limited sample at each redshift bin, covering a wide range of masses (Bauer et al. 2005).

Galaxies exist on Fig. 1 only when the SF induces detectable amounts of [OII] λ3727 emission. Our mass-selected galaxy samples, while not biased towards identifying star-forming galaxies, still show detectable SF in a majority $(50 - 80\%)$ of the galaxies at any epoch. Many studies focus on disentangling different stages in the lifetimes of individual galaxies. While this remains a difficult task, common trends in evolutionary paths have identified stages where detectable star formation occurs. One such stage is represented by a population of highly star forming, dust enshrouded, luminous IR galaxies (LIRGs) which are known to be much more common at $z > 1$ than they are today (e.g., Flores et al. 1999, Perez-Gonzalez et al. 2005). It is most likely that LIRGs correspond to short bursts of intense SF induced by recent merging or gas infall (Hammer et al. 2005). These brief bursts represent only occasional phases and not normal stages of SF in galaxy lifetimes, and we could possibly be detecting the low mass galaxies during LIRG phases.

The first studies of the evolution of the SFR from *Spitzer Space Telescope* 24 μm data have recently been published (Bell et al. 2005, Perez-Gonzalez et al. 2005). The SSFR evolution with stellar mass and redshift largely agrees with the work presented here for the low to intermediate mass galaxies, but show more scatter towards higher SSFRs in the high mass regime. While thermal IR observations detect the highly dust obscured objects missed by optical- and NIR-selected samples, a large uncertainty remains in converting the observed light into the total IR flux. The amount of dust heated by old stars is unknown. Since the most massive galaxies contain the largest populations of

old stars locally (e.g., Kennicutt et al. 1994) and at high redshifts (Drory et al. 2005), there is a possible tendency to overestimate the IR-derived SFR at higher stellar masses.

Large new surveys greatly improve our working understanding of galaxy evolution and stellar mass build up in the universe, but many uncertainties persist while we seek to understand the contributing components of new data. It remains important to continue multi-wavelength studies of galaxy evolution in seeking concordance among various methodologies.

References

Abazajian, K., et al. 2004, AJ, 128, 502

Bauer, A. E. and Drory, N. and Hill, G. J. and Feulner, G. 2005, ApJL, 621, L89

Brinchmann, J., & Ellis, R. S. 2000, ApJ, 536, L77

Cowie, L. L., Songaila, A., Hu, E. M., & Cohen, J. G. 1996, AJ, 112, 839

Drory, N. and Salvato, M. and Gabasch, A. and Bender, R. and Hopp, U. and Feulner, G. & Pannella, M. 2005, ApJ, 619L, 131D

Drory, N., Bender, R., Feulner, G., Hopp, U., Maraston, C., Snigula, J., & Hill, G. J. 2004a, ApJ, 608, 742

Drory, N., Bender, R., & Hopp, U. 2004b, astro-ph/0410084

Drory, N., Feulner, G., Bender, R., Botzler, C. S., Hopp, U., Maraston, C., Mendes de Oliveira, C., & Snigula, J. 2001b, MNRAS, 325, 550

Feulner, G., Goranova, Y., Drory, N., Hopp, U., & Bender, R. 2005, MNRAS, 358, L1

Feulner, G., Bender, R., Drory, N., Hopp, U., Snigula, J., & Hill, G. J. 2003, MNRAS, 342, 605

Flores, H. et al. 1999, ApJ, 517, 148F

Guzman, R., Gallego, J., Koo, D. C., Phillips, A. C., Lowenthal, J. D., Faber, S. M., Illingworth, G. D., & Vogt, N. P. 1997, ApJ, 489, 559

Hammer, F. and Flores, H. and Elbaz, D. and Zheng, X. Z. and Liang, Y. C. and Cesarsky, C. 2005 A&A, 430, 115H

Heidt, J., et al. 2003, A&A, 398, 49

Hopkins, A. M. 2004, ApJ, 615, 209

Kennicutt, R. C. 1998, ARA&A, 36, 189

Kennicutt, R. C. and Tamblyn, P. and Congdon, C. E. 1994, ApJ, 435, 22

Lilly, S. J., Le Fèvre, O., Hammer, F., & Crampton, D. 1996, ApJ, 460, L1

Madau, P., Ferguson, H. C., Dickinson, M. E., Giavalisco, M., Steidel, C. C., & Fruchter, A. 1996, MNRAS, 283, 1388

Maier, C., Lilly, S. J., Carollo, M., Stockton, A., & Brodwin, M. 2005, ApJ accepted, astro-ph/0508239

Noll, S., et al. 2004, A&A, 418, 885

Perez-Gonzalez, P. G., et al. 2005, ApJ, astro-ph/0505101

DISK GALAXIES AT HIGH REDSHIFT?

Max Pettini

Institute of Astronomy, Madingley Road, Cambridge, CB3 0HA, England
pettini@ast.cam.ac.uk

Abstract While many of the characteristics of the star-forming galaxies now being surveyed in large numbers at $z = 2 - 3$ are reminiscent of elliptical galaxies and bulges, the progenitors of today's spiral disks have proved more difficult to identify, probably because they were smaller and fainter at these early epochs. It will be many years yet before we can probe interstellar HI gas in 21 cm emission at these redshifts, but the HII regions of UV-bright galaxies will soon be mapped on kpc-scale from the ground with new instrumentation designed to work with laser-guided adaptive optics. This will be our best chance to measure disk-like rotation at high redshift.

Keywords: galaxies: high-redshift - galaxies: spiral - galaxies: kinematics and dynamics - galaxies: formation

1. Introduction

In the last few years the high redshift universe has spectacularly opened up to direct observations. Galaxies have been discovered at redshift up to nearly $z = 7$; large scale surveys have yielded thousands of galaxies with spectroscopic confirmation in well defined redshift intervals, including some which only a few years ago were considered inaccessible, such as the 'redshift desert' at $z \simeq 1.5 - 2.5$; and deep imaging campaigns have measured their emission over most of the electromagnetic spectrum from X-rays to radio wavelengths.

The main motivation common to all of these observational programmes is the desire to link the properties of high redshift galaxies with those we see around us today and thereby understand the physical processes at play in the formation and evolution of structure in the universe. It is perhaps a surprise to many of the participants of this meeting to realise that much of the effort so far has focused on the identification of the progenitors of today's elliptical galaxies and massive bulges, and that comparatively little attention seems to have been paid in direct imaging surveys to what might be the ancestors of disk galaxies like the Milky Way.

R. S. de Jong, Island Universes, 493–500.
© 2007 *Springer.*

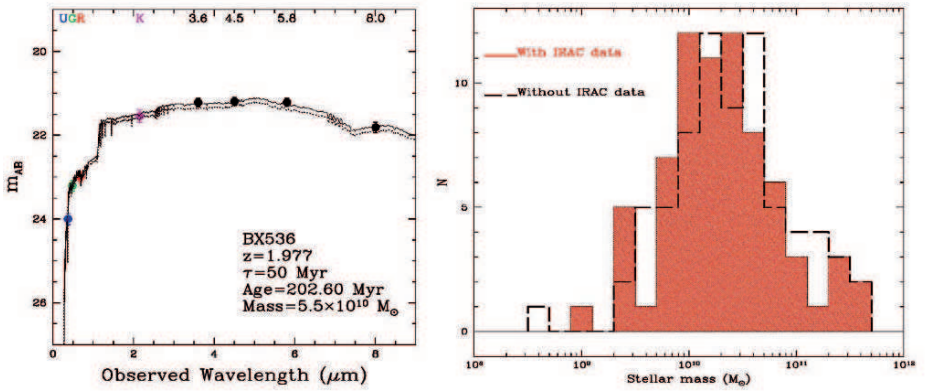

Figure 1. *Left:* Model spectral energy distributions (continuous line) which best fit the rest-frame UV to near-IR photometry of Q1700-BX536, a typical star-forming galaxy at $z\simeq2$. The bottom curve shows the result of fitting to the $UG\mathcal{R}K$ magnitudes only, excluding the *Spitzer* IRAC data points. The parameters values which characterise the best-fitting model—e-folding time scale of declining star formation, age, and assembled stellar mass—are given in the bottom right-hand corner. *Right:* Histograms of assembled stellar masses for the 72 BX galaxies with spectroscopic redshifts in the field of the $z_{\rm em}$=2.72 QSO HS1700+643. The median stellar mass of $z\simeq2$ galaxies brighter than $\mathcal{R}\simeq25.5$ is $2\times10^{10}M_\odot$. (From Shapley et al. 2005.)

2. Star-Forming Galaxies at $z\gtrsim2$: Ellipticals and Bulges in the Making

Galaxies directly detected in imaging surveys at optical, infrared, and sub-mm wavelengths all share many characteristics highly suggestive of an evolutionary link with today's spheroidal component of the galaxy population. While the results which I am about to summarise are mostly those obtained for the (rest-frame) UV-bright galaxies which constitute the 'Lyman break' ($\langle z\rangle = 3.0\pm0.3$) and 'BX' ($\langle z\rangle = 2.2\pm0.3$) samples of Steidel et al. (2003, 2004), the same considerations also apply to many of the objects uncovered by most other surveys targeting galaxies at these redshifts.

Their emission properties at X-ray (Reddy & Steidel 2004) and mid-IR (Reddy et al. 2006) wavelengths indicate star formation rates $\gtrsim10M_\odot$ yr^{-1} (for galaxies brighter than $\mathcal{R}=25.5$) and an average bolometric luminosity $\langle L_{\rm bol}\rangle\simeq3\times10^{11}L_\odot$. Their spectral energy distributions, which have now been determined from the rest-frame UV to the near-IR thanks to the highly successful *Spitzer* Space Telescope, indicate that these high star formation rates typically persist for several hundred million years, leading to the rapid assembly of stellar masses $M_*\gtrsim10^{10}M_\odot$ (see Figure 1) and to near-solar metallicities in the gas (Figure 2). In models of galaxy formation which couple cosmological simulations of dark matter halos with the physics and dynamics of the baryons (e.g., Blaizot et al. 2004; Mori & Umemura 2005) objects exhibiting these properties at $z=2-3$ naturally evolve to become today's massive and metal-rich elliptical galaxies.

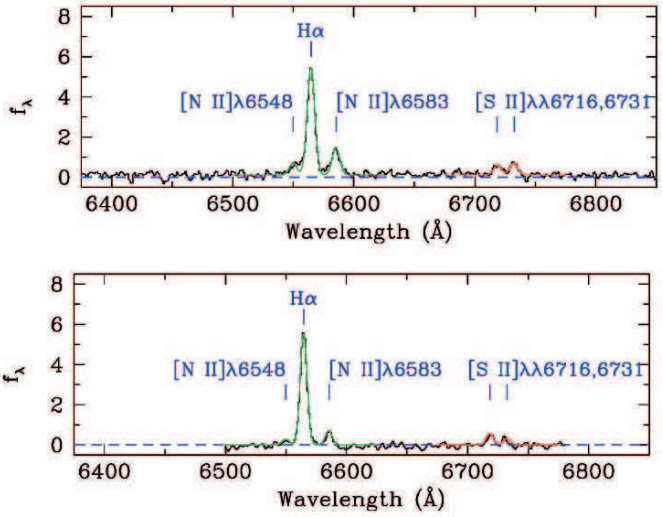

Figure 2. Composite spectra of BX galaxies at $z \simeq 2.2$ from the survey by Erb et al. (2006). *Upper Panel:* galaxies brighter than $K_s = 20$ have a mean ratio [N II]/H$\alpha = 0.25$ which indicates an oxygen abundance $12 + \log(\mathrm{O/H}) = 8.56$, or $\sim 4/5$ solar, if the local calibration of the $N2$ index with (O/H) applies to these galaxies. *Lower Panel:* galaxies fainter than $K_s = 20$ have [N II]/H$\alpha = 0.13$ and $12 + \log(\mathrm{O/H}) = 8.39$, or $\sim 1/2$ solar.

The closest, and best studied, spiral bulge is that of the Milky Way where the properties of individual stars can be determined. Most models which have been proposed to explain the distributions of stellar ages, metallicities, and element ratios (e.g., Ferreras, Wyse, & Silk 2003) share the same basic ingredients: (a) an early epoch of formation, at $z \sim 5$; (b) short infall timescales, $\tau < 0.5$ Gyr, leading to a rapid enrichment to near-solar metallicity and enhanced [α/Fe] ratios; and (c) significant outflow of gas and metals accompanying the collapse and star formation process, resulting in a final stellar mass $M_* \sim 10^{10} M_\odot$. These characteristics are very much in line with those determined for a typical UV-selected ('BX') galaxy at $z \sim 2$, although galaxies which *end up* with an assembled stellar mass of only $M_* \sim 10^{10} M_\odot$ are probably near, or below, the faint end of the observed luminosity distribution.

Perhaps the most compelling evidence linking the UV- and IR-bright galaxies at $z = 2 - 3$ with today's elliptical galaxies is provided by their clustering properties (see Figure 3). As shown by Adelberger et al. (2004), the high redshift populations are highly clustered, with correlation lengths $r_0 = 4.0 - 4.5 h^{-1}$ Mpc. In cosmological simulations, dark matter halos with these values of r_0 have masses $M_{\mathrm{DM}} = 10^{11.2} - 10^{12.3} M_\odot$; evolved forward in time their clustering and number density are a much better match to those of elliptical galaxies than spirals. There are also indications that in the largest galaxy overdensities at $z \simeq 2$ star formation started earlier than in the field, as expected within the general framework of hierarchical clustering theories of the

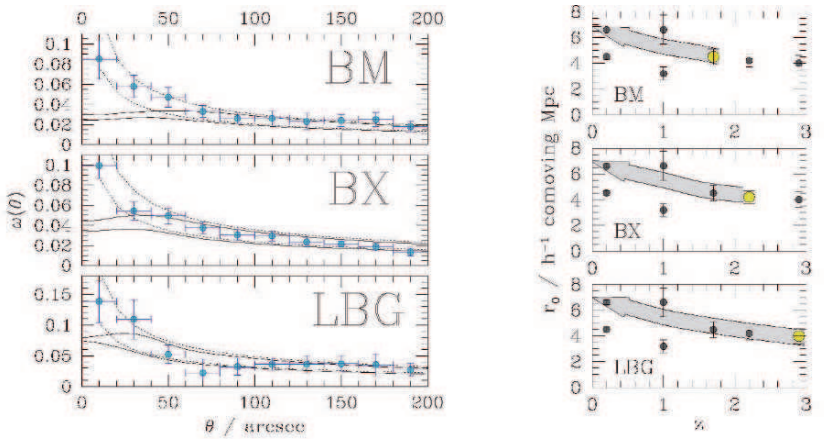

Figure 3. *Left*: Angular clustering on the sky of 'BM' ($\langle z \rangle = 1.7$), 'BX' ($\langle z \rangle = 2.2$), and Lyman break ($\langle z \rangle = 3.0$) galaxies (data points) and of dark matter halos from cosmological simulations (continuous lines). The simulations match the observations for halo masses in the range $M_{\rm DM} = 10^{11.2} - 10^{12.3} M_{\odot}$. *Right*: The arrows show the evolution seen in the simulations for halos within the mass ranges which match the observed galaxy clustering. The BM, BX, and LBG samples seem to trace the same objects—or, more precisely, the same halo mass range—through different evolutionary stages. When evolved to intermediate and low redshifts, their clustering matches that of elliptical galaxies in the DEEP and 2dF surveys (the two upper data points at $z = 1$ and 0.2), rather than that of galaxies which are still forming stars at these later epochs (lower data points). Figures reproduced from Adelberger et al. (2004).

evolution of structure. As a consequence, galaxies within these overdensities tend to have higher stellar masses and metallicities than the mean values for the population as a whole (Steidel et al. 2005).

2.1 Does Star Formation Take Place in Disks at $z = 2 - 3$?

In the standard picture whereby galaxies form via dissipative cooling of baryons within cold dark matter halos, star formation naturally takes place within a rotationally supported disk. Observationally, however, it has so far been difficult to prove conclusively that this in indeed the case. Occasionally, the nebular emission lines (mostly Hα and [O III]) from the HII regions of galaxies at $z = 2 - 3$ show spatially tilted profiles which are suggestive of ordered motions on scales of 5–10 kpc (Pettini et al. 2001; Erb et al. 2003). Some examples have been reproduced in Fig. 4. The interpretation of these kinematics as rotation is, however, far from clear-cut. A major difficulty is the inadequacy of the spatial resolution achieved so far, as evidenced by the finding that the velocity extent measured is highly dependent on the seeing (Erb et al. 2004). In no case has a flattening of these 'rotation curves' been detected unambiguously, presumably because the light is dominated by the inner, high surface brightness, regions. Of most concern is the lack of correlation between

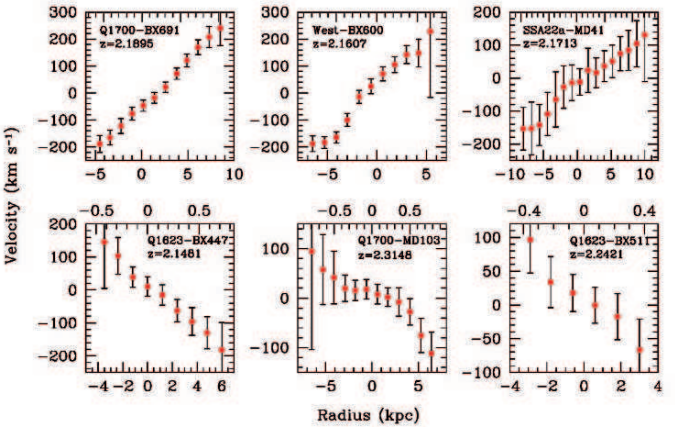

Figure 4. Examples of spatially resolved profiles of the Hα emission line in BX galaxies. Velocities are plotted relative to the central wavelength of the integrated Hα emission line, assumed to define the systemic redshift of the galaxy under consideration. Spatial offsets are measured relative to the centre of the continuum emission when available, or the spatial centre of Hα otherwise. The points shown are not independent, because the seeing was typically 0.5 arcsec FWHM. The standard 737 cosmology ($H_0 = 70\,\mathrm{km\ s^{-1}\ Mpc^{-1}}$, $\Omega_\mathrm{M} = 0.3$, $\Omega_\Lambda = 0.7$) was adopted to convert from arcsec on the sky to kpc at the redshift of each galaxy. Interpreted as rotation curves, the kinematics and linear extent of these galaxies imply dynamical masses $M_\mathrm{dyn} = v_c^2 r/G = (0.5 - 7) \times 10^{10} M_\odot$. However, the apparently ordered velocities could also be due to merging of protogalactic clumps.

the morphology of the galaxies and the incidence of ordered motions of their HII regions. Galaxies which in broad-band *HST* images have the appearance of highly inclined disks are no more likely to exhibit rotation along their major axes than galaxies with irregular or spheroidal morphology (Erb et al. 2004). An origin in merging protogalactic clumps is thus at least as plausible an explanation of the observed velocity patterns as rotating disks.

3. Damped Lyman alpha Systems: Early Stages in the Formation of Spiral Galaxies?

While an evolutionary link between star-forming galaxies at $z = 2 - 3$ and the spheroidal component of the local galaxy population is strongly suggested by the available evidence, an analogous connection for DLAs is still a matter for debate. The working hypothesis that in DLAs we see the progenitors of today's disk galaxies like the Milky Way (Wolfe et al. 1986), while consistent with the kinematics of the associated metal absorption lines (Wolfe et al. 2005), runs into some difficulties when confronted with the extensive set of metallicity measurements now available for DLAs (see Figure 5). Current models (e.g., Naab & Ostriker 2005) envisage the Milky Way disk to have been significantly smaller at $z = 2 - 3$ (that is, disk growth is from 'inside out'), and this would

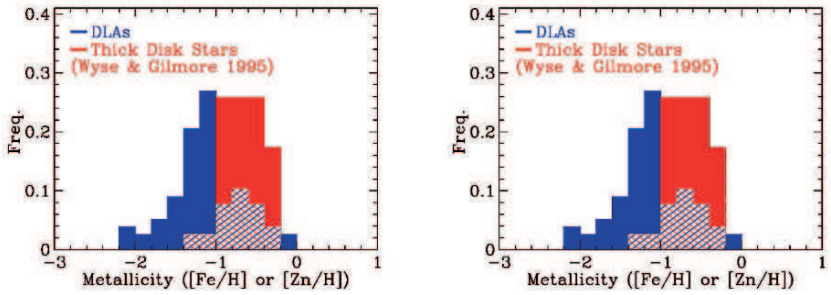

Figure 5. Metallicity distributions of DLAs and Milky Way thick (left panel) and thin (right panel) disk stars from the work by Akerman et al. (2005). The metallicity is measured from Zn in DLAs and Fe in Galactic stars. Approximately one half of the DLA measurements of [Zn/H] are upper limits; they have been included in the histograms as if they were detections.

indeed explain why direct detection of the stellar light from DLA host galaxies at $z > 1$ has proved so elusive (Wolfe et al. 2005 and references therein). However, even in the early stages of its evolution, the disk was already more metal rich than most DLAs, with $Z \simeq 1/3 Z_{\odot}$; the flat age-metallicity relation of disk stars implies that the epoch when the metallicity of the Milky Way was below this value was brief (e.g., Akerman et al. 2004). Consequently, there is little overlap between the metallicity distributions of the DLAs on the one hand, and of stars in the thin and thick disks of the Galaxy on the other (Fig. 5).

The low metallicities of most DLAs may be reconciled with the proposed origin in spiral galaxies if, during their assembly, disk galaxies were surrounded by extended envelopes (a halo, or a thick disk) of neutral gas which was metal-poor, or had a steep metallicity gradient. Such a scenario has been proposed by Wolfe et al. (2003) and may be the explanation for the very extended stellar disk structures recently found in galaxies such as M31 (Ibata et al. 2005). Simulations of the growth of disk galaxies through mergers of gas-rich subunits (e.g., Navarro 2004; Governato et al. 2005) can reproduce many of the characteristics of the Local Group of galaxies—it will be of considerable interest to examine in more detail the properties of the gaseous components of such mergers during this early build-up epoch with an eye to their possible interpretation as DLAs.

One of the most significant advances towards answering the long-standing question of which galaxies give rise to damped Lyα systems is the recent work by Zwaan et al. (2006) who tackled the problem 'from the other end', as it were, by considering the HI properties of local galaxies. Based on 21 cm maps of nearly 400 galaxies, obtained as part of the Westerbork HI survey of spiral and irregular galaxies (WHISP) and covering all Hubble types and a wide range in luminosity, the analysis by Zwaan et al. has shown that the distribution of luminosities of the galaxies producing DLAs is nearly flat from $M_B = -21$ to $M_B = -15$. Thus, at $z = 0$, galaxies spanning over two orders of magnitude

in luminosity evidently make roughly comparable contributions to the overall cross-section on the sky for DLA absorption. If this is also the case at high z, the heterogeneous nature of DLA absorbers provides a plausible explanation for the wide dispersion in their physical properties, including metallicity.

4. Summary and Outlook

In conclusion, it is certainly encouraging to reflect on the advances made over the last few years in charting the high redshift universe and in determining some important physical characteristics of the galaxies which inhabit it. Galaxies which are sufficiently bright to be detected in deep imaging surveys exhibit high star formation rates, of the order of tens of solar masses per year; rapid timescales of chemical enrichment and stellar mass assembly, of the order of a few hundred Myr; and the strong clustering appropriate to the most massive dark matter halos. These characteristics are broadly consistent with our ideas of how elliptical galaxies and the bulges of massive spirals may have formed when the universe was 1–2 Gyr old.

Contrasting these positive results, we have yet to find unequivocal evidence of disks at high redshifts, either in the kinematic properties of the HII regions of star-forming galaxies, or in the more general characteristics of damped Lyα systems, although there is mounting evidence that the latter are a varied population which may well include the progenitors of today's spirals like the Milky Way, as well as lower mass systems. But it would be overly pessimistic to end on a negative note. Admittedly, we are still many years away from developing the capability to trace at high redshifts the HI 21 cm rotation curves familiar to many of the participants of this meeting. However, recent advances in adaptive optics on 8-10 m telescopes have now turned into reality our long-held dream of overcoming the blurring effects of the Earth's atmosphere with large aperture, ground-based telescopes. Coupled to integral field near-IR spectrographs such as SINFONI on the ESO VLT and OSIRIS on the Keck II telescope, this state-of-the art technology should allow us to probe on kpc-scales the kinematics of the ionised gas in star-forming galaxies at $z = 2 - 3$. Exploratory tests suggest that such spatial resolution should be sufficient to distinguish between pure rotation and merging (see Figure 6). Even though the real situation is likely to be less black-and-white than the examples illustrated in Figure 6, exciting new findings in this area are undoubtedly just around the corner.

Acknowledgements It is a pleasure to acknowledge my collaborators in the various projects described in this review, particularly Kurt Adelberger, Chris Akerman, David Bowen, Sara Ellison, Dawn Erb, Naveen Reddy, Sam Rix, Alice Shapley and Chuck Steidel. I am very grateful to the conference organisers for financial support, which helped me take part in this stimulating and most enjoyable meeting, and for their patience with the preparation of this article.

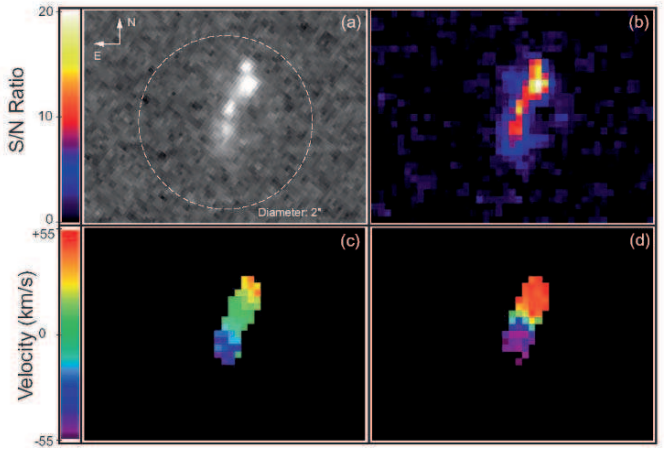

Figure 6. (a) *HST*-ACS B-band image of the z=2.2136 galaxy BX 1332 in the GOOD-N field. The other panels show maps of the S/N ratio (b), and velocity differences in the alternative cases of (c) a rotating disk, and (d) a bimodal velocity structure, expected after a four-hour integration with the laser-guided adaptive optics-fed near-IR spectrograph OSIRIS soon to come into routine operation on the Keck II telescope. (Reproduced from Law, Steidel,& Erb 2005).

References

Adelberger, K. L. et al. 2004, ApJ, 607, 226
Akerman, C. J., Carigi, L., Pettini, M., Nissen, P. E. & Asplund, M. 2004, A&A, 414, 931
Akerman, C. J., Ellison, S. L., Pettini, M., & Steidel, C. C. 2005, A&A, 440, 499
Blaizot, J. et al. 2004, MNRAS, 352, 571
Erb, D. K. et al. 2003, ApJ, 591, 101
Erb, D. K., Steidel, C. C., Shapley, A. E., Pettini, M., & Adelberger, K. L. 2004, ApJ, 612, 122
Erb, D. K. et al. 2006, ApJ, submitted
Ferreras, I., Wyse, R. F. G. & Silk, J. 2003, MNRAS, 345, 1381
Governato, F., Stinson, G., Wadsley, J., & Quinn, T. 2005, in The Fabulous Destiny of Galaxies: Bridging Past and Present, in press (astro-ph/0509263)
Ibata, R. et al. 2005, ApJ, submitted (astro-ph/0504164)
Law, D. R., Steidel, C. C., & Erb, D. K. 2005, AJ,
Mori, M., & Umemura, M. 2005, Nature, submitted
Naab, T., & Ostriker, J. P. 2005, MNRAS, in press (astro-ph/0505594)
Navarro, J.F. 2004, in Penetrating Bars through Masks of Cosmic Dust, p. 655
Pettini, M. et al. 2001, ApJ, 554, 981
Reddy, N. A., & Steidel, C. C. 2004, ApJ, 603, L13
Reddy, N. A. et al. 2006, ApJ, submitted
Shapley, A. E. et al. 2005, 626, 698
Steidel, C. C. et al. 2005, ApJ, 626, 44
Steidel, C. C. et al. 2004, ApJ, 604, 534
Wolfe, A. M., Gawiser, E., & Prochaska, J. X. 2003, ApJ, 593, 235
Wolfe, A. M., Prochaska, J. X., & Gawiser, E. 2005, ARAA, 43, 861
Wolfe, A. M., Turnshek, D. A., Smith, H. E., & Cohen, R. D. 1986, ApJS, 61, 249
Wyse, R. F. G., & Gilmore, G. 1995, AJ, 110, 2771
Zwaan, M. A. et al. 2006, MNRAS, in press (astro-ph/0510127)

LOCAL GALAXIES AS DAMPED LY-α ANALOGS

M. A. Zwaan[1*], J. M. van der Hulst[2], F. H. Briggs[3,4], M. A. W. Verheijen[2] and E. V. Ryan-Weber[5]

[1] *ESO, Garching b. München, Germany.*
[2] *Kapteyn Astronomical Institute, University of Groningen, The Netherlands*
[3] *RSAA, Mount Stromlo Observatory, Weston, Australia*
[4] *Australian National Telescope Facility, Epping, Australia*
[5] *Institute of Astronomy, University of Cambridge, UK*
* mzwaan@eso.org

Abstract We calculate in detail the expected properties of low redshift DLAs under the assumption that they arise in the gaseous disks of galaxies like those in the $z{\approx}0$ population. A sample of 355 nearby galaxies is analysed, for which high quality HI 21-cm emission line maps are available as part of an extensive survey with the Westerbork telescope (WHISP). We find that expected luminosities, impact parameters between quasars and DLA host galaxies, and metal abundances are in good agreement with the observed properties of DLAs and DLA galaxies. The measured redshift number density of $z{=}0$ gas above the DLA limit is $dN/Sdz = 0.045 \pm 0.006$, which compared to higher z measurements implies that there is no evolution in the comoving density of DLAs along a line of sight between $z{\sim}1.5$ and $z{=}0$, and a decrease of only a factor of two from $z{\sim}4$ to the present time. We conclude that the local galaxy population can explain all properties of low redshift DLAs.

Keywords: galaxies: ISM - quasars: absorption lines - galaxies: evolution

1. Introduction

The range of HI column densities typically seen in routine 21-cm emission line observations of the neutral gas disks in nearby galaxies is very similar to those that characterise the Damped Lyman-α Systems or DLAs with $N_{\rm HI} > 2 \times 10^{20}$ cm^{-2}. An attractive experiment would therefore be to map the HI gas of DLA absorbing systems in 21-cm emission, and measure the DLAs' total gas mass, the extent of the gas disks and their dynamics. This would provide a direct observational link between DLAs and local galaxies, but unfortunately such studies are impossible with present technology (see e.g., Kanekar et al. 2001). The transition probability of the hyperfine splitting that causes

R. S. de Jong, Island Universes, 501–506.
© 2007 *Springer.*

the 21-cm line is extremely small, resulting in a weak line that can only be observed in emission in the very local ($z<0.2$) universe, with present technology. On the other hand, the identification of DLAs as absorbers in background QSO spectra is, to first order, not distance dependent because the detection efficiency depends mostly on the brightness of the background source, not on the redshift of the absorber itself. In fact, the lowest redshift ($z<1.7$) Lyman-α absorbers cannot be observed from the ground because the Earth's atmosphere is opaque to the UV wavelength range in which these are to be found. Furthermore, due to the expansion of the universe the redshift number density of DLAs decreases rapidly toward lower redshifts. Consequently, there are not many DLAs known whose 21-cm emission would be within the reach of present-day radio telescopes.

So, we are left with a wealth of information on the cold gas properties in local galaxies, which has been collected over the last half century, and several hundreds DLA absorption profiles at intermediate and high redshift, but little possibility to bridge these two sets of information. Obviously, most observers resort to the optical wavelengths to study DLAs but attempts to directly image their host galaxies have been notably unsuccessful (see e.g., Warren et al. 2001 and Møller et al. 2002 for reviews). A few positive identifications do exist, mostly the result of HST imaging.

Although the absolute number of DLAs at low z is small, the success rate for finding low-z host galaxies is better for obvious reasons: the host galaxies are expected to be brighter and the separation on the sky between the bright QSO and the DLA galaxy is likely larger. Early surveys for low-z DLA host galaxies consisted of broad band imaging and lacked spectroscopic follow-up (e.g., Le Brun et al.1997). Later studies aimed at measuring redshifts to determine the association of optically identified galaxies with DLAs, either spectroscopically (e.g., Rao et al. 2003), or using photometric redshifts (Chen & Lanzetta 2003). All together, there are now $\sim$20 DLA galaxies known at $z<1$. The galaxies span a wide range in galaxy properties, ranging from inconspicuous LSB dwarfs to giant spirals and even early type galaxies. Obviously, it is not just the luminous, high surface brightness spiral galaxies that contribute to the HI cross section above the DLA threshold. As explained above, we cannot study these galaxies in the 21-cm line on a case-by-case basis, but we can do a study of a statistical nature to see if the properties of DLAs and DLA galaxies agree with our knowledge of HI in the local universe.

2. 140,000 "DLAs" at $z=0$

Blind 21-cm emission line surveys in the local universe with single dish radio telescopes such as Parkes or Arecibo have resulted in an accurate measurement of $\Omega_{\rm HI}(z=0)$, which can be used as a reference point for higher redshift

DLA studies. $\Omega_{\rm HI}$ is simply calculated by integrating over the HI mass function of galaxies, which is measured with surveys such as HIPASS (Zwaan et al. 2005a). However, due to the large beam widths of the singe dish instruments, these surveys at best only barely resolve the detected galaxies and are therefore not very useful in constraining the column density distribution function of $z \approx 0$ HI. Hence, for this purpose we use the high resolution 21-cm maps of a large sample of local galaxies that have been observed with the Westerbork Synthesis Radio Telescope. This sample is known as WHISP (van der Hulst et al. 2001) and consists of 355 galaxies spanning a large range in HI mass and optical luminosity. The total number of independent column density measurements above the DLA limit is ∼140,000, which implies that the data volume of our present study is the equivalent of ∼140,000 DLAs at z=0!

Each galaxy in the sample is weighted according to the HI mass function of galaxies. We can now calculate the column density distribution function $f(N_{\rm HI})$,

$$f(N_{\rm HI}) = \frac{c}{H_0} \frac{\int \Phi(M_{\rm HI}) \Sigma(N_{\rm HI}, M_{\rm HI})\, dM_{\rm HI}}{dN_{\rm HI}}, \qquad (1)$$

where $\Sigma(N_{\rm HI}, M_{\rm HI})$ is the area function that describes for galaxies with HI mass $M_{\rm HI}$ the area in $\rm Mpc^{-2}$ corresponding to a column density in the range $N_{\rm HI}$ to $N_{\rm HI} + dN_{\rm HI}$, and $\Phi(M_{\rm HI})$ is the HI mass function. c/H_0 converts the number of systems per Mpc to that per unit redshift.

Figure 1 shows the resulting $f(N_{\rm HI})$ on the left, and the derived HI mass density per decade of $N_{\rm HI}$ on the right. For comparison with higher redshift observations, we also plot the results from two other studies. The Péroux (2005) measurements of $f(N_{\rm HI})$ below the DLA limit are the result of their new UVES survey for "sub-DLAs". The intermediate redshift points from Rao et al. (2005) are based on Mg II-selected DLA systems. The surprising result from this figure is that there appears to be only very mild evolution in the intersection cross section of HI from redshift z∼5 to the present. From this figure we can determine the redshift number density of $\log N_{\rm HI} > 20.3$ gas and find that $dN/dz = 0.045 \pm 0.006$, in good agreement with earlier measurements at z=0. Compared to the most recent measurements of dN/dz at intermediate and high z, this implies that the comoving number density (or the "space density times cross section") of DLAs does not evolve after z∼1.5. In other words, the local galaxy population explains the incidence rate of low and intermediate z DLAs and there is no need for a population of hidden very low surface brightness (LSB) galaxies or isolated HI clouds (dark galaxies).

The right hand panel shows that at z=0 most of the HI atoms are in column densities around $N_{\rm HI} = 10^{21}$ $\rm cm^{-2}$. This also seems to be the case at higher redshifts, although the distribution might flatten somewhat. The one point that clearly deviates is the highest $N_{\rm HI}$ point from Rao et al. (2005) at $\log N_{\rm HI} = 21.65$. The figure very clearly demonstrates that this point dominates

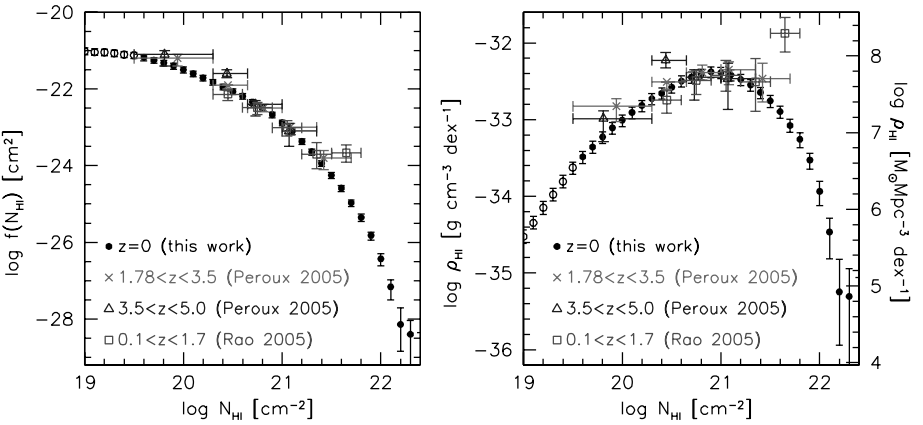

Figure 1. *Left:* The HI column density distribution function $f(N_{\rm HI})$. The solid dots are from our analysis of 21-cm maps of local galaxies, the other points are from various surveys at higher redshifts as indicated in the legend. All calculations are based on a $\Omega_{\rm m} = 0.3$, $\Omega_\Lambda = 0.7$ cosmology. *Right:* The contribution of different column densities (per decade) to the integral HI mass density. Note the very weak evolution in $\Omega_{\rm HI}$ from high z to the present.

the $\Omega_{\rm HI}$ measurement at intermediate redshifts. It is therefore important to understand whether the Mg II-based results really indicate that high column densities ($\log N_{\rm HI} \sim 21.65$) are rare at high and low redshift, but much more ubiquitous at intermediate redshifts, or whether the Mg II selection introduces currently unidentified biases.

3. Expected Properties of Low-z DLAs

Now that we have accurate cross section measurement of all galaxies in our sample, and know what the space density of our galaxies is, we can calculate the cross-section weighted probability distribution functions of various galaxy parameters. Figure 2 shows two examples. The left panel shows the B-band absolute magnitude distribution of cross-section selected galaxies above four different HI column density cut-offs. 87% of the DLA cross-section appears to be in galaxies that are fainter than L_*, and 45% is in galaxies with $L < L_*/10$. These numbers agree very well with the luminosity distribution of z<1 DLA host galaxies. Taking into account the non-detections of DLA host galaxies and assuming that these are $\ll L_*$, we find that 80% of the z<1 DLA galaxies are sub-L_*. The median absolute magnitude of a z=0 DLA galaxy is expected to be $M_B = -18.1$ ($\sim L_*/7$). The conclusion to draw from this is that we should not be surprised to find that identifying DLA host galaxies is difficult. Most of them (some 87%) are expected to be sub-L_* and many are dwarfs.

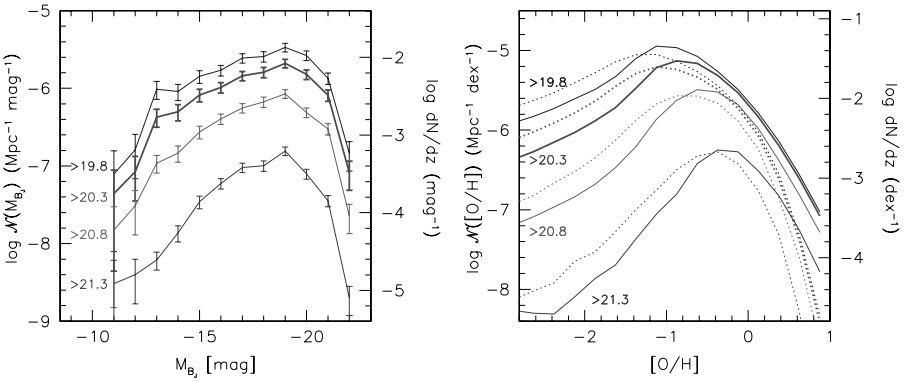

Figure 2. *Left:* The expected distribution of B-band absolute magnitudes of z=0 high HI column density systems. The lines plus errorbars show the product of cross sectional area and space density, which translates to the number of expected absorbers per Mpc per magnitude. The right axis shows the corresponding number of absorbers per unit redshift dN/dz. The different lines correspond to different column density limits, as indicated by the labels. The thick line corresponds to the classical DLA limit of $\log N_{\rm HI} > 20.3$. *Right:* The probability distribution of oxygen abundance [O/H] of HI absorbers. The solid lines refer to the approach of assuming fixed [O/H] gradients and the the dashed lines refer to varying gradients (see text).

Using similar techniques, we find that the expected median impact parameter of $\log N_{\rm HI} > 20.3$ systems is 7.8 kpc, whereas the median impact parameter of identified z<1 DLA galaxies is 8.3 kpc. Assuming no evolution in the properties of galaxies' gas disks, these numbers imply that 37% of the impact parameters are expected to be less than $1''$ for systems at z=0.5. This illustrates that very high spatial resolution imaging programs are required to successfully identify a typical DLA galaxy at intermediate redshifts.

The right panel in Figure 2 shows the probability distribution of oxygen abundance in z=0 DLAs. We constructed this diagram by assigning to every HI pixel in our 21-cm maps an oxygen abundance, based on the assumption that the galaxies in our sample follow the local metallicity–luminosity ($Z - L$) relation (e.g., Garnett 2002), and that each disk shows an abundance gradient of [O/H] of $-0.09\,{\rm dex\,kpc^{-1}}$ (e.g., Ferguson et al. 1998) along the major axis. The solid lines correspond to these assumptions, the dotted lines are for varying metallicity gradients in disks of different absolute brightness. The main conclusion is that the metallicity distribution for HI column densities $\log N_{\rm HI} > 20.3$ peaks around [O/H]=-1 to -0.7, much lower than the mean value of an L_* galaxy of [O/H]$\approx$ 0. The reason for this being that *1)* much of the DLA cross section is in sub-L_* galaxies, which mostly have sub-solar metallicities, and *2)* for the more luminous, larger galaxies, the highest interception probability is at larger impact parameters from the centre, where the

metallicity is lower. Interestingly, this number is very close to the z=0 extrapolations of metallicity measurements in DLAs at higher z from Prochaska et al. (2003) and Kulkarni et al. (2005). For the mean mass-weighted metallicity of HI gas with $\log N_{\rm HI} > 20.3$ at z=0 we find the value of $\log Z = -0.35 \pm 0.2$, also consistent with the z=0 extrapolation of $N_{\rm HI}$-weighted metallicities in DLAs, although we note this extrapolation has large uncertainties given the poor statistics from DLAs at z<1.5. These results are in good agreement with the hypothesis that DLAs arise in the HI disks of galaxies.

4. Conclusions

The local galaxy population can explain the incidence rate and metallicities of DLAs, the luminosities of their host galaxies, and the impact parameters between centres of host galaxies and the background QSOs.

This work is presented in much more detail in a forthcoming paper (Zwaan et al. 2005b).

References

Chen, H. & Lanzetta, K. M. 2003, ApJ, 597, 706

Ferguson A. M. N., Gallagher J. S., Wyse R. F. G., 1998, AJ, 116, 673

Garnett D. R., 2002, ApJ, 581, 1019

Kanekar N., Chengalur J. N., Subrahmanyan R., Petitjean P., 2001, A&A, 367, 46

Kulkarni V. P., Fall S. M., Lauroesch J. T., York D. G., Welty D. E., Khare P., Truran J. W., 2005, ApJ, 618, 68

Le Brun, V., Bergeron, J., Boisse, P., & Deharveng, J. M. 1997, A&A, 321, 733

Møller, P., Warren, S. J., Fall, S. M., Fynbo, J. U., & Jakobsen, P. 2002, ApJ, 574, 51

Møller P., Fynbo J. P. U., Fall S. M., 2004, A&A, 422, L33

Péroux, C., Dessauges-Zavadsky, M., D'Odorico, S., Kim, T., & McMahon, R. G. 2005, MNRAS, *in press*

Prochaska J. X., Gawiser E., Wolfe A. M., Castro S., Djorgovski S. G., 2003, ApJ, 595, L9

Rao, S. M., Nestor, D. B., Turnshek, D. A., Lane, W. M., Monier, E. M., & Bergeron, J. 2003, ApJ, 595, 94

Rao, S. M. 2005, astro-ph/0505479

van der Hulst J. M., van Albada T. S., Sancisi R., 2001, ASP Conf. Ser. 240: Gas and Galaxy Evolution, 240, 451

Warren S. J., Møller P., Fall S. M., Jakobsen P., 2001, MNRAS, 326, 759

Zwaan, M. A., et al. 2005a, MNRAS, 359, L30

Zwaan, M. A., van der Hulst, J. M., Briggs, F. H., Verheijen, M. A. W., Ryan-Weber, E. V., 2005b, MNRAS, *submitted*

THE GROWTH OF DISK GALAXIES

Disentangling Evolution and Selection Biases

Nicole P. Vogt[1*] and the DEEP Team[2]

[1] *New Mexico State University, Las Cruces, USA*
[2] *University of California, Santa Cruz, USA*
* nicole@nmsu.edu

Abstract We review the status of current observations of the fundamental parameters of intermediate redshift ($0.2 < z < 1.2$) spiral galaxies. Advances in instrumentation of 8–10m class telescopes have made possible detailed measurements of galaxy luminosity, morphology, kinematics and mass, in both the optical and the infrared passbands. By studying such well known star formation indicators as [OII]3727Å (in the optical) and Hα (redshifted to the infrared), the internal velocity structure and star formation rates of galaxies can be traced through this entire redshift regime. The combination of throughput and optimum seeing conditions yields spectra which can be combined with high resolution multiband imaging to explore the evolution of galaxies of various morphologies, and to place constraints on current models of galaxy formation and star formation histories.

Out to redshifts of $z = 1$, these data form a high redshift Tully-Fisher relation that spans four magnitudes and extends to well below L^*, with no obvious change in shape or slope with respect to the local relation. A comparison of disk surface brightness between local and high redshift samples yields an offset in accordance with distance-dependent surface brightness selection effects, as can the apparent change in disk size with redshift for disks of a given mass. These results support low Ω_0 models of formation, and provide further evidence for modest increases in luminosity with lookback time for the bulk of the field spiral galaxy population, given the limits imposed by the parent HST+WFPC2 imaging catalog.

Keywords: cosmology: observations — galaxies: formation — galaxies: distances and redshifts — galaxies: evolution — galaxies: structure

1. Introduction

Distant galaxies can be characterized observationally in terms of number counts, luminosity, color, size, and morphology from images, to which spectra

R. S. de Jong, Island Universes, 507–512.
© 2007 *Springer.*

add redshifts, line strengths, and, most critically, internal velocities. Potential changes from local populations include variations in counts, in the relative densities of various populations, and the apparent inclusion of "new" morphological types, as well as scaling changes in structural parameters for local galaxy morphological types (e.g., galaxy mass, luminosity, or size). Current disk galaxy studies call for anywhere from zero to three magnitudes of luminosity or surface brightness evolution (brightening) and factors of one or two decrease in disk size by redshifts of order one.

2. Sample Characteristics

The sample we discuss herein is comprised of 130 field galaxies at redshifts between 0.1 and 1.3, defined by moderate resolution Keck+LRIS spectroscopy at $R \sim 5,000$. Individual slitlets were placed upon each object to align with the galaxy major axes, as determined from previously acquired HST+WFPC2 V (V_{606}) and I (I_{814}) images. The target galaxies form a subset of the first phase of the Deep Extragalactic Exploratory Probe (DEEP) project survey, being drawn from a general redshift survey of 821 objects in the Groth Survey Strip (Weiner et al. 2005). HST optical imaging has been enhanced with NICMOS H-band imaging and STIS spectroscopy, with K-band imaging from Keck, UKIRT, and Subaru, and with ground-based *BVRIJHK* for a portion of the kinematic subsample.

Three features distinguish the parent redshift survey. First, the survey field forms a continuous band extending over 40×3 arcminutes on the sky (covering a range of 38 co-moving Mpc by redshift z=1). Second, the complete HST imaging in both V and I allows for the measurement of a uniform set of rest-frame colors and structural parameters out to redshifts $z \sim 1$. Third, the spectral resolution of 3–4Å (versus, for example, 10Å for the CFGRS and 40Å for the CFRS) enables both resolution of the [O II] λ3727 doublet feature (2.7 Å rest-frame split) and that detailed internal kinematic measurements be made for individual objects.

The key selection criteria for these objects are the general selection criterion of the parent redshift survey (namely $V + I \leq 48$), and an object elongation on the sky equivalent to an inclination angle of 30° for a disk galaxy. We emphasize that these objects were not chosen for large angular or physical size, nor for any particular morphology. The parent sample was chosen from an underlying HST imaging catalog to match the distribution of half light radii, bulge fractions, and morphological asymmetry (Vogt et al. 2005). The single variable with a clear selection bias is the position angle of target major axes on the sky, as all spectroscopic masks were laid out at the same angle on the sky and elongated objects were prioritized to have a position angle within 30° of this angle (to which individual slitlets could be aligned).

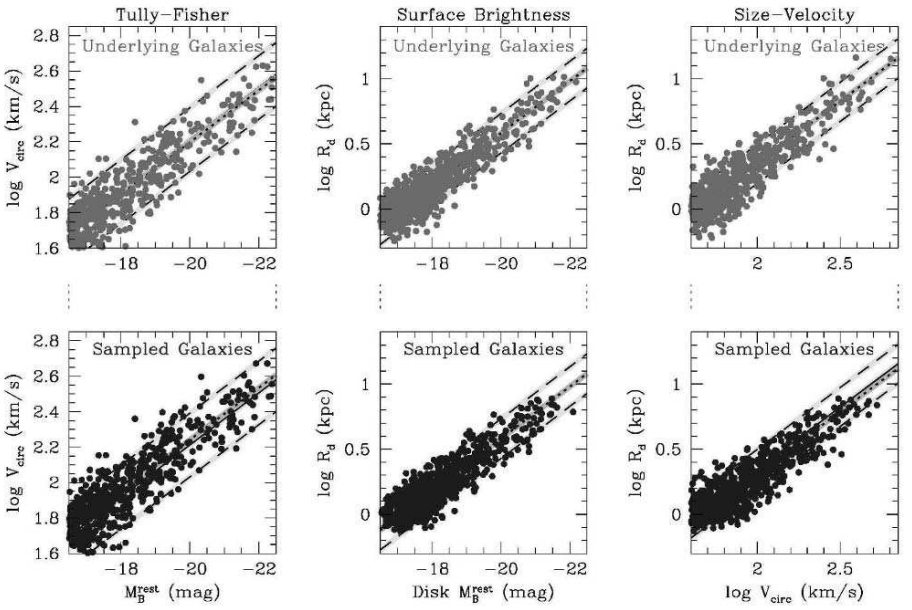

Figure 1. The modeled distribution of local disk galaxies in three fundamental parameter spaces; the top row shows a random selection of disk galaxies, while the bottom row incorporates the survey selection effects (fairly mild for nearby objects). For this and the next three figures, the yellow central line and dashed outlying lines ($\pm 2\sigma$) show the distribution of local galaxies, while the blue dotted line shows a fit to the zeropoint offset for the galaxies selected within each bin.

3. Data Analysis

The technique of deriving velocity profiles from the two-dimensional spectra is discussed in Vogt et al. (2005b). Briefly, profiles were fit to spatially resolved spectra of the emission lines [OII]3727, Hβ, [OIII]5007, and Hα. A grid of model velocity profiles for exponential disks was then fit to the two-dimensional spectra, allowing a best fit value to be determined for the key variable, the intrinsic velocity amplitude of the profile.

We then model the distribution of local disk galaxies in three fundamental planes, examining the Tully-Fisher relation (velocity vs. luminosity), the surface brightness relation (luminosity vs. size), and the velocity vs. size relation. We begin with a local luminosity function, and use local relations and their scatter to distribute galaxies throughout the relevant parameter space. We then apply an observational selection function as shown in Figures 1 and 2, which models the redshift-dependent change in sensitivity to galaxies for a survey which requires the acquisition of spatially resolved spectra.

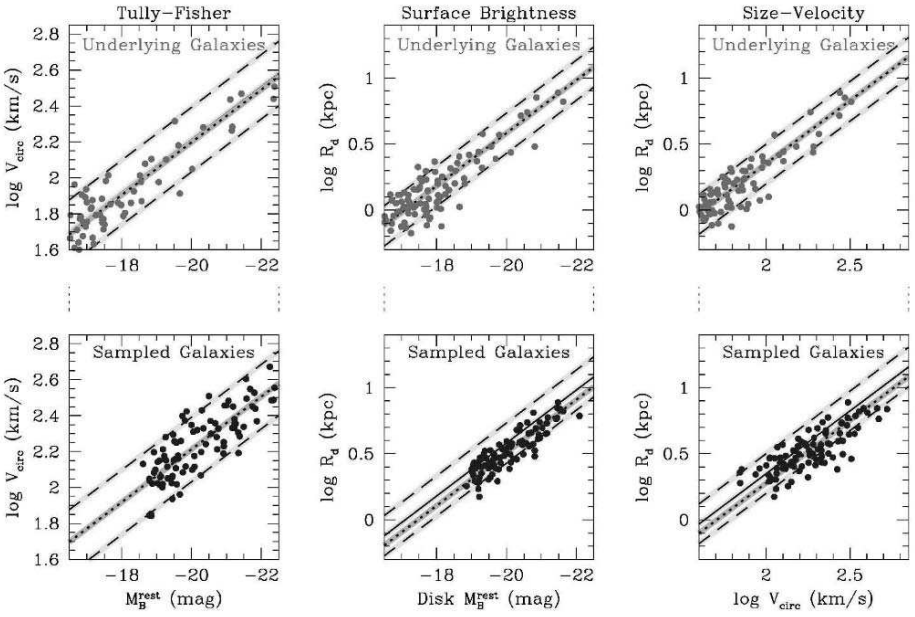

Figure 2. The modeled distribution of disk galaxies at a redshift of unity in three fundamental parameter spaces; the top row shows a random selection of objects drawn from the distribution of local galaxies, while the bottom row incorporates the survey selection effects in surface brightness, magnitude, and size. We observe a linear increase in zeropoint in the surface brightness and the size-velocity planes, driven strongly by the change in observable surface brightness, while the Tully-Fisher relation is relatively unchanged.

The observational selection function can be divided into three parts. First, we consider the modeled surface brightness sensitivity) of the HST+WFPC2 images (Simard et al. 1999), which is linear with redshift and imposes an increase in central surface brightness of 1.3 magnitudes by a redshift of one. Second, there is a magnitude limit for all objects imposed by the parent redshift survey of 24 magnitudes or brighter in $V + I$. Third, we take into account the size limitations which are a function of the additional need to obtain spatially resolved spectra. In order to analyze data, we require that the spectral flux of at least one emission line in each spectrum extend to $1''$ or more across the slitlet. We also require that the spectral flux extend out to two or more disk scale lengths along the galaxy major axes.

The angular and linear size requirements imposed to obtain spatially resolved profiles (e.g., rotation curves) act as a function of the radius to which star formation extends along the galaxy disks (a "gas radius"), rather than correlating directly with the more familiar model parameter of disk scale length. The relationship between the critical gas radius and the disk scale lengths is

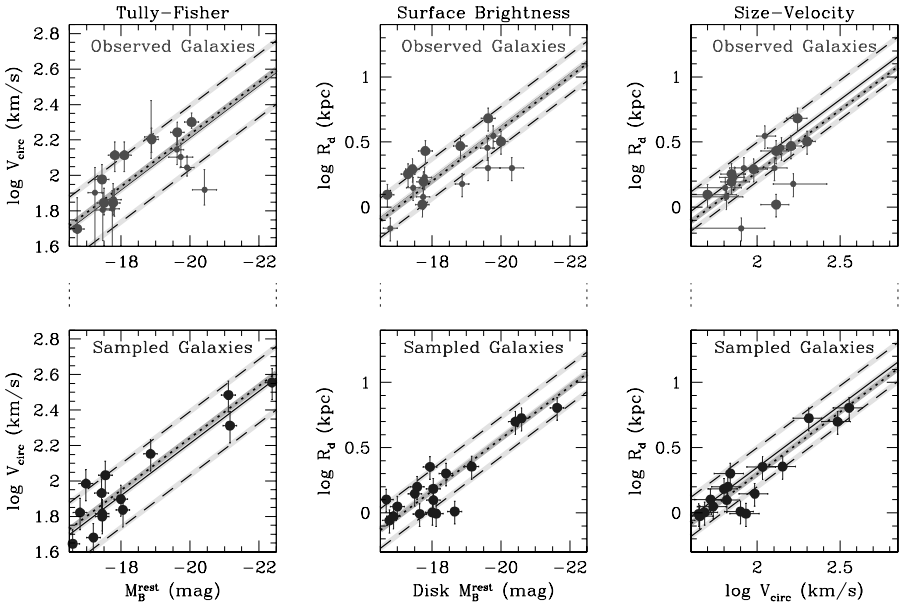

Figure 3. The observed and modeled distribution of disk galaxies around a redshift of 0.2 in three fundamental parameter spaces; the top row shows the actual galaxies observed within the survey, while the bottom row incorporates the redshift-dependent survey selection effects on a catalog of representative local galaxies (selecting as many galaxies as were observed, as they would appear at equivalent redshifts given no evolution in intrinsic properties). We are able to reproduce the offset from local relations in all planes purely by means of selection effects.

scattered locally as well as in the distant Universe, and also worth evaluating for redshift-dependent evolution. Because of the interaction between the angular and linear criteria, both galaxies with intrinsically small disk scales and galaxies with intrinsically large disk scale lengths can be affected by this selection effect. The combined effect can produced an artificially tight size distribution, and thus promote an underestimate of the intrinsic spread, particularly at high redshifts. Because the survey sensitivity at the faint end of the luminosity function decreases with redshift, the two types of constraints can be as important at low redshifts ($z \sim 0.3$) as at redshifts near to unity.

Figures 3 and 4 compare the distribution of our surveyed galaxies with galaxies drawn from the model local catalog to which our selection effects have been applied. We are able to account for the bulk of the apparent offsets in the surface brightness and size-velocity planes with these functions, while our Tully-Fisher relation does not show strong changes with redshift (also in agreement with the modeled distributions).

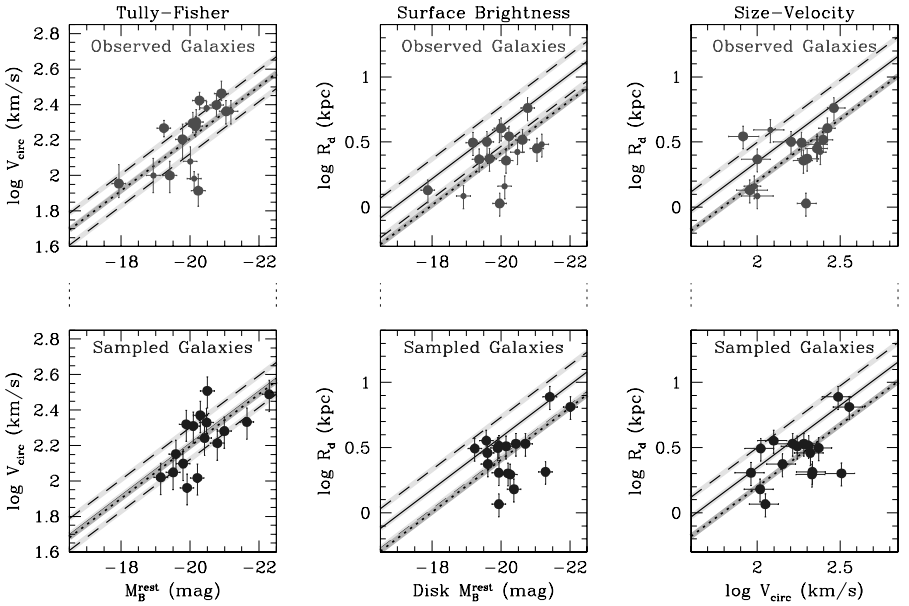

Figure 4. The modeled and observed distribution of disk galaxies around a redshift of unity in three fundamental parameter spaces; the top row shows actual galaxies observed within the survey, while the bottom row incorporates the redshift-dependent survey selection effects on a catalog of representative local galaxies (selecting as many galaxies as were observed, as they would appear at equivalent redshifts given no evolution in intrinsic properties). We are again able to reproduce the offset from local relations in all planes purely by means of selection effects.

In conjunction with these effects, we are required to invoke a modest decrease in disk scale lengths of $20 \pm 10\%$ by a redshift of one. We emphasize, however, that additional evolution may be hidden within the selection criteria, beyond the limits at which we can observe it.

References

Simard, L., et al. 1999, ApJ, 519, 563
Vogt, N. P., et al. 2005a, ApJS, 159, 41
Vogt, N. P., et al. 2005b, in preparation
Weiner, B. J.., et al. 2005, ApJ, 620, 595

ROTATION CURVES OF SPIRAL GALAXIES

Dark Matter & Angular Momentum

Susan A. Kassin[1*] and Roelof S. de Jong[2**]

[1] *UCO/Lick Observatory, University of California at Santa Cruz, USA*

[2] *Space Telescope Science Institute, Baltimore, USA*

* kassin@ucolick.org, ** dejong@stsci.edu

Abstract We decompose the rotation curves of 34 local bright spiral galaxies into baryonic and dark matter components. Analysis of the resulting dark-to-luminous matter distributions shows that they are self-similar once scaled to an appropriate radius. In addition, the radius where the dark matter contribution to the rotation curves equals that of the baryons correlates with galaxy properties such that galaxies with greater values are larger, brighter, faster rotators, more massive, and of earlier Hubble type. In comparing our data to a model for the dark matter distribution in galaxies, we find that fits are generally poor in the inner parts, and all but 2 galaxies are better fit if adiabatic contraction of the halos is performed.

We compare the integrated and detailed distribution of specific angular momentum, j, of these galaxies to that of dark matter halos from N-body simulations. The distribution of integrated j among galaxies is a factor of $\sim$2–3 less than that of the halos, and is consistent with the j of their inner 30%. The halos have excess j compared to the galaxies at radii beyond the inner few kiloparsecs.

Keywords: galaxies: fundamental parameters - dark matter - galaxies: kinematics and dynamics – galaxies: spiral – galaxies: stellar content

1. Introduction

The flatness of rotation curves has long been the most direct evidence for the existence of a dominant component of dark matter in spiral galaxies (Sofue & Rubin, 2001). However, the distribution of dark matter is poorly constrained, even in galaxies where the presence of dark matter is dominant (e.g., Verheijen, 1997). Interestingly, the main uncertainty in the distribution of dark matter stems from the poorly known stellar mass distribution (e.g., Verheijen, 1997). We use color-mass-to-light ratio (M/L) (Bell & de Jong 2001; Bell et al. 2003) relations to derive stellar mass profiles of galaxies. These color-M/L relations

R. S. de Jong, Island Universes, 513–518.
© 2007 *Springer.*

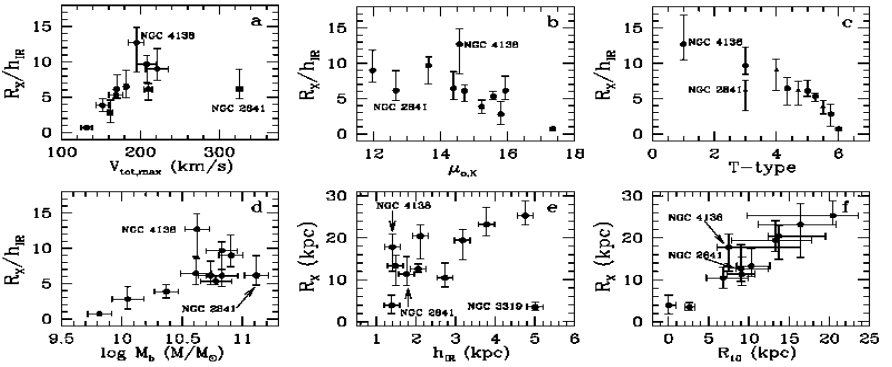

Figure 1. Relations between R_X/h_{IR}, R_X and galaxy properties. Error bars are due to the 0.1 dex uncertainty in the color-M/L relations. Fractions with values < 1 are added to the integer Hubble T-types.

were determined from the analysis of spectro-photometric spiral galaxy evolution models and give an upper limit to the baryonic mass present. With the distributions of stellar mass in galaxies reasonably well determined, given rotation curves, we can begin to investigate those of the dark matter.

Given this information, we can also investigate the specific angular momentum, j, content of galaxies. It has long been assumed in theories of galaxy formation that the total amount and radial distribution of j is conserved as baryons decouple from the dark matter and form into a disk. Here, we re-examine these assumptions.

2. Dark Matter in Bright Spiral Galaxies

For 34 local bright ($B < 12.5$ mag) spiral galaxies that have rotation curves in the literature, we derive their stellar mass distributions by applying color-M/L relations to radial $B-R$ color and K-band luminosity. When available, gas masses are included, otherwise we assume that the gas component is negligible. At those radii where the observed rotation speed of a galaxy is greater than that of its baryons, the additional gravitational component is assumed to be due to dark matter. The radial contribution of dark matter to the rotation curves is derived.

Dark Matter Scaling Relations

The quantities R_{10} and R_X are defined to be the radii where dark matter contributes 10% and 50% (the "cross-over radius") to the rotation curve of a galaxy. In Figure 1, R_X/h_{IR}, where h_{IR} is the near-infrared disk scale-length, and R_X are plotted versus galaxy properties. There are less points in these plots than galaxies in our sample since not all galaxies have an R_X

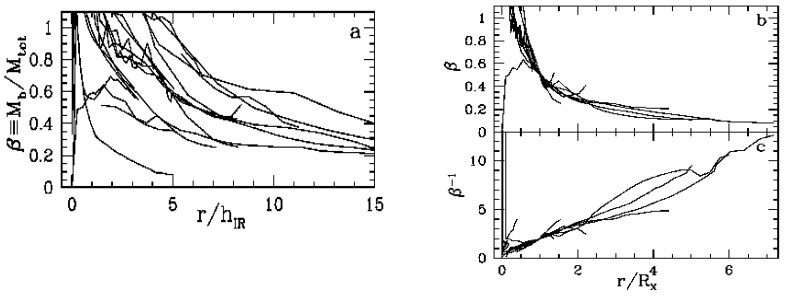

Figure 2. $\beta(r) \equiv M_b(r)/M_{tot}(r)$ and its inverse for galaxies with an appreciable dark matter contribution. The baryonic model over-predicts the observed rotation curve when $\beta(r) > 1$.

measurement. Galaxies with larger values of R_X are observed to rotate faster, be brighter, of earlier morphological type, more massive, larger, and have larger values of R_{10}. Two of the outliers in Figure 1, NGC 2841 and NGC 4138, are found to have signatures of kinematic disturbance. The third outlier, NGC 3319, is discussed in Kassin, de Jong & Weiner (2006).

Radial Behavior of Dark Matter

In Figure 2, the dimensionless parameter $\beta(r) \equiv M_b(r)/M_{tot}(r)$, where M_b is the baryonic mass and M_{tot} is the total mass, and its inverse, are plotted for galaxies with an appreciable dark matter contribution. In Figure 2b, $\beta(r)$ is plotted versus radius in units of R_X which causes the curves to overlap at $r = R_X$. The regularity that is observed can be explained in terms of exponential disks and flat rotation curves. The rotation curve of a galaxy is nearly flat beyond $r \sim 2h_{IR}$. Much of the baryonic mass is also enclosed at $r \sim 2h_{IR}$, causing the baryonic rotation curves to be roughly Keplerian ($V_b(r) \propto 1/r$) beyond this radius. Therefore, beyond $\sim 2h_{IR}$, it should be the case that $\beta(r) \propto 1/r$, which is what we observe. The $\beta(r)$ curves overlap nicely when plotted versus radius normalized to R_X because R_X is located beyond $2h_{IR}$. We parameterize the trend of β^{-1} with r/R_X in a simple universal manner: $\beta^{-1} = 1.71(r/R_X) + 0.021$.

Comparison with NFW Model for Halo Density Distributions

We compare the dark matter distributions with the Navarro, Frenk & White (1996; NFW) analytical function designed to fit numerical N-body simulations of dark matter halos. To do this, for each galaxy, we fit its observed rotation curve with a total mass rotation curve created from the addition of its baryonic rotation curve to a grid of halo models. We repeat the fits for halos that are adiabatically contracted according to the distributions of baryons in the galaxies (Blumenthal et al. 1986). The majority of the fits have poor χ^2 values, and all but 2 galaxies are better fit if adiabatic contraction is not performed. The

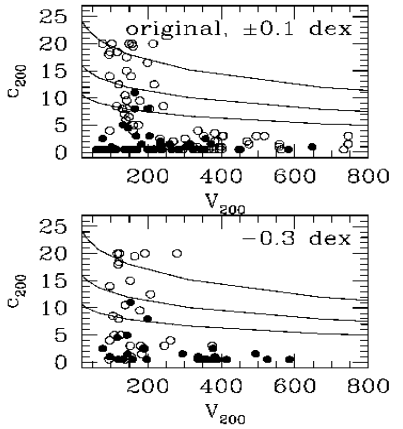

Figure 3. Best-fit halo parameters for different normalizations of the color-M/L relations ($\pm$0.1, -0.3 dex). Filled symbols are those fits with adiabatic contraction. Curves are the expected range of halo parameters from simulations.

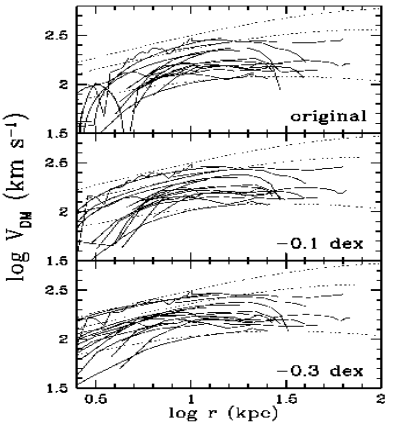

Figure 4. Dark matter rotation curves for different normalizations of the color-M/L relations (solid lines) and NFW halos for $c_{200} = 10$ and $V_{200} = 100$, 300, 500 km/s (dotted lines).

NFW has 2 free parameters that we fit for: concentration (c_{200}) and velocity (V_{200}). In Figure 3, we plot these values for the the best-fit halos along with the range of these parameters found in numerical simulations (Bullock et al., 2001). Even without adiabatic contraction, the best-fit concentrations are low compared to those in simulations. This can also be concluded from Figure 4 where dark matter rotation curves and NFW halo models for $c_{200} = 10$ are plotted. Even though the NFW models are too concentrated to match the inner parts of galaxies, they fare quite well in the middle to outer parts. In order for the NFW models with the predicted concentrations to better match the dark matter distributions, a normalization of the color-M/L relations even lower than -0.3 dex, where baryons contribute very little to the total mass in the inner parts of galaxies, would have to be implemented. This, however, cannot be the case for all galaxies (Kassin, de Jong & Weiner (2006); de Jong & Bell 2006).

3. Specific Angular Momentum in Bright Spiral Galaxies

Integrated Specific Angular Momentum, j_{tot}

We derive "minimum" and "maximum" j_{tot} measurements for the 34 galaxies. For $j_{tot,min}$, the last radius used in the J calculation is the last measured rotation curve radius. For $j_{tot,max}$, it is where the baryonic mass of a galaxy is ≈ 0; the rotation curve is extended with V_{flat} (the velocity of the flat region of the rotation curve) to this radius. These two j_{tot} measurements do not differ very much for our data (Figure 6). In Figure 5, they are plotted versus V_{flat}

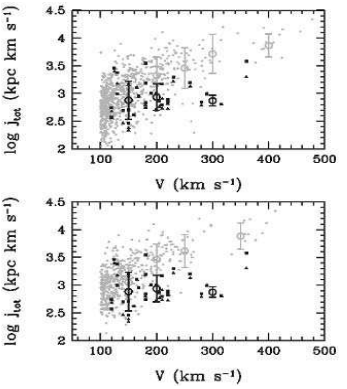

Figure 5. Integrated j versus V_{flat} for galaxies and halos. Galaxies are plotted in black, and halos in grey. Halos with $V = V_{max}$ and $V = V_{virial}$ are in the upper and lower plots, respectively. Averages are plotted as large open circles.

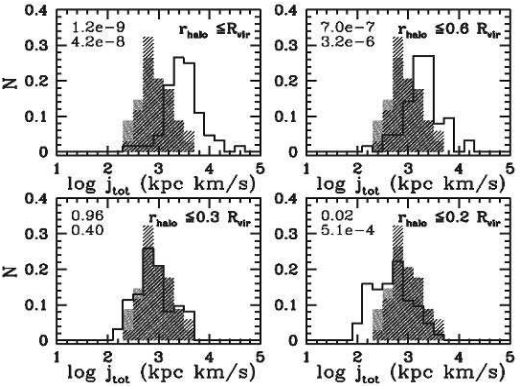

Figure 6. Distributions of j_{tot} among galaxies and fractions of halos. Histograms for the halos are clear; those for $j_{tot,min}$ and $j_{tot,max}$ are shaded and striped, respectively. K-S statistics are in the upper left corners for comparison of the halos with $j_{tot,min}$ (top) and $j_{tot,max}$ (bottom).

and are compared to the j_{tot} and V of dark matter halos. The dark matter halos are from a numerical N-body simulation of B. Allgood for ΛCDM, $\sigma_8 = 0.8$, $h = 0.7$, $L_{box} = 80h^{-1}$ Mpc, and $f_{res} = 1.2h^{-1}$ kpc. Galaxies tend to have less j_{tot} at a given V; the difference is a factor of 2.4 at 200 km/s if V_{max} of the halos is used, and a factor of 3.4 if V_{virial} is used. In Figure 6, we plot the distributions of $j_{tot,min}$ and $j_{tot,max}$ among galaxies. They are compared to the j_{tot} within different fractions of the virial radius of dark matter halos in the mass range $10^{12} < M_{halo} < 10^{13} M_{\odot}$. The j_{tot} distributions of the galaxies follow that of the inner 30% of dark matter halos.

Detailed Distribution of Specific Angular Momentum

N-body numerical simulations predict a universal functional form for the cumulative mass distribution of j in dark matter halos, $M(< j)$ (Bullock et al., 2001). We assume that baryons initially had this distribution, and later collapsed into a disk while conserving $j(r)$. The surface mass density of the resulting disk is compared with observations. To calculate the predicted surface mass density, $\Sigma_p(r)$, consider a mass element dM, then $dM = \Sigma_p(r)\, 2\pi r dr = M(< j)\, dj$. Solving for $\Sigma_p(r)$, we obtain:

$$\Sigma_p(r) = \frac{M_{virial} f_b \mu v(r)}{2\pi r} \left[\frac{1}{j_o + rv(r)} - \frac{rv(r)}{(j_o + rv(r))^2} \right] \qquad (1)$$

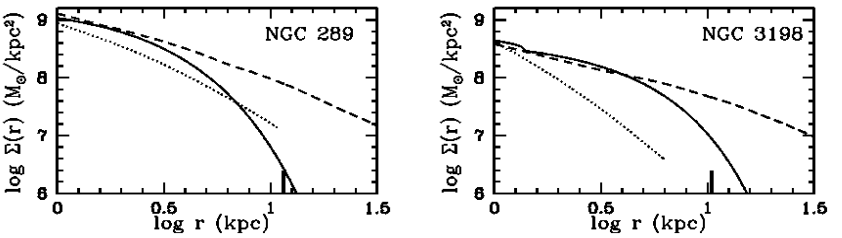

Figure 7. Observed (solid line) and predicted surface mass density distributions under the assumption of detailed j conservation for 2 representative galaxies. The predictions are for μ values of 1.1 (dotted line) and 2 (dashed line), which span its 90% range. The normalization of the predictions is arbitrary. R_{25} is marked with a bar on the x-axis.

where $v(r)$ is the rotation curve of the disk, j_{max} the maximum j, $j_o = j_{max}(\mu - 1)$, M_{virial} the virial mass, f_b the fraction of baryons that form the disk, and μ a shape parameter. We examine the shape of $\Sigma_p(r)$ which is determined by μ. The parameters M_{virial} and f_b only affect the normalization, and j_{max} affects the radial extent of the disk. Given the rotation curve of a galaxy, we calculate its $\Sigma_p(r)$ with Equation 1 and compare it to the galaxy's observed surface mass density. Two representative galaxies are plotted in Figure 7. While the slopes of the $\Sigma_p(r)$'s generally match the observations in the inner few kpc of the galaxies, they are too steep in the outer parts.

Acknowledgements We would like to thank Eric Bell, James Bullock, Mike Fall, David Koo, James Pizagno, Richard Pogge, Sandra Faber, and Ben Weiner for their valuable comments.

References

Bell, E. F., McIntosh, D. H., Katz, N., & Weinberg, M. D. 2003, ApJS, 149, 289
Bell, E. F., de Jong, R. S. 2001, ApJ, 550, 2
Blumenthal, G. R., Faber, S. M., Flores, R., & Primack, J. R 1986, ApJ, 301, 2712
Bullock et al. 2001, ApJ, 555, 240
de Jong, R. S., Bell, E. F. 2006, these proceedings, p. 107
Kassin, S. A., de Jong, R. S., Weiner, B. J. 2006, ApJ, 643, 804
Navarro, J. F., Frenk, C. S., & White, S. D. M. 1996, ApJ, 462, 563
Sofue, Y. & Rubin, V. 2001, ARAA, 39, 137
Verheijen, M. A. W. 1997, Ph.D. thesis, Rijksuniversiteit Groningen

THE EVOLUTION OF DISK GALAXIES IN CLUSTERS AND THE FIELD

Steven P. Bamford[1*], Alfonso Aragón-Salamanca[1] and Bo Milvang-Jensen[2]

[1] *School of Physics and Astronomy, University of Nottingham, UK*

[2] *Max-Planck-Institut für extraterrestrische Physik, Garching, Germany*

* ppxspb@nottingham.ac.uk

Abstract We describe our project to examine the evolution of distant disk galaxies, and present the results of our work based on the Tully-Fisher relation. Comparing matched cluster and field samples we find evidence that the cluster galaxies are on average 0.7 ± 0.2 mag brighter than those in the field. Considering the field sample alone we find a brightening with redshift amounting to 1.0 ± 0.5 mag by $z = 1$, which is likely to be an upper limit, considering the selection effects. We also give brief details of the ESO Distant Clusters Survey (EDisCS) and describe our plans for expanding our studies using data from this survey.

Keywords: galaxies: evolution - galaxies: clusters - galaxies: kinematics and dynamics

1. Our Project

The broad aim of this project is to investigate disk galaxy evolution, as a function of both redshift and environment, using rotation velocity as a baseline for the comparison of various galaxy properties. To achieve this we have obtained VLT/FORS2 multi-slit spectroscopy for a large number of bright emission-line galaxies in the fields of six clusters with redshifts $0.2 \lesssim z_{cl} \lesssim 0.8$. Rotation velocities were measured by fitting the [OII] emission line using a synthetic rotation curve method called $\mathrm{ELFIT2PY}$, which is based on the algorithms of $\mathrm{ELFIT2D}$ by Simard & Pritchet (1999). The results of these fits have been thoroughly examined to determine their quality, and to reject measurements which are deemed unreliable. Photometry and structural parameters are measured on imaging from a range of sources, primarily FORS2 and HST. Full details of the sample selection and data analysis are given in Bamford et al. (2005a) and Milvang-Jensen et al. (2003). Our final sample consists of 111 emission-line galaxies with secure rotation velocity measurements, and covers the redshift range $0.1 \lesssim z \lesssim 1$.

R. S. de Jong, Island Universes, 519–522.
© 2007 *Springer.*

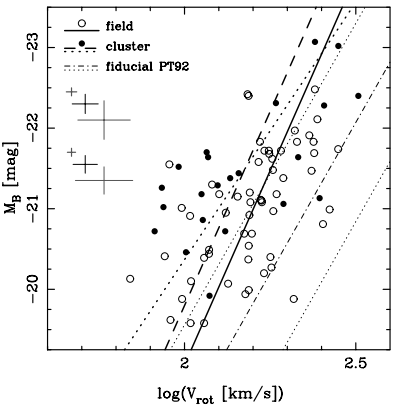

Figure 1. The TFR for our matched samples of field (open points) and cluster (filled points) galaxies. The thin dot-dashed line indicates the fiducial local relation of PT92, with its 3σ scatter delimited by thin dotted lines. Fits to the matched field sample (solid line) and cluster sample (constrained to the field slope: dashed line, free slope: dotted line) are marked. The two sets of error bars indicate the 10th-, 50th- and 90th-percentile errors for field (top) and cluster (bottom) points.

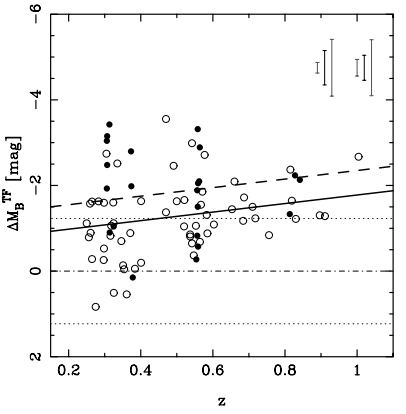

Figure 2. The residuals from the fiducial TFR of PT92 for our matched TFR samples of field (open points) and cluster (filled points) galaxies. The thin lines correspond to those in Fig. 1. Thick lines show fits to the full field TFR sample (solid line) and the cluster sample, constrained to the field slope (dashed line). The two sets of error bars indicate the 10th-, 50th- and 90th-percentile errors for field (left) and cluster (right) points.

2. Cluster Study

There is now much evidence indicating a transformation of star-forming spirals into passive S0 galaxies in cluster environments. However, the detailed form of this evolution and the mechanisms responsible are still far from certain. An interesting possibility is that the interaction causes an enhancement of the star-formation rate prior to its eventual truncation. To examine this question, we have compared the B-band Tully-Fisher ($M_B - \log V_{\rm rot}$) relation (TFR) for 'matched' samples of field and cluster spirals (Bamford et al. 2005a).

Figure 1 shows our TFR for 58 field and 22 cluster galaxies covering similar ranges in redshift ($0.25 \leq z \leq 1.0$) and luminosity ($M_B \leq -19.5$ mag). The cluster galaxies show an offset from the field sample, such that they are 0.7 ± 0.2 mag brighter for a given rotation velocity. Figure 2 presents this in terms of residuals from the local fiducial relation of Pierce & Tully (1992; hereafter PT92), versus redshift. The offset persists, at a 3σ significance level, even when evolution in the field sample is accounted for, as shown by Fig. 3.

This result implies a phase of enhanced luminosity (and hence star-formation) in the early stages of a spiral's interaction with the cluster environment.

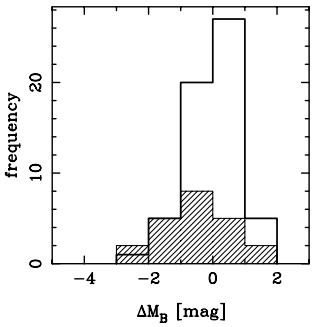

Figure 3. Histogram of the residuals of our field (open histogram) and cluster (hatched histogram) data from the fiducial TFR of PT92, with field evolution subtracted (i.e., the residuals from the solid line in Fig. 2). Note that the cluster distribution is clearly offset from that of the field.

3. Field Study

Studies examining the evolution of the global star formation rate (SFR) density of the universe find a substantial increase of a factor of ≥ 10 from $z = 0$–1 (e.g., Heavens et al. 2004). Is this trend simply due to an evolution in the star-formation rates of individual giant spirals, or is some other process or population responsible? Does the evolution depend on galaxy mass?

To investigate this we have again used the TFR, to look for changes in the relation between M_B (a proxy for SFR) and $V_{\rm rot}$ (a proxy for total mass), as described fully in Bamford et al. (2005b).

Our TFR for 89 field spirals with $0.1 \leq z \leq 1$ is shown in Fig. 4. The slope is not significantly different to that measured locally, i.e., no evidence for mass-dependent evolution. Examining the TFR residuals versus z (Fig. 2), or fitting the TFR intercept in several redshift bins (Fig. 5), we find a B-band brightening of 1.0 ± 0.5 mag, for a given $V_{\rm rot}$, by $z \sim 1$. Due to selection effects this is an upper limit to the true evolution, but still implies slower SFR evolution than measured globally.

This suggests that the global SFR evolution of the universe is *not* driven by the SFR decline in giant spirals.

4. Future Work with EDisCS

The ESO Distant Cluster Survey (EDisCS) is a study of galaxies in and around $\sim$20 clusters at $0.4 \leq z_{cl} \leq 1.0$. These clusters were optically selected using the Las Campanas Distant Cluster Survey Gonzalez et al. 2001, and thus have a wide range of properties.

For each cluster we have a wealth of imaging and spectroscopy data. Many projects are underway using these data, including studies of morphology,

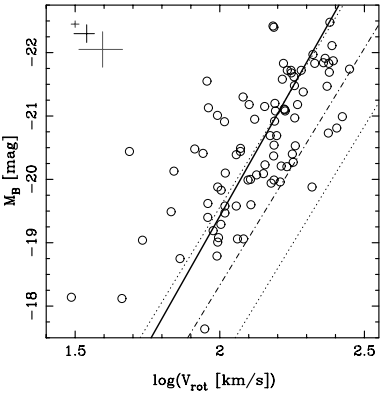

Figure 4. The TFR for our full field TFR sample. The thin lines indicate the local fiducial TFR of PT92, as in Fig. 1. A fit to the points is marked by the thick solid line. The error bars give the 10th-, 50th- and 90th-percentile errors on the points.

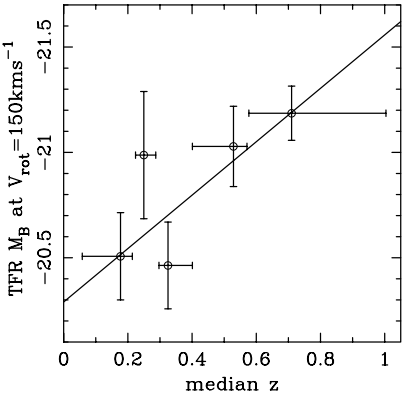

Figure 5. The intercept of TFR fits to subsamples of our field sample in five redshift bins. The fits were performed with constant slope, equal to the PT92 value. Horizontal error bars indicate the width of each redshift bin, with the point at the median redshift. Vertical error bars give the uncertainty on the fitted intercepts. The solid line is a fit to the points.

luminosity functions, colour-magnitude diagrams, cluster substructure, velocity distributions, lensing masses and stellar populations.

From the spectra we are now measuring reliable rotation velocities, in order to perform detailed investigations into the evolution of various galaxy properties with respect to this useful baseline. With more than 5 times as many galaxies, we will have the statistical power to vastly improve upon the studies shown above. The addition of HST morphologies, homogeneous colours, spectral indices and a variety of clusters with well characterised properties, will allow unprecedented studies of disk galaxy evolution with environment and redshift.

References

Bamford, S.P., et al. 2005a, MNRAS, 361, 109
Bamford, S.P., Aragón-Salamanca, A. & Milvang-Jensen, B. 2005b, submitted to MNRAS
Gonzalez, A.H., et al. 2001, ApJS, 137, 117
Halliday, C., et al. 2004, A&A, 427, 397
Heavens, A., et al. 2004, Nature, 428, 625
Milvang-Jensen, B., et al. 2003, MNRAS, 339, L1
Pierce, M.J. & Tully, R.B. 1992, ApJ, 387, 47
Simard, L. & Pritchet, C.J. 1999, PASP, 111, 453

INVESTIGATION OF AGE AND METALLICITY GRADIENTS AND DUST EXTINCTION IN DISC GALAXIES IN THE HUBBLE DEEP FIELD

Barbara Cunow

Department of Mathematical Sciences, University of South Africa, South Africa
cunowbhl@unisa.ac.za

Abstract Using HST data, disc scalelengths in the UV, optical and NIR wavelength regions are used to study age and metallicity gradients and dust extinction in disc galaxies of intermediate redshifts in the Hubble Deep Field North. The observed colour gradients are compared to model calculations of dusty disc galaxies. First results indicate that the age and metallicity gradients in the HDF galaxies differ from the age and metallicity gradients found in local spiral galaxies.

Keywords: galaxies: abundances – galaxies: dust extinction – galaxies: stellar content – galaxies: structure

1. Introduction

It has been known for a long time that the discs of local spiral galaxies tend to become bluer with increasing radius. Such colour gradients can be caused by stellar population gradients and by dust extinction. Studies have indicated that the stars in the outer regions of the disc are younger and/or less metal-rich than the stars in the inner regions, and that dust extinction also contributes to the observed colour gradients. During the last years, a number of investigations of the colours of intermediate and high-redshift galaxies have been done (e.g., Abraham et al. 1999, Moth & Elston 2002). However, it is not clear yet in general, what age and metallicity gradients are present and how large the dust extinction is. In this work, the colour gradients in disc galaxies of the Hubble Deep Field North (HDF-N) are investigated.

The method used here is the one applied in Cunow (2004), where colour gradients in the discs of local spiral galaxies were measured as a function of the inclination angle. The comparison between the colour gradients of face-on galaxies with those of edge-on galaxies allows to separate between colour

R. S. de Jong, Island Universes, 523–526.
© 2007 *Springer.*

gradients caused by age and metallicity gradients and colour gradients due to dust extinction.

2. Colour Gradients of the HDF Galaxies

The sample consists of 32 disc galaxies in the HDF-N, chosen from the list of van den Bergh et al. (2000). 23 galaxies have redshifts $0.3 < z < 0.6$ and are referred to as Sample HDF 1, and the other 9 galaxies have $0.8 < z < 1.1$ and are referred to as Sample HDF 2. The morphological types cover the interval from Sa to Scd, the absolute magnitudes in the B rest frame lie in the range $-22.2 \leq M_B \leq -17.3$, and the whole range from face-on to edge-on view is covered. The sample properties are similar to those of the local spiral galaxies studied in Cunow (2004).

The data are the U_{300}, B_{450}, V_{606}, I_{814} HDF images and the J_{110} and H_{160} NICMOS images of the HDF field (HST GO program 7818). For each galaxy and filter, the disc scalelength r_D is determined by fitting an exponential law to the outer part of the surface brightness profile, and the apparent ellipticity ϵ of the disc region is measured. r_D and ϵ are corrected for the PSF by using model exponential discs and smoothing them with the PSF.

The colour gradients in the disc are represented by the scalelength ratios $r_D(F_1)/r_D(F_2)$, where F_1 and F_2 are two different wavelength regions with F_1 being bluer than F_2. It is found that the colour gradients of most HDF galaxies are small. For Sample HDF 1, the scalelength ratios increase slightly from face-on to edge-on view. For $\epsilon < 0.5$ we have $r_D(F_1)/r_D(F_2) \approx 1$, and for $\epsilon > 0.5$ one measures $r_D(F_1)/r_D(F_2) > 1$. For Sample HDF 2, $r_D(F_1)/r_D(F_2) \approx 1$ for all inclination angles.

3. Model Calculations

Images of model galaxies in the B_{450}, V_{606}, I_{814}, J_{110} and H_{160} bands (U_{300} was excluded because of the red leak of the filter) were calculated using the procedures described in Cunow (2004). Each model galaxy consists of a luminous stellar disc and a dust disc, and the radial colour gradients in the stellar disc are obtained from the radial age and metallicity gradient in the disc and models of stellar evolution. The images are calculated for the average redshift of each HDF sample, and r_D and ϵ are measured for each image.

The age and metallicity gradient is given by the variation of the average age $<A>$ and metallicity Z with radius R. The colour gradients are obtained as follows. For each R, the star formation history (SFH) is calculated. It is assumed that the SFH has an exponential shape with a star formation time scale u which is determined by $<A>$ and the age of the oldest stars in the galaxy t_0. The colours at R are obtained from the SFH at R and the colours of a single stellar population (SSP) with metallicity $Z(R)$. The SSP colours

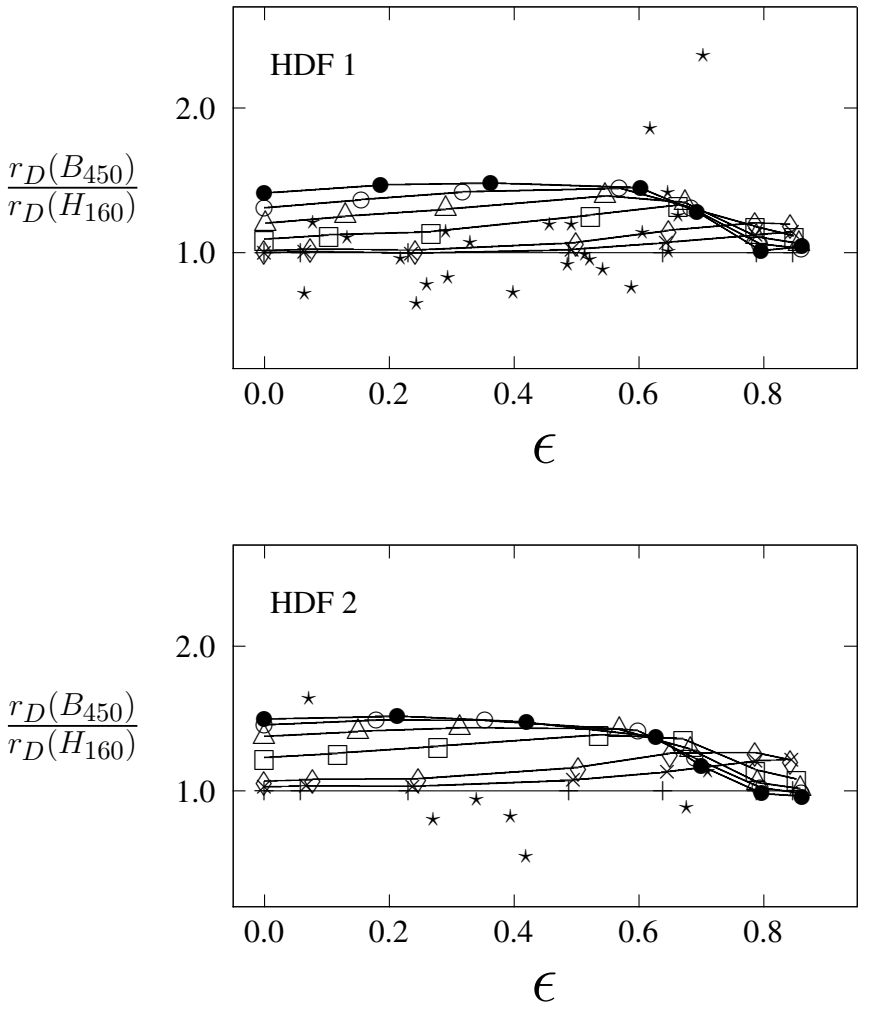

Figure 1. Disc scalelength ratios plotted against apparent ellipticity $\epsilon(H_{160})$ for Samples HDF 1 and HDF 2, and for the models with no age or metallicity gradient. The data points are denoted by $\star$. Central face-on optical depth in the rest frame B band, τ_0^B, for the models: $+$ for $\tau_0^B = 0$, $\times$ for $\tau_0^B = 0.5$, $\Diamond$ for $\tau_0^B = 1$, $\Box$ for $\tau_0^B = 3$, $\triangle$ for $\tau_0^B = 5$, $\circ$ for $\tau_0^B = 7$, and $\bullet$ for $\tau_0^B = 10$.

are determined from SSP model spectra which are redshifted to the average redshift of the sample, and the HDF and NICMOS filter curves.

The models were calculated for various age and metallicity gradients. For the dust properties, the average values for the Milky Way Galaxy were used.

In addition, younger versions of the models A−10M0 and A0M−30 of Cunow (2004) which represent the local non-active galaxies best, were calculated. They were obtained by determining $<A>(R)$ for t_0 of the HDF samples from $<A>(R)$ and t_0 for the local galaxies using the assumption that $u(R)$ does not change with time.

4. Results

The HDF data can be reproduced by (i) the models with no age or metallicity gradient and no or little dust, (ii) the models with a positive age or metallicity gradient, i.e. with stars that are older or more metal-rich with increasing distance from the centre, and any amount of dust, and (iii) the models with a small negative age or metallicity gradient and no dust. The models with a large negative age or metallicity gradient, and the younger versions of the best-fitting models for the local non-active galaxies do not reproduce the data, because the scalelength ratios of the models are systematically too large.

Figure 1 shows the comparison between the data and the models with no age or metallicity gradient. The scalelength ratios of the models with optically thin discs are in agreement with the data points, but for the models with optically thick discs the model points lie above the data.

These results indicate that the discs of the HDF galaxies have small age and metallicity gradients and small amounts of dust, or positive age and metallicity gradients and any amount of dust. This differs from what is found in Cunow (2004) for the local non-active spiral galaxies, and indicates that the disc galaxies in the HDF have age and metallicity gradients in the stellar disc which are different from those in local spiral galaxies.

Acknowledgements I thank the South African National Research Foundation NRF and the University of South Africa for financial support. The HDF images were obtained by the Hubble Deep Field Team, STScI, NASA, and the NICMOS images were taken for the HST GO program 7818.

References

Abraham R.G., Ellis R.S., Fabian A.C., Tanvir N.R., Glazebrook K. 1999, MNRAS 303, 641
Cunow B. 2004, MNRAS 353, 477
Moth P., Elston R.J. 2002, AJ 124, 1886
van den Bergh S., Cohen J.G., Hogg D.W., Blandford R. 2000, AJ 120, 2190

PHOTOMETRIC PROPERTIES OF CLUMPY GALAXIES IN THE HUBBLE ULTRA DEEP FIELD

Debra Meloy Elmegreen

Department of Physics & Astronomy, Vassar College, Poughkeepsie, NY, USA
elmegreen@vassar.edu

Abstract Galaxies in the Hubble Ultra Deep Field (UDF) larger than 10 pixels (0.3 arcsec) have been classified according to morphology. There are 884 galaxies, including spirals, ellipticals, chains, clump-clusters, doubles, and tadpoles; 399 disk galaxies in the Tadpole field were also measured. Linear structures dominate at faint magnitudes. Distributions of axial ratios are compared to nearby samples. 30% of ellipticals are clumpy, and 10-30% of spirals are barred. Radial profiles and clump properties are measured for disk galaxies. Spiral and clump-cluster galaxies are dominated by giant clumps of 10^9 M_o. Galaxy redshifts, star formation histories, and masses are modeled for 10 clump clusters by comparing photometric colors and magnitudes with redshifted stellar population models.

Keywords: galaxies: high-redshift - galaxies: evolution - galaxies: structure

1. Introduction

Understanding the properties of galaxies at high redshift is critical for understanding galaxy evolution that led to the local universe. The advent of high resolution deep imaging surveys is revolutionizing our exploration of galaxies in the early universe. Here we present photometric properties of clumpy galaxies observed in the Hubble Ultra Deep Field for comparison with nearby galaxies. Following previous efforts at classifying galaxy morphology in the Hubble Deep Field (HDF)-North (Abraham et al. 1996a,b) and South (WIlliams et al. 1996; Volonteri et al. 2000) and the Hawaiian Deep Field (Cowie, Hu, & Songaila 1995), we divided UDF galaxies according to 6 different morphological classes: spiral, elliptical, chain, double, clump-cluster, and tadpole.

R. S. de Jong, Island Universes, 527–530.
© 2007 *Springer.*

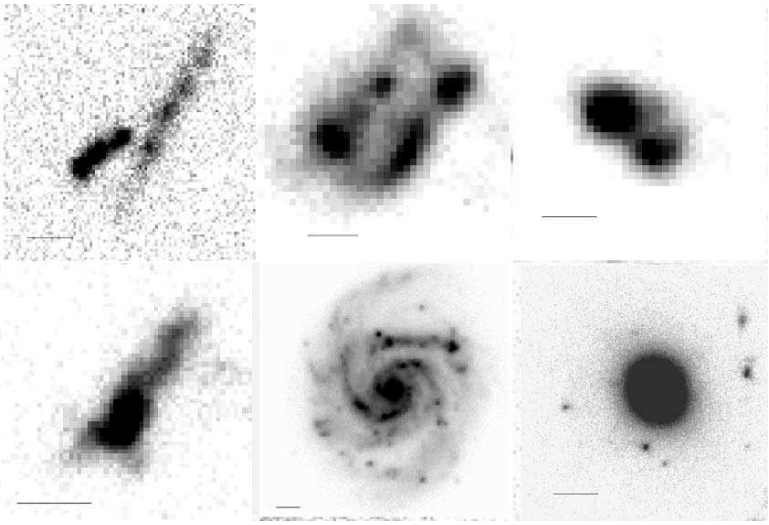

Figure 1. Galaxy morphologies in the Ultra Deep Field: chain, clump cluster, double, tadpole, spiral, elliptical.

2. Data and Photometry

Images of the Ultra Deep Field were made with the Hubble Advanced Camera for Surveys in four passbands, B, V, i, z in over 400 orbits (Beckwith et al. 2004). These reach about 1.5 mag deeper than the HDFs and provide 0.03 arcsec px^{-1} resolution. We selected all 884 galaxies with major axes greater than 10 pixels in i_{775} band in order to have sufficient detail for classification. We also measured 399 galaxies in the HST ACS field of the Tadpole galaxy, (UGC10214; Tran et al. 2004). Photometry was done in all bands for the integrated galaxies out to the 2-σ contour limit of 26 mag arcsec^{-2}. Color-color and color-magnitude diagrams were constructed for each type (Elmegreen et al. 2004a,b; 2005a). Substructure within each galaxy was identified by eye and photometry was done on each clump, amounting to about 1500 individual regions.

Barred Galaxies

We find that 10 to 30% of disk galaxies are barred in the UDF and Tadpole fields (Elmegreen et al. 2004), which is consistent with the local fraction and with the GOODS/GEMS results out to redshift 1 (Jogee et al. 2004). Some of the higher redshift galaxies have poorly formed spiral structure. Bars are also present in some clump cluster galaxies.

Clumpy Ellipticals

Out of 100 ellipticals in the UDF, 30 have clumps indicating mergers. The clumps have masses of about 10^8 M_o and ages of about 1 Gyr. The axial ratios of the elliptical sample are the same as for local ellipticals, indicating that ellipticals very quickly relaxed to their present shapes (Elmegreen et al. 2005b).

Lyman Break Galaxies

In the UDF, 30 galaxies were V-band dropouts and 13 were i-band dropouts. These Lyman Break Galaxies therefore have redshifts of 4 or 5, respectively. Star formation rates were estimated from Madau et al. (1998) relations, and ranged from 6 to 20 M_o yr^{-1} for V-band dropouts, to 23 to 190 M_o yr^{-1} for i-band dropouts (Elmegreen et al. 2005a).

Clump Clusters

Color evolution models were made using the stellar templates of Bruzual & Charlot (2003) in order to compare with the color-color and color magnitudes of 10 clump cluster galaxies and their embedded clumps (Elmegreen & Elmegreen 2005). We find that the clumps have masses of about 10^9 M_o and ages of $<$1 Gyr, with sizes of 1-2 kpc. These are much more massive than the largest clumps in current-day galaxies.

Radial Profiles

The scale lengths were determined for all low inclination spiral galaxies (Elmegreen et al. 2005c). They averaged about 2.4 kpc, which is smaller than for local galaxies (van der Kruit 1987). This indicates that galaxies must grow with time. Clump cluster galaxies do not have exponential light distributions along their major axes. However, ellipse fits show that some have exponential profiles when azimuthally averaged. The individual clump magnitudes and positions were measured in each spiral and clump cluster galaxy, and show an exponential distribution for both galaxy types. This result suggests that clumps dissolve with time to form the exponential disks.

3. Conclusions

Linear structures dominate at faint magnitudes. Chain galaxies appear to be edge-on clump cluster galaxies. Face-on spiral galaxies, if present, are lost due to surface brightness dimming effects. Axial ratios for chain and clump cluster galaxies as well as distant spiral galaxies, compared to local values for disk galaxies, suggest the presence of thick disks. Axial ratios for high redshift elliptical galaxies suggest that they relaxed early, to the present distributions. The fraction of barred spiral galaxies is approximately the same as the local

value for strong bars, 10-30%, out to about redshift z=1. Star-forming clumps appear to be much larger and more massive than the biggest clumps in local galaxies; they are typically 10^9 M_o with ages <1 Gyr and sizes of 1 kpc. Lyman Break Galaxies are mostly peculiar galaxies, and have star formation rates from 10-100 M_o yr^{-1} compared with a few M_o yr^{-1} for normal nearby galaxies.

Acknowledgements The author thanks collaborators Bruce Elmegreen and undergraduates Thomas Ferguson, Ellen Foster, Douglas Rubin, Meredith Schaffer, and David Vollbach, and acknowledges support from the Vassar College Research Fund.

References

Abraham, R., Tanvir, N., Santiago, B., Ellis, R., Glazebrook, K., & van den Bergh, S. 1996a, MNRAS, 279, L47

Abraham, R., van den Bergh, S., Glazebrook, K., Ellis, R., Santiago, B., Surma, P., & Griffiths, R. 1996b, ApJS, 107, 1

Beckwith, S.V.W. et al., 2004,ftp://archive.stsci.edu

Bruzual, G. & Charlot, S. 2003, MNRAS, 344, 1000

Cowie, L., Hu, E., & Songaila, A. 1995, AJ, 110, 1576

Elmegreen, B.G., & Elmegreen, D.M. 2005, ApJ, 627, 632

Elmegreen, B.G., & Elmegreen, D.M. 2005d, ApJ, in press

Elmegreen, B.G., Elmegreen, D.M., & Hirst, A.C. 2004b, ApJ, 612, 191

Elmegreen, D.M., Elmegreen, B.G., & Hirst, A.C. 2004a, ApJ, 604, L21

Elmegreen, D.M., Elmegreen, B.G., & Sheets, C.M. 2004b, ApJ, 603, 74

Elmegreen, D.M., Elmegreen, B.G., & Ferguson, T.E., 2005b, ApJL, 623, L71

Elmegreen, D.M., Elmegreen, B.G., Rubin, D.S., & Schaffer, M. 2005a, ApJ, in press

Elmegreen, D.M., Elmegreen, B.G., Vollbach, D., Foster, E., & Ferguson, T. 2005c, ApJ, in press; astro-ph/0508216

Jogee, S. et al. 2004, ApJL, 615, 105

Madau, P., Pozzetti, L., & Dickinson M., 1998, ApJ, 106, 116

Tran, H. et al. 2003, ApJ, 585, 750

Volonteri, M., Saracco, P., & Chincarini, G. 2000, A&AS, 145, 111

van der Kruit, P.C. 1987, A&A. 173, 59

Williams, R., et al. 1996, AJ, 112, 1335

THE BIVARIATE BRIGHTNESS DISTRIBUTION OF GALAXY DISKS

J. Liske[1*], S.P. Driver[2] and P.D. Allen[2]

[1] *ESO, Garching bei Muenchen, Germany*

[2] *RSAA, Mount Stromlo Observatory, Australia*

* jliske@eso.org

Abstract Using the results of a bulge-disk decomposition of 10 000 galaxies with $B <$ 20 mag from the Millennium Galaxy Catalogue, we recover the space-density of galaxy disks as a joint function of luminosity and effective surface brightness.

Keywords: galaxies: structure - galaxies: fundamental parameters - surveys

1. Introduction

The bivariate brightness distribution (BBD) quantifies the space density of galaxies as a joint function of luminosity and surface brightness (SB) and is hence an extension of the luminosity function. The BBD is linked to the mass and angular momentum distributions of galaxies and the different formation processes of different galaxy types or components are predicted to be encoded in their BBDs (e.g., Dalcanton et al. 1997; Mo et al. 1998; de Jong & Lacey 2000). Hence the BBD is a useful test-bed for galaxy formation models. Constructing the BBDs of disks and bulges separately is of particular interest in this respect. However, at z=0 this requires high-quality, wide-field imaging data with well known selection limits, and a corresponding redshift survey to high completeness.

2. Data: The Millennium Galaxy Catalogue

The Millennium Galaxy Catalogue (MGC; Liske et al. 2003; Driver et al. 2005) is a deep, wide-field B-band imaging survey conducted with the Wide Field Camera on the INT, covering 37.5 deg^2 in $\sim$1.25 arcsec seeing to a limiting isophote of 26 mag arcsec^{-2}. The galaxy sample used here is defined as the 10 095 MGC galaxies that have $B < 20$ mag.

Public datasets (such as SDSS and 2dFGRS) together with our own redshift survey, mainly using 2dF, have yielded redshifts for 96.05% of this sample.

R. S. de Jong, Island Universes, 531–534.
© 2007 *Springer.*

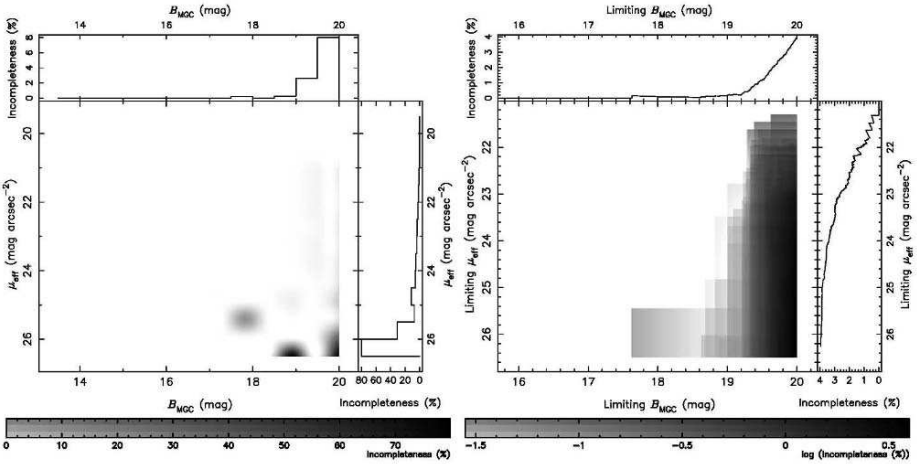

Figure 1. The MGC's overall redshift incompleteness is 96.05%. The left panel shows the incompleteness as a function of magnitude and surface brightness. Despite our single-slit observations some magnitude and SB-dependent bias still remains. We account for this in the analysis. The right panel shows the incompleteness as a function of *limiting* magnitude and SB. From the top sub-panel we can see that for $B < 19.2$ mag the incompleteness is only 0.21%.

This also includes a single-slit campaign on Gemini, the NTT and the ANU 2.3m in an attempt to mitigate the severity of the SB bias in the redshift completeness, which is inevitably introduced by using a fibre-fed MOS such as 2dF (see Fig. 1). The median redshift of our sample is 0.12.

The excellent MGC image quality enables us to decompose all galaxies with $B < 20$ mag into bulges and disks using GIM2D (Simard 1998). The MGC is currently one of the largest samples for which quantitative morphology is available. The 2D surface brightness profile is modelled as the sum of a Sersic bulge and an exponential disk, convolved with the seeing (see P. Allen's contribution to these proceedings for details). We have confirmed the reliability of this process using independent duplicate observations of ~ 700 objects in the overlap regions of neighbouring MGC fields.

3. Preliminary Results

We use the bivariate stepwise maximum likelihood method of Driver et al. (2005) to construct the BBD of the disk components of galaxies. A full analysis of all relevant selection limits is still pending, but here we conservatively set the low-SB and maximum size limits to the same values as in Driver et al.'s analysis of the total-galaxy BBD, i.e. $\mu_{\rm lim} = 25.25$ mag arcsec^{-2} and $r_{\rm max} = 15$ arcsec. These are not absolute detection limits but rather the limits to which accurate photometry is possible. The minimum size limit is

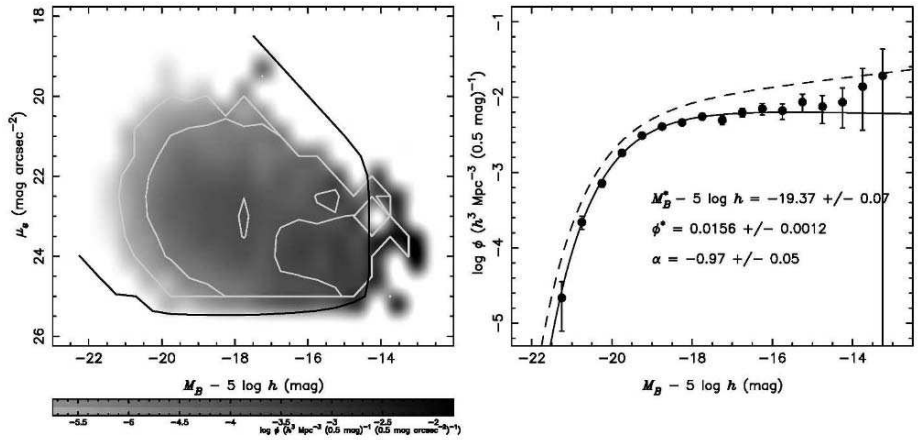

Figure 2. The contours and image in the left panel both show the bivariate brightness distribution of galaxy disks as derived from the MGC. The thick solid line encloses that part of parameter space which is probed by at least 100 objects and represents our selection limit. Integrating the BBD over surface brightness yields the disk luminosity function in the right panel. The solid line shows the best-fit Schechter function with parameters indicated. The dashed line shows the total MGC luminosity function for comparison.

determined by GIM2D's capability of recovering a component half-light radius, and we set it to 0.7 times the FWHM of the seeing. Within these limits we have a complete sample of 5721 disks with $0.013 < z < 0.18$.

The resulting BBD of galaxy disks is shown in Fig. 2 (left panel). It exhibits a well defined shape: at a given luminosity the distribution of surface brightness is Gaussian, i.e. the size distribution of disks is log-normal. The peak of the surface brightness distribution shifts to fainter values at lower luminosities. This SB-luminosity relation is described by $\mu^* = 21.78 + 0.5(M_B + 20)$ mag arcsec^{-2}. Clearly, the next step is to perform a detailed comparison of these and other features of the disk BBD with the predictions of galaxy formation models.

References

Dalcanton, J. J., Spergel, D. N., and Summers, F. J. 1997, ApJ, 482, 659.

de Jong, R. S., and Lacey, C. 2000, ApJ, 545, 781.

Driver, S. P., Liske, J., Cross, N. J. G., De Propris, R., and Allen, P. D. 2005, MNRAS, 360, 81.

Liske, J., Lemon, D. J., Driver, S. P., Cross, N. J. G., and Couch, W. J. 2003, MNRAS, 344, 307.

Mo, H. J., Mao, S., and White, S. D. M. 1998, MNRAS, 295, 319.

Simard, L. 1998, In Albrecht, R., Hook, R. N., and Bushouse, H. A., editors, *ASP Conf. Ser. 145, Astronomical Data Analysis Software and Systems VII*, volume 145, page 108. Astronomical Society of the Pacific.

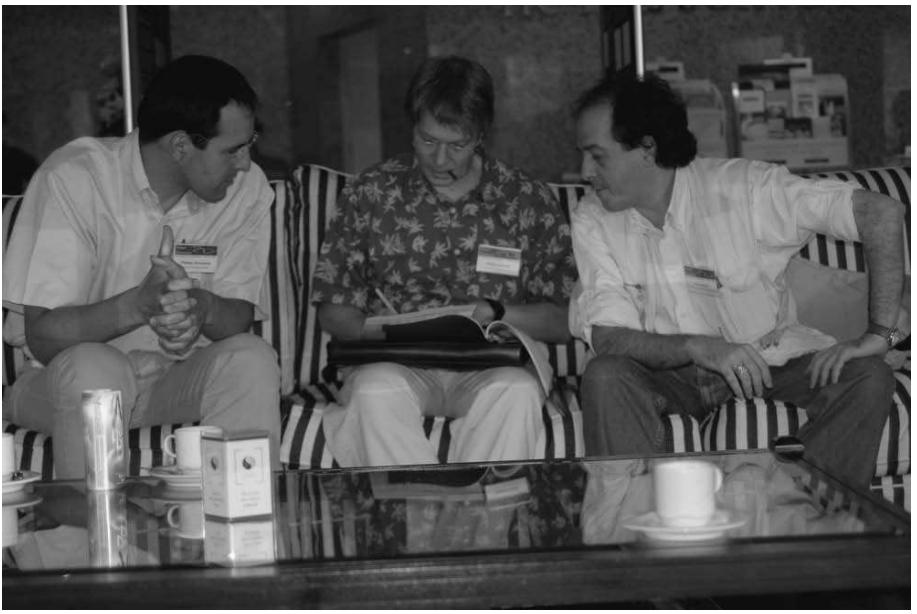

Philippe Héraudeau, Preben Grosbøl, and Panos Patsis work with pen and paper.

Robert Braun and Eric Murphy rely on a laptop.

VIII

FORMATION MODELS OF DISK GALAXIES

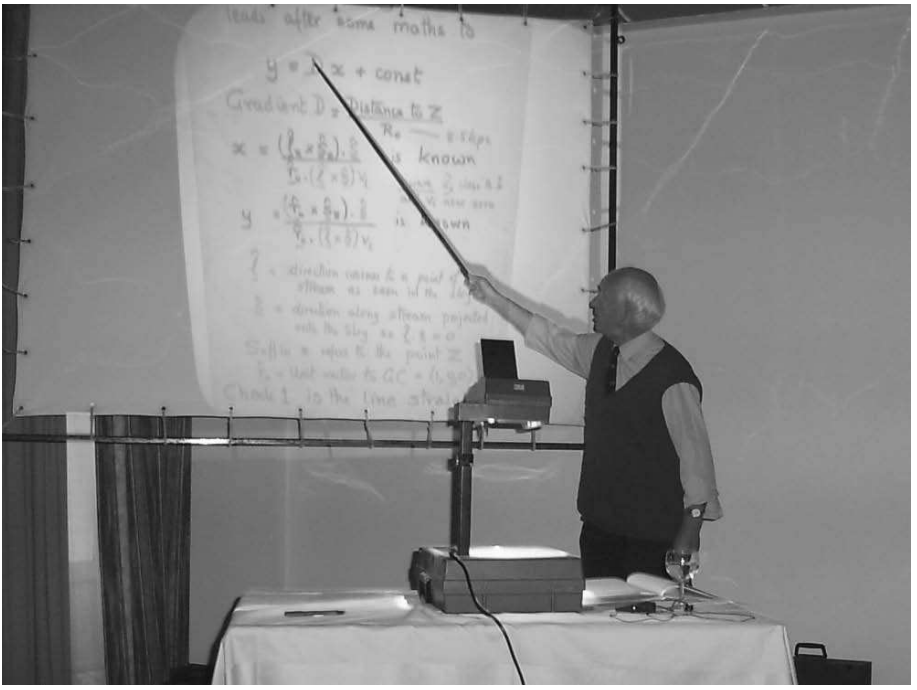

Donald Lynden-Bell delivering his lecture.

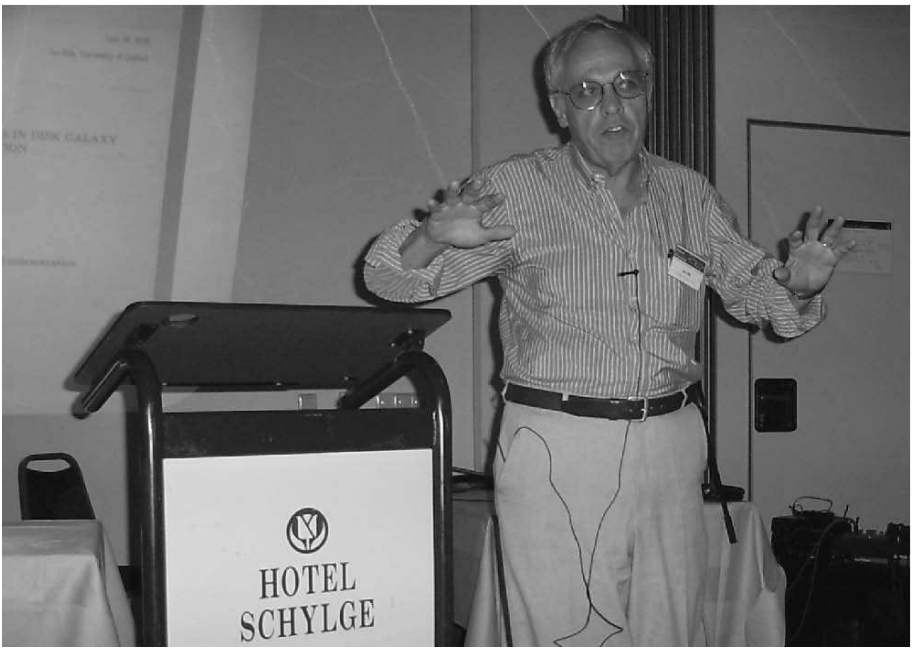

Joe Silk stressing a point.

AN ANALYTICAL PERSPECTIVE ON GALAXY FORMATION

Joseph Silk

Department of Physics, University of Oxford, UK
silk@astro.ox.ac.uk

Abstract Galaxy formation theory is a mysterious art. It is driven by phenomenology and by numerical simulations of dark matter clustering under gravity. Once the complications of star formation are incorporated, the theory becomes so complex that the brute force approach of numerical simulations needs to be supplemented by physical insights into the nature of such processes as feedback. I present here a few analytical perspectives that may shed some light on the nature and implications of global star formation for galaxy formation.

Keywords: galaxies: formation - galaxies: evolution - stars: formation

1. Introduction

Fundamental questions in galaxy formation theory remain unresolved. Why do massive galaxies assemble early? And how can their stars form rapidly, as inferred from the α/Fe abundance ratios? Where are the baryons? And if, as observations suggest, they are in the intergalactic medium, both the photo-ionised Lyman α forest and the collisionally ionised warm-hot intergalactic medium (WHIM), how and when is the intergalactic medium (IGM) enriched to 0.1 of the solar value? Can the galaxy luminosity function be reconciled with the dark matter halo mass function? Does the predicted dark matter concentration allow a simultaneous explanation of both the Tully-Fisher relation and the luminosity function? And for that matter, is the dark matter consistent with barred galaxy and low surface brightness dwarf galaxy rotation curves? The observational data that motivates many of these questions can be traced back to the colour constraints on the interpretation of galaxy SEDs by population synthesis modelling (Sandage 1986; Larson 1986).

The galaxy distribution is bimodal in colour, and this can be seen very clearly in studying galaxy clusters. The presence of a red envelope in distant clusters of galaxies testifies to the early formation of massive ellipticals. A major recent breakthrough has been the realisation from UV observations

R. S. de Jong, Island Universes, 537–544.
© 2007 *Springer.*

with GALEX that many ellipticals, despite being red, have an ongoing trickle of star formation. Most field galaxies, and galaxies on the outskirts of clusters, are blue and are actively forming stars.

The general conclusion is that there must be two modes of global star formation: quiescent and starburst. The inefficient, long-lived, quiescent mode is motivated by cold gas accretion and global disk instability. The low efficiency is due to negative feedback. The disk mode is relatively quiescent and continues to form stars for a Hubble time. The starburst mode is necessarily efficient. It is motivated by mergers, including observations and simulations, as well as by CDM theory. The high efficiency is due to positive feedback, but how is the feedback provided?

2. Open Issues in Galaxy Formation

Consider first the baryon fraction in the universe. There is a universal prediction from high z. In fact four methods, involving primordial nucleosynthesis, the cosmic microwave background temperature fluctuations, the Lyα forest component of the IGM, and the gas fraction in massive galaxy clusters, all conspire to give a baryon fraction of $15 \pm 3\%$.

In contrast, both in our own galaxy and in M31, two of the best studied galaxies, we find a baryon fraction of $6 - 8\%$. Formation of galactic disks requires a baryon fraction of 10% or more for effective dissipation. These baryons seem not to be present, at least in the inner parts of galaxies, today. A clue comes from studies of the low redshift IGM which contains around half of the baryon content of the universe. The IGM is enriched today to about $[Z] \sim -1$. In massive clusters, where the intracluster medium (ICM) amounts to several times the mass in stars, it is enriched to about 30% of the solar value, and this is true to $z \sim 1$.

The simplest explanation is that a mass in baryons roughly equal to that in stars was enriched and ejected in early winds from forming galaxies. In clusters, the enrichment and ejection efficiency was larger than in the field. This is reminiscent of the two modes of star formation. The disk mode is inefficient and not responsible for substantial winds, at least from massive disks. The starburst mode drove the winds, and was responsible for much of the enrichment. In the clusters, which are dominated by elliptical and S0 galaxies, these winds occurred earlier and more widely than in the field.

Serious questions remain. How did the winds occur? Is there indeed a clean distinction between the two modes of star formation, or is there a continuum, from mini-starbursts to ultraluminous starbursts? Can the powerful starbursts account for early spheroid assembly? And what is the role of SMBHs in starbursts? Why do quiescent star forming and starbursting galaxies fit on the same law that relates star formation rate per unit area to gas surface density?

In the following, I will develop some tentative answers. The quiescent mode is motivated by cold gas accretion and global disk instability, and this naturally leads to a series of ministarbursts. The low efficiency due to negative feedback is induced by supernova heating of the multiphase interstellar medium. The powerful starburst mode is motivated by mergers of gas-rich galaxies, that effectively concentrate the gas reservoir in the merged systems. The high efficiency is due to positive feedback from AGN-driven outflows. These outflows trigger further star formation and supernovae, so that ultraluminous starbursts are a synergetic combination of SMBHs and spheroid formation that culminates in the formation of spheroids whose stellar masses and chemical evolution are coupled to the masses of the SMBHs.

3. Nature of the Feedback: Disks

In the quiescent mode, the clumpy nature of accretion suggests that ministarbursts might occur. In fact, what is more pertinent is the runaway nature of supernova feedback in a cold gas-rich disk. Initially, exploding stars compress cold gas and stimulate more star formation. Negative feedback is eventually guaranteed in part as the cold gas supply is exhausted and also as the cold gas is ejected in plumes and fountains from the disk.

Global simulations have inadequate dynamical range to follow the multiphase interstellar medium, supernova heating and star formation. The following toy model provides an analytical description of disk star formation. I assume that self-regulation applies to the hot gas filling factor $1 - e^{-Q}$, where Q is the porosity and is defined by

$$\begin{aligned}&(\text{ SN bubble rate}) \times (\text{maximum bubble 4-volume }) \\ &\quad \propto (\text{star formation rate})\,(\text{turbulent pressure})^{-1.4}\,.\end{aligned}$$

One can now write the star formation rate as (Silk 2003) $\alpha_S\, rotation\, rate \times gas\, density$ with $\alpha_S \equiv Q\epsilon$. Here $\epsilon = (\sigma_{gas}/\sigma_f)^{2.7}$, where the fiducial velocity dispersion

$$\sigma_f \approx 20\mathrm{kms}^{-1}\left(\mathrm{E_{SN}}/10^{51}\right)^{0.6}\left(200\mathrm{M}_\odot/\mathrm{m_{SN}}\right)^{0.4}\,.$$

The star formation efficiency $Q\epsilon$ is

$$0.02\left(\frac{\sigma_{gas}}{10\,\mathrm{kms}^{-1}}\right)\left(\frac{v_c}{400\,\mathrm{kms}^{-1}}\right)\left(\frac{m_{SN}}{200\mathrm{M}_\odot}\right)\left(\frac{10^{51}\mathrm{ergs}}{E_{SN}}\right).$$

The observed mean value is 0.017 (Kennicutt 1998).

To extract the wind, one might expect that the outflow rate equals the product of the star formation rate, the hot gas volume filling factor, and the mass loading factor. This reduces to $\sim Q^2\epsilon\dot{M}_*$, or $\dot{M}_{outflow} \approx f_L\alpha_S^2\epsilon^{-1}M_{gas}\Omega$. If Q is of order 50%, then the outflow rate is of order the star formation rate, but this evidently only is the case for dwarf galaxies.

Ejection

Ejection via early winds is inferred to account for both the enriched intracluster gas, the warm/hot intergalactic medium and the nearby Lyman α forest. For the case of the intergalactic medium in low density environments at $z \sim 0$, the observations, most notably of OVI and CIII in the Lyman α forest (Danforth et al. 2005) and OVII and OVIII absorption in the WHIM (Nicastro et al. 2005), require that the metallicity $[Z] \gtrsim 0.1$. The IGM results require considerable heavy element ejection from typical field galaxies since roughly half of the cosmic baryons are involved, or more than 3 times the baryons in stars.

Observations of Lyman break galaxies find offsets to the blue of the gas absorption relative to the stellar absorption features, and also broad gas absorption line widths (Adelberger et al. 2003). This suggests that early winds from L_* galaxies are a common phenomenon in the early universe. Since these galaxies seem to be strongly clustered, their mass loss is most likely to be relevant to ICM enrichment.

At least phenomenologically, the "missing" baryons *could* be in the WHIM. Typical field galaxies almost certainly are responsible for IGM enrichment. Indeed, the Milky Way and several nearby galaxies provide case studies for a history of minor mergers and galactic fountains. The gas which is expelled from the disks is most likely still trapped in the halos. Dwarf galaxy starbursts are supernova energy-driven outflows. However, there is a severe theoretical difficulty, in that ejection from L_* galaxies is not supported by hydrodynamical simulations with SN feedback (Springel & Hernquist 2003). Some additional input is required, and this most likely is provided by AGNs.

4. Nature of the Feedback: Spheroids

Spheroids are assembled early, and massive spheroids are assembled rapidly. Why is star formation so efficient and what physics provides the high efficiency that distinguishes massive from low mass spheroids that results in the enhancement of $[\alpha/Fe]$?

I argue that the ultraluminous starburst mode is most likely the culprit. Ultraluminous infrared galaxies (ULIRGs), with luminosities of order $10^{13}\mathrm{L}_\odot$ and star formation rates of order $1000\mathrm{M}_\odot\,\mathrm{yr}^{-1}$ are known to be triggered by major mergers between gas-rich galaxies. Tidal torques drive much of the gas into a dense core via angular momentum loss associated with shocks and strong dissipation. The star formation is highly efficient, as measured from the gas content. An extended stellar spheroid forms in the core: evidence for this comes from the distribution of the young star clusters that tracks the V-band light as well as the de Vaucouleurs profile seen in the near-infrared that develops within 100 Myr in the merging systems (Schweizer 2005).

In fact, this is far from the complete story. One has now to pose the question: why is star formation so efficient in the ultraluminous starburst mode? The answer is far from obvious. Supernovae result in inefficient star formation, in disks. This is confirmed by theory and observation. The same is true in low mass spheroids. The feedback is negative: gas is heated and ejected. However, in massive protospheroids, theoretical multiphase simulations demonstrate that winds are quenched by cooling. The analytical discussion of porosity shows that feedback is suppressed. So if supernovae cannot do the job, what else can?

The SMBH connection

The best evidence that points towards a distinct mechanism for spheroid star formation comes from the correlation between SMBH and spheroid velocity dispersion. The spheroid stars are old and formed when the galaxy formed. Hence the SMBHs, which accounts via the empirical correlation for approximately 0.001 of the spheroid mass, must have formed in the protogalaxy more or less contemporaneously with the spheroid. Supermassive black hole growth is certainly favoured in the gas-rich protogalactic environment.

SMBHs provide an intriguing possibility for stimulating a new and powerful mode of star formation. Accretion onto the SMBH occurs via a disk. The accretion disk fuels the growing SMBH, and twin relativistic jets are accelerated from the vicinity of the SMBH along the minor axis of the accretion disk. These jets are the fundamental power source for the high non-thermal luminosities and the huge turbulent velocities measured in the nuclear emission line regions in active galactic nuclei and quasars. The jets drive hot spots at a velocity of order 0.1c that impact the protogalactic gas. These are probably disruptive, but the jets are surrounded by hot cocoons that engulf and overpressure ambient protogalactic clouds (Saxton 2005). These clouds collapse and form stars. The speed of the cocoon as it overtakes the ambient gas clouds greatly exceeds the local gravitational velocity. In this way, a coherent and positive feedback is provided via triggering of massive star formation and supernovae on a short time-scale (Silk 2005).

If this is correct, the ULIRG phenomenon involves both spheroid formation and SMBH growth associated with the gas-rich proto-spheroid phase. The ULIRG winds are AGN momentum-driven and are self-limiting, with the rate of mass ejected inevitably being of order the star formation rate. The SMBH-triggered associated outflow generates the $M_{SMBH} \approx 10^6 \sigma_7^4 M_\odot$ relation, where σ_7 denotes the spheroid velocity dispersion in units of 100 km/s (Silk & Rees 1998).

Another toy model

To make these arguments less qualitative, consider the following toy model. A jet of luminosity L_J drives a hot spot at speed v_J into the multiphase protogalactic gas core. Following Begelman & Cioffi (1989), one can describe this situation by momentum balance: $L_J/v_J = \rho_a R_h^2 v_w^2$, where R_h is the hot spot width, ρ_a is the ambient gas density, and v_w is the wind velocity. Now there is a critical momentum flux above which the protogalactic gas is expelled from the protogalaxy. This condition is

$$L_{cr}/v_J = GMM_g/r = f_g\sigma_g^4/G.$$

If we identify the jet luminosity with the Eddington luminosity, we obtain $L_{cr}/v_J = L_{Edd}/c = 4\pi G\kappa^{-1}M_{BH}$, where κ is the electron-scattering opacity. It follows that $M_{SMBH} = f_g\sigma_g^4\kappa/4\pi G^2$. This is in fact the observed correlation between M_{SMBH} and σ_g in both slope and normalisation.

There is no good reason to believe that the jet outflow is Eddington-limited. In fact the accretion, presumably for a brief phase, almost certainly is not. Empirically, we know this because one has to form SMBHs in excess of $3 \times 10^9 \mathrm{M}_\odot$ by $z \sim 6$. We indeed may reasonably expect that the jet-driven flow is super-Eddington:

$$\frac{L_J}{L_{cr}} = f_c \left(\frac{v_w}{\sigma_g}\right)^2 \left(\frac{R_h}{R_c}\right)^2,$$

where f_c is the baryon compression factor in the core and R_c is the cocoon width. Eventually, perhaps after only 10^7 yr, the outflow is Eddington-limited, and

$$M_{SMBH} = \frac{\kappa}{4\pi G^2}\sigma^4 \left(\frac{M_g}{M}\right)\left(1 - f_L\alpha_S(\frac{\sigma_f}{\sigma_{gas}})^{2.7}(v_w/\sigma_g)\right).$$

Supernova-triggered galactic outflows are prevalent until

$$\sigma_{gas} \approx (f_L\alpha_S v_w)^{1/4}\sigma_f^{-0.7} \sim 100\mathrm{km\,s^{-1}};$$

at larger gas turbulence velocities, black hole outflow-initiated outflows must dominate. Self-regulation of jet outflow (positive) and SN (negative) feedback means that $\dot{M}_*^E \sim L_J/cv_w \propto v_w^2\sigma_g^2$. This expression explicitly provides the ingredient missing in earlier formulations of starbursts, and yields the needed boost in star formation efficiency.

Anti-hierarchical formation

One of the greatest challenges in galaxy formation theory is to account for the systematically earlier and more rapid formation of the massive galaxies. This is precisely the opposite of what is found for the evolution of the mass

function and for chemical evolution. Hierarchical galaxy formation predicts that massive halos form later and more slowly. The star formation prescriptions hitherto used in numerical and semi-analytical modeling similarly predict that chemical evolution is slower in the more massive systems.

SMBH-triggered star formation provides a means of circumventing this problem. The novel feature is that the SMBHs themselves form anti-hierarchically, as indeed is observed (Hasinger et al. 2005). One arrives at a theoretical explanation by considering the Compton-cooled wind core. This provides the mass reservoir out of which the disk accretes and the SMBH can continue to grow. One finds that the mass reservoir scales as the 2/3 power of SMBH mass. Hence the most massive SMBHs have the largest reservoir per unit mass for growth, and one may plausibly imagine that they will achieve run-away growth by accretion before the lower mass SMBHs have formed. If the SMBHs grow anti-hierarchically, and trigger star formation, then so should the spheroids.

5. Conclusions

Starbursts are ubiquitous. The star formation rate is limited by the local gas supply. This favours a series of (mini)-bursts if the gas supply is stochastic. In disks, the star formation efficiency is low because of negative SN-driven feedback. Both spheroids and disks form inside-out. However, the star formation in massive spheroids is efficient because of positive AGN-driven feedback.

The self-regulation hypothesis yields the star formation rate. Winds lead to saturation of the global star formation rate and the supermassive black hole mass, and provide an explanation for the observed correlation between SMBH and spheroid. In ultraluminous starbursts, the maximum luminosity from star formation $\sim 1000 \mathrm{L}_{\odot} \mathrm{yr}^{-1}$, and this is of order the Eddington luminosity. The spheroid mass saturates at $M_{BH} \sim 0.001 M_{spheroid}$. The supermassive black hole correlation with σ_g is a consequence of gas accretion, SMBH growth and AGN feedback-triggered star formation in the protospheroid.

That the gas ejected is of order the mass in stars is a plausible outcome of starbursts. However, the mechanism differs between small spheroids and disks, and for massive spheroids. In the former case, the outflows are energy-driven, by the porosity of the hot SN-heated bubbles. In the latter case, the flows are momentum-driven by the AGN outflow pushing on the dense, cooled interface with the protogalaxy. The momentum-driven ouflows from ULIRGs scale as $v_w \propto L_J^{1/2} \propto (\dot{M}_*^E)^{1/2}$. This is similar to the observed envelope for ULIRG superwinds. The Compton-cooled outflows provide a dense gas reservoir for forming spheroid cores. The outflow cores control downsizing of M_{BH} and consequently M_* in the spheroid.

Acknowledgement I thank C. Maraston and D. Thomas for discussions of many of the issues covered here.

References

Adelberger, K., Steidel, C., Shapley, A., Pettini, M. 2003, ApJ 584, 45
Begelman, M. C., Cioffi, D. F. 1989, ApJL, 345, L21
Danforth, C., Shull, J., Rosenberg, J., Stocke, J. 2005, ApJ submitted (astro-ph/0508656)
Hasinger, G., Miyaji, T., Schmidt, M. 2005, A&A in press (astro-ph/0506118)
Kennicutt, R.C. 1998, ApJ 498, 541
Larson, R. 1986, MNRAS 218, 409L
Nicastro, F. et al. 2005, ApJ 629, 700
Sandage, A. 1986, A&A 161, 89
Saxton, C., Bicknell, G., Sutherland, R.,Midgley, S., 2005, MNRAS 359, 781
Schweizer, F., 2005, *Starbursts: From 30 Doradus to Lyman Break Galaxies*, Astrophysics & Space Science Library, Springer, Dordrecht, 329, p.143
Silk, J. 2003, MNRAS 343, 249
Silk, J. 2005, MNRAS in press (astro-ph/0509149)
Silk, J. M. Rees, M. 1998, A&A 331, L1
Springel, V., Hernquist, L. 2003, MNRAS 339, 289

Katia Ganda, Isabel Pérez, and Tony Wong having a good time.

X-RAYS FROM DISK GALAXY HALOS, Lyα FROM FORMING GALAXIES, AND THE z$\sim$1 TULLY-FISHER RELATION

Jesper Sommer-Larsen

Dark Cosmology Centre, Niels Bohr Institute, University of Copenhagen, Denmark
jslarsen@tac.dk

Abstract Extended, soft X-ray emission from the halo of a very large disk galaxy has been detected. The luminosity and surface brightness distribution is in excellent agreement with predictions by recent, cosmological galaxy formation models. Predicted Lyα emission, associated with "cold" accretion of filamentary gas onto galaxies, is discussed in relation to Lyα "blobs". Finally, the predicted evolution of the Tully-Fisher relation, going from z=0 to 1, is discussed in relation to recent observations.

Keywords: cosmology: theory - galaxies: formation - X-rays: galaxies - methods: numerical - galaxies: kinematics and dynamics

1. X-ray Emission from Disk Galaxy Haloes

Disk galaxies continue forming to the present day, as evidenced by, e.g., infall of high-velocity clouds and satellite galaxies. Self-consistent models of disk galaxy formation predict that, at present, part of the inflowing gas originates as hot and dilute, low-metallicity halo gas, slowly cooling out and accreting onto the disk (e.g., Abadi et al. 2003, Sommer-Larsen et al. 2003, Governato et al. 2004, Robertson et al. 2004). The X-ray luminosity of the hot halo is predicted to increase strongly with the mass of the galaxy, and the haloes of the most massive galaxies should be detectable with current X-ray instruments (Toft et al. 2002, Rasmussen et al. 2004). Searches for this hot halo gas have so far failed to detect such soft X-rays, challenging our current understanding of galaxy formation. Moreover, it has been suggested that disk galaxies of total mass less than a few times $10^{11} M_{\odot}$ form primarily through accretion of cold gas, resulting in reduced halo X-ray emission (e.g., Birnboim & Dekel 2003; Keres et al. 2005 – see also next section). On the other hand, the recent detection of a warm-hot phase of the intergalactic medium shows the presence of a reservoir of hot and dilute gas at galactic distances (Nicastro

R. S. de Jong, Island Universes, 545–550.
© 2007 *Springer.*

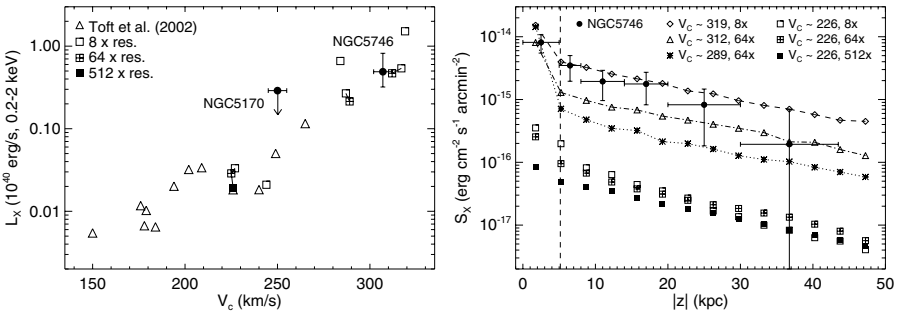

Figure 1. Left: Predicted and observed 0.3-1.5 keV luminosities of X-ray haloes as a function of disc circular velocity. All X-ray luminosities have been calculated within the same physical aperture as used for NGC 5746. The filled circles are from the observations of NGC 5746 and NGC 5170 (1-σ upper limit of $L_X < 2.9\ 10^{39}$ erg/s, 0.3-2 keV), while other symbols are the predictions from simulations with a range of different resolutions and circular velocities: Triangles are for simulations with low-metallicity chemical composition while squares are for simulations with self-consistent chemical evolution run at 8, 64, and 512 times the original resolution (Sommer-Larsen, Gotz & Portinari 2003) corresponding to gas particle masses of 7.5 10^5, 9.4 10^4 and 1.2 10^4 $M_\odot$, respectively. Results from simulations re-run at higher resolution are connected with lines. Open squares, except the simulated galaxy with a circular velocity of $\sim$225 km/s, are for simulations run with a universal baryon fraction of 0.15. All other simulations were run with a baryon fraction of 0.1. Right: Predicted and observed surface brightness profile of X-ray haloes as function of the distance to the disc mid-plane. Filled circles are NGC 5746 data while other symbols mark simulations with different resolutions and circular velocities. The vertical dashed line indicates D25 of NGC 5746.

et al. 2005). Furthermore, absorption of the OVI line in quasar spectra (Wakker et al. 2004), and the head-tail structure of some high-velocity clouds in the halo of the Milky Way (Bruns et al. 2000) provide circumstantial evidence that the Milky Way is surrounded by an extended hot halo.

As a test of current disk galaxy formation models we used the Chandra X-ray telescope to study the most promising candidate spiral galaxy for detecting halo X-ray emission, NGC 5746. We also studied a similar, but less massive galaxy, NGC 5170, as a test of our procedure. The galaxies are massive and nearby (NGC 5746 is an SBb galaxy at d=29.4 Mpc and has V_c=307$\pm$5 km/s; NGC 5170 is an Sc galaxy at d=24.0 Mpc and has V_c=250$\pm$5 km/s). Both galaxies are quiescent, showing no signs of either starburst activity, interaction with other galaxies, or an active galactic nucleus. The disks of the galaxies are viewed almost perfectly edge-on.

Diffuse, soft X-ray emission extending more than 20 kpc from the stellar disc was detected around NGC 5746. A total of about 200 net counts in the 0.3-2 keV band were detected from the halo of NGC 5746, corresponding to a 4.0-σ detection. The same observing technique and data analysis revealed no

diffuse emission around the less massive galaxy NGC 5170. Moreover, from Fig. 1 it follows that the agreement between observations and models is very good. Full discussions of the results will be presented in Pedersen et al. (2005), and Rasmussen et al. (2005).

2. "Cold" Accretion, and Lyα Properties of Forming Galaxies

Most of the Lyα photons produced in young galaxies originate from photo-ionized HII regions around young, massive stars. In recent years, however, it has been realized that not all gas, which ends up as cold and star-forming in galaxies, has been shock-heated to temperatures $T \sim 10^6$ K, before it is accreted onto the galaxy. Rather, the gas is accreted at densities and rates, such that gas remains at $T \sim 10^4$ K during the accretion, cooling mainly by abundant Lyα emission (e.g., Birnboim & Dekel 2003; Keres et al. 2005). So a fraction of the Lyα photons produced in and around young galaxies originate from cooling, almost neutral gas – we find this fraction to be typically of order 10%. In Fig. 2 (left) is shown, for a high-resolution galaxy formation simulation, the temperature distribution of gas before it is accreted onto the

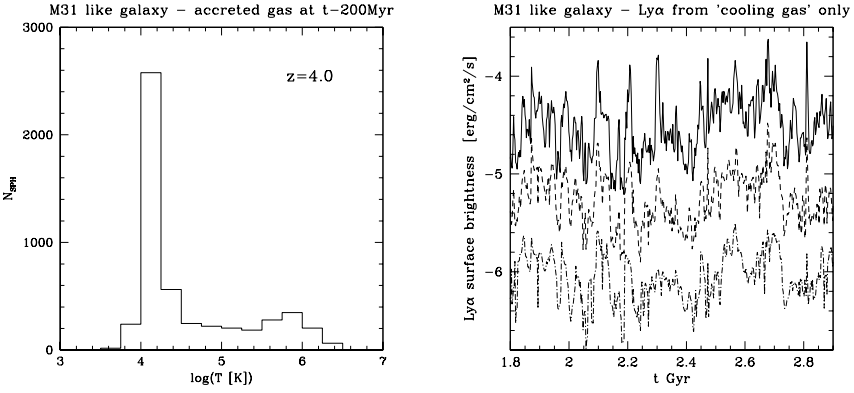

Figure 2. Left: Temperature distribution of gas particles, prior to accretion onto a number of starforming proto-disks in a M31 like proto-galaxy. Shown is (at a time 200 Myr before the z=4 frame) temperatures of gas particles, which at z=4 are located in the starforming proto-disks at densities $n_H > 10$ cm^{-3}, and which 200 Myr prior to this have not been accreted onto the proto-disks yet. Right: Lyα surface brightness of "cooling" radiation from the region around a M31 like proto-galaxy at $z \sim 3$, versus time. Top curve shows the peak surface brightness; second and third averages over circular regions of radii 10 and 20 kpc, respectively, centered at the position of the peak Lyα surface brightness.

proto-disks of a M31 like proto-galaxy, at z=4. As can be seen, at this redshift, the majority of the gas is, in fact, accreted "cold".

Can Lyα emission associated with "cold" accretion be observed? In recent years a number of so-called Lyα "blobs" have been detected (Keel et al. 1999, Steidel et al. 2000, Francis et al. 2001, Matasuda et al. 2004, Palunas et al. 2004, Dey et al. 2005). These are systems with spatial extents of up to 100 kpc, and Lyα luminosities of up to 5 10^{43} erg/s. In all cases, but one (see below), counterparts (like optical, IR, X-ray or radio) have been detected. Various mechanisms have been proposed, like i) QSO illumination (e.g., Haiman & Rees 2001; Weidinger et al. 2004), ii) galactic super-winds (e.g., Mori et al. 2004; Wilman et al. 2005), or iii) cold accretion. In the case of a z=3.15 blob, discovered by Nilsson et al. (2005), there are no other sources associated with the object going from X-rays (Chandra) to 8 μm emission (Spitzer). The blob has a linear extent of about 50 kpc and a typical surface brightness of 4 10^{-4} erg/s/cm^2, at the source. Moreover, a galaxy of photometric redshift 3.0 is situated at a projected distance of about 40 kpc from the blob, and may, given the uncertainty in the photometric redshift, be physically associated with the blob.

To test whether this blob can be filamentary gas being accreted "cold" onto a companion galaxy, we conducted the following experiment: for a M31 like proto-galaxy we calculated the Lyα surface brightness, in a 100x100 kpc (projected) region centered on the proto-galaxy, of "cooling" radiation only (so all contributions from regions with young stars were removed, as well as all emission, in general, from gas closer than 10 kpc to any star-forming region). The result is shown in Fig. 2 (right), at $z \sim$3, for a period of about 1 Gyr, with time resolution of just 2.5 Myr. As can be seen from the figure, we can get to within about an order of magnitude of the observed surface brightness level. This is interesting, and may point to a cold accretion origin of the blob Lyα emission, just on a larger scale, such as filamentary gas accretion onto a galaxy group – this option is currently being investigated. Given that in a search volume of about 40000 comoving Mpc^3, only one such blob has been detected, it is actually comforting, that we could *not* reproduce the blob characteristics, by cold accretion onto this, randomly selected, M31 like galaxy.

3. The $z \sim 1$ Tully-Fisher Relation

Considerable effort has been spent in recent years to determine the evolution of the zero-point and slope of the disk galaxy Tully-Fisher relation going from z=0 to $z \sim 1$ (e.g., Vogt 1999; Barden et al. 2003, Milvang-Jensen et al. 2003; Bohm et al. 2004; Bamford et al. 2005). The observational results span a range from almost no evolution to about 1.1 mag fading in the B-band. Such observational information provides important constraints on models of galaxy

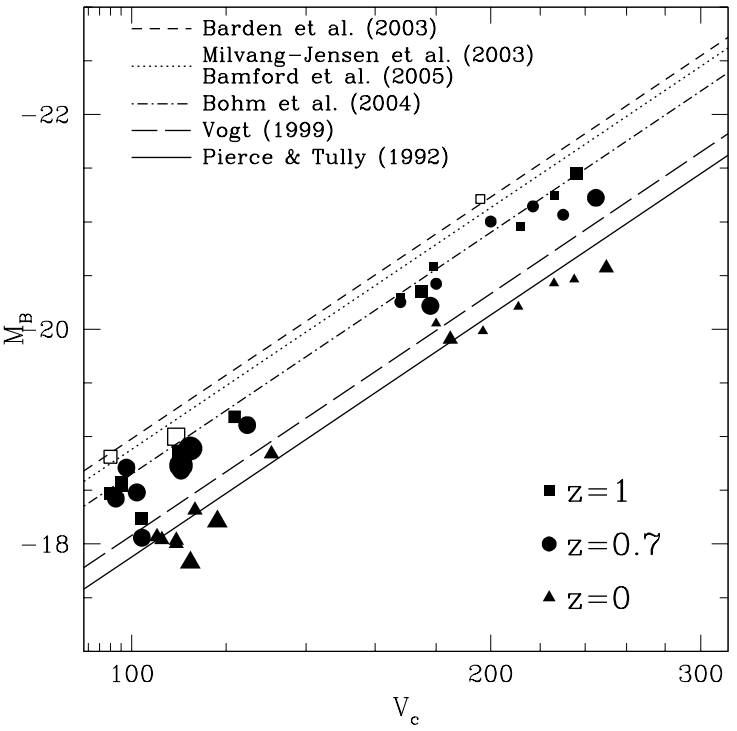

Figure 3. Tully-Fisher relations from observations, as well as, simulations. Solid line: B-band z=0 TF relation of Pierce & Tully (1992) for Sc galaxies (B–V∼0.55), shifted downwards by 0.6 mag to enable a comparison to the model disk galaxies which have B–V=0.6-0.75 (∼Sb type). Other lines show the differential evolution of the zero-point of the B-band TF going to $z \sim 1$, reported by various authors (the slopes have been forced to be as for the z=0 TF relation). Results of models, invoking feedback, self-consistent treatment of chemical evolution and metal-dependent radiative cooling, and assuming a universal baryon fraction of 0.15 (Portinari & Sommer-Larsen 2005) are shown by various symbols. Filled symbols correspond to z=0, 0.7 and 1. Open symbols refer to disk galaxies, which were too disturbed at z=1 to enable determination of the TF quantities; hence these were determined at z=0.8 instead. Smallest symbols correspond to the original resolution of Sommer-Larsen et al. (2003), medium sized and large to 8 and 64 times higher mass resolution, respectively.

formation and evolution, in particular no or only very mild evolution points to scenarios with considerable, continuing disk growth, going from z=1 to 0.

Given this, it is clearly of interest to compare to what fully cosmological galaxy formation simulations, incorporating feedback, non-instantaneous chemical evolution, metal-dependent radiative cooling etc. predict. We have recently engaged in such a study, and show the first results in Fig. 3; the full results will be presented in Portinari & Sommer-Larsen 2005. The preliminary conclusion based on the results shown in Fig. 3 is that our results for z=0.7 and

1.0, relative to the z=0 results are nicely bracketed by the various observational determinations at $z \sim 1$. Moreover, we find that the stellar *mass* TF relation shows essentially no evolution going from z=1 to 0, since an increase in stellar mass leads to an increase in V_c as well. This is in agreement with the findings of Conselice et al. (2005).

Acknowledgements I thank my collaborators on the various projects for providing material to this contribution.

References

Abadi, M. G. et al. 2003, ApJ, 591, 499
Bamford S.P., Milvang-Jensen B., Aragon-Salamanca A., Simard L., 2005, MNRAS 361, 109
Barden M., Lehnert M.D., Tacconi L., Genzel R., White S., Franceschini A., 2003, submitted to ApJ Letter (astro-ph/0302392)
Birnboim, Y. & Dekel, A. 2003, MNRAS, 345, 349
Bruns, C., Kerp, J., Kalberla, P. M. & Mebold, U. 2000, A&A, 357, 120
Bohm A., Ziegler B.L., Saglia R.P., R., Fricke K.J., Gabasch A., Heidt J., Mehlert D., Noll S. & Seitz S. 2004, A&A, 420, 97
Conselice C.J., Bundy K.E., Richard S., Brichmann J., Vogt N.P., Phillips A.C., 2005, ApJ 628, 160
Dey, A. et al. 2005, ApJ, 629, 654
Francis, P. J. et al. 2001, ApJ, 554, 1001
Governato, F. et al. 2004, ApJ, 607, 668
Keel, W. C. et al. 1999, AJ, 118, 2547
Keres, D., Katz, N., Weinberg, D. H. & Dave, R. 2005, MNRAS, 363, 2
Matasuda, Y. et al. 2004, AJ, 128, 569
Milvang–Jensen B., Aragon–Salamanca A., Hau G.K.T., Jørgensen I., Hjorth J., 2003, MNRAS 339, L1
Nicastro, F. et al. 2005, Nature, 433, 495
Nilsson, K., Fynbo, J. P. U., Moller, P., Sommer-Larsen, J. & Ledoux, C. 2005, A&A, to be submitted
Palunas P. et al. 2004, ApJ, 602, 545
Pedersen, K., Rasmussen, J., Sommer-Larsen, J., Toft, S., Benson, A. J. & Bower, R. G. 2005, New Astronomy, submitted
Pierce M.J., Tully R.B. 1992, ApJ 387, 47
Portinari, L. & Sommer-Larsen, J. 2005, MNRAS, to be submitted
Rasmussen et al. 2004, MNRAS, 349, 255
Rasmussen, J., Sommer-Larsen, J., Pedersen, K., Toft, S., Benson, A. J. & Bower, R. G. 2005, ApJ, to be submitted
Robertson, B. et al. 2004, ApJ, 606, 32
Sommer-Larsen, J., Gotz, M. & Portinari, L. 2003, ApJ, 596, 46
Steidel, C. C. et al. 2000, A&A, 391, 13
Toft et al. 2002, MNRAS, 335, 799
Vogt N.P., 1999, in The Hy Redshift Universe, A.J. Bunker and W.J.M. van Breugel (eds.), ASP Conf. Series vol. 193, p. 145
Wakker, B. P. et al. 2004, contribution to the Extra-planar Gas Conference, Dwingeloo (astro-ph/0409586)

GAS RICH MERGERS IN DISK FORMATION

C. B. Brook[1], V. Veilleux[1], D. Kawata[2], H. Martel[1] and B. K. Gibson[3]

[1] *Université Laval, Canada*

[2] *Carnegie Observatories, USA*

[3] *Swinburne University, Australia*

Abstract In order to explain disk galaxy formation within the hierarchical structure formation, it seems that gas rich mergers must play an important role. We review here our previous studies which have shown the importance of mergers at high redshift being gas rich, in the formation of both the stellar halo and thick disk components of disk galaxies. Regulation of star formation in the building blocks of our galaxy is required to form a low mass low metallicity stellar halo. This regulation results in high redshift, gas rich mergers during which the thick disk forms. In these proceedings, we categorise stars from our simulated disk galaxy into thin and thick disk components by using the Toomre diagram. Rotation velocity, metallicity and age histograms of the two populations are presented, along with alpha element abundances (oxygen, silicone, magnesium), age-height above the plane, age-radius, metallicity-height, and metalicity-radius gradients.

Keywords: galaxies: formation - methods: N-body simulations - galaxies: abundances - galaxies: interactions

1. Introduction

The overcooling problem (White & Rees 1978), coupled with the ineffectiveness of implemented feedback algorithms in regulating star formation (Katz & Gunn 1991) have been central to the difficulties of simulating disk galaxies in a cold dark matter (CDM) Universe. Without sufficient feedback, stars form rapidly in the earliest collapsing dark matter halos, which subsequently merge; angular momentum is transferred to the dark matter halo, and the resultant disk is significantly smaller (in scalelength), and has less angular momentum, than those observed. Feedback from supernovae, stellar winds, quasars etc, has proven to be difficult to simulate, yet the effects of feedback are essential in the formation of disk galaxies. Recent models incorporate these processes without attempting to detail the complex multiphase gas physics involved. This has highlighted the importance of regulating star formation in the "building blocks" of galaxies. (note: We use the term "building blocks"

R. S. de Jong, Island Universes, 551–556.
© 2007 *Springer.*

when refering to early forming small galaxies which will have merged or been accreted to the final galaxy at redshift 0. By contrast, the term "satellites" is reserved for those small galaxies which are found orbiting the central galaxy at z=0).

To tackle these problems, Thacker & Couchman (2000) turned off cooling for a fixed time in gas within the Smooth Patricle Hydrodynamical smoothing kernel of a supernova event, resulting in increased angular momentum in the simulated disk galaxy. Brook et al. 2004a (see section 2) examined constraints on such feedback models provided by the Milky Way's stellar halo. Sommer-Larsen and collaborators have examined other implementations of feedback, and also shown the importance of regulating cooling at early epochs (Sommer-Larsen, Götz, & Portinari 2003). Governato et al. (2004) highlights the importance of resolution in simulating disk galaxies. Implementing these findings has allowed models such as those presented in this conference by Jesper Sommer-Larsen and Fabio Governato to make progress in reproducing disk galaxies with properties approaching those of observed disks. Although feedback recipes differ, a crucial ingredient in these improved models is the regulation of star formation in galactic building blocks. The implications is that early mergers are gas rich...

2. Gas Rich Mergers and the Stellar Halo

In Brook et al. (2004a) we simulated disk galaxy formation *using identical initial conditions* with two different feedback methods. Using thermal feedback following Katz & Gunn (1991), star formation is rapid when the building blocks collapse (figure 1), with the stars rapidly reaching relatively high metallicities, and accreting preferentially to the halo meaning a massive, metal rich stellar halo is formed. In the adiabatic feedback model, which follows Thacker & Couchman (2000), star formation is regulated in low mass building blocks, which remain gas rich when accreted at high redshift, and galaxies form with a low mass, low metallicity stellar halo. The dissipative gas accretes on to the forming (thick) disk.

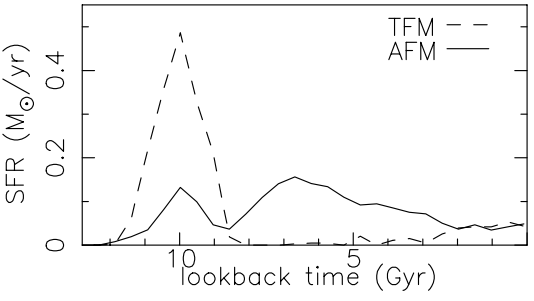

Figure 1. Star formation histories of a galactic building block in the Adiabatic and Thermal Feedback Models. The ability of the AFM to regulate star formation in galactic building blocks is a crucial ingredient in creating disk galaxies with low mass, low metallicity stellar halos (from Brook et al. 2004a).

James Bullock presented a model in which he and his collaborators have modelled the stellar halo using the assumption that stellar halo stars are accreted from galactic building blocks. They use cosmologically motivated merger histories to set the timing, mass, and orbits of the accretions onto an analytic potential. Star formation rates in individal building blocks and satellites are motivated by the mass accretion histories of their host dark matter halos. Bullock & Johnston (2005) find that star formation in building blocks prior to accretion must be highly regulated, in order to match the properties of the Milky Way's stellar halo; early mergers/accretions are gas rich. The growth and accretion histories of building blocks are systematically different than those of sattelites, and they show in Font et al. (2005) that such differences can naturally explain the difference in alpha elements between the stellar halo and the Milky Way's dwarf galaxies (see e.g. the contribution to these proceedings of Kim Venn).

3. Gas Rich Mergers and the Thick Disk

The emerging evidence that old thick disk stars seem to envelope the majority, and perhaps all disk galaxies, means that the formation of thick disks may be an integral stage in disk galaxy formation. Understanding thick disk formation may thus be a key insight in unravelling disk galaxy formation. In previous papers, we have proposed that the thick disk forms during gas rich mergers, which were frequent at high redshift in a CDM Universe (Brook et al. 2004a; Brook et al. 2005a). This formation scenario was shown to be consistent with observations of both the Galactic and extra-galactic thick disks.

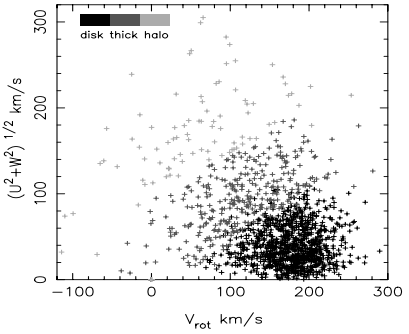

Figure 2. The Toomre diagram of simulation solar neighbourhood stars. Our categoristion of stars as thin disk, thick disk and halo are indicated.

In these previous studies, we used the abrupt increase in the velocity dispersion-age relation of solar neighbourhood stars, apparent in both the simulations and observations, as an indication of the time of thick disk formation. By selecting stars according to their age, we were able to relate dynamical and chemical properties of the stellar components, to the dominant processes which were occurring during their birth. This allowed us to show that thick disk stars form during gas rich merger events at high redshift, while disk stars

form in a later, more quiescent epoch. In these procedings, we categorise stars from our simulated disk galaxy into thin and thick disk components by using the Toomre diagram, as shown in figure 2. Rotation velocity, metallicity and age histograms of the two populations are presented, along with alpha element abundances (oxygen, silicone, magnesium), age-height above the plane, age-radius, metallicity-height, and metalicity-radius gradients. These are consistent with those in Brook et al. 2005) using different selection criteria for the components, in this case better mimicking observational techniques. The conclusions of that paper remain valid.

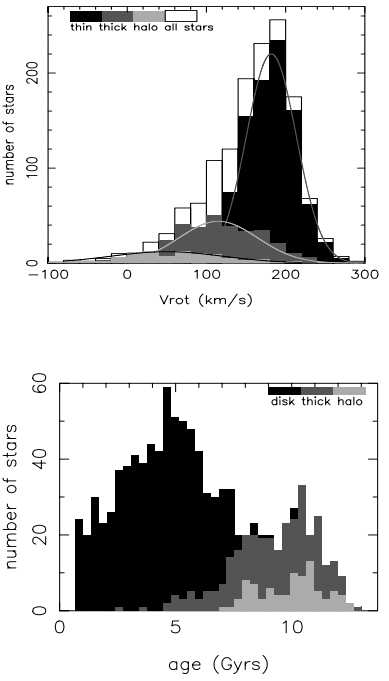

Figure 3. Rotational velocity (*top left*), metallicity (*top right*), and age (*left*) histograms of simulation solar neighbourhood stars, depicting disk stars (black), thick disk (dark grey) and halo stars (light grey) as selected from the Toomre diagram.

In these proceedings, Alyson Brooks traces thick disk stars in their simulated disk galaxy, and finds that only around 5% of such stars have been accreted directly from stars in building blocks, implying that direct accretion plays a minor, role in thick disk formation. Kim Venn shows that thick disk stars have high α element abundances at relatively high Fe values. This may be explained by the merging epoch during which the thick disk forms driving increased star formation rates. The observations of Debra Elmegreen hint that the progenitors of todays disk galaxies were clumpy, resembling our simulations redshifts at $z \sim 2$. Her interpretation that Hubble Deep Field disk galaxies are thicker than their local counterparts adds weight to theories such as ours in which thick disks are formed early (Elmegreen et al. 2005). Julianne Dalcanton presented evidence for the existence of counter-rotating thick disks (Yoachim

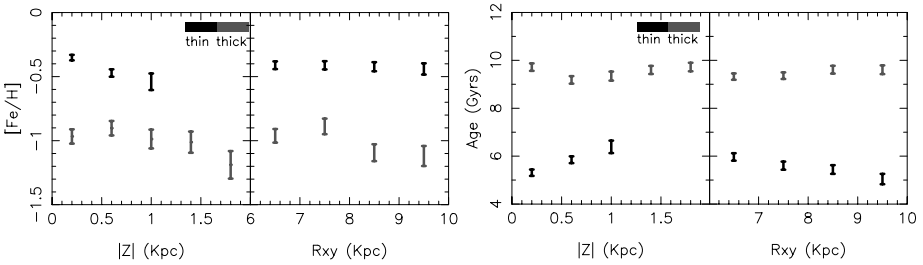

Figure 4. Disk and thick disk metallicity and age gradients in the radial (R_{xy}) and perpendicular (|Z|) directions, showing in particular no gradient with height for thick disk stars.

& Dalcanton 2005). This provides further constraints on thick disk formation scenarios. We have a study underway which hopes to determine which thick disk formation scenarios are favoured by such observations.

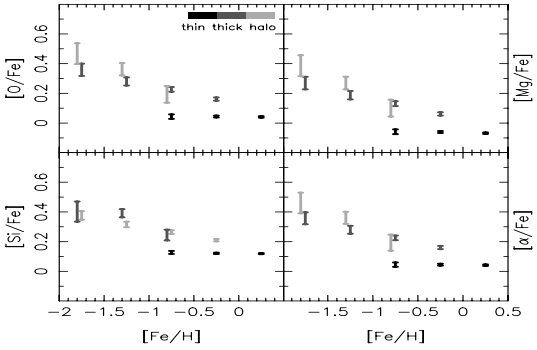

Figure 5. The plots of α elements vs $[Fe/H]$ show that thick disk stars are α enhanced compared to those in the thin disk.

4. Gas Rich Mergers and the Thin Disk

Feedback at early epochs also results in enrichment of the IGM, with gas which falls later onto the disk regions being enriched by gas ejected or tidally stripped from the galactic building blocks, relieving the g-dwarf problem (Brook et al. 2004a). Subsequent "inside out" growth of the thin disk in the relatively quiescent period since $z \sim 1$ results in the flattening of the spiral galaxies. This is explored in relation to our simulated disk galaxies in Brook et al. (2006).

5. Conclusion

If we are to accept ΛCDM cosmology, it seems necessary to invoke gas rich mergers to explain many properties of disk galaxies. It is necessary that mergers of building blocks which collapse at high redshift in CDM remain gas

rich in creating low mass, low metallicity stellar halos, with observed chemical abundances. The stellar disk that emerges from the chaotic merging period that characterises ΛCDM between redshifts ∼2 and ∼1, is relatively hot. The rapid star formation induced by these events results in high α abundances in stars where iron levels are relatively high, in this emergent thick disk. Gas leftover (gas that is heated during this epoch, rather than forming stars) is pre-enriched and falls later onto the thin disk, thus alleviating the G-dwarf problem.

That gas rich mergers are important in galaxy formation is not a surprise in the sense that it has become clear that, for CDM to work, then the conversion of gas to stars must become very inefficient as we move toward smaller mass objects. Such processes are required to explain the multitude of evidence that is pointing toward "downsizing", in which star formation occurs over longer timescales in low mass objects. It must be remembered that 80% of the Milky Way's stars form quiessently from gas in the thin disk,which forms through dissipative processes. We thus conclude that in low density environments, where disk galaxies form, there is growing evidence that the "building blocks" of such galaxies in a cold dark matter Universe remain gas rich. In this manner, there is found a bridge between the two classical galaxy formation paradigms, rapid collapse as proposed in Eggen, Lynden-Bell & Sandage (1962), and the hierarchical build up proposed in Searle & Zinn (1978) and White & Rees (1998).

Acknowledgements CB thanks Fabio Governato, Alyson Brooks, Julianne Dalcanton, James Bullock, and Kim Venn for stimulating discussions and making Island Universes a fun conference.

References

Brook, C. B., Gibson, B. K., Martel, H., & Kawata D. 2005, ApJ,
Brook, C. B., Kawata, D., Gibson, B. K., & Flynn C. 2004a, MNRAS, 349, 52
Brook, C. B., Kawata, D., Gibson, B. K., & Freeman K. 2004b, ApJ, 612, 894
Brook, C. B., Kawata, D., Martel, H., Gibson, B. K., & Bailin J. 2005, submitted ApJ
Bullock, J. S., & Johnston, K. V. 2005 ApJ submitted, astroph/0506467
Elmegreen, D. M., Elmegreen, B. G., Rubin, D. S., & Schaffer, M. A. 2005, ApJ, 631, 85
Eggen,O. J., Lynden-Bell, D. & Sandage, A. R. 1962 ApJ 136, 748
Yoachim, P., & Dalcanton, J. J., 2005 ApJ, 624, 701
Font, A., Johnston, K. V., Bullock, J. S., & Robertson, B., 2005 ApJ submitted, astroph/0506467
Governato, F. et al. 2004, ApJ, 607, 688
Katz, N., & Gunn, J. E. 1991, ApJ, 377, 565
Katz, N. 1992, ApJ, 391, 502
Searle, L. & Zinn, R. 1978 ApJ 225, 357
Sommer-Larsen, J., Götz, M., & Portinari, L. 2003, ApJ, 596, 47
Thacker, R. J., & Couchman, H. M. P. 2000, ApJ, 545, 728
White, S. D. M., & Rees, M. J. 1978, MNRAS, 183, 341

COSMOLOGICAL SIMULATIONS OF GALAXY FORMATION II: MATCHING THE OBSERVATIONAL PROPERTIES OF DISK GALAXIES

Fabio Governato[1,2*], Beth Willman[3**] and Lucio Mayer[4***]

[1] *INAF-Brera, Milano, Italy*

[2] *University of Washington, Seattle, USA*

[3] *NYU, Gotham City, USA*

[4] *Institute fur Astronomie, ETH Zurich, Switzerland*

* fabio@astro.washington.edu, ** bw427@nyu.edu, *** lucio@phys.ethz.ch

Abstract We have used fully cosmological, high resolution N-body + SPH simulations to follow the formation of disk galaxies with a rotational velocity between 140 and 280 km/s in a ΛCDM universe. The simulations include gas cooling, star formation (SF), the effects of a uniform UV background and a physically motivated description of feedback from supernovae (SN). The host dark matter (DM) halos have a spin and last major merger redshift typical of galaxy sized halos as measured in recent large scale N–Body simulations. Galaxies formed rotationally supported disks with realistic exponential scale lengths and fall on the I-band and baryonic Tully-Fisher relations. The combination of UV background and SN feedback drastically reduced the number of visible satellites orbiting inside a Milky Way sized halo, bringing it fair agreement with observations. Feedback delays SF in small galaxies and more massive ones contain older stellar populations. The current star formation rates as a function of galaxy stellar mass are in good agreement with those measured by the SDSS.

Keywords: galaxies: formation - galaxies: evolution - methods: N-body simulations - galaxies: fundamental parameters

1. Introduction

N–Body/gas-dynamical simulations have become the primary tools with which to model galaxy formation in a cosmological context. They are necessary to follow the internal structure of galaxies as well as the complex interplay between baryon cooling and feedback. These studies are of fundamental importance to answer a number of challenges faced by the hierarchical model of structure formation: (a) early numerical simulations of galaxy formation

R. S. de Jong, Island Universes, 557–564.
© 2007 *Springer.*

Table 1. Summary of the properties of the three cosmological halos. [a]: Circular velocity at virial radius. [b]: number of gas and star particles changes slightly depending on ϵSN. [1&2]: smaller softening/larger N values are for a z=0.5 ultra-high resolution run.

Run	Virial Mass M$\odot$	Vc[a] km/s	spin λ	z of last major merger	ϵ kpc	N^b_{tot} at z=0 dark+gas+stars
DWF1	1.6 10^{11}	70	0.01	2.2	0.3	$\sim$ 860.000
MW1[1]	1.15 10^{12}	134	0.04	2.5	0.6-0.3[1]	$\sim$ 700.000 - 4.000.000[2]
GAL1	3.1 10^{12}	185	0.035	2.75	1.	$\sim$ 480.000

reported a catastrophic loss of angular momentum in the baryonic component, leading to the formation of galaxies with very small disk scale lengths and dominant spheroidal components (e.g., Navarro & Steinmetz 2002); (b) dark matter-only simulations predict over an order of magnitude more subhalos around Milky Way-like galaxies than the number of dwarfs observed around the Milky Way and M31 (Moore et al. 1998., Willman et al. 2004); and (c) observations show that more massive late-type galaxies have older stellar populations than less massive late-type galaxies (MacArthur et al. 2004). This finding is at face value in contradiction with the fact that in CDM scenarios less massive halos form first. *These very different aspects of the formation and evolution of galaxies need to be simultaneously addressed by simulations of galaxy formation*.

2. Code and Simulations

We used GASOLINE (Wadsley, Quinn & Stadel 2004), a smooth particle hydrodynamic (SPH), parallel treecode that is both spatially and temporally adaptive with individual particle time steps. The code includes a treatment of i) Compton and radiative cooling, ii) star formation and a supernova (SN) feedback, and iii) a UV background from QSOs and star forming galaxies following an updated version of the Haardt & Madau model predictions (1996, Haardt 2005, private communication). The facts that supernova feedback and the UV background can reduce gas retention and accretion in halos with low virial temperature makes them possible solutions to the problems mentioned in the introduction (e.g., Benson et al. 2002). The current implementation of star formation and feedback from stellar process is described in detail in Stinson et al. (2005). Feedback follows qualitatively the algorithm implemented by Thacker & Couchman (2000). We assume that the energy released into the ISM stops the gas from cooling and forming stars over some timescale, thereby the gas will just expand adiabatically. The time scale for the cooling shutoff and the amount of mass affected are now physically motivated and chosen following McKee & Ostriker (1977). The only two free parameters in our algorithm are star formation efficiency and the fraction of SN energy dumped

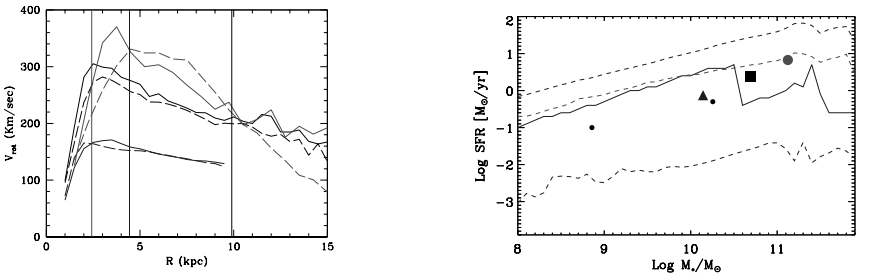

Figure 1. Left Panel: Azimuthally averaged rotation velocity of cold gas (solid line) and stars younger than 6.5 Gyrs (dashed line). From top to bottom: GAL1,MW1,DWF1. The vertical lines show 2.2 disk scale lengths for each simulated galaxy, the point at which the rotation velocity V_{TF} is measured. Right panel: The present day star formation rate of our simulated galaxies vs their stellar mass compared with the SDSS sample in Brinchmann et al. 2005. (blue triangle: DWF1, solid square: MW1, red circle: GAL1, solid dots: simulated small galaxies within the high res region of MW1.

into the ISM. These parameters are tuned to reproduce the properties present day disk galaxies (Governato et al. 2005) and are then applied to cosmological simulations. The SN efficiency parameter (ϵSN) was varied from 0.2 to 0.6. Best overall results were obtained with ϵSN = 0.4 to which all plots refer unless otherwise noted. A Miller Scalo IMF is assumed. Cosmological galaxies were simulated in a ΛCDM concordance cosmology using the "renormalization" technique to maximize the resolution in the region of interest (Katz & White 1993). *Three DM halos were selected with the criteria of a) a last major merger (defined as a 3:1 mass ratio) at redshift 2.2 $< z <$ 2.75, and b) no halos of similar or larger mass within a few virial radii*. The physical and numerical parameters of our runs are summarized in Table 1.

The last major merger redshift (z_{lmm}) range is typical for galaxy sized DM halos in a concordance cosmology, as recently shown in large N-body simulations by Li, Mo & van den Bosch (2005) and Maller et al. (2005). Global magnitudes for our models were obtained coupling the star formation histories (SFH) of our simulations with GRASIL (Silva et al. 1998), a code to compute the spectral evolution of stellar systems taking into account the effects of dust reprocessing.

3. Results

Disks and Star Formation Rates: At the final time, the three galaxies have formed a substantial disk component well fit by an exponential profile outside the inner 1-2 kpc. The stellar disks follow exponential profiles out to 2.5–3 scale lengths. All three galaxies also have extended disks of cold gas with

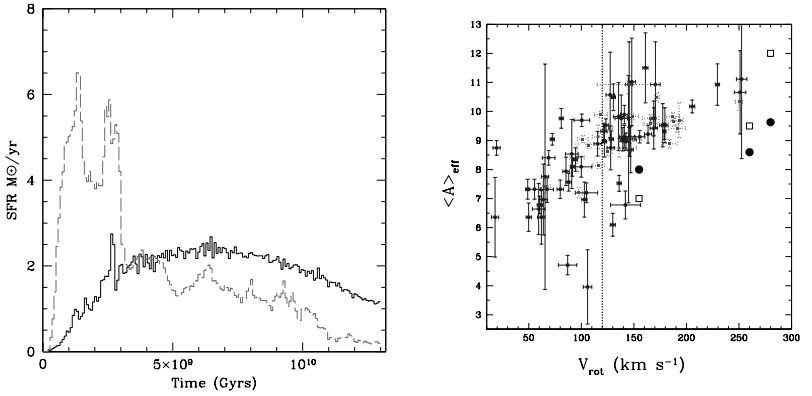

Figure 2. Left panel: Star formation rate of all stars within 4 disk scale heights from the disk plane in two different runs of DWF1. Black solid line: strong SN feedback (ϵSN=0.6); Magenta long-dashed: no feedback, no UV. The addition of feedback smooths out the peak in SF otherwise present at high redshift and during the last major merger event at z=2.3. Feedback delays the conversion of gas into stars until gas accumulates and cools in the potential well of the main progenitor. The run with feedback has a present day SFR almost ten times higher. Right panel: Average and median age of stellar populations vs galaxy circular velocity. Solid and empty circles show values for our simulated galaxies. Data points with error bars are from MacArthur et al. 2004.

exponential scale lengths larger than even the youngest component of the stellar disks. Beyond 3 scale lengths, the stellar disk declines rapidly even for young stars. Such disk profiles are quite common in observed spiral galaxies with 150 $< v_c <$ 250 km/s (Pohlen & Trujillo 2006).

Within the inner 1-2 kpc, the two smaller galaxies (DWF1 and MW1) exhibit a steep central "bulge" component. Due to its small physical size, it is possible that this bulge component is affected by resolution. We confirmed this possibility by comparing to a run of MW1 that uses a force resolution of 0.3 kpc and eight times better mass resolution (this resolution is unprecedented for SPH simulations of individual galaxies in a cosmological context). While this ultra-high resolution run produces a galaxy with a very similar disk scale length and rotation curve, the central concentration of baryons within the central kpc (and thus the central steepening of the profile) is reduced (see Governato et al. 2005). We also investigated the effect of SN feedback strength on the final galaxy properties. The stellar profile and size of the final disks in the more massive galaxies (MW1 and GAL1) is only weakly dependent on the strength of SN feedback because the adopted efficiency for supernovae heating is too low to generate large scale winds and mass loss in massive halos. The fact that the final stellar and cold gas masses compare very well with the Milky Way thus argues in favor of such relatively moderate effect of feedback

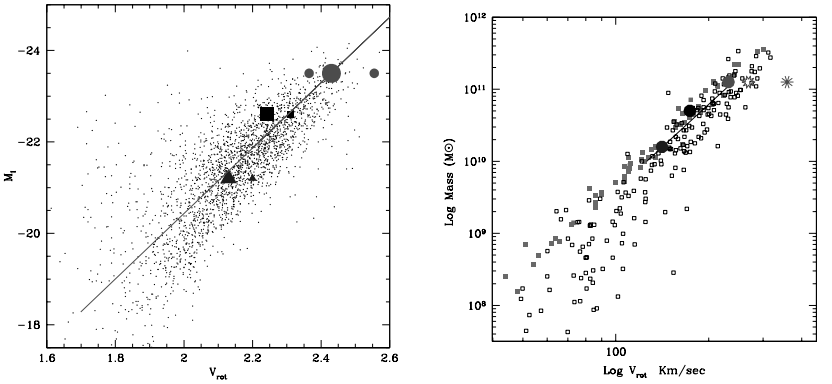

Figure 3. Left panel: The Tully-Fisher relation. Small dots are from a recent data compilation by Giovanelli & Haynes. The red line is a fit to data in Giovanelli et al (1997). Solid triangle: DWF1; Solid Square: MW1; Solid/Starred Dot: GAL1. Bigger dots shows V_{rot} measured at $3.5R_d$ (as in the observational data). Smaller dots show V_{rot} measured at $2.5R_d$. The rightmost red dot uses the stellar peak velocity. Right Panel: The baryonic TF relation. Solid triangle: DWF1; Solid Square: MW1; Solid Dot: GAL1; Empty circles: McGaugh et al. 2000, Magenta squares: McGaugh et al. 2005. The solid line is a best fit from data in Gurovich et al. 2004. Simulation data points include all stars and cold gas within their bulges & disks components.

at these mass scales. However, the dwarf galaxy disk stellar profile is drastically affected by varying amount of SN feedback. When ϵSN is increased to 0.6, the stellar density profile of DWF1 is best described by a single exponential profile with a shorter scale length than that measured with ϵSN = 0.4. Unlike the disk sizes, the strength and longevity of dynamical bars in all three galaxies increases remarkably with decreasing strength of the feedback. SN feedback also plays a major role in shaping the star formation histories (SFHs) of our simulated galaxies, particularly that of DWF1, the lowest mass galaxy in the set. The right panel of Fig. 1 shows that the simulated z=0 SFRs are in good agreement with those measured from the SDSS over a large range of stellar masses (Brinchmann et al. 2005). The left panel of Fig. 2 compares the SFH of DWF1 in the cases without SN feedback and with the strongest feedback adopted in our study (ϵSN = 0.6). Early star formation is significantly reduced by feedback, as the relative strength of SF bursts during major merger events. We verified that lowering the efficiency of star formation during mergers preserves a large quantity of cold gas that rapidly settled in rotationally supported disks. Fig. 2 (right panel) also shows that our simulations follow the trend observed by MacArthur et al. (2004): galaxies with less massive stellar component also tend to have younger stellar populations. The inclusion of feedback and its differential effect at different galaxy masses reproduces the observed "anti-hierarchical" trend within a cosmological context.

The Abundance of Milky Way Satellites: A combination of radiative feedback from the cosmic UV background and SN winds drastically reduces the number of satellites within the virial radius of the MW1 galaxy to the point where it is in agreement with observations, although the satellites are too bright compared to those of the Milky Way. The satellites resolved in these runs (V_{max} > 25 km/s) exhibit extended and sporadic star formation histories, similar to those observed in Milky Way dwarfs.

Rotation curves and the Tully–Fisher relation: The azimuthally averaged rotation curves of galaxies simulated including SN feedback are shown in the left panel of Fig. 1. This figure shows that gas rotational velocities are very similar to stellar ones for models with feedback. However, gas and stellar velocities are often different for models without feedback, because stars have higher velocity dispersions and cold gas is often completely misaligned with the main stellar component. The rotation curves combined with the disk scale lengths of intermediate age disk stars allow us to compare our galaxy models against two fundamental relation for normal galaxies: (1) the Tully-Fisher (TF) relation that links the characteristic rotation velocity of a galaxy with its total magnitude or baryonic disk+bulge mass (Giovanelli & Haynes 1997) and (2) the "baryonic TF" relation (McGaugh 2002, McGaugh 2005), which takes into account that smaller galaxies are more gas rich and that stars account for only a fraction of their disk total mass (Fig. 3). Early simulations reported severe difficulties in matching the normalization of the above relations, as the central rotational velocities of the simulated galaxies were too high due to an excess of matter at the center of galaxies. This was possibly due to excessive baryon cooling and angular momentum loss and the subsequent adiabatic contraction of the DM component. High resolution simulations in which only a weak feedback was included, such as those of Governato et al. (2004) and Abadi et al. (2003), showed a small, but consistent shift from the TF relation with galaxies being too centrally concentrated compared to real ones. Our new set of simulations successfully matches both relations. *Matching the Tully-Fisher relation is possibly the most important conclusion of the work presented here.* This match shows that our simulations produce a realistic distribution of stars, baryons and dark matter within the central few kpc of disk galaxies. Much progress remains to be made before galaxy formation is fully understood. However, once sufficient resolution and some of the complexities of star formation and SN feedback are introduced in numerical simulations, the ΛCDM scenario is able to create galaxies that share some of their structural properties with the real ones.

Acknowledgements FG was a Brooks Fellow when this project started. FG was supported in part by NSF grant AST-0098557 and the Spitzer Telescope Theory Grant. Simulations were run at ARSC. We thank our collaborators for allowing us to show results before publication.

References

Abadi M. G., Navarro J. F., Steinmetz M., Eke V. R., 2003a, ApJ, 591, 499

Benson A. J., Frenk C. S., Lacey C. G., Baugh C. M., Cole S., 2002, MNRAS, 333, 177

Brinchmann J. et al. 2004, MNRAS, 351, 1151

Giovanelli, R. et al. 1997, AJ, 113, 53

Governato F., Mayer L., Wadsley J., Gardner J. P., Willman B., Hayashi E., Quinn T., Stadel J., Lake G., 2004, ApJ, 607

Governato F., Stinson G., Wadsley J. & Quinn, T. 2005 (astro-ph/0509263)

Gurovich, S., McGaugh, S. S., Freeman, K. C., Jerjen, H., Staveley-Smith, L., & De Blok, W. J. G. 2004, PASA, 21, 412

Haardt F., Madau P., 1996, ApJ, 461, 20

Li, Y., Mo H.J. and van den Bosch, F. 2005 (astro-ph/0510372)

Katz, N., & White, S. D. M. 1993, ApJ, 412, 455

MacArthur L. A., Courteau S., Bell E., Holtzman J. A., 2004, ApJS, 152, 175

Maller A., et al. 2005, (astro-ph/0509474)

McGaugh, S. S., Schombert, J. M., Bothun, G. D., & de Blok, W. J. G. 2000, ApJL, 533, L99

McGaugh, S. S. 2005, ApJ, 632, 859

McKee C. F., Ostriker J. P., 1977, ApJ, 218, 148

Moore, B., Ghigna, S., Governato, F., Lake, G., Quinn, T., Stadel, J., & Tozzi, P. 1999, ApJL, 524, L19

Navarro J. F., Steinmetz M., 2000, ApJ, 538, 477

Pohlen M. and Trujillo I., these proceedings, p. 253. (astro-ph/0509057)

Silva, L., Granato, G. L., Bressan, A., & Danese, L. 1998, ApJ, 509, 103

Stinson G., et al. 2005, submitted.

Thacker R. J., Couchman H. M. P., 2000, ApJ, 545, 728

Wadsley J. W., Stadel J., Quinn T., 2004, New Astronomy, 9, 137

Willman, B., et al. 2005, AJ, 129, 2692

Willman, B., Governato, F., Dalcanton, J. J., Reed, D., & Quinn, T. 2004, MNRAS, 353, 639

Fabio Governato contemplating some galaxy formation models.

COLLAPSE OF THE PRIMORDIAL GAS CLOUDS IN THE PRESENCE OF UV RADIATION FIELD

Jaroslaw Stasielak[1*], Slawomir Stachniewicz[2**] and Marek Kutschera[2,1***]

[1] *Institute of Physics, Jagiellonian University, Krakow, Poland*

[2] *Astrophysics Division, H.Niewodniczański Institute of Nuclear Physics, Krakow, Poland*

* stasiela@th.if.uj.edu.pl, **Slawomir.Stachniewicz@ifj.edu.pl, *** Marek.Kutschera@ifj.edu.pl

Abstract Our goal is to study the effects of the UV radiation from the first stars, quasars and hypothetical Super Heavy Dark Matter (SHDM) particle decays on the formation of primordial bound objects in the Universe. We trace the evolution of a spherically symmetric density perturbation in the Lambda Cold Dark Matter and MOND model, solving the frequency-dependent radiative transfer equation, non-equilibrium chemistry, and one-dimensional gas hydrodynamics. We concentrate on the destruction and formation processes of the H_2 molecule, which is the main coolant in the primordial objects.

Keywords: dark matter - early universe - radiative transfer

1. Introduction

The existence of the first objects is a direct consequence of the growth of the primordial density fluctuations. At the beginning, there are linear density perturbations which expand with the overall Hubble flow. Subsequently, these perturbations can grow and form primordial clouds. Clouds with enough density contrast decouple from this flow and start to collapse. The kinetic energy of the infalling gas is dissipated through shocks and the cloud becomes pressure supported. The further evolution of the cloud is determined by its ability to cool sufficiently fast. Clouds which could not cool fast enough will stay in a pressure-supported stage and will not form any stars. The existence of the efficient cooling mechanism is necessary to continue the collapse of the cloud, its subsequent fragmentation and star formation.

In our work we are interested in the first generation of stars which are still forming in the low mass clouds when first luminous objects already exist. These objects are made from the primordial gas so they are metals free. It is simply because the first stars did not have much time to produce them. These objects could be irradiated by the UV and X-rays radiation produced by the

R. S. de Jong, Island Universes, 565–568.
© 2007 *Springer.*

first stars, quasars and hypothetical Super Heavy Dark Matter (SHDM) particle decays (Doroshkevich & Naselsky 2002; Shchekinov & Vasiliev 2004).

In the absence of metals, the most important cooling mechanism for low-mass primordial clouds is so called 'H_2 cooling', i.e. cooling by radiation of excited rotational and vibrational states of H_2 molecule. The presence of initial mass fraction of the molecular hydrogen H_2 of only 10^{-6} is enough to trigger the final collapse of low mass clouds.

However, molecular hydrogen is fragile and can easily be photo-dissociated by photons with energies of 11.26 - 13.6 eV (Lyman and Werner bands)(Shull & Beckwith 1982). Destruction of the H_2 would stop collapsing of the low mass clouds and decrease star formation rate. On the other hand X-rays radiation can increase production of the H_2 by enhancement of free electrons fraction. From above we see that the UV and X-rays radiation background alters the subsequent growth of cosmic structures. It regulates star formation rate so it has important implication to the re-ionization history of the Universe (Cen 2003). It is therefore crucial to determine quantitatively the consequences of radiation feedback on the formation of early generation objects.

Feedback of the UV background to the collapse of the spherically symmetric primordial gas cloud was studied by many authors (Tajri & Umemura 1998; Kitayama & Ikeuchi 2000; Kitayama et al. 2000; Kitayama et al. 2001; Omukai 2001). However their calculation was simplified. They have been using the so called self-shielding function (Draine & Bertoldi 1996). Our approach includes solving the frequency-dependent radiative transfer equation in the 'exact' way. We also try to check the evolution of the collapsing cloud in the MOND model.

2. Description of the Code

In the Newtonian case dynamics is governed by the following equations:

$$\frac{dM}{dr} = 4\pi r^2 \varrho, \tag{1}$$

$$\frac{dr}{dt} = v, \tag{2}$$

$$\frac{dv}{dt} = -4\pi r^2 \frac{dp}{dM} - \frac{GM(r)}{r^2}, \tag{3}$$

$$\frac{du}{dt} = \frac{p}{\varrho^2}\frac{d\varrho}{dt} + \frac{\Lambda}{\varrho}, \tag{4}$$

where r is the radius of a sphere of mass M, u is the internal energy per unit mass, p is the pressure and ϱ is the mass density. Here eq.(1) is the continuity equation, (2) and (3) give the acceleration and (4) accounts for the energy conservation. The last term in the eq.(4) describes cooling/heating of the gas, with Λ being the energy absorption (emission) rate per unit volume.

Λ consist of two parts, that is, the radiative cooling Λ_{rad} and the chemical cooling Λ_{chem}. The former can be written as

$$\Lambda_{rad}\left(m\right) = -\varrho \frac{\partial L\left(m\right)}{\partial m}. \tag{5}$$

The luminosity $L\left(m\right)$ is obtained by solving radiative transfer equation.

The net chemical cooling rate Λ_{chem} is given by

$$\Lambda_{chem} = \varrho \frac{\partial \epsilon_{chem}}{\partial t} \tag{6}$$

where ϵ_{chem} is the chemical binding energy per unit gas.

We use the equation of state of the perfect gas

$$p = (\gamma - 1)\varrho u, \tag{7}$$

where $\gamma = 5/3$, as the primordial baryonic matter after recombination is assumed to be composed mainly of monoatomic hydrogen and helium, with the fraction of molecular hydrogen H_2 always less than 10^{-3}.

In case of modified gravity (MOND) we do not include the dark component but it is necessary to modify equation (3). Details are shown in Stachniewicz & Kutschera (2005).

In the simulations we have used the code described in Stachniewicz & Kutschera (2001), based on the codes described by Thoul & Weinberg (1995) and Haiman, Thoul & Loeb (1996). This is a standard, one-dimensional, second-order accurate Lagrangian finite-difference scheme.

We start our calculations at $z = 500$ or the end of the radiation-dominated era. We use our own code to calculate the initial chemical composition and initial gas temperature. Initial overdensities may be calculated from the power spectrum which may be obtained e.g. using the CMBFAST program by Seljak & Zaldarriaga (1996).

We apply initial density profiles in the form of a single spherical Fourier mode used also by Haiman, Thoul & Loeb (1996)

$$\varrho_b(r) = \Omega_b \varrho_c (1 + \delta \frac{\sin kr}{kr}), \tag{8}$$

where ϱ_c is the critical density of the Universe, $\varrho_c = 3H^2/8\pi G$ with H being the actual value of the Hubble parameter. As the initial velocity we use the Hubble velocity:

$$v(r) = Hr. \tag{9}$$

In our calculations we include nine species: H, H^-, H^+, He, He^+, He^{++}, H_2, H_2^+ and e^-. Full list of relevant chemical reactions, appropriate formulae,

reaction, photoionization and photodissociation rates is given in Stachniewicz & Kutschera (2001).

3. Radiative Transfer Equation in Spherical Symmetry

In addition to eq. (1) - (4) we solve non-relativistic, time-independent equation for radiation transport in spherical geometry:

$$\mu \frac{\partial I_\nu}{\partial r} + \frac{1-\mu^2}{r} \frac{\partial I_\nu}{\partial \mu} = \varrho \left\{ j_\nu (r) - \kappa_\nu (r) I_\nu \right\}, \tag{10}$$

where $I_\nu = I_\nu (r, \mu)$ is the intensity of radiation of frequency ν, at radius r and in the direction $\mu = \cos\theta$, where θ is the angle between the outward normal and photon direction. $\kappa_\nu (r)$ is the emissivity and $j_\nu (r)$ opacity at radius r.

Our scheme of solving this equation is similar to method from Mihalas & Mihalas (1984) and York (1980). Detailed results will be described in a paper, which is in preparation.

References

Cen R., 2003, ApJ 591, 12
Doroshkevich A. G., Naselsky P. D., 2002 (astro-ph/0201212)
Draine B. T., Bertoldi F., 1996, ApJ 468, 269
Haiman Z., Thoul A. A., Loeb A., 1996, ApJ 464, 523
Kitayama T., Ikeuchi S., 2000, ApJ 529, 615
Kitayama T., Tajiri Y., Umemura M., Susa H., Ikeuchi S., 2000, MNRAS 315, L1
Kitayama T., Susa H., Umemura M., Ikeuchi S., 2001, MNRAS 326, 1353
Mihalas D., Mihalas B. W., 1984, 'Foundations of Radiation Hydrodynamics', pages 378-381, (New York: Oxford Univ. Press)
Omukai K., 2001, ApJ 546, 635
Shull J. M., Beckwith S., 1982, Ann. Rev. Astron. Astrophys. 20, 163
Seljak U., Zaldarriaga M., 1996, ApJ 469, 437
Shchekinov Y. A., Vasiliev E. O., 2004, A&A 419, 19
Stachniewicz S., Kutschera M., 2001, Acta Phys. Pol. B 32, 227
Stachniewicz S., Kutschera M., 2005, MNRAS 362, 89
Tajiri Y., Umemura M., 1998, ApJ 502, 59
Thoul A. A., Weinberg D. H., 1995, ApJ 442, 480
York H. W., 1980, A&A 86, 286

IX

CONFERENCE SUMMARY

Mike Disney giving his congratulations speech to Piet van der Kruit at the barbecue held in the beach restaurant “De Branding”.

ISLAND UNIVERSES

Tim de Zeeuw

Leiden Observatory, The Netherlands
dezeeuw@strw.leidenuniv.nl

Keywords: galaxies: spiral

1. In the Footsteps of Kapteyn

This has been an exciting conference covering a large range of topics on the properties of disk galaxies, much of it related to pioneering work done by Piet van der Kruit, the Jacobus C. Kapteyn Distinguished Professor of Astronomy at the University of Groningen. Let me therefore first say a few words about Piet, and then highlight some of the main results presented here this week.

Piet received his PhD degree with Jan Oort in Leiden in 1971, at the time when the Westerbork Synthesis Radio Telescope came on line. He was one of the first to publish data obtained with it, and rapidly established himself as an authority in radio studies of nearby galaxies. In the late seventies, Piet shifted his attention to optical studies of disk galaxies. Together with Leonard Searle, he wrote an influential set of papers which established that stellar disks are truncated at about four exponential scale-lengths, and that the vertical scale-height of disks is constant with radius. He obtained early stellar kinematic measurements of disks with Ken Freeman, and was quick to use new instrumental approaches. An example is his realization that the imager on the Pioneer 10 interplanetary probe could be used to measure the surface brightness distribution and scale-length of the Milky Way. Piet supervised the production of about a dozen high-quality PhD theses, and he continues to be active in research. This is a remarkable achievement considering his major management and science policy activities in the past two decades. These included a stint as dean of the Faculty of Science in Groningen, directing the Kapteyn Institute for a decade, chairing the boards of ASTRON and NOVA, and many advisory and oversight functions on the international level, most recently as President of the ESO Council and Chair of the ALMA Board.

It is appropriate to record that Piet also made some remarkable discoveries in statistics. The legendary papers with Leonard Searle have Piet as first author on all of them due to the use of the *van der Kruit guilder*. The discovery paper is reproduced in Figure 1, and exemplifies Piet's style: concise and to the point.

R. S. de Jong, Island Universes, 571–578.
© 2007 *Springer.*

Curiosités Numismatiques (Monte Carlo), No. 427. (1982)

THE VAN DER KRUIT GUILDER

by

P.C.van der Kruit
L.Searle

Summary The van der Kruit guilder is described.

1. Introduction.

In this monograph we describe the recently discovered van der Kruit guilder.

2. Description.

The van der Kruit guilder is shown in figure 1.

Front Back

Fig. 1.

3. Conclusion.

This concludes our description of the van der Kruit guilder.

Acknowledgement We thank Méta Morphose for her continued interest.

Reference

Searle,L. and van der Kruit,P.C. 1983, The Searle Shilling, Curiosités Numismatiques, Monte Carlo, No.432.

Figure 1. The paper on the van der Kruit guilder cited in the influential series of papers on *Surface-photometry of edge-on spiral galaxies* by van der Kruit & Searle (1981a, b, 1982a, b). It was not needed in Paper V of the series, in which Piet used Pioneer 10 data to measure the scalelength of the Milky Way (van der Kruit 1986).

2. Structure and Evolution of Disk Galaxies

This conference saw many new (and some old) results on disk galaxies. The talks and poster contributions demonstrated clearly that these systems are quite complex *Island Universes*, and that their properties pose a considerable challenge to the theory of galaxy formation (as reviewed by Freeman and Silk). In these concluding remarks, I draw attention to some results on the various components of these galaxies, briefly comment on new insights provided by ongoing panchromatic surveys, and close with a glimpse into the future.

Stellar Disks

The basic properties of the surface brightness distribution of stellar disks were established by Freeman (1970) and van der Kruit & Searle (1981a, b, 1982a, b), based on photographic photometry. Various speakers addressed recent work in this area. Three types of surface brightness profiles are seen, namely the pure exponential profile (corresponding to the canonical Freeman disk) extending out to as much as nine scalelengths (Pohlen). Many galaxies instead have a double exponential profile, with the outer slope steeper than the inner slope; these are essentially the truncated profiles discovered by van der Kruit & Searle, and reminiscent of Freeman's 'Type II' curves. A third class of galaxies also displays double exponential profiles, but these have an outer slope that is shallower than the inner slope. Pérez reported evidence that the ratio of inner to outer scalelengths is fairly constant out to a redshift of about one.

At least during this conference, there appeared to be some confusion on whether studies of face-on objects and those of edge-on systems (where the effect of the line-of-sight integration is different) agree. There is also some uncertainty about the relative numbers in each of the three classes of galaxies. We heard initial reports on automated measurements of the structural properties of disks in very large samples, including the Sloan Digital Sky Survey and the Millennium Galaxy Catalogue (Allen). This should resolve the inclination issues and establish the relative importance of the three classes.

A fascinating new development in this area is provided by detailed studies of the nearest galaxies, based on star counts. This allows disks to be traced to very faint (integrated) magnitudes. Heroic counts in M31 by Ferguson's team, based on the wide-field mosaic obtained with the Isaac Newton Telescope on La Palma, and related work by Guhathakurta and colleagues, not only traces various streams of stars in the halo of the nearest large spiral galaxy, but also revealed tantalizing evidence for a giant extended structure perhaps as large as 100 kpc. It is not yet clear whether this is a giant disk or a metal-poor halo, or how it formed, but spectroscopy obtained at 8-10m class telescopes provides kinematics and [Fe/H] measurements, and should clarify this soon.

Some disk galaxies display UV and Hα emission which extends well beyond the Holmberg radius, suggesting recent star formation in the 'Outer Banks' (Zaritsky). It is not clear whether the presence of these stars is in harmony with the canonical threshold for star formation (Kennicutt 1998), or whether there is a link with the presence of a flaring or warped HI disk.

Thick Disks

In addition to the standard stellar disk, most spirals contain a thick disk of modest mass. The mass fraction appears to increase in galaxies with a circular velocity below about 120 km/s, and spectroscopic observations with Gemini show that some thick disks counter-rotate relative to the main disk of the galaxy (Dalcanton). This strongly suggests an external origin, and resembles the situation in S0 galaxies, where a number of cases are known of counter-rotating disks with different scaleheights.

The run of [α/Fe] versus [Fe/H] indicates that the thick disk of the Milky Way cannot have formed by accretion of small stellar lumps (Venn). The inference is that all these structures formed via *wet* accretion, i.e., an accretion of perhaps a small satellite, but involving gas. The theorists, of course, reminded us that they thought this all along, but it is gratifying to see that high-resolution simulations are now being carried out to compare this scenario in detail with observed galaxies (Bullock, Brook, Governato, Sommer–Larsen).

Bars

Nearly 70% of disk galaxies contain a large-scale stellar bar (Knapen). This influences the dynamics in the disks, allows efficient redistribution of angular momentum, and can drive gas to the center (as do interactions) which can trigger a starburst, sometimes in a spectacular ring (Falcon–Barroso, Allard). The bars themselves slow down and change shape due to friction by the halo. Determining the rate of slowing down has been a long-standing problem, but recent work by Sellwood and Athanassoula appears to have sorted this out—at last. However, it is not yet clear whether this result is consistent with the constant bar fraction observed in galaxies since redshift one (Bell).

Impostor Bulges

It has become clear in the past decade that the bulges of disk galaxies comprise a mix of structures, with subclassifications into classical and 'pseudo' bulges, bars and 'peanuts'. The nomenclature is colorful but the nature of the central regions remains a subject of confusion. Perhaps as many as half of all disk galaxies have 'classical' bulges with a de Vaucouleurs' $R^{1/4}$ surface brightness profile and substantial rotation. These appear quite similar to small E/S0 galaxies. High-resolution imaging with the Hubble Space Telescope

(HST) revealed that the remaining 'bulges' have approximately exponential light profiles, and may in fact be small disks with a central star cluster (Carollo 1999). These structures are sometimes referred to as pseudo-bulges (Kormendy & Kennicutt 2004), but their definition may need further clarification, as the label is often connected to preconceived notions on formation. Perhaps a new name is useful, as emphatic statements made during this conference that the speaker believes that such-and-such a galaxy has 'a real pseudo bulge' are not very illuminating to the uninitiated.

Elmegreen argued that bars do not transform into bulges today, as some scenarios have it, while Bureau reminded us that 'an end-on peanut looks like a bulge', so that a central bar may in some cases *be* the bulge.

A related topic which, however, was not discussed during this conference is the presence/absence of supermassive black holes in the nuclei of disk galaxies, and the relation with the nature of the central regions.

Extraplanar Gas and Warps

Extended extraplanar gas is seen in nearby edge-on galaxies in HI (Fraternali/Sancisi) and in Hα and X-rays (Dettmar). The properties appear consistent with the theory of galactic fountains and winds, and it is not evident that in-situ star formation is needed in the halo, as has been suggested. It will be interesting to investigate the effect of the odd run-away O/B star that escapes from the disk population at high speed, and finds itself in the halo before expiring in a supernova explosion.

Binney reviewed the origin of warps, in a talk which was interrupted by one of the more spectacular rainstorms seen in the Low Countries in the past decade, and saw more than half the audience run to their rooms to close the windows. After a simple "my goodness" Binney continued unfazed by this behavior, and demonstrated that warps are most likely caused by the torques on the dark halo related to the local cosmic inflow pattern. This may provide a way to read more of the fossil record of the formation of, e.g., the Local Group, and, in any case, is clear evidence that disk galaxies are, in fact, not isolated island universes.

Dark Halos

Studies of dark halos based on HI rotation curves are now mature (de Blok). It seemed to me, at least, that the field needs to move beyond the 'cusp wars' regarding the central structure of dwarf and low-surface-brightness galaxies, and the arguments whether it is the observers who do their measurements wrong, or the theorists who are missing key ingredients in their N-body simulations. I was impressed to see recent progress in this area using an approach pioneered by Piet and developed further by his student Bottema, namely the measurement

of the stellar $M/L_\star$ of the disk (e.g., Bottema 1993). This requires measuring the vertical velocity dispersion, which breaks the degeneracy between the contributions of the stellar and halo mass to the observed rotation curve. Comparison of the resulting dynamical $M/L_\star$ with the value inferred from the colors and line-strengths sets important limits on the IMF (de Jong), and on the specific angular momentum content of the halo (Kassin). Multi-slit, or, even better, integral-field spectroscopy is the next step, as it simultaneously constrains the shape of the velocity ellipsoid and the value of $M/L_\star$. We were treated to a preview on this by Verheijen and Bershady.

The Milky Way

Kapteyn's own Island Universe received relatively little attention at this conference. Binney discussed the kinematics of disk stars in the Milky Way, and Venn showed evidence that the stellar halo cannot have formed by dissolving present-day dwarf spheroidals, dIrr or LMC clones. But a detailed comparison of Milky Way properties with simulations of galaxy formation constitute a key test of the entire formation paradigm (Bullock, Sommer–Larsen, Governato). There is much room for further work here.

3. Panchromatic Surveys

The recent launch of the GALEX and Spitzer space telescopes has enabled high-quality imaging of galaxies from the UV via the optical and the infrared to CO/HI in the millimeter and radio regime (Kennicutt, Regan, Murphy, Matthews, Braun). The near and mid-infrared maps allow separation of stars and dust, and provide a test of the dust extinction derived from groundbased NIR data (Alves) and other methods (Holwerda). The panchromatic maps obtained as part of surveys such as the SINGS Legacy Program in principle provide good estimates of the spectral energy distribution as function of position, of star formation rates, constrain the lifetime of embedded phases of massive star formation, and delineate the cosmic-ray structure, all as a function of Hubble type. The challenge is to model all this in detail, and Dopita showed us the way forward here, in a comprehensive presentation with impressive graphics.

The next step is to obtain similar panoramic information for nearby galaxies at much higher spectral resolution. This has been available at radio wavelengths for over three decades, and the deployment of integral-field spectrographs allows the optical community to finally catch up. Examples of the value of such studies were presented by Falcon–Barroso, Ganda, and Verheijen. Despite Kennicutt's suggestion that the SINGS/HUGS community is the team to join, even he agreed that the darker forces employing all-seeing eyes such as SAURON should be watched with interest, if not trepidation.

Much ongoing work addresses properties of galaxies to high redshift, and we were treated to a whirlwind overview on the last day of the conference. These studies observe galaxy evolution over much of the history of the Universe, but at the expense of limited spatial resolution. Most objects found to date are the progenitors of present-day spheroids (Pettini), although disks have been detected to a redshift of about two (Abraham/Kassin) and the Damped-Lyman-α (DLA) systems seen in the spectra of distant quasars resemble local galaxies with HI (Zwaan). There is substantial evidence for inside-out formation (Bell/Trujillo), but proper correction for selection bias is critical (Vogt) and one should keep in mind that the evolution of a population is not the same as the evolution of the individual objects (Bell). I was impressed by the recent progress on determining metallicities in disks to redshifts as large as three, reported by Kewley, and by similar studies for the intergalactic medium summarized by Fall. Both speakers made it clear that the samples are not as large as one would want, and that selection effects are important.

4. The Future

Ongoing and planned spectroscopic studies of the resolved stellar populations in the Milky Way and Local Group galaxies will teach us much. Panchromatic surveys of nearby galaxies complemented by integral-field spectroscopic studies in the optical and near-infrared are now possible, and the new adaptive-optics assisted instruments SINFONI, NIFS and OSIRIS on 8-10m class telescopes will allow extension of spatially resolved studies of the integrated light of galaxies to substantial redshifts. Theoretical models and simulations need to fit the observations in detail, and this appears within reach, not only for accretion of individual satellites in the early history of Local Group galaxies, but also for the evolution of populations of cluster and field objects.

The Herschel Space Observatory will be launched in a few years, followed in about 2013 by the James Webb Space Telescope. Both will be complemented by ALMA. This will provide a major jump in sensitivity and resolution at infrared and submillimeter wavelengths, further enabling studies of galaxy evolution to high redshift. The launch of GAIA in 2011 will result in a three-dimensional stereoscopic survey of the entire Milky Way and its halo, which will reveal the fossil record of formation of our own galaxy with unprecedented precision. All this bodes well for the future, and there clearly is much scope for further pioneering work by Piet.

Acknowledgements It is a pleasure to congratulate Roelof de Jong with organizing such a stimulating conference, to thank Jesus Falcon–Barroso, Leonie Snijders and Remco van den Bosch for assistance with the manuscript, and to thank Piet and Corry for a longstanding and warm friendship.

References

Bottema R., 1993, A&A, 275, 16
Carollo C.M., 1999, ApJ, 523, 566
Freeman K.C., 1970, ApJ 160, 811
Kennicutt R.C., 1998, ARA&A, 36, 189
Kormendy J., Kennicutt R.C., 2004, ARA&A, 42, 603
van der Kruit P.C., Freeman K.C., 1986, ApJ, 303, 556
van der Kruit P.C., Searle L., 1981a, A&A, 95, 105
van der Kruit P.C., Searle L., 1981b, A&A, 95, 116
van der Kruit P.C., Searle L., 1982a, A&A, 110, 61
van der Kruit P.C., Searle L., 1982b, A&A, 110, 79
van der Kruit P.C., 1986, A&A, 157, 230

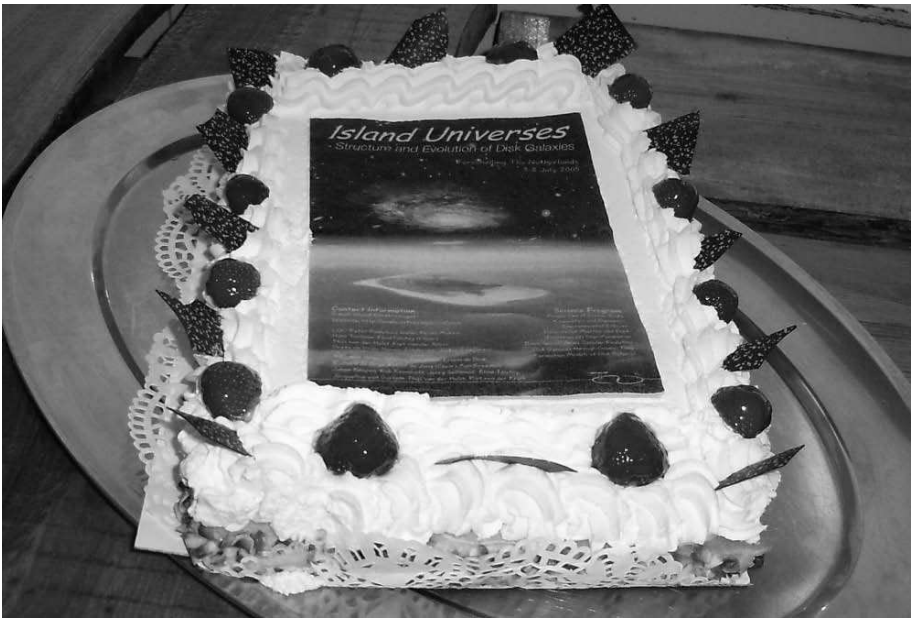

Dessert after the barbecue: Island Universes cake!

Index

Astrophysics and Space Science Proceedings

Volume 1: ***Diffuse Matter from Star Forming Regions to Active Galaxies***, edited by T.W. Hartquist, J.M. Pittard, S.A.E.G. Falle
Hardbound ISBN 978 1-4020-5424-2, December 2006

Volume 2: ***Solar, Stellar and Galactic Connections between Particle Physics and Astrophysics***, edited by A. Carramiñana, F.S. Guzmán, and T. Matos
Hardbound ISBN 978 1-4020-5574-4, December 2006

Volume 3: ***Island Universes***, ***Structure and Evolution of Disk Galaxies*** edited by R. de Jong
Hardbound ISBN 978 1-4020-5572-0, December 2006

For further information about this book series we refer you to the following web site: www.springer.com